Concentration and fractionation of Rare Earth Elements in alkaline complexes : the role of fluids

Cyrielle Bernard

THÈSE

En vue de l'obtention du

DOCTORAT DE L'UNIVERSITÉ DE TOULOUSE

Délivré par : *l'Université Toulouse 3 Paul Sabatier (UT3 Paul Sabatier)*

Présentée et soutenue le *23 octobre 2020* **par :**

Cyrielle BERNARD

Concentration et fractionnement des Terres Rares dans les complexes alcalins : le rôle des fluides

---

JURY

Kathryn	GOODENOUGH	British Geological Survey	Rapportrice
Alexandre	TARANTOLA	Université de Lorraine	Rapporteur
Michel	GRÉGOIRE	Université Toulouse 3	Examinateur
Anne-Sylvie	ANDRÉ-MAYER	Université de Lorraine	Examinatrice
Didier	BÉZIAT	Université Toulouse 3	Directeur de thèse
Guillaume	ESTRADE	Université Toulouse 3	Co-directeur de thèse
Stefano	SALVI	Université Toulouse 3	Invité
Julien	BERGER	Université Toulouse 3	Invité

École doctorale et spécialité :
SDU2E : Sciences de la Terre et des Planètes Solides
Unité de Recherche :
Géosciences Environnement Toulouse (UMR5563)
Directeurs de Thèse :
Didier BÉZIAT, *Guillaume ESTRADE* et *Stefano SALVI*

Acknowledgements

Although this manuscript is written in English, you will have to forgive me but I would like to thank everyone who accompanied me during these three years in French, my native language.

J'adresse tout d'abord un immense merci à mes encadrants, MM. Guillaume Estrade, Stefano Salvi et Didier Béziat. Guillaume, pour ton guidage constant, depuis les couloirs labyrinthiques de l'OMP lors de notre première rencontre jusqu'à l'aboutissement de ce manuscrit, tu m'as permis de trouver la sortie sans me brûler les ailes. Stefano, pour avoir toujours trouvé du temps pour moi, même au beau milieu d'une pandémie, entre un HDR, un conseil de laboratoire et 3 articles à relire. Et Didier, pour tes conseils avisés, même après la retraite : vers l'infini et au-delà !

Je remercie beaucoup Kathryn Goodenough et Alexandre Tarantola pour avoir accepté d'être les rapporteurs de ce travail. Votre lecture attentive et vos commentaires ont permis d'améliorer la version finale de ce travail de longue haleine.

Je remercie également les nombreuses personnes qui contribué à la bonne réalisation des analyses dans ce travail. Merci à Philippe de Parseval et Sophie Gouy pour leur implication et leur curiosité constante sur mon travail. Merci aussi à Thierry Aigouy pour son aide et sa réactivité lors des séances MEB, pour le meilleur et pour le pire (!). Merci également à Fabienne de Parseval pour la fabrication des lames minces sur lesquelles j'ai passé tant d'heures. Merci à David Chew et Foteini Drakou du Trinity College, Irlande, pour leur aide dans la réalisation de cartographies ICPMS. Merci à Chris Harris de l'Université de Cape Town, Afrique du Sud, ainsi que Etienne Deloule, Gaston Giuliani, Michel Champenois et Nordine Bouden du CRPG Nancy pour les analyses isotopiques. J'aimerais également remercier toutes les personnes qui m'ont aidée ponctuellement dans mes analyses : Sabine Choy pour l'accompagnement au broyage et à la séparation magnétique de mes roches, François Martin pour les analyses Mössbauer des pyroxènes, Claudie Josse et Teresa Hungria pour les observations MET dans ces mêmes pyroxènes, Yves Auda pour son accompagnement patient dans l'écriture

du programme informatique pyroxènes, Corinne Routaboul pour les analyses de spectroscopie infrarouge sur les elpidites, Franck Poitrasson pour son aide à propose d'Evisa, et Aurélie Marquet pour les analyses LA-ICPMS. J'adresse ma gratitude à Marc de Rafélis pour son tutorat en tant qu'enseignant. Enfin, j'aimerais remercier Margot Munoz, Loïc Drigo, Carine Baritaud et Anne-Marie Cousin qui, même sans être directement connectés à mon doctorat, ont toujours été disponibles et souriants en toute situation.

Un doctorat ne peut s'effectuer sans compagnons de route avec qui partager les bons et les moins bons moments. J'ai eu la chance de partager un bureau international et soudé avec Salomé, Aruã, Gina et Benjamin. Merci pour votre bonne humeur, le bureau H137 n'a pas fini d'entendre des discussions passionnées la bouche pleine de gâteaux ! J'adresse une pensée particulière à Salomé : nous avons commencé notre thèse en même temps et, quelques guacamoles plus tard, nous la finissons ensemble. Je remercie également Steven et Gaétan qui m'ont, entre autres, suivie dans la folle aventure du Student Chapter. Nos péripéties espagnoles défilent dans ma tête... à une vitesse plus ou moins raisonnable ! Je remercie aussi Adrien, stagiaire devenu camarade par son sérieux et sa gentillesse. Merci également à tous ceux que j'ai côtoyés le temps d'une discussion ou d'un café : Anissa, Dahédrey, Sylvain, Rémi, Paty, Beatriz, Loïs, Vianney, et les autres. Enfin, merci à ceux qui étaient là avant : Samuel, mon jumeau semi-géologue; Aurélie, qui j'en ai bien peur ne comprendra jamais ma passion pour "les cailloux"; et Guilhem et Stellina, les meilleurs colocataires que l'on puisse souhaiter.

Je ne peux évidement pas conclure ces remerciements sans envoyer une vague de gratitude à ma famille. Merci à mes parents, Nicole et Frédéric, qui ont cru en moi depuis le tout début. Vous avez été présents à chaque nouvelle étape de ma vie, encourageants et fiers quoi qu'il arrive. Vous m'avez donné les moyens de naviguer par moi-même dans ce monde et pour ça je ne vous remercierai jamais assez. Merci à mes sœurs, Candice et Lucile. Vous êtes le moteur qui me permet d'avancer, et je suis fière de vous.

Enfin, merci à toi Nicolas, qui m'accompagne depuis déjà bien trop longtemps. Ton soutien indéfectible m'a permis d'aller plus loin que jamais.

Abstract

The rare earth elements (REE) are critical resources used in many modern technologies, including high tech and renewable energy infrastructure. Their worldwide production is currently mostly restricted to China and Australia. The REE are divided in two groups, i.e. light REE (LREE, La-Eu) and heavy REE (HREE, Gd-Lu), the latter being rarer and with more industrial uses. REE deposits can be primary high temperature (igneous, carbonatites and alkaline systems) or secondary low temperature (placers and ion-adsorption). Type and grade of REE resources depends on many parameters including primary igneous source, magmatic processes, hydrothermal fluids circulation, and/or weathering. Among primary high temperature deposits, alkaline granites and associated pegmatites are the richest in HREE. Although it is accepted that magmatic processes are fundamental in concentrating the REE, the role of hydrothermal fluids in concentrating and fractionating these elements remains unclear.

This manuscript investigates the importance and characteristics of hydrothermal fluids in concentrating and fractionating the REE relatively to magmatic and source processes. To do so, petrography and fluid inclusions are studied in six alkaline complexes worldwide, namely Amis (Namibia), Evisa (Corsica), Khan Bogd (Mongolia), Strange Lake (Canada), and Ambohimirahavavy and Manongarivo (Madagascar). The comparison of these complexes allows to draw general conclusions about REE enrichment and fractionation in alkaline complexes.

This study shows that the main mineralogy is similar in all complexes and is made of quartz, alkali feldspar, Na-amphiboles, aegirine, and a complex zirconosilicate (elpidite or an eudialyte-group-mineral, EGM). Despite local variations, many accessory minerals are also common to most of these alkaline complexes, such as pyrochlore-group-minerals, zircon, and Fe and/or Ti-oxides. Amphibole, EGM, elpidite and feldspars grew exclusively during magmatic stage. Quartz and aegirine are zoned and grew from magmatic to hydrothermal stages; feldspars and primary zirconosilicates got hydrothermally altered. Primary

zirconosilicates are commonly replaced by an assemblage of secondary minerals forming pseudomorphs. They present a wide variety of chemistries (silicates, oxides, halides, carbonates, phosphates). The detailed study of zoning and alteration of amphiboles and aegirine, which is the topic of a published paper, shows that hydrothermal fluids do mobilize and fractionate the REE. A quantitative estimation confirms their high importance compared with magmatic processes. A similar study of zircon highlights the local influence of these processes, as the REE composition of zircon in pseudomorphs depends on the REE composition of the replaced mineral. These observations point out the importance of studying rock-forming minerals such as pyroxenes and amphiboles to unravel geological events controlled by common processes.

Composition and origin of hydrothermal fluids is explored through microthermometric and SEM studies of fluid inclusions in quartz of the six complexes. They reveal that although their salinity varies a lot, fluids circulate at a relatively low temperature (< 400 °C). All investigated complexes experienced the circulation of at least two fluids, one Na- and K-rich, and one Ca- and Na-rich. At the Malagasy complexes and Strange Lake, it has been established that the Na-K-bearing fluid is orthomagmatic and the Ca-Na-bearing one is secondary.

In conclusion, this work shows that REE enrichment and fractionation in alkaline granites and associated pegmatites is linked to the circulation of a Na-K-rich and a Ca-Na-rich fluid, at temperatures below 400 °C. This fluid contains REE ligands such as F, OH, Cl that fractionate the REE. Their influence is mostly local, but evidences such as REE-bearing phase in fractures point to a more global mobilization and fractionation.

Résumé

Les terres rares (TR) sont des métaux critiques utilisés dans les nouvelles technologies, dont les énergies renouvelables, et produites surtout en Chine et en Australie. Les TR sont divisées en TR légères (La-Eu) et TR lourdes (Gd-Lu). Ces-dernières sont plus rares, et ont plus d'applications. Les gisements de TR peuvent être primaires, formés à haute température (ignés, carbonatites, systèmes alcalins) ou secondaires, de plus basse température (placers, argiles à adsorption d'ions). Le type et le tonnage des gisements de TR dépendent de nombreux paramètres comme la source du magma, les processus magmatiques, la circulation de fluides hydrothermaux, et/ou l'altération. Les granites alcalins sont les gisements primaires les plus riches en TR lourdes. Actuellement, si le rôle des processus magmatiques est accepté pour la concentration et le fractionnement des TR, celui des fluides hydrothermaux pose question.

Ce manuscrit se concentre sur l'importance relative des fluides hydrothermaux par rapport aux processus magmatiques pour le comportement des TR. Pour cela, une étude détaillée de la pétrographie et des inclusions fluides de six complexes alcalins est effectuée. Ces complexes sont Amis (Namibie), Evisa (Corse), Khan Bogd (Mongolie), Strange Lake (Canada), et Ambohimirahavavy et Manongarivo (Madagascar). La comparaison entre ces six complexes permet une conclusion générale sur l'origine de l'enrichissement et du fractionnement des TR dans les complexes alcalins.

Cette étude montre que la minéralogie principale des six complexes est similaire. Elle est formée de quartz, feldspath alcalin, amphibole-Na, aégyrine, et d'un zirconosilicate complexe (elpidite ou eudialyte). La plupart des minéraux accessoires sont communs à tous les complexes, avec quelques variations. Les principaux sont le pyrochlore, le zircon, et les oxydes de Fe et/ou Ti. L'amphibole, l'eudialyte, l'elpidite et les feldspaths se sont formés au stade magmatique. Le quartz et l'aégyrine sont zonés et ont cru du stade magmatique à hydrothermal ; les feldspaths et les zirconosilicates primaires ont été altérés au stade hydrothermal.

Ces-derniers sont souvent remplacés par un assemblage de minéraux variés (silicates, oxydes, halides, carbonates, phosphates) formant des pseudomorphoses. L'étude détaillée de la zonation et l'altération des amphiboles et des aégyrines, qui fait l'objet d'un article publié, montre que les fluides hydrothermaux mobilisent et fractionnent en effet les TR. Une estimation quantitative confirme leur importance par rapport aux processus magmatiques. Une étude similaire sur le zircon montre que ces processus sont principalement locaux, car la composition en TR du zircon dans les pseudomorphoses dépend du minéral qu'il remplace. Ces conclusions démontrent l'importance de l'étude de minéraux communs afin de mieux contraindre les processus géologiques.

La composition et l'origine des fluides hydrothermaux fait l'objet d'une étude au travers de l'analyse microthermométrique et MEB d'inclusions fluides piégées dans du quartz. Cette étude montre que bien que la salinité des fluides varie beaucoup, ils circulent tous à une température relativement basse (< 400 °C). Au moins deux fluides ont circulé dans les six complexes, l'un riche en Na et K, et le second en Ca et Na. A Madagascar et Strange Lake, il a été établi que le fluide riche en Na et K est orthomagmatique, tandis que celui riche en Ca et Na est secondaire.

En conclusion, ce manuscrit montre que l'enrichissement et le fractionnement des TR dans les granites et pegmatites alcalins sont liés à la circulation de deux fluides, riches en Na-K ou Ca-Na, à des températures inférieures à 400 °C. Ce deuxième fluide contient des ligands de TR comme F, OH ou Cl, connus pour transporter les TR. Leur influence est en grande partie locale, mais certains indices comme la présence de phases à TR dans des fractures montre que la mobilisation et le fractionnement peuvent avoir lieu à plus grande échelle.

Contents

Acknowledgements iii

Abstract v

Résumé vii

List of Figures xv

List of Tables xix

1 Introduction 1

1.1 Generalities on alkaline complexes 1

1.1.1 Definition of alkaline rocks with focus on granitoid 1

1.1.2 Formation and emplacement of peralkaline complexes 3

1.1.3 Common mineralogy and petrology of alkaline rocks 6

1.2 Pegmatites formation 7

1.2.1 Description and classification of pegmatites 7

1.2.2 Formation of pegmatites 10

1.3 Generalities on rare earth elements 14

1.3.1 The rare earth elements, critical resources 14

1.3.2 Geochemistry of the REE 16

1.3.2.1 Physical properties of the REE 16

1.3.2.2 Mineralogy of the REE 18

1.3.3 Rare earth elements deposits types 20

1.3.4 Challenges of REE exploitation 21

1.3.4.1 Environmental and public health concerns 21

1.3.4.2 Possible solutions 24

1.4 Control on REE concentration and fractionation in alkaline granitoid deposits 25

1.5 Aims of this study and selection of alkaline complexes 27

1.6 Thesis organisation 29

2 Geological and petrological context **33**
2.1 The Amis complex, Namibia 33
2.1.1 Geological setting of the Brandberg and Amis plutons 33
2.1.2 Petrology of Amis rocks: arfvedsonite granite and alkaline pegmatite 35
2.1.3 Magmatic vs hydrothermal contribution 37
2.2 The Evisa complex, Corsica 39
2.2.1 Geological setting of the Evisa plutons 39
2.2.2 Petrology of main Evisa rocks: hypersolvus granite, subsolvus granite, and pegmatites 39
2.2.3 Magmatic granitic source and hydrothermal circulations . . . 43
2.3 The Khan Bogd complex, Mongolia 44
2.3.1 Geological setting of the Khan Bogd plutons 44
2.3.2 Petrology of Khan Bogd rocks: alkaline granites and pegmatite 45
2.3.3 Magmatic vs hydrothermal contribution 48
2.4 Manongarivo and Ambohimirahavavy complexes, Madagascar . . . 50
2.4.1 Geological setting of northwestern Malagasy plutons 50
2.4.2 Petrology of Malagasy alkaline oversaturated rocks: granites and pegmatites 52
2.4.3 Magmatic vs hydrothermal contribution 55
2.5 The Strange Lake complex, Canada 57
2.5.1 Geological setting of the Strange Lake plutons 57
2.5.2 Petrology of Strange Lake rocks: hypersolvus granite, subsolvus granite, and pegmatites 59
2.5.3 Magmatic vs hydrothermal contribution 61
2.6 Synthesis on magmatic vs hydrothermal contributions to REE enrichment in the six studied alkaline complexes 65

3 Comparative petrological study **69**
3.1 General methods and samples description 69
3.1.1 Methods 69
3.1.2 Samples preliminary description 71
3.2 Main mineralogy 74
3.3 Primary REE-bearing minerals 80

3.3.1 Primary REE-bearing minerals identification 80
3.3.2 Primary zirconosilicates: eudialyte-group minerals, elpidite . 86
3.4 Pseudomorphs and secondary REE-bearing minerals 91
3.4.1 Presentation of pseudomorphs found in the six alkaline complexes 91
3.4.1.1 Pseudomorphs after primary zirconosilicates 92
3.4.1.2 Pseudomorphs after primary minerals other than zirconosilicates 99
3.4.2 Focus on Khan Bogd 103
3.5 Mineral paragenesis of the six studied complexes 105

4 Detailed study of minerals with REE zonations common to all complexes: amphibole, pyroxene and zircon 115
4.1 Alkali pyroxenes and amphiboles: a window on Rare Earth Elements and other High Field Strength Elements behavior through the magmatic-hydrothermal transition of peralkaline granitic systems . . 116
4.2 Oxygen isotopes as tracers for amphiboles and pyroxene origin . . . 163
4.2.1 Presentation of O stable isotopes and their applications 163
4.2.2 Application of O isotopes to alkaline amphibole and pyroxene 165
4.2.3 In situ isotopic measurements 168
4.3 Zircon as an indicator of REE enrichment 168
4.3.1 Petrography of zircon 169
4.3.2 Major and trace elements in zircon 180
4.3.2.1 Compositional variations within single zircon crystals 180
4.3.2.2 Comparison of zircon compositions in a same complex 180
4.3.2.3 Comparison between complexes 189
4.3.3 REE in zircon 189
4.3.4 Discussion on the origin of zircon types highlighting REE enrichment and fractionation processes 193
4.3.4.1 Type-SG zircon 193
4.3.4.2 Type-P zircon 195
4.3.4.3 Type-I zircon 198
4.3.5 What zircon tells us about REE behavior at the magmatic-hydrothermal transition 198

4.4 Estimation of the contribution of hydrothermal fluids to the REE budget of alkaline complexes . . . 199
4.4.1 Mass-balance calculation on pseudomorphs . . . 199
4.4.2 Estimation of the proportion of REE in hydrothermal minerals 200
4.4.2.1 Methodology . . . 200
4.4.2.2 Results and discussion . . . 202
4.4.2.2.1 Magmatic vs hydrothermal REE budget . . 202
4.4.2.2.2 Discussion on the method . . . 203

5 Fluid inclusion study 205
5.1 Introduction . . . 205
5.2 Geological context . . . 207
5.3 Sample selection and method . . . 208
5.3.1 Sample selection . . . 208
5.3.2 Methods . . . 210
5.4 Petrography of selected samples . . . 211
5.4.1 General mineralogical description . . . 211
5.4.2 Petrography of fluid inclusions types and assemblages . . . 214
5.4.2.1 The Amis complex, Namibia . . . 214
5.4.2.2 The Evisa complex, Corsica . . . 220
5.4.2.3 The Khan Bogd complex, Mongolia . . . 220
5.4.2.4 The Ambohimirahavavy complex, Madagascar . . . 221
5.4.2.5 The Manongarivo complex, Madagascar . . . 224
5.4.2.6 The Strange Lake complex, Canada . . . 224
5.5 Results . . . 227
5.5.1 Identification of populations and microthermometry data . . . 227
5.5.1.1 The Amis complex, Namibia . . . 227
5.5.1.2 The Evisa complex, Corsica . . . 229
5.5.1.3 The Khan Bogd complex, Mongolia . . . 230
5.5.1.4 The Ambohimirahavavy complex, Madagascar . . . 233
5.5.1.5 The Manongarivo complex, Madagascar . . . 234
5.5.1.6 The Strange Lake complex, Canada . . . 236
5.5.2 SEM study of solids in fluid inclusions . . . 237
5.5.3 Evaporate salt mounds . . . 239
5.6 Discussion . . . 243

5.6.1 Fluid features common to all complexes from this study . . . 243
5.6.2 Fluid circulations in the six complexes . . . 247
5.6.2.1 The Amis complex, Namibia . . . 247
5.6.2.2 The Evisa complex, Corsica . . . 248
5.6.2.3 The Khan Bogd complex, Mongolia . . . 249
5.6.2.4 The Ambohimirahavavy complex, Madagascar . . . 250
5.6.2.5 The Manongarivo complex, Madagascar . . . 251
5.6.2.6 The Strange Lake complex, Canada . . . 251
5.6.3 Comparison of the characteristics of complexes of this study with the literature . . . 252
5.6.3.1 Summary of fluid properties in silica-saturated alkaline complexes . . . 252
5.6.3.2 Comparison with the literature: fluids in silica-undersaturated alkaline complexes and peraluminous pegmatites . . . 252
5.6.4 Other mineralized systems with interaction of a granitic melt with hydrothermal fluids: epithermal and porphyry deposits 253
5.7 Conclusion . . . 254

6 Thesis synthesis: contribution of magmatic and hydrothermal stages on REE behavior in alkaline granitic complexes 257
6.1 Magmatic vs hydrothermal mineral paragenesis . . . 257
6.2 REE concentration at magmatic and hydrothermal stages . . . 258
6.3 REE fractionation by hydrothermal fluids . . . 261
6.4 Properties of fluids in alkaline systems . . . 261
6.5 The mobility of other HFSE in fluids of alkaline systems . . . 263
6.6 A recipe for REE enrichment and fractionation in alkaline granites and associated pegmatites . . . 264

Conclusions and perspectives 269

Conclusions et perspectives 271

Bibliography 271

Appendices 295

A List of minerals mentioned in the manuscript **297**

B Glossary of unusual terms used in the manuscript **301**

C Program used to determine the proportion of pyroxene in a thin section **303**

List of Figures

1.1 Geodynamic contexts of alkaline and carbonatite rocks 3
1.2 Major REE deposits and occurences worldwide 4
1.3 Pseudomorphs after EGM and elpidite 6
1.4 Internal zonation of pegmatites 10
1.5 Common industrial uses of REE 14
1.6 Worldwide rare earth production between 1992 and 2019 15
1.7 Periodic table of elements 17
1.8 REE in a nutshell 18
1.9 Proportions of the different families of REE-bearing minerals 20
1.10 Geodynamic contexts of REE deposits 21
1.11 Whole-rock Yb/La vs Yb contents of different alkaline complexes worldwide 23
1.12 Map of location, age and geological context of emplacement of the six selected complexes 29

2.1 Map of the Amis and Brandberg complexes, Namibia 34
2.2 Presentation of the main rocks that can be found in the Amis complex, Namibia 36
2.3 Y/Ho vs La/Ho ratios in melt inclusion glasses and whole rock from the Amis Complex, Namibia 38
2.4 Map of the Evisa complex, Corsica 40
2.5 Presentation of the main rocks that can be found in the Evisa complex, Corsica 42
2.6 Map of the Khan Bogd complex, Mongolia 45
2.7 Presentation of the main rocks that can be found in the Khan Bogd complex, Mongolia 47
2.8 Geodynamic hypothesis for the formation of the Khan Bogd plutons, Mongolia 48

2.9 Map of the Ambohimirahavavy and Manongarivo complexes, Madagascar . . . 51
2.10 Presentation of the main rocks that can be found in the Ambohimirahavavy and Manongarivo complexes, Madagascar . . . 53
2.11 Map of the Strange Lake complex, Canada . . . 58
2.12 Presentation of the main rocks that can be found in the Strange Lake complex, Canada . . . 60
2.13 Alteration/precipitation path for the fluid exsolved from the Strange Lake magma . . . 63
2.14 Spider diagram of whole rock pegmatites and granites . . . 66

3.1 Main minerals common to all six studied complexes . . . 74
3.2 Quartz overgrowths in granitic samples . . . 76
3.3 Quartz overgrowths and zonations in pegmatitic samples . . . 77
3.4 Peculiar zonations in quartz of granites of two complexes . . . 78
3.5 Zonations of alkali feldspars in the different complexes . . . 79
3.6 Ternary diagrams of PGM from the six complexes . . . 82
3.7 Presentation of the main primary REE-bearing minerals . . . 85
3.8 Photographs of EGM . . . 87
3.9 Photographs of elpidite . . . 88
3.10 Ternary diagrams of elpidite . . . 91
3.11 Complex pseudomorphs after a magmatic zirconosilicate . . . 93
3.12 Ternary diagrams of armstrongite and gittinsite . . . 95
3.13 Zirconosilicates and quartz pseudomorphs after a magmatic zirconosilicate . . . 96
3.14 Photographs showing the zonations in fluorite . . . 99
3.15 Pseudomorphs after primary minerals other than zirconosilicates . . . 102
3.16 Characterization of REE-Zr phase in fractures at Khan Bogd . . . 104
3.17 Comparison of the paragenesis of the six complexes . . . 108
3.18 Detailed paragenesis of all six complexes studied . . . 114

4.1 δ^{18}O values of important geological reservoirs . . . 164
4.2 δ^{18}O versus δD of waters of different origins . . . 166
4.3 Photographs of zircons from Amis . . . 172
4.4 Photographs of zircons from Evisa . . . 173
4.5 Photographs of type-II zircons from Khan Bogd . . . 175

4.6 Photographs of zircons from Ambohimirahavavy 176
4.7 Photographs of zircons from Manongarivo 178
4.8 Photographs of zircons from Strange Lake 179
4.9 Binary diagrams showing zircons composition at Amis 183
4.10 Binary diagrams showing zircons composition at Evisa 184
4.11 Binary diagrams showing zircons composition at Khan Bogd 185
4.12 Binary diagrams showing zircons composition at Ambohimirahavavy 186
4.13 Binary diagrams showing zircons composition at Manongarivo . . . 187
4.14 Binary diagrams showing zircons composition at Strange Lake 188
4.15 Zircon spider diagrams 190
4.16 Estimation of the percentage of REE in hydrothermal minerals 202

5.1 Examples of zonations and fluid inclusions in fluorite and aegirine . 212
5.2 Quartz overgrowths 213
5.3 Quartz overgrowths in granitic samples 215
5.4 Quartz overgrowths and zonations in pegmatitic samples 216
5.5 Photographs of representative FI in quartz from Amis 218
5.6 Photographs of representative FI in quartz from Evisa 219
5.7 Photographs of representative FI in quartz from Khan Bogd 222
5.8 Photographs of representative FI in quartz from Ambohimirahavavy 223
5.9 Photographs of representative FI in quartz from Manongarivo 225
5.10 Schematic representation of FI in quartz from Strange Lake 226
5.11 Diagrams of salinities and temperatures of FI from Amis 228
5.12 Diagrams of salinities and temperatures of FI from Evisa 230
5.13 Diagrams of salinities and temperatures of FI from Khan Bogd 231
5.14 Evolution of an LVS FI evolution under cooling at Khan Bogd 232
5.15 Diagrams of salinities and temperatures of FI from Ambohimirahavavy 234
5.16 Diagrams of salinities and temperatures of FI from Manongarivo . . 235
5.17 Diagrams of salinities and temperatures of FI from Strange Lake . . . 236
5.18 SEM photographs and spectra of opened inclusions at Khan Bogd . . 238
5.19 SEM photographs and spectra of decrepitated FI at Amis 239
5.20 SEM photographs and spectra of decrepitated FI at Evisa 240
5.21 SEM photographs and spectra of decrepitated FI at Khan Bogd 240
5.22 SEM photographs and spectra of decrepitated FI at Ambohimirahavavy 241
5.23 SEM photographs and spectra of decrepitated FI at Manongarivo . . 242

5.24 Diagrams of salinities and temperatures of FI from the six studied complexes 245

6.1 Synthesis of the steps for REE enrichment and fractionation 265

List of Tables

1.1 Classification of pegmatites according to Černý and Ercit (2005) . . . 7
1.2 Classification of pegmatites according to Dill (2015) 8
1.3 Selected REE-minerals, chemical formulas, preferential geological settings and key-occurrences 19
1.4 Classification of rare earth deposits 22

2.1 Summary of geological and geodynamic context of the six studied complexes 67

3.1 List of standards used for EPMA calibration 70
3.2 List and description of selected samples for this study 73
3.3 Analyses of primary REE-bearing minerals of the six studied complexes 84
3.4 Analyses of primary zirconosilicates, EGM and elpidite 90
3.5 Analyses of secondary zirconosilicates 98
3.6 Summary of the main REE-bearing minerals found in each complex . 107

4.1 Whole crystals δ^{18}O values from this study 167
4.2 Petrographic characteristics of zircon 170
4.3 Mean zircon compositions 181
4.4 Mass-balance calculations on pseudomorphs 200

5.1 Samples selected for the FI study 209
5.2 Main properties of FI measured in this study 246

Chapter 1

Introduction

1.1 Generalities on alkaline complexes

1.1.1 Definition of alkaline rocks with focus on granitoid

Alkaline rocks are defined by their high contents of Na_2O and K_2O. They can be basic (typically basalts) or felsic (granitoids). This work focuses only on differentiated alkaline rocks, where sodic and potassic minerals are typically feldspathoids, alkali amphiboles (riebeckite, arfvedsonite), and alkali pyroxenes (aegirine) (Dostal, 2017). Alkaline granitoids can be either silica-oversaturated, i.e. granites and rhyolites containing quartz and alkali amphiboles or pyroxenes; or silica-undersaturated, i.e. syenites, trachytes and phonolites containing normative feldspathoids or acmite (Le Maitre et al., 2004). These two alkaline series are often found together in the same complex (Estrade, 2014; Marks et al., 2011; Marks and Markl, 2017; Ponthus, 2018) and can be either metaluminous, i.e. molar (Na_2O+K_2O) < Al_2O_3, or peralkaline, i.e. molar (Na_2O+K_2O) > Al_2O_3 (Le Maitre et al., 2004; Marks et al., 2011).

Alkaline rocks are also described to be agpaitic or miaskitic. Many classifications (e.g. Le Maitre et al., 2004; Sørensen, 1997; Ussing, 1912) have led to confusion on the definition of these terms. Historically, these terms were only used for SiO_2-undersaturated rocks, but their use for alkaline granitoids has recently been extended (Marks et al., 2011). In this work, 'agpaitic' refers to rocks containing complex zirco- and/or titanosilicates (e.g. eudialyte-group minerals, of general formula $Na_{15}(Ca,REE)_6(Fe,Mn)_3Zr_3Si_{26}O_{72}(O,OH,H_2O)_3(Cl,OH)_2$), whereas 'miaskitic' refers to rocks made of zircon and/or Ti-oxides (Marks and Markl, 2017). If both zircon and complex zirconosilicates occur, the rock is definied as transitional agpaitic. Agpaitic rocks are rarer and emplaced at

shallower levels than miaskitic ones. They are also younger: although the oldest occurrence found so far is 2176.0 ± 2.7 Ma old (Nechalacho deposit, Canada, Timofeev and Williams-Jones, 2015), most agpaitic rocks are less than 400 Ma old (Marks and Markl, 2017). The agpaitic or miaskitic nature depends on the fO_2, $aSiO_2$, peralkalinity, and aH_2O of the peralkaline melt. Agpaitic rocks formation necessitates reduced conditions (they are then CH_4 rich, which is confirmed by the study of fluid inclusions), low aH_2O, and high salinities of the melt. This low aH_2O and fO_2 inhibits fayalite, magnetite and hematite formation, which leaves enough Fe available to crystallize alkaline amphiboles and pyroxene. This rises peralkalinity and lowers $aSiO_2$, which in turn drive high halogen and HFSE amounts. On the contrary, miaskitic rocks need high fO_2, which promotes a high aH_2O. This water enrichment compared to agpaitic rocks drives an early exsolution of water-rich fluids that deplete the peralkaline melt in halogens and thereby in HFSE and REE. Consequently, miaskitic rocks are less concentrated in rare metals than their agpaitic equivalent (Marks et al., 2011; Marks and Markl, 2017; Migdisov et al., 2016).

Thus, alkaline granitoids, particularly the agpaitic ones, are enriched in incompatible rare metals, in some cases in spectacular amounts. These elements include the rare earth elements (REE) and high field strength elements (HFSE, namely Nb, Ta, Zr, Hf, U, Th, Sn, Ti) for which they represent a potentially important economic resource (Dostal, 2017), even though they represent less than 1 % of the total estimated volume of igneous rocks worldwide (Fitton and Upton, 1987). Peralkaline granitoids are more evolved than metaluminous ones, hence they can concentrate more the incompatible rare metals, in particular the REE. The highest rare metal concentrations are usually hosted by pegmatites, where mineralization consists in a variety of rare-metal bearing minerals. The main mechanism responsible for the high rare metal content in alkaline melts is known to be magmatic, i.e. mainly controlled by differentiation processes, but the light-heavy REE fractionation is still vastly discussed (Chakhmouradian and Wall, 2012; Dostal, 2017; Verplanck and Van Gosen, 2011). In this study, silica-saturated peralkaline granitoids have been chosen to understand the fractionation mechanism between light-REE (LREE, from La to Eu) and heavy-HREE (HREE, from Gd to Lu and Y).

1.1.2 Formation and emplacement of peralkaline complexes

Alkaline magmatism is found in many geodynamic contexts (Fig 1.1) such as continental rifts (e.g. Madagascar, Estrade et al., 2014a; Namibia, Schmitt et al., 2002), hot-spots (e.g. Azores, Ridolfi et al., 2003), large igneous provinces (e.g. Kerguelen, Ponthus, 2018), back-arcs and post-collisional terranes (e.g. Mongolia, Kynicky et al., 2011; Corsica, Bonin et al., 1978). Alkaline complexes with the higher HFSE grades are however mostly concentrated in continental rifts (Vasyukova and Williams-Jones, 2020). Alkaline rocks can be found in close association with carbonatites (Fig 1.2) which can also contain significant concentrations of REE (Balashov and Glaznev, 2006; Marks and Markl, 2017; Sørensen, 1974).

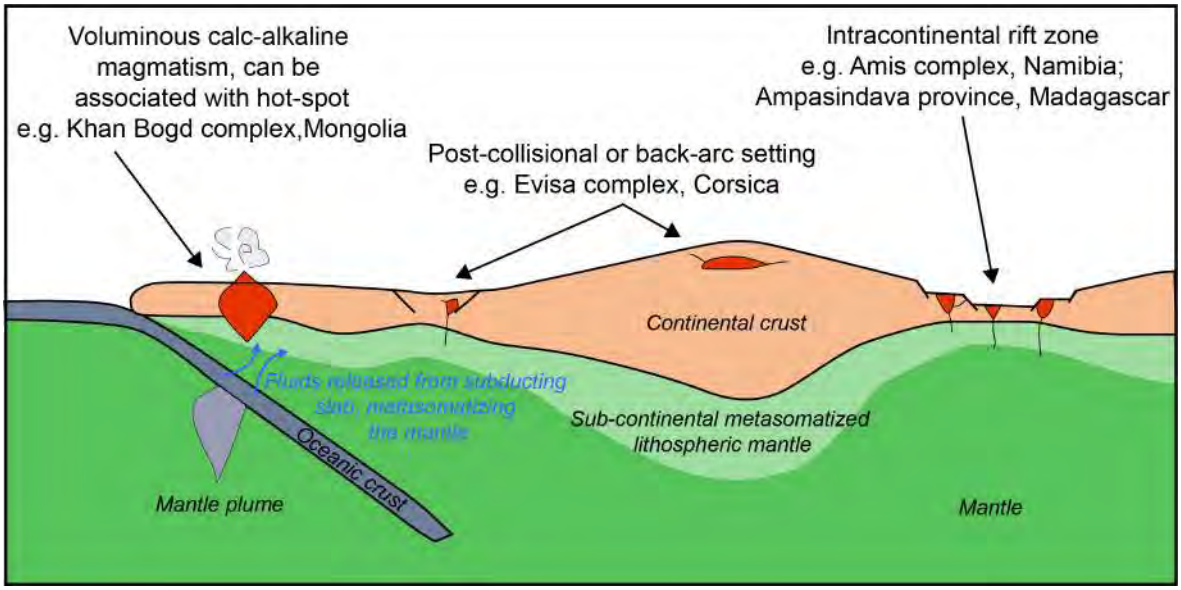

Figure 1.1 Schematic cross-section illustrating the main environments of formation of alkaline and carbonatite rocks, adapted from Goodenough et al. (2016)

Historically, the first accepted theory as to the origin of alkaline rocks evoked a superficial formation by reaction "of common mafic magma with limestone", because of its regular association with carbonatites (Bowen, 1945). More generally, this mechanism implied interactions between a mantellic magma and its environment. With additional studies on peralkaline complexes in different contexts, this theory has been rethought and improved. The role of the mantle as a source for peralkaline magmas has then been known for a long time and supported by petrological, geophysical and isotopic arguments (e.g. Balashov and Glaznev, 2006; Bowen, 1945; Green and Ringwood, 1968; Kramm and Kogarko, 1994). The magma source has been determined as a metasomatically enriched depleted mantle,

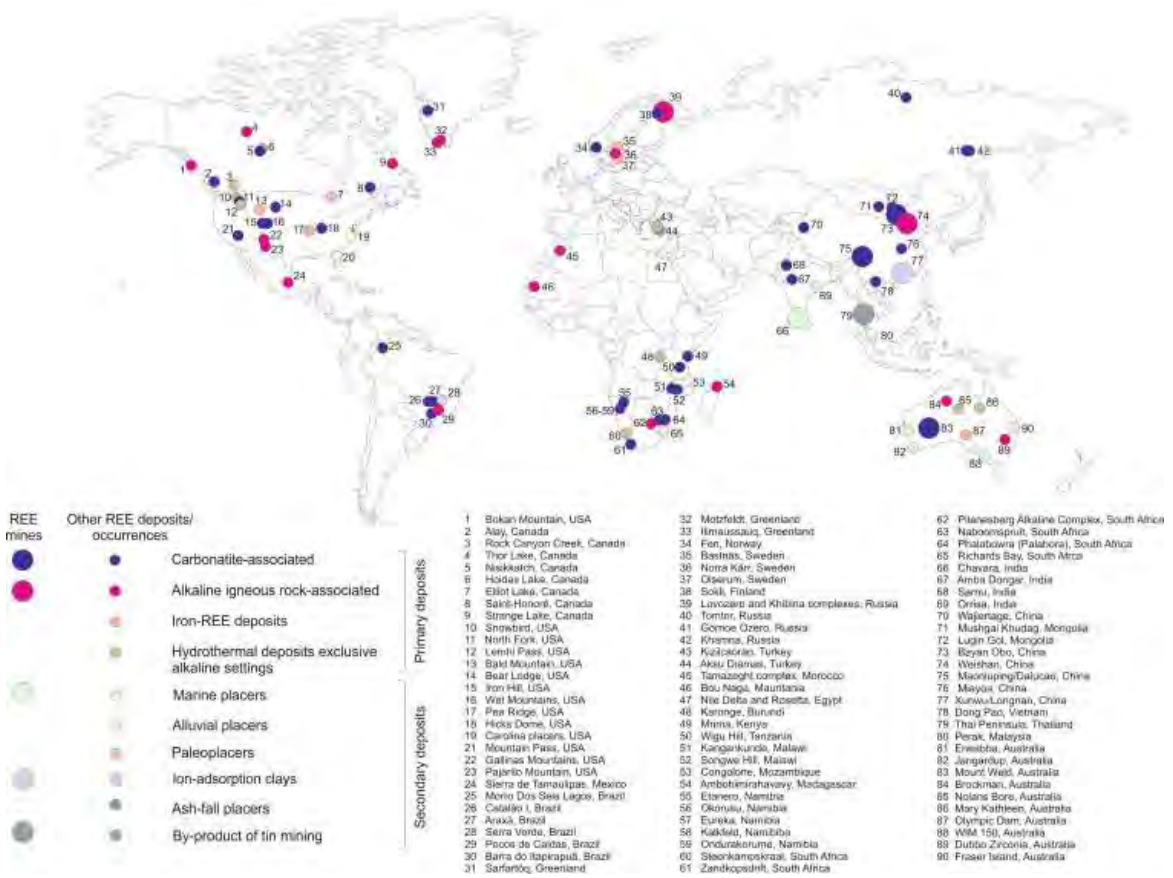

Figure 1.2 A map showing the type and location of the major REE deposits and occurences worldwide, from Elliott et al. (2018)

or a mantle plume. Isotopic studies show that the most HFSE-rich alkaline rocks have high $\delta^{18}O$ and high initial $^{86}Sr/^{87}Sr$ values (e.g. Siegel et al., 2017; Trumbull et al., 2004), which shows they have undergone crustal assimilation. This model, in addition to explaining part of the observed HFSE enrichment, also elucidates the spatial association of silica under-saturated and over-saturated rocks that can be observed on the field (Balashov and Glaznev, 2006; Foland et al., 1993; Vasyukova and Williams-Jones, 2020).

Whichever the mode of formation, after its production, the magma ascends until the upper crust. Until the 21^{st} century, it was thought that this magma ascended either by diapiring thanks to the difference of density between the magma and surrounding rocks, or passively because of subsidence of rock blocks into the reservoir. In both cases, the shape of plutons would be annular or elliptic, and controlled by pre-existing structures and shearing in the upper crust (Bonin, 1990b). More recent studies have highlighted the tabular shape of intraplate plutons, thereby showing the relative independence of their set up with tectonics, along

with their incremental emplacement linked to deep magmatic processes that are still unresolved (Annen et al., 2015; de Saint Blanquat et al., 2011; Menand et al., 2015). Magmas can also reach up to the surface through dikes and lodes, producing alkaline lavas through crustal contamination. Eventually, late and hence much more differentiated melts crystallize as pegmatites and aplites in fractures, dykes and sills (Fig 1.1).

Alkaline magmas progressively crystallize throughout the entire emplacement process, and fractional crystallization is a key process to ultimately form the highly differentiated alkaline granitoids and, among them, alkaline pegmatites. Vasyukova and Williams-Jones (2020), based on the study of the Strange Lake complex, demonstrated that in order to form HFSE-enriched alkaline rocks, two steps are required. The first one is that plagioclase stops crystallizing before Ca is entirely consumed from the melt, in order to allow the formation of an immiscible Ca-fluoride melt that sequesters the LREE and Y. The second one is the crystallization of arfvedsonite, which drives the agpaicity of the melt. After their emplacement, peralkaline magmas can undergo a phase of subsolidus interaction with fluids (Bonin, 1990b) of orthomagmatic and, less commonly, external origin. Evidence includes presence of pseudomorphs, i.e., assemblages of secondary minerals with exotic chemistry (e.g. REE-fluorocarbonates, zirconosilicates, phosphates, oxides) replacing primary phases (Fig 1.3), and of fluid inclusions, the analysis of which provides important information on the composition of the circulating fluids. These are generally mainly aqueous, with variable amounts of CH_4, CO_2, halogens (F, Cl), alkalis, and water-soluble components (e.g. Estrade et al., 2015; Salvi and Williams-Jones, 1997; Vasyukova and Williams-Jones, 2016). Peralkaline magmas have notably high solubility coefficients for halogens carried by circulating fluids, which can drive to higher enrichment in REE and other HFSE, along with formation of an exotic secondary mineralogy. Vasyukova and Williams-Jones (2020) even infer that in order to enrich alkaline rocks in HFSE, the fluid needs to be aqueous-carbonic and acidic.

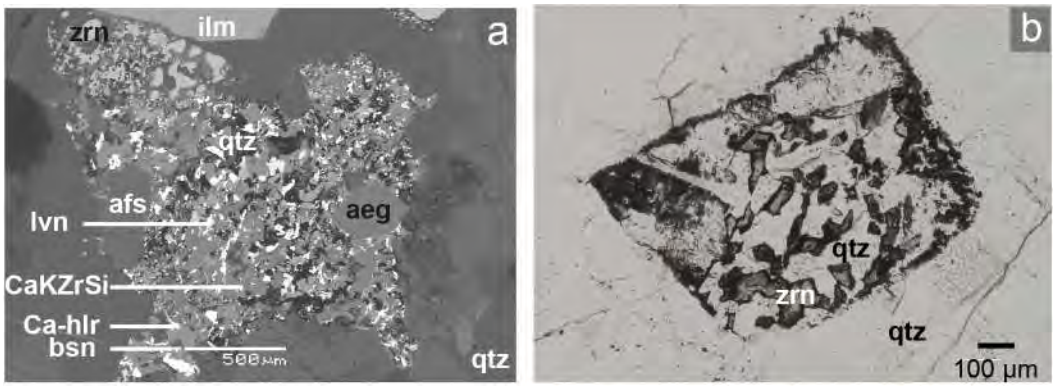

Figure 1.3 BSE and optical microscope images of pseudomorph of HFSE-bearing minerals after eudialyte-groupe mineral (a) and elpidite (b). Abbreviations: qtz: quartz; zrn: zircon; afs: alkali feldspar; aeg: aegirine; arf: arfvedsonite; Ca-hlr: calciohilairite; lvn: låvenite; ilm: ilmenite; bsn: bastnäsite-(Ce)

1.1.3 Common mineralogy and petrology of alkaline rocks

According to Le Maitre (2002), a rock is considered alkaline if it contains either modal feldspathoids and/or alkali amphiboles or pyroxenes, or normative feldpsathoids or acmite. Alkaline rocks are divided between metaluminous and peralkaline, depending on their chemistry. Metaluminous alkaline rocks are defined by the presence of hastingsite and biotite, assemblages of quartz, katophorite, magnesioriebeckite, sodic hedenbergite, ilmenite, magnetite and fayalite are found (Sørensen, 1974). Peralkaline rocks have a high sodium activity, hence K-feldspar, albite, perthites, quartz, alkali pyroxene (aegirine), and alkali amphiboles are common minerals. Hydrothermal albitization of feldspars process may be locally severe (Sørensen, 1974). Aenigmatite, astrophyllite, zircon and biotite are minor but often present accessory minerals, except in the most evolved peralkaline rocks where biotite is unstable. Along with these phases, fluorite, pyrochlore-group minerals (PGM), cryolite, and many zirconosilicates such as elpidite ($Na_2ZrSi_6O_{15}.3H_2O$), eudialyte-group minerals, or armstrongite ($CaZrSi_6O_{15}{\cdot}2H_2O$) can be found, but only rarely in high quantities (Bonin, 1990b; Markl et al., 2010; Marks et al., 2011; Nicholls and Carmichael, 1969).

1.2 Pegmatites formation

1.2.1 Description and classification of pegmatites

The word 'pegmatite' comes from the Greek "to make rigid by binding together", which refers to the intergrowth of quartz and feldspar commonly found in pegmatites. To this day, the most recent definition of pegmatites is proposed by London (2018, page 350): "Pegmatite is an essentially igneous rock, mostly of granitic composition, that is distinguished from other igneous rocks by (1) the extremely coarse and systematically variable size of its crystals, or (2) by an abundance of crystals with skeletal, graphic, or other strongly directional growth habits, or (3) by a prominent spatial zonation of mineral assemblages, including monominerallic zones. Any one of these textural attributes might be sufficient to define a pegmatite body, but they tend to occur together".

Table 1.1 Classification of pegmatites according to Černý and Ercit (2005)

Class / *Subclass*		Typical mineralization	P, T conditions
Abyssal (AB)		REE, Zr, U, Th, Ti	4-9 kbar, 700-800 °C
Muscovite (MS)		-	5-8 kbar, 580-650 °C
Muscovite-Rare-element (MSREL)		REE, Ti, Li, Be, Zr, B, Nb, Ta F	3-7 kbar, 520-650 °C
Rare-element (REL)	**NYF**	REE, U, Th, Be, Nb, Ta, F	2-4 kbar, 450-650 °C
	LCT	Li, Cs, Be, Sn, Hf, Nb, Ta, B, P, F	
Miarolitic (MI)		REE, Ti, Li, Be, Zr, B, F	1,5-3 kbar, 400-500 °C

Pegmatites occur as dikes and veins never bigger than one kilometre thick. Because of their high natural abundance, most studies focused on peraluminous pegmatites, so alkaline ones are still vastly unknown. This lack of knowledge may also be because of the difficulty to apprehend and experimentally reproduce the many possible combinations of alkali and carbonates, which modify melt structure (Thomas et al., 2012). The next paragraphs focus on granitic pegmatites only.

The most common classification for pegmatites is provided by Černý and Ercit (2005), and granitic pegmatites are divided in five categories based on their depth of emplacement and trace elements content: abyssal (high to low pressure, high temperature), muscovite (high pressure and temperature), muscovite-rare-element (moderate pressure and temperature), rare-element (low temperature and pressure),

Table 1.2 Classification of pegmatites according to Dill (2015)

ORE BODY

Host rock lithology	Metamorphic rocks		Metamorphic rocks	Metamorphic and magmatic rocks	Magmatic rocks	Remarks
1 st order term **Type of pegmatitic/ aplitic rock**	**Pseudopegmatite/ pseudoaplite**	**Metapegmatite/ metaaplite**	**Pegmatoid/ aploid**	**Pegmatite/ aplite**	**Plutonic pegmatite/ aplite**	**Mandatory**
	Aplitic: grain size ≤ host rock and homogeneous Pegmatitic : grain size >> host rock and heterogeneous				Aplitic: grain size < host rock Pegmatitic : grain size >> host rock host rock and heterogeneous	
Specific type of host rock	*Gneiss, amphibolite , eclogite* *e.g., pegmatoid- (cordierite-sillimanite-gneiss)*				*Granite, syenite, granodiorite*	*Optional*
Determination	Mapping in the field the ore-host rock relation and measuring the grain size by visual examination					
2 th order term **Shape and structure**	**Tabular, schlieren, stock-like, pockets, vein-type, pipes, chimneys, floors** e.g. Sc-Nb aplite tabular, quartz-albite pegmatoid tabular				**Miarolitic, pod-like, pockets, vein-type, schlieren** e.g. topaz granite pegmatite miarolitic	**Mandatory**
Internal structure	Unzoned - rimmed-complex/ ungraded-complex/ graded (e.g. UST)					
Size (thickness)	*cm-sized, dm-sized , meter-sized*					*Optional*
Determination	Mapping in the field the shape by visual examination and measuring the morphological increments and size with a yardstick					
3 th order term **Chemical qualifier** **Rare metal pegmatites** ***sensu lato***	**Sn, W, Ta, Nb, Sc, Be, Li, Cs, Rb, REE ,Y, U, Th, B, F, P, Zr** **e.g. Nb-Li pegmatite, (Sc-U)-Nb-P aploid**					**Mandatory** Can be linked to the "Chessboard classification scheme of mineral deposits", using alpha-numerical codes
Determination	By visual inspection of rock-forming minerals, including hand lens for accessory minerals (put in brackets) Rock-forming and accessory minerals ⇒ chemical symbols (e.g. beryl, euclase ⇒ Be, Li mica ⇒ Li, allanite ⇒ REE, if necessary LREE)					
4 th order term **Mineralogical qualifier** **Industrial mineral**	**quartz, feldspar, foid, garnet, zeolite, mica, corundum, graphite** **e.g. (andalusite)-quartz-feldspar metapegmatite, graphite- feldspar-quartz pegmatite**					**Mandatory** Can be linked to the "Chessboard classification scheme of mineral
pegmatites						deposits", using alpha-numerical codes
Specific type of minerals for gemstone-bearing pegmatites , fine-tuning and genetic interpretation	*e.g. Al pegmatite (ruby), F-Sn-W granite pegmatite (topaz>fluorite), Li-Nb-P pegmatite (triphylite), Li-Nb-P pegmatite (amblygonite)*					*Optional - Composite of level 3 and 4*
Determination	See 3 nd order term for determination					

ORE COMPOSITION

and miarolitic (very low pressure; Table 1.1). Rare-element pegmatites are also divided in two families: lithium-caesium-tantalum (LCT) pegmatites, and niobium, yttrium, fluorine (NYF) pegmatites that have high REE and HFSE contents, but are rarely enriched enough to be considered as economic resources for these metals. This study focuses on NYF pegmatites, which are systematically close to the granitic pluton, and main ore minerals are zirconosilicates such as elpidite. Same as LCT pegmatites, NYF pegmatites are commonly altered by a late-stage, F- and CO2-rich orthomagmatic fluid. Some authors suggest that rather than fluids, immiscible silicate and fluoride melts were produced and are the origin for pegmatites (Goodenough et al., 2019; Vasyukova and Williams-Jones, 2014).

However, Dill (2015) argues that the classification from Černý and Ercit is not adequate because it mixes chemistry (MS, MSREL and REL), depth (AB) and texture (MI) characteristics of pegmatites. Instead, he proposes another classification with 4 order terms in which all these elements are taken into account together (Table 1.2). The two first order terms are based on physical parameters: the first one is based on

the type of surrounding rocks (metamorphic or magmatic) as well as the grain size of pegmatites, and the second one on the structure of pegmatites. Order terms 3 and 4 are based on pegmatites chemistry, including respectively which rare metal they are made of, and what is their main mineralogy. Based on this classification, the rocks from this study are defined as plutonic granitic, zoned vein-type, REE-HFSE pegmatites (amphibole-aegirine-quartz-feldspar). Although it is more adequate, the pegmatites classification by Dill is still not commonly used, probably due to its complexity.

Pegmatites can be of various compositions following the chemistry of the igneous body they genetically come from. Even between pegmatites originating from the same igneous body, and inside a single pegmatite, differences are found. Zonations are of two natures: regional, and internal. Regional zonation is marked by an increasing differentiation of pegmatites with distance to the igneous body they are linked to. Internal zonation affects mineralogy as much as texture inside the pegmatite. Depending on the dip of the pegmatite, the shape of this internal zonation varies: if the pegmatite is steeply dipping due to its emplacement in the brittle crust, the zonation is concentric; but if the pegmatite is shallowly dipped, it is then layered (Brisbin, 1986). In peraluminous pegmatites, from the margins to the core, one can see the border zone, the wall zone, the intermediate zone, and the quartz core, with sometimes aplitic texture in between. These zones, except for aplite, are symmetric (London, 2008, 2014, Fig 1.4a). Based only on texture, this internal zonation of peraluminous pegmatites can be compared to the one of hydrothermal veins coarse grains in the core, crystals growing towards it, and mineralogical layering parallel to pegmatite borders. However, no common pattern for peralkaline pegmatites was highlighted in the literature, and their internal zonation remains seemingly random (Fig 1.4b,c).

Mineralogically speaking, granitic pegmatites resemble granitic plutons in the way that they contain quartz, feldspars and sometimes biotite as main phases. Quartz is mostly interstitial or skeletal, except in pegmatites cores where it occurs as massive lenses. Alkaline feldspars usually grow inward from the pegmatite margins, whereas plagioclase more often forms spherical structures or grow parallel to the margins. In NYF pegmatites, it is standard to find a single ternary feldspar (anorthite, albite, or orthose). Accessory minerals in pegmatites are borosilicates (tourmaline), phosphates (apatite for all pegmatites, monazite and xenotime for NYF and LCT ones), and oxides (cassiterite, columbo-tantalite,

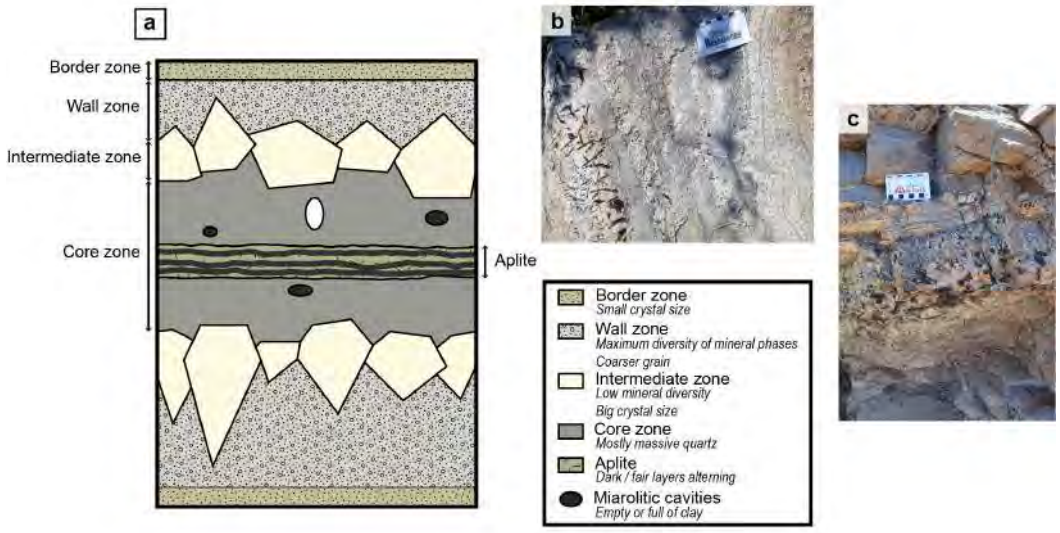

Figure 1.4 Diagram and field photographs showing internal zonation of pegmatites. (a) Schematic view of a type metaluminous pegmatite according to London (2014); (b) Photograph of an alkaline pegmatite from the Ambohimirahavavy complex, Madagascar; (c) Photograph of an alkaline pegmatite from the Khan Bogd complex, Mongolia

PGM, ilmenite, magnetite, etc.). Although common in granites, Fe-Ti oxides are uncommon in pegmatites. Rare-element pegmatites can contain up to a hundred minerals. Minerals specific to NYF alkaline pegmatites are F-rich (fluorite, lepidolite, topaz, and any hydroxylated mineral in which F substituted for OH groups), gadolinite-(Y), alkaline pyroxenes (aegirine) and amphiboles (arfvedsonite, riebeckite), and minor phases such as phyllosilicates, carbonates, sulphides, and zeolites (Černy, 1991; London, 2008).

1.2.2 Formation of pegmatites

The mechanism of pegmatites formation has been investigated since the end of the 19^th century, but there is still no consensus. In addition, models were based mostly on metaluminous pegmatites, hence many shadow zones still remain on peralkaline pegmatites. Historically, one of the first models for pegmatite formation was exclusively hydrothermal, formalized by Roedder in 1984 but known since at least Crosby and Fuller (1897). Based on the high resemblance between textures of pegmatite and hydrothermal vein, pegmatitic minerals were thought to precipitate from an H_2O-CO_2-NaCl fluid issued from surrounding rocks. However, the absence

of systematic hydrothermal alteration along with the study of fluid/melt inclusions show that if there is a hydrothermal phase, it only occurs at the end of the emplacement and therefore cannot be its cause.

In 1949, Cameron formulated the opposite hypothesis of an origin exclusively igneous, followed by Jahns in 1953. They said that the different zones in pegmatites are formed by crystallisation on the walls of a magmatic chamber. Thereby, they thought pegmatites are formed only by fractionated crystallisation, in a nearly closed system, with a non-existent to minor late role of fluids. Cameron did not check his model with the texture of pegmatites, but Jahns did and found that the coarse-grained texture of pegmatites is due to a low viscosity melt, explained by a high concentration in H_2O, F, and Li_2O, that enhance ions diffusivity and allows big crystals to grow inwardly (London, 2014; Thomas et al., 2012).

Vlasov, in 1961, chose to trust the igneous model, and proposed a classification of five types of pegmatites, with an increasing complexity linked to the distance to the parent igneous body and the differentiation. He though nuanced his model by admitting that rare minerals come from an unknow replacement process. Baker, in 1998, also rested on the igneous model to explain regional zonation of pegmatites. He affirmed that if the pluton is big enough to significantly heat host rocks, dikes will form, but never further than 10 km away. Because these dikes occur late during the cooling of the pluton, only the most differentiated melts will remain to fill them, and the further from the igneous body, the more differentiated the melt.

Another model, already formulated by Landes in 1933, was then brought up by Jahns and Burnham (1969). It states that only an igneous phase fills pegmatitic dykes, but this phase is so evolved that it contains a high concentration of H_2O, and hence an aqueous interface forms between the solid rocks and the melt. Layering in pegmatites and aplites would then be the consequence of quenching of a melt that lost potassium for the aqueous phase, from which K-feldspar could grow. Late hydrothermal events would enrich rare-element pegmatites in various rare-element bearing minerals. This explanation is in accordance with the amount of silica necessary to grow quartz and feldspar crystals, and with fluid and melt inclusions. However, the compositions proposed would give a cooling time of more than a thousand years, compared to the few years that is observed in nature; and the extraction of only K and no Na in the fluid is today known impossible (Burnham and Nekvasil, 1986; London, 2014; Thomas et al., 2012). Hence, this model is the closest one to the current hypothesis, but still needs refinement.

Burnham and Nekvasil (1986) proposed an alternative for this dual origin: most of the pegmatite would be igneous, but the quartz core would be around 60 % hydrothermal, from a fluid that would have dissolved silicium and alkalis from the associated melt. They confessed though that they had no idea of actual processes of transport and deposition.

Another hypothesis was made by Wilkinson et al. (1996). They argued about the existence of a K_2O-CO_2-SiO_2-H_2O fluid with a polymerized structure forming a Si-rich gel. This gel, due to its high viscosity, would prevent any convection in the dyke, leaving diffusion as the only possibility of ions movement. This would then lower the nucleation rate, allowing less but bigger crystals to grow. The last part of this fluid would be highly enriched in silicium, thereby coherent with the quartz core found in peraluminous pegmatites. However, values of the solubility of quartz in water imply that huge amounts of water must transit through the dyke in order to get such a Si-rich gel, which seems highly unlikely.

Today, two main models predominate, proposed by London (2018) and by Thomas et al. (2000). In 1991, Černý wrote that pegmatites petrology is "a process encompassing magmatic, supercritical, hydrothermal and gaseous phenomena in unique chemical systems", which is exactly what both models tend to prove.

London (2008) proposes that pegmatites crystallize from a granitic melt already enriched in HFSE, from margins to centre. His hypothesis is based on experiments in which melts of granitic composition were cooled below their liquidus temperatures and crystallized with textures similar to pegmatites (e.g. London and Morgan, 2017; Sirbescu et al., 2017). London affirms that since pegmatites crystallize in dykes, with cold surrounding rocks, the melt cools appreciably before crystallization begins. Hence, the melt viscosity is very high, and elements including HFSE have a low diffusivity. Elements that are incompatible with respect to the growing quartz and feldspar are concentrated next to the crystallization front, and cannot dilute in the remaining melt before complete cooling due to its viscosity, thus forming a boundary layer. Constitutional zone refining occurs in the boundary layer, decreasing activities of elements concentrated in this layer, regardless of their concentration. This leads to a partition coefficient crystal/melt close to zero, and to an extremely high concentration of these elements, including fluxing ones. The accumulation of B, P, and/or F causes an increase in the solubility of H_2O in the melt. Liquidus undercooling being an irregular process, it can explain the unequal size and composition of pegmatite layers. The limitations of this model is brought

by the study of melt and fluid inclusions, that indicate high concentrations of H_2O and fluxing elements during the entire cooling process instead of only in the end. A high concentration of H_2O would also lower the viscosity, diluting the boundary layer. Finally, constitutional zone refining proved to be unstable, and pegmatites are thought to form by several injections when there is only one in this model (Thomas and Davidson, 2015; Thomas et al., 2012; Thomas et al., 2006b).

The hypothesis of Thomas and Davidson (2016) builds on the study of melt and fluid inclusions. They found that pegmatites can contain from 20 to 50 % H_2O, against around 10 % occurring in granites. Hence, they conclude pegmatites form from a high temperature, silicated magma enriched in H_2O and fluxing elements (traditionally B, P, and F, but also H_2O, OH^-, CO_2, HCO_3^-, CO_3^{2-}, SO_4^{2-}, PO_2^{3-}, H_3BO_3, Cl, Li, Na, K, Rb, Cs, and Be according to Thomas et al., 2012). These lower the viscosity of the melt, allowing a higher rate of diffusion of chemical elements. The process of Ostwald ripening is then very effective, i.e. smaller crystals are dissolved to allow bigger ones to grow (Jain and Hughes, 1978). The layers observed in pegmatites would be due to a change of conditions in the environment (P, T, pH, etc) which may have either additive or multiplicative effects. The difference of temperature between the melt and host rocks leads to quenching on the margins, thereby isolating the inside of the pegmatite and leaving it cool more slowly to form giant crystals (Thomas and Davidson, 2015). The main argument against this model is the concentration of Be in the melt inclusions of studied pegmatites, which is much more important than in the original granitic melt. This may lead to think that studied minerals were accidently trapped and do not represent the actual composition of the melt. Plus, no experiment has ever been able to reproduce this model (London, 2015).

Consequently, mechanisms of formation of pegmatites are still under debate, each theory having its pros and cons. Also, it is important to mention that both models focus mostly on metaluminous compositions, which leaves peralkaline pegmatite genesis vastly unknown.

1.3 Generalities on rare earth elements

1.3.1 The rare earth elements, critical resources

Rare earth elements are classified among the most critical raw materials today because of their high demand and their low available supply (European Commission, 2018). They are used in many modern technologies linked to the energy transition (Goodenough et al., 2018; Lucas et al., 2014), but their production is quite restricted worldwide. The demand for rare earth oxides was estimated to 123,100 tons REO in 2016 and keeps growing every year (Goodenough et al., 2018). Rare earth elements are typically used for their their magnetic, luminescence and redox properties in many fields, the largest applications being permanent magnets, catalysts, polishing powders and rechargeable battery electrodes (Fig 1.5; Lucas et al., 2014; Wall, 2014).

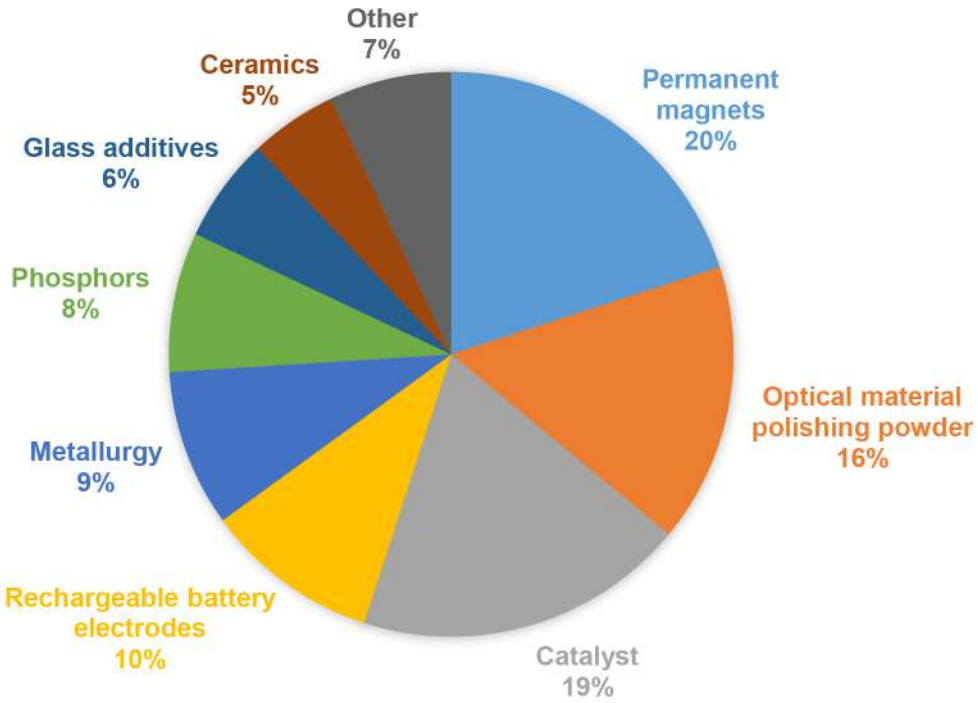

Figure 1.5 A diagram representing the most common industrial uses of REE, the main REE used, and the percentage of their world consumption, data from Lucas et al. (2014) and Wall (2014)

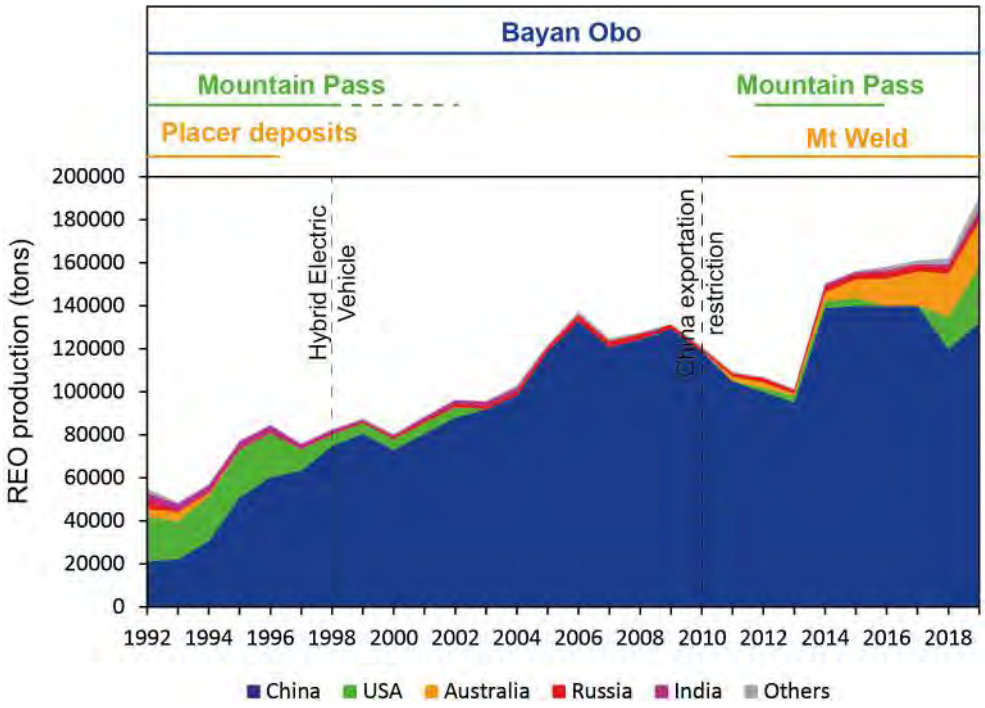

Figure 1.6 A graph showing the worldwide rare earth production between 1992 and 2019, with the proportion supplied from major REE producing countries and the most important deposits. The contribution of ion adsorption REE deposits to global production is also shown. From British Geological Survey, 1998, 2003, 2008, 2013, 2018, 2019; U.S. Geological Survey, 2019, 2020

Rare earth element deposits are usually low grade and low tonnage compared to other mined resources. The only known exception is the giant deposit of Bayan Obo, China (> $1.7x10^7$ tonnes REE_2O_3, Smith et al., 2016). REE exploitations are then small-scale and rarely attract large mining companies. The production of REE has increased since the beginning of their exploitation in the 1950s, and the main producing sites have changed over time (Wall, 2014). Placers in Western Australia and India were the only source of early production in the 1950s. The Mountain Pass carbonatite deposit in the USA dominated production in the 1960s to 1970s before its closure. In the 1980s, the Bayan Obo carbonatite in China became the first producing site. Since the 1980s, other Chinese producing sites opened, resulting in China being the dominant producer and supplying 80.7 % of the world's REE in 2017. In 2010, China restricted REE exportation, claiming that these restraints were to preserve the environment. This resulted in a drastic increase of REE prices and a general awareness of the REE supply vulnerability (Humphries, 2013). Since 2015, Mount Weld in Australia is a growing producer, and reached 9.2 % of the world's REE production in 2017 (Fig 1.6; British Geological Survey, 2019; Marquis,

2019). Although Brazil and Vietnam are the most important country in terms of REE reserves after China (18.3 % of the world known reserves in 2018), the exploitation and production of REE remains low (respectively 0.59 and 0.24 %, U.S. Geological Survey, 2019). Two thirds of actual REE exploration projects are in alkaline rocks and carbonatites, which represents only a small part of the more than 550 of these complexes known in the world (Fig 1.2).

1.3.2 Geochemistry of the REE

1.3.2.1 Physical properties of the REE

Rare Earth Elements are a family of 16 elements with similar properties including lanthanides (La to Lu) and Y (Fig 1.7). Some classifications also include Sc despite its geochemical behaviour that can differ from the other REE. Despite their name, the REE can be quite common in the Earth's upper crust; for example, Ce is respectively 2.3 and 3.7 times more abundant than Cu and Pb (Rudnick and Gao, 2003). However, as a result of the Oddo-Harkins effect (which is also valid for all elements; Harkins, 1917; Oddo, 1914), REE with odd atomic numbers are always less abundant than REE with even atomic numbers (Fig 1.8a), to the extent that they are less abundant than 94 % of other elements in the Solar System (Anders and Grevesse, 1989). For example, Tb and Tm are respectively two and five times less abundant in the continental crust than Mo (Chakhmouradian and Wall, 2012). Consequently, REE concentrations provide jigsaw patterns (Fig 1.8a) difficult to analyse, and are always normalized to a reference value. The choice of the reference is free and depends entirely on the goal of the study: it can be primitive mantle, CI chondrite, shales, etc. Promethium is never found in nature and is only produced artificially.

REE are mostly trivalent (3+ valence), with the exception of Ce and Eu that can be quadrivalent (Ce^{4+}) and divalent (Eu^{2+}) respectively. REE have relatively small atomic radii and a high cationic charge that provide them a high field strength (defined as atomic radius divided by cationic charge; Lottermoser, 1992), and are hence part of the HFSE. HFSE regroup REE, Nb, Ta, Zr, Hf, U, Th, Sn, and Ti and are usually all considered as incompatible elements during magmatic processes, i.e. they do not easily enter solid crystals and tend to get richer in melts as magmas differentiate (Linnen et al., 2014). Consequently, most evolved magmas such as peralkaline melts are enriched in HFSE, including REE.

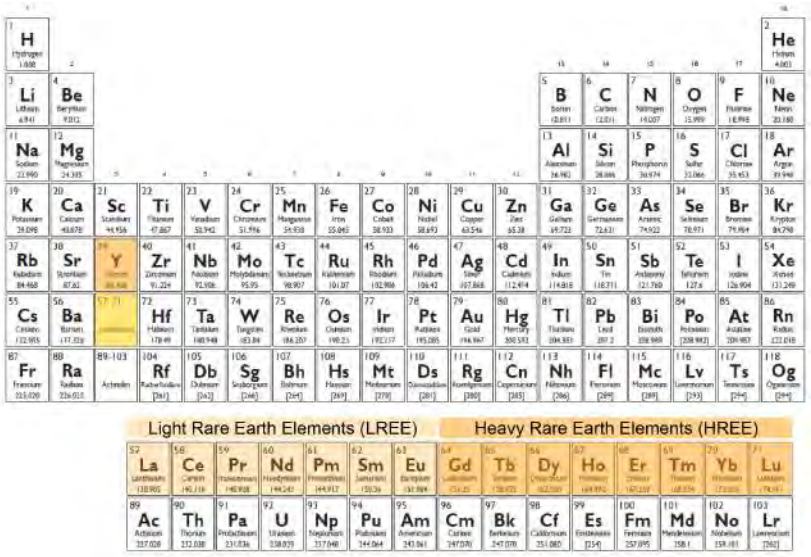

Figure 1.7 Periodic table of elements, the REE are highlighted

The REE are traditionally divided in two categories, namely, light-REE (LREE) and heavy-REE (HREE). The limit between LREE and HREE is set around Eu, but varies depending on the authors. In this work, LREE are considered to be from La to Eu, and HREE from Gd to Lu plus Y. LREE have bigger atomic radii but smaller atomic numbers, meaning they have lighter atomic masses compared to HREE that have smaller atomic radii and higher atomic numbers (Fig 1.8b). This important ionic radii reduction from La to Lu is called "lanthanide contraction" (Goldschmidt, 1925). It is related to the imperfect shielding properties of 4f electrons of REE that results in increasing the attraction of outer electrons toward the nucleus. This difference in atomic radii makes LREE more incompatible than HREE: being bigger, it is more difficult for them to enter crystal structures.

Lanthanide contraction and the Oddo-Harkins effect result in variable behaviours of REE in partitioning and concentrating in melts, growing crystals, and fluids and in their final concentration in the Earth's crust (Chakhmouradian and Wall, 2012). This difference in behaviour is also exploited in industrial separation. Because the Earth's crust is produced by partial melting of the upper mantle and LREE are more incompatible than HREE, in most natural systems of the crust LREE are generally more enriched than HREE (Rudnick and Gao, 2003), while the upper mantle is depleted in LREE (Workman and Hart, 2005). REE have long been considered as immobile as they are not soluble in aqueous solutions. However, studies of natural and artificial samples showed they are able to form stable aqueous complexes with ligands such as Cl^-, F^-, OH^-, CO_3^{2-} or PO_4^{3-} (Gysi et al., 2016;

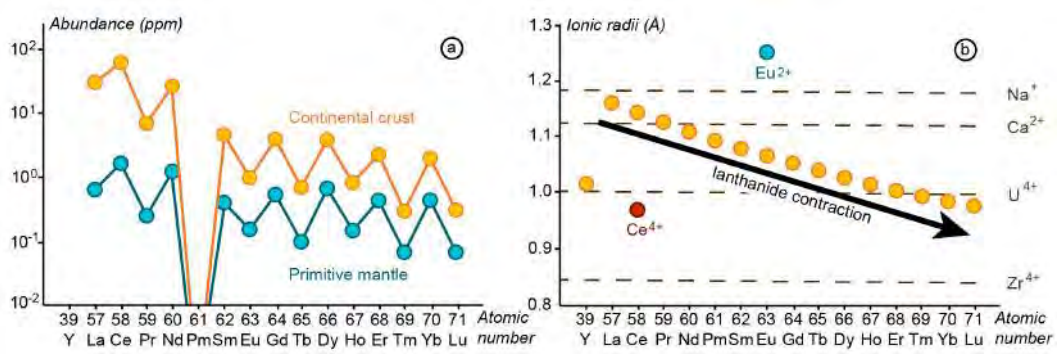

Figure 1.8 REE in a nutshell, adapted from Chakhmouradian and Wall (2012). (a) A diagram showing REE abundances in the Earth's primitive mantle (McDonough and Sun, 1995) and continental crust (Rudnick and Gao, 2003) and the Oddo-Harkins effect; (b) A diagram showing the ionic radii of REE cations in eight-fold coordination against their atomic number and compared with other common elements (Shannon, 1976)

Migdisov et al., 2016; Salvi and Williams-Jones, 1990; Wood, 1990). The behaviour of REE in hydrothermal fluids is then still not fully understood to this day.

1.3.2.2 Mineralogy of the REE

Rare earth elements are present as trace elements in most minerals. They are never native, but still can enter the mineralogical formula of silicates, carbonates, oxides, phosphates, fluorides, borates and sulfates (Table 1.3, Fig 1.9). In agreement with the preference of LREE for large coordination numbers (7-11), they are found mostly in carbonates and phosphates, whereas the preference of HREE for smaller coordination numbers (6-8), makes them occur preferentially in oxides. Silicates structures are varied, hence they are dispersed in the whole coordination number spectrum and can incorporate LREE as much as HREE (Kanazawa and Kamitani, 2006). To this day, over 350 REE minerals have been described (CNMC, 2020), but only 10 minerals are currently mined (Castor and Hedrick, 2006) despite research to improve this number (Davris et al., 2017a; Davris et al., 2017b). The most well-known are bastnäsite-(Ce), monazite-(Ce), and xenotime-(Y). The vast majority of REE-bearing minerals are actually made of Ce, Y, La, or Nd. In addition, some minerals contain high levels of REE substituting for other elements of similar radius and/or charge. Apatite, zircon and PGM are some examples.

Table 1.3 Selected REE-minerals with idealized chemical formulas, preferential geological settings and key-occurrences, from Marquis (2019)

Mineral Formula	Geological Setting	Notable Example(s)
	SILICATE	
Allanite (REE-rich Epidote) $(Ca, REE)Al_2Fe^{2+}(Si_2O_7)(SiO_4)O(OH)$	Hydrothermal vein REE deposits.	Hoidas Lake (Canada)
Britholite (Apatite supergroup) $(REE,Ca)_5[(Si,P)O_4]_3(OH,F,Cl)$	Peralkaline feldspathoid rocks.	Kipawa (Canada)
Steenstrupine $Na_{14}LREE_6Mn^{2+}{}_2Fe^{3+}{}_2Zr(PO4)_7Si_{12}O_{36}(OH)_2.3H_2O$	Peralkaline feldspathoid rocks.	Kvanefjeld (Ilimaussaq, Greenland)
Gadolinite $Fe(2+)Be_2REE_2(SiO_4)_2O_2$	Granitic pegmatites.	Strange Lake (Canada), Ytterby (Sweden), Barringer Hill (USA)
Zircon $(Zr, HREE)SiO_4$	Placers and peralkaline syenitic rocks (both altered and unaltered).	Nechalacho (Canada), Eneabba (Australia), Poços de Caldas (Brazil)
Eudialyte $Na_{15}Ca_6Fe_3Zr_3Si(Si_{25}O_{73})(O,OH,H_2O)_3(Cl,OH)$	Peralkaline feldspathoid rocks.	Kipawa (Canada), Kringlerne (Ilimaussaq, Greenland)
	OXIDE	
Cerianite CeO_2	Carbonatite and peralkaline feldspathoid rocks, also in laterites and ion adsorption deposit regolith profiles.	Nechalacho (Canada), Huashan Deposit (China)
Loparite $(LREE,Na,Ca)_2(Ti,Nb)_2O_6$	Peralkaline feldspathoid rocks	Lovozero (Russia)
Pyrochlore Group $(Na, Ca, REE)_2Nb_2O_6F$	Various occurrences – peralkaline feldspathoid, granitoid and carbonatite rocks.	Strange Lake (Canada), Zudong Intrusion (IAD protolith, China)
Euxenite Group $(HREE,Ca)(Nb,Ta,Ti)_2O_6$	Granite pegmatites.	Třebíč Pluton (Czech Republic)
Fergusonite $HREENbO_4$	Carbonatites plus associated fenites and phoscorites, peralkaline granites and associated pegmatites, laterites.	Strange Lake (Canada), Pitinga (Brazil)
Samarskite Group $(HREE,Fe,U,Th,Ca)(Nb,Ta,Ti)O_4$	Metasomatic carbonates and peralkaline feldspathoid rocks, and granitic pegmatites.	Bayan Obo (China), Nechalacho (Canada), Barringer Hill (USA)
Aeschynite $(REE,Ca,Fe,Th)(Ti,Nb)_2(O,OH)_6$	Metasomatic carbonates and peralkaline feldspathoid rocks.	Bayan Obo (China), Khibina (Russia)
	PHOSPHATE	
Apatite Group $(Ca, REE)_5(PO4)_3(F,OH)$	Alkaline, peralkaline and carbonatite igneous complexes.	Khibina (Russia)
Monazite $(LREE, Th)PO_4$	Carbonatites and associated metasomatic rocks, laterites and placers.	Mountain Pass (USA), Bayan Obo (China), Eneabba (Australia), Mount Weld (Australia), Steenkampskraal (South Africa), Kangankunde (Malawi)
Xenotime $(HREE)PO_4$	Carbonatites and associated metasomatic rocks, laterites and placers.	Lofdal (Namibia), Ak-Tyuz (Kazakhstan), Pitinga (Brazil), Mount Weld (Australia)
	CARBONATE, FLUORCARBONATE & FLUORIDE	
Bastnäsite $LREE(CO_3)F$	Carbonatites and altered peralkaline feldspathoid rocks.	Mountain Pass (USA), Bayan Obo (China), Weishan (China), Maoiuping (China), Nechalacho (Canada)
Parisite $CaLREE_2(CO_3)_3F_2$	Carbonatites and associated metasomatic rocks, plus hydrothermal REE deposits.	Mountain Pass (USA), Bayan Obo (China), Weishan (China), Snowbird (USA).
Synchysite $Ca(LREE,HREE)(CO_3)_2F$	Associated with carbonatites and altered peralkaline syenitic and granitic rocks.	Lugin Gol (Mongolia), Nechalacho (Canada), Ak-Tyuz (Kazakhstan)
Burbankite $(Na, Ca)_3(Sr, Ba, Ce)_3(CO_3)_5$	Associated with carbonatites.	Poços de Caldas (Brasil)
Ancylite $LREESr(CO_3)_2(OH)\cdot H_2O$	Associated with peralkaline feldspathoid rocks.	Khibina (Russia), Ilimaussaq (Greenland)

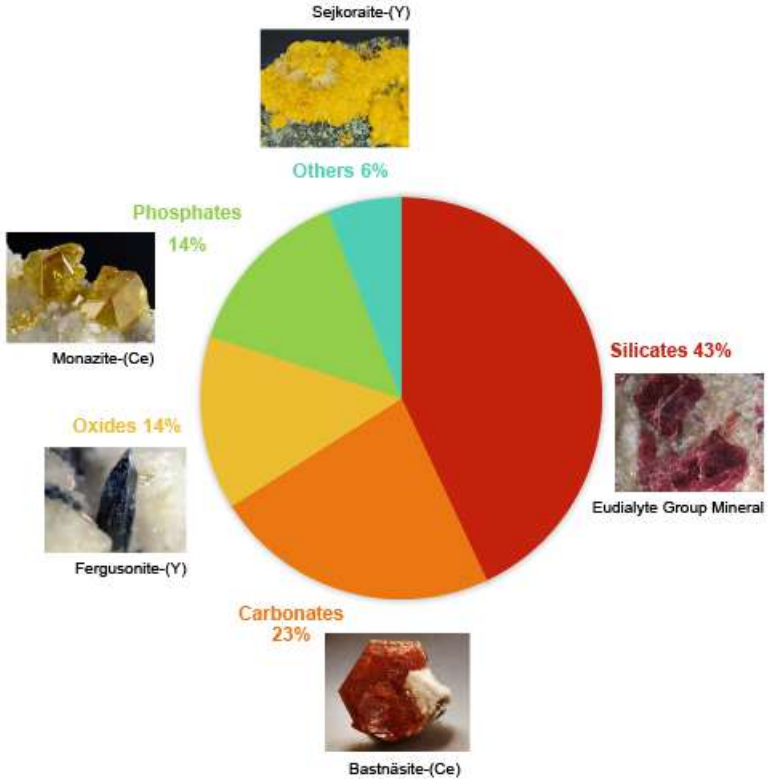

Figure 1.9 A diagram showing the proportions of the different families of REE-bearing minerals, with macroscopic photographs of an example of mineral for each family, data from Chakhmouradian and Wall (2012) and photographs from mindat.org (accessed 01/2020)

1.3.3 Rare earth elements deposits types

REE deposits are classically divided into two groups (Fig 1.2 and Table 1.4; Bloodworth, 2010; Kanazawa and Kamitani, 2006; Linnen et al., 2014; Marquis, 2019), namely, high-temperature primary (magmatic and hydrothermal) or low-temperature secondary (sedimentary and weathering). Primary deposits include alkaline rocks, carbonatites, iron-oxides REE, and hydrothermal veins (Table 3). Primary magmatic deposits can also be affected by hydrothermal fluids, causing a REE enrichment through mechanisms that are still not fully understood to this day (Verplanck and Van Gosen, 2011). Secondary deposits typically include placers, laterites, and ion-adsorption clays. A summary of geodynamic contexts of REE deposits is provided in Fig 1.10.

Type and grade of REE resources provided by these deposits depends on the primary igneous source, the degree of partial melting and fractional crystallization in the melt, hydrothermal fluids circulation, weathering, and geodynamic setting (Goodenough et al., 2016; Kogarko, 1990; Marks and Markl, 2017; Smith et al., 2016;

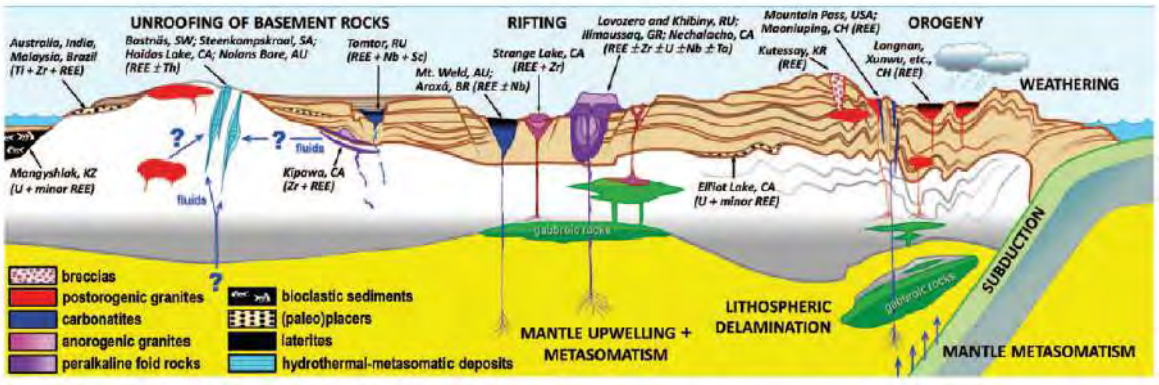

Figure 1.10 Schematic view of geodynamic contexts REE deposits can be found in, from Chakhmouradian and Wall (2012)

Wall and Zaitsev, 2004). For example, ion-adsorption clays are poorly concentrated in REE, but their exploitation is easy and relatively cheap. Alkaline granites and associated pegmatites are the richer deposits in HREE (Fig 1.11). Table 1.4 provides a summary of the characteristics of the different REE deposits along with key-examples.

1.3.4 Challenges of REE exploitation

1.3.4.1 Environmental and public health concerns

Despite being used in green technologies, the REE exploitation is no exception to usual environmental mining issues. The REE are mined in open-pits, often as by- and co-products of other ores. For example, at the Bayan Obo deposit, REE are by-products of iron ore mining; at Elliot Lake, Canada, they were by-products of uranium (Marquis, 2019; Wall, 2014). Main mined REE minerals are bastnäsite-(Ce) and monazite-(Ce). The extraction process of igneous deposits includes the isolation of REE ore (mostly by flotation techniques), acid attack, leaching, solid/liquid separation, solvent extraction, and heating. It leads to the separation of each REE and its transformation into pure oxide, phosphate and fluoride (Lucas et al., 2014). Different extraction methods are used for secondary deposits as they are less consolidated; they include excavation by bucket (often underwater for placers) and crushing. There are only few details available of mining techniques for ion adsorption deposits in China as they are often small scale, manual exploitation (Wall, 2014). Physical digging causes destruction on mining sites, and used chemicals for extraction and separation can be released in waters and soils. The

Table 1.4 A classification of rare earth deposits with key-examples, adapted from Kanazawa and Kamitani (2006), Jébrak and Marcoux (2008), and Marquis (2019)

Deposit group	Deposit type	Main characteristics	REE resources	Main REE minerals	Genetic model	Examples of major deposits	Reference
Primary	Alkaline rock	Abundant alkali minerals, high differenciation	Generally low grade (<2 wt% REE_2O_3); granites contain more HREE	Zircon, xenotime-(Y), fergusonite-(Y), allanite-(Y), bastnäsite-(Ce), eudialyte group minerals	Magmatic/hydrothermal	Khibina and Lovozero, Russia; Strange Lake, Canada; Ilímaussaq, Greenland	Salvi and Williams-Jones 1990, Kogarko 2002, Goodenough et al. 2016, Smith et al. 2016
	Carbonatites	At least 50 % of carbonate minerals	LREE	Bastnäsite-(Ce), monazite-(Ce), synchisite-(Ce), apatite	Magmatic/hydrothermal	Mountain Pass, USA; Bayan Obo, China	Castor 2008, Smith 2007
	Iron-Oxide-Gold-Copper (IOCG)	Magmatic with magnetite, or hydrothermal rich in Cu, Au, U	All REE	Bastnäsite-(Ce), monazite-(Ce), xenotime-(Y), britholite-(Ce)	Magmatic/hydrothermal	Olympic Dam, Australia	Castor and Hedrick 2006
	Hydrothermal (not associated with alkaline rocks)	Hydrothermal phosphate, quartz and fluorite veins which can carry a wide variety of metals	LREE	Apatite, monazite-(Ce)	Hydrothermal	Nolans Bore and Browns Range, Australia	Huston et al. 2016
Secondary	Placer	Mechanical accumulation of resistant heavy minerals redeposited and concentrated during sedimentation processes in river, estuarine or shallow marine environments	All REE	Monazite-(Ce), xenotime-(Y)	Physical weathering, erosion, transport and redeposition	Elliot Lake, Canada; Manavalakuruchi, India	Wall 2014, Sengupta and Van Gosen 2016
	Laterite, bauxite	Clay and iron-rich soils formed under tropical climate. Bauxites are laterites with > 40 % Al_2O_3	All REE	Clays and secondary apatite, rhabdophane-(Ce, Y)	Weathering	Mount Weld, Australia	Lottermoser 1990, Cocker 2014
	Ion-adsorption	Near surface chemically weathered granitoid rocks (biotite and muscovite granites)	HREE	Clays	Weathering of REE-rich granitoids	Longnan, China	Sanematsu et al. 2013, Marquis et al. 2017

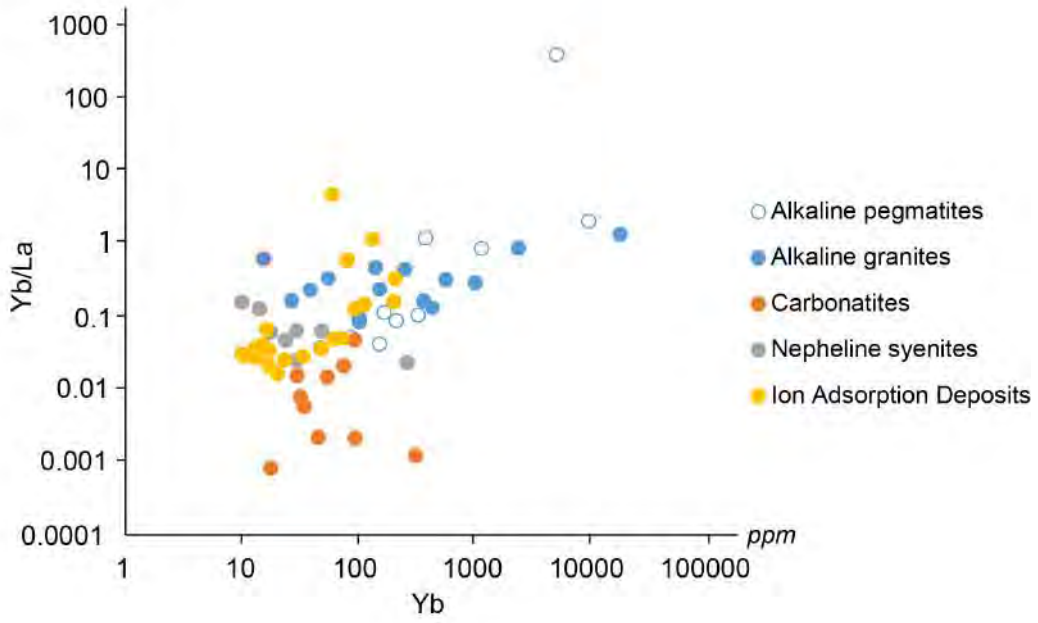

Figure 1.11 A logarithmic diagram plotting chondrite-normalized (Sun and McDonough, 1989) values of whole-rock Yb/La vs Yb contents for different alkaline complexes worldwide. Five groups are distinguished: alkaline granites, alkaline pegmatites, carbonatites, nepheline syenites, and ion-adsorption deposits. Data are from this study plus bibliography (Boily and Williams-Jones, 1994; Chengyu et al., 1990; Estrade, 2014; Estrade et al., 2014b; Hatch, 2015; Ishihara et al., 2008; Jahn et al., 2001; Kogarko et al., 2002; Kynicky et al., 2011; Li et al., 2010; Liu et al., 2015; Mikhailova et al., 2017; Moore et al., 2015; Poitrasson et al., 1995; Sanematsu et al., 2013; Schmitt et al., 2002; Sørensen and Larsen, 1987; Vasyukova and Williams-Jones, 2014; Wang et al., 2010; Xu et al., 2017; Yang et al., 2003; Zaitsev et al., 2015)

extraction of REE also produces heavy metals-rich clay dust (Keith-Roach et al., 2015). Another issue of REE exploitation is their common association with U and Th in high quantities, occurring in the structure of REE minerals as well as separated minerals (Chakhmouradian and Wall, 2012). Uranium and Th are concentrated in mining wastes and emit radioactivity and Rn. Miners and local populations are more likely to develop cancers, as it has been established in the historical trial of Bukit Merah, Malaysia (Ichihara and Harding, 1995). The REE themselves are not usually considered toxic, although some uses can become dangerous if prolongated. For example, the main reported issue is with Ce used in polishing powders which has been documented to accumulate in the bone, liver, heart, and cause lung problems. It is important to have these considerations in mind in order to not look at life through rose-tinted glasses as to green technologies.

1.3.4.2 Possible solutions

Considering ecological damages of open-pit REE exploitation, it is important to increase the control of exploitations, as the Chinese government did to limitate the proliferation of small-scale exploitations, and punish illegal prospection (Chakhmouradian and Wall, 2012). Mining rehabilitation is also fundamental to allow the nature to rebuild itself. Phytomining, i.e. bioharvesting of metals from crops grown in soils from ancient mines, is a working example of rehabilitation (Sheoran et al., 2009).

Finding alternative materials to lower or suppress REE in our technologies is now fundamental considering the criticality of REE available resources. Alternatives can be found to replace partially or totally the REE in current technologies, or to design new technologies that do not need REE. To this day, substitution of REE is not always possible due to the high performance provided by these metals. Found substitutes also have to be cheaper than REE, which is another limitation. However, research is under way and some solutions have already been found, such as in magnets in which Nd can now be reduced or totally replaced by iron nitride or ferrite (Wall, 2014; Weber and Reisman, 2012).

Recycling is another way to reduce our need to extract the REE. It has many advantages, among which slowing down the depletion of natural resources and the filling of landfills, limiting the production of waste products, and lowering the amount of energy necessary to obtain pure REO (up to 90 % less, Lucas et al., 2014). However, to this day the recycling technology is not sufficient to provide all the REE we need, hence it can only be complementary of REE mining (Grosse, 2010). Some materials, such as phosphor powders and rechargeable batteries, are easier to recycle for REE, and some countries, like Japan, are more active in REE recycling (Chakhmouradian and Wall, 2012). However, and despite the efforts of researchers to improve REE-recycling technologies, in 2011 only 1 % of the total extracted REE were recycled (Binnemans et al., 2013; Mueller et al., 2015). After the 2010 crisis, this number increased, but is still low (Lucas et al., 2014). Several explanations have been raised to understand this phenomenon, among which: property issues, i.e. sellers are not concerned by the becoming of their merchandise; difficulty of finding informations on who you should give your material to be recycled; long lifetimes of merchandises with significant amounts of REE; absence of regulation; low yield of most REE components (e.g. less than 0.1 wt% for mobile phones); and impossibility

to recycle only one REE (e.g. the recycling of Nd magnets results in the extraction of Nd along with La and Ce which are then oversupplied; Binnemans et al., 2013; Chakhmouradian and Wall, 2012; Garcier and Verrax, 2017). REE-recycling is hence a good solution to limitate REE extraction from natural resources, but still needs improvement and control.

1.4 Control on REE concentration and fractionation in alkaline granitoid deposits

It is commonly accepted that the high levels of REE in alkaline granitoid deposits are explained by a magmatic source already enriched in rare metals, magmatic processes, and, to some extent, remobilization by hydrothermal fluids (Chakhmouradian and Zaitsev, 2012).

In alkaline granitoid deposits, as mentioned in section 1.1.2, the source of melts is known to be mantellic (Balashov and Glaznev, 2006; Foland et al., 1993). In this case, a regular partial melting of the mantle would not lead to the formation of high concentrations of REE and HFSE. Hence, a metasomatic pre-enrichment of these elements in the mantle is required. The origin of this metasomatic event is not fully understood, but several hypotheses exist. Among them, the recycling of oceanic and continental crust and the delamination and downwelling of subcontinental lithosphere are good candidates. Anyways, metasomatism is recognized to enrich the mantle in either sodium or potassium. The first one reduces the mantle rocks by removing ferric iron in garnets, thereby forming aegirine, whereas the second one oxidizes the mantle by depleting garnets in Al_2O_3 and forming phlogopite. Associated with low partial melting degrees of the mantle and differentiation of the resulting magma, this redox change participates in the extreme enrichment in halogens, REE, and HFSE of the magmas (Markl et al., 2010; Marks and Markl, 2017).

Purely magmatic processes also play a significant role in the REE enrichment of alkaline rocks. A low rate of partial melting of the source will highly enrich the resulting magma in incompatible elements, including the REE. This has been observed for example in basalts, that were enriched in LREE if produced in an extensional setting (<1 % partial melting) compared to oceanic basalts (Chakhmouradian and Zaitsev, 2012). Fractional crystallization in magmatic

chamber also enhances the enrichment in REE as minerals with low REE concentration crystallize, leaving the REE in the remaining melt. The unusual HREE enrichment of some peralkaline granites for example is enhanced by fractional crystallization of feldspars (e.g. $^{plagioclase/melt}D_{Ce}$ is 0.1 to 0.4 and $^{plagioclase/melt}D_{Lu}$ is 0.02 to 0.06; Bédard, 2006). Light-heavy REE fractionation in alkaline granitoids is often explained by the low solubility of monazite-(Ce) in silicated magmas. Hence, LREE are either trapped in monazite-(Ce) and are never incorporated in the magma, or they are removed from the melt during early stages by crystallization of monazite-(Ce). Eventually, melt-melt or fluid-melt immiscibility is another effective way to concentrate REE: if one liquid has a lower affinity for the REE, they will concentrate in the second liquid. This is the case for carbonate-silicate systems, in which the REE, and in particular the HREE, partition into the silicate phase (Chakhmouradian and Zaitsev, 2012; Veksler et al., 2012).

Long underestimated, hydrothermal fluids are suspected to play a significant role in concentrating REE in economic amounts and in fractionating LREE-HREE. The geochemical behaviour of REE in aqueous hydrothermal fluids, including mobilization, transport, and deposition, is controlled by several factors: concentration of volatile components, availability, concentration and nature of complexing agents (mainly F^-, CO_3^{2-}, Cl^-, SO_4^{2-} and PO_3^-), time of residence of REE in the fluid, and physical parameters of the environment such as pH, temperature, pressure, alkalinity (Kogarko, 1990). The study of fluid inclusions, although reported in very few papers, gives direct evidences as to the composition and minimal temperature of REE-rich fluid. Mineral assemblages provide indirect evidences that chloride and sulphate enhance REE solubility in fluid phases and may play a role in specific enrichment in HREE (Broom-Fendley et al., 2016). Today, it is proved that no matter the magmatic or meteoric origin of aqueous fluids, REE are transported as complexes formed mainly with chloride and sulphate, but also with carbonate, fluoride, phosphate and oxalate. Hydroxyl is also an important ligand specific to alkaline rocks due to their high pH. The stability of all those complexes varies according to the ligand, the environment conditions, and the heavy or light nature of the REE, thereby leading to a fractionation. For example, HREE-F^{2+} complex is more stable than LREE-F^{2+} complex at ambient temperature, while it is the opposite at high temperatures. The same effect has been observed for chloride complexes, but not for sulphate ones. In addition, experiments showed that as HREE are heavier than LREE, with an equal residence time in the fluid,

LREE are transported on longer distances than HREE. REE can also occur in significative concentrations as ions at low temperatures. Finally, thermodynamic calculations showed that a high alkalinity in the fluid keeps volatile elements into a single fluid phase (Kogarko, 1990; Lottermoser, 1992; Migdisov et al., 2016). While early-stage alterations of alkaline rocks are K-feldspathization, albitization, and biotitization, late-stage induced alterations like sericitization and chloritization produce fluids enriched in REE-complexing agents, which highly enhances REE mobility. Considering solubility factors, changes in the environment are responsible for favoured deposition of REE, along with crystallographic control (Lottermoser, 1992). Minerals structures have affinities that vary from one REE to another, which is one more source of REE fractionation. An example of change in the environment can be the neutralization of acidity of a REE-F^{2+} rich aqueous solution, which destabilizes the complexes and causes the deposition of REE fluoride minerals. This neutralization can be due to the circulation in carbonate rocks, or to a mixing with another high-pH fluid. Thereby, fluoride is considered more as a depositional ligand than a transport one. The main depositional mechanisms include precipitation of minerals containing the ligands, fluid mixing, cooling, and fluid-rock interaction (Broom-Fendley et al., 2017; Migdisov et al., 2016).

Fractionation of the REE during hydrothermal phase seems to originate from mobilization (stability and nature of ligands in the fluid), transport (long time of residence), and deposition (stability of REE-bearing minerals, crystallographic control) mechanisms. However, many unknowns remain regarding the precise behaviour of REE at high temperatures, in carbonate-bearing solutions, or even of the stability of the different REE complexes in fluids. Plus, the importance of these mechanisms compared to magmatic ones are still to be understood.

1.5 Aims of this study and selection of alkaline complexes

We have seen in the preceeding sections that the rare earth elements are considered a critical resource, mostly due to a constantly growing demand and Chinese monopoly of supply market. We have also seen how low recycling and substitution of the REE can only make this criticity stronger in the years to come. For all of these reasons, it is necessary to improve our knowledge on the

formation of economic REE-deposits and, given that REE extraction occurs mostly in ion-adsorption clay deposits in China, focusing in particular on alternative deposit types. As shown above, ideal candidates are carbonatites and associated alkaline rocks, as they are found on all continents and are often enriched enough in REE to be exploited. In particular, silica-saturated alkaline rocks are preferentially enriched in HREE compared to LREE, making them key targets for industrial applications. Therefore, one of the goals of this study is to understand the processes leading to this peculiar heavy versus light REE-fractionation.

Another aspect that is still not fully understood is how alkaline granitoid rocks form and how they reach such economic concentrations in REE. As reviewed above, the initial global REE concentration is acceptedly of magmatic origin and depends on the magmatic source of the rock. Therefore, because pegmatites differenciate from the last and most evolved melts, they are even richer in REE. But pegmatite formation is still debated, notably concerning the presence or not of a water phase (London, 2008; Thomas et al., 2006b). This is of capital importance because, as reviewed above, fluids, whether orthomagmatic or external to the intrusion, have the ability to transport the REE via ligands such as Cl^- and F^-. However, the specific role of these ligands, and whether they interact with other chemical species present in the fluids (e.g. mixed complexes), still need documentation. Questions that need answering include: what is the form of the main ligands for REE in hydrothermal fluids? How much REE can be mobilized compared to magmatic processes? Do fluids fractionate the REE? To what extent? In order to help providing answers to these questions, this study focuses on understanding the physical and chemical properties of the fluids that allegedly transported the REE in peralkaline rocks.

To apprehend these objectives, this thesis focuses on six alkaline complexes, all showing signs of hydrothermal fluid circulations. They all comprise silica-saturated rocks, but were emplaced in different geodynamic contexts and at different periods of time, and were chosen so to represent a spectrum of the known alkaline complexes (Fig 1.12). By using this strategy, if a common pattern is found it could confidently be related to a general process. The goal of this work is to understand the general mobilization and fractionation processes of REE in hydrothermal fluids during the history of alkaline silica-saturated rocks. This will allow to evaluate the respective contribution of magmatic and hydrothermal processes in concentrating the REE in these rocks. To achieve this goal, the approaches used in this thesis

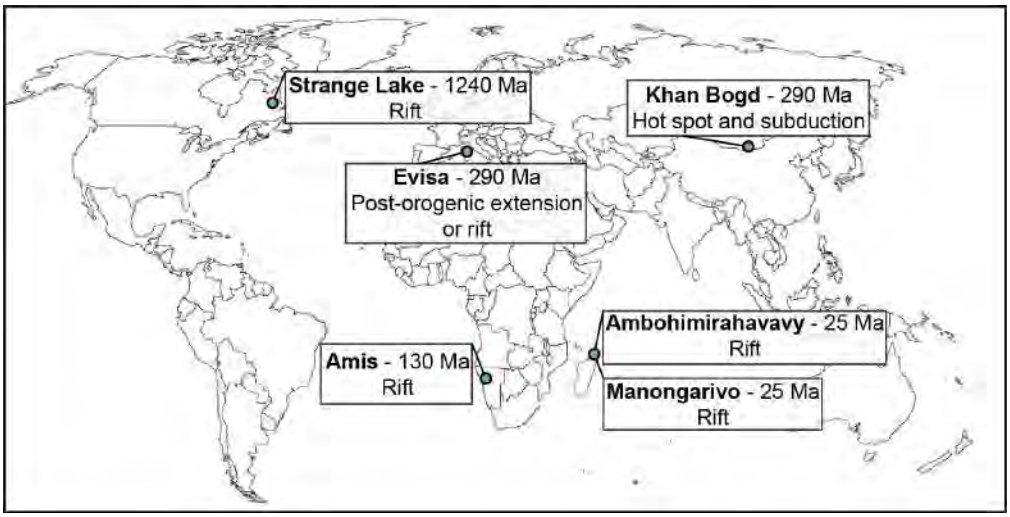

Figure 1.12 A worldwide map showing the location, age and geological context of emplacement of the six alkaline complexes selected for this study

are based on careful petrological and geochemical studies of both REE-bearing and main common minerals as well as on the study of fluid inclusions from all six complexes.

1.6 Thesis organisation

In order to better constrain the timing of REE concentration and fractionation in alkaline granites and pegmatites, Chapter 2 provides a detailed description of each selected alkaline complex. Their geological setting, main mineralogy and magmatic-hydrothermal evolution is provided as described in the existing literature. This state of the art permits to understand the similarities (e.g. melt source, main mineralogy) and differences (e.g. magmatic processes, composition of the circulating hydrothermal fluid) between the studied complexes.

Chapter 3 focuses on the petrology of the complexes to understand the extent of the similarities between the six studied complexes. After a description of analytical methods and studied samples, the textures and compositions of main minerals, i.e. quartz, alkali feldspars, amphiboles and pyroxene, are described. Quartz and pyroxene are zoned, and feldspars are widely albitized. The chapter goes on with the analysis of primary REE-bearing minerals, with an emphasis on primary zirconosilicates, i.e., eudialyte-group minerals and elpidite. These minerals are commonly altered into an assemblage of secondary hydrothermal minerals

forming pseudomorphs. Other minerals, such as amphibole or narsarsukite, can also be replaced by secondary minerals in pseudomorphs. The nature and REE concentration of these secondary minerals give precious information about the timing of REE concentration and fractionation, as well as on the composition of circulating hydrothermal fluids. This detailed petrological analysis allows me to propose a paragenesis for each complex.

Chapter 4 focuses on specific minerals that have the ability to grow from magmatic to hydrothermal stages and to incorporate significant amounts of REE, i.e., amphiboles, pyroxene, and zircon. Their study provides an accurate timing for REE concentration and fractionation in such complexes. Amphiboles and pyroxene are studied in a paper published in the journal *Contributions to Mineralogy and Petrology*. Amphiboles are found not zoned and exclusively magmatic in this study, whereas pyroxene in pegmatites is zoned in all complexes, no matter their geological emplacement context. The zonation is made of a core rich in Zr, Ca, Sn, Hf and REE, and sector-zoned rims rich either in Ti and Ca or in Fe depending on the sector. The core is found to be magmatic, and the rims hydrothermal in origin. The lower concentration of REE in the rims indicates most of enrichment occurs on the magmatic stage, but light-heavy REE fractionation occurs on the hydrothermal stage. This study allows to understand the general process for REE enrichment and fractionation in alkaline silica-saturated complexes worldwide. In order to confirm the dual origin of pyroxene, further analyses of oxygen isotopy are performed on crushed whole pyroxene crystals as well as in situ in the different zones. The results do not show any difference on whole crystals analysis. Following the same reasoning than for amphiboles and pyroxene, zircon textures and composition are analyzed in another section. Three types of zircon were found in the complexes: type-SG, which regroups euhedral magmatic crystals that can be hydrothermally altered; type-P, made of secondary euhedral, dendritic and botryoidal crystals in pseudomorphs; and type-I, made of secondary anhedral interstitial crystals. The main results show that the REE composition of type-P zircon depends mostly on the composition of the primary replaced mineral and therefore cannot be used to infer the composition of the fluid it grew from. The chapter is concluded with a calculations to estimate the contribution of hydrothermal fluids to the REE budget of each complex. A mass balance calculation is performed between primary zirconosilicates and secondary pseudomorphs. An image analysis program was developed exclusively for this PhD in order to estimate a more hydrothermal REE

budget at the sample scale. All calculations show that the majority of the REE, and even more HREE, present in the rocks of the six studied complexes is contained in hydrothermal minerals.

Chapter 5 focuses on understanding the properties of hydrothermal fluids that circulated in the six studied complexes in order to check whether or not they share common patterns that would allow them to mobilize, deposit and fractionate the REE. To do so, fluid inclusions are studied using microthermometry and SEM. This investigation reveals that although their salinity varies significantly from one complex to another as well as within a same sample, fluids circulate at a relatively low temperature (<400 °C). All investigated complexes experienced the circulation of two fluids, one Na- and K-rich, and one Ca- and Na-rich. For the Malagasy complexes and Strange Lake, it has been established that the Na-K-bearing fluid is orthomagmatic and the Ca-Na-bearing one is meteoric. For the other complexes, available data did not allow determination of a timing. The relative contribution of the two fluids to the REE budget, however, could not be investigated.

Chapter 6 summarizes the observations made in the previous chapters and proposes a recipe for REE enrichment in alkaline granites and associated pegmatites. It shows that from the study of aegirine core-to-rim zonation, zircon composition, primary zirconosilicates and PGM hydrothermal alteration, and mass-balance calculation, it is possible to conclude that the absolute quantity of REE in alkaline complexes depends primarily on magmatic source and processes, but that there is an extensive remobilization and concentration of these elements by hydrothermal fluids. Evidences for local (sample-scale) as well as global (complex-scale) influence of hydrothermal fluids were found, hence the scale over which the REE are mobilized and fractionated by fluids is still an open question. Fluid inclusions in the different complexes provide various entrapment temperatures, all under 400 °C, as well as different salinities. The composition of hydrothermal fluids is common to the six studied complexes, with one fluid rich in NaCl and KCl, and a second one rich in $CaCl_2$ and NaCl. Known ligands for the REE such as F, Cl, OH, CO_3^{2-} and S were found in some complexes, but the general observation, i.e., that HREE are more mobilized than LREE in fluids of the six complexes of this study, is not explained by the present knowledge of REE ligands. This chapter also discusses the mobilization of HFSE other than REE by the fluids, such as Ti and Th.

Chapter 2

Geological and petrological context

2.1 The Amis complex, Namibia

2.1.1 Geological setting of the Brandberg and Amis plutons

The Brandberg complex is one of more than 20 occurrences of anorogenic alkaline rocks in Namibia (Woolley, 2001). It is a 20 km wide circular complex of hornblende-biotite metaluminous granite that can reach up to 2573 m above sea level (Pirajno, 2015). The pluton emplaced 132.5 to 130.5 My ago in metasediments of the Damara orogen ($\sim$ 550 My; Miller, 1983) and volcanic rocks from the Etendeka igneous province, which are more or less contemporary of the pluton (Schmitt et al., 2000).

The Amis complex intrudes this granite in its south-west side (see Fig 2.1), but is the same range of age. It is of particular interest because of its specific high enrichment in HFSE, volatiles (H_2O, F) and REE. The Amis complex is made up of about 3 km^2 of peralkaline rocks, with a main part consisting of arfvedsonite granite, plus alkaline pegmatite-aplite occurrences and dikes that have very similar composition to the main granite. Many dikes and sills extend beyond the complex, with a maximum thickness of 50 m and a maximum length of 1.5 km for the thinest; this shows the low viscosity of the magma emplaced.

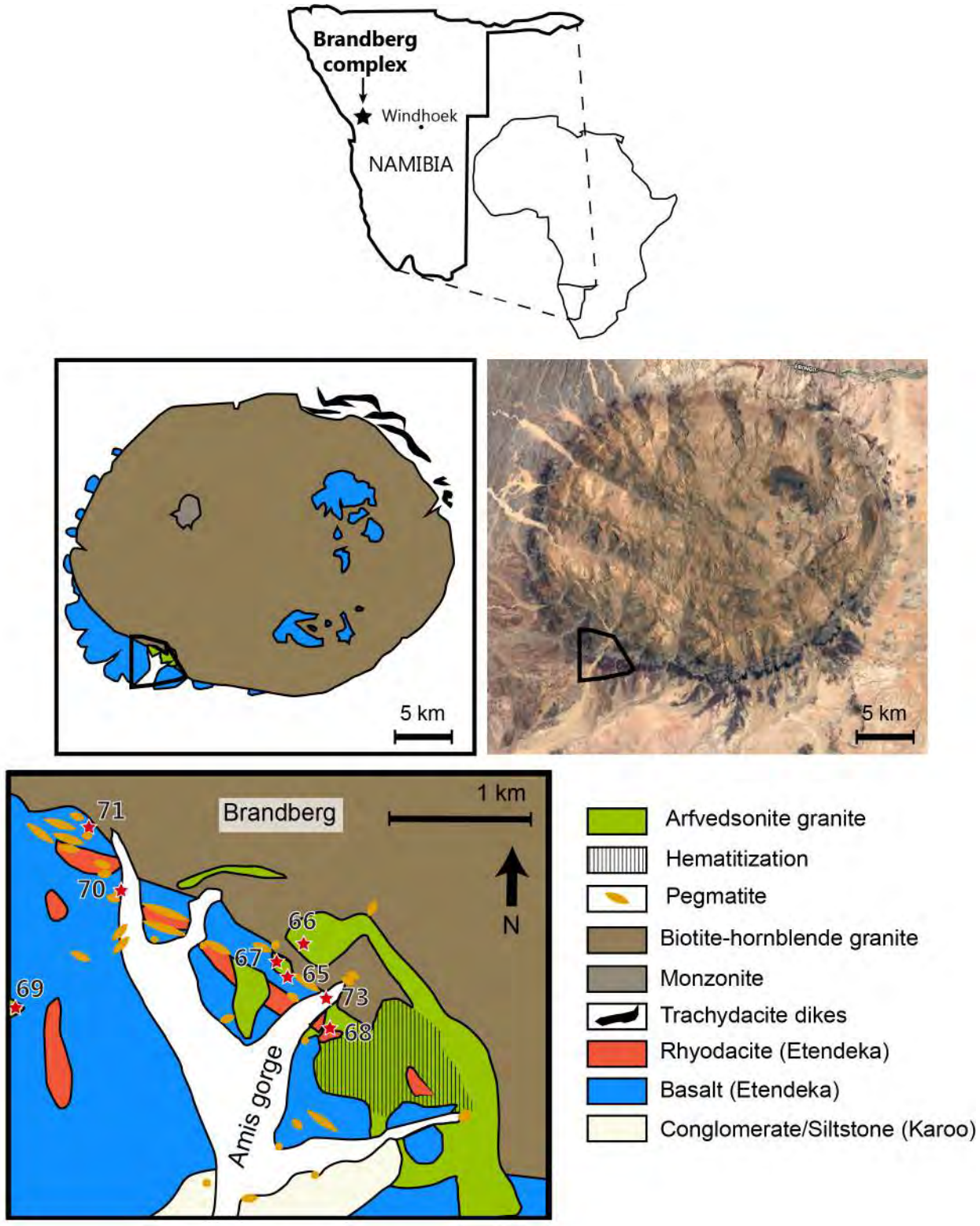

Figure 2.1 Localization, satellite image and geological map of the Amis and Brandberg complexes, modified after Schmitt et al. (2002). Stars provide the location of samples analyzed in this study

2.1.2 Petrology of Amis rocks: arfvedsonite granite and alkaline pegmatite

The petrological and chemical compositions of the two main rock types, namely arfvedsonite granite and alkaline pegmatite are very alike, and their distinction is mainly based on textural arguments and mineralization potential. Arfvedsonite granite is medium-grained, while pegmatite occurs as both coarse and fine-grained dikes (Fig 2.2). They are both rich in REE, other HFSE and volatiles (H_2O, F). The main felsic minerals in both rock types are quartz, albite and microcline, which makes them subsolvus granite and pegmatites. Main mafic minerals are Na-amphibole (arfvedsonite) and Na-pyroxene (aegirine), usually arranged around the latter (Pirajno, 2015). The arfvedsonite granite shows arfvedsonite layering, with layers of 1 meter to several cm (Fig 2.2b,e).

Accessory minerals in the arfvedsonite granite are common to both layer types. They are REE-bearing fluorite intergrown with bastnäsite-(Ce), PGM, monazite-(Ce), xenotime-(Y), scarce zircon, and dalyite. They are all interstitial, except for PGM. Alkaline pegmatites, mostly concentrated in the north-western part of the Amis complex, are especially rich in REE Zr, Nb and U and contain typical radial clusters of aegirine and associated astrophyllite (Fig 2.2c,d,f) along with a lot of accessory minerals such as ilmenite, PGM, thorite, gadolinite-(Y), wulfenite, hematite, and zircon (Schmitt et al., 2002; Woolley, 2001). Association of zircon and quartz clearly replaces a primary mineral, forming pseudomorphs; however, having been completely replaced, this mineral has not been identified yet. Two types of PGM are distinguished by Schmitt et al. (2002) in pegmatite. The first one is found as euhedral inclusion in zircon, hence it is older, and its composition is similar to that of PGM in the arfvedsonite granite. It is interpreted as magmatic. The second type of PGM is anhedral and enriched in Ti and HREE to the detriment of Nb. This type of PGM is of late-magmatic to secondary origin, but Schmitt et al. did not give any evidence in favour of one or the other origin. Thorite also seems particularly enriched in HREE.

Four granite and 4 pegmatite samples were kindly provided by Dr. Sam Broom-Fendley from the Camborne School of Mines, England, for this study. They are located on Fig 2.1.

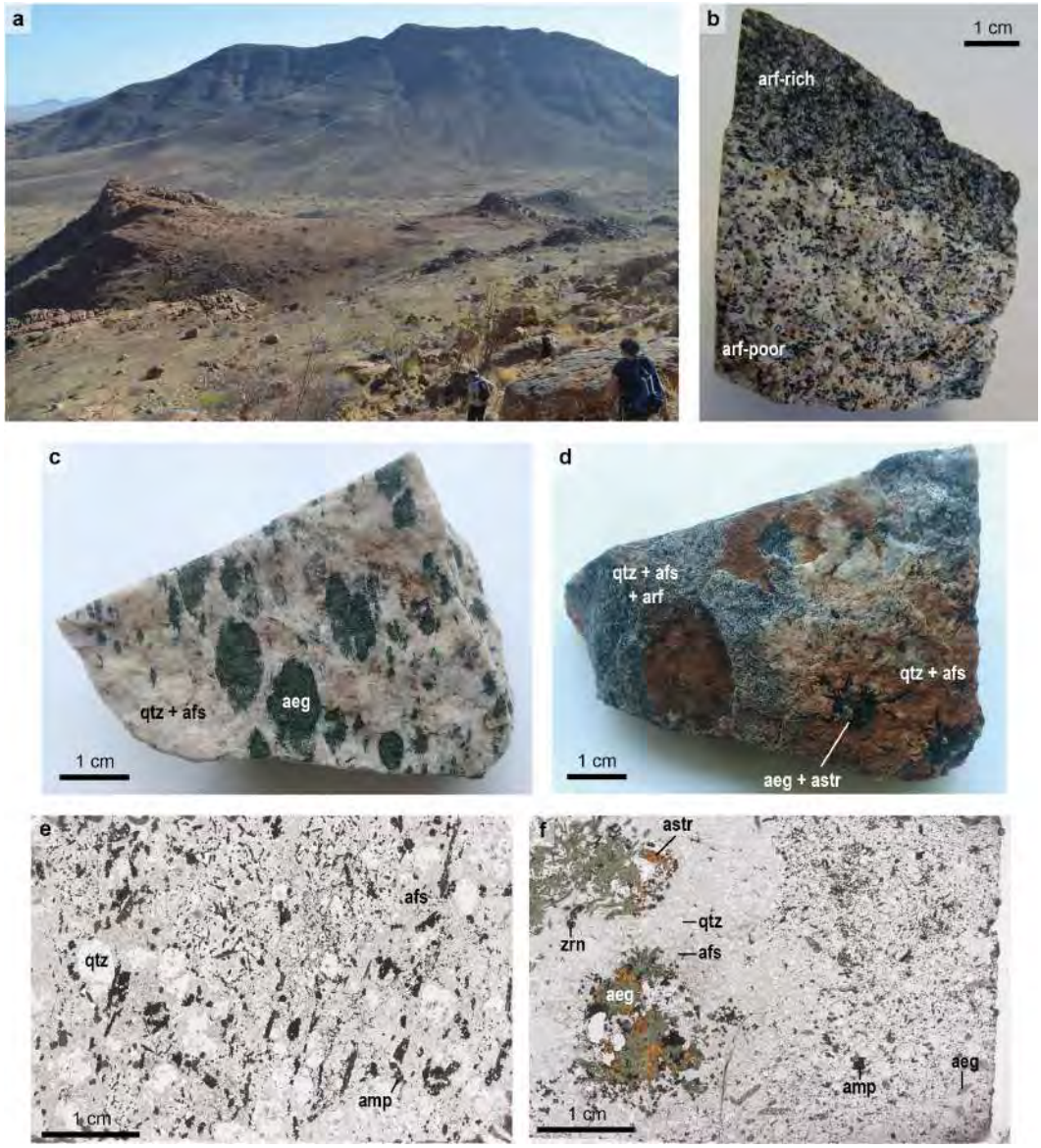

Figure 2.2 Presentation of the main rocks that can be found in the Amis complex. (a) General field view of the complex, photograph courtesy of Sam Broom-Fendley; (b) Arfvedsonite granite, with its basal part depleted in amphibole, sample SOS069; (c) Pegmatite with clusters of aegirine, sample SOS070b; (d) Pegmatite with an arfvedsonite zone and a radial aegirine cluster zone, sample SOS071; (e) Thin section of arfvedsonite granite, sample SOS069; (f) Thin section of pegmatite with radial aegirine cluster, sample SOS071. Abbreviations: qtz: quartz; afs: alkali feldspar; aeg: aegirine; arf: arfvedsonite; astr: astrophyllite; zrn: zircon; amp: amphibole

2.1.3 Magmatic vs hydrothermal contribution

Amis and Brandberg granites are derived from the same source, which is different from the Paraná-Etendeka lavas one. The complexes are interpreted to originate from a basaltic melt which experienced differentiation and assimilation of crustal material in a rifting context (Schmitt et al., 2000). Schmitt et al. (2002) focused on the study of melt inclusions in alkaline pegmatite and found that the bulk composition of melt inclusions is very similar to that of whole-rock composition of the arfvedsonite granite as to major elements. Based on this result as well as on the fact they have not found any primary fluid inclusion, they infer that magmatic processes, including crystal fractionation, would be the only process responsible for HFSE enrichment.

However, these authors admit that the higher concentrations of H_2O, F and Cl in melt inclusions than in the arfvedsonite granite indicates that volatiles loss must have occurred during fractionation of the residual peralkaline melt, which would have caused a relative enrichment in HFSE and would be the source for alkaline pegmatite. In addition, they evoke two hydrothermal events that must have affected the complex. This is consistent with the presence of mineral alterations in arfvedsonite granite and alkaline pegmatite, such as the replacement of arfvedsonite by quartz-hematite overgrowths. The study of the Y/Ho and La/Ho ratios inquires on the intervention of a fluid as well as on its composition. Indeed, in magmatic systems Y^{3+} and Ho^{3+} behave coherently, hence the ratio Y/Ho should be constant and equal to the chondritic ratio. In hydrothermal fluids, their concentration depends on the stability of the complex they formed, hence the ratio will deviate from the chondritic value. The way it deviates indicates the fluid major composition, as Y does not behave the same in fluorine-rich solutions than in carbonate-rich ones for example. Hence considering that the La/Ho and Y/Ho ratios in melt inclusions are lower than they are in chondrites (Fig 2.3), along with the high concentration of HREE in late-stage minerals such as bastnäsite-(Ce), Schmitt et al. (2002) propose the intervention of a carbonate-rich fluid that took preferentially LREE. Since these melt inclusions ratios are similar to those of pegmatite, they infer this fluid must be orthomagmatic. In the arfvedsonite granite, although based on 2 measurements, Schmitt et al. observe that these ratios vary considerably. The constant Y/Ho and increasing La/Ho trend (Fig 2.3) is interpreted as the footprint of a postmagmatic F-rich fluid

in which HREE complexes are more stable. This relatively depleted the primary mineralogy in HREE by solving them, before reprecipitating them in minerals such as fluorite, fluocerite-(Ce) and bastnäsite-(Ce) (increasing Y/Ho and decreasing La/Ho, Fig 2.3).

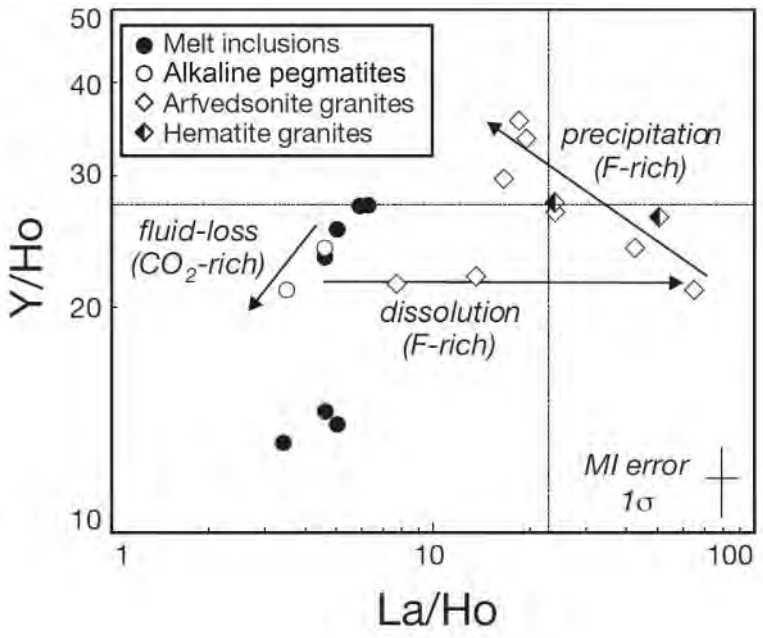

Figure 2.3 Y/Ho vs La/Ho ratios in melt inclusion glasses and whole rock from the Amis Complex (1σ error for SIMS analysis of melt inclusions is indicated) from Schmitt et al. (2002). Dashed lines indicate Y/Ho and La/Ho chondritic ratios. Note that four out of seven melt inclusions have near-chondritic Y/Ho ratios

However, based on oxygen isotope ratios on quartz and pyroxene-amphibole in the arfvedsonite granite that are consistent with equilibrium at magmatic temperatures, they specify that the impact of hydrothermal fluids on REE redistribution was only local (∼10 m). However, this analyze was only made on minerals identified as magmatic, and not on REE-bearing minerals. On the other hand, Diehl (1990) proposes that the influence of hydrothermal fluids extended over the entire complex, forming aegirine clusters in alkaline pegmatite. He suggests that an oxidizing, fluorine and rare-metal bearing fluid would destabilize arfvedsonite and metasomatically replace it with aegirine and astrophyllite.

The initial high REE and HFSE content of the rocks of the Amis complex is hence considered purely magmatic in the literature, but the origin of high concentration and fractionation of the REE is still debated.

2.2 The Evisa complex, Corsica

2.2.1 Geological setting of the Evisa plutons

The Evisa complex (dated to 290 My by U-Pb on zircon; Cocherie et al., 2005; Poitrasson et al., 1998) is about 20 km^2, oriented NE-SW and located above a deep fracture which caused its peculiar elongated shape (Quin, 1969). It was emplaced among metaluminous granitoids after the Variscan collision in an extensional post-orogenic context or rifting (Rossi et al., 2010). The complex mainly comprises hypersolvus (contains only one alkali feldspar type) and subsolvus (contains two types of alkali feldspar, albite and microcline) peralkaline granites rich in REE-bearing minerals such as monazite-(Ce), apatite, and allanite-(Ce) (Bonin, 1990b). Intrusions have a morphology in domes shaped by surface erosion (Fig 2.5a). The hypersolvus granite occurs elongated along the eastern edge of the subsolvus one and is about 2 km wide (Fig 2.4). Poitrasson et al. (1998) estimated that it was emplaced at about 0.5 kbar (1.5 km) and between 900 and 700 °C, which led to formation of chilled margins at the contact with the host rocks. In addition to these two granite varieties, the Evisa complex contains lindinosite fragments (a melanocratic peralkaline granite with about 60 % of Na- amphibole, Le Maitre et al., 2004), fayalite-bearing pegmatites, and granitic pegmatites (Bonin, 1980). Pegmatites are mostly found at the center of the two main granites and have diffused boundaries with them (Bonin, 1990b). Finally, late dikes of different natures intersect the entire complex. They include mafic (dolerites) and felsic (microgranites, rhyodacites, rhyolites) dike varieties, plus quartz veins (Rossi et al., 2010; Vellutini et al., 1996).

2.2.2 Petrology of main Evisa rocks: hypersolvus granite, subsolvus granite, and pegmatites

The hypersolvus granite is coarse-grained (1-4 mm) (Rossi et al., 2010; Vellutini et al., 1996; Fig 2.5b,h), but microgranite is found locally, on the edges of the pluton or in dikes (Quin, 1969). The hypersolvus granite is mainly made up of 30-40 % of euhedral quartz, 60-70 % perthitic feldspar and a few percentages of ferromagnesian

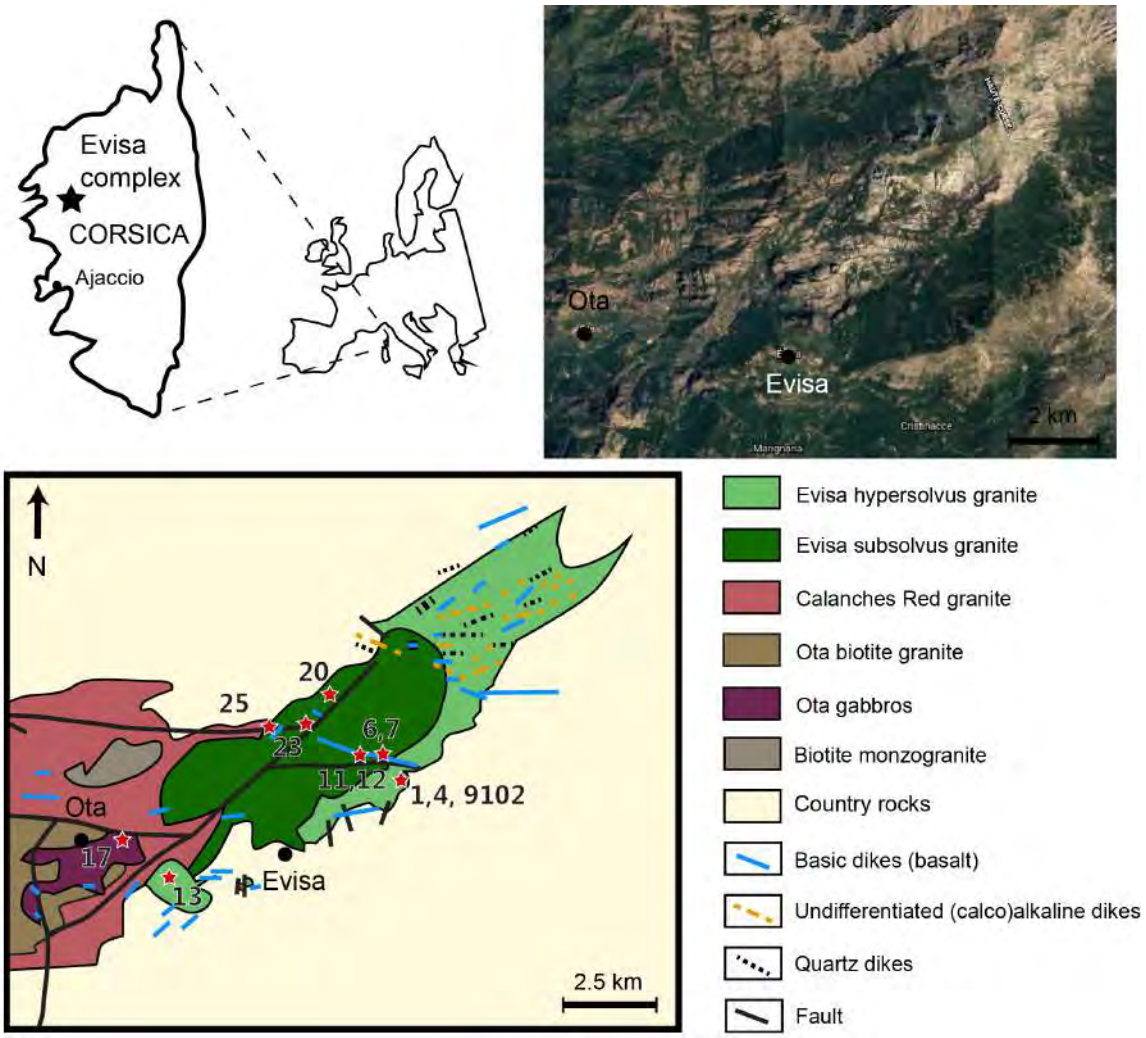

Figure 2.4 Localization, satellite image and geological map of the Evisa complex and surrounding granites, modified after Rossi et al. (2010) and Vellutini et al. (1996). Stars provide the location of samples analyzed in this study

minerals (arfvedsonite, leakeite, biotite) associated with astrophyllite. Accessory minerals are oxides (locally in high quantities, Fig 2.5c; hematite, cassiterite, rutile, fergusonite-(Ce), PGM), sulphides (pyrite, pyrrhotite, chalcopyrite, galena), sulphates (barytine), phosphates (apatite, monazite-(Ce), xenotime-(Y)), halides (fluorite, cryolite, bastnäsite-(Ce)), and silicates (allanite-(Ce, La, Nd), aenigmatite, epidote, låvenite, chevkinite-(Ce), stilpnomelane, titanite, zircon; Bonin, 1990b; Poitrasson, 2002). The hypersolvus granite contains some pegmatites at the top of its domes, which are composed of the same mineralogy than the hypersolvus granite, including a high amount of iron oxides (Fig 2.5e).

The subsolvus granite leucocratic rock speckled with 2-3 mm long rods of arfvedsonite (Rossi et al., 2010; Fig 2.5b). Quin (1969) describes three textures for

this granite: fine-grained, containing short and thick albite, and coarse-grained. These textures are observed progressively respectively from the rim to the core of the granite (Vellutini et al., 1996). A peculiar feature of this subsolvus granite is the presence of a decimeter-thick layer of Na-amphibole-rich pegmatite on its surface, in contact with host rocks (Vellutini et al., 1996). The mineralogy of the subsolvus granite is comparable to that of the hypersolvus one, with a few exceptions: distinct albite and orthoclase occurs instead of perthite; aegirine partially or fully replaces arfvedsonite according to the following reaction.

$$arfvedsonite + O_2 \rightarrow aegirine + oxides + quartz + vapor \tag{2.1}$$

In addition to producing aegirine, reaction 2.1 increases the total amount of quartz in the rock. Astrophyllite and biotite are absent, while elpidite occurs, though it is partially to totally pseudomorphosed by secondary minerals (Bonin, 1990b). In subsolvus pegmatite (Fig 2.5j), arfvedsonite was entirely replaced by aegirine, in which case the pegmatite is surrounded by a fenitized zone developed in the subsolvus granite, similar to the one surrounding aegirine clusters in the Amis complex (Bonin and Platevoet, 1988). The subsolvus granite also occurs as a hydraulic breccias associated with hematite-fluorite veins, cemented by a granitic groundmass rich in arfvedsonite (Fig 2.5g,k). This breccia represents a continuum between magmatic stage, at which granitic minerals continue to grow, and hydrothermal stage, characterized by hematite and fluorite (Bonin, 1988). Lindinosite pieces are found inside the granite and can measure up to 500 m in thickness. The roof of the domes are especially rich in dikes made of granite with albitic and chloritic alteration (Bonin, 1990b; Fig 2.5d).

In addition to the hypersolvus and subsolvus granitic pegmatites, fayalite-bearing pegmatites are also found in the granite roofs. They contain pockets of giant quartz, alkali feldspar, and fayalite crystals in a red, hematite- and chlorite-rich matrix that can be interpreted as previous miarolitic cavities (Fig 2.5f). Fayalite crystals can measure up to 50 cm and are altered to hematite.

Two hypersolvus granite, 5 subsolvus granite and 5 pegmatite samples from the central part of the complex were collected during a field campaign in September 2018. They are located on Fig 2.4.

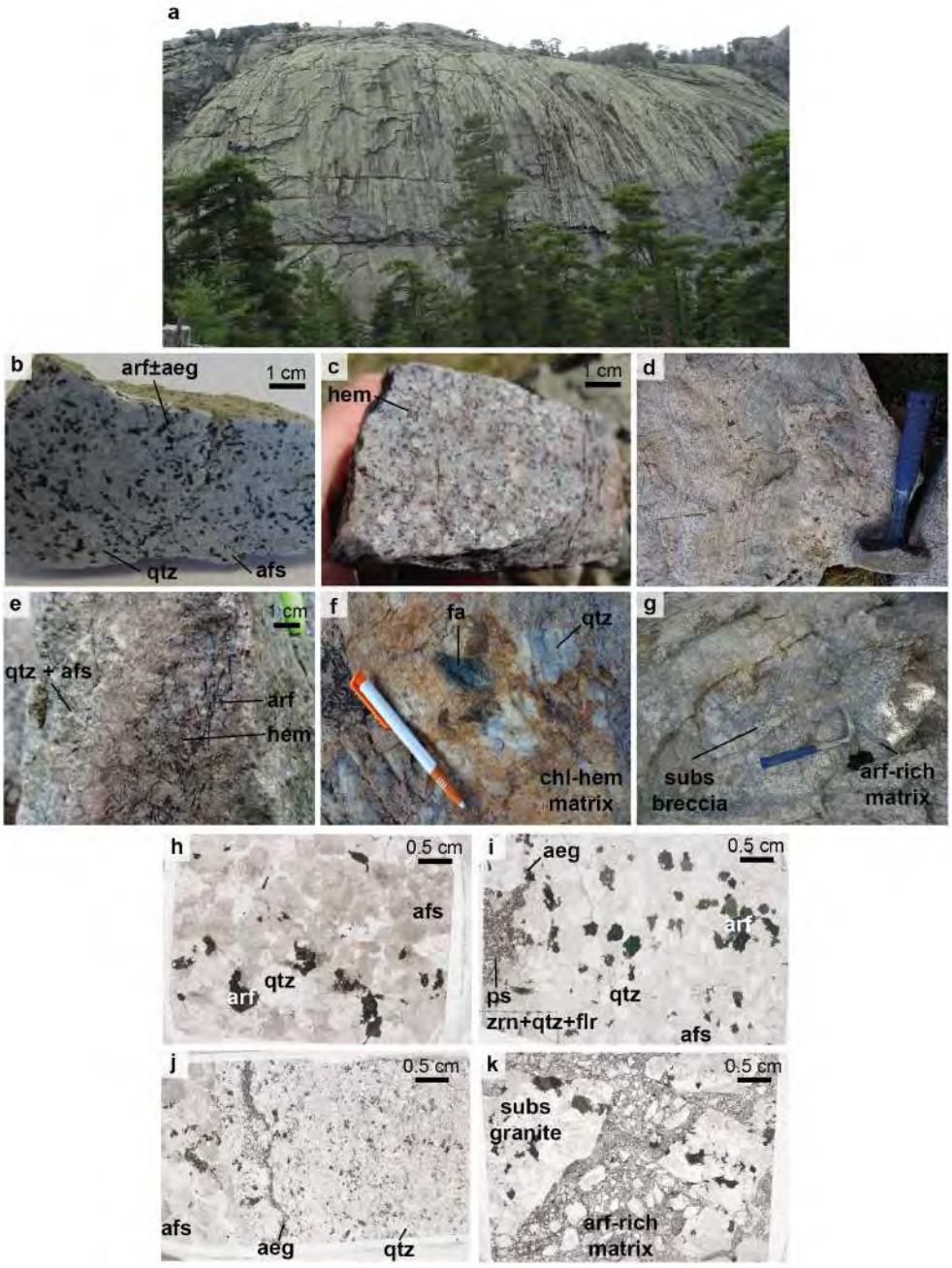

Figure 2.5 Presentation of the main rocks found in the Evisa complex. (a) Dome of the Evisa subsolvus granite, looking north; (b) Hand sample of subsolvus granite, with white sticks of arfvedsonite ± replaced by aegirine; (c) Hypersolvus granite stained with hematite; (d) Pegmatite in the subsolvus granite; (e) Pegmatite in the hypersolvus granite; (f) Fayalite-bearing pegmatite; (g) Breccia of subsolvus granite, cemented by a a granitic groundmass rich in arfvedsonite; (h) Thin section of hypersolvus granite, sample EV1801; (i) Thin section of subsolvus granite with a zircon, quartz and fluorite pseudomorph, sample EV18123B; (j) Thin section of aegirine-bearing pegmatite, sample EV1817A; (k) Thin section of breccia of subsolvus granite, sample EV1808. Abbreviations: qtz: quartz; afs: alkali feldspar; aeg: aegirine; arf: arfvedsonite; hem: hematite; fa: fayalite; chl: chlorite; subs: subsolvus;zrn: zircon; flr: fluorite; ps: pseudomorph

2.2.3 Magmatic granitic source and hydrothermal circulations

Two hypotheses have been proposed for the source of these granites but are still debated: the most widespread is a mantle source with low crustal contamination; the other one is a residual crustal source from which a granitic magma and most of the water had already been removed (Vellutini et al., 1996).

Several authors have reported two main hydrothermal events at Evisa. A comparison between Sm-Nd and Rb-Sr datations showed that the Rb-Sr system has been reset at 249±3 Ma, which would be the age of the first hydrothermal event which occurred at the end of crystallization of the complex (Poitrasson et al., 1998). Peralkaline fluids, most likely related to the intrusion of the subsolvus granite, briefly circulated and altered mostly the hypersolvus granite. During this first and restricted hydrothermal event, feldspars were mostly affected and partially replaced by aegirine.

The second and more important hydrothermal event occurred around 200 Ma and was also evidenced by Sm-Nd datations (Bonin et al., 2008; Poitrasson et al., 1998). This hydrothermal event affected both granites. It was characterized by F-rich fluids, as shown by the presence of the hydraulic breccias associated with hematite-fluorite veins. The albitic and chloritic alteration of pegmatites at the top of the domes shows this fluid must have had a high activity in Si and Na (Bonin, 1980, 1990b; Bonin and Platevoet, 1988). This second hydrothermal event triggered the replacement of the primary zirconosilicate elpidite by a secondary assemblage (Bonin, 1990b). It is interesting to note that this secondary hydrothermal event matches the beginning of the opening of the Liguro-Piemont basin in the Alps and has been recorded in other areas of the Alpine Chain (Poitrasson et al., 1998).

The role of these events in mobilizing and fractionating the REE in the Evisa complex has not been further investigated. It is however known that higher amounts of REE are found in the subsolvus granite than in the hypersolvus one (respectively 174 vs 94 ppm of Y, and 194 vs 106 ppm of Ce; Bonin, 1990a). Furthermore, studies in more southern Corsican alkaline granites of similar ages have shown a local influence (∼1 km) of remobilization and fractionation of the REE, with the alteration of REE-bearing primary minerals (e.g. allanite-(Ce, La, Nd)) and the recrystallization of HREE-bearing minerals (e.g. allanite-(Y); Poitrasson, 2002; Poitrasson et al., 1998). However, according to those studies the whole-rock concentration of REE was not affected, confirming a limited influence of the fluids.

Hence, it is likely that the overall amount of REE in the Evisa complex originates from magmatic processes (source and fractional crystallization), but that local concentrations as well as LREE/HREE fractionation can be caused by late- to post-magmatic hydrothermal circulations.

2.3 The Khan Bogd complex, Mongolia

2.3.1 Geological setting of the Khan Bogd plutons

The Khan Bogd complex is among the largest alkaline granite plutons in the world, with a surface of 1500 km^2. It has been investigated for mining purposes and estimates indicate grades between 0.3 and 4.5 % REE, the highest grade being located at the top of the granites plutons (estimation of the tonnage is not available, Kovalenko and Yarmolyuk, 1995). To my knowledge, only three publications exist in the western literature on this complex (Gerdes et al., 2017; Kovalenko et al., 2006; Kynicky et al., 2011), on which is based the short description that follows. Khan Bogd is located in the southern Gobi Desert, at the transition between island-arc calc-alkaline differentiated volcanics (329$\pm$5 My) and rift-related bimodal basalt–comendite–alkali granite association (318-290 My). The complex was dated by U-Pb on zircon at approximately 290 Ma (Kovalenko et al., 2006). The pluton consists of three ring bodies: a western peralkaline arfvedsonite granite, in which many aegirine granitic pegmatites occur parallel to the external contacts, an eastern peralkaline aegirine granite, and an alkaline porphyritic granite (Fig 2.6). The absence of pegmatite in the eastern ring tends to show that they were emplaced at the same time.

The general tectonic setting is controlled by the intersection of the Gobi–Tien Shan Rift Zone with an oblique fracture zone. According to preliminary gravity measurements, the pluton is flat with its base subsiding towards the northwest: it is 7 km deep on its northwestern part, 4.5 km deep in its central part, and 1-2 km deep in its southeastern part. The contact of the pluton with bimodal complex volcanics host rocks is sharp and made of volcanics and granite breccias, xenoliths, and a metamorphic aureole of hornfels sometimes cut by dikes. All these observations point to an active emplacement followed by an uplift of at least 2 km (Kovalenko et al., 2006; Kynicky et al., 2011).

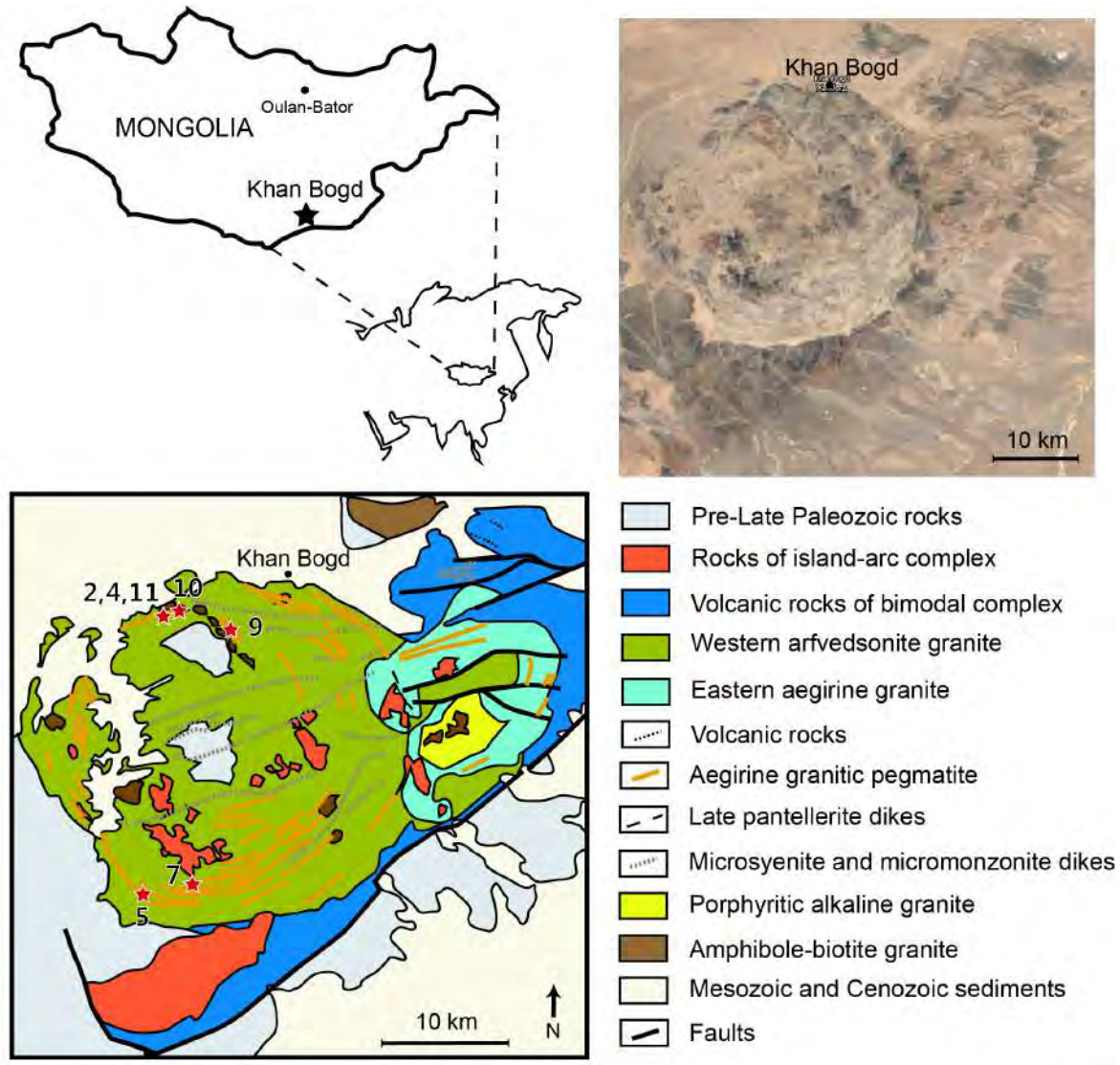

Figure 2.6 Localization, satellite image and geological map of the Khan Bogd complex, modified after Kovalenko et al. (2006). Stars provide the location of samples analyzed in this study

2.3.2 Petrology of Khan Bogd rocks: alkaline granites and pegmatite

The major mineralogy of the Khan Bogd peralkaline plutons consists of perthitic alkali feldspar (microcline with albite exsolutions, up to 35 modal %), quartz (48–53 modal %), arfvedsonite (up to 12 modal %, Fig 2.7d,h) which is, in its eastern part, replaced by aegirine (up to 11 modal %). Accessory minerals are titanite, rutile, apatite, zircon, and zirconosilicates including elpidite, armstrongite and gittinsite (Kynicky et al., 2011). Metasomatically altered samples also contain Fe–Mn oxides,

calcite and REE fluorcarbonates (bastnäsite-(Ce), parasite-(Ce) and synchysite-(Ce)). The peralkaline granites are agpaitic, they both have Na-Ca zirconosilicates as the main accessory phases showing the high degree of differentiation of the magma. The Na-Ca zirconosilicates, present in both ring-bodies and pegmatites, are primary Ca-poor and REE-rich elpidite locally replaced by an assemblage of either early Ca-enriched elpidite - armstrongite - gittinsite - quartz or late calcite - zircon, forming pseudomorphs. Primary elpidite is however much better preserved than the primary zirconosilicates of the other alkaline complexes presented in this manuscript (Fig 2.7b,f). Both peralkaline ring-bodies are enriched in HREE compared to LREE. The porphyritic granite is similar to the peralkaline granites, but is much more altered to white mica, and is miaskitic since its main accessory mineral is primary zircon.

Pegmatites occur at the top of domes of the western granitic body, either as zoned lenses (5-100 m long, Fig 2.7e) or as layered dikes (Fig 2.7a-c,f,g). Their mineralogical composition is similar to that of alkaline granites, with more aegirine replacing arfvedsonite (Kynicky et al., 2011; Vaglio et al., 2007). Lenses of pegmatites are made of a thin border zone including arfvedsonite and aegirine crystals embedded in albitized microcline and quartz, and a quartz core zone (Fig 2.7e). An alteration halo is present around pegmatites, but is restricted to a few cm wide, which is thin compared with alteration halos around carbonatites and porphyries than can reach up to 100 m.

Three granite and 7 pegmatite samples from the sides of the western ring of the complex were collected by Guillaume Estrade during a High Tech Alk Carb field campaign in September 2017. They are located on Fig 2.6.

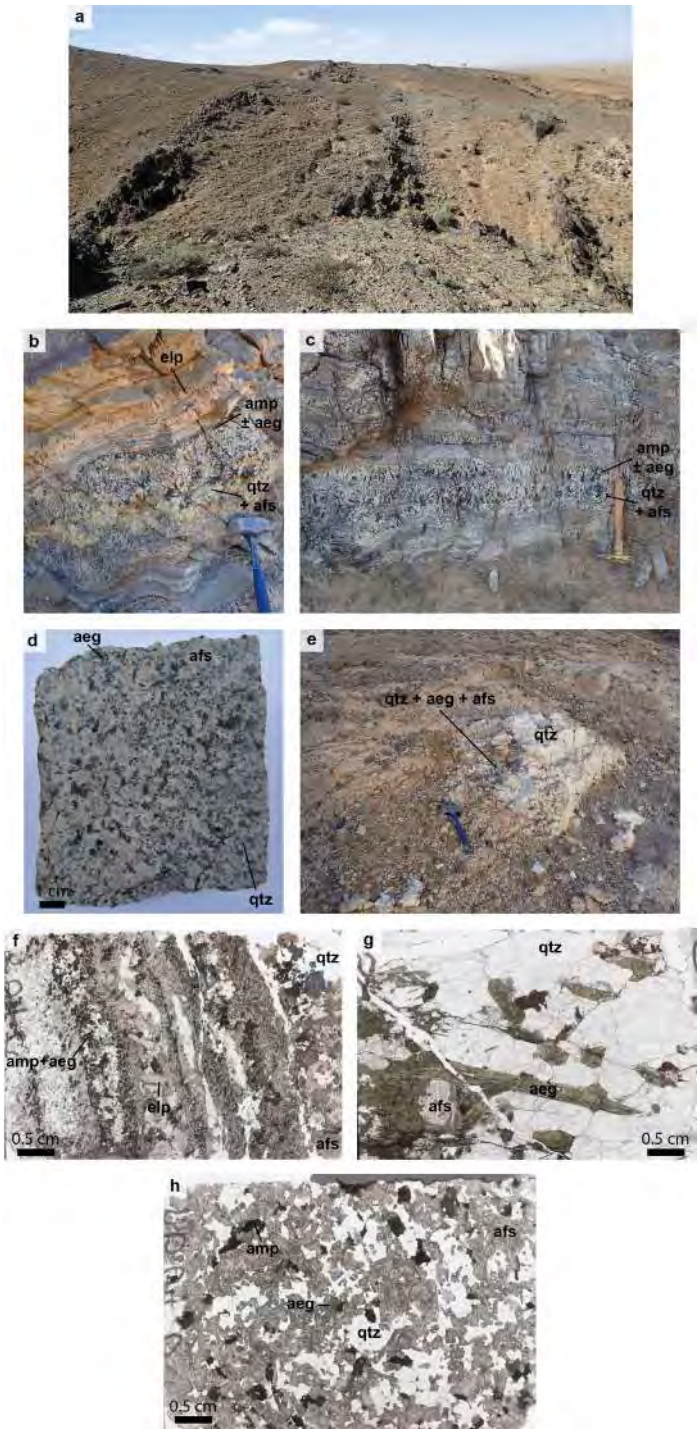

Figure 2.7 Photographs of the main alkaline rocks found in the Khan Bogd complex. (a) Set of parallel WSW-ENE pegmatite dikes on the northern part of the complex, close to the location of sample 10 (Fig 2.6); (b) Mineralogical layering in a dike of pegmatite with beige elpidite crystals; (c) Mineralogical layering in a dike of pegmatite with cm-sized arfvedsonite crystals; (d) hand sample of alkaline granite, sample KB07A; (e) Lens of pegmatite hosted in the Western arfvedsonite granite, with a quartz core and aegirine, feldspar and quartz rims; (f) Thin section of an elpidite-bearing pegmatite, sample KB04A; (g) Thin section of pegmatite, sample KB07D; (h) Thin section of alkaline granite, sample KB04D. Photographs a, b, c, e by Guillaume Estrade. Abbreviations: elp: elpidite; amp: amphibole; aeg: aegirine; qtz: quartz; afs: alkali feldspar

2.3.3 Magmatic vs hydrothermal contribution

Field observations allowed Kovalenko et al. (2006) to propose the following emplacement sequence for the Khan Bogd complex: (1) island-arc basalt–andesite–rhyolite complex formed in relation with the South Mongolian Hercynides continental active margin; (2) volcanic rocks of the bimodal basalt–comendite complex erupted on top; (3) alkaline magma emplaced and spread nearly horizontally, forming the western arfvedsonite-bearing granite and associated pegmatites; (4) The residual alkali magma reached the eastern part of the ring granite, forming the aegirine-bearing ring. Meanwhile, pantellerite, microsyenite, micromonzonite and then porphyritic alkaline granite dikes formed in the western ring along faults; (5) Kynicky et al. (2011) propose the release of a silica-saturated orthomagmatic fluid.

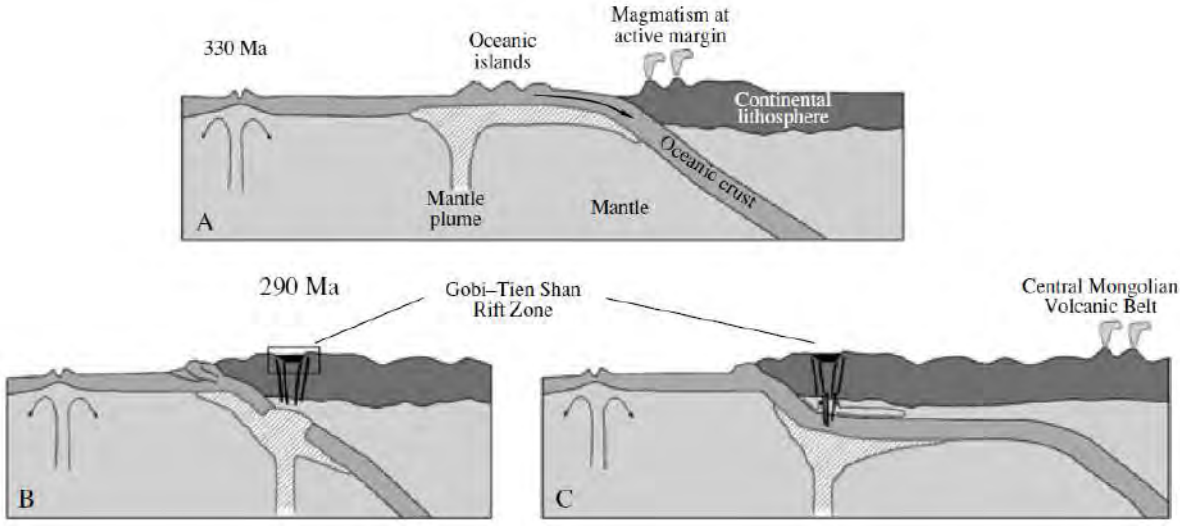

Figure 2.8 The two geodynamic hypothesis for the formation of the Khan Bogd plutons proposed by Kovalenko et al. (2006). (a) Situation of the Khan Bogd zone at 330 Ma; (b) Hypothesis 1 at 290 Ma: the mantle plume crosses the sinking slab; (c) Hypothesis 2 at 290 Ma: the mantle plume heats the slab, lowers its sinking angle and triggers its partial melting

To form such a large amount of differentiated alkali granite, the volume of parental basaltic magma must have been huge, almost similar to the one of medium-sized trap provinces. Hence, a low degree of partial melting is unlikely since it would then be necessary to consider even larger masses of the initial substrate and extremely large volumes of primary basaltic magmas (Gerdes et al., 2017). The source of the Khan Bogd plutons is linked to both a mantle plume and the active continental margin of the South Mongolian Hercynides, but the exact

process is still under discussion. A first hypothesis proposes that oceanic islands blocked the subduction and broke the slab, allowing the mantle plume to cross it, forming a structure similar to an asthenospheric window that would have been the source of the rift-related magmatism and the Khan Bogd pluton (Fig 2.8b). A second hypothesis suggests that the mantle plume heated the slab and thereby lowered its sinking angle. This provoked partial melting of the sinking oceanic lithosphere and of the mantle wedge. Either way, geochemical studies indicate that extensive crustal contamination occurred, generating the alkali granitic magma (Fig 2.8c; Kovalenko et al., 2006). Considering the unlikelihood of a low degree of partial melting of the mantellic source of the parental magma of Khan Bogd alkaline granites, and even while considering crustal contamination, it is necessary to appeal to another process to explain their relatively high concentrations in REE.

Fractional crystallization can explain the global enrichment of the peralkaline granites in alkalis and rare metals compared to the porphyritic granite. However, it cannot account for the observed preferential enrichment in HREE compared to LREE. Indeed, fractionation of zircon (the main accessory phase of the porphyritic granite) would have driven LREE enrichment and Zr depletion of the resulting granites.

Another explanation for the REE fractionation, which is not incompatible with the first one, is provided by the circulation of a low-temperature, acidic orthomagmatic fluid that altered the granites and pegmatites at Khan Bogd. The alteration occurred in two steps, as shown by the progressive replacement of (1) primary elpidite into Ca- and REE-rich secondary elpidite or armstrongite (about 0.45 wt% REE; Mesto et al., 2014), and (2) secondary Ca -bearing zirconosilicates into zircon associated with either calcite or gittinsite plus quartz. In addition, many secondary LREE-fluorcarbonates are associated with these replacement phases. Hence, considering that secondary phases after elpidite are Ca-rich and associated with calcite and fluorcarbonates, Kynicky et al. (2011) concluded for the circulation of an orthomagmatic Ca–CO_2–F-rich fluid. Calcium may have been provided by volcanic and sedimentary country rocks.

2.4 Manongarivo and Ambohimirahavavy complexes, Madagascar

2.4.1 Geological setting of northwestern Malagasy plutons

Since the amalgamation of Madagascar, its magmatic history is made of two episodes. The first one is dated at 92–84 Ma, during the separation of the island from India. It produced basalts and rhyodacite found for example at Morondava and Androy and considered as large igneous provinces. The second one is of Cenozoic age (Eocene-present), linked to a rifting event, and comprises mafic and felsic more evolved magmatic rocks, ranging from tholeiitic to alkaline compositions. This last magmatic event occurred mostly in the northern (intrusive and volcanic rocks) and central (only volcanics) parts of Madagascar. The Ampasindava alkaline province is made of many ring-shaped intrusions of Cenozoic age emplaced into Mesozoic-Cenozoic sedimentary rocks of the Antsiranana basin and known as the Isalo group. These sediments, of marine-shelf carbonates and marine-fluvial siliciclastic composition (marl, limestone, siltstone), emplaced above a Proterozoic basement made of metamorphosed volcanoclastic sequences and high-grade metasediments (Cucciniello et al., 2016; Thomas et al., 2009).

The first geological study of the Ampasindava province in northwestern Madagascar was made at the beginning of the 20^{th} century by Alfred Lacroix in his book *Minéralogie de Madagascar*, in which he acknowledged the Ampasindava region as the most interesting petrographic province he knew (Lacroix, 1923). Due to the recent discovery of rare metals in economic concentrations, the province spotted the attention of a German mining exploration company, Tantalus Rare Earths AG (Estrade et al., 2014b). Ambohimirahavavy and Manongarivo complexes are the biggest complexes of the Ampasindava province (Fig 2.9a). With respectively about 18 km across and 270 km^2, they are made of the accumulation of many plutonic and volcanic evolved alkaline rocks that were emplaced at circa 24 Ma by $^{40}Ar/^{39}Ar$ on feldspar (Cucciniello et al., 2016; Rakotovao, 2009; Thomas et al., 2009).

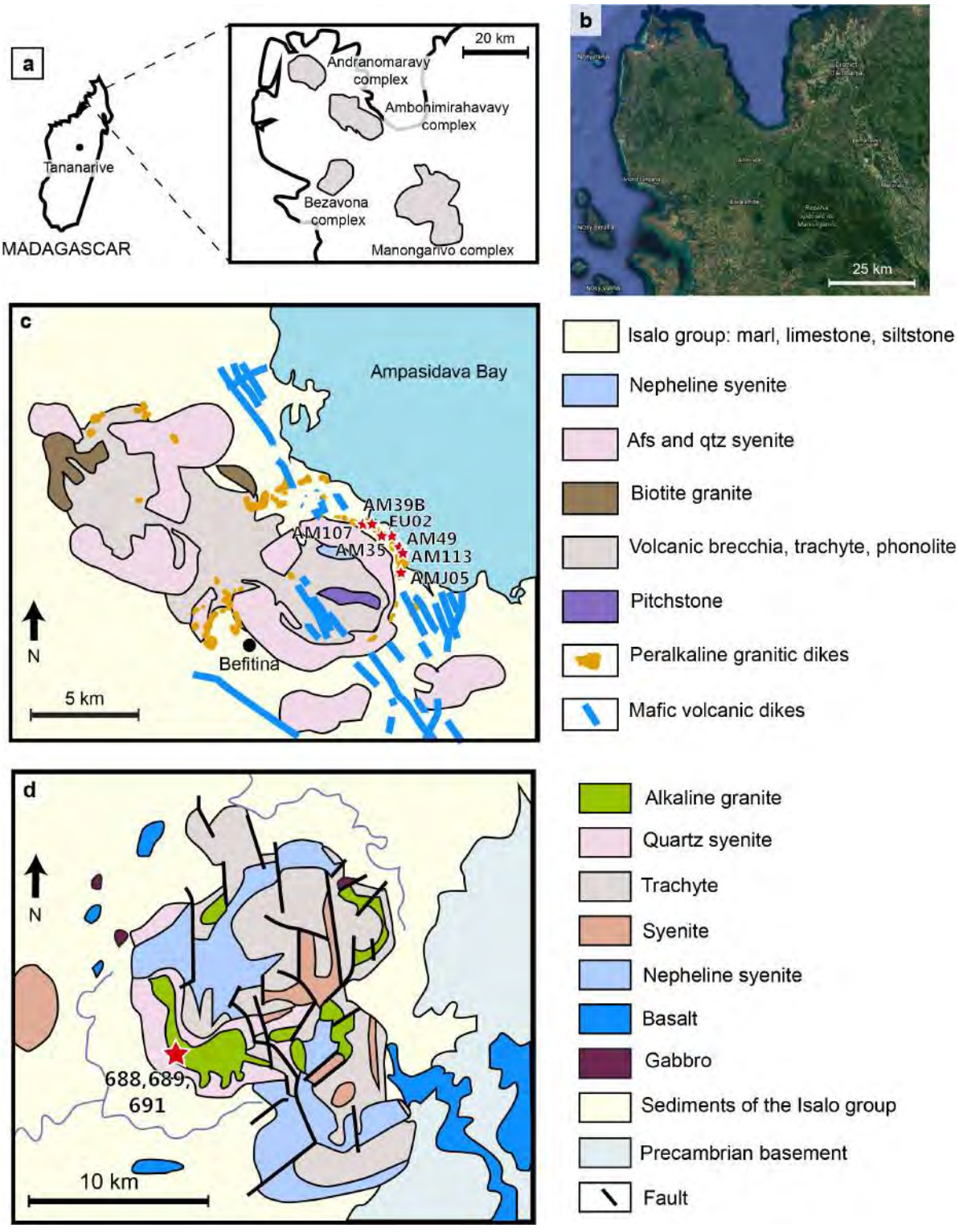

Figure 2.9 Localization (a), satellite image (b) and geological map of the Ambohimirahavavy (c) and Manongarivo (d) complexes, modified after Donnot (1963) and Estrade et al. (2015). Stars provide the location of samples analyzed in this study

Syenites form the major part of the Ambohimirahavavy complex and occur as two ring-shaped intrusions beside one another (Fig 2.9b). The northwestern one has the highest relief of the complex and is made of an assembly of syenite and biotite granite. The southeastern circular intrusion with about 7 km of diameter is the most studied and concentrates the most varied rocks. The center part is covered with volcanic breccias of trachytic composition that fills in a caldera along with dikes of camptonite, alkali basalt, hawaiite and mugearite. The Ambohimirahavavy complex is surrounded by a 2 km-wide occurrence of dikes of mafic, syenitic and granitic compositions (Estrade, 2014; Marquis, 2019).

Despite being the largest intrusion in the area, the Manongarivo complex is not well documented, probably because of its peculiar inaccessibility. Similarly to the Ambohimirahavavy complex, it is made of two ring-shaped intrusions side by side: the northern and main part is named Bekolosy-Andaimpotsy intrusion, and the southern one is the Antsatrotro (Donnot, 1963; Fig 2.9c). Together, they form a three leaves clover-like shape. It is made of a central caldera-like depression filled with volcanic breccias, and plutonic rocks organized in sills evolving towards a more silica-rich composition from core to rim. It mostly intrudes sedimentary rocks of the Isalo groups, but its southern part is connected to an extended basaltic area. Many faults, either radial or circular, affect the complex (Cucciniello et al., 2016; Donnot, 1963; Estrade, 2014; Marquis, 2019; Rakotovao, 2009).

2.4.2 Petrology of Malagasy alkaline oversaturated rocks: granites and pegmatites

Only one petrography study of Manongarivo, to this day, have been carried on, and is unpublished (Bollaert, 2019). The following sections then mostly apply to the Ambohimirahavavy complex, although the unpublished petrography study indicates both complexes have a similar mineralogy.

Plutonic rocks are nepheline syenite, alkali feldspar syenite, quartz alkali feldspar syenite, biotite granite, peralkaline granite and pegmatites, when volcanics are trachyte, phonolite, pitchstone, camptonite, hawaiite, mugearite, rhyolite and basalt. In both syenite rings the rocks become more enriched in SiO_2 from the center to the rims of the complex: from nepheline syenite to quartz syenite (Fig 2.10e) to granite (Fig 2.10b,f), and finally to pegmatite (Estrade, 2014; Fig 2.10c,g). Volcanics and undersaturated-syenites have generally low concentrations in HFSE and REE.

Granites and associated pegmatites are the most enriched in REE and other HFSE (Estrade et al., 2014b). They locally form a REE-rich skarn at their contact with carbonate-rich sediments (Estrade et al., 2015). Ion adsorption ore is also present and developed from supergene alteration of REE-rich granites and pegmatites. This study focuses on HFSE and REE-rich lithologies, i.e. alkaline granites and associated pegmatites, hence further description is only given for these rocks.

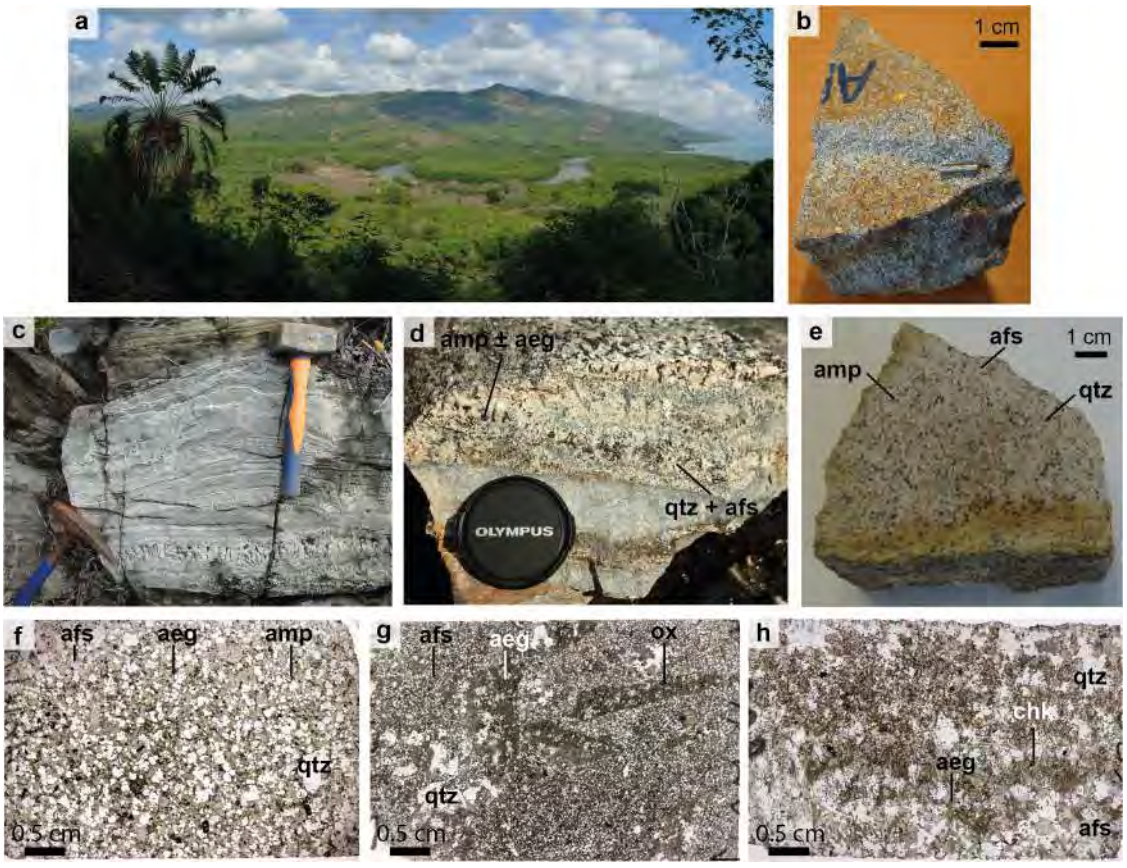

Figure 2.10 Presentation of the main alkaline rocks found in the Ambohimirahavavy and Manongarivo complexes. (a) General view of the Ambohimirahavavy complex, looking NW. The land behind the meander is the Southeastern syenite body; (b) Hand sample of alkaline granite, sample AM107; (c) Layered pegmatite from Ambohimirahavavy with big arfvedsonite crystals; (d) Pegmatite from Manongarivo, sample 691; (e) Hand sample of quartz-saturated syenite, sample 695; (f) Thin section of alkaline granite from Ambohimirahavavy, sample AM107; (g) Thin section of pegmatite from Ambohimirahavavy, sample AM113B; (h) Thin section of pegmatite from Manongarivo, sample 688. Photographs by Guillaume Estrade and Stefano Salvi. Abbreviations: amp: amphibole; aeg: aegirine; qtz: quartz; afs: alkali feldspar; ox: Fe- and/or Ti-oxide; chk: chevkinite-(Ce)

The granites of Ambohimirahavavy and Manongarivo are fine-grained and composed of Na-amphiboles, Na-pyroxene, perthitic alkali feldspar, and quartz (Fig 2.10b,f). Accessory minerals are biotite, bastnäsite-(Ce), rutile, apatite, monazite-(Ce), xenotime-(Y), Eudialyte Group Minerals (EGM), zircon, baddeleyite, chevkinite-(Ce), columbite, fluorcalciopyrochlore, ilmenite-pyrophanite, parisite-(Ce), synchisite-(Ce), thorite, fluorapatite, fergusonite-(Y), fluorite, nacareniobsite-(Ce), cerite-(Ce), hematite, and turkestanite (Bollaert, 2019; Donnot, 1963; Estrade et al., 2014a; Estrade et al., 2014b; Estrade et al., 2015; Marquis, 2019; Rakotovao, 2009). Na-amphiboles are locally replaced by Na-pyroxene or secondary minerals assemblage of quartz, calcite, Fe–Mn carbonate, titanomagnetite, rutile, sphalerite and pyrite. In granitic pegmatites, Na-amphiboles are arfvedsonite and fluoroarfvedsonite (Estrade, 2014). Na-pyroxene is also locally partly replaced by quartz, calcite, Fe-Ca-Mg carbonates, and Fe-oxide (Estrade et al., 2018).

Three types of peralkaline granites are distinguished at Ambohimirahavavy by Estrade et al. (2014b): (1) GR-I, a coarse-grained miaskitic granite, with HFSE-bearing minerals being zircon, PGM, monazite-(Ce) and chevkinite-(Ce). It contains on average 875 ppm REE, 1270 ppm Zr, and 220 ppm Nb; (2) GR-II, a transitional agpaitic to miaskitic pegmatitic granite with EGM replaced by Zr-Ca-bearing phases, REE-Ca-F-bearing phases, and ultimately by zircon and quartz. GR-II shows mineralogical layering and is intermediate between GR-I and GR-III. It contains on average 2000 ppm REE, 18600 ppm Zr, and 520 ppm Nb. Lacroix referred to this granite as 'fasibitikite'; (3) GR-III, an agpaitic pegmatitic granite with EGM, nacareniobsite-(Ce) and turkestanite. It is the most enriched in HFSE (19700 ppm Zr, and 3800 ppm Nb) and REE (14580 ppm) (Estrade et al., 2014b). The replacement of EGM in GR-I and GR-II forms three types of pseudomorphs based on the replaced and replacing minerals: (1) dendritic and botryoidal porous zircon, with Al, Fe and Ca trapped in the pores, in a quartz matrix, replacing EGM; (2) zircon, quartz, and rare-metal bearing minerals also replacing EGM; (3) zircon, REE fluorcarbonates, fergusonite-(Y), allanite-(Ce), PGM, monazite-(Ce), Nb-rich titanite and an unidentified zirconosilicate replacing aegirine-augite. This third category occurs only in GR-I intruding limestone.

The texture of granitic pegmatites varies a lot, both inside a single dike (0.02 to 1 m thick) and between two of them. The textures range from microgranular, coarse-grained, pegmatitic, and aplitic to laminated (Fig 2.10c,d,g,h). These pegmatites are systematically rich in HFSE-bearing minerals (Estrade, 2014).

Similarly to Khan Bogd, an alteration halo of a few cm is present around pegmatites.

Three granite and 4 pegmatite samples from the southern part of the Ambohimirahavavy complex were collected by Guillaume Estrade. Due to poor outcropping conditions and low occurrence of pegmatites, this work is based only on 3 pegmatite samples from Manongarivo. The samples from Ambohimirahavavy were selected according to previous studies from Estrade et al. (2014, 2014b). They are located on Fig 2.9.

2.4.3 Magmatic vs hydrothermal contribution

Two hypotheses have historically been proposed as to the emplacement mode of these complexes. They may have been formed either from the Seychelles-Comores evolving hot spot (Emerick and Duncan, 1982), or from old and deep lithospheric fractures (Nougier et al., 1986). A more recent study (Estrade, 2014) dated the age of emplacement of nepheline syenites (24.2 $\pm$ 0.6 Ma) compared to pegmatites (23.5 $\pm$ 6.8 Ma) and extrusive rocks (17 Ma to present) and tends to rule out the hot spot hypothesis. Alkaline complexes in northwestern Madagascar are aligned along a NW-SE path oriented N130 parallel to the Sandrakota shear zone, a major tectonic zone active during the East African Orogeny around 540 Ma (Rakotovao, 2009; Thomas et al., 2009), and to most mafic dikes. Along with the actual global NW-SE seismicity trend (de Wit, 2003), these observations confirm Nougier's hypothesis of old lithospheric fractures reactivated during a rifting period (Estrade, 2014).

Estrade et al. (2014) proposed a first interpretation as to the origin and evolution of the complexes of the Ampasindava province. The parental melt of the complexes would have been generated by low degrees of melting (2-10 %) of an incompatible element-enriched metasomatized mantle source with residual minerals enriched in volatiles such as amphibole and phlogopite. Fractional crystallization would have produced the silica-undersaturated rocks, whereas silica-oversaturated rocks could have originated from the same melt, with crustal contamination. The fractionation of plagioclase and alkali feldspar from this silica-saturated magma would have formed the most evolved peralkaline rocks of the complexes. In this scenario, the silica-undersaturated melt would have crystallized at 1000-700 °C, and the oversaturated syenitic one at 860-570 °C.

Marquis (2019) proposed a different model, but in which the source of the

parental melt of the complexes would still be a metasomatized mantle. She agrees on a low degree of partial melting that formed an alkali basaltic/basanitic parental melt. This magma got trapped at a shallow level during its ascension. This entrapment would have enhanced alkali feldspar fractionation, resulting in the production of a peralkaline, volatile-rich melt that interacted with the upper, already crystallized parts of the magmatic chamber as well as with country rocks. The interaction would have given birth to the silica-saturated series, including alkaline pegmatites that would have continued to evolve during their emplacement as dikes.

However, those processes are still not enough to explain the extreme REE and other HFSE enrichment of pegmatites. Two additional processes are proposed by Marquis (2019) and Estrade (2014). The first one is the immiscibility between silicate- and salt-rich melts, the latter sequestrating the REE and thereby keeping them in residual melts, from which pegmatites crystallize.

The presence of pseudomorphs made of zircon, quartz, and REE-enriched secondary minerals and replacing early magmatic EGM, together with the presence of porous zircons enriched in Al, Fe, Ca, (elements that do not generally enter zircon structure), and PGM enriched in REE along fractures (Estrade et al., 2018; Estrade et al., 2014b), point in addition to late- to post-magmatic alteration. According to recent studies, an orthomagmatic fluid affected the complexes in the very last stages of magmatic evolution, while low-temperature pegmatites crystallized (Estrade, 2014; Estrade et al., 2018; Marquis, 2019). The presence of aegirine replacing arfvedsonite indicates that the circulating fluid must have been rich in Na^{+} and Fe^{3+}. Alteration of EGM also enriched the fluid in Ca^{2+}, F^{-}, and Cl^{-}, at least locally, before reprecipitating these elements in various secondary phases such as fluorite and bastnäsite-(Ce).

In conclusion, REE mineralization was controlled by several processes. Magmatic source, partial melting, fractional crystallization and differentiation on one hand, immiscibility silicate/salt-melts and hydrothermal alteration on the other hand, contributed to the global enrichment in REE and other HFSE of the Malagasy complexes.

2.5 The Strange Lake complex, Canada

2.5.1 Geological setting of the Strange Lake plutons

The Strange Lake complex is a well-known resource of critical metals in Northeastern Canada, on the border between Quebec and Labrador. Reserves are estimated at 278 Mt grading 0.93 % REE_2O_03 of which 39 % are HREE, and 214 Mt at 0.85 % REE_2O_3 in total (Gowans et al., 2017). The complex also contains significant amounts of other mineralizations with about 30 Mt grading at 3.25 % ZrO_2, 0.56 % Nb_2O_5, and 0.12 % BeO (Salvi et al., 2005). It was first discovered by the Iron Ore Company of Canada in 1979 who was originally searching for uranium (Salvi et al., 2005). The Strange Lake complex is an anorogenic igneous body emplaced at a shallow level around 1240±2 Ma (Mesoproterozoic, U-Pb on zircon) in the Rae Province of the Canadian Shield, between Aphebian gneiss and Elsonian monzonites (Miller, 1996). Main characteristics such as structure, mineralogy and chemistry are similar to those of peralkaline complexes developed in the Gardar rift in Greenland. Based on these elements, the complex is commonly presented as the Labrador extension of the Gardar anorogenic igneous event (Boily and Williams-Jones, 1994; Pillet et al., 1989; Salvi and Williams-Jones, 1995). The complex consists of 36 km^2 of three concentric highly differentiated peralkaline granitic plutons, partially surrounded by an outwardly-dipping fracture associated with a fluorite and hematite breccia similar to the one found at Evisa.

These three plutons are distinguished based on feldspar mineralogy. The core of the complex consists of the oldest intrusive part, a hypersolvus granite (Fig 2.12b), while a largely metasomatized transsolvus granite (perthite plus two distinct alkali feldspars) surrounds it. Finally, a subsolvus granite (Fig 2.12c,d,g) forms the majority of the complex. The transsolvus granite was formerly considered as subsolvus, because perthite only occurs in minor amounts, as only recently recognized (Vasyukova and Williams-Jones, 2016; Fig 2.11). Highly evolved pegmatites concentrate in the subsolvus granite. These three magmatic events correlate with a progressive enrichment in REE and HFSE: mineralization-poor hypersolvus granite, transsolvus granite, and subsolvus mineralization-rich granite (Miller, 1986). The three magmatic intrusions form a reverse zoning caused by the

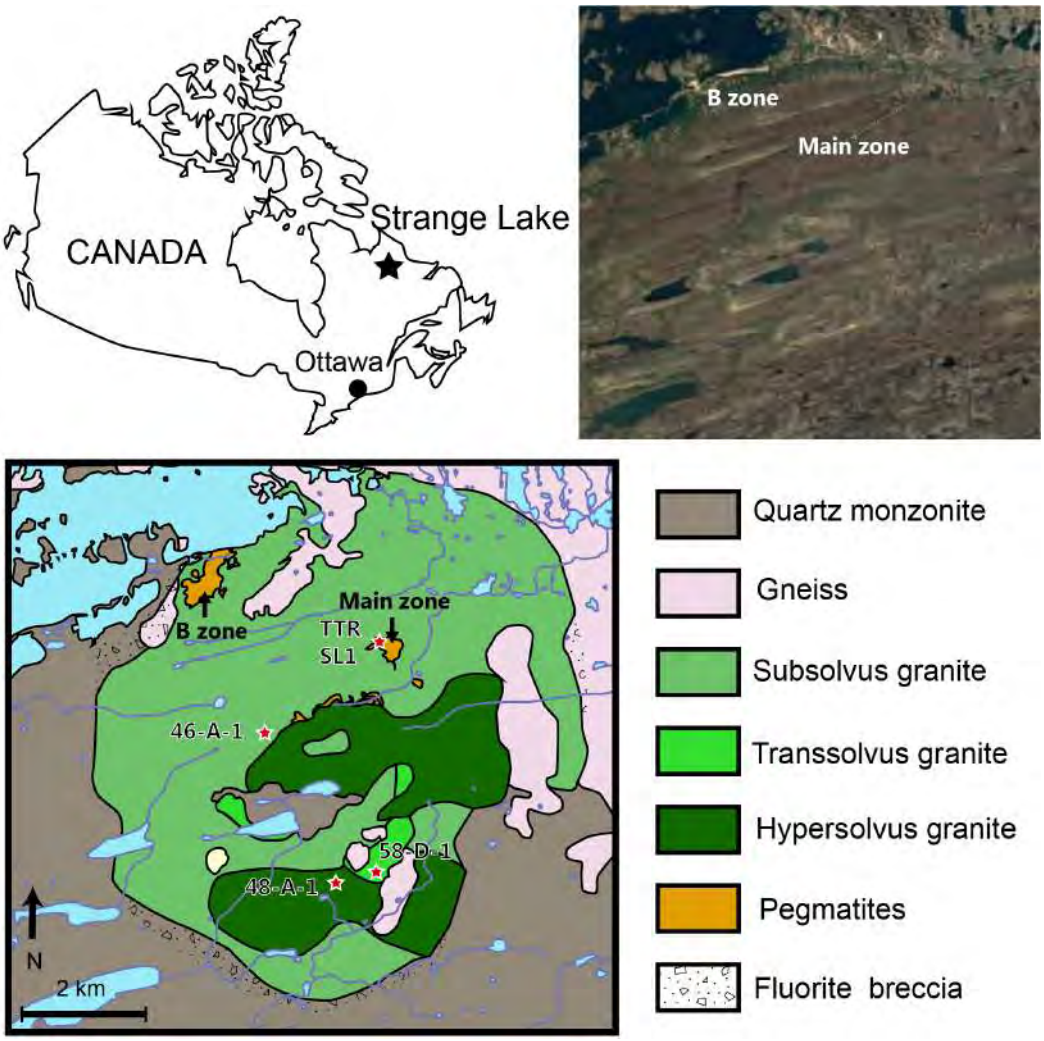

Figure 2.11 Localization, satellite image and geological map of the Strange Lake complex, modified after Vasyukova et al. (2016). Stars provide the location of samples studied in this work

latter melt, saturated with H_2O, forcing its way up around the already emplaced hypersolvus pluton rather than inside it (Gysi et al., 2016; Siegel et al., 2017).

The most REE and HFSE enriched part of the complex are pegmatites occurring either as 10 to 50 cm thick dikes cutting mainly the subsolvus granite, or as 6 to 20 m wide bodies in the center (Main zone) and northwest parts (B zone, $\sim$0.4 km^2 discovered in the late 2010s and currently the main target for exploration) of the complex. The B zone alone contains some 20 Mt of ore grading at 1.44 wt% REE_2O_3, including 50 % of HREE, and up to 2.59 % ZrO_2 and 0.34 % Nb_2O_5; the Main zone was estimated at 30 Mt 3.25 % ZrO_2, 1.3 % REE_2O_3, 0.56 % Nb_2O_5, and 0.12 % BeO in 1995 (Boily and Williams-Jones, 1994; Gowans et al., 2017; Salvi et al., 2005).

2.5.2 Petrology of Strange Lake rocks: hypersolvus granite, subsolvus granite, and pegmatites

All three granite types are mostly leucocratic, fine- to medium-grained, and silica- saturated. Enclaves of a melanocratic, finer grained granite but with similar mineralogy occur locally (Fig 2.12c; Salvi and Williams-Jones, 1990). The main phases of the Strange Lake complex are quartz, Na-amphibole, aegirine, and alkali feldspar (albite, orthoclase, microcline and/or perthites). Amphibole is ferro–ferri-katophorite mainly interstitial in the hypersolvus granite, and occurs as phenocrysts of arfvedsonite and ferro–ferri leakeite in the trans- and subsolvus granite (Siegel et al., 2017). It also occurs as cumulate layers up to 20 cm thick in the B zone. Accessory minerals include aenigmatite, astrophyllite, fluorite, thorite, PGM, gadolinite, kainosite, gagarinite-(Ce,Y), bastnäsite-(Ce), zajacite-(Ce), monazite-(Ce), fluornatropyrochlore, narsarsukite, titanite, fluorbritholite-(Ce), fluorite, ferriallanite-(Ce), chevkinite-(Ce), and låvenite (Gowans et al., 2017; Salvi and Williams-Jones, 1997; Salvi et al., 2005). In addition, the granites contain from 5 (hypersolvus) up to 30 % (subsolvus) zirconosilicates, namely elpidite, gittinsite, armstrongite, catapleiite, Ca-catapleiite, dalyite, hilairite, vlasovite, and zircon. Elpidite is magmatic, and in the shallower parts of the complex has been replaced by pseudomorphs mostly made of gittinsite and quartz. Armstrongite appears to be an intermediate phase between elpidite and gittinsite. Pseudomorphs can also locally contain zircon, fluorite, and/or bastnäsite-(Ce). Narsarsukite is replaced by pseudomorphs of titanite and quartz (Salvi and Williams-Jones, 1995). Except for narsarsukite and titanite, titanosilicates are commonly found in the northern part of the hypersolvus granite. Amphibole is locally replaced by hematite, aegirine, quartz and REE, HFSE and Ca-bearing minerals.

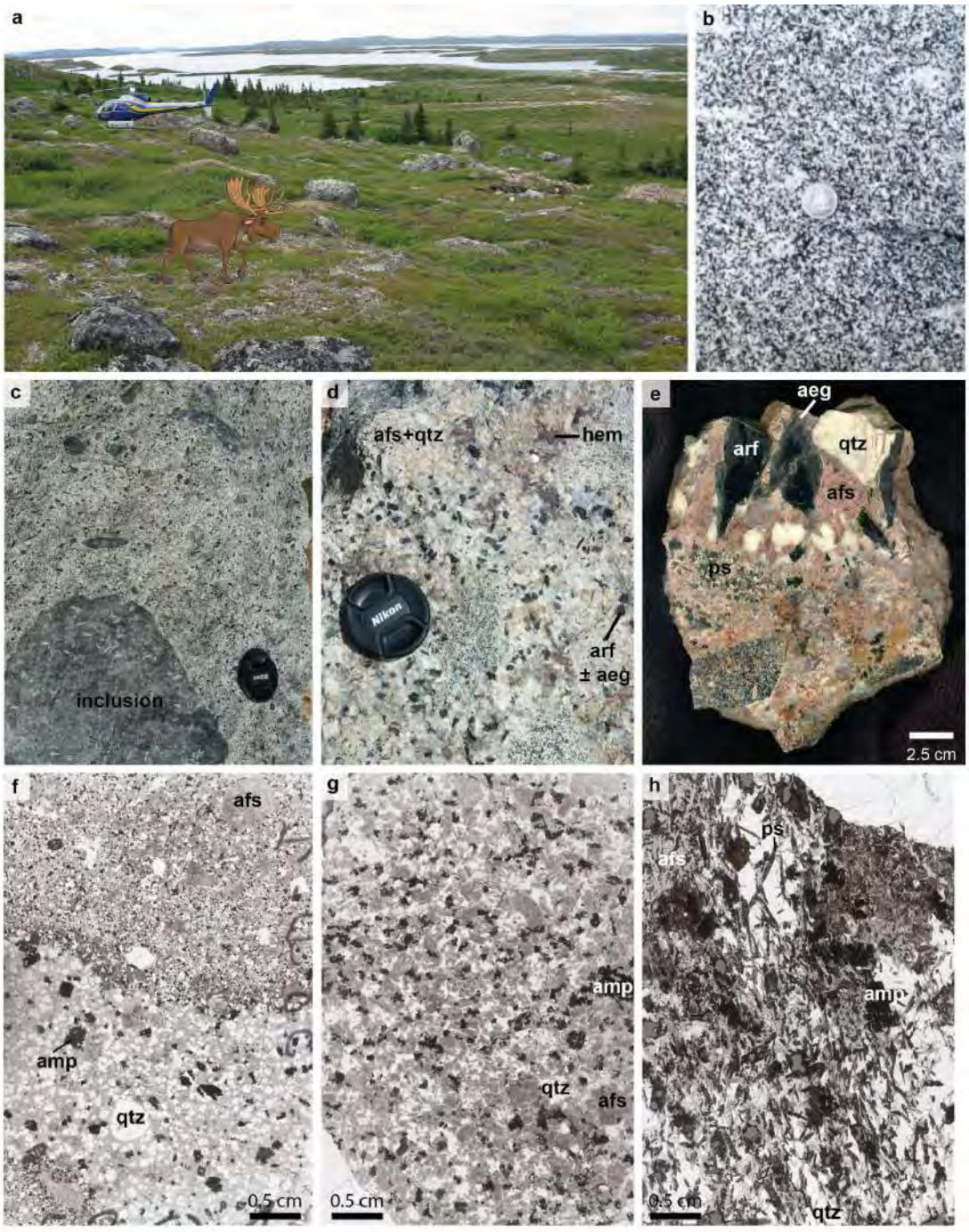

Figure 2.12 Presentation of the main alkaline rocks found in the Strange Lake complex. (a) A view of Lac Brisson from the northern edge of the complex, with its local wildlife (photograph by Peter Cashin); (b) Fresh hypersolvus granite; (c) Subsolvus granite with inclusions of a melanocratic variety; (d) Altered subsolvus granite with pegmatitic patches and hematite alteration; (e) Hand sample of a pegmatite from the Main zone; (f) Thin section of hypersolvus granite, sample 58-D-1; (g) Thin section of subsolvus granite, sample 46-A-1; (h) Thin section of pegmatite with boat-shaped pseudomorphs of gittinsite and quartz after elpidite, sample TTR16. Photographs (b)-(e) were taken by Stefano Salvi. Abbreviations: afs: alkali feldspar; qtz: quartz; hem: hematite; arf: arfvedsonite; aeg: aegirine; ps: pseudomorph

Pegmatites are of granitic composition and the largest of them, observed in drill core in the B zone as well as in a trench in the Main zone, show a well-defined mineral zonation (Fig 2.12e,h). Borders have a granitic composition with a high proportion of zirconosilicates, whereas the core part is made up mainly of quartz, fluorite, and LREE-fluorcarbonates. Fluorite and quartz in the cores occur as phases filling former fractures and are often associated with fluorite–fluocerite-(Ce) solid solutions in alternating REE-poor (fluorite) and REE-rich (fluorite–fluocerites) layers. Smaller, unzoned pegmatites present a composition that resembles that of the border of zoned pegmatites, with more quartz (Gysi and Williams-Jones, 2013; Gysi et al., 2016).

Rocks from Strange Lake used in this thesis consist of 1 hypersolvus granite, 1 transolvus granite, 2 subsolvus granite, and 4 pegmatite samples, collected by Stefano Salvi and kindly provided by Anthony Williams-Jones and Olga Vasyukova. Sample selection was based taking into consideration previous studies done on the complex (Salvi and Williams-Jones, 1990, 1995, 2006; Siegel et al., 2017). Samples locations are provided on Fig 2.11.

2.5.3 Magmatic vs hydrothermal contribution

Magmatic processes were long known to play a role in REE and other HFSE enrichment at Strange Lake, as the last granite to emplace (subsolvus) is also the richest in REE and HFSE mineralization (Miller, 1996). In addition, the occurrence of pseudomorphs at Strange Lake had been first interpreted to represent transformations at the magmatic stage (Birkett et al., 1992; Miller, 1996), mostly because at the time it was common knowledge that HFSE were extremely immobile elements, i.e. could not be transported in a fluid. However, the textural relationships, along with fluid inclusion evidence and the presence of secondary fluorite, forced the scientific community to recognize that the rocks in the complex underwent extensive hydrothermal alteration, in particular the subsolvus and transsolvus varieties (Boily and Williams-Jones, 1994; Gysi and Williams-Jones, 2013; Miller, 1986; Roelofsen and Veblen, 1999; Salvi and Williams-Jones, 1995).

Several authors have carried out follow up investigations to sharpen our understanding of the processes involved and highlighted the input of hydrothermal activity to the mineralization, in the form of two events. These include studies of bulk-rock chemistry, alteration phases, fluid inclusions, melt inclusions, numerical

simulations of fluid–rock interaction, and O-isotopic studies. The complexity of textural relationships among secondary minerals is part of the explanation for the high amount of available models for the hydrothermal sequence at the Strange Lake complex. The most recent model is provided by Vasyukova et al. (2019) as follows, and is illustrated in Fig 2.13.

(I) Magmatic stage saw the emplacement and evolution of all three granitic plutons. Feldspar fractionation in the hypersolvus granite led to the increase of H_2O and volatiles and incompatible elements, including the REE, in the melt. Volatiles accumulated along the walls on the magmatic chamber, fracturing them and leading to the formation of pegmatites at the roof (Gysi et al., 2016).

(IIa) The first hydrothermal event did not affect REE and other HFSE concentration. It is attributed to the circulation of a basic (pH$\sim$10), hot ($\geq$ 425 to $\sim$360 °C; Fig 2.13) brine enriched in Be, K, Al, Rb, Zr and Pb (Salvi and Williams-Jones, 2006; Vasyukova and Williams-Jones, 2016). It is interpreted as the circulation of a high salinity ($\sim$23 wt% NaCl) orthomagmatic fluids released during crystallization of pegmatites.

(IIb) During cooling, from $\sim$360 to $\sim$310 °C, this fluid got oxidized, causing the replacement of arfvedsonite by aegirine (Fig 2.13). This replacement released significant F, K, Rb and Li. In the fluid, the absence of enrichment in F, K and Rb along with the removal of LREE, Be, Zr, Hf, Nb and Pb indicate these elements were directly consumed by precipitating minerals such as fluocerite-(Ce) (LREE and F), gadolinite-(Ce) (LREE and Be), zircon (Zr and Hf) and pyrochlore (Nb and Pb), and by K-metasomatism. Due to the consumption of Na during the replacement of arfvedsonite by aegirine, the salinity decreased to half.

(III) The replacement of arfvedsonite by aegirine during cooling enhanced oxidation, and carbonic phases evolved from CH_4-dominated to CH_4 with higher order hydrocarbons to CO_2-dominated at $\sim$300 °C (Fig 2.13; Salvi and Williams-Jones, 2006; Vasyukova and Williams-Jones, 2016). This replacement was accompanied by a drop of pH from $\sim$10 to $\sim$3 and the precipitation of nahcolite at a salinity of $\sim$14 wt%. The ongoing drop in pH (Fig 2.13) drove nahcolite dissolution, which released Na and caused Na-metasomatism and another drop in salinity ($\sim$4 wt%).

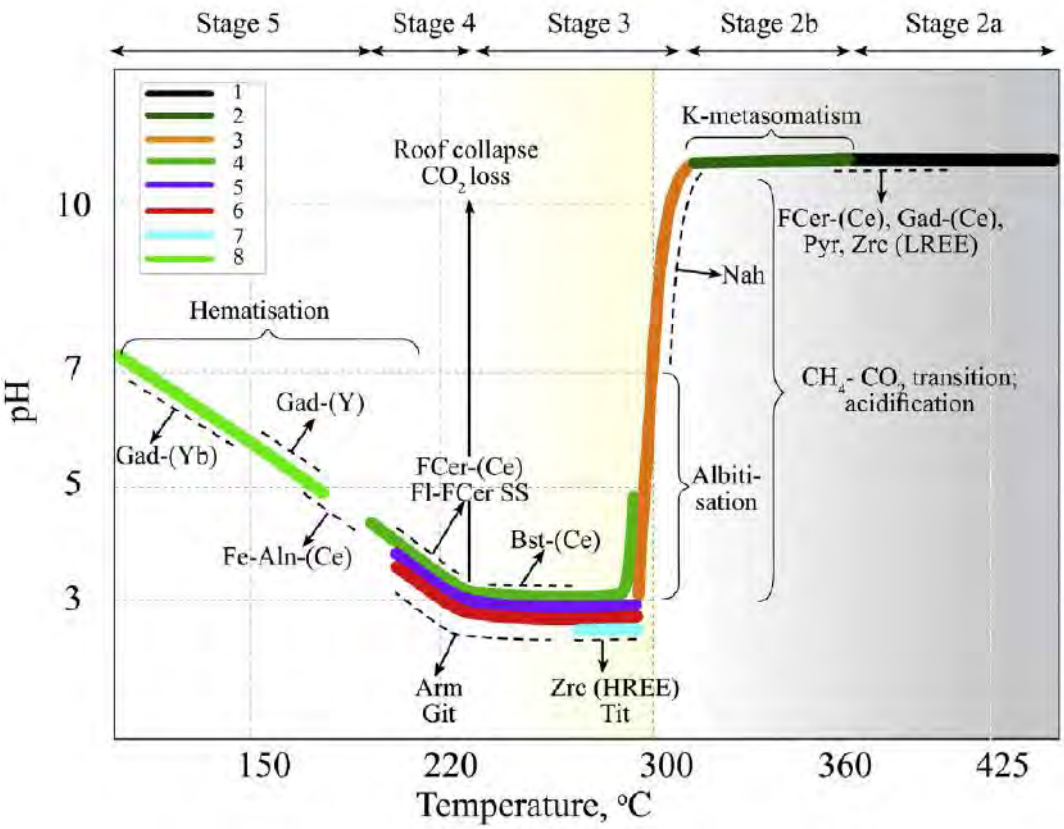

Figure 2.13 pH-temperature diagram illustrating the alteration/precipitation path for the fluid that exsolved from the Strange Lake magma (pegmatite), from Vasyukova and Williams-Jones (2019). The main processes that controlled the composition of the fluid and the precipitation of new phases are indicated by colours 1–8 in the legend: (1) exsolution of a reduced aqueous-carbonic fluid from the magma; (2) alteration of arfvedsonite to aegirine; (3) conversion of CH_4 and higher hydrocarbons to CO_2, and saturation of the fluid in nahcolite, and then CO_2; (4) alteration of arfvedsonite to ferroceladonite; (5) dissolution of fluorite; (6) alteration of elpidite to zircon and, in turn, gittinsite; (7) alteration of narsarsukite to titanite; (8) alteration of arfvedsonite to aegirine and hematite. The dashed black lines indicate the intervals during which particular minerals precipitated. Abbreviations: FCer: fluocerite; Gad: gadolinite; Pyr: pyrochlore; Zrc: zircon; Nah: nahcolite; Bst: batnäsite; Arm: armstrongite; Git: gittinsite; Fl: fluorite; Fe-Aln: ferriallanite

The rapid drop in pH also caused the dissolution of REE-rich fluorite and consequent reprecitation of REE-poor fluorite. This in turn released Ca, Sr, F and REE to the fluid, which led to the alteration of narsarsukite to titanite (consuming Ca and LREE) and to the alteration of elpidite to zircon and quartz (Salvi and Williams-Jones, 1990; zircon consuming F and HREE). In addition, the two reactions released minor Zr, Hf and Nb (Migdisov et al., 2011; Timofeev and Williams-Jones, 2015). The increasing CO_2, F and REE in the fluid induced precipitation of bastnäsite-(Ce), which in turn increased the molar Ca/F ratio of

the fluid and replaced elpidite and zircon to gittinsite and armstrongite. The simultaneous alteration of arfvedsonite and microcline to ferroceladonite enhanced the concentrations of Fe, Li and Mn in the fluid.

(IV) This stage begins with the loss of a CO_2 gas-saturated fluid due to the pluton roof collapse, at ∼230 °C (Fig 2.13). This fluid reacted with the surrounding granite (Vasyukova and Williams-Jones, 2018), modifying its composition and locally depositing ferroceladonite and bastnäsite-(Ce). The high concentration of the fluid in Zr, Ca and F may reflect equilibration with vlasovite and fluorite in the granite.

Stages (IV) and (V) are still not well-defined, except for the REE behavior. The removal of CO_2 caused an increase in pH (Migdisov and Williams-Jones, 2014), which in turn drove the precipitation of fluocerite-(Ce) and fluorite-fluocerite-(Ce) solid solution. This precipitation collected REE, and mostly LREE, from the remaining fluid phase. Simultaneously, arfvedsonite got replaced by ferroceladonite and other phyllosilicates, causing Fe accumulation in the fluid until oxidation was sufficient for extensive hematization (Fig 2.13). Since there was no gas left in the system, it is impossible to infer at which temperature hematization actually began. The only constraint is the maximum temperature at which hematite was stable, which is 230 °C.

(V) This stage is associated with brittle deformation, probably linked to the collapse of the roof of the pluton, and is considered as a secondary fluid. This fluid, according to Gysi et al. (2016) was meteoric in origin. During this stage, hematization occurred throughout pegmatites and the subsolvus granite. Arfvedsonite got replaced by aegirine and hematite at a maximum temperature of ∼180 °C. The precipitation of ferriallanite-(Ce) consumed a lot of LREE from the fluid, while gadolinite-(Y) consumed MREE. Heavy-REE were still highly concentrated in the fluid at this stage, which implies the precipitation of a HREE-rich mineral, probably gadolinite-(Yb), after entrapment of the fluid. Finally, fluorite and hematite precipitated, forming the cement of the breccia that surrounds the complex.

In addition to these observations, bulk-rock analyzes coupled with a 2-D geochemical model of the complex (Gysi et al., 2016) show that the LREE are dispersed, while HREE and Zr are unequally distributed. This hydrothermal stage has hence played a significant role in the specific HREE enrichment of the Strange Lake complex.

2.6 Synthesis on magmatic vs hydrothermal contributions to REE enrichment in the six studied alkaline complexes

From the study of the six alkaline granitic complexes, it appears that their level of study is highly variable (Tab 2.1). From one extreme to the other, the Strange Lake complex has been studied since 1986 (Miller, 1986), while the only available descriptions for the Manongarivo complex were published in 1963 by Donnot in a book regrouping a description of all intrusive alkaline complexes of the Ampasindava Province and in 2009 by Rakotovao in her PhD. Consequently, many models followed one another to understand the emplacement of the Strange Lake and, to a lesser extent, the Ambohimirahavavy complexes. On the other hand, a few models are available for the Amis, Evisa and Khan Bogd complexes, and none for the Manongarivo complex. The level of study of the complexes is also linked to the economic interest of mining companies who can afford research studies in order to later extract REE ore (Tab 2.1). The observed REE concentration and fractionation vary with the complex and the type of rock (Fig 2.14). Pegmatites are systematically richer in REE than granites, except at Ambohimirahavavy where the granite contains more HREE. Pegmatites from Strange Lake, Amis and Evisa have a flat to HREE-enriched spectrum. Granite and pegmatite from Strange Lake contain much more REE than the same rocks in the other complexes, and rocks from Khan Bogd contain less REE than the others on average. Aside from Strange Lake, the pegmatite from Manongarivo contains a lot of LREE, and the pegmatite from Amis contains much HREE.

Although they emplaced in different geodynamic complexes, it appears that the melt source of the six studied alkaline complexes is systematically the upper, metasomatized mantle. The role of crustal contamination is debated, as it has been identified at Amis and Khan Bogd, is discussed at Madagascar, and has not occurred at Evisa according to the most widespread theory. If present, crustal contamination can be a source for the REE in alkaline granitic complexes. Feldspars fractionation, identified at Khan Bogd, Strange Lake and Madagascar and not discussed in the other complexes, is a key process for REE-enrichment in alkaline complexes. Indeed, plagioclase crystallization withdraws mostly Ca, Al and Eu (Eu^{2+} substitutes for

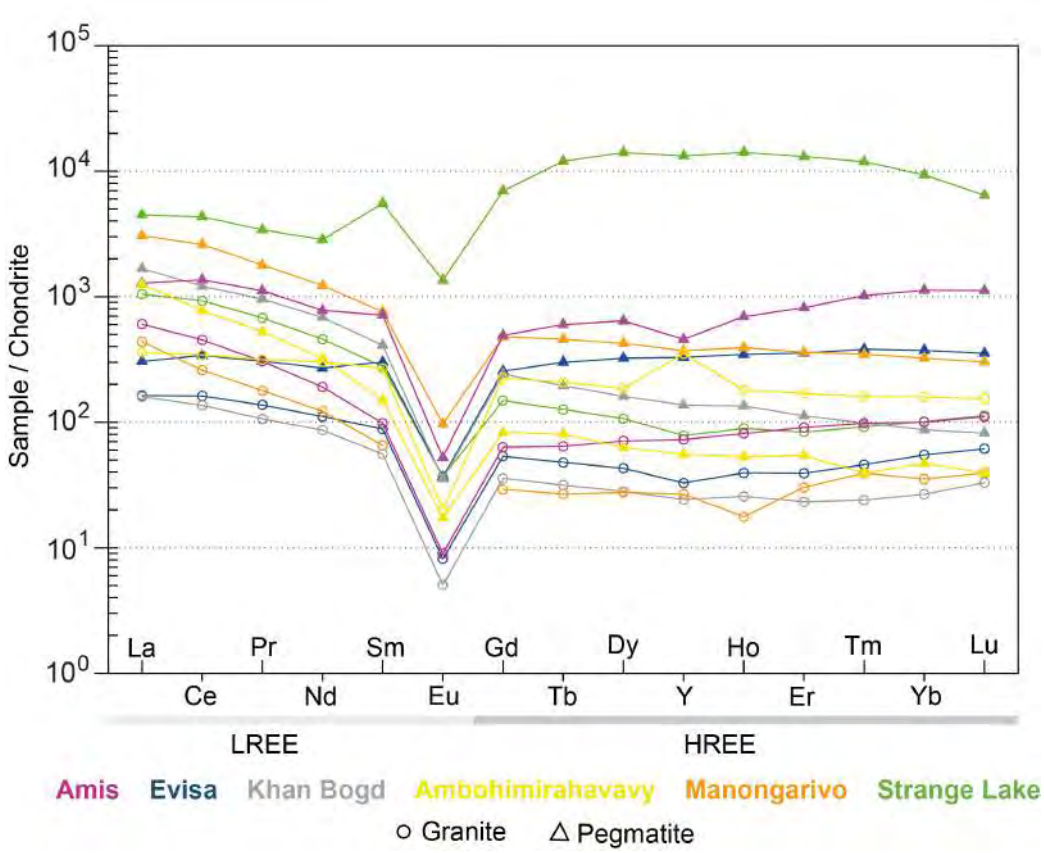

Figure 2.14 Spider diagram of whole rock pegmatites and granites of the six complexes of this study, chondrite-normalized (Sun and McDonough, 1989). Data from Ambohimirahavavy are from Estrade et al. (2014a; granite) and Estrade et al. (2014b; pegmatite); data of the granite from Amis are from Schmitt et al. (2002). Granites from Evisa and Strange Lake are subsolvus and hypersolvus respectively

Ca^{2+} in plagioclase) from the melt, which gets relatively enriched in alkalis. This increase in alkalis leads to a transition from plagioclase to alkali feldspar. Alkali feldspar in turn withdraws mostly K from the melt, increasing Na in the residual magma as fractional crystallization progresses. Hence, the residual magma enriches in Na as well as in incompatible elements, among which are the REE (except for Eu). The major disagreement as to magmatic processes in alkaline melts is the rate of partial melting. Indeed, this parameter was studied at Madagascar and Khan Bogd. According to Kovalenko et al. (2006) and Marquis (2019), alkaline magmas of these complexes are produced by a relatively high rate of partial melting. Estrade (2014) suggests on the contrary that the Ambohimirahavavy complex was produced with a low degree of partial melting. This discussion is essential, because a lower rate of partial melting implies that incompatible elements, including the REE, are more concentrated in the newly generated melt.

Table 2.1 A summary of geological and geodynamic context of the six complexes studied in this manuscript

Complex name	Amis	Evisa	Khan Bogd	Ambohimirahavavy	Manongarivo	Strange Lake
Location	Namibia	Corsica	Mongolia	Madagascar	Madagascar	Canada
Age	130 Ma	290-249 Ma	290 Ma	25 Ma	25 Ma	1240 Ma
Size	3 km²	20 km²	1500 km²	120 km²	270 km²	36 km²
Geodynamic context	Rift	Rift or Post-orogenic extension	Hot spot and subduction	Rift	Rift	Rift
Level of the pluton outcropping	Roof	Roof + middle	Roof	Roof + volcanites	Roof + volcanites	Roof
Mineralization	REE	REE	REE	REE	REE	Zr, REE, Nb, Be
Owner company	-	-	-	Tantalus Rare Earths AG	-	Torngat Metals Ltd.
Magmatic source and processes	Upper, metasomatized mantle + crustal contamination	Upper, metasomatized mantle or Continental crust with granitic melts and H_2O extracted	Upper, metasomatized mantle + crustal contamination	Upper, metasomatized mantle + crustal contamination and melt-melt immiscibility debated	?	Upper, metasomatized mantle
Hydrothermal circulations	Orthomagmatic, CO_3-rich; Post-magmatic, F-rich	Orthomagmatic; Post-magmatic, F-rich	Orthomagmatic, Ca-, CO_2-, F-rich	Orthomagmatic, Ca-, F-, Cl-rich	?	Orthomagmatic, Ca-, Na-, CH_4/CO_2-rich; Post-magmatic Ca-, F-rich
Level of study	Limited	Good	Limited	Good	Almost inexistent	Very good
References	Schmitt et al., 2002	Bonin et al., 1978 Bonin & Platevoet, 1988 Poitrasson et al., 1998	Kovalenko et al., 2006 Kynicky et al., 2011 Gerdes et al., 2017	Estrade et al., 2014 Marquis, 2019	Donnot, 1963	Salvi & Williams-Jones, 1990 Gysi et al., 2016 Vasyukova et al., 2019

A new important source for REE enrichment evoked by Marquis (2019) at Ambohimirahavavy is magmatic immiscibility. She proposed the separation of silicate- and a salt-rich immiscible melts. The salt-rich melt having the ability to form stable complexes with the REE, they would be kept in this late residual melt, from which pegmatites crystallize.

Although their role are still debated, all six complexes have undergone alteration by at least one orthomagmatic fluid, and sometimes a second, late hydrothermal fluid (identified at Amis, Evisa, and Strange Lake). The composition of the fluids that circulated was measured in fluid inclusions at Ambohimirahavavy and Strange Lake, and inferred from the study of secondary mineral assemblages in the other complexes. The resulting conclusions are similar for all the complexes, although they do not always have the same timing. For example, F^- is described in all complexes, but in the orthomagmatic fluid at Khan Bogd and Madagascar, and in the post-magmatic fluid at Amis, Evisa and Strange Lake. The significant presence of Na^+ and Fe^{3+} in an orthomagmatic fluid is reported at Evisa, Madagascar and Strange Lake, and Ca^{2+} was identified at Khan Bogd, Madagascar and Strange Lake. Locally, CO_2 and/or CH_4 were reported at Khan Bogd and Strange Lake, and CO_3^{2-} at Amis. No matter the fluids composition, at least one hydrothermal event per site is reported to have affected the entire complex. This statement is questioned only at Amis, where Schmitt et al. (2002) affirm that hydrothermal processes are local whereas Diehl (1990) is in favour of a large scale event. Independently of its orthomagmatic or late origin, the F-, Ca-rich fluid is systematically observed to mobilize and fractionate the REE. The scale of this process compared to magmatic ones is still a matter of debate.

Chapter 3

Comparative petrological study

3.1 General methods and samples description

3.1.1 Methods

Granite and pegmatite samples from all six complexes were selected in order to investigate the role of fluids in concentrating, mobilizing and fractionating the REE. Pegmatites from all complexes are heterogeneous in texture, i.e. they show mineralogical layering visible from the scale of the outcrop to that of a thin section, whereas granites are generally homogeneous. In pegmatites, the layers have grain sizes ranging from a few µm to about 40 cm and locally more. Therefore, to obtain meaningful data, samples for this study were selected from zones of relatively fine grain size (less than a few cm). However, alkaline rocks, and in particular pegmatites, are characterized by complex mineralogical assemblages, and paragenesis are often difficult to interpret. Based on chemical analyses as well as on textural relationships such as inclusions, zonations, rim dissolution or crystal shape, this work proposes where possible a sequence of events for the emplacement and evolution of the six studied complexes. A list of the selected samples is provided in Tab 3.2.

Polished thin sections were prepared from all samples from the six complexes and were studied using classic petrographic techniques, i.e. plain polarized light (PPL) and crossed polarized light (XPL) microscopy, cathodoluminescence (CL), Scanning Electron Microscopy (SEM), microprobe (EPMA), and Laser-Ablation Inductively Coupled Plasma Mass Spectrometry (LA-ICPMS) in order to determine mineral textural relationships and composition.

Cathodoluminescence observations were carried out using an optical HC6-LM microscope with a voltage of 14 kV and a beam current ranging between 0.07

Table 3.1 A list of standards used for EPMA calibration

Element	Standard
Al	Corindon
Ca	Wollastonite
Ce	Monazite-(Ce)
Cl	Tugtupite
Dy	$DyPO_4$
Er	$ErPO_4$
F	Topaze
Fe	Hematite
Gd	$GdPO_4$
Hf	HfZr
K	Sanidine
Mg	Periclase
Mn	Pyrophanite
Na	Albite
Nb	Nb metal
Nd	Monazite-(Nd)
Pb	Synthetic $Pb_2P_2O_7$
Si	Wollastonite
Sn	Cassiterite
Ta	Ta metal
Th	Thorianite
Ti	Pyrophanite
U	Uraninite
Y	Xenotime-(Y)
Yb	Xenotime-(Yb)
Zn	Sphalerite
Zr	Zircon

and 0.15 nA. SEM images in back-scattered electron (BSE) mode were collected with a Jeol JSM6360LV SEM coupled with a Bruker silicon drift detector and interpreted with the Esprit software at the GET laboratory, using an accelerating voltage of 20 kV, and a detection time of 40 s. Mineral compositions were determined at the Centre Raymond Castaing in Toulouse, using a CAMECA SX Five electron microprobe, with an accelerating voltage of 15 kV, a beam current of 20 nA for pyroxene, zircon and Ca-zirconosilicates and 10 nA for amphibole and Na-zirconosilicates, and a beam diameter of about 2 μm. Specific attention was given to Na in order to avoid its migration under the beam. Quantitative elemental maps of aegirine crystals were performed on the same instrument, using an accelerating voltage of 15 kV, a beam current of 20 nA and 100 nA for major and minor elements respectively. Counting time was 1 s on each pixel with a step of 0.5 to 4 μm depending on crystal size. Standards used for calibrations ate listed in Table 3.1. Uncertainties were calculated using the method of Ancey et

al. (1978). Trace element concentrations were determined in situ by LA-ICPMS (GET laboratory) on 30 μm polished thin-sections, using a New Wave Research ESI 213 laser coupled to a Thermo-Fisher Element-XR high-resolution ICP-MS. Laser beam diameter varied from 30 to 50 μm depending on mineral size, and data were acquired by ablating lines instead of spots in order to prevent intersecting solid inclusion or internal zoning. NIST synthetic glass certified reference materials SRM 610 and SRM 612 were used as external and secondary standards, respectively. Each analysis was normalized using ^{29}Si values previously determined by EMPA. The relative precision ranged from 5 to 10 %. Trace elements maps of aegirine crystals were performed at the Trinity College in Dublin using photon machines G2 193 nm UV laser with a Helex two-volume cell coupled to a Thermo iCAPQ ICP-MS. Laser beam diameter was 12 μm, and NIST synthetic glass certified reference materials SRM 610 was used as external standard. Analysis were semi-quantitative and compared to microprobe data to obtain the real concentration. Fourier Transform Infrared Spectroscopy (FTIR) maps of elpidite were performed at the Plateforme scientifique et technique of the University of Toulouse with an MCT detector with a resolution of 8 cm^{-1}, and were corrected with the Kramers-Kronig transformation. In addition, samples were sent to the SARM Nancy to perform whole-rock analyses of major and trace elements. Rock samples were crushed and melted with $LiBO_2$ at 980 °C before being placed in an acid HNO_3 (1 $mol.L^{-1}$) - H_2O_2 ($\sim$0.5 % v/v) - glycerol ($\sim$10 % v/v) solution and analyzed with a Thermo Fischer ICap 6500 ICP-OES for major elements, and a Thermo Elemental X7 ICP-MS for trace elements according to the method by Carignan et al. (2001). Fluorine and Cl were analyzed by potentiomeric dosage with a Radiometer Analytical Meterlab SAC950/ION450, and Li with an AAS Varian 220FS flame.

3.1.2 Samples preliminary description

Petrographic observations show that pegmatites and granites are all dominated by quartz, alkali feldspar (perthites, albite, orthoclase, and/or microcline) that are commonly strongly albitized, plus Na-amphiboles (typically arfvedsonite and leakeite) and, mostly in pegmatites, aegirine. Common accessory minerals in both rock types include zircon, PGM and Fe- and/or Ti-oxides. Other minerals present mostly in pegmatites include Ca and Na zirconosilicates (EGM, elpidite,

gittinsite, armstrongite), fluorite, astrophyllite and REE-bearing minerals: silicates (chevkinite-(Ce), allanite-(Ce, Nd), britholite-(Y)); carbonates (bastnäsite-(Ce) and parisite / synchysite-(Ce)), oxides (aeschynite-(Y)), and phosphates (monazite-(Ce) and xenotime-(Y)). The presence of hydrothermal circulations is shown by the systematic alteration of some primary minerals and by the presence of secondary mineral assemblages. Sodic amphibole is commonly replaced by aegirine and Fe- and/or Ti-oxides. Primary zirconosilicates, namely elpidite, EGM, or unknown, are altered into a variety of REE-bearing phases forming pseudomorphs. A remaining question is whether or not it is possible to infer the nature of the primary mineral in rocks it was completely pseudomorphed, based only on the nature of the secondary phases.

Table 3.2 A list and description of selected samples for this study. Abbreviations: qtz: quartz; afs: alkali feldspar; arf: arfvedsonite; lkt: leakeite;aeg: aegirine; zrn: zircon; git: gittinsite; flr: fluorite;amp: amphibole; chl: chlorite; ep: epidote

Complex	Sample #	Description	Main mineralogy
Amis, Namibia	SOS065	Contact between arfvedsonite granite and country-basalts	qtz, afs, arf
	SOS066	Aplite through arfvedsonite granite	qtz, afs, arf
	SOS067	Fine-grained felsic vein in basalt	qtz, afs, lkt
	SOS068	Aplite through arfvedsonite granite	qtz, afs, arf, aeg
	SOS069	Arfvedsonite granite	qtz, afs, arf
	SOS070	Pegmatite	qtz, afs, lkt, aeg
	SOS071	Pegmatite with aegirine clusters	qtz, afs, lkt
	SOS073	Fluorite-bearing granite	qtz, afs, arf
Evisa, Corsica	EV1801	Hypersolvus granite	qtz, afs, arf
	EV1804	Pegmatite in the hypersolvus granite	qtz, afs, Na-amp, aeg
	EV1805	Lindinosite	
	EV1806	Subsolvus granite	qtz, afs, Na-amp, aeg
	EV1807	Subsolvus granite	qtz, afs, Na-amp, aeg
	EV1808	Fluorite-hematite granitic breccia	qtz, afs, Na-amp, aeg
	EV1811	Pegmatite in the subsolvus granite	qtz, afs, Na-amp, aeg
	EV1812	Subsolvus granite	qtz, afs, Na-amp, aeg
	EV1813	Altered pegmatite	qtz, afs, Na-amp, aeg
	EV1817	Aegirine-bearing aplite	qtz, afs, aeg
	EV1820	Subsolvus granite	qtz, afs, Na-amp, aeg
	EV1821	Lindinosite	
	EV1823	Subsolvus granite with big pseudomorphs	qtz, afs, arf, aeg
	EV1825	Pegmatite in the subsolvus granite	qtz, afs, Na-amp, aeg
	EV9102	Hypersolvus granite	qtz, afs, Na-amp, aeg
Khan Bogd, Mongolia	KB02	Pegmatite	qtz, afs, arf
	KB04A, C	Elpidite-bearing pegmatite	qtz, afs, arf, aeg, elp
	KB04B	Pegmatite	qtz, afs, arf, aeg
	KB04D	Granite	qtz, afs, arf, aeg
	KB05	Quartz core of a pegmatite	qtz
	KB07A	Granite	qtz, afs, arf, aeg
	KB07B	Quartz core of a pegmatite	qtz
	KB07C, D	Aegirine-rich pegmatite	qtz, afs, aeg
	KB09A	Pegmatite	qtz, afs, arf, aeg
	KB09B	Arfvedsonite granite	qtz, afs, arf
	KB10B	Contact between pegmatite and country-rock schist	qtz, afs, arf, aeg
	KB11	Aplite with aegirine + arfvedsonite	qtz, afs, arf, aeg
Ambohimirahavavy, Madagascar	AM35	Aegirine-bearing pegmatite	qtz, afs, lkt, aeg, zrn
	AM49	Pegmatite	qtz, afs, lkt, aeg
	AM107	Amphibole-bearing granite	qtz, afs, lkt, aeg
	AM113A	Pegmatite	qtz, afs, lkt, aeg
	AMJ05	Amphibole-bearing granite	qtz, afs, lkt, aeg
	AMJ45	Aegirine-bearing granite	qtz, afs, lkt, aeg
	EU02	Eudialyte-bearing granite	qtz, afs, aeg, EGM
Manongarivo, Madagascar	688	Pseudomorphs and aegirine-bearing aplite	qtz, afs, aeg
	689	Pseudomorphs and aegirine-bearing aplite	qtz, afs, aeg
	691	Granite with aegirine + amphibole	qtz, afs, arf, aeg
Strange Lake, Canada	46-A-1	Subsolvus granite	qtz, afs, arf
	48-A-1	Hypersolvus granite	qtz, afs, arf
	58-D-1	Hypersolvus granite	qtz, afs, arf, aeg
	SL1-20	Pegmatite with big pseudomorphosis and altered amphibole	qtz, afs, arf, aeg, git, flr
	SL1a	Pegmatite with pseudomorphosis	qtz, afs, arf, aeg, git, flr
	SL1b	Altered subsolvus granite	qtz, afs, aeg, flr
	TTR16	Pegmatite with pseudomorphosis	qtz, afs, arf, aeg, git, flr
	TTR20	Fluorite-bearing pegmatite	qtz, afs, aeg, git, flr

3.2 Main mineralogy

Main minerals, i.e. rock-forming minerals, are those that can be seen with the naked eye in macroscopic samples. These are quartz, alkali feldspar, Na-amphiboles, and aegirine. Amphiboles are not zoned for the most part and appear dark blue to dark green under PPL (Fig 3.1a). Aegirine is green and can be core-to-rim and sector zoned under PPL (Fig 3.1b), or replace amphiboles. Since these two minerals can also incorporate a lot of REE, their zonations and interactions are studied in detail in Chapter 4. Optical microscopy does not show any zonation in quartz and alkali feldspar; however, zonations are revealed in both minerals by CL, consisting of a second generation of quartz overgrowing the primary one, and of a core-to-rim zonation in alkali feldspars (Figs 3.2, 3.3, 3.4).

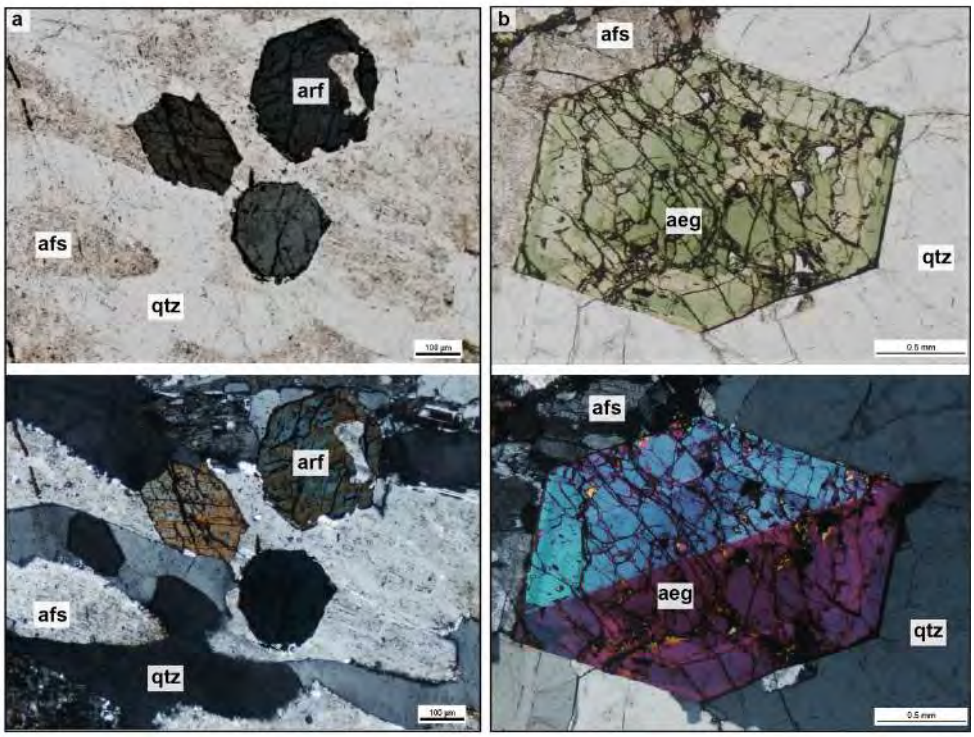

Figure 3.1 Main minerals common to all six studied complexes under PPL (top) and XPL (bottom). (a) Not zoned basal sections of arfvedsonite cogenetic with quartz and alkali feldspar from Evisa (EV1804C); (b) Zoned aegirine cogenetic with quartz and alkali feldspar from Khan Bogd (KB07D). Abbreviations: qtz: quartz; arf: arfvedsonite; aeg: aegirine; afs: alkali feldspar

Core-to-rim zonations in quartz are common to all complexes in granites (Fig 3.2), while in pegmatites they are present only at Amis, Evisa and Madagascar (Fig 3.3). Zonation is not visible under PPL, but is revealed with CL. In granites, the core appears navy blue while the rims are dark blue, except at Ambohimirahavavy where it is the opposite. The rims are thin compared to the core at Amis and Khan Bogd, whilst the core is less developed in the other granites. In addition, the core at Ambohimirahavavy is rich in inclusions of alkali feldspar, aegirine and Na-amphibole. At Strange Lake, alkali feldspar inclusions are located close to the core-rim transition, inside the rim. Granites from Ambohimirahavavy and Strange Lake also have quartz cores clearly delimited, in contrast to the other granites where the core-rim limit is blurry. All of these elements indicate that the core grew in two major steps. The difference in color is due to different activator elements. In quartz, the nature of activator elements is still debated, but studies point to a high amount of Ti (Rusk et al., 2006), or a high ratio Ti/Fe (Marshall and Mariano, 1988), being responsible for the observed blue color. In addition, some peculiar zonations were found in quartz crystals of granites from Strange Lake and Khan Bogd. At Strange Lake, some crystals contain a ring-shaped zonation in the middle, with lighter quartz forming the rim (Fig 3.4a,b). This may be an evidence for an episodic event during quartz crystallization. Considering the irregular shape of the outer side of the light blue ring (Fig 3.4b), it is likely that it experienced some dissolution before recrystallization. At Khan Bogd, the granite contains some quartz with a wavy-shaped zonation (Fig 3.4c,d).

In pegmatites, the same overgrowth is observed only at Amis, Evisa and Madagascar (Fig 3.3). The core at Ambohimirahavavy is also the only one to be darker than the rims. At Khan Bogd and Strange Lake, the quartz close to sealed fractures appears lighter, suggesting a second generation of quartz sealed the first one. Considering alkaline pegmatites crystallization processes are complex, it is not surprising to note that quartz zonations/overgrowths are more complex as well. The study of trace elements in those quartz would thereby be interesting to document the composition of the crystallization environment.

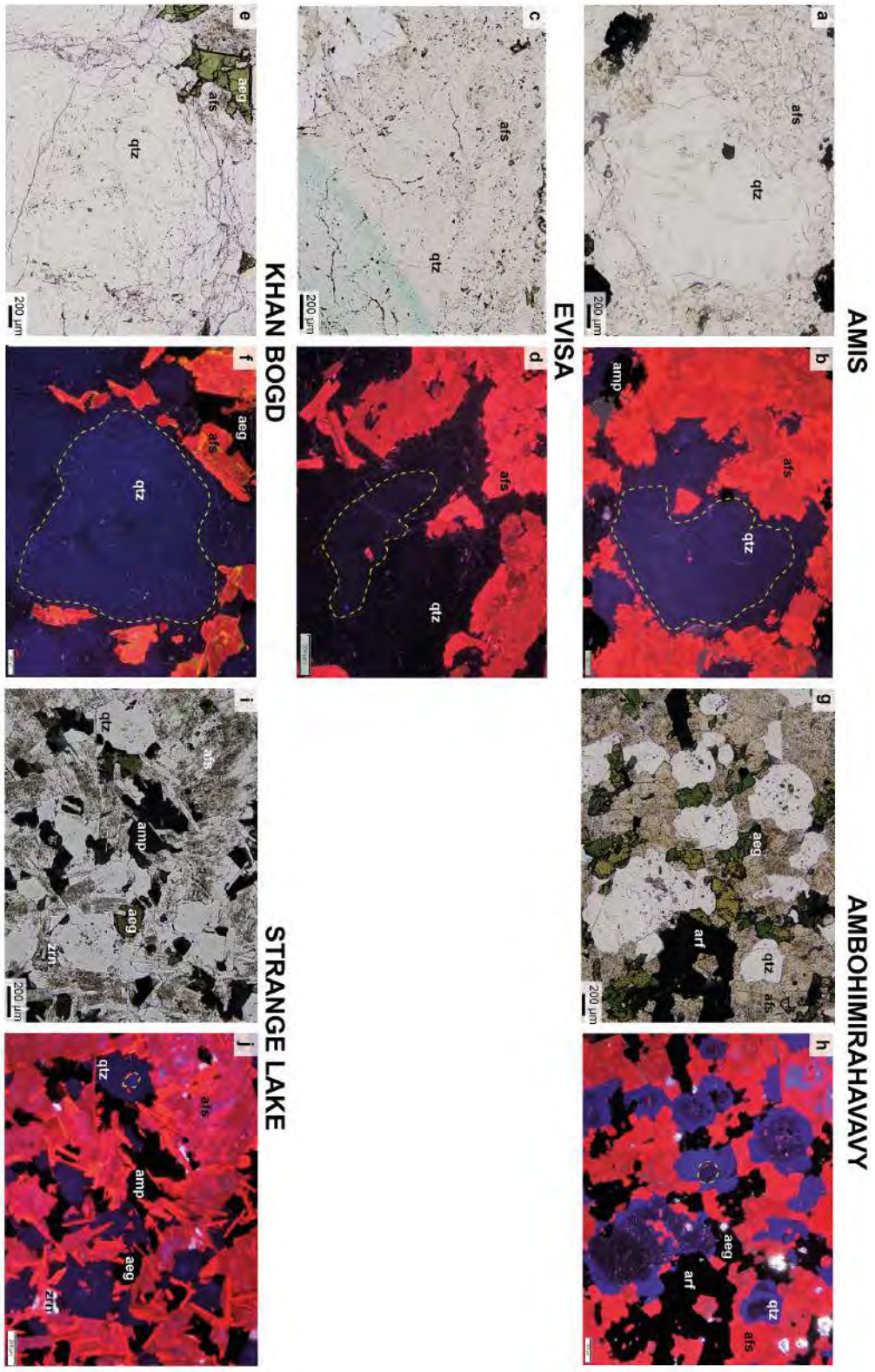

Figure 3.2 Quartz overgrowths in granitic samples. (a), (c), (e), (g), and (i) are PPL views; (b), (d), (f), (h), and (j) are CL images. The yellow dashed line gives an idea of the limit between the core and the overgrowth. (a), (b) Amis (SOS069); (c), (d) Evisa (EV1823B); (e), (f) Khan Bogd (KB07A); (g); (h) Ambohimirahavavy (AM107); (i), (j) Strange Lake (58-D-1). Abbreviations: qtz: quartz; arf: arfvedsonite; aeg: aegirine; afs: alkali feldspar; amp: amphibole; zrn: zircon

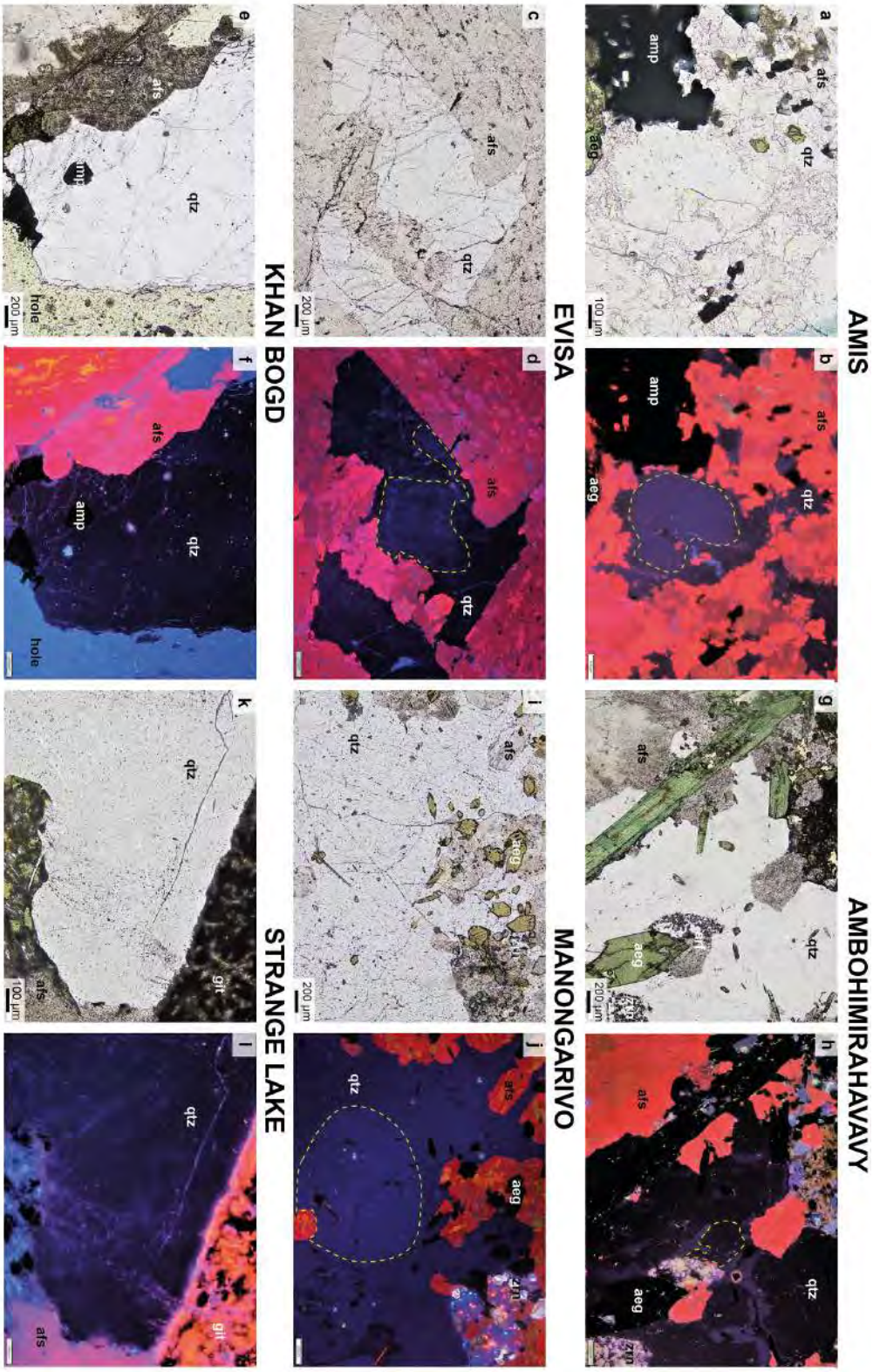

Figure 3.3 Quartz overgrowths and zonations in pegmatitic samples. (a), (c), (e), (g), (i), and (k) are PPL views; (b), (d), (f), (h), (j), and (l) are CL images. The yellow dashed line gives an idea of the limit between the core and the overgrowth. (a), (b) Amis (SOS071); (c), (d) Evisa (EV1825A); (e), (f) Khan Bogd (KB04B); (g); (h) Ambohimirahavavy (AM35); (i), (j) Manongarivo (688); (k), (l) Strange Lake (SL1-20). Abbreviations: qtz: quartz; amp: amphibole; aeg: aegirine; afs: alkali feldspar; zrn: zircon; git: gittinsite

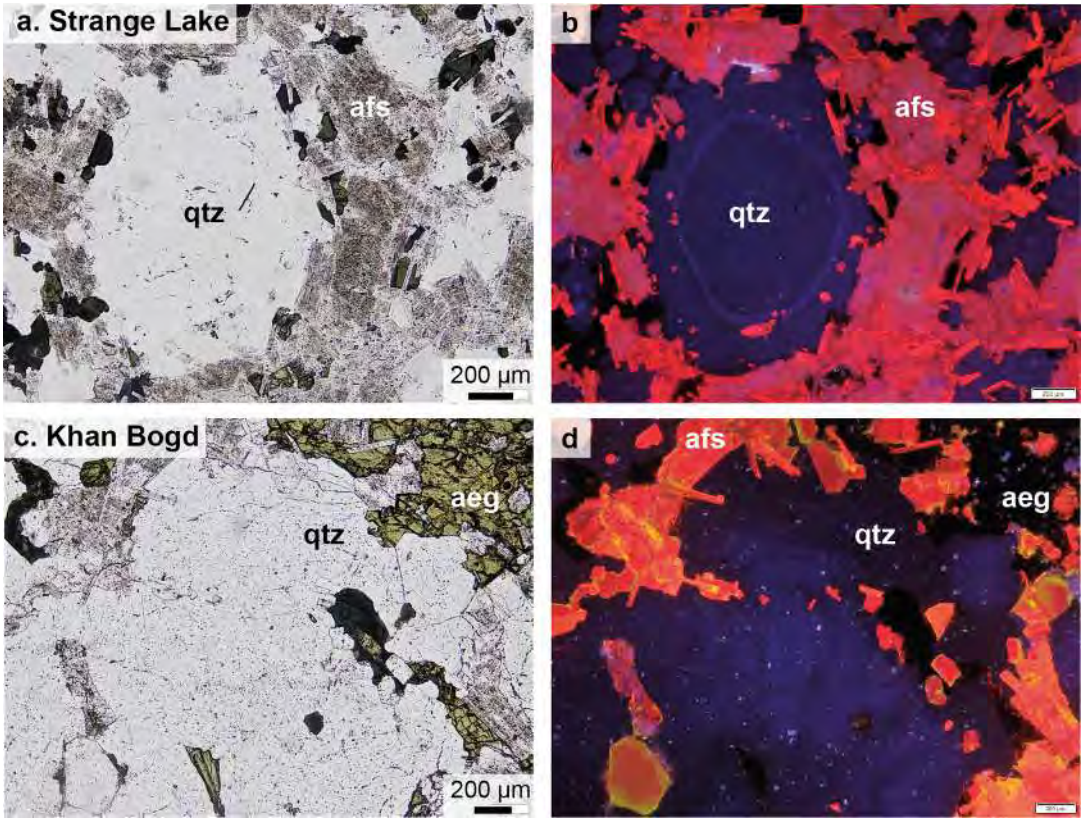

Figure 3.4 Peculiar zonations in quartz of granites of two complexes. (a) and (c) are PPL views; (b) and (d) are CL. (a), (b) Three zones in a quartz crystal from Strange Lake (58-D-1); (c), (d) Wavy-shaped zonation in a quartz crystal from Khan Bogd (KB07A). Abbreviations: qtz: quartz; aeg: aegirine; afs: alkali feldspar

Feldspars can also reveal different colors with CL linked to their composition. They mostly display a strong red color due to the presence of Fe^{3+} in alkali feldspars (Marshall and Mariano, 1988; Fig 3.5). The variations in the red color intensity depend on the amount of Fe^{3+}, which is usually attributed to hydrothermal alteration, which causes albitization of existing feldspars. At Khan Bogd and Manongarivo, alkali feldspars often show core-to-rim zonations from red to green and yellow (Fig 3.5f,j), which are the sign of the presence of Mn^{2+} or Fe^{2+}, characteristic of plagioclase (Marshall and Mariano, 1988). In these two complexes as well as at Ambohimirahavavy, amphiboles and pyroxene are also rich in Mn compared to the other complexes (see 4). In addition, it is common at Strange Lake and occasional at Amis to find feldspar fluorescing in blue (Fig 3.5l), which shows that the feldspar is K-rich and contains Ti^{4+} (Marshall and Mariano, 1988). Based on their texture, K-feldspar crystals are likely remains of previous feldspars preserved from the global albitization.

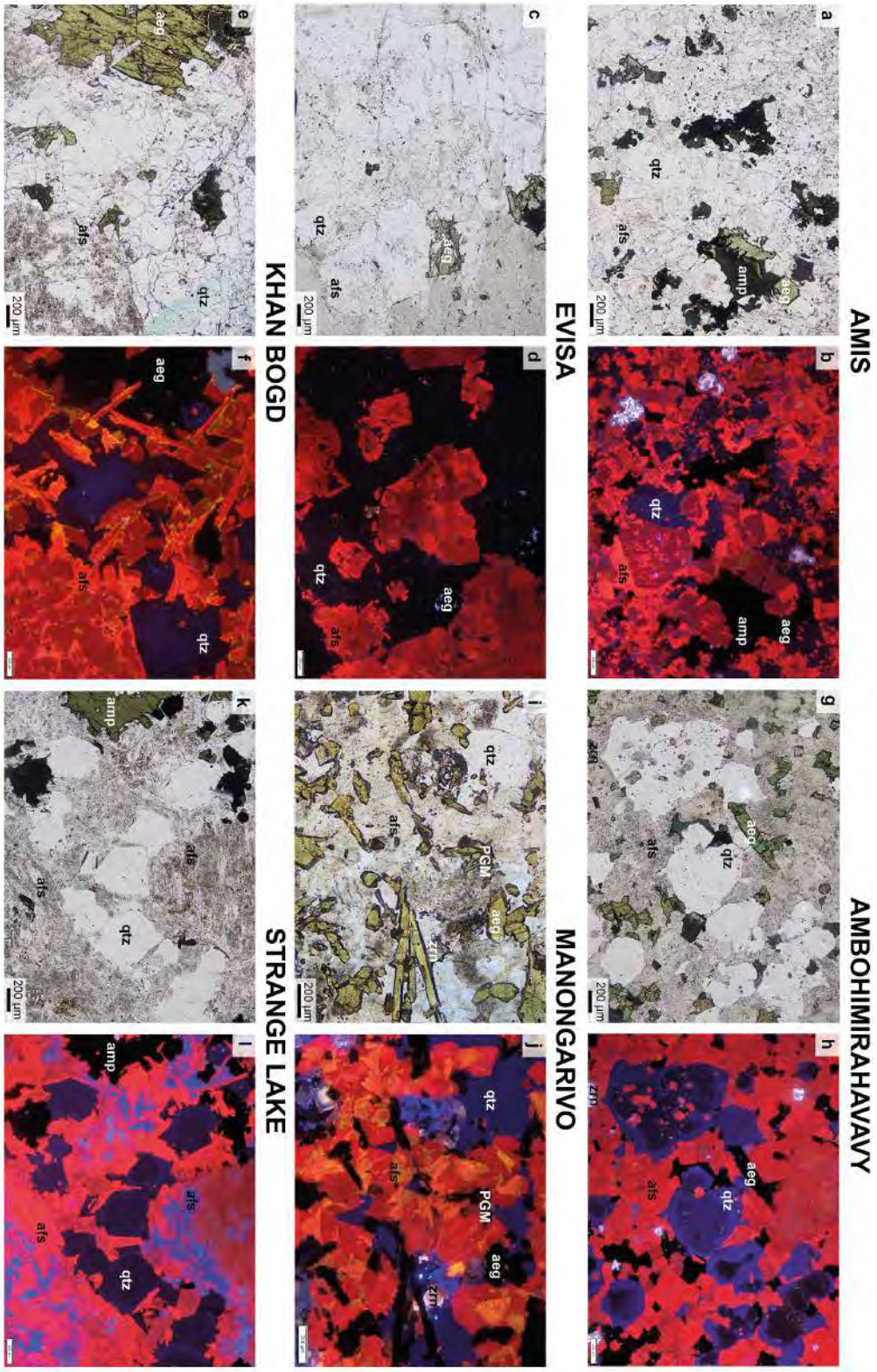

Figure 3.5 Zonations of alkali feldspars in the different complexes. (a), (c), (e), (g), (i), and (k) are PPL views; (b), (d), (f), (h), (j), and (l) are CL images. (a), (b) Amis (SOS071); (c), (d) Evisa (EV1823B); (e), (f) Khan Bogd (KB07A); (g); (h) Ambohimirahavavy (AM107); (i), (j) Manongarivo (688); (k), (l) Strange Lake, (58-D-1). Abbreviations: qtz: quartz; aeg: aegirine; afs: alkali feldspar; zrn: zircon; amp: amphibole; PGM: pyrochlore group minerals

3.3 Primary REE-bearing minerals

3.3.1 Primary REE-bearing minerals identification

Based on petrological observations, REE-bearing minerals present in all complexes were identified and a chronology of crystallization has been established. Euhedral minerals growing in equilibrium with magmatic quartz and feldspars, sometimes altered or being replaced, are considered primary, i.e. they crystallized from a melt. Pyrochlore group minerals, Ca- and Na-zirconosilicates, monazite-(Ce), chevkinite-(Ce) and allanite-(Ce, Nd) are the primary minerals typically considered as most concentrated in magmatic REE. A summary of the main primary REE-bearing minerals in each complex is provided in Tab 3.6.

Pyrochlore group minerals were observed in all complexes, in granites and pegmatites. This oxide forms typical euhedral crystals yellowish to brown in color under PPL (Fig 3.7a). Crystals are usually relatively small (20-200 μm across) and occur in equilibrium with quartz and feldspars. According to the classification by Atencio et al. (2010), PGM are fluorcalciopyrochlore (Tab 3.3). PGM can incorporate a significant amount of REE, such as at Amis where it can contain up to 27 % of oxides of REE (REO), with both LREE and HREE (Schmitt et al., 2002; Tab 3.3). In all six studied complexes, PGM are systematically altered to a Pb-, REE-richer variety, called fluornatropyrochlore (Fig 3.7b, 3.6). PGM at Ambohimirahavavy are poorer in REE than at Strange Lake and Amis (Tab 3.2, Fig 3.20). At Ambohimirahavavy, Estrade et al. (2014) also mention the growth of feriallanite-(Ce) and fergusonite-(Y) at the expense of PGM. The primary origin of fluorcalciopyrochlore is also confirmed at Manongarivo, Strange Lake and Amis by the literature (e.g. respectively, Donnot, 1963; Miller, 1996; Schmitt et al., 2002). PGM compositions differ between granites and pegmatites of a same complex. PGM in granites are systematically richer in REE, Nb and poorer in Pb (i.e. less altered) than PGM in pegmatites, except at Ambohimirahavavy where PGM in pegmatites are richer in REE (Fig 3.6). Notable composition differences are also present between complexes. At Amis, PGM are rich in REE and Ti compared to the other complexes (Fig 3.6). In addition, two types of PGM were found and described by Schmitt et al. 2002. According to these authors, the first one is included in zircon, proving without any doubt its magmatic origin; the second is anhedral,

richer in Ti (and poorer in Nb; Tab 3.3, Fig 3.6), and present only in pegmatites. From these observations, the Ti-rich PGM appear to have grown later than the other PGM, but there is no evidence as to its hydrothermal origin: it is probably a late-magmatic mineral. No PGM as rich in Ti as described by Schmitt et al. was found among the samples in this study, although they are not located inside zircons but in equilibrium with quartz and feldspars. PGM from Amis and in granites at Evisa are rich in Y_2O_3 compared to the other complexes (20 vs 0.5 % on average, respectively). PGM from Manongarivo are surprisingly different from PGM at Ambohimirahavavy (e.g. different CaO, TiO_2, Ce_2O_3 contents), even though the two complexes formed in similar conditions and at the same time. PGM in pegmatites from Evisa contain more CaO than other PGM, and those from Strange Lake are richer in Na. At Khan Bogd, PGM are especially rich in Si and poor in Nb. However, this study is only preliminary: in order to better understand the variation in elements concentrations and at what timing they occur, it is important to study zonations in PGM crystals.

In this study, primary monazite-(Ce), of formula $Ce(PO_4)$, was found only at Manongarivo and Amis, but it was also reported at Strange Lake and Ambohimirahavavy in the literature (Donnot, 1963; Estrade, 2014; Miller, 1996; Tab 3.3). This phosphate occurs as translucent with a high relief under PPL. It can occur as sparse primary subhedral crystals in association with magmatic quartz and feldspars (Fig 3.7c), as well as secondary anhedral crystals in pseudomorphs. Monazite-(Ce) grains are never bigger than 400 μm across. It is sector zoned (Fig 3.7d) and alteration to REE fluorcarbonates has been reported at Ambohimirahavavy (Estrade et al., 2014b). Monazite-(Ce) typically contains 70 % REO at Ambohimirahavavy, the vast majority of which being LREE (Estrade et al., 2014b; Tab 3.3).

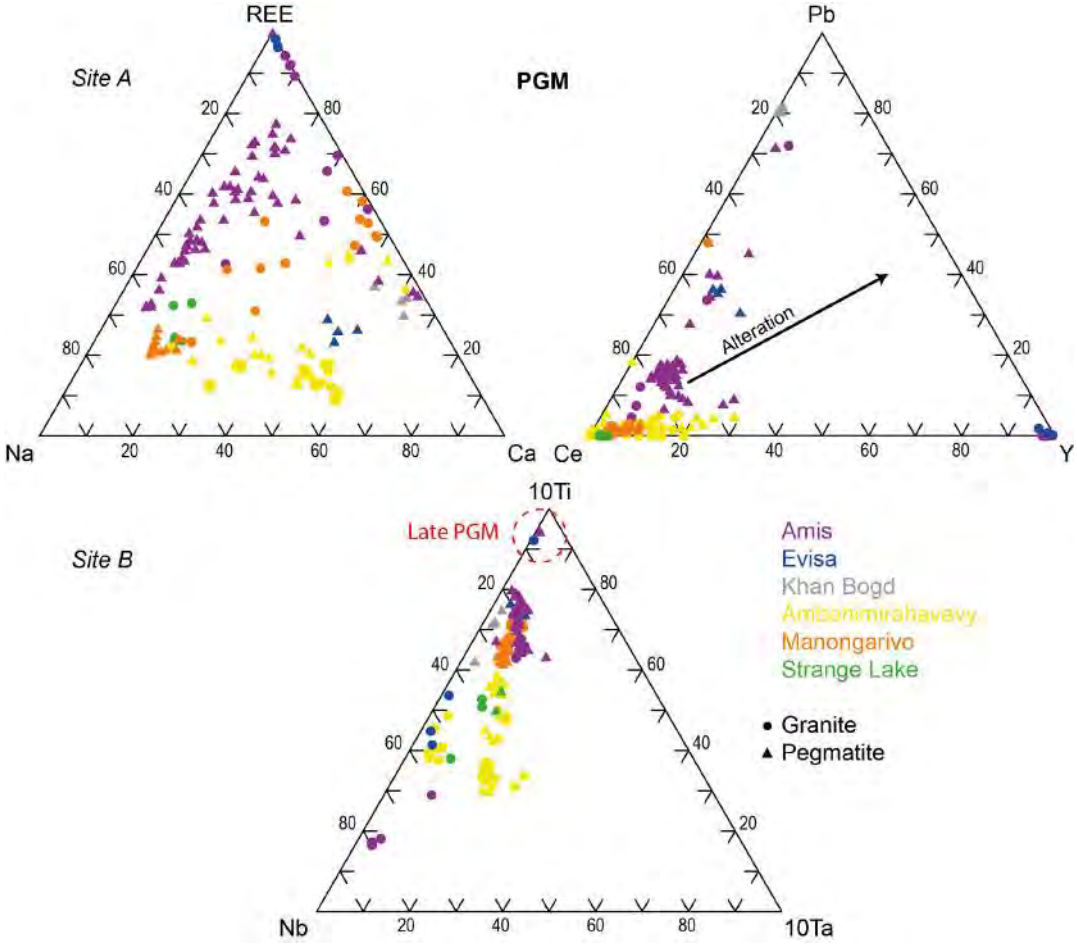

Figure 3.6 Ternary diagrams of PGM from the six complexes. Data are from this study as well as from Gysi et al. (2016) and Schmitt et al. (2002); additional data about Ambohimirahavavy and Manongarivo were provided by Guillaume Estrade and Soatsitohaina Rakotovao. Elements are in apfu normalized to 100 %. Coefficients were added for some elements for a better visualization of the data; global tendencies are unaffected

Chevkinite-(Ce), a silicate of formula $Ce_4(Ti,Fe^{2+},Fe^{3+})_5Si_4O_{22}$, was found at Evisa, Ambohimirahavavy, and Manongarivo in this study, but only in small quantities. It has also been reported in a fluid inclusion at Strange Lake (Vasyukova and Williams-Jones, 2016). It is generally dark brown to black under PPL and does not appear to be affected by alteration (Fig 3.7e). It occurs as euhedral crystals (up to 700 μm across) cogenetic with other minerals (quartz, feldspar, aegirine, PGM; Fig 3.7f), but also as interstitial anhedral crystals. Inclusions of thorite as euhedral crystals indicate chevkinite-(Ce) crystallization during main magmatic phase, whilst its occurrence as interstitial grains rather points out to a late magmatic origin. Additional composition analyses would be necessary to confirm this hypothesis.

Chevkinite-(Ce) typically contains 40 % REO on average at Evisa, most of it being LREE. The low amount of LREE at Manongarivo (26.45 %) is an analisis artifact as La was not analyzed (Tab 3.3). Chevkinite-(Ce) from Manongarivo is rich in Mn; no significant difference in composition was found between chevkinite-(Ce) crystals of the different complexes (Tab 3.3).

Allanite-(Ce, Nd), where present, is secondary in all studied complexes. However, this silicate of formula $Ca(Ce,Nd)Al_2Fe^{2+}Si_3O_{12}(OH)$ was found in the hypersolvus granite of Evisa as extremely altered euhedral crystals (Fig 3.7g). It is usually found in association with amphibole. Poitrasson et al. (1998) described allanite crystals totally replaced by monazite-(Ce) and fluocerite-(Ce), and also associated with amphiboles (Fig 3.7h). In hypersolvus samples of this study, allanite-(Ce) was found partially replaced by britholite-(Ce), another REE-bearing silicate (Fig 3.7g). Based on its alignment on the Sm-Nd isochron of the whole rock and the feldspars, allanite must be magmatic in origin at Evisa (Poitrasson et al., 1998). Allanite contains 25 % REO at Evisa (Tab 3.3), which is lower than the average composition of 38 % ("Allanite-(Ce)", 2020). This allanite also contains less Al and more Ti, Ca and Fe (Tab 3.3).

Calcium- and Na-zirconosilicates (mostly elpidite or EGM) are primary minerals common to most complexes which can contain significant concentrations of REE. Primary zirconosilicates are partially or totally altered in all complexes, forming pseudomorphs; the next section is dedicated to their study.

Table 3.3 Analyses of primary REE-bearing minerals of the six studied complexes where they exist. Results presented for this study were acquired with EPMA. Data from Webmineral are presented for comparison. n.a.: not analyzed; b.d.l.: below the detection limit ("Allanite-(Ce)", 2020; "Chevkinite-(Ce)", 2020; Estrade et al., 2014b; Gysi et al., 2016; "Monazite-(Ce)", 2020; Schmitt et al., 2002; Vasyukova and Williams-Jones, 2019)

Complex	Amis					Evisa				Khan Bogd	Ambohimirahavavy				Manongarivo			Strange Lake			Reference		
Mineral	PGM	PGM (altered)	PGM	PGM	PGM	PGM	PGM	Chevkinite-(Ce)	Allanite-(Ce)	PGM	PGM	PGM (altered)	Monazite-(Ce)	Chevkinite-(Ce)	PGM	PGM	Chevkinite-(Ce)	PGM	PGM	Chevkinite-(Ce)	Monazite-(Ce)	Chevkinite-(Ce)	Allanite-(Ce)
Source	Schmitt et al. (2002)	Schmitt et al. (2002)	Schmitt et al. (2002)	This study	This study	This study	This study	Poitrasson, unpublished	Poitrasson, unpublished	This study	Estrade et al. (2014)	Estrade et al. (2014)	Estrade et al. (2014)	Estrade et al. (2014)	This study	Rakotovao, unpublished	This study	Gysi et al. (2016)	Gysi et al. (2016)	Vasyukova et al. (2015)	Webmin	Webmin	Webmin
Analyzes no.	*2*	*3*	*3*	*4*	*53*	*4*	*4*	*7*	*1*	*4*	*9*	*9*	*3*	*4*	*14*	*14*	*3*	*24*	*18*	*76*			
Rock nature	Granite	Granite	Pegmatite	Granite	Pegmatite	Granite	Pegmatite	Granite	Granite	Pegmatite					Pegmatite	Granite	Pegmatite	Granite	Pegmatite	Granite			
Wt%																							
SiO_2	0.09	2.41	0.01	0.72	0.47	2.66	0.41	20.30	28.92	13.65	b.d.l.	b.d.l.	0.55	18.55	0.91	0.68	17.78	0.94	1.23	19.8		19.94	29.32
ZrO_2	0.12	0.30	b.d.l.	0.79	b.d.l.	b.d.l.	b.d.l.	n.a.	n.a.	0.80	n.a.	n.a.	b.d.l.	0.27	0.88	n.a.	0.28	0.34	0.35	0.3			
CaO	3.26	2.77	0.58	0.93	1.11	0.27	6.08	2.79	8.99	3.15	11.23	12.44	b.d.l.	0.89	2.84	4.74	0.36	3.57	4.72	1.2		3.72	5.47
Na_2O	0.51	1.06	0.16	0.01	1.39	0.01	1.47	n.a.	n.a.	0.19	3.90	4.14	n.a.		6.80	2.27	0.19	7.49	8.67	n.a.			
TiO_2	9.64	8.59	24.28	0.76	9.31	7.87	9.72	18.49	4.27	3.80	2.61	2.85	b.d.l.	8.08	7.09	9.16	16.60	4.60	5.02	16.4		16.57	
Al_2O_3	n.a.	n.a.	n.a.	b.d.l.	0.10	0.21	0.03	0.35	6.49	0.26	n.a.	n.a.	n.a.	n.a.	0.04	0.00	0.01	n.a.	n.a.	n.a.			18.66
K_2O	n.a.	n.a.	n.a.	n.a.	n.a.	n.a.	n.a.	0.02	n.a.	n.a.	n.a.	n.a.	n.a.	n.a.	n.a.	n.a.	n.a.	n.a.	n.a.	n.a.			
FeO total	1.16	1.86	0.32	0.01	0.25	1.88	0.84	8.53	21.88	2.99	0.52	0.46	b.d.l.	14.53	0.37	0.68	7.86	0.46	b.d.l.	12.2		13.71	8.76
MnO	n.a.	n.a.	n.a.	b.d.l.	0.12	b.d.l.	1.09	0.36	0.40	0.13	n.a.	n.a.	b.d.l.	b.d.l.	0.46	0.00	3.73	0.06	0.03	n.a.			
MgO	n.a.	n.a.	n.a.	b.d.l.	b.d.l.	0.05	b.d.l.	n.a.	0.00	0.16	n.a.	n.a.	n.a.	n.a.	b.d.l.	n.a.	0.01	n.a.	n.a.	n.a.		0.67	
F	1.16	1.24	0.53	0.09	2.31	0.1	0.28	n.a.	n.a.	b.d.l.	3.33	3.94	b.d.l.	b.d.l.	3.12	n.a.	b.d.l.	2.83	3.31	0.2			
H_2O	n.a.	n.a.	n.a.	n.a.	n.a.	n.a.	n.a.	n.a.	n.a.	n.a.	n.a.	n.a.	n.a.	n.a.	n.a.	n.a.	n.a.	n.a.	n.a.	n.a.			1.47
Nb_2O_5	53.68	47.52	33.64	45.83	47.89	39.23	42.48	n.a.	n.a.	24.39	59.85	61.12	b.d.l.	8.13	49.03	50.31	1.24	57.05	55.75	2.0			
Ta_2O_5	3.72	3.21	1.47	0.58	3.18	0.36	2.20	n.a.	n.a.	0.39	4.10	4.32	b.d.l.	0.60	2.41	2.73	0.1	2.38	3.48	n.a.			
Y_2O_3	0.42	0.83	14.39	21.35	0.88	24.33	1.08	1.51	0.27	0.13	0.44	0.42	b.d.l.	0.14	0.72	0.25	0.04	0.23	0.18	b.d.l.			5.51
La_2O_3	3.61	2.75	0.93	n.a.	n.a.	n.a.	n.a.	8.76	6.60	n.a.	1.95	1.45	29.15	15.11	n.a.	3.21	n.a.	4.52	4.25	13.9	16.95	18.92	
Ce_2O_3	9.32	7.80	3.16	0.65	9.38	0.46	7.39	18.77	12.91	4.89	4.99	3.90	32.63	23.42	11.43	8.89	26.45	10.79	10.42	23.5	34.16	23.15	32.04
Pr_2O_3	0.91	0.70	0.40	n.a.	n.a.	n.a.	n.a.	2.18	1.30	n.a.	b.d.l.	b.d.l.	2.23	1.86	n.a.	1.18	n.a.	0.99	0.99	2.3			
Nd_2O_3	2.49	1.89	1.53	n.a.	n.a.	n.a.	n.a.	8.14	4.22	n.a.	1.99	1.55	5.63	5.60	n.a.	4.11	n.a.	2.40	2.38	7.0	14.01		
Sm_2O_3	0.40	0.28	0.56	n.a.	n.a.	n.a.	n.a.	1.39	0.38	n.a.	b.d.l.	b.d.l.	b.d.l.	b.d.l.	n.a.	0.48	n.a.	0.21	0.21	0.7			
Gd_2O_3	0.23	0.26	2.25	n.a.	n.a.	n.a.	n.a.	n.a.	n.a.	n.a.	b.d.l.	b.d.l.	n.a.	n.a.	n.a.	n.a.	n.a.	0.09	0.14	0.4			
Tb_2O_3	b.d.l.	0.01	0.39	n.a.	n.a.	n.a.	n.a.	n.a.	n.a.	n.a.	n.a.	n.a.	n.a.	n.a.	n.a.	n.a.	n.a.	n.a.	n.a.	n.a.			
Dy_2O_3	0.12	0.15	2.71	n.a.	n.a.	n.a.	n.a.	n.a.	n.a.	n.a.	n.a.	n.a.	n.a.	n.a.	n.a.	n.a.	n.a.	0.12	b.d.l.	b.d.l.			
Yb_2O_3	0.02	0.10	1.22	n.a.	n.a.	n.a.	n.a.	n.a.	n.a.	n.a.	n.a.	n.a.	n.a.	n.a.	n.a.	n.a.	n.a.	n.a.	n.a.	n.a.			
Σ REO	*17.52*	*14.77*	*27.54*	*22.00*	*10.26*	*24.79*	*8.47*	*40.75*	*25.68*	*5.02*	*9.37*	*7.32*	*69.64*	*46.13*	*12.15*	*18.12*	*26.49*	*19.35*	*18.57*	*47.80*	*65.12*	*42.07*	*37.55*
PbO	1.48	10.55	0.56	b.d.l.	3.38	0.38	6.42	n.a.	n.a.	28.93	b.d.l.	b.d.l.	n.a.	n.a.	0.27	0.83	0.1	n.a.	n.a.	n.a.			
ThO_2	0.19	0.20	5.20	6.00	0.74	1.05	1.87	1.41	0.39	0.06	0.29	0.52	0.91	0.69	0.61	0.27	b.d.l.	0.10	b.d.l.	n.a.	5.50	2.19	
UO_2	4.68	4.31	0.91	0.16	5.10	0.98	6.90	0.08	0.00	1.60	3.53	2.45	n.a.	n.a.	1.42	1.27	b.d.l.	0.59	0.14	n.a.			
P_2O_3	n.a.	n.a.	n.a.	n.a.	n.a.	n.a.	n.a.	n.a.	n.a.	n.a.	n.a.	n.a.	29.83	n.a.	n.a.	b.d.l.	n.a.	n.a.	n.a.	n.a.	29.55		
WO_3	n.a.	n.a.	n.a.	2.68	0.49	2.75	0.23	n.a.	n.a.	b.d.l.	n.a.	n.a.	n.a.	n.a.	0.09	n.a.	n.a.	n.a.	n.a.	n.a.			
Total	*97.21*	*98.79*	*95.20*	*80.56*	*86.10*	*82.59*	*88.49*	*93.08*	*97.02*	*85.52*	*98.73*	*99.56*	*100.93*	*97.87*	*88.49*	*91.07*	*74.75*	*99.76*	*101.27*	*99.90*	*100.17*	*98.87*	*101.23*

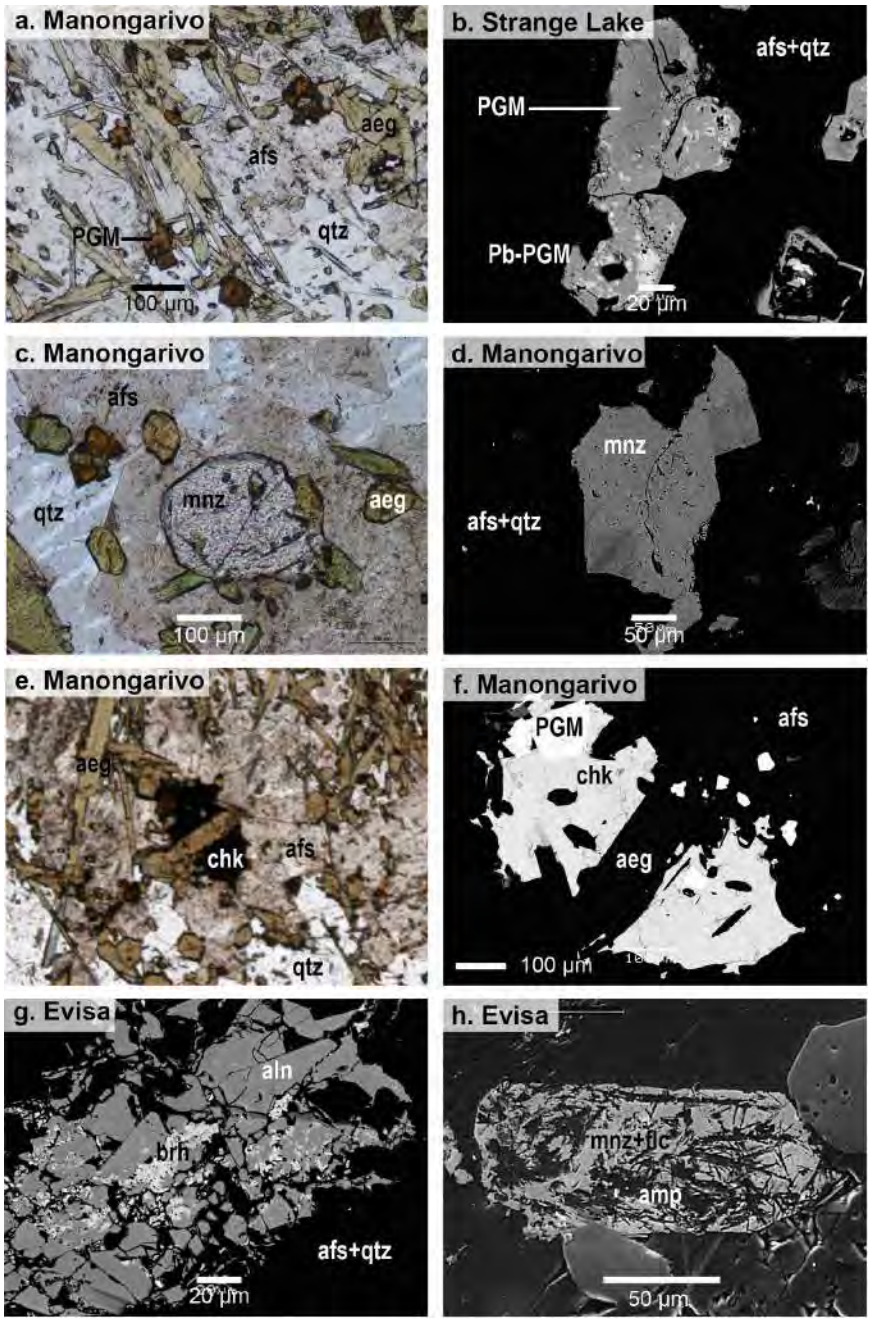

Figure 3.7 Presentation of the main primary REE-bearing minerals. (a), (c), (e), and (i) are PPL views; (b), (d), (f), (g), (h) and (j) are BSE-SEM images. (a) PGM crystals, Manongarivo (688); (b) Altered PGM crystal, Strange Lake (SL1-20); (c) Monazite-(Ce), Manongarivo (688); (d) Monazite-(Ce), Manongarivo (688); (e) Chevkinite-(Ce), Manongarivo (688); (f) Same chevkinite-(Ce) crystal ; (g) Allanite-(Ce) altered into britholite, Evisa (EV9102); (h) Pseudomorph of monazite-(Ce) + fluocerite-(Ce) after allanite-(Ce), Evisa (from Poitrasson et al. (1998)); (i) EGM crystal filled with inclusions, Ambohimirahavavy (EU02); (j) Same EGM crystal. Abbreviations: PGM: pyrochlore group minerals; mnz: monazite; chk: chevkinite; brh: britholite; aln: allanite; flc: fluocerite; amp: amphibole; EGM: eudialyte-group minerals

3.3.2 Primary zirconosilicates: eudialyte-group minerals, elpidite

Calcium and/or Na zirconosilicates were present in all six studied complexes as early magmatic phases but the nature, localization and amounts of zirconosilicates varies from one complex to another. Some primary zirconosilicates have been observed in the samples from this study, and others are totally replaced, hence their identification is based on previous papers.

The only primary zirconosilicates described in alkaline complexes, both silica-saturated and undersaturated, are EGM and elpidite. These two minerals never occur at the same stage in a same complex. To my knowledge only a handful of studies focus on why they cannot crystallize together. According to Michel-Lévy (1961), EGM can only crystallize in a restricted range of Na concentration, and only above 440 °C, whilst elpidite crystallizes under 380 °C. Borst et al. (2016) compare conditions of formation of EGM and gittinsite, a Ca-rich zirconosilicate whose structure is close to elpidite, and indicate that H_2O activity is another parameter to take into account. Although it is not mentioned in the studies, it is obvious that a low concentration of Ca favors elpidite compared with EGM.

The complex of Ambohimirahavavy includes agpaitic pegmatitic granitic dykes (called GR-III, Estrade et al., 2018; Estrade et al., 2014b), described for the first time by Alfred Lacroix in his series of books *Minéralogie de Madagascar* (1923) and extremely rich (>10 vol%) in eudialyte-group minerals (EGM, of formula $Na_{15}(Ca,REE)_6(Fe,Mn)_3Zr_3Si_{26}O_{73}(O,OH,H_2O)_3(Cl,OH)_2$). Although common in SiO_2-undersaturated syenites, EGM occurrences are rare in alkaline granites (Estrade et al., 2018). The EGM in sample EU02, collected in a core in this GR-III, occur as big euhedral crystals of up to 2 mm. They are colorless under PPL, and contain many inclusions in their core (Fig 3.8a,b). Inclusions are made a wide variety of minerals including alkali feldspars, aegirine, allanite-(Ce), monazite-(Ce), quartz, fluorapatite, nacareniobsite-(Ce), and thorite (Fig 3.8c). The EGM crystals in this sample are not altered. Chemical study show this eudialyte is four times richer in REE (∼7 wt%; Tab 3.4) on average, and poorer in Ca (4 to 8 wt%; Tab 3.4), than reported EGM from nepheline syenites (Estrade et al., 2018). Eudialyte-group minerals are also present in transitional miaskitic granitic dykes (called GR-II, Estrade et al., 2018; Estrade et al., 2014b) of Ambohimirahavavy, but they are almost systematically completely pseudomorphed. Pseudomorphs are described in detail in 3.4.

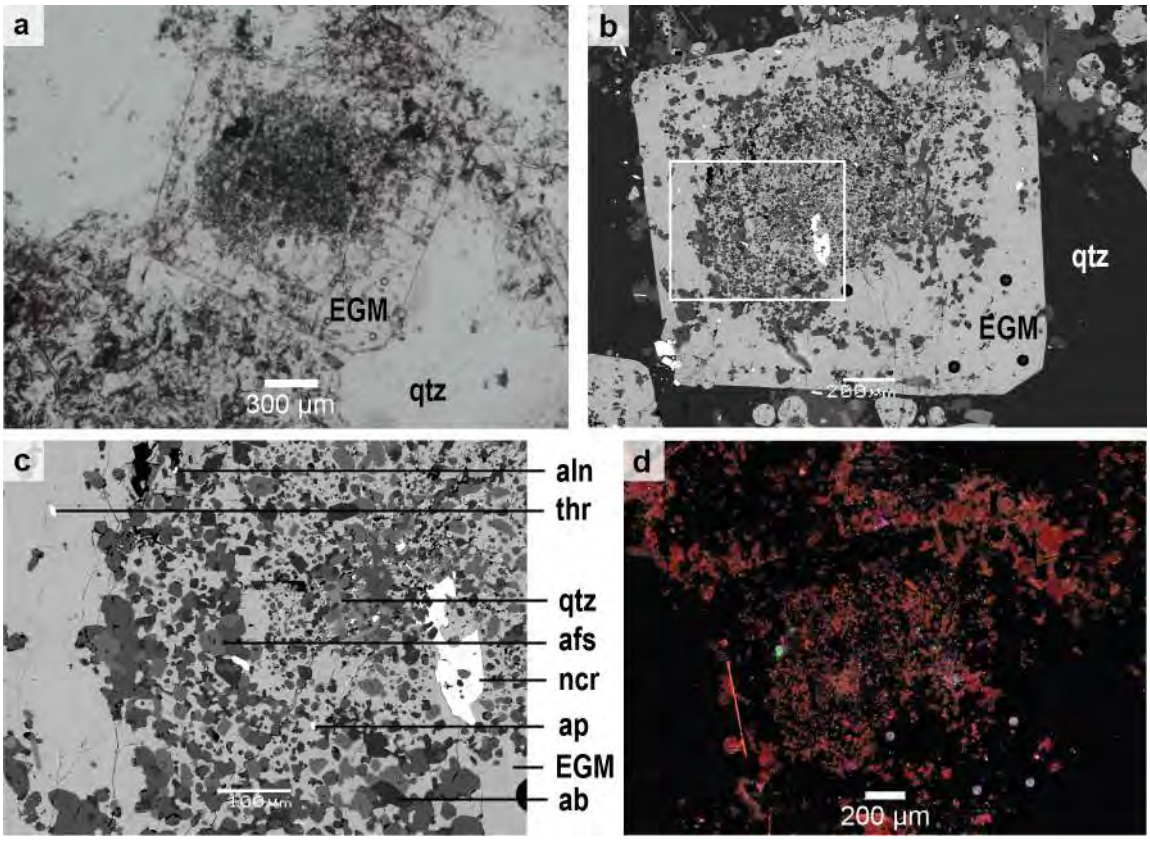

Figure 3.8 An eudialyte-group mineral crystal seen under different conditions. (a) PPL; (b) SEM, the white square is the limit of the zoomed image (c); (d) CL. Abbreviations: thr: thorite; ncr: nacareniobsite-(Ce); ap: fluorapatite; ab: albite

In the Manongarivo complex pseudomorphs can be observed, similar to those at Ambohimirahavavy in that they also contain a wide diversity of secondary, REE-bearing phases. This suggests the previous presence of a primary zirconosilicate that has been entirely altered. In his report about the northwestern alkaline complexes of Madagascar, Donnot (1963) draws a parallel between the pseudomorphs of Manongarivo and those of Ambohimirahavavy. Relying of the work of Lacroix (1923), he mentions that the high amounts of Zr-rich and REE-rich phases in the pseudomorphs must come from a former Zr-bearing mineral. No primary Zr-bearing mineral was found among the samples of this study, but another study by Bollaert (2019, unpublished) reports the presence of euhedral EGM crystals (up to 1 mm) with inclusions of vlasovite and aegirine. No chemical analyses are available on EGM from Manongarivo.

In the Khan Bogd complex, EGM is not present, but another complex zirconosilicate, elpidite ($Na_2ZrSi_6O_{15}{\cdot}3H_2O$), is. It occurs as beige euhedral crystals of up to 2 mm across (Fig 3.9a,e). It has been found fresh only in pegmatite

among the samples of this study, but has also been reported in granite (Kynicky et al., 2011). Elpidite is commonly altered along preexisting fractures (Fig 3.9b) and extensively replaced by secondary minerals, namely zircon, quartz, and armstrongite (Fig 3.9a-d). Zircon is rarely in direct contact with fresh elpidite, and the same observation was made at Strange Lake by Salvi and Williams-Jones (1995). Altered elpidite has a whiter colour than the fresh one under PPL (Fig 3.9a,e). This mineral is highly hydrated (9 to 11 % H_2O), but altered zones are even richer in OH groups (Fig 3.9f; Tab 3.4), demonstrating that alteration must have been hydrothermal. Although no REE appears in the elpidite formula, the mineral can still contain significant concentrations, and crystals in pegmatites are especially enriched in HREE compared to granitic ones (Kynicky et al., 2011). Although new analyses from this study provide REE contents much lower than the study from Kynicky et al. (2011), it confirms that altered elpidite contains more HREE (380 ppm Y) and Ca (1.68 %) than fresh elpidite (14 ppm Y and 0.58 % CaO; Tab 3.4; Fig 3.10).

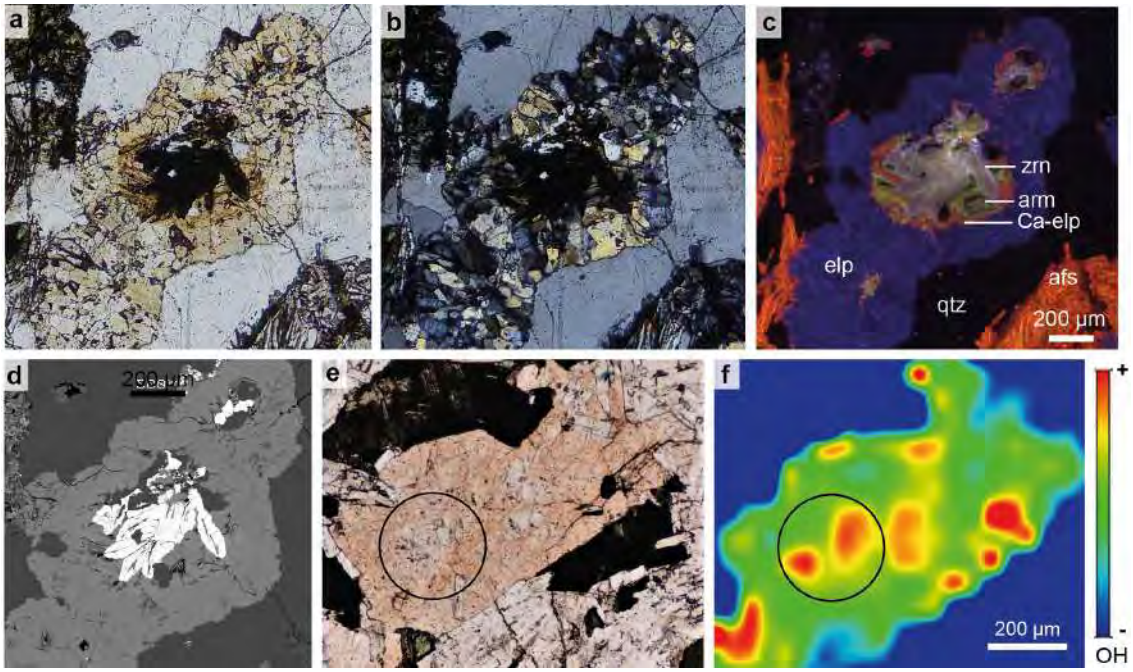

Figure 3.9 Altered elpidite at Khan Bogd, samples KB04A and KB04C. (a), (b), (c) and (d) show one crystal, and (e) and (f) a second one. (a) Optical microscope of an elpidite altered to secondary phases in its core; (b) XPL; (c) CL; (d) SEM; (e) Optical microscope of an elpidite crystal more altered in its whiter core; (f) Infrared spectroscopy showing the relative abundance of OH group in the elpidite crystal, the circle matches the circled zone in (e). Abbreviations: zrn: zircon; arm: armstrongite; elp: elpidite

Elpidite also occurs in pegmatites at Strange Lake, as large (up to 5 mm), boat-shaped crystals. Similarly to Khan Bogd, it is highly altered to a more Ca-rich elpidite (Fig 3.10) and secondary armstrongite and more generally gittinsite forming pseudomorphs. The alteration is important, to the extent that no elpidite grain was found in the pegmatitic B zone (Gysi et al., 2016). Elpidite from Strange Lake contains 9 to 10 % H_2O (Salvi and Williams-Jones, 1995), and its REE content was only recently analyzed by Vasyukova and Williams-Jones (2019). This analysis reveals that elpidite from Strange Lake contains less total REE than at Khan Bogd (1770 vs 3200 ppm respectively), and that it is enriched in HREE (1470 ppm) compared to LREE (4 ppm; Tab 3.4).

Pegmatites from the Amis complex also contain pseudomorphs, but no relicts of complex zirconosilicates were identified. There is no published work mentioning a primary zirconosilicate either. However, considering the abundance of globular pseudomorphs as well as their high zircons content, it is reasonable to assume they replace a previous magmatic zirconosilicate. The exact nature of this mineral remains unknown.

No primary zirconosilicate was found in the samples at Evisa, but the presence of pseudomorphs in the subsolvus granite and associated pegmatites suggests that there may have been, similar to the case at Manongarivo. Bonin (1988) however, did identify elpidite occurring as yellowish needles aggregates in miarolitic cavities of the subsolvus granite. It is thus possible that the pseudomorphs formed after elpidite, similarly to Strange Lake. Unfortunately, Bonin did not analyze REE in the elpidite (Tab 3.4), but the Al content he reports is much higher than at Khan Bogd and Strange Lake (0.25, 0.03 and 0.01 % respectively; Tab 3.4). Since he could only analyze elpidite with EPMA, it is possible that the lack of elements provokes an artificial deviation from the alteration trend drawn by elpidite at Khan Bogd and Strange Lake (Fig 3.10). No pseudomorphs nor elpidite were observed in the hypersolvus granite.

Table 3.4 Analyses of primary zirconosilicates EGM and elpidite, from this study as well as the literature of the six studied complexes if they exist. Results presented for this study were acquired with EPMA for major elements, and LA-ICPMS for traces. Data from Webmineral are presented for comparison. n.a.: not analyzed; b.d.l.: below the detection limit (Bonin and Platevoet, 1988; "Elpidite", 2020; Estrade et al., 2018; "Eudialyte", 2020; Kynicky et al., 2011; Salvi and Williams-Jones, 1995

Complex	Amis	Evisa	Khan Bogd				Ambohimirahavavy		Manongarivo	Strange Lake		Reference	
Mineral		Elpidite	Elpidite	Ca-elpidite	Elpidite	Ca-elpidite	EGM	EGM		Elpidite	Ca-elpidite	Elpidite	EGM
Source		Bonin (1988)	This work	This work	Kynicky et al. (2011)	Kynicky et al. (2011)	This work	Estrade et al. (2018)		Vasyukova et al. (2019)	Salvi et al. (1995)	Webmin	Webmin
Rock type		Granite	Pegmatite	Pegmatite	Pegmatite	Pegmatite	GR-III	GR-III		Granite	Granite		
Major (wt%)													
Analyzes #		9	17	18	7	7	1	12		4	1		
SiO_2		60.33	58.86	58.65	62.40	60.52	62.71	50.22		56.4	63.40	60.11	48.45
ZrO_2		19.97	20.13	19.81	21.57	18.83	19.75	10.94		20.0	17.05	20.55	12.42
CaO		0.22	0.58	1.68	0.25	2.21	4.65	7.74		0.1	1.93		8.48
Na_2O		9.11	8.92	7.52	6.19	5.41	2.59	11.39		9.1	7.87	10.33	12.49
TiO_2		n.a.	0.03	0.04	0.13	0.02	0.00	0.18		0.0	0.20		
Al_2O_3		0.25	0.03	0.04	n.a.	n.a.	1.23	0.00		0.0	n.a.		
K_2O		n.a.	0.13	0.14	0.11	0.05	0.15	0.41		0.0	0.21		
FeO total		n.a.	0.10	0.21	0.22	0.07	0.18	4.24		0.2	0.29		4.34
MnO		n.a.	0.03	0.03	b.d.l.	0.02	0.07	1.88		0.0	0.07		2.14
MgO		n.a.	0.01	0.01	n.a.	n.a.	0.03	n.a.		n.a.	0.65		
F		n.a.	n.a.	n.a.	n.a.	n.a.	n.a.	n.a.		0.2	n.a.		
Cl		n.a.	0.19	0.19	n.a.	n.a.	n.a.	2.18		n.a.	n.a.		1.79
H_2O		n.a.	n.a.	n.a.	n.a.	n.a.	n.a.	n.a.		n.a.	n.a.	9.01	1.36
Trace (ppm)													
Analyzes #		9	3	5	7	7	1	12		4	1		
Nb		n.a.	8.7	18	n.a.	n.a.	6010	16300		83	4600		
Ta		n.a.	9.3	10	n.a.	n.a.	n.a.	n.a.		n.a.	n.a.		
Sn		n.a.	28	45	n.a.	n.a.	260	n.a.		n.a.	n.a.		
Y		n.a.	14	384	2200	7900	3250	16000		292	n.a.		11400
La		n.a.	1.0	2.9	379	615	n.a.	12100		0.1	n.a.		
Ce		n.a.	3.0	4.9	757	10993	130	26200		0.7	n.a.		82700
Pr		n.a.	2.5	0.8	93	119	n.a.	n.a.		0.1	n.a.		
Nd		n.a.	6.2	6.8	387	397	n.a.	10100		0.9	n.a.		
Sm		n.a.	4.9	10	114	107	n.a.	2800		0.7	n.a.		
Eu		n.a.	0.9	0.8	8	10	n.a.	n.a.		1.4	n.a.		
Gd		n.a.	6.0	23	175	169	n.a.	2900		1.4	n.a.		
Tb		n.a.	4.6	5.0	24	27	n.a.	n.a.		1.3	n.a.		
Dy		n.a.	9.0	39	267	275	n.a.	n.a.		30	n.a.		
Ho		n.a.	7.2	11	88	87	n.a.	n.a.		18	n.a.		
Er		n.a.	8.7	48	309	313	640	n.a.		164	n.a.		
Tm		n.a.	9.9	5.0	49	51	n.a.	n.a.		73	n.a.		
Yb		n.a.	7.1	95	282	253	1550	n.a.		1039	n.a.		
Lu		n.a.	4.4	16	34	31	n.a.	n.a.		146	n.a.		
Σ REE		n.a.	*89*	*652*	*5165*	*21347*	*5570*	*70100*		*1768.6*	n.a.		*94100*
Pb		n.a.	7.1	50	n.a.	n.a.	n.a.	n.a.		3.4	n.a.		
Th		n.a.	1.6	5.3	n.a.	n.a.	n.a.	n.a.		35	n.a.		
U		n.a.	8.5	63	n.a.	n.a.	2970	n.a.		n.a.	n.a.		
Hf		n.a.	3900	4170	4400	4100	3160	1300		4133	n.a.		
Total		*89.88*	*89.42*	*88.82*	*91.83*	*89.67*	*93.15*	*97.95*		*86.6*	*92.12*	*100.00*	*100.88*

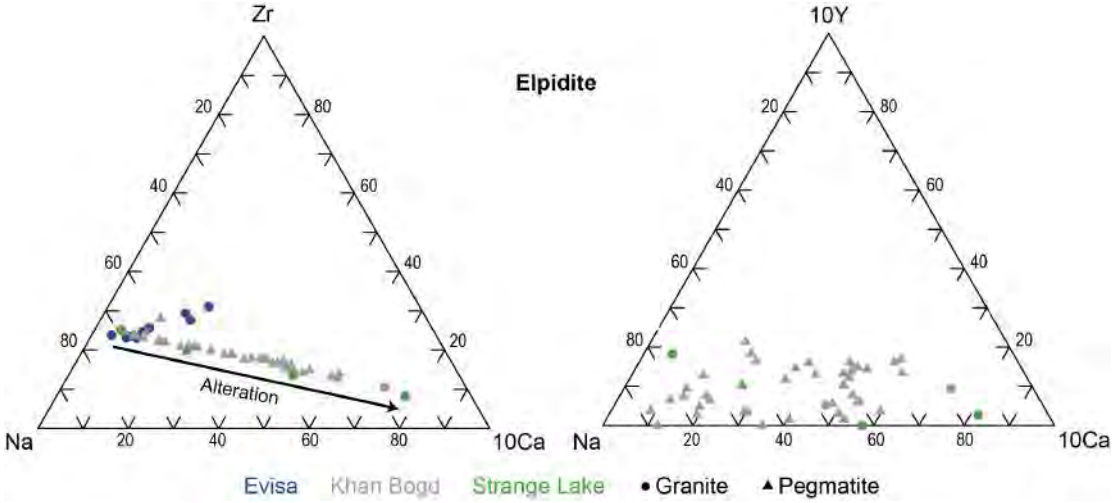

Figure 3.10 Ternary diagrams of elpidite at the complexes where it occurs as primary, namely, Evisa, Khan Bogd and Strange Lake. Data are from this study as well as from Bonin (1988); Kynicky et al. (2011); Roelofsen and Veblen (1999); Salvi and Williams-Jones (1995); Vasyukova and Williams-Jones (2019). Elements are in apfu normalized to 100 %. Y was not measured in elpidite from Evisa. Coefficients were added for some elements for a better visualization of the data; global tendencies are unaffected

3.4 Pseudomorphs and secondary REE-bearing minerals

3.4.1 Presentation of pseudomorphs found in the six alkaline complexes

In this study, a pseudomorph is intended as an assemblage of secondary minerals replacing an earlier mineral of which it has retained the shape. Pseudomorphs are usually recognized by the high quantity of crystals in a small zone confined by sharp boundaries which are interpreted as the edges of the original crystal. Pseudomorphs are acknowledged as the sign of hydrothermal alteration as they contain a high variety of minerals and can be connected by fractures throughout the rock (e.g. Estrade et al., 2014b; Kynicky et al., 2011; Salvi and Williams-Jones, 1990; e.g. Fig 3.11f for fractures). Based on the mineral replaced as well as on the secondary mineralogy, three main types of pseudomorphs were found in the six studied complexes: (1) after Na-amphibole, (2) complex mineralogy after the primary zirconosilicate, and (3) zircon and quartz after the primary zirconosilicate. They occur in granites as much as in pegmatites. At Strange

Lake, a fourth type was found, after narsarsukite (Salvi and Williams-Jones, 1995); and at Amis, the granitic sample SOS073 contains biotite-bearing pseudomorphs of an unknown origin. More details about pseudomorphs in all six studied complexes are given in the following sections.

3.4.1.1 Pseudomorphs after primary zirconosilicates

All six studied complexes contain, or used to contain, a primary zirconosilicate, namely elpidite or EGM. These are now partially or totally replaced by an assemblage of secondary minerals. The assemblage is made of two to tens of minerals forming a dark cluster unidentifiable under the microscope.

Assemblages regrouping an important quantity of different minerals were found in the Malagasy complexes replacing EGM (Fig 3.11a,b), at Evisa after elpidite (Fig 3.11c,d), and at Amis after an unknown zirconosilicate (Fig 3.11e,f). At Amis, pseudomorphs of this type were only found in sample SOS073, a fluorite-bearing granite which was collected from a river bed (Fig 2.1). Considering its unknown origin, this sample will not be further investigated in this manuscript. This type of pseudomorph occurs as dark alteration spots in the rock (Fig 3.11a,c,e), making their content difficult to analyze based only on optical microscope observations. The wide variety of minerals contained in these pseudomorphs was identified with an SEM-EDS. Secondary phases are generally much smaller than the original one (Fig 3.11b,d,f). They include silicates (e.g. quartz, britholite-(Ce, Y), zircon, vlasovite, calciohilairite, etc), halides (fluorite), phosphates (monazite-(Ce), xenotime-(Y)), carbonates (e.g. bastnäsite-(Ce), parasite-(Ce), etc), and oxides (e.g. aeschynite-(Ce, Y), hematite, etc). Amorphous phases can also be present, such as the unknown CaKZrSi phase on Fig 3.11b.

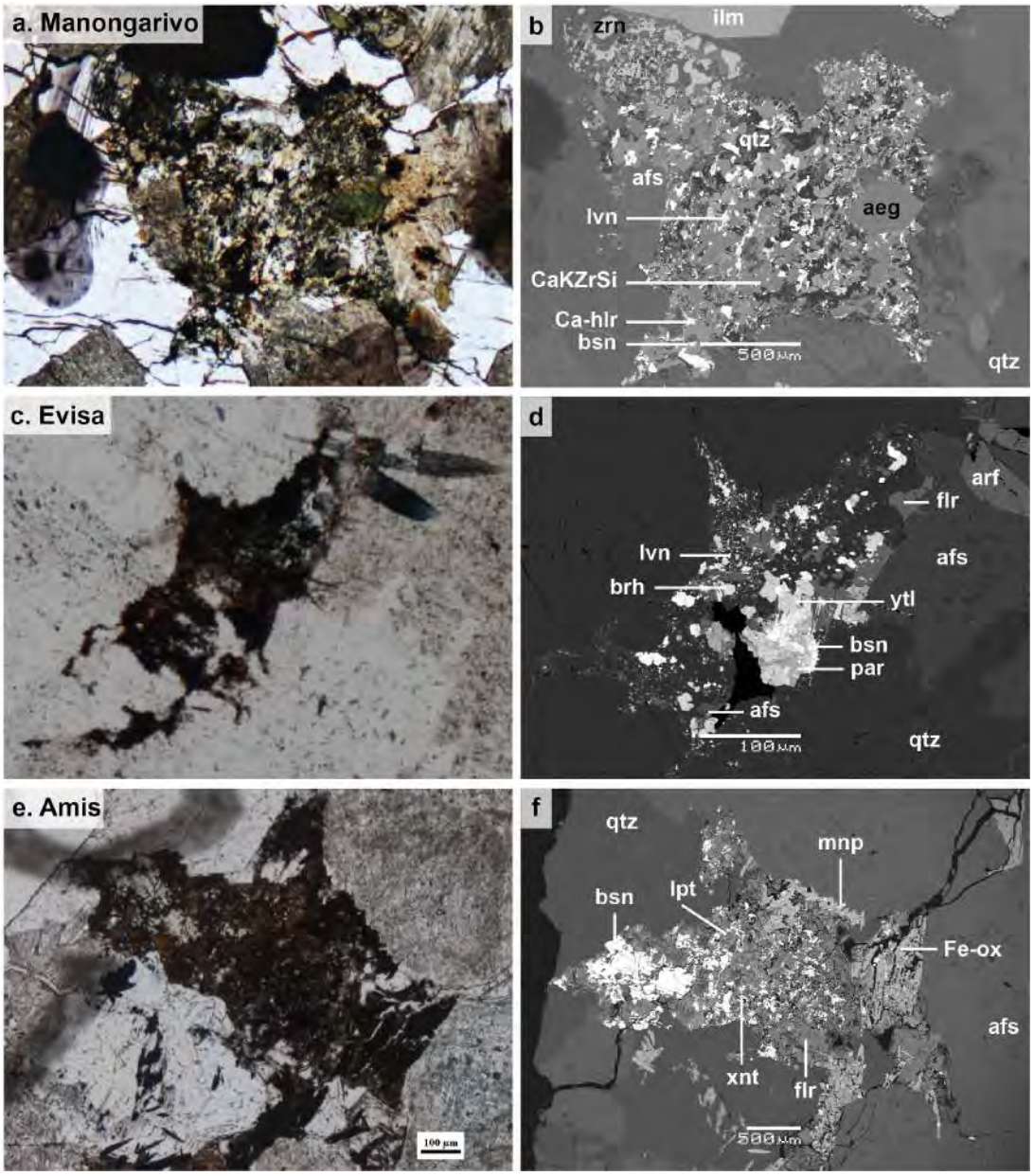

Figure 3.11 Photographs of complex pseudomorphs after a magmatic zirconosilicate. (a), (c) and (e) are PPL views, (b), (d) and (f) are BSE-SEM images. (a), (b) Pseudomorph after EGM, Manongarivo (689); (c), (d) Pseudomorph after elpidite, Evisa (EV1804C); (e), (f) Pseudomorph after an unknown zirconosilicate, Amis (SOS073). Abbreviations: ilm : ilmenite ; qtz : quartz ; afs : alkali feldspar ; aeg : aegirine ; bsn : bastnäsite-(Ce); brh: britholite-(Ce); arf: arfvedsonite; Ca-hlr: calciohilairite; flr: fluorite; par: parisite-(Ce); xnt: xenotime-(Y); lvn: låvenite; ytl: yttrialite-(Y); lpt: laptevite-(Ce); mnp: maoniupingite-(Ce)

Pseudomorphs containing mainly calcic zirconosilicates and quartz were exclusively observed in two complexes where the primary zirconosilicate is elpidite, namely, Strange Lake and Khan Bogd (but not Evisa). The calcic zirconosilicates are mostly gittinsite and, less commonly, armstrongite. The REE content in armstrongite

and gittinsite is highly variable inside a same complex (Fig 3.12). The replacement of elpidite by armstrongite and gittinsite has been well documented in the literature (Gysi et al., 2016; Kynicky et al., 2011; Salvi and Williams-Jones, 1995) and occurs according to the following reactions:

$$Na_2ZrSi_6O_{15} \cdot 3H_2O + Ca + 5H_2O \rightarrow CaZrSi_2O_7 + 2Na + 4H_4SiO_4 \tag{3.1}$$

i.e.

$$elpidite + Ca + 5H_2O \rightarrow gittinsite + 2Na + 4H_4SiO_4 \tag{3.2}$$

or

$$Na_2ZrSi_6O_{15} \cdot 3H_2O + Ca \rightarrow CaZrSi_6O_{15} \cdot 3H_2 + 2Na \tag{3.3}$$

i.e.

$$elpidite + Ca \rightarrow armstrongite + 2Na \tag{3.4}$$

At Strange Lake, in most of the altered rocks the replacement is complete and dominated by gittinsite (Fig 3.13b-d; Tab 3.5), where it occurs under PPL as dark-green rosettes grouped in the boat-shaped legacy of elpidite; whereas at Khan Bogd, elpidite is only partially altered, mostly to dark-pink anhedral armstrongite (Tab 3.5) and zircon and quartz towards the core (Fig 3.9a-d). Armstrongite and gittinsite at Strange Lake are richer in HREE than the other complexes (Tab 3.5). Evidence for partial alteration of elpidite, involving armstrongite as an intermediate phase, has been discussed by Salvi and Williams-Jones (1995) at Strange Lake (Tab 3.5). In order to form quartz, reaction 3.1 would for example need to be turned into reaction 3.5:

$$Na_2ZrSi_6O_{15} \cdot 3H_2O + Ca \rightarrow CaZrSi_2O_7 + 2Na + 4SiO_2 + 3H_2O \tag{3.5}$$

i.e.

$$elpidite + Ca \rightarrow gittinsite + 2Na + 4SiO_2 + 3H_2O \tag{3.6}$$

which, based on molar volume of the interacting minerals, would lead to a significant volume reduction, forming pore space which is not observed. Hence, Salvi and Williams-Jones (1995) concluded the quartz precipitated somewhat later, directly from the circulating fluid. Reaction 3.1, producing silica in its dissolved form, could be a source for this quartz. In the presence of this kind of Ca-,

Zr-dominated pseudomorph, it is therefore possible to assert that the replaced mineral was elpidite, even if there is no crystal left in the rock. Consequently, the absence of such secondary mineral assemblages in pseudomorphs at Amis could indicate that the primary zirconosilicate was not elpidite. Considering only elpidite and EGM were reported as primary zirconosilicates in alkaline complexes, both SiO_2-saturated and undersaturated (e.g. at Ilímaussaq, Marks and Markl, 2015), it is likely that the primary zirconosilicate at Amis was EGM.

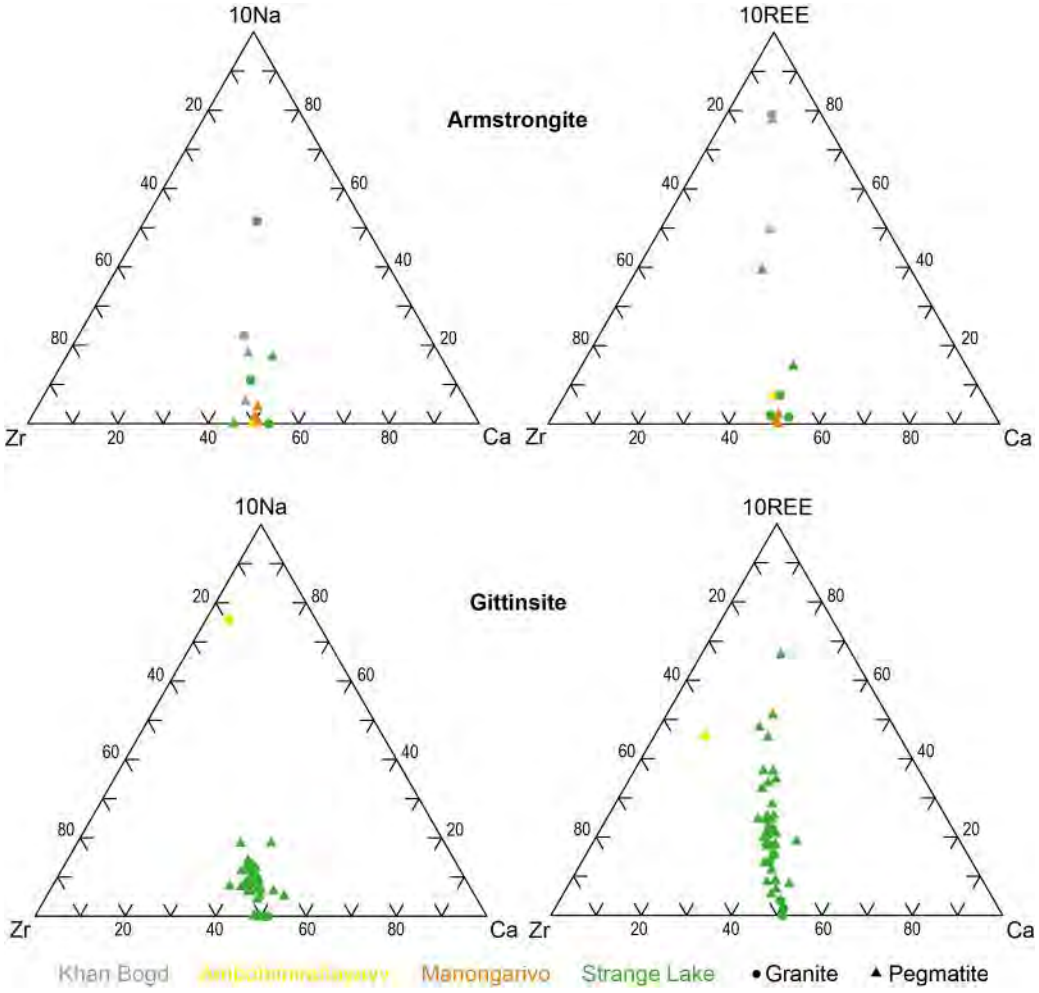

Figure 3.12 Ternary diagrams of armstrongite and gittinsite at the complexes where they were reported, namely, Khan Bogd, Ambohimirahavavy, Manongarivo and Strange Lake. Data are from this study as well as from Estrade et al. (2018); Gysi et al. (2016); Kynicky et al. (2011); Roelofsen and Veblen (1999); Salvi and Williams-Jones (1995). Elements are in apfu normalized to 100 %. Coefficients were added for some elements for a better visualization of the data; global tendencies are unaffected

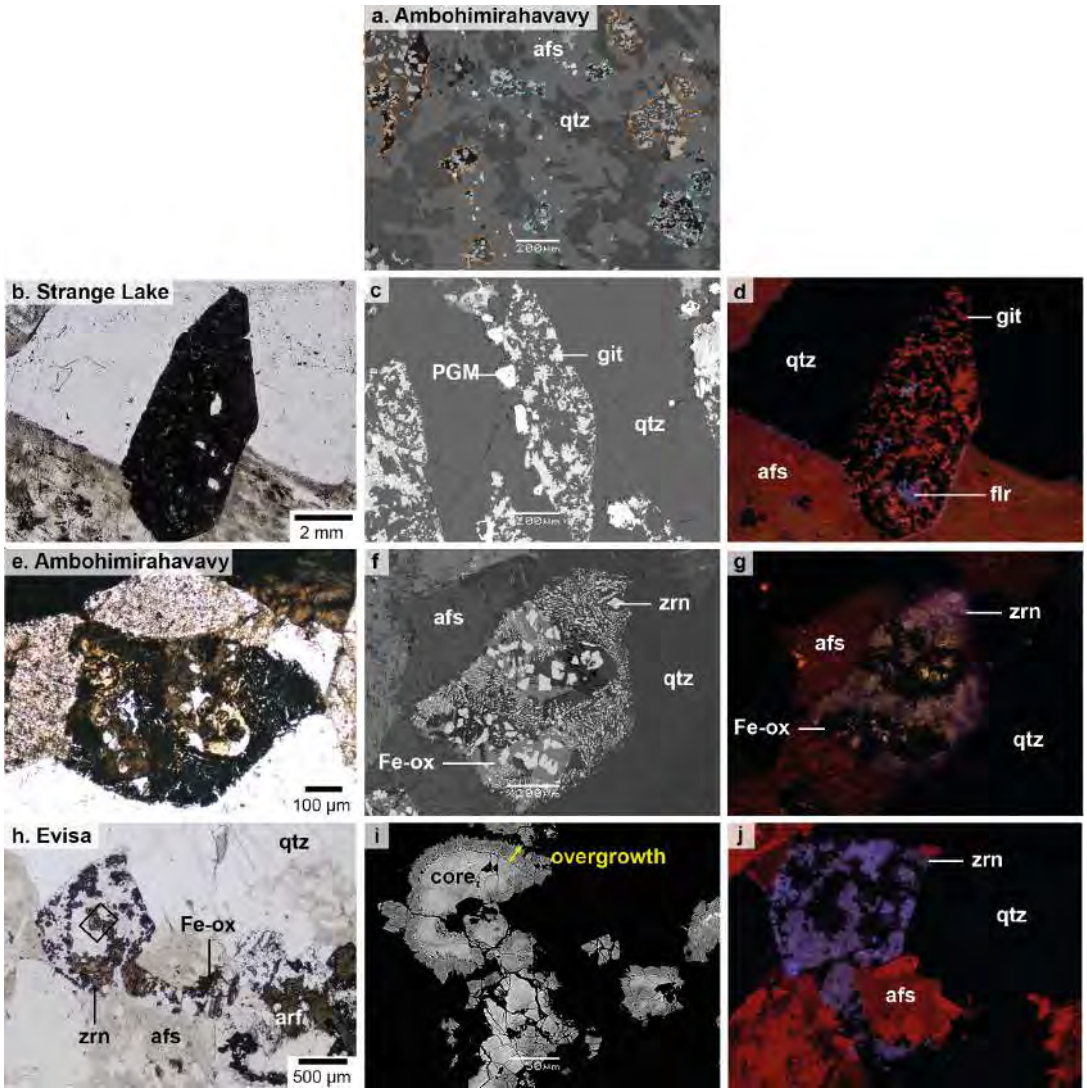

Figure 3.13 Photographs of zirconosilicates and quartz pseudomorphs after a magmatic zirconosilicate. (b), (e) and (h) are plain polarized light (PPL) views, (a), (c), (f) and (i) are BSE-SEM images, and (d), (g), (j) are CL photographs. (a) A general view of pseudomorphs at Ambohimirahavavy (AM113A1); main pseudomorphs are circled in blue if they contain many phases, and in orange if they contain only zircon and quartz; (b), (c), (d) Gittinsite and quartz pseudomorphs after elpidite at Strange Lake (SL1-20); (e), (f), (g) Pseudomorph made of quartz and dendritic and euhedral zircon, Ambohimirahavavy (AMJ05); (h), (i), (j) Pseudomorph made of quartz and zircon with overgrowths, Evisa (EV1812). Abbreviations: git: gittinsite; afs: alkali feldspar; qtz: quartz; pcl: pyrochlore group minerals; zrn: zircon; flr: fluorite

The gittinsite pseudomorphs at Strange Lake can also locally contain Fe-oxides and fluorite (Gysi and Williams-Jones, 2013; Miller, 1996; Fig 3.14c-f). Fluorite was also found in zircon and quartz pseudomorphs at Evisa. If present, fluorite is zoned under CL from blue to purple (Fig 3.14). Luminescence in fluorite is caused by the presence of REE. A blue luminescence is attributed to LREE, while a purple

one is linked to the presence of HREE, and mostly Dy^{3+} and Tb^{3+}. At Strange Lake, Vasyukova and Williams-Jones (2016, 2019) inferred from the composition of one fluid inclusion with many solids that fluorite crystallized from a fluoride melt that separated from a silicate melt. This fluoride-silicate melt immiscibility would have occurred early in the emplacement of the pluton. The fluoride melt crystallized after the silicate one, forming fluorbritholite-(Ce) and fluorite. Finally, an aqueous fluid exsolved from the silicate melt altered the inclusion, dissolving previously formed minerals and replacing fluorbritholite-(Ce) with fluocerite-(Ce), bastnäsite-(Ce), gagarinite-(Y) and fluorite. Considering the affinity of the REE for F in aqueous fluids (Migdisov et al., 2016), this late alteration is likely to have contributed to mobilization and local concentration of the REE at Strange Lake. Fluorite observed in all complexes of this study is purple in its core, and has lighter blue, altered rims (Fig 3.14). With these considerations in mind, it is possible to conclude that light blue fluorite crystallized after the purple one, during the dissolution-reprecipitation hydrothermal episode described by Vasyukova and Williams-Jones. Hence, the first generation of fluorite is enriched in HREE, while the second generation is richer in LREE.

Both EGM and elpidite can also be replaced by an assemblage made exclusively of zircon and quartz. These pseudomorphs can coexist with pseudomorphs made of many phases (Fig 3.13a). Zircon in these pseudomorphs can be euhedral or dendritic, locally in the same pseudomorph (Fig 3.13e-g). At Evisa, ternary zircon was even observed with overgrowths on top of secondary euhedral zircon crystals (Fig 3.13h-j). Considering zircon can be primary as well as occur in pseudomorphs and incorporate a significant amount of REE, it documents REE enrichment throughout the complexes emplacement. Hence, a more detailed study is provided in Chapter 4.

Table 3.5 Analyses of secondary zirconosilicates, from this study as well as the literature of the six studied complexes if they exist. Results presented for this study were acquired with. Data from Webmineral are presented for comparison. n.a.: not analyzed; b.d.l.: below the detection limit ("Armstrongite", 2020; "Calciohilairite", 2020; Estrade et al., 2018; "Gittinsite", 2020; Gysi et al., 2016; Kynicky et al., 2011; "Vlasovite", 2020)

Complex	Amis	Evisa	Khan Bogd		Ambohimirahavavy			Manongarivo				Strange Lake						Reference			
Mineral			Armstrongite	Gittinsite	Armstrongite	Gittinsite	Vlasovite	Armstrongite	Altered armstrongite	Calciohilairite	Mn-Calciohilairite	Armstrongite	Gittinsite	Gittinsite	Calciohilairite	Vlasovite	Unknown	Armstrongite	Gittinsite	Calciohilairite	Vlasovite
Source			Kynicky et al. (2011)	Kynicky et al. (2011)	Estrade et al. (2018)	Estrade et al. (2018)	This work	This work	This work	This work	This work	Gysi et al. (2016)	This work	Gysi et al. (2016)	This work	Gysi et al. (2016)	This work	Webmin	Webmin	Webmin	Webmin
Analyzes #			7	7	10	4	1	3	5	11	4	3	43	28	4	29	4				
Rock type			Pegmatite	Pegmatite	Pegmatite	GR-III	Pegmatite	Pegmatite	Pegmatite	Pegmatite	Pegmatite	Pegmatite	Pegmatite	Pegmatite	Granite	Granite	Granite				
Major (wt%)																					
SiO_2			59.48	40.07	40.28	63.63	59.27	60.98	61.67	44.32	39.38	60.00	36.00	39.37	42.14	55.30	50.02	60.71	40.13	43.58	56.48
ZrO_2			19.24	39.58	33.29	19.70	28.13	19.74	17.00	28.98	32.92	19.00	33.26	36.57	32.02	27.70	18.34	20.75	41.15	29.79	28.96
CaO			8.13	16.76	14.98	2.36	0.02	9.26	3.82	13.17	12.85	7.26	13.01	17.50	5.18	b.d.l.	3.83	9.44	18.73	13.56	
Na_2O			0.05	0.15	b.d.l.	2.60	13.58	0.02	0.09	0.03	b.d.l.	b.d.l.	0.11	b.d.l.	1.37	13.60	1.03				14.56
TiO_2			0.03	0.11	b.d.l.	b.d.l.	0.11	0.06	0.04	0.07	0.21	0.12	0.09	0.07	0.15	b.d.l.	3.75				
Al_2O_3			n.a.	n.a.	1.11	b.d.l.	0.02	0.27	0.07	0.19	0.58	0.70	0.22	0.14	0.07	b.d.l.	0.20				
K_2O			0.06	0.06	b.d.l.	b.d.l.	0.08	0.05	n.a.	0.03	n.a.	b.d.l.	0.04	b.d.l.	0.10	0.11	0.14				
FeO total			0.34	0.45	1.13	0.14	1.12	0.24	0.06	0.08	0.27	0.16	0.82	0.31	2.33	0.03	1.15				
MnO			0.04	0.05	1.37	b.d.l.	0.07	0.14	0.07	0.04	4.12	0.06	1.41	0.72	0.29	b.d.l.	0.11				
MgO			n.a.	n.a.	n.a.	n.a.	0.02	0.01	n.a.	0.01	n.a.	n.a.	0.22	n.a.	0.03	n.a.	0.18				
F			n.a.	n.a.	n.a.	n.a.	n.a.	n.a.	n.a.	n.a.	n.a.	4.94	n.a.	0.10	n.a.	0.16	n.a.				
Cl			n.a.	n.a.	b.d.l.	b.d.l.	n.a.	n.a.	n.a.	n.a.	n.a.	n.a.	n.a.	n.a.	n.a.	n.a.	n.a.				
H_2O			n.a.	n.a.	n.a.	n.a.	n.a.	n.a.	n.a.	n.a.	n.a.	n.a.	n.a.	n.a.	n.a.	n.a.	n.a.	9.10		13.07	
Trace (ppm)																					
Nb_2O_5			n.a.	n.a.	b.d.l.	b.d.l.	b.d.l.	1443	3326	975	2850	890	12605	2567	825	b.d.l.	5680				
Ta_2O_5			n.a.	n.a.	n.a.	n.a.	b.d.l.	b.d.l.	n.a.	b.d.l.	n.a.	n.a.	b.d.l.	n.a.	b.d.l.	n.a.	b.d.l.				
SnO			n.a.	n.a.	n.a.	n.a.	770	1083	1020	0	1540	n.a.	5615	n.a.	2388	n.a.	1457				
Y_2O_3			3700	4900	1900	14400	b.d.l.	b.d.l.	23368	711	9492	14200	22220	1600	16563	b.d.l.	3640				
La_2O_3			1992	519	b.d.l.	b.d.l.	n.a.	n.a.	n.a.	n.a.	n.a.	b.d.l.	n.a.	433	n.a.	b.d.l.	n.a.				
Ce_2O_3			3778	963	2200	b.d.l.	400	330	n.a.	219	n.a.	1500	4579	1233	608	b.d.l.	4585				
Pr_2O_3			364	104	n.a.	n.a.	n.a.	n.a.	n.a.	n.a.	n.a.	n.a.	n.a.	n.a.	n.a.	n.a.	n.a.				
Nd_2O_3			1503	321	1900	n.a.	n.a.	b.d.l.	520	1025	2610	1300	1474	167	547	b.d.l.	630				
Sm_2O_3			386	96	b.d.l.	b.d.l.	n.a.	n.a.	n.a.	n.a.	n.a.	80	n.a.	b.d.l.	n.a.	b.d.l.	n.a.				
Eu_2O_3			10	8	n.a.	n.a.	n.a.	n.a.	n.a.	n.a.	n.a.	b.d.l.	n.a.	533	n.a.	b.d.l.	n.a.				
Gd_2O_3			355	101	b.d.l.	b.d.l.	n.a.	390	1510	648	b.d.l.	1700	2535	b.d.l.	1970	b.d.l.	920				
Tb_2O_3			36	17	n.a.	n.a.	n.a.	n.a.	n.a.	n.a.	n.a.	n.a.	n.a.	n.a.	n.a.	n.a.	n.a.				
Dy_2O_3			445	181	n.a.	n.a.	n.a.	b.d.l.	300	250	12110	3600	9082	b.d.l.	657	b.d.l.	2480				
Ho_2O_3			117	60	n.a.	n.a.	n.a.	n.a.	n.a.	n.a.	n.a.	n.a.	n.a.	n.a.	n.a.	n.a.	n.a.				
Er_2O_3			394	246	n.a.	n.a.	n.a.	440	1845	425	950	2200	5221	333	1117	b.d.l.	n.a.				
Tm_2O_3			63	47	n.a.	n.a.	n.a.	n.a.	n.a.	n.a.	n.a.	n.a.	n.a.	n.a.	n.a.	n.a.	n.a.				
Yb_2O_3			485	300	n.a.	n.a.	n.a.	b.d.l.	5640	b.d.l.	2510	2500	7571	1300	623	b.d.l.	b.d.l.				
Lu_2O_3			63	31	n.a.	n.a.	n.a.	n.a.	n.a.	n.a.	n.a.	b.d.l.	n.a.	400	n.a.	b.d.l.	n.a.				
Σ REO			*13691*	*7892*	*6000*	*14400*	*400*	*1160*	*33183*	*3278*	*27672*	*27080*	*52682*	*5999*	*22085*		*12255*				
PbO			n.a.	n.a.	11500	b.d.l.	b.d.l.	b.d.l.	514	110	3565	n.a.	6307	n.a.	3860	n.a.	64395				
ThO_2			n.a.	n.a.	n.a.	n.a.	n.a.	253	b.d.l.	610	258	n.a.	440	n.a.	1553	n.a.	673				
UO_2			n.a.	n.a.	b.d.l.	b.d.l.	n.a.	540	1502	115	88	n.a.	1074	n.a.	630	n.a.	1038				
HfO_2			6400	8200	8300	3200	n.a.	n.a.	n.a.	n.a.	n.a.	4400	n.a.	10000	n.a.	6900	n.a.				
P_2O_5			n.a.	n.a.	n.a.	n.a.	n.a.	n.a.	n.a.	n.a.	n.a.	500	n.a.	20	n.a.	b.d.l.	n.a.				
Total			*89.38*	*98.84*	*94.74*	*90.19*	*102.54*	*91.23*	*86.77*	*87.41*	*93.93*	*95.48*	*93.05*	*96.63*	*86.81*	*97.59*	*87.30*	*100.00*	*100.01*	*100.00*	*100.00*

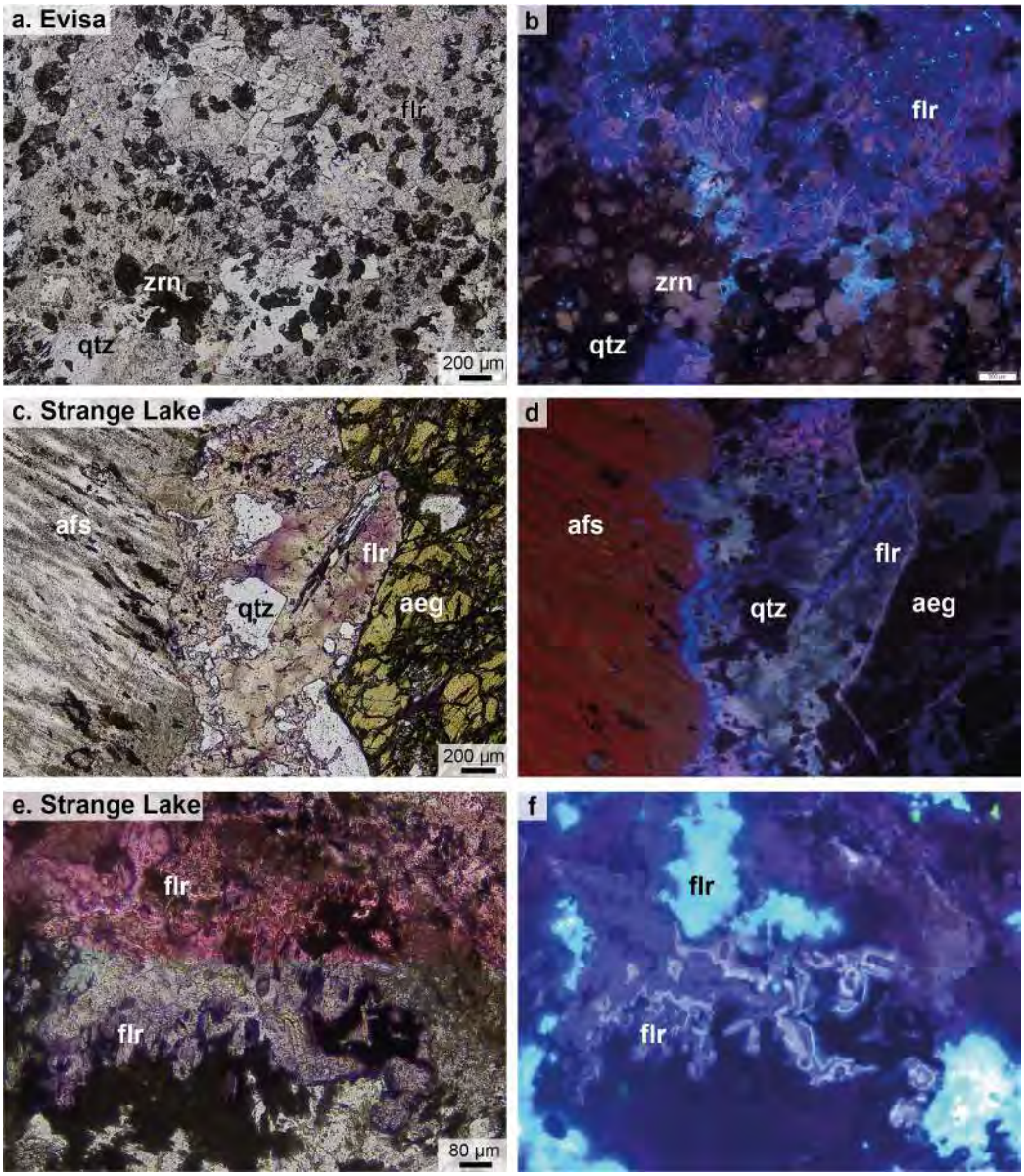

Figure 3.14 Zonations of fluorite in 2 complexes. (a), (c), and (e) are PPL views, (b), (d), and (f) are CL images. (a), (b) Fluorite in a zircon + quartz pseudomorph at Evisa (EV1823B); (c), (d) Fluorite in a pegmatite from Strange Lake (SL1-20); (e), (f) Zoned fluorite in a pegmatite from Strange Lake (TTR20). Abbreviations: qtz: quartz; afs: alkali feldspar; zrn: zircon; flr: fluorite

3.4.1.2 Pseudomorphs after primary minerals other than zirconosilicates

Pseudomorphs can also form after other minerals than zirconosilicates in the same rocks than pseudomorphs after zirconosilicates. They were found to form after amphibole in all complexes, and after narsarsukite ($Na_2(Ti,Fe)Si_4(O,F)_{11}$) at Strange Lake. There are probably other types of pseudomorphs, but the complexities of

these replacements make it very difficult to distinguish them and no study so far has pointed to other types of replacement in these complexes.

Pseudomorphs after amphibole are present in pegmatites and granites of all six complexes, but the nature of the secondary assemblage depends on the primary amphibole. In the studied complexes, arfvedsonite and leakeite are the major amphiboles. In pegmatites, amphiboles are all totally to partially replaced, whereas in granites, both altered and unaltered occurrences can be observed. Arfvedsonite is mainly replaced by an assemblage of aegirine, quartz and Fe- and/or Ti-oxides (magnetite, hematite, ilmenite, titanite, rutile; Fig 3.15a,b). Arfvedsonite is also known to react directly with quartz to form aegirine, but without producing any oxide. The presence of oxides indicates the reaction occurring is more likely similar to:

$$Na_3Fe_4^{2+}Fe^{3+}Si_8O_{22}(OH)_2 + 2H_2O \rightarrow 9NaFe^{3+}Si_2O_6 + 2Fe^{2+}Fe_2^{3+}O_4 + 6SiO_2 + 5H_2 \tag{3.7}$$

i.e.

$$arfvedsonite + 2H_2O \rightarrow 9aegirine + 2magnetite + 6quartz + 5H_2 \tag{3.8}$$

(Salvi and Williams-Jones, 1996). The intervention of a fluid is therefore necessary to produce those pseudomorphs. In addition to the main minerals, zircon, fluorite, sphalerite and REE-bearing minerals (bastnäsite-(Ce), britholite-(Y), parisite-(Ce)) were punctually found in the complexes. In most cases, leakeite, which contains less iron than arfvedsonite, is not replaced by aegirine, but rather by an assemblage of Fe- and/or Ti-oxides, fluorite, and/or REE-bearing minerals such as aeschynite-(Y). Titanium-oxides in these pseudomorphs are present in low amounts ($\leq$ 1 %, Fig 3.15c-f), but their presence can be surprising considering there is no primary Ti-bearing mineral. From Fig 3.15d, it is possible to estimate total TiO_2 in the primary amphibole and compare it with total TiO_2 in Ti-oxides, in order to understand the source for Ti. Personal EPMA analyses give an average of 0.62 % TiO_2 in leakeite from Evisa. Considering titanite forms approximatively 1 % of the pseudomorph and contains 30.29 % TiO_2 on average ("Titanite", 2020), the total TiO_2 required to make titanite in a pseudomorph is 0.01 x 30.29 = 0.31 % TiO_2. Hence, TiO_2 in secondary titanite is likely to originate from the primary leakeite. In this example at Evisa, a half of the TiO_2 disappears with the hydrothermal replacement; it is therefore likely that Ti is mobilized by fluids, and this may be the source for Ti-oxides found in pseudomorphs after primary zirconosilicates. In addition, alkali

amphibole can also be replaced by a more calcic amphibole, like ferri-kaersutite (Fig 3.15c,d).

Pseudomorphs with biotite, quartz, zircon and Fe- and/or Ti-oxides were found in the granite SOS066 from Amis (Fig 3.15e,f). No other biotite was found in other samples from Amis, or any of the other complexes, and this sample was collected at a location where the Amis arfvedsonite granite intrudes the Brandberg biotite-hornblende granite (Fig 2.1). Except for biotite instead of aegirine, the assemblage is similar to that of pseudomorphs after arfvedsonite. It is thus possible that the original mineral was also an amphibole, but richer in K, which lead to the formation of biotite instead of aegirine.

As mentioned, narsarsukite was also reported to be a primary magmatic mineral replaced by an assemblage of titanite and quartz. This mineral was only reported at Strange Lake and is replaced according to the reaction:

$$Na_2(Ti_xFe^{3+}_{1-x})Si_4O_{10}(OH,F) + xCa \rightarrow xCaTiSiO_5 + (4-x)SiO_2 + 2Na + (1-x)Fe^{3+} \tag{3.9}$$

i.e.

$$narsarsukite + xCa \rightarrow xtitanite + (4-x)quartz + 2Na + (1-x)Fe^{3+} \tag{3.10}$$

(Gysi et al., 2016; Salvi and Williams-Jones, 1996). Calcium necessary for this reaction was introduced by the late-stage Ca-metasomatism reported at Strange Lake (Gysi et al., 2016; Salvi and Williams-Jones, 1990).

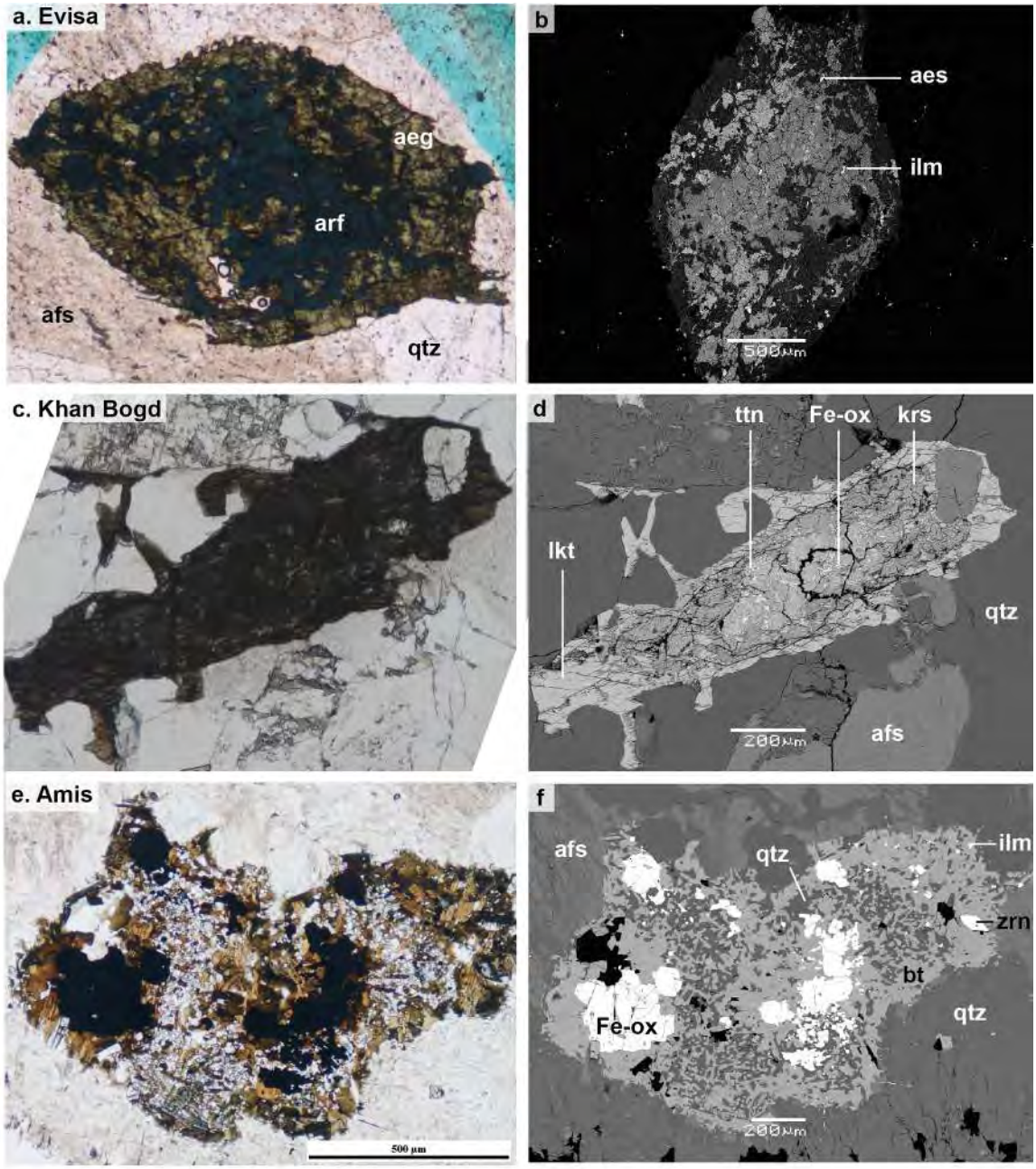

Figure 3.15 Pseudomorphs after primary minerals other than zirconosilicates, found in all six studied alkaline complexes. (a), (c) and (e) are PPL views, and (b), (d) and (f) are SEM images. (a-b) Arfvedsonite replaced by aegirine and Fe-Ti oxides, Evisa (EV1813); (c-d) Leakeite altered to kaersutite and Fe-Ti oxides, Khan Bogd (KB09A); (e-f) Probable K-amphibole pseudomorphosed to biotite, zircon, quartz and Fe- and/or Ti-oxides, Amis (SOS066). Abbreviations: aes: aeschynite-(Y); ilm: ilmenite; lkt: leakeite; ttn: titanite; krs: kaersutite; bt: biotite; qtz: quartz; zrn: zircon; afs: alkali feldspar

3.4.2 Focus on Khan Bogd

At Khan Bogd, in pegmatites, elpidite can be totally replaced by zircon and quartz, replaced only partially in its core, or fresh. Elpidite is first replaced by armstrongite, its calcic mineral equivalent, then by zircon and quartz (Fig 3.9a-d). No remaining elpidite was found in granitic samples, hence analyses were made on elpidite crystals from pegmatites only (Tab3.4). The results show that elpidite does not immediately turn into armstrongite, but becomes more and more calcic (and less and less sodic) with alteration, before being totally replaced. The same observation was made by Kynicky et al. (2011) at Khan Bogd, and by Salvi and Williams-Jones (1995) and Roelofsen and Veblen (1999) at Strange Lake. Roelofsen and Veblen conclude from these observations that there is a solid solution between elpidite and armstrongite, which is confirmed by the crystal chemistry study of Mesto et al. (2014). Analyses listed in Tab 3.4 also highlight the enrichment in REE, and mostly HREE, in altered elpidite from pegmatites. Infrared spectroscopy analyses show that the hydration of elpidite becomes more important with the intensity of alteration (Fig 3.9e-f). This observation confirms that the Ca-, HREE-rich variety of elpidite, observed in the partial replacements, is indeed hydrothermal. Hence, it proves that, at least at Khan Bogd, a Ca-rich hydrothermal fluid was able to mobilize and locally concentrate and fractionate REE.

Another interesting observation is the presence of a Zr-HREE-rich phase, crystallized in thin hairline fractures that form a dense network of cm scale affecting the rocks (Fig 3.16). This texture indicates a secondary, hydrothermal origin for this phase. An attempt was made to analyze its composition by EPMA, but because of its very small size, its occurrence as fractures filling, and its likely hydrated composition, only a partial composition was measured (Fig 3.16d). Although these fractures affect the entire rock, i.e., they cross several minerals, the Zr-REE phase occurs mostly in fractures that are not in quartz (Fig 3.16). In particular, it has been observed in Na-amphibole, alkali feldspar (Fig 3.16a-c), and aegirine (Fig 3.16e-h).

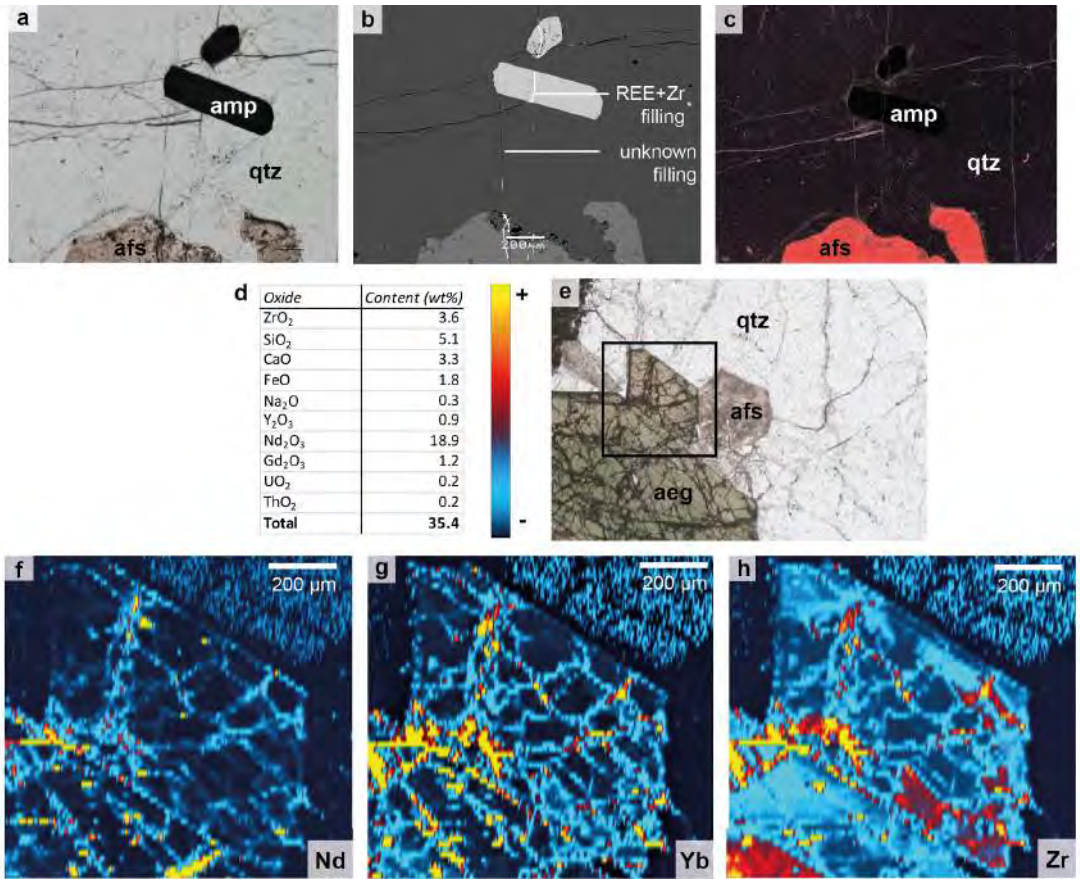

Figure 3.16 Characterization of REE-Zr phase in fractures at Khan Bogd. (a) PPL view of the fractures affecting pegmatite KB02; (b) SEM image of the same zone, the phase is only deposited outside of quartz; (c) CL image of the same zone, a different phase is deposited inside quartz; (d) Partial composition of the phase deposited outside of quartz; (e) PPL view of the fractures affecting pegmatite KB07D, the square shows the position of the following images. (f) Detail of image (e), LA-ICPMS map of Nd; (g) Detail of image (e), LA-ICPMS map of Yb; (h) Detail of image (e), LA-ICPMS map of Zr. The scale is relative inside of a same image only and is indicated by the colorbar next to (c). Abbreviations: amp: amphibole; qtz: quartz; afs: alkali feldspar; aeg: aegirine

It seems that circulating fluid reacted with host minerals to trigger the precipitation of this phase. Given the nature of the different minerals into which the unknown phase precipitated, it is possible that Na was the triggering factor as it is the only element common to alkali amphibole, aegirine, and alkali feldspar, and it is not present where this phase did not precipitate. Nonetheless, the Zr-REE phase was also found in fractures in quartz, although to a much smaller extent, away from the alkali-bearing minerals, suggesting that the fluid transported at least Zr and REE to some distance.

3.5 Mineral paragenesis of the six studied complexes

From the observation of textures, habitus and chemistry of the minerals present in all six complexes, it is possible to infer the following paragenesis for each complex (Fig 3.17 and 3.18). Personal observations were complemented with descriptions in the literature for significant minerals, such as primary zirconosilicates (Bollaert, 2019; Bonin and Platevoet, 1988; Estrade et al., 2014b; Gysi and Williams-Jones, 2013; Kynicky et al., 2011; Salvi and Williams-Jones, 2006; Salvi et al., 2005). The ensemble of the data permits to draw the following conclusions.

(1) Main minerals, namely quartz, alkali feldspar, Na-amphiboles and aegirine, are common to all studied complexes. Despite local variations, many accessory minerals are also common to most of these alkaline complexes. Given the high number of accessory minerals found in the different complexes, this work will emphasis on REE-bearing accessory minerals. Among accessory minerals, PGM are common primary minerals, zircon occurs as primary or secondary, and Fe- and/or Ti-oxides are secondary after amphiboles for the most part. Secondary phases after primary zirconosilicates present a wide variety of chemistries (silicates, oxides, halides, carbonates and phosphates) to be related with their precipitation from a fluid in a pseudomorph. Oxides and phosphates are present in all complexes. Halides are present in smaller quantities at Khan Bogd, which is something to remember for fluid inclusions study as F is known to contribute to REE mobilization in fluids (Migdisov et al., 2016). Ca-carbonate minerals are more present in the complexes where host rocks are calcic, namely, Evisa (calco-alkaline monzogranites), Khan Bogd (calco-alkaline volcanics), and Malagasy complexes (limestones of the Isalo group). Malagasy complexes are the only ones to be hosted exclusively in sediments, and contain less Ti-bearing minerals than the others. Rocks from Evisa also contain more secondary sulfides than the other complexes. Minerals rich in K, Ca are more commonly found in granites, as pegmatites are even more differentiated and therefore depleted in these elements.

(2) The only minerals to grow exclusively on the magmatic stage are Na-amphibole, EGM, elpidite, and feldspars. The zonation in quartz and aegirine records two main events, and feldspars and primary zirconosilicates alteration indicates all these complexes underwent at least one hydrothermal stage. In addition, the wavy-shaped zonation of some quartz crystals at Khan Bogd favors

an unstable environment of crystallization, such as a hydrothermal fluid. Hence, it is likely that quartz and aegirine core grew in equilibrium with the main minerals during the magmatic phase, and their rims overgrew during a later, hydrothermal event. More evidences are provided for aegirine in Chapter 4. This hydrothermal event may have occurred continuously with the magmatic stage at Amis, Evisa and Khan Bogd, and after a break at Ambohimirahavavy and Strange Lake. This would explain the difference of limitation between core and rim.

(3) The composition of pseudomorphs, which are hydrothermal in origin, depends on the nature of the primary mineral. Elpidite is mostly replaced by an agpaitic assemblage of gittinsite and quartz, while pseudomorphs after EGM contain a wide variety of minerals including silicates, halides, oxides, phosphates and carbonates. These two zirconosilicates cannot be found together in a same rock. Both zirconosilicates can also be replaced by a miaskitic assemblage of zircon and quartz. Amphiboles are replaced by another amphibole or by Fe- and/or Ti-oxides with aegirine. Finally, at Strange Lake, narsarsukite is replaced by titanite and quartz. Hence, it is possible to identify the primary mineral, or at least its nature (zirconosilicate if the pseudomorph is made of zircon and quartz), even where it was completely replaced.

(4) Many secondary minerals contain an important quantity of REE (Tab 3.5, 3.6), to be related to the concentration of REE in the primary zirconosilicates (Tab 3.4). Secondary minerals after non-zirconosilicate phases, i.e. after amphibole or narsarsukite, do not contain significant REE concentrations, similarly to the phase they hydrothermally grew from. These observations are in favor of a mobilization only local of the REE by fluids. However, fractures filling and partial replacement of elpidite by a Ca-richer phase at Khan Bogd imply a general fluid circulation process mobilizing and fractionating the REE. Hence, it is possible to assert that hydrothermal alteration locally concentrates the REE in REE-bearing minerals such as bastnäsite-(Ce). The role of hydrothermal fluids in concentrating the REE at the scale of granites and pegmatites needs more study and is discussed in Chapter 4.

(5) Heavy-REE secondary minerals located in pseudomorphs are especially concentrated at Strange Lake and Evisa. The most abundant HREE-minerals are fluorite, britholite-(Y) and kainosite-(Y) at Strange Lake, and britholite-(Y), okanoganite-(Y), yttrialite-(Y) and xenotime-(Y) at Evisa. Secondary minerals usually containing LREE or no REE such as fluorcalciopyrochlore, fluorite, bastnäsite-(Ce), thorite or titanite, can contain significant HREE concentrations

at Amis. Two generations of fluorite are present at Evisa and Strange Lake, the first one being enriched in HREE and the second one in LREE. At least in these complexes, the enrichment in HREE in secondary minerals leaves no doubt as to the role of hydrothermal fluids in fractionating the REE. All secondary phases are clues as to the characteristics of circulating hydrothermal fluids and will need to be taken into account while studying fluid inclusions.

Table 3.6 A summary of the main primary and secondary REE-bearing minerals found in each complex. The description is based on personal observations complemented with descriptions found in the literature. Minerals are sorted from the most to the less abundant. Abbreviations: zrn: zircon; xnt: xenotime-(Y); mnz: monazite-(Ce); bsn: bastnäsite-(Ce); aln: allanite-(Ce); elp: elpidite; chk: chevkinite-(Ce); flr: fluorite; brh: britholite-(Ce); par: parisite; ytl: yttrialite-(Y); arm: armstrongite; ap: fluorapatite; aes: aeschynite-(Ce); git: gittinsite

Complex	Primary REE minerals	Secondary REE minerals
Amis, Namibia	Unknown zirconosilicate, zrn, PGM	zrn, xnt, mnz, bsn, aln
Evisa, Corsica	elp, zrn, PGM, chk, aln	zrn, flr, brh, bn, par, ytl
Khan Bogd, Mongolia	elp, zrn, PGM	arm, zrn, bsn, par, mnz
Ambohimirahavavy, Madagascar	EGM, zrn, PGM, mnz, chk	zrn, bsn, ap, mnz, aln
Manongarivo, Madagascar	EGM, zrn, PGM, mnz, chk	zrn, bsn, aes, mnz
Strange Lake, Canada	elp, PGM, mnz, chk	git, flr, brh

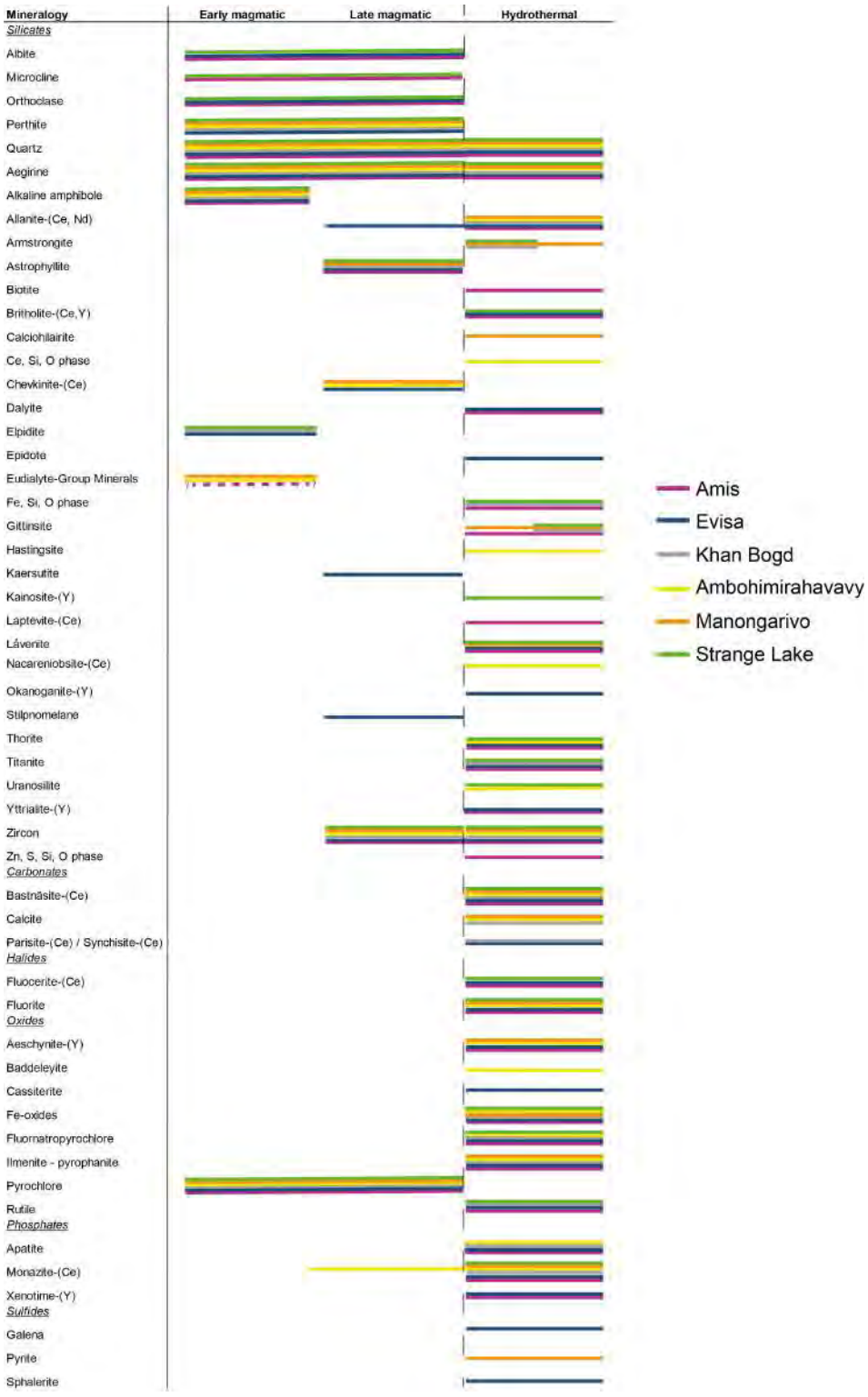

Figure 3.17 Comparison of the paragenesis of all six complexes studied: Amis (Namibia), Evisa (Corsica), Khan Bogd (Mongolia), Ambohimirahavavy (Madagascar), Manongarivo (Madagascar), and Strange Lake (Canada). Paragenesis are based on new observations as well as on existing descriptions (Bollaert, 2019; Bonin and Platevoet, 1988; Estrade et al., 2014b; Gysi and Williams-Jones, 2013; Kynicky et al., 2011; Salvi and Williams-Jones, 2006; Salvi et al., 2005)

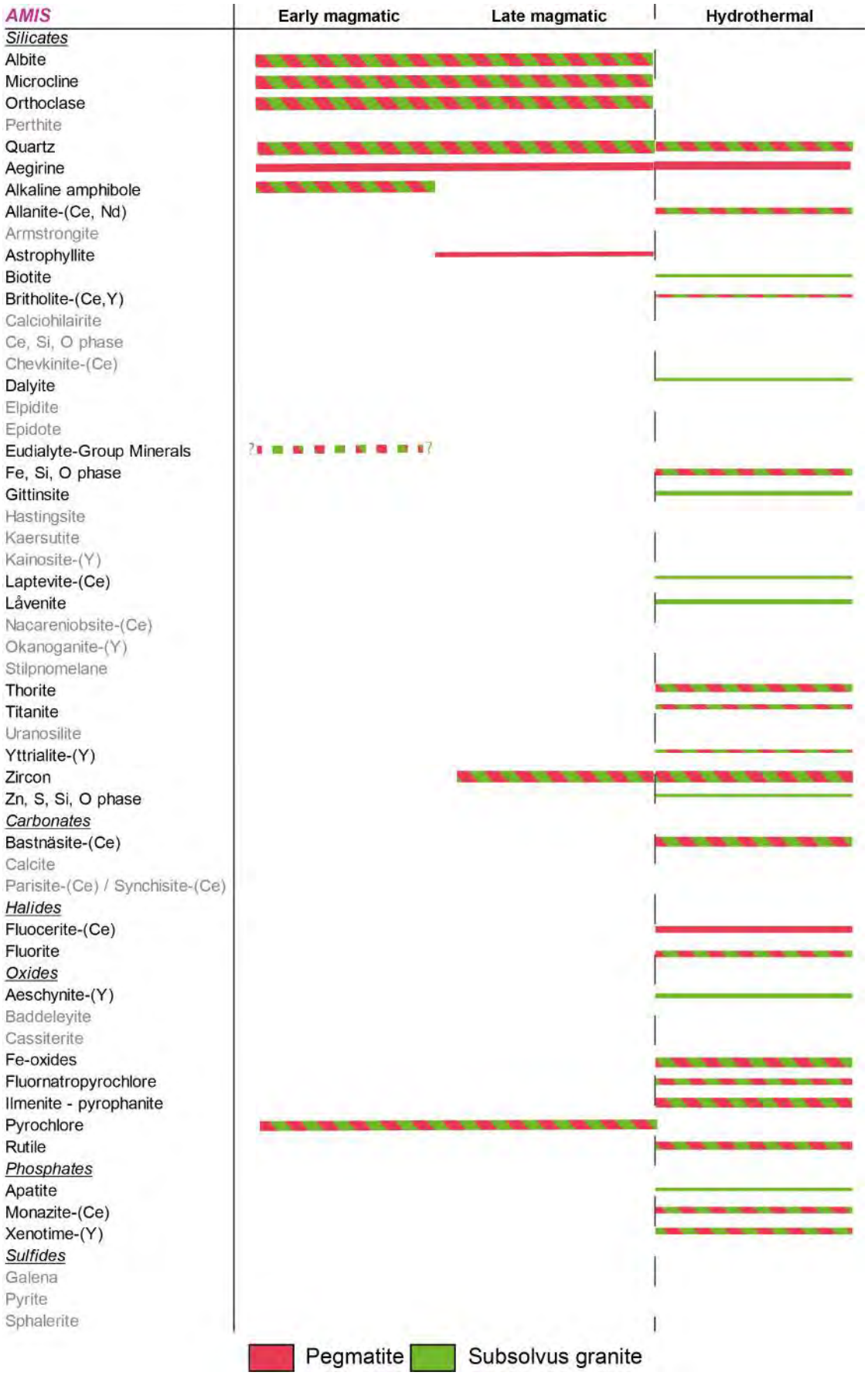
AMIS
Early magmatic
Late magmatic
Hydrothermal
Silicates
Albite
Microcline
Orthoclase
Perthite
Quartz
Aegirine
Alkaline amphibole
Allanite-(Ce, Nd)
Armstrongite
Astrophyllite
Biotite
Britholite-(Ce,Y)
Calciohilairite
Ce, Si, O phase
Chevkinite-(Ce)
Dalyite
Elpidite
Epidote
Eudialyte-Group Minerals
Fe, Si, O phase
Gittinsite
Hastingsite
Kaersutite
Kainosite-(Y)
Laptevite-(Ce)
Låvenite
Nacareniobsite-(Ce)
Okanoganite-(Y)
Stilpnomelane
Thorite
Titanite
Uranosilite
Yttrialite-(Y)
Zircon
Zn, S, Si, O phase
Carbonates
Bastnäsite-(Ce)
Calcite
Parisite-(Ce) / Synchisite-(Ce)
Halides
Fluocerite-(Ce)
Fluorite
Oxides
Aeschynite-(Y)
Baddeleyite
Cassiterite
Fe-oxides
Fluornatropyrochlore
Ilmenite - pyrophanite
Pyrochlore
Rutile
Phosphates
Apatite
Monazite-(Ce)
Xenotime-(Y)
Sulfides
Galena
Pyrite
Sphalerite
Pegmatite
Subsolvus granite

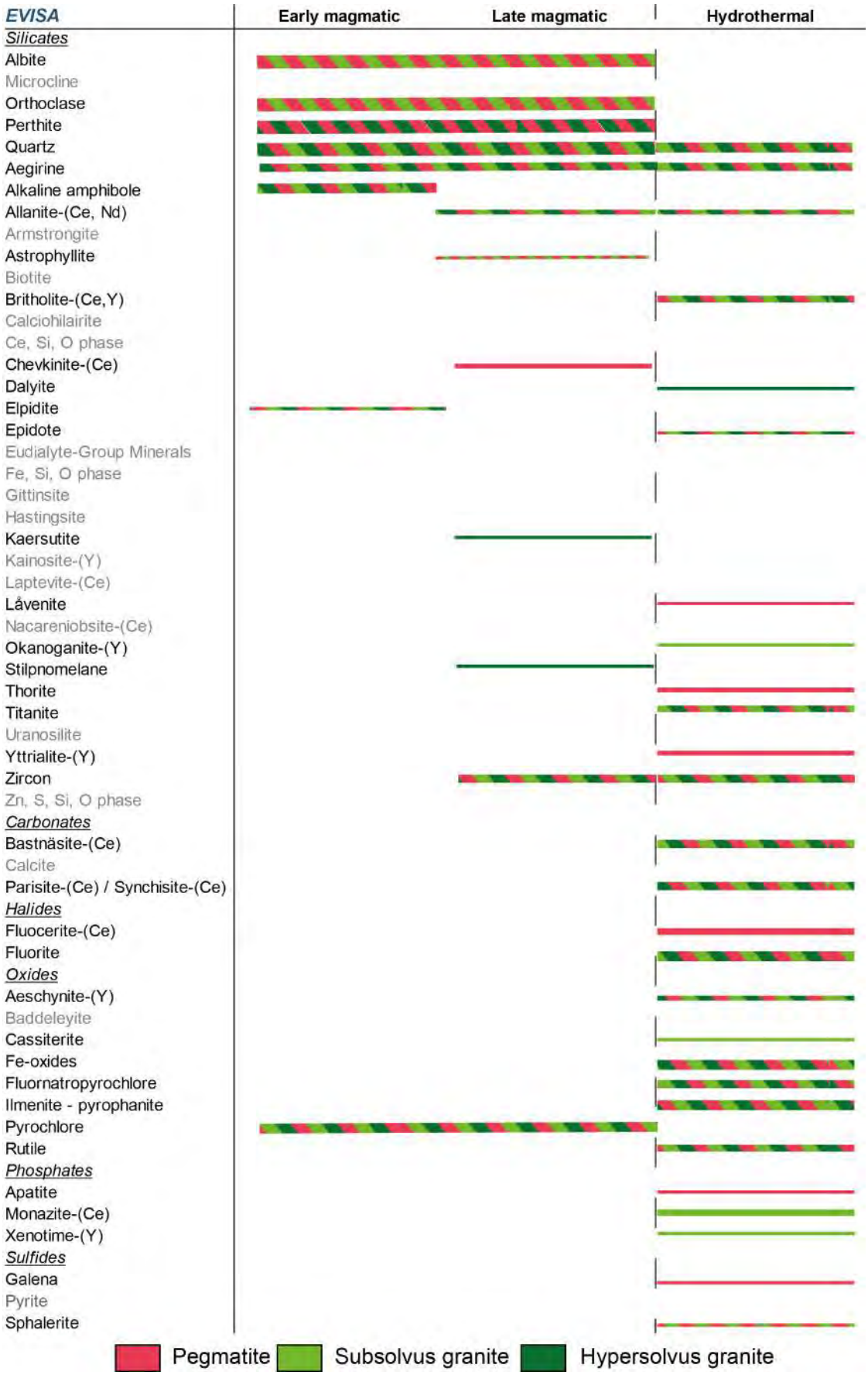
EVISA
Early magmatic
Late magmatic
Hydrothermal
Silicates
Albite
Microcline
Orthoclase
Perthite
Quartz
Aegirine
Alkaline amphibole
Allanite-(Ce, Nd)
Armstrongite
Astrophyllite
Biotite
Britholite-(Ce,Y)
Calciohilairite
Ce, Si, O phase
Chevkinite-(Ce)
Dalyite
Elpidite
Epidote
Eudialyte-Group Minerals
Fe, Si, O phase
Gittinsite
Hastingsite
Kaersutite
Kainosite-(Y)
Laptevite-(Ce)
Låvenite
Nacareniobsite-(Ce)
Okanoganite-(Y)
Stilpnomelane
Thorite
Titanite
Uranosilite
Yttrialite-(Y)
Zircon
Zn, S, Si, O phase
Carbonates
Bastnäsite-(Ce)
Calcite
Parisite-(Ce) / Synchisite-(Ce)
Halides
Fluocerite-(Ce)
Fluorite
Oxides
Aeschynite-(Y)
Baddeleyite
Cassiterite
Fe-oxides
Fluornatropyrochlore
Ilmenite - pyrophanite
Pyrochlore
Rutile
Phosphates
Apatite
Monazite-(Ce)
Xenotime-(Y)
Sulfides
Galena
Pyrite
Sphalerite
Pegmatite
Subsolvus granite
Hypersolvus granite

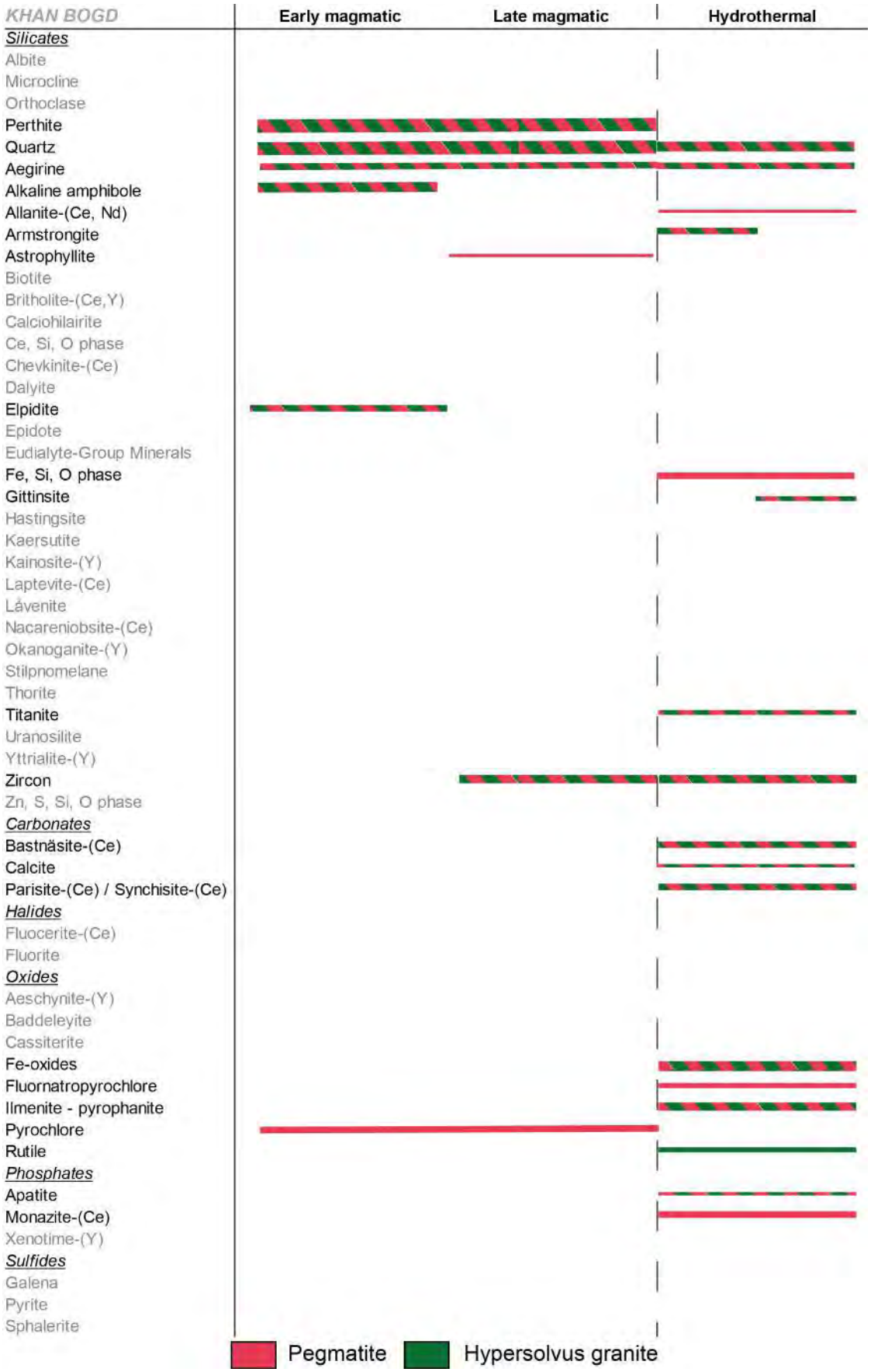
KHAN BOGD
Early magmatic
Late magmatic
Hydrothermal
Silicates
Albite
Microcline
Orthoclase
Perthite
Quartz
Aegirine
Alkaline amphibole
Allanite-(Ce, Nd)
Armstrongite
Astrophyllite
Biotite
Britholite-(Ce,Y)
Calciohilairite
Ce, Si, O phase
Chevkinite-(Ce)
Dalyite
Elpidite
Epidote
Eudialyte-Group Minerals
Fe, Si, O phase
Gittinsite
Hastingsite
Kaersutite
Kainosite-(Y)
Laptevite-(Ce)
Låvenite
Nacareniobsite-(Ce)
Okanoganite-(Y)
Stilpnomelane
Thorite
Titanite
Uranosilite
Yttrialite-(Y)
Zircon
Zn, S, Si, O phase
Carbonates
Bastnäsite-(Ce)
Calcite
Parisite-(Ce) / Synchisite-(Ce)
Halides
Fluocerite-(Ce)
Fluorite
Oxides
Aeschynite-(Y)
Baddeleyite
Cassiterite
Fe-oxides
Fluornatropyrochlore
Ilmenite - pyrophanite
Pyrochlore
Rutile
Phosphates
Apatite
Monazite-(Ce)
Xenotime-(Y)
Sulfides
Galena
Pyrite
Sphalerite
Pegmatite
Hypersolvus granite

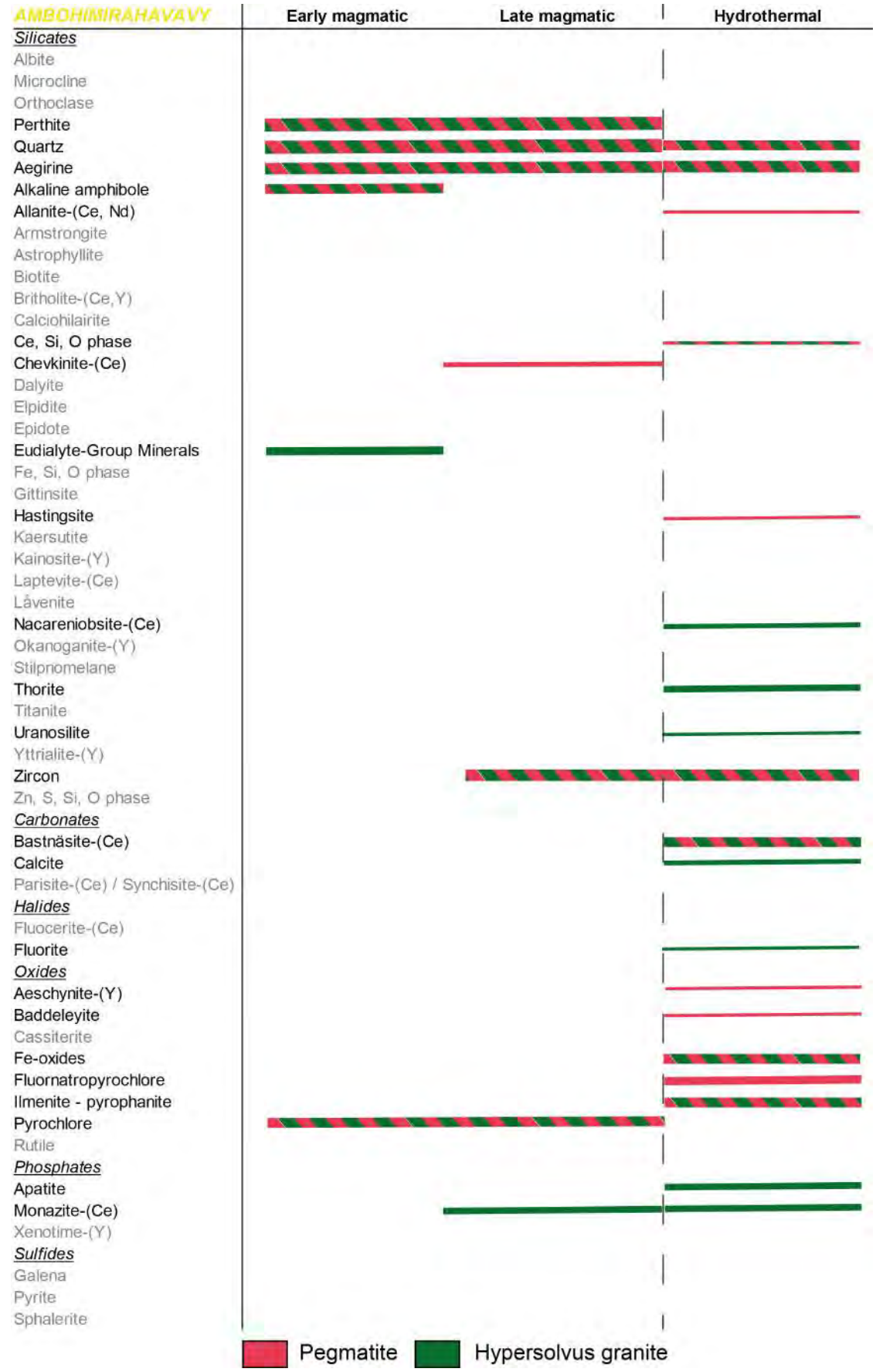
AMBOHIMIRAHAVAVY
Early magmatic
Late magmatic
Hydrothermal
Silicates
Albite
Microcline
Orthoclase
Perthite
Quartz
Aegirine
Alkaline amphibole
Allanite-(Ce, Nd)
Armstrongite
Astrophyllite
Biotite
Britholite-(Ce,Y)
Calciohilairite
Ce, Si, O phase
Chevkinite-(Ce)
Dalyite
Elpidite
Epidote
Eudialyte-Group Minerals
Fe, Si, O phase
Gittinsite
Hastingsite
Kaersutite
Kainosite-(Y)
Laptevite-(Ce)
Låvenite
Nacareniobsite-(Ce)
Okanoganite-(Y)
Stilpnomelane
Thorite
Titanite
Uranosilite
Yttrialite-(Y)
Zircon
Zn, S, Si, O phase
Carbonates
Bastnäsite-(Ce)
Calcite
Parisite-(Ce) / Synchisite-(Ce)
Halides
Fluocerite-(Ce)
Fluorite
Oxides
Aeschynite-(Y)
Baddeleyite
Cassiterite
Fe-oxides
Fluornatropyrochlore
Ilmenite - pyrophanite
Pyrochlore
Rutile
Phosphates
Apatite
Monazite-(Ce)
Xenotime-(Y)
Sulfides
Galena
Pyrite
Sphalerite
Pegmatite
Hypersolvus granite

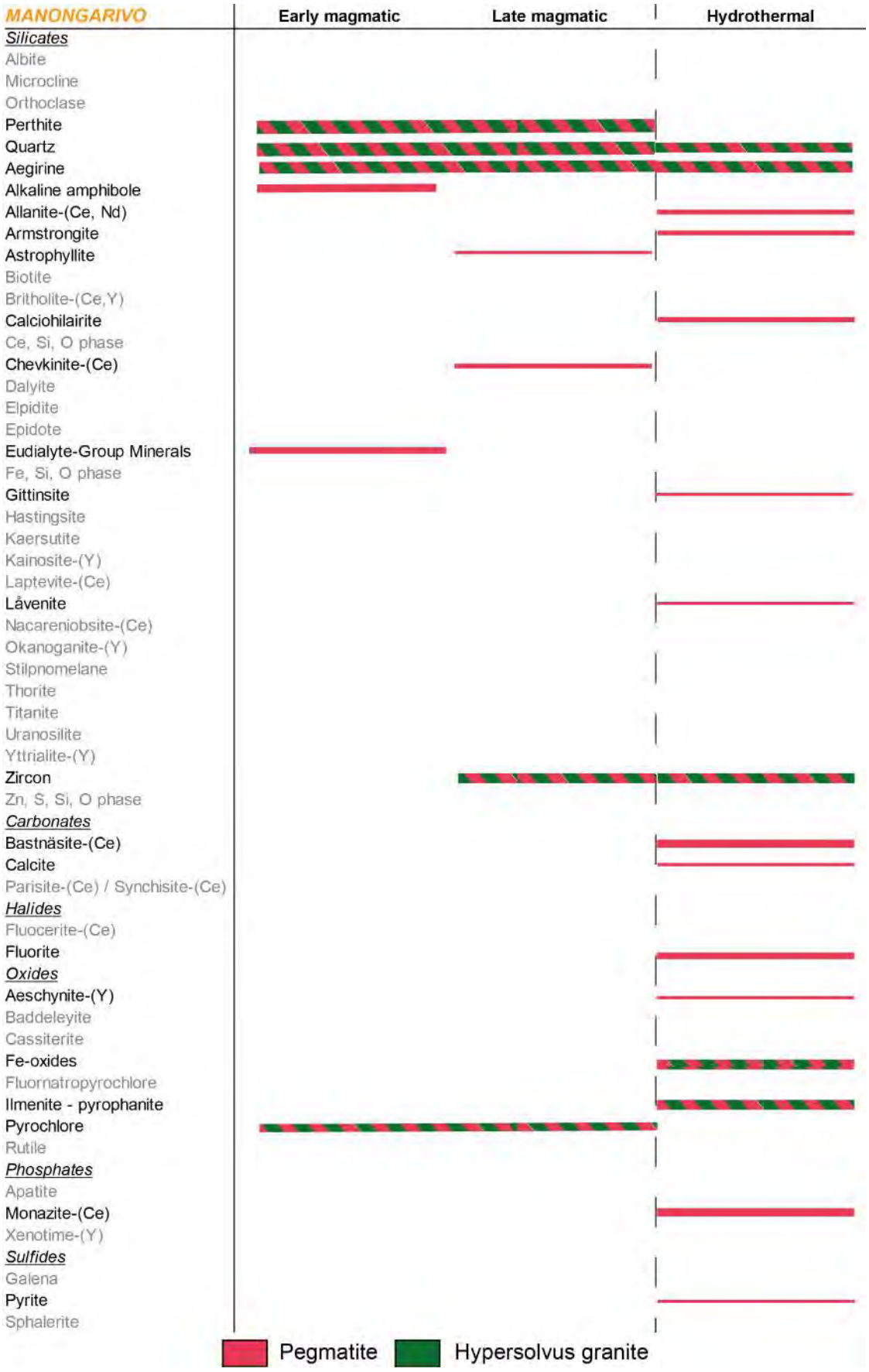
MANONGARIVO
Early magmatic
Late magmatic
Hydrothermal
Silicates
Albite
Microcline
Orthoclase
Perthite
Quartz
Aegirine
Alkaline amphibole
Allanite-(Ce, Nd)
Armstrongite
Astrophyllite
Biotite
Britholite-(Ce,Y)
Calciohilairite
Ce, Si, O phase
Chevkinite-(Ce)
Dalyite
Elpidite
Epidote
Eudialyte-Group Minerals
Fe, Si, O phase
Gittinsite
Hastingsite
Kaersutite
Kainosite-(Y)
Laptevite-(Ce)
Låvenite
Nacareniobsite-(Ce)
Okanoganite-(Y)
Stilpnomelane
Thorite
Titanite
Uranosilite
Yttrialite-(Y)
Zircon
Zn, S, Si, O phase
Carbonates
Bastnäsite-(Ce)
Calcite
Parisite-(Ce) / Synchisite-(Ce)
Halides
Fluocerite-(Ce)
Fluorite
Oxides
Aeschynite-(Y)
Baddeleyite
Cassiterite
Fe-oxides
Fluornatropyrochlore
Ilmenite - pyrophanite
Pyrochlore
Rutile
Phosphates
Apatite
Monazite-(Ce)
Xenotime-(Y)
Sulfides
Galena
Pyrite
Sphalerite
Pegmatite
Hypersolvus granite

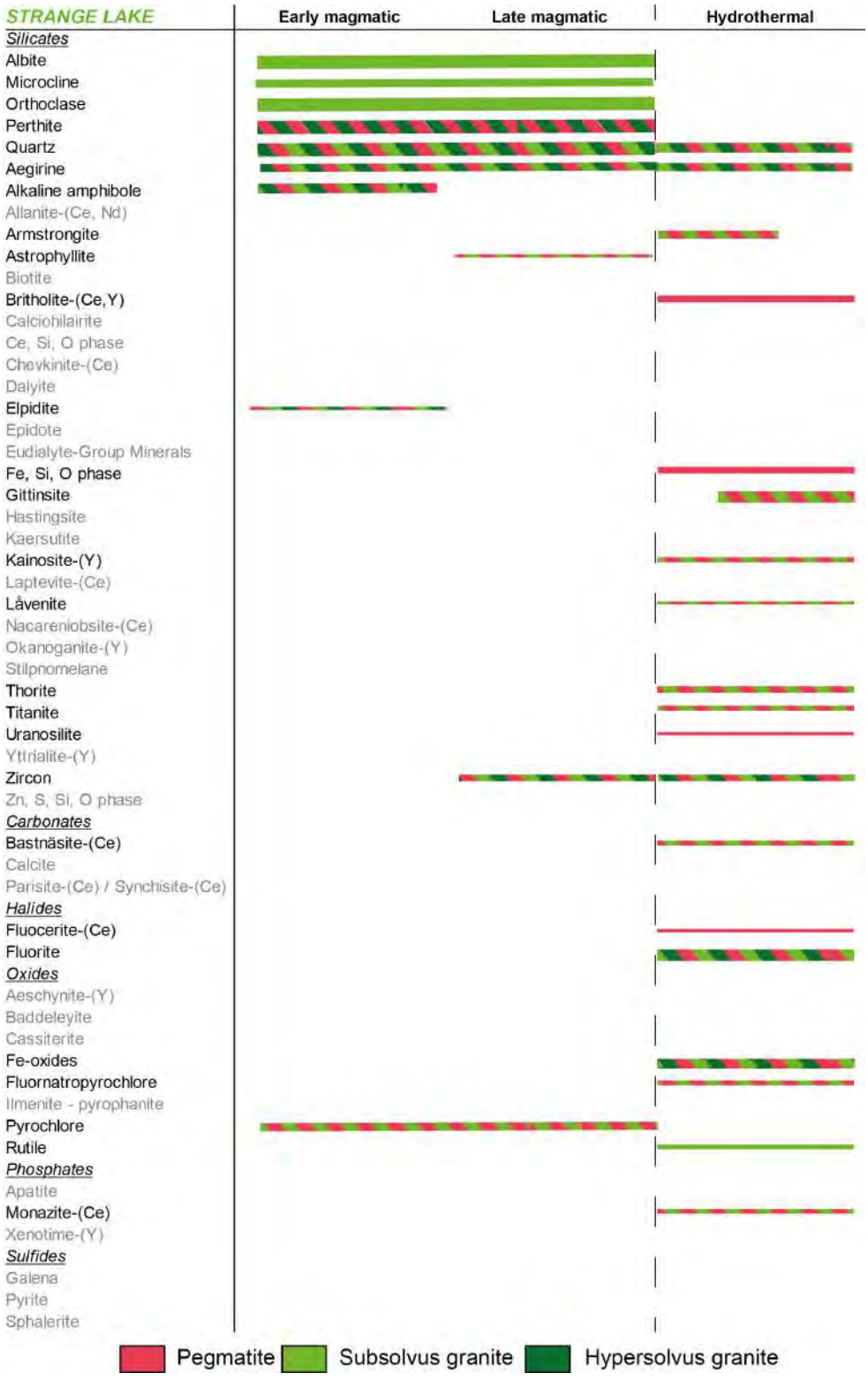

Figure 3.18 Detailed paragenesis of all six complexes studied: Amis (Namibia), Evisa (Corsica), Khan Bogd (Mongolia), Ambohimirahavavy (Madagascar), Manongarivo (Madagascar), and Strange Lake (Canada). Paragenesis are based on new observations as well as on existing descriptions (Bollaert, 2019; Bonin and Platevoet, 1988; Estrade et al., 2014b; Gysi and Williams-Jones, 2013; Kynicky et al., 2011; Salvi and Williams-Jones, 2006; Salvi et al., 2005). Minerals in grey do not occur in the complex, but does in other complexes of the study. A distinction is made between the different rock types of the complexes: pink bars are for pegmatite, and green ones are for granite

Chapter 4

Detailed study of minerals with REE zonations common to all complexes: amphibole, pyroxene and zircon

High-Field Strength Elements (HFSE), including the REE, are critical raw material today as they have a wide panel of uses and a restricted number of suppliers (Goodenough et al., 2018; Lucas et al., 2014). Among the REE, HREE have more applications but are even rarer. The main known HREE deposits are restricted to ion-adsorption deposits in China (Chakhmouradian and Wall, 2012; U.S. Geological Survey, 2019), hence it is important to document other REE occurrences worldwide. Alkaline igneous rocks are known to concentrate REE and, in particular, silica-saturated rocks have a high Yb/La ratio, i.e. they are enriched in HREE. Pegmatites are known to form from the last and most evolved part of a melt, and as such they typically concentrate the highest amounts of HFSE, including REE.

Alkaline silica-saturated rocks remain widely undocumented in comparison to their silica-undersaturated equivalent. It is known that magmatic processes play a role in pre-enrichment of alkaline rocks in REE and other HFSE (Marks and Markl, 2017). However, some studies point out the role of hydrothermal fluids in mobilizing, concentrating and fractionating the REE (e.g. Migdisov et al., 2016; Salvi and Williams-Jones, 1990). The relative importance of these two processes is still debated and this study is a new contribution towards solving this question.

The goal of the work that forms the basis for the following Chapter is to link the REE and other HFSE contained in common minerals to the major events that impact these rocks, i.e. to the magmatic-hydrothermal transition, using the six selected alkaline complexes. Ideal candidates to do so are pyroxene, amphibole and zircon,

because of their ubiquitous presence in these rocks and because they have been documented to form during a large span of the evolution of alkaline rocks, from early magmatic to late hydrothermal stages (e.g. Nielsen 1979; Jones and Peckett 1981; Ranløv and Dymek 1991; Marks et al. 2004). In addition, these minerals incorporate a relatively high amount of REE and other HFSE compared to other rock-forming minerals (e.g. alkali feldspar and quartz).

4.1 Alkali pyroxenes and amphiboles: a window on Rare Earth Elements and other High Field Strength Elements behavior through the magmatic-hydrothermal transition of peralkaline granitic systems

Manuscript published in the journal *Contributions to Mineralogy and Petrology*

This paper provides detailed petrography and major and trace element analytical data of amphibole and pyroxene of six alkaline complexes worldwide in order to link their REE and other HFSE content with the magmatic-hydrothermal transition. These data allowed to identify three different amphiboles, namely fluoro-arfvedsonite, ferro-ferri-fluoro-leakeite, and ferro-ferri-katophorite, depending on the complex they grew in. Pyroxene is aegirine in all complexes, and two types were identified in each complex: type I is found only in pegmatites and stands for euhedral crystals with core-to-rim and sector zoning; type II stands for anhedral, oscillatory zoned aegirine crystals associated with Fe- and/or Ti-oxides and at time replacing amphibole. Type I aegirine is made of a core, named zone A, systematically rich in Ca, Sn, Hf, Zr and depleted in Na, Al and Fe^{3+} compared to the rims, and rims, in which sector zoning occurs. An additional zone, called B, is present between the core and the rims at Khan Bogd only; it shows random oscillations of many elements including Ti and Mn. In the rims, zone C matches crystallographic sectors (110) and (010) and is rich in Ti and Ca; zone D matches

crystallographic sector (100) and is richer in Fe. Rims of type I aegirine also contain fluid inclusions and, at Ambohimirahavavy, inclusions of secondary, REE-rich minerals. Both aegirine and amphibole are globally rich in Na and Fe^{3+}, and contain significant amounts of REE, and mostly HREE.

Based on these observations as well as on numerous descriptions from the literature (e.g. Estrade, 2014; Kovalenko et al., 2006; Schmitt et al., 2002; Siegel et al., 2017), we could infer that amphiboles grew exclusively at the magmatic stage. Understanding the crystallization sequence of aegirine was trickier. The sharp compositional change between the core and the rims in type I aegirine suggests a sudden change in the crystallizing environment. The rims C and D contain fine oscillatory zoning, fluid inclusions, and, at Ambohimirahavavy, mineral inclusions that match the composition of those met in hydrothermal pseudomorphs (e.g. zircon, bastnäsite-(Ce)). Therefore, we infer that type I aegirine has a magmatic core (zone A) and hydrothermal rims (zones C and D). Changes in elements composition between the different zones is due to crystallo-chemical properties of aegirine as well as to competition and composition of the crystallization environment, either magmatic or hydrothermal. Type II aegirine forming after amphibole is known to be hydrothermal (Salvi and Williams-Jones, 1990). Considering that zoning patterns are the same for all type II aegirine crystals and that they are systematically found associated with Fe- and/or Ti- oxides, we consider that they all grew replacing amphibole, totally or partially. Hence, we consider type II aegirine as entirely hydrothermal.

Once it was clear which zones of the crystals grew during the magmatic phase and which grew during hydrothermal circulation, we could analyze the REE and other HFSE compositions in the different zones, and infer the timing of concentration and fractionation of the REE. It appears that the REE are more concentrated in the magmatic core of type I aegirine. However, REE are also present in the hydrothermal rims, in lower concentration but with an additional fractionation. Given the overwhelming evidence for circulation of an orthomagmatic fluid in all complexes, we propose that fractionation results from variations in fluid composition, especially in Cl^-, F^-, and CO_3^{2-} which have the ability to form more or less stable aqueous complexes with the REE (Migdisov et al., 2016).

This study highlights REE concentration and fractionation processes common to all six studied alkaline complexes, despite different geological emplacement contexts and mineralogies. It also documents the timing of REE concentration and fractionation in such complexes, which necessitate the intervention of a hydrothermal fluid.

Contributions to Mineralogy and Petrology (2020) 175:81
https://doi.org/10.1007/s00410-020-01723-y

ORIGINAL PAPER

Alkali pyroxenes and amphiboles: a window on rare earth elements and other high field strength elements behavior through the magmatic-hydrothermal transition of peralkaline granitic systems

Cyrielle Bernard[1] · Guillaume Estrade[1] · Stefano Salvi[1] · Didier Béziat[1] · Martin Smith[2]

Received: 15 January 2020 / Accepted: 3 August 2020

Abstract

Peralkaline granites and pegmatites are a prime repository of REE and HFSE, critical raw materials. Although it is accepted that magmatic processes are fundamental in concentrating these metals, the role of hydrothermal fluids in concentrating and fractionating these elements remains unclear. This paper investigates the global reproducibility of the magmatic-hydrothermal evolution of alkaline silica-saturated systems using alkali pyroxene and amphiboles from six alkaline complexes. These minerals contain significant amounts of REE and other HFSE, and pyroxene is stable throughout the magmatic and hydrothermal stages. Amphibole consists of mostly unzoned arfvedsonite, leakeite, and katophorite, while pyroxene is always aegirine. Two types of aegirine were defined. In all complexes, type-I aegirine is zoned; its core is enriched in Ca, REE, Zr, Hf, Sc and Sn, and the rims in Na, Fe^{3+} and contains secondary rare-metal bearing minerals and fluid inclusions. Type-II aegirine replaces amphibole and is oscillatory zoned. We interpret the amphiboles and REE-rich cores of type-I aegirine to have grown during the magmatic stage, whereas the rims of REE-poorer type-I and II aegirine are formed during the hydrothermal stage. During magmatic crystallization, REE intake into amphiboles and pyroxene as well as LREE-HREE fractionation were favored by their crystallographic properties and by competition among them and other minerals. During subsequent hydrothermal stages, REE and other HFSE were remobilized, locally reconcentrated and fractionated in mineral pseudomorphs and secondary pyroxene. These observations point out the importance of studying rock-forming minerals such as pyroxenes and amphiboles to unravel geological events controlled by common processes globally.

Keywords Peralkaline granite · Pegmatite · Pyroxene · Amphibole · Rare earth elements · High field strength elements

Introduction

High Field Strength Elements (HFSE, namely Nb, Ta, Zr, Hf, U, Th, Sn, and Ti), and in particular Rare Earth Elements (REE), are among raw materials considered the most critical today (European Commission 2018). They are used in many modern technologies linked to the transition to renewable energy infrastructure (Lucas et al. 2014; Goodenough et al. 2018), but their production is quite restricted, worldwide. REE deposits can be primary (igneous, carbonatites and alkaline systems) or secondary (placers and ion-adsorption) (Chakhmouradian and Wall 2012) and economic concentrations of heavy REE (HREE, Gd to Lu) are rather rare compared to those of light REE (LREE, La to Eu). The latter occur in high amounts mostly in carbonatites and placer deposits and are commonly hosted in

Communicated by Gordon Moore.

Electronic supplementary material The online version of this article (https://doi.org/10.1007/s00410-020-01723-y) contains supplementary material, which is available to authorized users.

✉ Guillaume Estrade
guillaume.estrade@get.omp.eu

[1] GET, CNRS, UPS, Université de Toulouse III, Toulouse, France

[2] School of Environment and Technology, University of Brighton, Brighton BN2 4GJ, UK

fluorcarbonates such as bastnäsite-(Ce), parisite-(Ce) and synchysite-(Ce), and phosphate such as monazite-(Ce). Ion-adsorption deposits provide most of the global HREE production (Chakhmouradian and Wall 2012; U. S. Geological Survey 2019). In alkaline igneous rocks, REE are hosted mainly in monazite-(Ce), xenotime-(Y), fergusonite-(Y), loparite-(Ce) and eudialyte-group minerals (EGM) (Larsen and Sørensen 1987; Chakhmouradian and Wall 2012). Most alkaline igneous rocks are silica-undersaturated, with the silica-saturated variety (i.e., granitic) being quite rare (e.g. Larsen and Sørensen 1987; Ranløv and Dymek 1991; Foland et al. 1993; Kramm and Kogarko 1994; Sheard et al. 2012). However, it is the latter that have high Yb/La ratios compared to other varieties (Fig. 1). Pegmatites, which form from the last and most evolved part of silica-saturated melts, concentrate the highest amounts of REE and other HFSE.

There is a general consensus in the literature that magmatic processes play a role for a pre-enrichment of alkaline rocks in REE and other HFSE (Marks and Markl 2017). These include sourcing from undepleted, more or less metasomatized mantle, crustal contamination, fractional crystallization, and melt-melt immiscibility during magma cooling (Bonin 2007; Nardi and Bitencourt 2009; Chakhmouradian and Zaitsev 2012; Veksler et al. 2012). There is also evidence that hydrothermal processes may play a key role in concentrating these elements to ore grades (e.g. Salvi and Williams-Jones 1990; William-Jones et al. 2012). However, to date, the relative importance of magmatic versus hydrothermal processes is still debated, partly because the processes occurring at the magmatic-hydrothermal transition are hard to document and most studies were carried out in the laboratory (e.g. Migdisov et al. 2016).

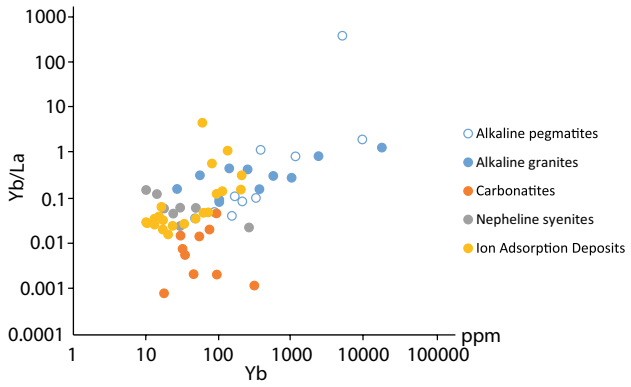

Fig. 1 A logarithmic diagram plotting chondrite-normalized (Sun and McDonough 1989) values of whole-rock Yb/La vs Yb contents for different alkaline complexes worldwide. Five groups are distinguished: alkaline granites, alkaline pegmatites, carbonatites, nepheline syenites, and ion-adsorption deposits. Data are from this study plus from Estrade et al. (2014b), Boily and Williams-Jones (1994), Estrade (2014), Kynicki et al. (2011), Poitrasson et al. (1995), Vasyukova and Williams-Jones (2014), Schmitt et al. (2002), Moore et al. (2015), Yang et al. (2003), Xu et al. (2017), Liu et al. (2015), Zaitsev et al. (2014), Kogarko et al. (2002), Li et al. (2010), Sørensen et al. (1987), Hatch (2015), Sanematsu et al. (2013), Ishihara et al. (2008), Wang et al. (2010), and Chengyu et al. (1990)

To fill this gap, it is important to understand the timing of concentration of the REE in natural occurrences. To do so, in this paper we propose for the first time a detailed study of common minerals that carry REE and other HFSE from the magmatic through the hydrothermal stages, from six silica-saturated alkaline occurrences worldwide. The goal is to make out the meaning of textures and link them to the major events that impacted the selected complexes, i.e. the magmatic-hydrothermal transition. Once it is clear which zones of the crystals grew during the magmatic phase and which grew during hydrothermal circulations, we can analyze the REE and other HFSE compositions in the different zones, and infer the timing of concentration and fractionation of the REE. Ideal candidates to do so are the pyroxene and amphibole mineral groups, because of their ubiquitous presence in these rocks and because they have been documented to form during a large span of the evolution of alkaline rocks, from early magmatic to late hydrothermal stages (e.g. Nielsen 1979; Jones and Peckett 1981; Ranløv and Dymek 1991; Marks et al. 2004). In addition, they incorporate a relatively high amount of REE and other HFSE compared to other rock-forming minerals (e.g. alkali feldspar and quartz), even though they are not considered as ore as their partition coefficients for HFSE (except Eu) are not high enough (Fedele et al. 2015). Primary zirconosilicates can also incorporate high levels of HFSE and are common in alkaline rocks, however, they are frequently altered to secondary minerals during the hydrothermal stage. Hence, pyroxenes and amphiboles are the best minerals to evidence the behavior of HFSE throughout the entire process of alkaline granite and pegmatite crystallization.

Geological background

The six alkaline igneous complexes on which this work focuses are: Ambohimirahavavy (Estrade et al. 2014a) and Manongarivo (Donnot 1963) in Madagascar, Amis in Namibia (Schmitt et al. 2002), Evisa in Corsica (Bonin et al. 1978), Khan Bogd in Mongolia (Kovalenko et al. 2006), and Strange Lake in Canada (Currie 1985). These complexes were chosen because all present evidence of hydrothermal circulation and contain high amounts of REE (from 800 ppm in a granite from Khan Bogd to 12% in a pegmatite from Strange Lake, unpublished data). All complexes contain peralkaline rocks, i.e. their ratio of $(Na_2O + K_2O)/Al_2O_3$ is > 1. Some of them have been the subject of in-depth studies, such as the Strange Lake complex which was first studied in the late 1980's (e.g. Miller 1996; Salvi and Williams-Jones 1990) and still is today (Vasyukova and Williams-Jones

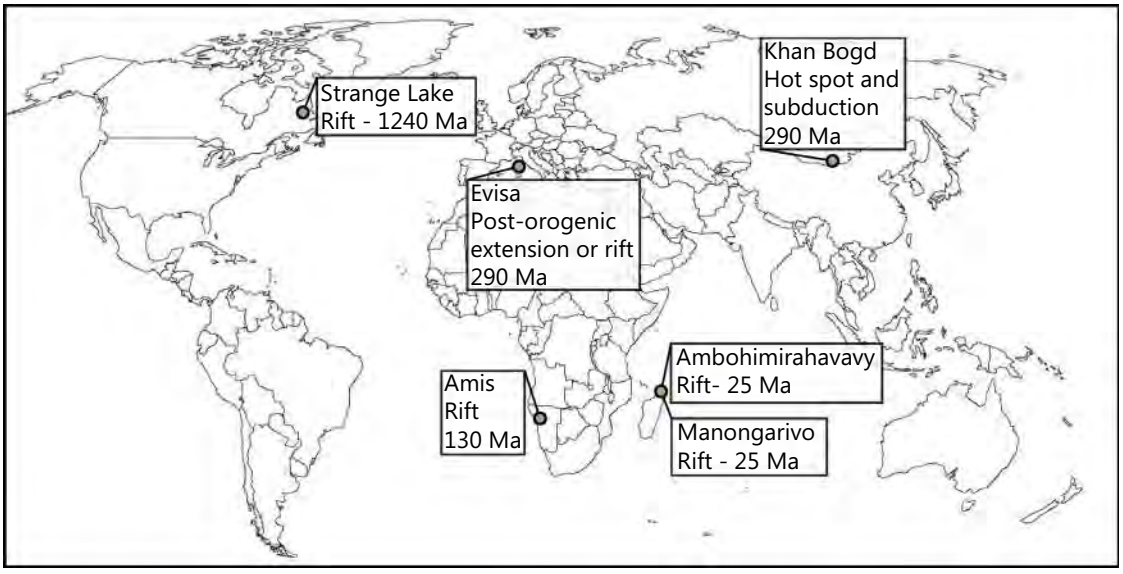

Fig. 2 Map localizing the six complexes studied in this paper. The geodynamic context and ages are given below their names in the rectangular boxes

2020); others are poorly known, as is the case for the Manongarivo complex, for which the only available information is a mere mention in a French compilation (Donnot 1963).

Although they were emplaced in different geodynamic complexes and at different periods (Fig. 2), it appears that the melt source was a metasomatized upper mantle for all six complexes. Crustal contamination and feldspars fractionation, if occurring, are two processes that can enrich alkaline granites in REE. However, the rate of partial melting at the origin of these complexes is still debated, which is an essential parameter given that a lower rate implies a greater accumulation of incompatible elements, REE included, in the newly generated melt. All complexes underwent at least one alteration episode from an orthomagmatic fluid, and some of them an additional late hydrothermal event (identified at Amis, Evisa, and Strange Lake). The composition of the fluids that circulated was measured in fluid inclusions at Ambohimirahavavy and Strange Lake, and inferred from the study of secondary mineral assemblages for the other complexes. The presence of significant amounts of Na^+ and Fe^{3+} in an orthomagmatic fluid is reported for Evisa, the two Malagasy complexes and Strange Lake, and Ca^{2+} was identified at Khan Bogd, Madagascar and Strange Lake. Locally, CO_2 and/or CH_4 were reported at Khan Bogd and Strange Lake, and CO_3^{2-} at Amis. The resulting conclusions are similar for all the complexes: independently of its orthomagmatic or late origin, a F-, Ca-rich fluid is systematically observed and inferred to have mobilized and fractionated the REE. The importance of this process compared to magmatic ones in concentrating and fractionating the REE is still a matter of debate. Comparing six complexes that were emplaced in different geodynamic settings and witnessed different fluid conditions (composition, temperature), is a strategy to highlight common features to better constrain and generalize the timing of REE and other HFSE enrichment in alkaline complexes. Below, follows a rapid summary of the main geological features of each complex; more detailed information is provided in Online Resource 1.

Amis complex, Namibia

The Amis complex and the larger Brandberg complex onto which it is juxtaposed are of the same age (132.5–130.5 My) and are hosted in metasediments of the Damara orogen (~ 550 My; Miller 1983) and volcanic rocks from the Paraná-Etendeka igneous province. Three granite and four pegmatite-aplite samples were used for this study. The Amis complex is mainly made of an arfvedsonite granite and aegirine-rich pegmatite-aplites. The Amis complex is highly enriched in REE, other HFSE and volatiles (H_2O, F). Pegmatites and aplites in the north-western part of the Amis complex are particularly enriched in REE mineralizations and uranium. Schmitt et al. (2002) infer that hydrothermal fluids had a very limited impact on the rocks of Amis complex. They affirm that minerals are all mainly magmatic, with the exception of replacement of arfvedsonite by quartz-hematite overgrowths. Based on the study of melt inclusions, they propose that the main process of REE and other HFSE enrichment is magmatic. In contrast, Diehl (1990) proposed that hydrothermal fluids played a significant role, and inferred the replacement of arfvedsonite by aegirine.

Evisa complex, Corsica

The Evisa complex (290 My; Cocherie et al. 2005) was emplaced among metaluminous granitoids. We collected seven granite and five pegmatite samples from the central part of the complex. The complex mainly comprises hypersolvus (perthitic feldspar) and subsolvus (albitic and alkali feldspar) peralkaline granites (Bonin 1990) and associated pegmatites rich in REE-bearing minerals such as monazite-(Ce), apatite, and allanite-(Ce). The hypersolvus granite probably experienced two hydrothermal events: a minor, early episode at the end of crystallization, and a more important second episode, characterized by F-rich fluids, around 200 My (Poitrasson et al. 1998; Bonin et al. 2008). The subsolvus granite is intrusive into the perthitic unit and only experienced the second hydrothermal event, which triggered the replacement of the primary zirconosilicate elpidite by a secondary assemblage (Bonin 1990).

Khan Bogd complex, Mongolia

The Khan Bogd complex is located in the southern Gobi Desert, at the transition between island-arc calc-alkaline differentiated volcanics (329 ± 5 My) and rift-related bimodal basalt–comendite–alkali granite association (318–290 My), and is dated at approximately 290 Ma (Kovalenko et al. 2006). It is among the largest alkaline granite plutons in the world, with a surface area of 1500 km^2. We collected three granite and seven pegmatite samples, mostly on the western side of the complex. The pluton consists of two ring bodies: a western peralkaline arfvedsonite-bearing granite and a later emplaced, eastern aegirine granite. They are both associated with pegmatites. The pluton has been investigated for mining purposes and estimates indicate grades between 0.3 and 4.5% REE, the highest grade being located at the top of the granite plutons (estimation of the tonnage is not available, Kovalenko and Yarmolyuk 1995). The origin of this pluton is linked to a mantle plume and the continental subduction of the South Mongolian Hercynides, but the exact magmatic process is still debated (Kovalenko et al. 2006; Kynicky et al. 2011). Kynicky et al. (2011) propose the release of a silica-saturated orthomagmatic fluid that, similarly to Evisa, triggered the replacement of primary elpidite.

Manongarivo and Ambohimirahavavy complexes, Madagascar

Ambohimirahavavy and Manongarivo are the biggest complexes of the Ampasindava province in north-western Madagascar, yet are not well documented. They were emplaced at circa 24 Ma into marine-shelf carbonates and marine-fluvial siliciclastic sediments of the Isalo Group (Thomas et al. 2009; Cucciniello et al. 2016). We collected three granite and four pegmatite samples from the southern part of the Ambohimirahavavy complex. Due to poor outcropping conditions and low occurrence of pegmatites, we could only obtain three pegmatite samples from Manongarivo. The samples from Ambohimirahavavy were selected according to previous studies from Estrade et al. (2014a,2014b). Both complexes were likely emplaced in a rifting context and are made of two ring-shaped intrusions side by side, composed of nepheline syenite, alkali feldspar syenite, biotite granite, peralkaline pegmatites, and various volcanic rocks. Due to the recent discovery of rare metals in economic concentrations in ion-adsorption clays, the province drew the attention of a mining exploration company (Estrade et al. 2014b). Granite and pegmatite dykes are the most enriched lithologies in REE and other HFSE. An orthomagmatic fluid metasomatized the complexes in the very last stages of magmatic evolution (Estrade et al. 2014b) and caused the replacement of primary zirconosilicates (eudialyte-group minerals (EGM) at Ambohimirahavavy, unknown at Manongarivo) by an assemblage of secondary HFSE-bearing minerals (Lacroix 1923; Rakotovao et al. 2009; Estrade et al. 2018).

Strange Lake complex, Canada

The Strange Lake complex was emplaced 1240 My ago into Paleoproterozoic gneisses and quartz monzonite (Miller 1996) and is considered to represent an extension of the Gardar rift in Greenland (Pillet et al. 1989; Boily and Williams-Jones 1994; Siegel et al. 2017a). We chose three granite and four pegmatite samples which were selected according to previous studies from Salvi and Williams-Jones (1990, 1995, 2006). The Strange Lake complex consists of a hypersolvus granite, while a younger, largely metasomatized transsolvus granite (rare perthite plus two distinct feldspars, previously classified as subsolvus, e.g. Boily and Williams Jones 1994) surrounds it, forming the majority of the complex (Gysi et al. 2016; Siegel et al. 2017b). These plutons are partially bounded by an outwardly-dipping fracture associated with fluorite and hematite breccia. Two zones of pegmatites have been reported: the Main zone in the center of the complex, and the B zone on the north-western edge. These magmatic events correlate with a progressive enrichment in REE and other HFSE, from HFSE-poor hypersolvus granite to HFSE-rich transsolvus granite and pegmatites (Miller 1996). Most of the REE are concentrated in the pegmatites. Reserves are estimated at 278 Mt grading 0.93% REE_2O_3 of which 39% are HREE, and 214 Mt at 0.85% REE_2O_3 in total (Gowans et al. 2017). The complex also contains significant amounts of ZrO_2, Nb_2O_5, and BeO. Two main extensive hydrothermal events affected the complex. The first event is attributed to circulation of a hot (≥ 300 °C)

orthomagmatic brine consisting of K- and Na-enriched aqueous and carbonic phases (Salvi and Williams-Jones 2006; Vasyukova and Williams-Jones 2019). The second hydrothermal event consists of a cooler fluid (100–200 °C) resulting from mixing of a meteoric fluid and a fluid originating from the granites (Gysi et al. 2016).

Features common to pegmatites and granites from all six complexes

Pegmatites in all complexes are heterogeneous in texture, i.e. they show mineralogical layering visible from the scale of the outcrop to that of a thin section (Fig. 3), whereas granites are generally homogeneous. In pegmatites, the layers have grain sizes ranging from a few μm to about 40 cm and locally more (Fig. 3). Therefore, to obtain meaningful data, samples for this study were selected from zones of relatively fine grain size (less than a few cm).

All pegmatites and granites are dominated by quartz, alkali feldspar (perthites, albite, orthoclase, and/or microcline) that are commonly strongly albitized, plus alkali amphiboles and, mostly in pegmatites, aegirine (Fig. 4). Common minerals in both rock types include zircon, pyrochlore group minerals (PGM) and Fe- and Ti-oxides. Other minerals present mostly in pegmatites include Ca and Na zirconosilicates, fluorite, astrophyllite and REE-bearing minerals [typically bastnäsite-(Ce), monazite-(Ce), xenotime-(Y), chevkinite-(Ce), allanite-(Ce), aeschynite-(Y), fergusonite-(Y), britholite-(Y), synchysite-(Ce)]. Ti-bearing minerals such as chevkinite-(Ce) and astrophyllite show signs of alteration such as dissolved edges (Fig. 4a).

Ca and Na zirconosilicates, which are characteristic minerals of agpaitic rocks, are mostly eudialyte-group minerals (EGM) at Ambohimirahavavy (Lacroix 1923; Estrade et al. 2018), and elpidite at Evisa, Khan Bogd and Strange Lake (Bonin 1988; Salvi and Williams-Jones 1990; Grigor'eva et al. 2011). These zirconosilicates were partially to totally replaced by secondary miaskitic mineral assemblages, which commonly form pseudomorphs (Poitrasson et al. 1998; Estrade et al. 2014b; Gysi et al. 2016). The mineralogy of the pseudomorphs varies in the different complexes and consists either of different Zr- and/or REE-bearing minerals (Fig. 4b), or exclusively zircon plus quartz, i.e. typical miaskitic mineral assemblage (Fig. 4c). Both pseudomorph types are found in all complexes, except in Amis where our samples only contain the miaskitic zircon-quartz type. Elpidite can also be extensively replaced by other zirconosilicates, namely armstrongite and gittinsite (e.g. Salvi and William-Jones 1995), whereas EGM is only partially replaced by these phases. At Khan Bogd, cathodoluminescence reveals the elpidite is altered from its core, replaced by zircon and armstrongite (Fig. 4d). Pseudomorphs from Evisa consist of Ca-rich mineral assemblages such as fluorite and parisite-(Ce), the latter growing mostly at the expense of bastnäsite-(Ce). At Manongarivo and Amis, the precursor mineral has not been identified because partial replacement has not been observed in these complexes, so far.

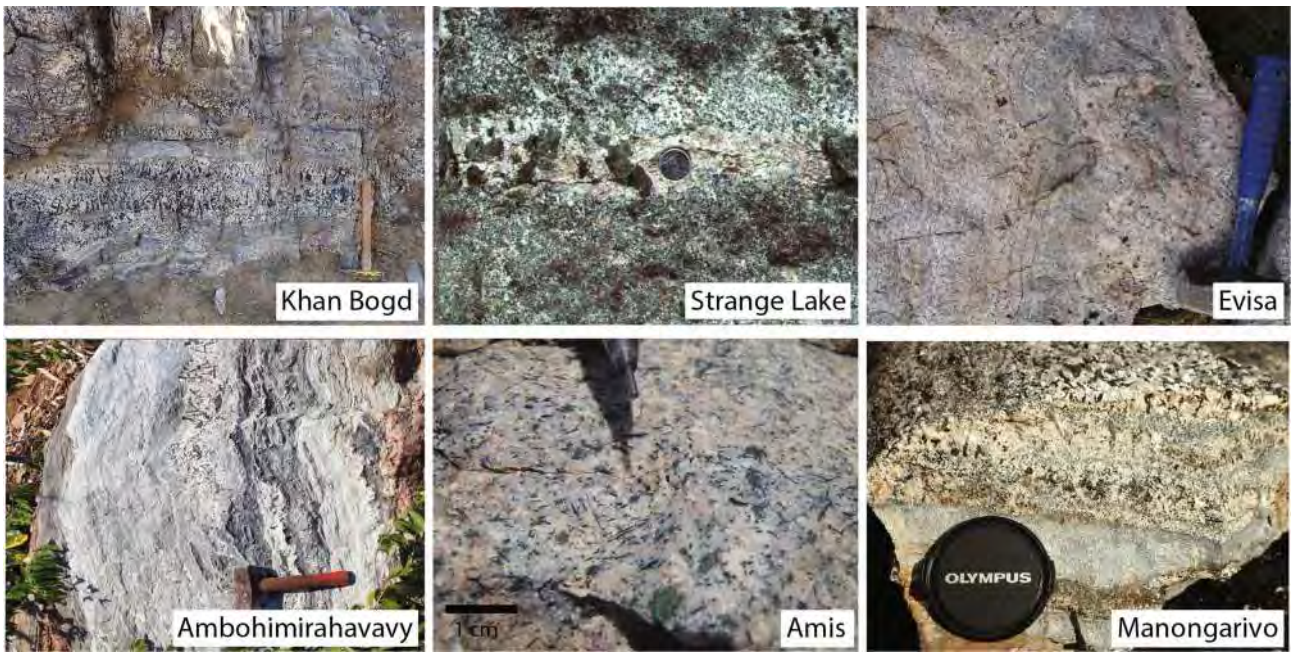

Fig. 3 Photographs of outcrop or hand samples of pegmatites from the six complexes. Most display a well-marked layering defined by mineralogy and textural variations

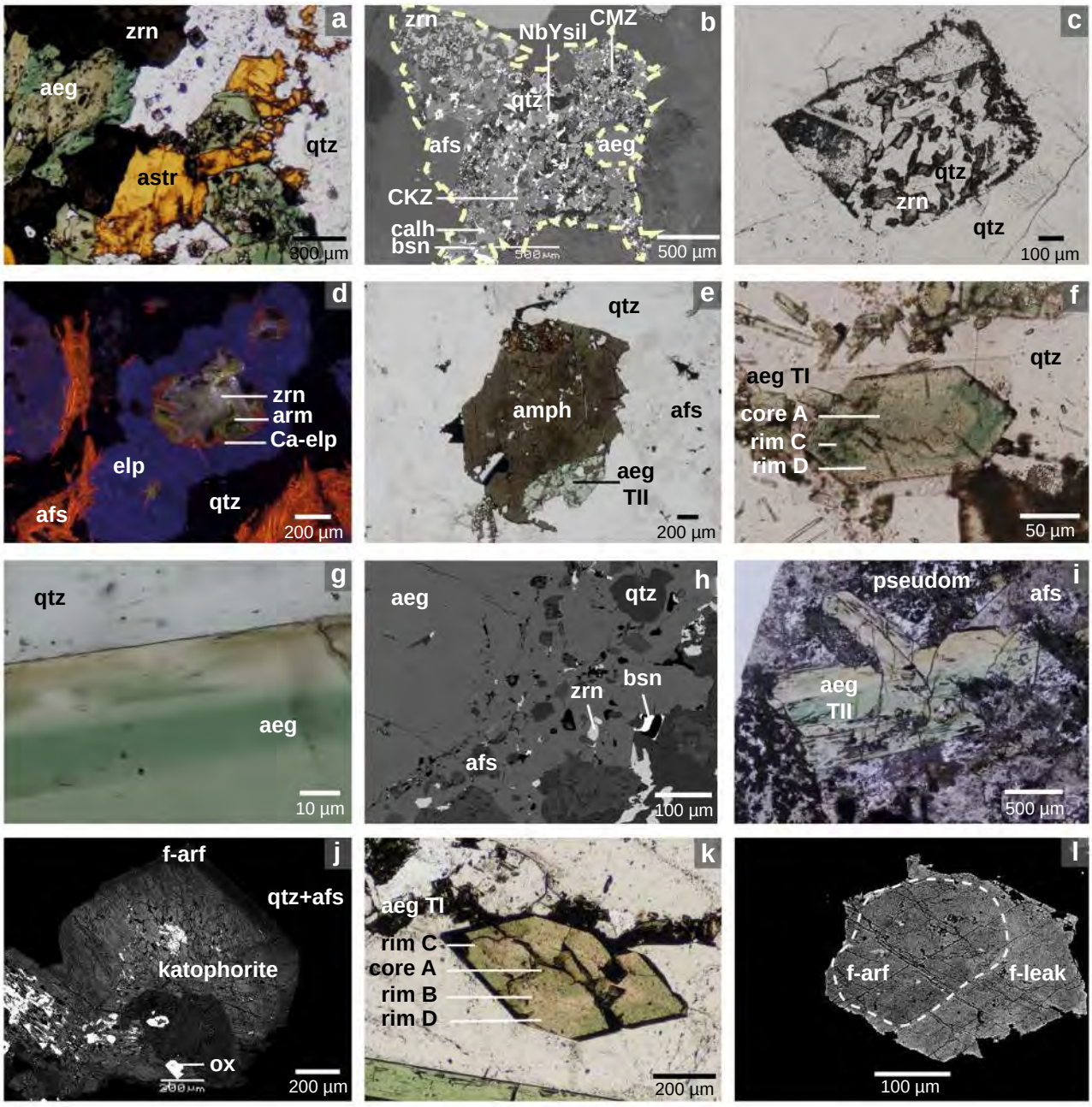

Fig. 4 **a** Altered astrophyllite from Amis, **b** REE-bearing pseudomorph (Manongarivo), **c** Zircon-quartz pseudomorph (Evisa), **d** Elpidite (Khan Bogd), altered to armstrongite and zircon in its center, **e** Arfvedsonite replaced by type-II aegirine (Evisa), **f** A type-I aegirine showing core-to-rim zoning (Ambohimirahavavy), **g** Two tiny fluid inclusions in the rim of a type-I crystal of aegirine (Khan Bogd), **h** Mineral inclusions contained within the rim of a type-I aegirine (Ambohimirahavavy) that are of the same nature than minerals in REE-bearing pseudomorph, **i** A single crystal of type-II aegirine (Strange Lake), **j** Zoned amphibole, from katophorite in the core to arfvedsonite in the rims (Evisa), **k** A type-I aegirine showing core-to-rim zoning with zone B (Khan Bogd), **l** Zoned amphibole, from arfvedsonite in the core-to-leakeite in the rims (Evisa). Photographs **a**, **c**, **e**, **f**, **g**, **i** and **k** were taken with an optical microscope; photographs **b**, **h**, **j** and **l** with SEM EDS; and **d** with optical cathodoluminescence. pseudom: pseudomorph; zrn: zircon; aeg: aegirine; amph: amphiboles; qtz: quartz; afs: alkali feldspar; bsn: bastnäsite-(Ce); arf: arfvedsonite; ox: Ti- and Fe-oxides; calh: calciohilairite; CKZ: unidentified Ca- and K-bearing zirconosilicates; CMZ: unidentified Ca- and Mn-bearing zirconosilicates; NbYsil: unidentified Nb- and Y-bearing silicate; arm: armstrongite; elp: elpidite; astr: astrophyllite

Analytical methods

Polished thin sections were prepared from all samples from the six complexes and were studied using transmitted light microscopy, cathodoluminescence, scanning electron microscopy (SEM), microprobe, and laser-ablation inductively coupled plasma mass spectrometry (LA-ICPMS) to determine mineral textural relationships and amphiboles and pyroxene zoning.

SEM images in back-scattered electron (BSE) mode were collected with a Jeol JSM6360LV SEM coupled with a Bruker silicon drift detector and interpreted with the Esprit software at the Géosciences Environnement Toulouse laboratory, using an accelerating voltage of 20 kV, and a detection time of 40 s.

Mineral compositions were determined at the Centre Raymond Castaing in Toulouse, using a CAMECA SX Five electron microprobe (EPMA), with an accelerating voltage of 15 kV, a beam current of 20 nA for pyroxene, 10 nA for amphibole, and a beam diameter of about 2 µm. Quantitative elemental maps were performed on the same instrument, using an accelerating voltage of 15 kV, a beam current of 20 nA and 100 nA for major and minor elements respectively. Counting time was 1 s on each pixel with a step of 0.5–4 µm depending on crystal size. Uncertainties were calculated using the method of Ancey et al. (1978). Standards used for calibration as well as detection limits based on repeated measurements are provided in Online Resource 2.

To resolve the oxidation state of iron measured by microprobe, calculations of the valence were made following Droop (1987). To verify these measurements, a ^{57}Fe Mössbauer spectrum was collected at the Laboratoire de Chimie de Coordination—University of Toulouse on a constant-acceleration conventional spectrometer, at 80 K and with a 1.85 GBq source of ^{57}Co, over a ± 12 mm/s range with 512 channels. The spectra were acquired via a compact detector c-system and recorded with a Canberra multichannel analyzer, coupled to a computer with Recoil Mossbauer Analysis Software 1.05 from Lagarec and Rancourt (1997). Uncertainties were calculated using the covariance matrix. Pyroxene end-members were then calculated following Mann et al. (2006). Amphiboles end-members were calculated using the spreadsheet available from Locock (2014).

Trace element concentrations were determined in situ by LA-ICPMS at the Géosciences Environnement Toulouse laboratory, University of Toulouse, on 30-µm polished thin sections, using a New Wave Research ESI 213 laser coupled to a Thermo-Fisher Element-XR high-resolution ICP-MS. Laser beam diameter varied from 30 to 50 µm depending on mineral size, and data were acquired by ablating lines instead of spots to prevent intersecting solid inclusion or internal zoning. NIST synthetic glass certified reference materials SRM 610 and SRM 612 were used as external and quality control standards, respectively. Each analysis was normalized using SiO_2 values previously determined by EMPA. The relative precision ranged from 5 to 10% and detection limits, based on repeated measurements, are provided in Online Resource 3. Trace elements maps were performed at the Trinity College in Dublin according to the method provided in Ubide et al. (2015) using photon machines G2 193 nm UV laser with a Helex two-volume cell coupled to a Thermo iCAPQ ICP-MS. Laser beam spot for maps was 12 µm square, scan speed 8 µm/s and repetition rate 41 Hz. NIST SRM 610 glass was used as standard. A beam size of 12 µm square typically allows a spatial resolution of 7–10 µm in x and y. This relatively new ablation technique removes only 3–4 µm of material, which allows several maps to be performed on the same area. A first map with all REE and other HFSE was first established, before acquiring a second map with only five elements to obtain a better signal. LA-ICP-MS maps provide detailed spatial information on zonation in crystals that would not be available otherwise. Analysis were semi-quantitative and compared to microprobe data to obtain the real concentration.

To check for the absence of REE mineral inclusions in the pyroxene, we analyzed one sample from the Amis complex by scanning transmission electron microscopy (STEM) at the Centre Raymond Castaing in Toulouse. Unlike TEM, with STEM the electron beam is focused on a specific point of the sample and scans its surface instead of being focused on the entire surface. This allows a better resolution as well as local chemical identification (e.g. Pennycook and Nellist 2011). The focused ion beam (FIB) was used to prepare the sample for STEM. The FIB is a Hélios 600i operated at 5 kV, and the TEM a JEOL cold-FEG JEM-ARM200F operated at 200 kV equipped with a Cs probe corrector reaching a spatial resolution of 0.078 nm. Images were acquired in high-angle dark field (HAADF) as well as bright field (BF) modes. EDX spectra were recorded on a JEOL CENTURIO SDD detector.

Amphibole and pyroxene textural and chemical description

Textural features

Amphiboles

Amphiboles occur in granites and pegmatites as well-developed euhedral crystals (Fig. 4e). No significant textural difference was found between amphiboles of the six

complexes. They all appear pleochroic, dark green or dark blue to black under plain polarized light (PPL). Their size is highly variable from one complex to another as well as inside pegmatites (typically ranging from 20 µm to 10 cm), but is always comparable with the size of quartz and alkali feldspar crystals in the same rock. Except at Evisa (Fig. 4j), amphiboles are not zoned, but they display dissolution/corrosion textures on their rims. They commonly have small quartz and feldspar inclusions, and are in equilibrium with these minerals. Replacement of amphiboles by aegirine and Ti- and/or Fe-oxides is a common feature of peralkaline granitoids (Marks and Markl 2017) and occurs in all pegmatites and some granites (Fig. 4e).

Pyroxene

Pyroxene is ubiquitous in pegmatites and granites of all six complexes but present three different textural features. (1) In pegmatites which contain only minor amphibole, it occurs as light to dark green euhedral crystals under PPL ranging from 50 µm to 10 cm. These pyroxene crystals present a core-to-rim zonation pattern, with additional sector zoning in the rims, which are visible under PPL (Fig. 4f). Similarly to amphiboles, these crystals are in equilibrium with quartz and alkali feldspar grains. In the rims of this pyroxene, we also found fluid inclusions (Fig. 4g) and mineral inclusions that match the composition of those met in pseudomorphs (Fig. 4b and h). These pyroxene crystals were found in all studied complexes but Strange Lake. At Khan Bogd, these crystals present an additional zoning area between the core and the sector-zoned rims (Fig. 4k). (2) In some pegmatites, pyroxene occurs as anhedral crystals of size similar to the one we just described. These crystals are oscillatory zoned, from yellowish to green under PPL (Fig. 4i). They commonly include Fe- and/or Ti- oxides. (3) In granites as well as in some pegmatites, anhedral pyroxene is found replacing amphibole (Fig. 4e). This pyroxene is also weakly oscillatory zoned. As it replaces amphibole only partially, it's size is smaller than the previously described pyroxene crystals and depends on the original amphibole size. This pyroxene is associated with Fe- and/or Ti- oxides and can sometimes keep the 120° cleavages from the original amphibole.

Based on occurrence, size, color, zoning and mineralogical associations, we distinguish two main types of pyroxene in the six complexes we focus on in this study. Type-I matches euhedral zoned pyroxene, and our study focuses mainly on this type. Based on the observation that they present anhedral shape, oscillatory zoning, and are associated with Fe- and/or Ti- oxides, we regroup anhedral single pyroxene crystals and pyroxene replacing amphibole under the denomination type-II.

Major element composition

Amphiboles

Since they present the same textural features, all amphiboles were identified based solely on their chemistry, following the classification of Hawthorne et al. (2012) and in accordance with Leake et al. (1997). The general formula of amphibole is $AB_2C_5T_8O_{22}W_2$ where, in this study, A = Na; B = Na, Ca; C = Fe^{2+}, Fe^{3+}, Li; T = Ca, Al; and W = OH, F. The rootname is given to these amphiboles based on the composition of the sites A, B and C, and the prefix is added according to the composition of the sites C and W. By strictly following these rules, it appears that some complexes contain only one amphibole type, common to granites and pegmatites, and some contain different amphiboles (Table 1). Ambohimirahavavy (ferro-ferri-fluoro-leakeite; $Na_3Fe_4LiSi_8O_{22}F_2$), Manongarivo and Strange Lake (fluoro-arfvedsonite; $Na_3Fe_5Si_8O_{22}F_2$), and Khan Bogd [arfvedsonite; $Na_3Fe_5Si_8O_{22}(F,OH)_2$] contain only one amphibole. At Amis, amphibole is ferro-ferri-fluoro-leakeite in pegmatites and fluoro-arfvedsonite in the granite. At Evisa, granites and pegmatites contain a zoned amphibole with a core of fluoro-arfvedsonite and a rim of ferro-ferri-fluoro-leakeite (Fig. 4l). In addition, the hypersolvus granite from Evisa contains zoned crystals with ferro-ferri-katophorite [$Na_2Ca(Fe^{2+},Mg)_4Fe^{3+}(Si_7Al)O_{22}(OH)_2$] in their core and fluoro-arfvedsonite in their rims (Fig. 4j).

However, it is important to keep in mind that amphibole is a solid solution, thereby two amphiboles can have different names but be close in composition, and inversely can have the same name but present a compositional range. To avoid these artificial hiatuses and subsets, we focused on the concentration of elements involved, when attributing amphibole names in this study. Hence, the distinction between katophorite and other amphiboles is based on the Ca/(Ca + Na) ratio; being > 0.25 (close to 0.4), this makes it a Na–Ca amphibole, compared to values < 0.1 for other amphiboles, which are then considered Na-amphiboles. Thereby, ferro–ferri–katophorite at Evisa exhibits a significant compositional gap with the other amphiboles from this study. The distinction between Na-amphiboles is more subtle, and is based on the amount of Li and Fe^{2+}/Fe^{3+} ratio in the C site. Ideally, leakeite has 1 Li apfu; this value is on average 0.6 apfu at Ambohimirahavavy and Evisa, and 0.7 apfu at Amis. Arfvedsonites from the other complexes have average Li contents of 0.1–0.3 apfu, validating the distinction proposed here, although these values are intermediate between the two categories. The prefixes ferro- and ferri- refer to the presence of Fe^{2+} and Fe^{3+}, respectively, in

Table 1 Mean values for the major and trace element composition, obtained by microprobe and LA-ICPMS respectively, of amphiboles from pegmatites and granites from the six complexes

Complex	Ambo	Amis		Evisa			KB	M	SL
Type	F-f-f-lea	F-arf	F-f-f-lea	F-arf	F-f-f-lea	F-f-Kato	Arf	F-arf	F-arf
Wt.%									
Samples No.	**11**	**108**	**30**	**110**	**41**	**4**	**86**	**45**	**134**
SiO_2	51.50	50.13	51.70	50.56	51.03	49.95	50.17	49.42	49.78
TiO_2	0.84	1.14	1.49	0.70	0.62	0.70	0.92	1.44	0.93
Al_2O_3	0.33	0.69	0.51	0.88	0.83	1.14	0.16	0.58	0.67
K_2O	0.93	1.27	1.74	1.26	1.46	0.77	2.02	1.37	1.50
Fe_2O_3	13.60	9.98	12.62	11.31	13.45	10.25	9.09	7.00	7.97
FeO	16.70	22.84	17.02	22.39	19.20	25.89	23.83	25.96	25.38
MnO	1.99	0.51	0.76	0.42	0.59	0.53	1.66	1.92	0.75
MgO	0.15	0.05	0.24	0.23	0.33	0.09	0.13	0.44	0.11
CaO	0.24	0.19	b.d.l	0.46	0.31	1.04	0.43	0.36	0.58
Na_2O	10.40	8.98	8.57	7.87	7.78	6.44	8.03	8.86	8.76
F	1.85	3.21	3.38	2.10	2.54	0.75	1.72	2.07	2.52
Cl	b.d.l	b.d.l	b.d.l	b.d.l	b.d.l	b.d.l	b.d.l	b.d.l	b.d.l
Total	98.54	99.00	98.08	98.19	98.15	97.56	98.18	99.44	98.96
ppm									
Samples No.	**15**	**15**	**23**	**21**	**4**	**3**	**17**	**10**	**17**
Li	9800	4800	9600	6100	8800	2500	5100	700	1939
Be	8	22	79	13	29	51	b.d.l	4	22
Sc	12	15	13	4	5	11	8	13	10
Zn	2562	2927	17,114	2315	1702	2788	1680	1191	3333
Ga	4	10	8	8	6	19	3	5	10
Rb	69	28	80	21	15	17	30	15	21
Sr	b.d.l	b.d.l	b.d.l	22	b.d.l	b.d.l	36	24	b.d.l
Y	51	96	75	42	62	266	31	22	94
Zr	2009	743	1286	442	287	360	977	298	1015
Nb	397	111	127	57	53	189	24	116	106
Sn	42	53	360	71	30	45	10	4	45
Ba	1	2	5	1	b.d.l	2	1	b.d.l	2
La	6	6	8	3	4	34	2	10	21
Ce	14	30	137	11	16	107	5	25	63
Pr	2	4	3	2	3	20	1	4	9
Nd	8	23	14	11	17	94	3	15	41
Sm	2	8	5	4	10	34	1	3	11
Eu	b.d.l	0.3	0.2	0.3	0.2	1	b.d.l	b.d.l	1
∑LREE	32	71	167	31	50	290	12	57	146
Gd	1	10	7	4	16	36	b.d.l	2	8
Tb	0.3	2	2	1	3	6	0.2	0.3	2
Dy	4	13	17	6	11	44	3	3	14
Ho	2	4	4	2	2	10	1	1	4
Er	11	18	19	10	11	35	8	6	20
Tm	3	5	5	3	4	7	2	2	5
Yb	39	55	70	36	48	71	29	18	69
Lu	9	12	17	9	10	14	7	4	16
∑HREE + Y	120	215	216	113	167	489	81	58	232
Hf	79	38	68	19	12	18	34	9	39
Ta	5	2	3	1	1	4	0.4	2	1
Pb	9	12	97	4	4	21	2	1	9
Th	0.2	3	6	1	1	4	b.d.l	b.d.l	1
U	b.d.l	0.2	2	0.1	0.1	0.4	b.d.l	b.d.l	0.1

no. number of replicates, *F-arf* fluoro-arfvedsonite, *F-f-f-lea* ferro–ferri–fluoro–leakeite, *F-f-kato* ferro–ferri–katophorite, *b.d.l* below detection limit, *Ambo* Ambohimirahavavy, *KB* Khan bogd, *M* Manongarivo, *SL* Strange Lake

the C site.The prefix fluoro- indicates that the F concentration is systematically higher than the concentration of other elements in the W site. In this study, the amounts of F and OH, respectively, are close to 1.1 and 0.9 apfu in arfvedsonite from all complexes but Khan Bogd, where it is closer to 0.9 apfu F and 1.1 apfu OH. Strictly complying with the definition would result in two different names (F and OH varieties), which would vary with each complex. However, this would lead to add unnecessary confusion to the nomenclature, therefore, because the compositional differences are only minor, we chose to ignore this parameter.

Within a given category, amphiboles are globally similar in composition in all complexes, including Fe^{2+}/Fe^{3+} (around 3 for fluoro-arfvedsonite, 2 for leakeite, and 3.5 for katophorite), with only local variations (Table 1). Chlorine was not detected by microprobe analyses in any of the amphiboles. The main distinction regarding major element composition is found in (fluoro)-arfvedsonite from Manongarivo and Khan Bogd, which both have high contents of Mn (respectively 1.92 and 1.66% vs 0.50% in the other complexes, Fig. 5d) and Fe^{2+}/Fe^{3+} (4.00 and 5.90 vs 2.40). Amphibole from Ambohimirahavavy is also rich in Mn (1.99%) but does not show a high Fe^{2+}/Fe^{3+} value. Fluoro-arfvedsonite from Amis is as rich in F as ferro-ferri-fluoro-leakeite from all other complexes (around 1.6 apfu), which is unusual (Deer et al. 1997b). Amphiboles from pegmatites are generally slightly richer in HFSE, Li and Fe^{3+} than amphiboles from granites.

Pyroxene

Based on composition, pyroxene in granites and pegmatites consists of 85–97% aegirine end-member. Therefore, according to the classification of Morimoto (1988), we will refer to it as aegirine in the following sections of this paper. Pyroxene from Ambohimirahavavy and Khan Bogd is more Ca-rich than the other complexes, but it is still classified as aegirine.

Type-I aegirine crystals show a characteristic zoning pattern in pegmatites from all locations: a core-to-rim zoning visible in BSE images (Fig. 6n) and a sector zoning visible even by optical microscopy (Fig. 6o). This pattern defines 3 main zones, where zone A is the core and zones C and D form sector-zoned rims. Zone C matches the crystallographic sector (110), and zone D sector (100) (Ubide et al. 2019). In a few cases, an additional zone matching the crystallographic sector (010) is also present (e.g. ESM 6). All zones are optically distinguished by different tones of green, attributed to different Ti contents (Fig. 6g) (e.g. Strong 1969; Ferguson 1973; Nielsen 1979). The contacts between different zoning are sharp in all occurrences (Fig. 6). Zone A, the core, is systematically enriched in Ca, Sn, Hf, Zr (Fig. 7a–c, g) and depleted in Na, Al and Fe^{3+} compared to the other zones (Table 3). In pegmatites, we measured up to 2 wt% ZrO_2 in aegirine cores; although uncommon, Zr-rich aegirine was also described in other localities such as in nepheline syenites from the Motzfeldt Centre, South Greenland (Jones and Peckett 1981; up to 7 wt% ZrO_2) and in metaluminous trachytes from the Warrumbungle Volcano, Australia (Duggan 1988; up to 14.5 wt% ZrO_2). Sector zone C is particularly enriched in Ti and Ca (Fig. 6e, g), while D is in Fe (Fig. 6c). Two major growth layers are visible in the rims with, in sector C, Ti and Ca decreasing towards the rims of each layer (Fig. 6e, g). Al content is low in aegirine from all six complexes (about 0.3% Al_2O_3 compared to standard average values of 1.2% reported in aegirine; e.g. Deer et al. 1997a). At Khan Bogd, an additional zone, referred to as zone B, is found between the core and the sector-zoned rims of the crystals (Fig. 4k); it shows random oscillations due to variations in many elements, including Ti and Mn. The same zoning pattern, including zone B, was also observed by Ranløv and Dymek (1991) in nepheline syenite from the Narssaq Peninsula. However, they only documented variations in Zr, Ti, Al, Na, Ca and Fe. Larsen (1976) and Piilonen et al. (1998) respectively described a core-to-rim zoning in aegirine from nepheline syenite in the Ilímaussaq and Mont Saint-Hilaire complexes. They report cores enriched in Ca, Fe^{2+}, Mg, Mn and Zr compared to rims, which in turn contain higher Al, Ti, Na and Fe^{3+}. Shearer and Larsen (1994) supplemented the description of aegirine from Ilímaussaq, by reporting Sr and REE enrichment in cores compared to rims. In our analyses, we did not observe a systematic difference in Mn and Sr contents between core and rims.

Type-II aegirine is not sector-zoned but shows oscillatory zoning and we observed a wide variety of compositions depending on which layer was analyzed (Table 2). This zoning is irregular, with no core, made of compositionally varying layers with variable thickness. No common pattern was found among any type-II aegirine crystals, beside their heterogeneity. Many elements are involved, including Fe, Mn, Ca, and Ti (see Online Resource 8). No significant chemical differences were found between type-II aegirine from granites and pegmatites. Type-II aegirine is commonly depleted in Ti and Sn compared to type-I aegirine, except at Khan Bogd. Mg is commonly found in higher concentration in type-II aegirine (Table 2). No significant compositional difference was found between type-II aegirine replacing amphibole in granite and those in pegmatites. At Strange Lake, all observed aegirine crystals are of type-II (Table 2; Salvi and Williams-Jones 1990; Roelofsen 1997).

Trace element composition

Amphiboles

Amphiboles from all six complexes have very similar trace element patterns (Table 1). Fluoro-arfvedsonite and

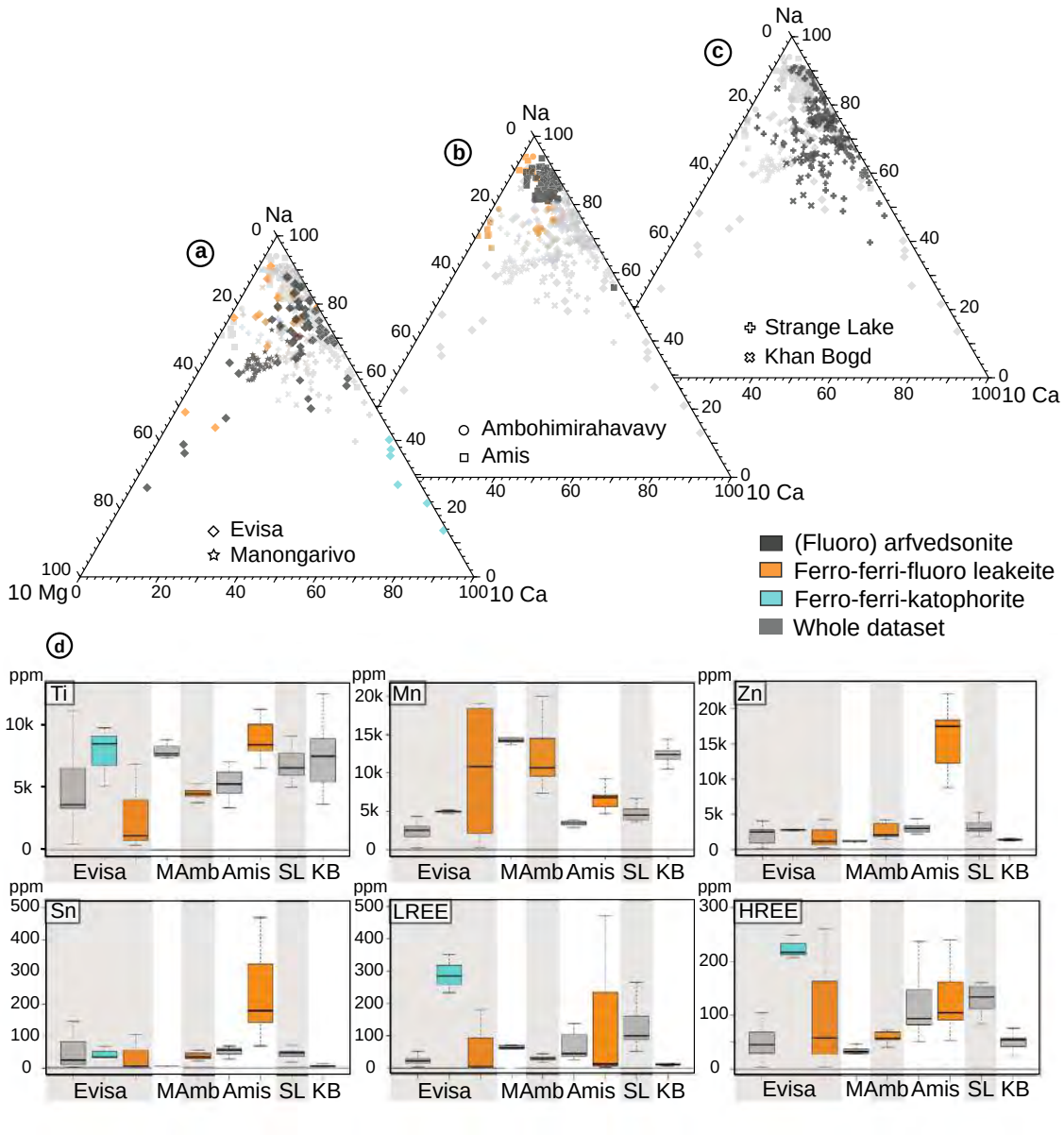

Fig. 5 Chemical composition of amphiboles. **a**–**c** Ternary diagrams representing amphibole poles for the **a** Evisa and Manongarivo complexes; **b** Ambohimirahavavy and Amis complexes; **c** Khan Bogd and Strange Lake complexes. Poles are plotted as 10 Mg and 10 Ca for a better visualization of the dataset. **d** Boxplots showing the trace-element composition of amphiboles from the different complexes. Thick black line represents the median, upper and lower boxplot limits the first and third quartile respectively, upper and lower dashed lines are the maximum and minimum values respectively, and the thin black line is the detection limit. Areas are shaded to distinguish data for each complex *M* Manongarivo, *Amb* Ambohimirahavavy, *SL* Strange Lake, *KB* Khan Bogd

ferri-fluoro-leakeite have practically the same composition, with Li contents alone being responsible for the transition from one kind to the other. This cation enters the amphibole structure according to the substitution: $^{C}Li^{+} + {}^{C}Fe^{3+} = 2{}^{C}Fe^{2+}$, described by Hawthorne et al. (1996). Ferro-ferri-katophorite, which is more calcic than the two other amphiboles, relates to fluoro-arfvedsonite through the substitution: $^{B}Ca^{2+} + {}^{T}Al^{3+} = {}^{B}Na^{+} + {}^{T}Si^{4+}$ (Deer et al. 1997b). This last substitution increases the size of the C site, leaving more space to incorporate LREE. Similarly, the coupled substitution (Mg, Fe^{2+}) → Fe^{3+} occurring in the C site of amphiboles enhances HREE incorporation (Bottazzi et al. 1999; Siegel et al. 2017b). Amphibole chondrite-normalized REE patterns are systematically enriched in HREE relative to LREE, with a depression in medium REE (MREE, from Eu to Dy). This pattern is unusual compared to more Ca-rich amphibole compositions in which REE patterns are usually enriched in LREE or in MREE (e.g. Marks et al. 2004; Coint

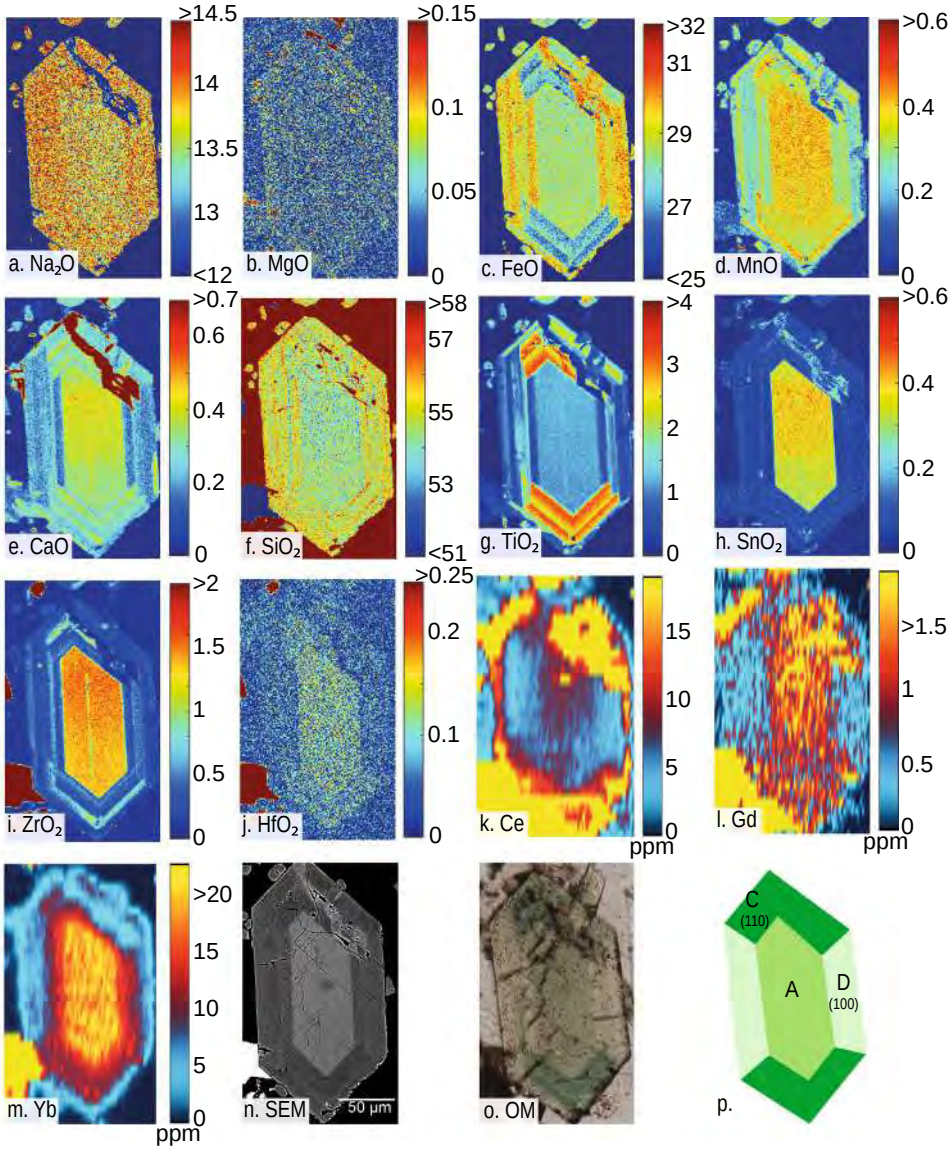

Fig. 6 Microprobe and LA-ICPMS maps on a type-I aegirine crystal at Ambohimirahavavy. Visible zonations were also found in the other complexes (see Supplementary material). 3 zones are distinguished: the core A, and the sector-zoned rims Cand D. Microprobe maps are in wt%, and LA-ICPMS maps are in ppm. Limits of aegirine on LA-ICPMS maps are blurry because the signal from the crystal and the matrix mix and do not reflect an actual concentration

et al. 2013). All spectra display a negative Eu anomaly suggesting early plagioclase fractionation (Fig. 8). The absolute REE concentrations, though somewhat varying from one complex to another, are quite similar (Fig. 8).

Despite their similar patterns, the absolute concentrations of REE and other HFSE can vary in amphiboles from one complex to the other. Fluoro-arfvedsonite from Manongarivo and Khan Bogd both have low quantities of Sn (4 and 10 ppm) and HREE (35 and 50 ppm on average). Fluoro-arfvedsonite from Manongarivo also has less LREE than fluoro-arfvedsonite from other complexes (11 vs 60 ppm on average). Ferro-ferri-katophorite from Evisa displays high enrichments in LREE and HREE (respectively 224 and 290 ppm) (Fig. 8). Ferro–ferri–fluoro–leakeite from Amis is notably different from other complexes in terms of trace elements: it is richer than ferro–ferri–fluoro–leakeite from other complexes in Ti (0.18 vs 0.07 apfu), Sn (360 vs 32 ppm), Zn (0.24 vs 0.05 apfu), Pb (97 vs 7 ppm), LREE (168 vs 37 ppm on average) and HREE (140 vs 83 ppm on average) (Table 1, Fig. 5d). Mn and Zn vary together on a 1:1 relation at Strange Lake, as mentioned in the paper by Hawthorne et al. (2001). Mn and Zn covary in amphiboles from Ambohimirahavavy and Amis as well, but in a different way (respectively 4:1 and 1:3), while at Manongarivo and Khan Bogd they do not appear to be related.

Pyroxene

Type-I aegirine, similarly to amphiboles, presents comparable trace elements patterns but different absolute concentrations, from one complex to the other (Table 2). Cores of type-I aegirine from the two Malagasy complexes have high Zr concentrations compared to other complexes (> 8000 vs 2700 ppm on average for the other complexes). Khan Bogd aegirine is

poorer in Li (17 vs 115 ppm), LREE (12 vs 80 ppm on average) and HREE (21 vs 125 ppm on average). Type-I aegirine from Amis, similarly to ferro-ferri-fluoro-leakeite in this complex, shows quite a different trace chemistry than aegirine from other complexes. Average Li is low (50 vs 115 ppm), while other metals are high, e.g. Zn (1780 vs 435 ppm), Sn (3740 vs 700 ppm), Pb (39 vs 7 ppm) and U (29 vs 0.5 ppm) (Table 2 and Fig. 7g). REE and Sc contents in cores of type-I aegirine (zone A) are higher than in the rims (zones B, C and D) for all complexes (Fig. 6, 9 and Table 3; similar maps of aegirine crystals from each complex are provided in Online Resource 4–8). Inside the rims, sector zone C is systematically enriched in REE compared to sector D (Fig. 6k, l, m). Nb and Ta do not have a constant behavior: their contents can be higher in sector zone C, be present only in fractures, or be enriched in an independent zonation, with all three cases being possible within the same sample. Similarly to amphiboles, the chondrite-normalized REE patterns of aegirine show high values for HREE relative to LREE, with lower medium REE. This particular pattern is known to be specific to Na- and Fe-enriched aegirine (Mahood and Stimac 1990; Shearer and Larsen 1994). The absolute REE concentrations, are quite similar from one complex to another, although small variations do exist (Fig. 9).

Trace element concentrations in type-II aegirine are highly dependent on the zoning pattern. This is notably true for Sn, Hf and Zr. Compared to type-I aegirine, Sn covaries with Ti instead of Zr. The shape of type-II aegirine REE patterns is similar to that of type-I, i.e. high HREE relative to LREE, with a depression in medium REE and a negative Eu anomaly. There is no common pattern in the REE contents of type-II aegirine: REE contents are higher in type-II than in type-I aegirine at Khan Bogd, generally lower at Evisa, and have similar values in Madagascar and at Amis (Fig. 7g).

To verify that the concentrations of REE measured in aegirine truly result from their incorporation in the crystal structure and not from small mineral inclusions, we used a STEM approach to investigate the core of a type-I aegirine, where REE are most concentrated. We did not detect any REE mineral inclusion, validating the premise that the REE are indeed incorporated in the pyroxene's structure. The main substitution involved in this process is common to type-I aegirine from all pegmatites. The classic aegirine substitution is

$$^{M2}Ca^{2+} + {}^{M1}\left(Mg^{2+},\ Fe^{2+}\right) \leftrightarrow {}^{M2}Na^{+} + {}^{M1}Fe^{3+}. \quad (1)$$

However, in aegirine from this study there is not enough Fe^{3+} to equilibrate this reaction, hence Al, Zr and Ti, present in aegirine, also contribute to compensate this deficiency, resulting in a new substitution mechanism:

$$^{M2}Ca^{2+} + {}^{M1}\left(Mg^{2+}, Fe^{2+}\right) \leftrightarrow {}^{M2}Na^{+} + {}^{M1}\left(Fe^{3+}, Al^{3+}, Zr^{4+}, Ti^{4+}\right). \quad (2)$$

However, REE can enter both M1 and M2 sites along with Fe^{3+} and Na^{+} (Beard et al. 2019). In clinopyroxenes, incorporation of REE, as well as other HFSE, is controlled by five crystal-chemistry driven mechanisms, with site parameters being determined by the size of the major elements. The first mechanism is decreasing temperature and increasing melt alkalinity, which usually lowers the REE compatibility. The second mechanism is similar to that for amphiboles and is defined by the substitution $Ca \rightarrow Na$, which increases the size of the M2 site leaving more space to incorporate LREE. It also decreases the size of the M1 site, making it more adequate to incorporate HREE. The third mechanism takes place in the M1 crystallographic site, where the combined substitution $(Mg, Fe^{2+}) \rightarrow Fe^{3+}$ leads to a charge effects that allows more HREE to enter this site along with Fe^{3+} (Marks et al. 2004; Beard et al. 2019). The fourth mechanism, described by Mollo et al. (2017), is also due to a charge effect. These authors propose the coupled substitution

$$^{M1}\left(Al, Fe^{3+}\right) + {}^{T}Al \leftrightarrow {}^{M2}\left(Mg, Fe^{2+}\right) + {}^{T}Si, \quad (3)$$

whereby the increase in Al at the expense of Si creates a charge deficiency compensated by the incorporation of REE in the M2 site. In addition, the growth from an environment rich in REE can result in incorporation of high levels of REE in aegirine. Indeed, the adsorption of REE onto aegirine surface during supersaturation may be too fast to equilibrate as crystal growth rate exceeds the internal diffusion rate (Smith et al. 2004).

All of the above mechanisms have the potential of favoring the incorporation of REE into pyroxene, however, aegirine in our study having low ^{T}Al and practically no Mg or Fe^{2+} in the M2 site, the mechanism of Mollo et al. is probably not significant in this case. The high REE concentration in aegirine of this study is therefore probably the result of the four other mechanisms that rely on size, charge, and kinetics effect at M sites of aegirine.

Ce anomalies

Some amphibole and aegirine chondrite-normalized spectra, mostly from one pegmatite sample from Amis, display a peak in Ce concentration (Figs. 8 and 9). The occurrence of this peak being restricted to a few samples, mass interference is excluded. In addition, ICP-MS signals showing peaks during ablation were all excluded so the presence of this Ce peak is not due to mineral inclusions. This peak may be due to the presence of Ce^{4+} instead of the usual Ce^{3+}. Indeed, Ce^{4+} has a smaller ionic radius (0.97 Å) than Ce^{3+} (1.143 Å) for an eight-fold coordination, thereby Ce^{4+} substitutes more easily with Fe^{2+} (0.92 Å) and Mg^{2+} (0.89 Å; Shannon 1976). The change in oxidation state is commonly interpreted to

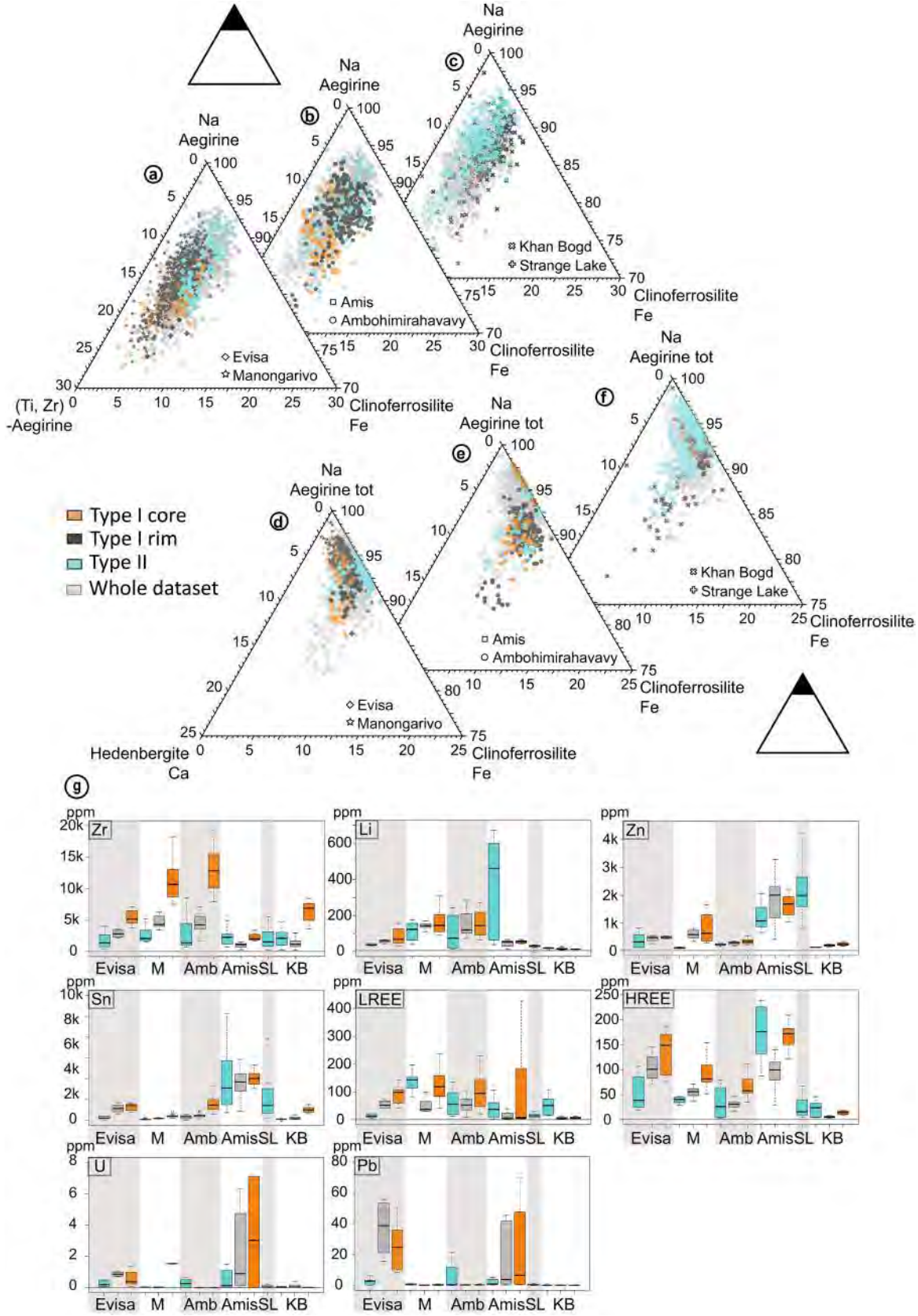
a
b
c
d
e
f
g
Na Aegirine
Na Aegirine tot
(Ti, Zr) -Aegirine
Hedenbergite Ca
Clinoferrosilite Fe
Evisa
Manongarivo
Amis
Ambohimirahavavy
Khan Bogd
Strange Lake
Type I core
Type I rim
Type II
Whole dataset
ppm
Zr
Li
Zn
Sn
LREE
HREE
U
Pb
Evisa M Amb AmisSL KB

◂**Fig. 7** Chemical composition of type-I and type-II aegirine crystals. Type-I aegirine is split between core and rim. Core and rim analyses are identified for type-I aegirine. **a**–**c** are for aegirine, (Ti, Zr)-aegirine, and clinoferrosilite; when figures; **d**–**f** are for aegirine + (Ti, Zr)-aegirine, hedenbergite, and clinoferrosilite. **a**, **d** complexes Evisa and Manongarivo; **b**, **e** complexes Ambohimirahavavy and Amis; **c**, **f** Khan Bogd and Strange Lake; **g** Box diagrams comparing the trace element contents of aegirine from the different complexes. Thick black line represents the median, upper and lower boxplot limits the first and third quartile respectively, upper and lower dashed lines are the maximum and minimum values respectively, and the thin black line is the detection limit. Colors are keyed to the legend given in **a**–**f**. Areas are shaded to distinguish data for each complex

indicate an increase in oxygen fugacity in the environment that can be either low temperature magmatic (< 600 °C, Trail et al. 2012) or hydrothermal (Xu et al. 2017).

Discussion

Origin of amphiboles

In the previous sections we have seen that three different amphiboles can be distinguished based on their major and trace chemistry: fluoro-arfvedsonite [$Na_3Fe_5Si_8O_{22}(F,OH)_2$], ferri-fluoro-leakeite ($Na_3Fe_4LiSi_8O_{22}F_2$), and ferro–ferri–katophorite [$Na_2Ca(Fe^{2+},Mg)_4Fe^{3+}(Si_7Al)O_{22}(OH)_2$]. All of them occur in granites and pegmatites as euhedral crystals and contain inclusions of quartz and feldspar grains (Fig. 4e), suggesting co-crystallization. Only amphiboles from Evisa have a variable composition, from fluoro-arfvedsonite or ferro-ferri-katophorite in cores, respectively to ferri-fluoro-leakeite or fluoro-arfvedsonite in the rims. In the other complexes, only one amphibole type is present in granites and in pegmatites. Based on textural observations, we believe these changes are the sign of magmatic evolution. Indeed, the concentration of Li and Na rises in the melt as differentiation occurs, until Li- and Na-rich amphiboles crystallize instead of their Li-poor, Mg-, Ca-rich equivalents. Based on various pieces of evidence, such as having a similar age to that of granite emplacement (Kovalenko et al. 2006), presence of melt inclusions (Schmitt et al. 2002), occurrence as well-developed euhedral crystals, and dissolution/corrosion textures (Estrade et al. 2014a; Gysi et al. 2016), it is accepted in the literature that amphiboles are magmatic phases in peralkaline granites. Hence, in accordance with our observations and those in the literature about the six studied complexes, we conclude that amphiboles of all types in our samples are magmatic. Their variation in trace element composition is directly linked to the environment they grew in, a highly evolved melt, enriched in incompatible elements. Among incompatible elements are the REE, which are known to be preferentially incorporated in alkaline amphiboles along with Na for LREE and Fe^{3+} for HREE (Bottazzi et al. 1999; Siegel et al. 2017b). Due to this crystallo-chemical control, amphiboles can incorporate a lot of REE at the magmatic stage, with a preference for HREE. Slight compositional differences in REE, Zn, Sn, Nb, Zr and Pb between amphiboles of the 6 complexes (Fig. 5d) likely reflect parental melt compositions. For example, the presence of ferro-ferri-katophorite in Evisa probably indicates an effect of melt contamination in Ca by the surrounding aluminous granites.

As previously described, amphiboles are commonly altered to Fe- and Ti-oxides and to type-II aegirine. Based on textural evidence that at Strange Lake this replacement occurs preferentially along cleavages in altered granites and pegmatites, as well as on mass-balance calculations, Salvi and Williams Jones (1990) identified this pyroxene occurrence as hydrothermal. Because we observed this replacement in all of our samples, it follows that a late hydrothermal event is a common feature in the complexes studied and, by extrapolation, most likely in alkaline rocks in general; indeed, a hydrothermal event was also documented in silica-undersaturated alkaline rocks such as at Ilímaussaq (e.g. Borst et al. 2016) or at Khibina and Lovozero (e.g. Arzamastsev et al. 2011.). Gysi et al. (2016) and Vasyukova and Williams-Jones (2019) show that at Strange Lake this event is due to a relatively high temperature, Ca-rich fluid. Based on the similarity of amphiboles alteration in all six complexes, we infer that the circulation of an orthomagmatic fluid is a process common to all complexes.

Origin of pyroxene

Core-to-rim zonation

Even though both types of aegirine identified in all complexes show some kind of zonation, only type-I shows a core-to-rim zonation, with a core enriched in Ca, Zr, Sn, Hf, Sc, REE and depleted in Na, Al and Fe compared to the rims (Fig. 6). The rims also have a higher Fe^{3+}/Fe^{2+} ratio than the core. This pattern is systematic for type-I aegirine crystals from all complexes. Type-II aegirine is oscillatory zoned and can replace amphibole.

The sharp compositional change between the core and the rims in type-I aegirine (Fig. 6) suggests a sudden change in the crystallizing environment. Based on the scarce presence of type-I aegirine where amphiboles are present, we infer that they grew in competition. Only the rims C and D contain fine oscillatory zoning (e.g. TiO_2 on Fig. 6g), fluid inclusions (Fig. 4g), and, at Ambohimirahavavy, mineral inclusions that match the composition of those measured in hydrothermal pseudomorphs [e.g. zircon, bastnäsite-(Ce), Fig. 4b and h]. Therefore, we infer that type-I aegirine has a magmatic core (zone A on Fig. 6p) while the rims are hydrothermal (zones C

Table 2 Mean values (number of analysis given in bold) for the major and trace element composition, obtained by microprobe and LA-ICPMS respectively, of aegirine from pegmatites and granites from six complexes worldwide in both pegmatites and granites

Complex	Ambo		Amis		Evisa		KB		M		SL
Type	T I	T II	T I	T II	T I	T II	T I	T II	T I	T II	T II
Wt.%											
Samples No.	**238**	**9**	**94**	**58**	**58**	**91**	**127**	**154**	**592**	**39**	**229**
SiO_2	52.40	52.56	52.52	52.45	52.34	52.69	52.38	52.31	52.29	52.41	51.92
TiO_2	1.08	0.62	1.46	1.13	1.35	1.04	0.94	0.94	1.66	0.74	1.18
Al_2O_3	0.25	0.29	0.25	0.27	0.32	0.46	0.26	0.27	0.23	0.26	0.35
K_2O	b.d.l	b.d.l	b.d.l	b.d.l	b.d.l	b.d.l	b.d.l	b.d.l	b.d.l	b.d.l	b.d.l
Fe_2O_3	26.00	27.18	28.02	27.40	25.39	27.25	27.51	27.16	26.64	28.57	28.07
FeO	6.08	4.99	3.60	4.38	5.98	4.92	4.79	5.12	4.07	4.23	3.63
MnO	0.25	0.61	0.11	0.14	0.16	0.19	0.25	0.36	0.85	0.31	0.36
MgO	b.d.l	0.05	b.d.l	0.06	b.d.l	0.03	0.03	0.03	0.03	b.d.l	b.d.l
CaO	0.75	0.63	b.d.l	0.49	0.69	0.11	0.37	0.95	0.48	0.88	0.19
Na_2O	12.57	12.68	13.39	12.94	12.62	13.06	12.93	12.62	13.06	12.88	13.09
Total	99.38	99.62	99.40	99.27	98.87	99.74	99.47	99.73	99.32	100.31	98.79
ppm											
Samples No.	**54**	**11**	**32**	**36**	**15**	**10**	**41**	**8**	**27**	**11**	**18**
Li	151	146	50	315	111	89	17	19	153	112	22
Be	1	15	19	30	13	22	8	b.d.l	4	b.d.l	2
Sc	21	13	14	32	17	15	12	22	20	18	11
Zn	301	449	1777	1231	412	375	222	171	807	96	2253
Ga	10	7	9	13	14	10	7	7	11	6	12
Rb	1	10	b.d.l	6	2	2	b.d.l	b.d.l	b.d.l	b.d.l	13
Sr	16	b.d.l	b.d.l	31	b.d.l	b.d.l	b.d.l	b.d.l	b.d.l	b.d.l	25
Y	22	25	30	96	52	10	6	12	32	29	32
Zr	8709	3606	1633	2195	4005	2049	2504	2180	8077	2737	4580
Nb	27	87	83	32	12	109	5	5	7	2	724
Sn	1011	310	3739	3520	1077	488	389	122	307	110	1828
Ba	b.d.l	2	b.d.l	25	11	3	2	1	b.d.l	b.d.l	1
La	12	10	11	4	4	4	1	5	7	13	4
Ce	36	32	47	21	18	9	6	17	29	49	44
Pr	7	5	4	4	4	2	1	4	6	10	3
Nd	32	22	16	19	26	8	3	20	37	55	15
Sm	7	5	5	8	11	3	1	5	10	14	6
Eu	0.2	0.1	0.3	1	1	b.d.l	b.d.l	0.2	0.5	1	0.4
∑LREE	94	74	83	56	64	25	12	51	90	142	73
Gd	6	3	5	9	13	4	2	4	9	11	5
Tb	1	1	1	3	2	0.6	0.2	1	1	2	1
Dy	4	5	9	21	14	3	1	3	7	9	7
Ho	1	1	2	5	3	0.9	0.2	1	2	2	2
Er	6	6	10	23	13	4	2	2	8	5	8
Tm	2	2	4	7	4	2	1	1	3	1	2
Yb	25	24	75	101	52	33	7	9	36	13	29
Lu	6	6	26	27	14	10	2	3	10	4	7
∑HREE + Y	73	72	161	292	165	67	21	36	108	74	92
Hf	343	136	172	177	185	84	110	85	319	119	125
Ta	9	3	14	2	1	14	1	0.1	2	0.5	29
Pb	3	28	39	3	24	3	0.2	0.1	1	1	14
Th	0.2	1	5	5	9	1	0.1	0.1	0.4	1	1
U	0.04	0.2	29	1	1	1	0.1	0.1	1	0.03	2

Granites only comprise type-II aegirine. T I, T II aegirine type-I, II

no. number of replicates, *b.d.l* below detection limit, *Ambo* Ambohimirahavavy, *KB* Khan bogd, *M* Manongarivo, *SL* Strange Lake

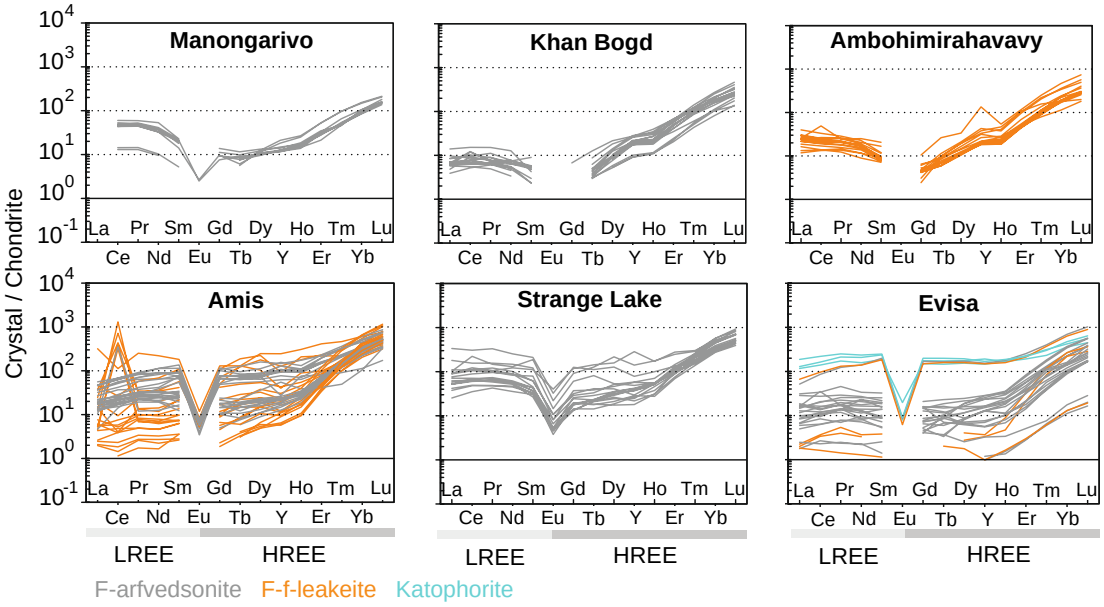

Fig. 8 Logarithmic diagrams plotting chondrite-normalized REE composition obtained by LA-ICP-MS for amphiboles (normalization from Sun and McDonough 1989) for all six complexes

and D in Fig. 6p). Zone B being only present at Khan Bogd, it will be discussed lower in this section. Chemical zoning in aegirine of our rocks matches that observed by Piilonen et al. (1998) in aegirine from Mont Saint-Hilaire, which they describe as a magmatic pyroxene overgrown by hydrothermal fibrous aegirine. More details about each element in the different zones is provided in the following paragraphs.

The variations in Na, Ca, Al, and Fe can be explained by a common process. Type-I aegirine magmatic cores are enriched in Ca, and its hydrothermal rims are richer in Na, Al and Fe^{3+}. Evidence such as widespread feldspar albitization, fluid inclusions composition, and the hydrothermal growth of aegirine without amphibole indicate that circulating hydrothermal fluids are oxidizing (above the magnetite-hematite buffer), of relatively high pH and rich in NaCl among other phases (Salvi and Williams-Jones 1996; Smith 2007; Estrade 2014; Gysi et al. 2016). Depletion in Ca and enrichment in Na and Fe while moving on from aegirine magmatic core to hydrothermal rims can then be explained by intake of Na from the hydrothermal fluids and simultaneous crystallization of Ca-rich secondary minerals in the pseudomorphs [fluorite, bastnäsite-(Ce)]. This process increases the amount of aegirine end-member compared to hedenbergite end-member which, along with the hydrothermal environment being more oxidizing than the silicate melt, increases the Fe^{3+}/Fe^{2+} ratio in the rims. The absolute amount of Al is very low in aegirine of this study, so the observed increase in this element in aegirine rims can be linked only to charge effects, with Al^{3+} being incorporated along with Fe^{3+}.

Because of their similar behavior, Zr and Hf both occur in the same growth zones. Based on the many arguments in favor of a magmatic core and hydrothermal rims, we propose two hypotheses as to the crystallization timing of type-I aegirine. Jones and Peckett (1981) asserted that formation of Zr-enriched aegirine is enhanced by low oxygen fugacity, and can only occur if no other Zr-bearing phase is growing. Pseudomorphs after primary zirconosilicates were found around aegirine crystals (Fig. 4b), hence it is impossible that aegirine grew after the magmatic zirconosilicates. Our first hypothesis is that, in accordance with the observations made by Jones and Peckett (1981), type-I aegirine cores grew before magmatic zirconosilicates, in the magma chamber. In the absence of any mineral Zr has a strong affinity for, Zr partitioned mostly into aegirine. These primary phenocrysts were brought into pegmatites, where primary zirconosilicates began to crystallize, incorporating most of the available Zr. Moving on to the hydrothermal stage, primary zirconosilicates were destabilized and replaced by minerals richer in Zr, including zircon, which form the pseudomorphs. Aegirine rims were then in competition with zircon, which has a high Zr uptake and therefore accounts for the decrease in Zr concentration in aegirine rims. In this hypothesis, aegirine necessarily stopped growing during their migration from the magma chamber to the pegmatites, or it would have resulted in another zonation in the magmatic

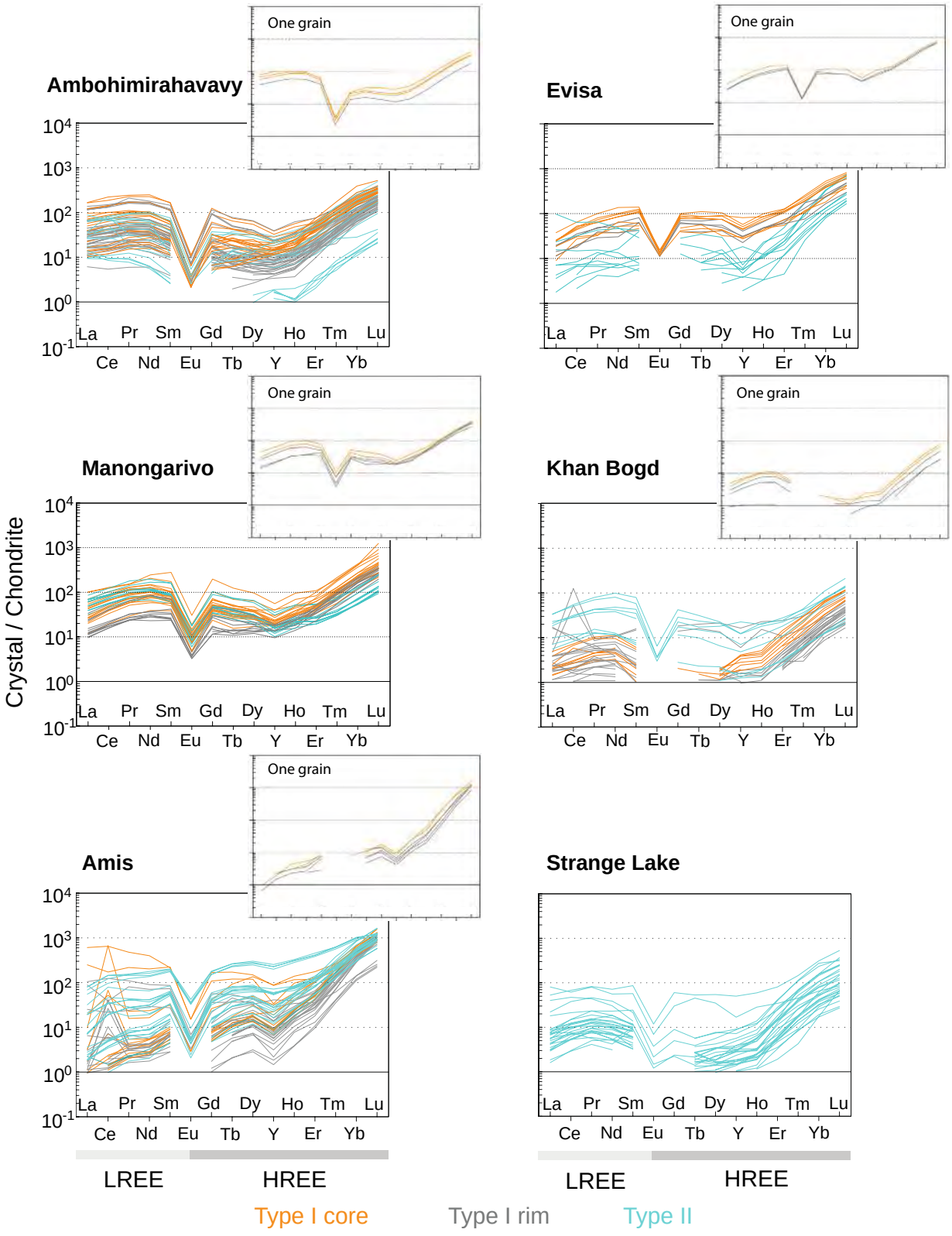

Fig. 9 Logarithmic diagrams plotting chondrite-normalized REE composition obtained by LA-ICPMS for aegirine (normalization from Sun and McDonough 1989) for all six complexes. Large spectra presents all LA-ICP-MS analyses for type-I and type-II aegirine, whereas small spectra on the side show an example of analyses performed on a single type-I crystal

Table 3 Mean composition of cores and rims of type-I aegirine from five complexes

Complex	Ambo		Amis		Evisa		KB		M	
Position	Core	Rim	Core	Rim	Core	Rim	Core	Rim	Core	Rim
ppm										
Samples No.	**22**	**32**	**12**	**20**	**8**	**7**	**8**	**21**	**16**	**11**
La	14	9	19	4	5	3	1	1	11	4
Ce	44	28	83	10	26	10	3	7	41	16
Pr	8	5	6	1	6	3	1	0.4	9	4
Nd	40	24	26	6	39	14	3	2	52	21
Sm	9	5	7	2	15	7	0.5	1	15	6
Eu	0.2	0.2	0.4	0.1	1	1	b.d.l	b.d.l	1	0.3
∑LREE	116	72	142	23	90	37	7	11	129	51
Gd	6	5	7	3	15	11	b.d.l	2	13	5
Tb	1	1	2	1	3	2	b.d.l	0.4	2	1
Dy	6	3	13	4	17	10	0.4	1	10	5
Er	1	1	3	1	4	2	0.2	0.2	2	1
Tm	8	4	14	6	16	9	2	1	10	6
Ho	3	1	5	3	5	3	1	0.2	3	2
Yb	34	17	94	56	61	44	9	3	44	27
Lu	8	4	30	22	15	12	2	1	13	7
Y	28	15	44	16	72	32	5	3	41	24
∑HREE + Y	95	51	212	110	207	124	19	12	138	78
La/Lu	2	2	0.6	0.2	0.3	0.3	0.3	1	0.8	0.5
Ca	8047	5512	243	215	6759	3062	3787	2310	3757	2902
Fe^{3+}	176,488	185,270	193,648	198,633	171,056	184,386	190,956	192,603	182,306	190,588
Hf	529	158	176	169	241	130	319	58	471	168
Na	91,898	93,417	99,084	99,024	91,997	94,713	93,401	95,708	96,060	97,171
Sn	1547	475	4020	3459	1297	857	1026	223	415	199
Zr	12,974	4444	2253	1013	5406	2604	6389	1340	11,397	4757
Al	931	1362	1096	1539	1657	1762	1567	1361	1072	1393

no. number of replicates, *b.d.l* below detection limit, *Ambo* Ambohimirahavavy, *KB* Khan bogd, *M* Manongarivo

core. Our second hypothesis is that aegirine core and primary zirconosilicates grew at the same time. In this case the conclusions of Jones and Peckett (1981) do not apply. This may be because their study was based on rocks from the magmatic chamber of Ilímaussaq which had plenty of time to equilibrate during crystallization, whereas our study is based on pegmatites, which crystallize quickly. Anyhow, in this hypothesis the competition between the two minerals resulted in the preference of Zr to go into primary zirconosilicates, but because of the high content of Zr in the melt and its low mobility (Duggan 1988), affinity for aegirine was still high enough to enrich it up to the 2 wt% that we have measured. The subsequent hydrothermal stage is similar to the one in our previous hypothesis, with higher Zr uptake by zircon rather than by zirconosilicates accounting for the decrease in Zr concentration in aegirine rims. A similar behavior was observed for Sn and is most likely due to a similar phenomenon. No Sn-based mineral was found in pseudomorphs, but Sn^{4+} can easily enter in the composition of secondary Ti-oxides because its radius is similar to the Ti^{4+} ion in eight-fold coordination (Shannon 1976). In addition, Sn is known to have a high solubility in Cl-rich fluids (e.g. Keppler and Wyllie 1991), making it easily mobilized. This results in a much higher Sn content in the magmatic zone A than in the rims of aegirine. At Amis, amphibole in pegmatite as well as aegirine are both enriched in Sn, Zn and Pb in comparison with the other complexes of this study (Fig. 7g). Ambohimirahavavy and Manongarivo have similar trace elements concentration (Fig. 7g) and formed in the same geological context, a few km away from each other. Both amphibole and pyroxene from Khan Bogd have low trace elements concentrations. All these observations tend to indicate that the variations of absolute concentration in REE, Zn, Sn, Zr, U and Pb between aegirine crystals of the 6 complexes (Fig. 7g), similarly to amphiboles, likely reflect parent melt compositions.

Sector zoning

Sector zoning occurs in the most outer rims in type-I aegirine, involves variations in Ti, Ca, Fe and REE, and was observed in all complexes. Many explanations have been invoked as to the origin of sector zoning, and the latest agree on the fact that it is linked to a crystal growth faster than element diffusion rates (Ubide et al. 2019). If this condition is respected, it will result a disequilibrium between the different crystal faces that will not all incorporate the same elements as it normally would (Strong 1969; Ferguson 1973; Larsen 1981). Elements are however incorporated on the different crystal faces in a matter so that charge balance is respected (Ubide et al. 2019). The crystallization rate could also impact the size of protosites (partially formed site on the surface of a growing crystal), which are in equilibrium with the crystallizing environment, and preferentially incorporate elements depending on their charge/radius ratio. If the growth rate is higher than ionic diffusion in the crystal, the protosites will not have enough time to re-equilibrate in size and incorporate different elements on the different faces of the crystal (Nakamura 1973). This higher growth rate is likely related to a lower temperature due to the change from magmatic to hydrothermal environment (Barkov and Martin 2015). However, these considerations must be taken carefully, as most of the research is based on augite and not aegirine.

Incorporation of Ti in aegirine is uncommon (Rønsbo et al. 1977; Dyulgerov and Platevoet 2006). Many explanations have been evoked: high temperature, low fO_2, high fO_2, low pressure, high activities of TiO_2 and SiO_2, high activity of alkalis, or a peculiar chemical composition of the environment such as low Zr and Na and high Ca (Ferguson 1973; Flower 1974; Larsen 1976; Rønsbo et al. 1977; Nielsen 1979; Brousse and Rançon 1984; Dyulgerov and Platevoet 2006). In our samples, a high temperature is ruled out as Ti incorporation occurs during the hydrothermal stage. As described in the previous section, Zr and Ca concentration are low in the crystallizing environment, and Na is high. Hence, and in accordance with Dyulgerov and Platevoet (2006), Larsen (1976), and Flower (1974), we suggest that in our rocks the incorporation of Ti into hydrothermal aegirine is favored by a high activity of Na and the low availability of Zr. Titanium may have been provided by the alteration of magmatic Ti-bearing minerals, such as astrophyllite (found at Manongarivo, Strange Lake, Khan Bogd and Amis, Fig. 4a) chevkinite-(Ce) (found at Ambohimirahavavy, Manongarivo and Evisa), or others such as narsarsukite, låvenite, and aenigmatite.

Oscillatory zoning

Oscillatory zoning is present in both types of aegirine. In type-I, it is found in the sector-zoned rims C [crystallographic sector (110)] and D [crystallographic sector (100)] as well as in zone B, intermediate between the core and the rims. Considering that zone B in type-I aegirine is only present in our samples in Khan Bogd, and was locally described in aegirine from the South Gardar Province, South Greenland by Ranløv and Dymek (1991), a general process to explain its formation is difficult to establish. Like zones C and D, zone B is poorer in Ca, Zr, Hf, Sn and REE than zone A. It is not specifically enriched in any element, but shows oscillatory zoning in Ti and Mn. We believe that zone B development is related to a specificity in the history of the Khan Bogd complex (Kynicky et al. 2011). In this complex, magmatic zone A aegirine would crystallize before or in competition with primary elpidite. At the hydrothermal stage, primary elpidite altered mostly into a secondary hydrated Ca- and REE-rich elpidite (Fig. 4i), and zone B grew simultaneously. The uptake of Ca and Zr by secondary elpidite from the fluid led to the lower concentration of these elements observed in zone B. The final stage, similarly to other complexes, was a more or less extensive pseudomorphism of elpidite and the formation of zones C and D on aegirine.

Oscillating concentrations in zones C and D are most likely produced by autocatalytic surface attachment, or boundary layer effect (Ortoleva et al. 1987; London 2008), which occurs when the crystal growth rate exceeds the diffusion rate of components in the fluid. Consider an initial solution saturated in component A, whose adsorption on the crystal surface is fast. As the adsorption progresses, the interface between the crystal and the solution becomes depleted in component A, and switches to saturation in component B. Component B is then adsorbed at the surface of the crystal, until the interface crystal-solution becomes saturated in component A again. This process results in a rhythmic but irregular zoning of aegirine crystals in zones C and D, consistent with a growth in a rapidly changing environment, which is a hydrothermal fluid.

Type-II aegirine either replaces amphibole or forms isolated crystals. Both kinds are found associated with Fe- and/or Ti- oxides, and are randomly zoned in many elements (Ti, Ca, Mn, Fe, Hf, Sn, Zr at least). The formation of aegirine from amphibole is known to be hydrothermal (e.g. Salvi and Williams-Jones 1990; Gysi et al. 2016). For arfvedsonite, it follows the reaction provided by Salvi and Williams-Jones (1997):

$$3Na_3Fe_5Si_8O_{22}(F,OH)_2 + 2H_2O = 9NaFeSi_2O_6 + 2Fe_3O_4 + 6SiO_2 + 5H_2. \quad (4)$$

The released Fe generally forms hematite or magnetite. Considering that zoning patterns are the same for all type-II aegirine crystals and that they are systematically found associated with Fe- and/or Ti- oxides, we consider that they all grew replacing amphibole, totally or partially. Hence, we consider type-II aegirine as hydrothermal.

REE behavior in amphiboles and aegirine

As mentioned in the introduction, amphiboles and pyroxenes, in agreement with their crystal-chemical parameters, can incorporate up to several hundreds of ppm of REE. In addition, their alkaline nature enhances the fractionation of light versus heavy REE through the preferential incorporation of HREE in their structure, resulting in the globally HREE-enriched patterns observed (Fig. 9; Beard et al. 2019). From the amphibole compositions, we know that the melt was rich in F (Table 1). Beard et al. (2020) showed that the more F in the melt, the lower the pyroxene-melt partition coefficient, hence the less REE are incorporated in pyroxene; this affects the LREE more than the HREE and hence contributes to the observed globally HREE-enriched patterns.

The REE compositional patterns observed in type-I aegirine are similar to the compositional trends for Zr, Hf and Sn, i.e. they are globally enriched in the core compared to the rims, except for Khan Bogd where the opposite is true (Fig. 10, Table 3). Given that the REE concentrations in aegirine at Khan Bogd are very low (2–7 ppm for Ce, 4–15 ppm for Y), we believe that this reverse trend is actually not significant (Fig. 10). The difference in REE concentration between aegirine zone A and zones B, C and D is due to the competition between aegirine and zirconosilicates for these elements, during the magmatic stage for zone A, and during the hydrothermal stage for the zones B, C and D. Scandium is sometimes grouped with REE, hence, it is not surprising to observe that, similarly to REE, it is enriched in the core of type-I aegirine.

During the hydrothermal stage, aegirine is in competition with an altered, REE-enriched elpidite for zone B, and with REE-bearing minerals in pseudomorphs [e.g. bastnäsite-(Ce)] for zones C—(110) and D—(100). We therefore suggest that it is a competition for REE between aegirine and coprecipitating minerals having each a different REE affinity which explains the variations in REE concentrations among the aegirine core-to-rim zones. REE are also affected by sector zoning and are more concentrated in zone C than D, along with Ti and Ca. Beard et al. (2019) studied experimentally the fractionation of REE in clinopyroxene in peralkaline melts and showed that the more Na and less Ca in M2 site of pyroxene, the smaller the M1 site, and the more HREE are incorporated. In addition, the authors mention that physico-chemical parameters not recorded in the composition of clinopyroxene, such as pressure, also play a significant role in the size of the M1 site. However, this mechanism is well defined only for pyroxenes whose aegirine component is not higher than 50%. In our samples, the substitution Ca → Na simply cannot be responsible for the zonation observed, as more REE are found in the C sector, where Ca concentration is also higher. In addition, in Ca-rich pyroxenes such as diopside and augite, Ca was not reported to fractionate between sectors (e.g. Ubide et al. 2019), which is another argument for the occurrence of a different exchange mechanism in our samples.

In addition to the above variations in bulk abundance, cores and rims also preferentially incorporate REE with lower or higher atomic numbers, creating a fractionation between the heavy and light REE. To evaluate this process, we calculated the percentages of REE enrichment or depletion from core-to-rim in type-I pyroxene. To do so, data obtained by LA-ICPMS were assigned either to the core or to the rim, based on their Zr content and zoning SEM observations. By comparing these two parameters, we were able to determine a threshold value, unique to each complex, below which a given aegirine analysis should be considered as rim, and above which core. These

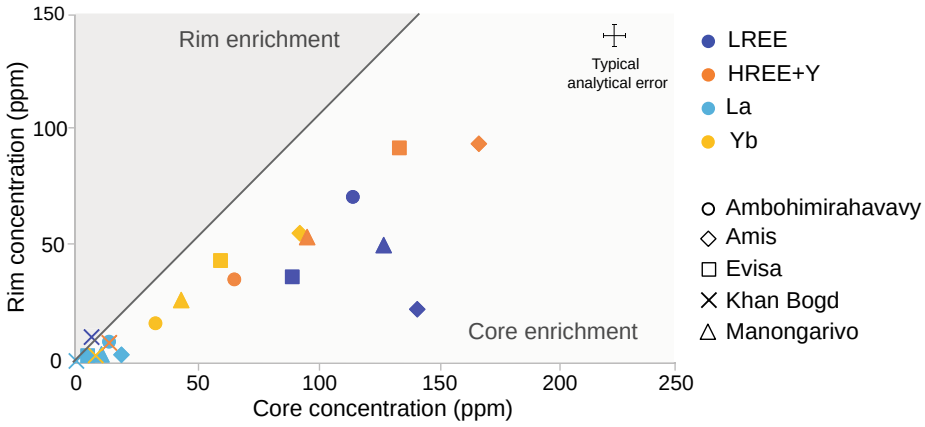

Fig. 10 Diagram plotting REE concentration obtained by LA-ICPMS in the core and rim of type-I pyroxene in five complexes. The typical analytical error is provided by the cross on the top right corner and is similar for all provided analyses

data were averaged out to obtain a single value each for core and rim (Fig. 10). Finally, we calculated the extent of loss or enrichment between core and rim for each REE, according to:

$$d = \frac{C - R}{C} \times 100 \quad (5)$$

where d represents the percentage difference between core and rim, C and R the mean values obtained for core and rim, respectively. Error bars shown in Fig. 11 were obtained using common error calculation formulae, namely (Eq. 6) for the mean and (Eq. 7) for the percentage.

$$\overline{\text{err}} = \sqrt{\frac{\sum_{x=1}^{n} \left(\text{err}_x\right)^2}{n}} \quad (6)$$

$$d_{\text{err}} = \frac{C - R}{C} \sqrt{\sqrt{\frac{\text{err}_C^2 - \text{err}_R^2}{(C - R)^2} + \frac{\text{err}_C^2}{C^2}}} \quad (7)$$

with $\overline{\text{err}}$ being the mean error, n the number of measurements, d_{err} the error on the percentage variation from core-to-rim, err_C the mean error on core data, and err_R the mean error on rim data. Resulting values indicate an enrichment in that element in the rim compared to the core when positive, while negative ones indicate a depletion (Fig. 11).

From the calculation of the percentage of depletion of REE from core-to-rim (Fig. 11) we see that Amis, Manongarivo and Evisa have a trend with a more important depletion of LREE than HREE: from 40–80% to 20–40% depletion, respectively. Ambohimirahavavy shows the opposite trend: around 30% of LREE depletion for 45% of HREE depletion. The latter trend is not as obvious as for other complexes, but it is still significant.

General model

We propose a global model of formation for amphiboles and aegirine in pegmatites (Fig. 12). During the magmatic stage, two hypotheses remain. In the first one, amphibole and zone A of type-I aegirine grew at early magmatic stage, concentrating Zr and REE. In the second hypothesis, type-I aegirine core, amphibole and zirconosilicates grew in competition. Most Zr was incorporated in the zirconosilicates, as well as REE if the primary zirconosilicates was EGM. However, highly differentiated alkaline melts being particularly enriched in Zr and REE, there is an extra supply in these metals which, combined with a fast crystallization, could be incorporated by the structures of amphiboles and aegirine (Fig. 12a).

During the orthomagmatic hydrothermal stage, amphiboles did not grow anymore, and type-I aegirine was in

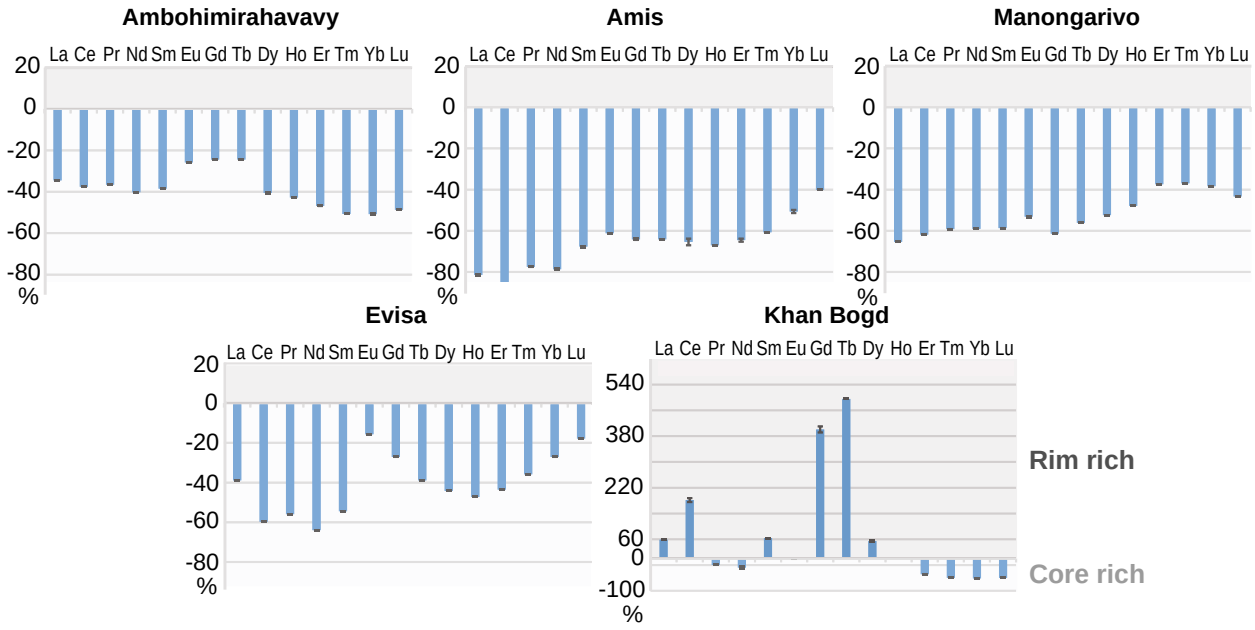

Fig. 11 Histograms plotting the difference of REE concentration between the core and the rims of type-I aegirine, and thereby REE fractionation from core-to-rim. Negative values stand for a higher REE concentration in the core, and positive ones for a higher concentration in the rims. The rim enrichment in Khan Bogd is an artifact. Calculated error is shown by black lines at the end of the histogram bars

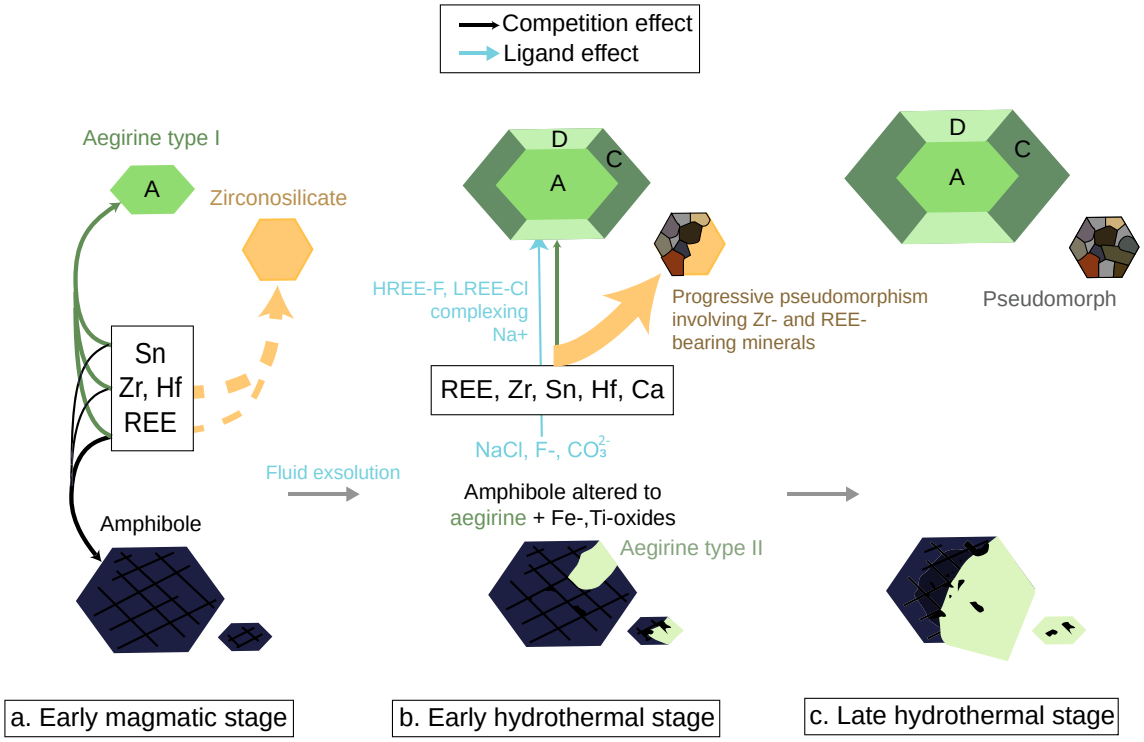

Fig. 12 A schematic illustration of a model for aegirine and amphiboles formation. The arrows signify transfer of elements (in the boxes) to the different minerals from the melt or fluid (light blue), the line thickness is proportional to the amount of transfer, and a dashed line indicates a possible transfer. Ligands in the fluids are also shown. During the early magmatic stage, the competition for REE, Zr, Hf, Zr and Sn is low to moderate (depending on the co-presence or not of amphibole, pyroxene and complex zirconosilicate) and allows a relative enrichment in these elements in type-I aegirine and, mostly for REE, in amphibole. During the hydrothermal stage, the competition for these elements is stronger as it involves zircon and REE-bearing minerals; consequently, type-I aegirine rims are globally depleted. Fluids composition leads to a different mobilization of light and heavy REE, originating REE fractionation. Meanwhile, hydrothermal fluids replace amphiboles by type-II secondary aegirine and Fe–Ti-oxides

competition with secondary Zr- and REE-bearing minerals (generally zircon and bastnäsite-(Ce)) that formed pseudomorphs after primary zirconosilicates. Since HFSE have much higher affinity for these secondary minerals, their concentrations globally decreased in the co-crystallizing aegirine rims. It is also during this stage that type-II aegirine crystals nucleated. Nevertheless, competition does not explain the observed LREE-HREE fractionation. Residual melt, depleted in incompatible elements, likely crystallized late quartz and feldspar.

Given the overwhelming evidence for circulation of an orthomagmatic fluid in all complexes, we propose that fractionation results from variations in fluid composition. From the presence of secondary minerals such as bastnäsite-(Ce) and fluorite, and the study of fluid inclusions at Ambohimirahavavy and Strange Lake (Estrade 2014; Vasyukova et al. 2016), we know that the fluids contained at least the anions Cl^-, F^-, and CO_3^{2-}. These species have the ability to form stable complexes with the REE, to different extents. F^- and CO_3^{2-} together are mostly depositional ligands (Migdisov et al. 2016), thus precipitate with REE typically forming the LREE-bearing bastnäsite-(Ce). On the other hand, Cl^- is a weak but abundant ligand that can transport LREE more easily than the heavy ones (Migdisov et al. 2016). If present as a transporting ligand, F^- also transports more LREE than HREE (Beard et al. 2020). We can thus infer that, depending on the relative concentrations of each ligand, fractionation of light vs heavy REE would be specific to each complex (Fig. 12b). As long as fluid flow continued, aegirine rims kept growing, although REE incorporation and LREE-HREE fractionation kept diminishing. By the time the hydrothermal stage waned, the two aegirine types were in equilibrium with the pseudomorphs and the partially replaced amphiboles (Fig. 12c).

Conclusions

By comparing amphibole and pyroxene in six alkaline complexes worldwide, our study highlights that despite different geodynamic contexts, mineralogy, and REE enrichment, there is a general crystallization process

common to all studied alkaline pegmatites. We believe this process can be generalized to all alkaline SiO_2-saturated pegmatites worldwide, with local variations in mineralogy and REE enrichment and fractionation rates. This crystallization process includes at least two main stages, respectively magmatic and hydrothermal.

From the study of the composition of amphibole and type-I aegirine core, we document the magmatic stage, during which a systematic primary enrichment in REE, HFSE and a LREE-HREE fractionation occurs. This enrichment is common to all complexes and linked to the properties of the extremely differentiated alkaline magma. The enrichment rate, however, differs from one complex to another. The REE fractionation is most likely due to crystallographic properties of aegirine and alkali amphiboles that preferentially incorporate HREE and do not represent an inherent property of the melt.

From the study of the texture and composition of type-I aegirine rims and type-II aegirine, we document similarities between complexes during the hydrothermal stage, at which amphiboles stop growing, type-I aegirine grows sector-zoned rims, and type-II aegirine begins replacing amphibole along with Fe- and Ti-oxides. The drop in REE concentration in hydrothermal aegirine of all complexes shows that REE hydrothermal enrichment is globally less effective than magmatic REE enrichment, but still effective. The observed REE fractionation in all complexes show that hydrothermal fluids also have the ability to fractionate LREE-HREE through their transportation associated with ligands such as F^-, Cl^-. The rate of fractionation as well as the amount of mobilized REE depends on the local properties of the circulating fluid(s). These observations show that hydrothermal flow is mandatory to enhance the concentration of the REE, and specially HREE, in alkaline pegmatites to ore levels.

Acknowledgements This work was supported by an INSU/TelluS grant from CNRS (French National Center for Scientific Research). We thank Anthony Williams-Jones, Olga Vasyukova and Sam Broom-Fendley for providing some of the rock samples from the Strange Lake and Amis complexes and David Chew who helped with LA-ICP-MS mapping. Kathryn Goodenough provided helpful discussion. We also wish to thank CPM reviewers Charles Beard and Adrian Finch for their suggestions and constructive criticisms, which greatly improved the final version of this manuscript.

References

Ancey M, Bastenaire F, Tixier R (1978) Application des méthodes statistiques en microanalyse. Microanal Microsc Électron Balayage 323:11–16

Arzamastsev AA, Arzamastseva LV, Zaraiskii GP (2011) Contact interaction of agpaitic magmas with basement gneisses: an example of the Khibina and Lovozero massifs. Petrology 19:109–133

Barkov AY, Martin RF (2015) Anomalous Cr-rich zones in sector-zoned clinopyroxene macrocrysts in gabbro, Mont Royal, Montreal, Quebec, Canada. Can Mineral 53:895–910

Beard CD, van Hinsberg VJ, Stix J, Wilke M (2019) Clinopyroxene/melt trace element partitioning in sodic alkaline magmas. J Petrol. https://doi.org/10.1093/petrology/egz052

Beard C, van Hinsberg V, Stix J, Wilke M (2020) The effect of fluorine on clinopyroxene/melt trace-element partitioning. Contrib Mineral Petrol. https://doi.org/10.1007/s00410-020-1672-5

Boily M, Williams-Jones AE (1994) The role of magmatic and hydrothermal processes in the chemical evolution of the Strange Lake plutonic complex, Quebec-Labrador. Contrib Mineral Petrol 118:33–47

Bonin B (1988) Peralkaline granites in Corsica: some petrological and geochemical constraints. Rendiconti Della Soc Ital Mineral Petrol 73:1191–1194

Bonin B (1990) Les granites des complexes annulaires, BRGM. Office des publications universitaires

Bonin B (2007) A-type granites and related rocks: evolution of a concept, problems and prospects. Lithos 97:1–29

Bonin B, Grelou-Orsini C, Vialette Y (1978) Age, origin and evolution of the anorogenic complex of Evisa (Corsica): a K–Li–Rb–Sr study. Contrib Mineral Petrol 65:425–432

Bonin B, Platevoet B, Poitrasson F, Renna MR (2008) Eurogranites-IGCP510 2008 Joint Field-meeting—Alkaline The Permian–Triassic A-type Volcanic–Plutonic Igneous Suite of Corsica. In: 33th International Geological Congress in Oslo, Norway Convention Centre, Lillestrom, Norway

Borst AM, Friis H, Andersen T et al (2016) Zirconosilicates in the kakortokites of the Ilímaussaq complex, South Greenland: implications for fluid evolution and high-field-strength and rare-earth element mineralization in agpaitic systems. Mineral Mag 80:5–30

Bottazzi P, Tiepolo M, Vannucci R et al (1999) Distinct site preferences for heavy and light REE in amphibole and the prediction of Amph/L D REE. Contrib Mineral Petrol 137:36–45

Brousse R, Rançon JP (1984) Crystallization trends of pyroxenes from agpaitic phonolites (Cantal, France). Mineral Mag 48:39–45

Chakhmouradian AR, Wall F (2012) Rare earth elements: minerals, mines, magnets (and more). Elements 8:333–340

Chakhmouradian AR, Zaitsev AN (2012) Rare earth mineralization in igneous rocks: sources and processes. Elements 8:347–353

Chengyu W, Dianhao H, Zhongxun G (1990) REE geochemistry in the weathered crust of granites, Longnan Area, Jiangxi Province. Acta Geol Sin - Engl Ed 3:193–209. https://doi.org/10.1111/j.1755-6724.1990.mp3002006.x

Cocherie A, Rossi P, Fanning CM, Guerrot C (2005) Comparative use of TIMS and SHRIMP for U–Pb zircon dating of A-type granites and mafic tholeiitic layered complexes and dykes from the Corsican Batholith (France). Lithos 82:185–219

Coint N, Barnes CG, Yoshinobu AS et al (2013) Use of trace element abundances in augite and hornblende to determine the size, connectivity, timing, and evolution of magma batches in a tilted batholith. Geosphere 9:1747–1765

Cucciniello C, Tucker RD, Jourdan F et al (2016) The age and petrogenesis of alkaline magmatism in the Ampasindava Peninsula and Nosy Be archipelago, northern Madagascar|SpringerLink. Mineral Petrol 110:309–331. https://doi.org/10.1007/s00710-015-0387-1

Currie KL (1985) An unusual peralkaline granite near lac Brisson, Quebec-Labrador. Curr Res 73–80

Deer WA, Howie RA, Zussman J (1997a) Rock-forming minerals: single-chain silicates, vol 2A. Geological Society of London, London

Deer WA, Howie RA, Zussman J (1997b) Rock-forming minerals: double-chain silicates, vol 2B. Geological Society of London, London

Diehl M (1990) Geology, mineralogy, geochemistry and hydrothermal alteration of the Brandberg alkaline complex. Geological Survey of Namibia, Namibia

Donnot M (1963) Côte Nord-Ouest du complexe intrusif alcalin; Ampasindava-Manongarivo

Droop GTR (1987) A general equation for estimating Fe 3+ concentrations in ferromagnesian silicates and oxides from microprobe analyses, using stoichiometric criteria. Mineral Mag 51:431–435

Duggan MB (1988) Zirconium-rich sodic pyroxenes in felsic volcanics from the Warrumbungle Volcano, Central New South Wales, Australia. Mineral Mag 52:491–496

Dyulgerov MM, Platevoet B (2006) Unusual Ti and Zr aegirine-augite and potassic magnesio-arfvedsonite in the peralkaline potassic oversaturated Buhovo-Seslavtzi complex, Bulgaria. Eur J Mineral 18:127–138

Estrade G (2014) Le complexe cénozoïque alcalin d'Ambohimirahavavy à Madagascar : origine, évolution et minéralisations en métaux rares. Toulouse 3

Estrade G, Béziat D, Salvi S et al (2014a) Unusual evolution of silica-under-and-oversaturated alkaline rocks in the Cenozoic Ambohimirahavavy Complex (Madagascar): mineralogical and geochemical evidence. Lithos 206:361–383

Estrade G, Salvi S, Béziat D et al (2014b) REE and HFSE mineralization in peralkaline granites of the Ambohimirahavavy alkaline complex, Ampasindava peninsula, Madagascar. J Afr Earth Sci 94:141–155

Estrade G, Salvi S, Béziat D (2018) Crystallization and destabilization of eudialyte-group minerals in peralkaline granite and pegmatite: a case study from the Ambohimirahavavy complex, Madagascar. Mineral Mag 82:375–399. https://doi.org/10.1180/minmag.2017.081.053

Fedele L, Lustrino M, Melluso L et al (2015) Trace-element partitioning between plagioclase, alkali feldspar, Ti-magnetite, biotite, apatite, and evolved potassic liquids from Campi Flegrei (Southern Italy). Am Mineral 100:233–249

European Commission (2018) Report on critical raw materials and the circular economy. http://ec.europa.eu/docsroom/documents/27348. Accessed 25 Apr 2018

Ferguson AK (1973) On hour-glass sector zoning in clinopyroxene. Mineral Mag 39:321–325. https://doi.org/10.1180/minmag.1973.039.303.08

Flower MF (1974) Phase relations of titan-acmite in the system Na_2O–Fe_2O_3–Al_2O_3–TiO_2–SiO_2 at 1000 bars total water pressure. Am Mineral J Earth Planet Mater 59:536–548

Foland KA, Landoll JD, Henderson CMB, Chen J (1993) Formation of cogenetic quartz and nepheline syenites. Geochim Cosmochim Acta 57:697–704. https://doi.org/10.1016/0016-7037(93)90380-F

Goodenough KM, Wall F, Merriman D (2018) The rare earth elements: demand, global resources, and challenges for resourcing future generations. Nat Resour Res 27:201–216. https://doi.org/10.1007/s11053-017-9336-5

Gowans RM, Lewis WJ, Zalnieriunas RV (2017) Quest Rare Minerals Ltd.: Strange Lake Resource Estimation

Grigor'eva AA, Zubkova NV, Pekov IV et al (2011) Crystal chemistry of elpidite from Khan Bogdo (Mongolia) and its K-and Rb-exchanged forms. Crystallogr Rep 56:832

Gysi AP, Williams-Jones AE, Collins P (2016) Lithogeochemical vectors for hydrothermal processes in the Strange Lake peralkaline granitic REE-Zr–Nb deposit. Econ Geol 111:1241–1276

Hatch GP (2015) TMR Advanced Rare-Earth Projects Index—Technology Metals Research. http://www.techmetalsresearch.com/metrics-indices/tmr-advanced-rare-earth-projects-index/. Accessed 27 Jun 2018

Hawthorne FC, Oberti R, Ungaretti L et al (1996) Fluor-ferro-leakeite, $NaNa_2$ (Fe_2+ 2Fe_3+ 2Li) $Si_8O_{22}F_2$, a new alkali amphibole from the Canada Pinabete pluton, Questa, New Mexico, USA. Am Mineral 81:226–228

Hawthorne FC, Oberti R, Cannillo E et al (2001) Li-bearing arfvedsonitic amphiboles from the Strange Lake peralkaline granite, Quebec. Can Mineral 39:1161–1170

Hawthorne FC, Oberti R, Harlow GE et al (2012) Nomenclature of the amphibole supergroup. Am Mineral 97:2031–2048

Ishihara S, Hua R, Hoshino M, Murakami H (2008) REE abundance and REE minerals in granitic rocks in the Nanling range, Jiangxi Province, southern China, and generation of the REE-rich weathered crust deposits. Resour Geol 58:355–372

Jones AP, Peckett A (1981) Zirconium-bearing aegirines from Motzfeldt, south Greenland. Contrib Mineral Petrol 75:251–255

Keppler H, Wyllie PJ (1991) Partitioning of Cu, Sn, Mo, W, U, and Th between melt and aqueous fluid in the systems haplogranite-H_2O–HCl and haplogranite-H_2O- HF. Contrib Mineral Petrol 109:139–150

Kogarko LN, Williams CT, Woolley AR (2002) Chemical evolution and petrogenetic implications of loparite in the layered, agpaitic Lovozero complex, Kola Peninsula, Russia. Mineral Petrol 74:1–24

Kovalenko VI, Yarmolyuk VV (1995) Endogenous rare metal ore formations and rare metal metallogeny of Mongolia. Econ Geol 90:520–529

Kovalenko VI, Yarmoluyk VV, Sal'nikova EB et al (2006) Geology, geochronology, and geodynamics of the Khan Bogd alkali granite pluton in southern Mongolia. Geotectonics 40:450–466

Kramm U, Kogarko LN (1994) Nd and Sr isotope signatures of the Khibina and Lovozero agpaitic centres, Kola Alkaline province, Russia. Lithos 32:225–242. https://doi.org/10.1016/0024-4937(94)90041-8

Kynicky J, Chakhmouradian AR, Xu C et al (2011) Distribution and evolution of zirconium mineralization in peralkaline granites and associated pegmatites of the Khan Bogd complex, southern Mongolia. Can Mineral 49:947–965

Lacroix A (1923) Minéralogie de Madagascar. A. Challamel (ed) Librairie maritime et coloniale

Lagarec K, Rancourt DG (1997) Extended Voigt-based analytic lineshape method for determining N-dimensional correlated hyperfine parameter distributions in Mössbauer spectroscopy. Nucl Instrum Methods Phys Res Sect B Beam Interact Mater Atoms 129:266–280

Larsen LM (1976) Clinopyroxenes and coexisting mafic minerals from the alkaline Ilimaussaq intrusion, South Greenland. J Petrol 17:258–290

Larsen LM (1981) Sector zoned aegirine from the Ilímaussaq alkaline intrusion, South Greenland. Contrib Mineral Petrol 76:285–291

Larsen LM, Sørensen H (1987) The Ilímaussaq intrusion—progressive crystallization and formation of layering in an agpaitic magma. Geol Soc Lond Spec Publ 30:473–488

Leake BE, Woolley AR, Arps CE et al (1997) Nomenclature of amphiboles; report of the Subcommittee on Amphiboles of the International Mineralogical Association Commission on new minerals and mineral names. Mineral Mag 61:295–310

Li X-H, Li W-X, Li Q-L et al (2010) Petrogenesis and tectonic significance of the 850 Ma Gangbian alkaline complex in South China: evidence from in situ zircon U–Pb dating, Hf–O isotopes and whole-rock geochemistry. Lithos 114:1–15

Liu Y, Chen Z, Yang Z et al (2015) Mineralogical and geochemical studies of brecciated ores in the Dalucao REE deposit, Sichuan Province, southwestern China. Ore Geol Rev 70:613–636. https://doi.org/10.1016/j.oregeorev.2015.03.006

Locock AJ (2014) An Excel spreadsheet to classify chemical analyses of amphiboles following the IMA 2012 recommendations. Comput Geosci 62:1–11
London D (2008) Pegmatites. Sp. Pub. 10. Can Miner 347
Lucas J, Lucas P, Le Mercier T et al (2014) Rare earths: science, technology, production and use. Elsevier, Amsterdam
Mahood GA, Stimac JA (1990) Trace-element partitioning in pantellerites and trachytes. Geochim Cosmochim Acta 54:2257–2276. https://doi.org/10.1016/0016-7037(90)90050-U
Mann U, Marks M, Markl G (2006) Influence of oxygen fugacity on mineral compositions in peralkaline melts: the Katzenbuckel volcano, Southwest Germany. Lithos 91:262–285. https://doi.org/10.1016/j.lithos.2005.09.004
Marks MA, Markl G (2017) A global review on agpaitic rocks. Earth-Sci Rev 173:229–258
Marks M, Halama R, Wenzel T, Markl G (2004) Trace element variations in clinopyroxene and amphibole from alkaline to peralkaline syenites and granites: implications for mineral–melt trace-element partitioning. Chem Geol 211:185–215
Migdisov A, Williams-Jones AE, Brugger J, Caporuscio FA (2016) Hydrothermal transport, deposition, and fractionation of the REE: experimental data and thermodynamic calculations. Chem Geol 439:13–42
Miller RM (1983) The Pan-African Damara Orogen of South West Africa/Namibia. Evol Damara Orogen South West Afr
Miller RR (1996) Structural and textural evolution of the Strange Lake peralkaline rare-element (NYF) granitic pegmatite, Quebec-Labrador. Can Mineral 34:349–371
Mollo S, Blundy JD, Giacomoni P et al (2017) Clinopyroxene-melt element partitioning during interaction between trachybasaltic magma and siliceous crust: clues from quartzite enclaves at Mt. Etna Volcano. Lithos 284–285:447–461. https://doi.org/10.1016/j.lithos.2017.05.003
Moore M, Chakhmouradian AR, Mariano AN, Sidhu R (2015) Evolution of rare-earth mineralization in the Bear Lodge carbonatite, Wyoming: mineralogical and isotopic evidence. Ore Geol Rev 64:499–521. https://doi.org/10.1016/j.oregeorev.2014.03.015
Morimoto N (1988) Nomenclature of pyroxenes. Mineral Petrol 39:55–76
Nakamura Y (1973) Origin of sector-zoning of igneous clinopyroxenes. Am Mineral 58:986–990
Nardi LVS, de Bitencourt M (2009) A-type granitic rocks in post-collisional settings in southernmost Brazil: their classification and relationship with tectonics and magmatic series. Can Mineral 47:1493–1503. https://doi.org/10.3749/canmin.47.6.1493
Nielsen TFD (1979) The occurrence and formation of Ti-aegirines in peralkaline syenites. Contrib Mineral Petrol 69:235–244
Ortoleva P, Merino E, Moore C, Chadam J (1987) Geochemical self-organization I; reaction-transport feedbacks and modeling approach. Am J Sci 287:979–1007
Pennycook SJ, Nellist PD (2011) Scanning transmission electron microscopy: imaging and analysis. Springer Science & Business Media, New York
Piilonen PC, McDonald AM, Lalonde AE (1998) The crystal chemistry of aegirine from Mont Saint-Hilaire, Quebec. Can Mineral 36:779–791
Pillet D, Bonhomme MG, Duthou JL, Chenevoy M (1989) Chronologie Rb/Sr et K/Ar du granite peralcalin du lac Brisson, Labrador central, Nouveau-Québec. Can J Earth Sci 26:328–332
Poitrasson F, Duthou J-L, Pin C (1995) The relationship between petrology and Nd isotopes as evidence for contrasting anorogenic granite genesis: example of the Corsican Province (SE France). J Petrol 36:1251–1274
Poitrasson F, Paquette J-L, Montel J-M et al (1998) Importance of late-magmatic and hydrothermal fluids on the Sm–Nd isotope mineral systematics of hypersolvus granites. Chem Geol 146:187–203
Rakotovao S, Rakotondrazafy R, Beziat D et al (2009) Pétrologie du complexe alcalin cénozoïque d'Ambohimirahavavy, presqu'île d'Ampasindava, nord-ouest de Madagascar. Mada-Géo 13:2–19
Ranløv J, Dymek RF (1991) Compositional zoning in hydrothermal aegirine from fenites in the Proterozoic Gardar Province South Greenland. Eur J Mineral. https://doi.org/10.1127/ejm/3/5/0837
Roelofsen JN (1997) The primary and secondary mafic silicates of two alkaline anorogenic complexes: Strange Lake (Quebec-Labrador) and Amba Dongar (Gujarat, India). PhD Thesis, McGill University Libraries
Rønsbo JG, Pedersen AK, Engell J (1977) Titan-aegirine from early Tertiary ash layers in northern Denmark. Lithos 10:193–204
Salvi S, William-Jones A (1995) Zirconosilicate phase relations in the Strange Lake (Lac Brisson) pluton, Quebec-Labrador, Canada: American Mineralogist. Am Mineral 80:1031–1040. https://doi.org/10.2138/am-1995-9-1019
Salvi S, Williams-Jones AE (1990) The role of hydrothermal processes in the granite-hosted Zr, Y, REE deposit at Strange Lake, Quebec/Labrador: evidence from fluid inclusions. Geochim Cosmochim Acta 54:2403–2418
Salvi S, Williams-Jones AE (1996) The role of hydrothermal processes in concentrating high-field strength elements in the Strange Lake peralkaline complex, northeastern Canada. Geochim Cosmochim Acta 60:1917–1932
Salvi S, Williams-Jones AE (1997) Fischer-Tropsch synthesis of hydrocarbons during sub-solidus alteration of the Strange Lake peralkaline granite, Quebec/Labrador, Canada. Geochim Cosmochim Acta 61:83–99
Salvi S, Williams-Jones AE (2006) Alteration, HFSE mineralisation and hydrocarbon formation in peralkaline igneous systems: Insights from the Strange Lake Pluton, Canada. Lithos 91:19–34
Sanematsu K, Kon Y, Imai A et al (2013) Geochemical and mineralogical characteristics of ion-adsorption type REE mineralization in Phuket, Thailand. Miner Deposita 48:437–451. https://doi.org/10.1007/s00126-011-0380-5
Schmitt AK, Trumbull RB, Dulski P, Emmermann R (2002) Zr-Nb-REE mineralization in peralkaline granites from the Amis Complex, Brandberg (Namibia): evidence for magmatic pre-enrichment from melt inclusions. Econ Geol 97:399–413
Shannon RD (1976) Revised effective ionic radii and systematic studies of interatomic distances in halides and chalcogenides. Acta Crystallogr 32:751–767
Sheard ER, Williams-Jones AE, Heiligmann M et al (2012) Controls on the concentration of zirconium, niobium, and the rare earth elements in the thor lake rare metal deposit, northwest territories, Canada. Econ Geol 107:81–104. https://doi.org/10.2113/econgeo.107.1.81
Shearer CK, Larsen LM (1994) Sector-zoned aegirine from the Ilimaussaq alkaline intrusion, South Greenland: implications for trace-element behavior in pyroxene. Am Mineral 79:340–352
Siegel K, Williams-Jones AE, Stevenson R (2017a) A Nd-and O-isotope study of the REE-rich peralkaline Strange Lake granite: implications for Mesoproterozoic A-type magmatism in the Core Zone (NE-Canada). Contrib Mineral Petrol 172:54
Siegel K, Williams-Jones AE, van Hinsberg VJ (2017b) The amphiboles of the REE-rich A-type peralkaline Strange Lake pluton–fingerprints of magma evolution. Lithos 288:156–174
Smith MP (2007) Metasomatic silicate chemistry at the Bayan Obo Fe–REE–Nb deposit, Inner Mongolia, China: contrasting chemistry and evolution of fenitising and mineralising fluids. Lithos 93:126–148
Smith MP, Henderson P, Jeffries TER et al (2004) The rare earth elements and uranium in garnets from the Beinn an Dubhaich

Aureole, Skye, Scotland, UK: constraints on processes in a dynamic hydrothermal system. J Petrol 45:457–484
Strong DF (1969) Formation of the hour-glass structure in augite. Mineral Mag 37:472–479
Sun S-S, McDonough W (1989) Chemical and isotopic systematics of oceanic basalts: implications for mantle composition and processes. Geol Soc Lond Spec Publ 42:313–345
Thomas RJ, De Waele B, Schofield DI et al (2009) Geological evolution of the Neoproterozoic Bemarivo Belt, northern Madagascar. Precambrian Res 172:279–300. https://doi.org/10.1016/j.precamres.2009.04.008
Trail D, Bruce Watson E, Tailby ND (2012) Ce and Eu anomalies in zircon as proxies for the oxidation state of magmas. Geochim Cosmochim Acta 97:70–87. https://doi.org/10.1016/j.gca.2012.08.032
Ubide T, McKenna CA, Chew DM, Kamber BS (2015) High-resolution LA-ICP-MS trace element mapping of igneous minerals: In search of magma histories. Chem Geol 409:157–168. https://doi.org/10.1016/j.chemgeo.2015.05.020
Ubide T, Mollo S, Zhao J et al (2019) Sector-zoned clinopyroxene as a recorder of magma history, eruption triggers, and ascent rates. Geochim Cosmochim Acta 251:265–283. https://doi.org/10.1016/j.gca.2019.02.021
US Geological Survey (2019) Rare Earths Statistics and Information. In: Miner. Commod. Summ. https://www.usgs.gov/centers/nmic/rare-earths-statistics-and-information. Accessed 28 Aug 2019
Vasyukova O, Williams-Jones AE (2014) Fluoride–silicate melt immiscibility and its role in REE ore formation: evidence from the Strange Lake rare metal deposit, Québec-Labrador, Canada. Geochim Cosmochim Acta 139:110–130
Vasyukova OV, Williams-Jones AE (2019) Closed system fluid-mineral-mediated trace element behaviour in peralkaline rare metal pegmatites: evidence from Strange Lake. Chem Geol 505:86–99
Vasyukova O, Williams-Jones A (2020) Partial melting, fractional crystallisation, liquid immiscibility and hydrothermal mobilisation–A 'Recipe' for the formation of economic A-Type granite-hosted HFSE deposits. Lithos 356:105300
Vasyukova OV, Williams-Jones AE, Blamey NJF (2016) Fluid evolution in the Strange Lake granitic pluton, Canada: implications for HFSE mobilisation. Chem Geol 444:83–100
Veksler IV, Dorfman AM, Dulski P et al (2012) Partitioning of elements between silicate melt and immiscible fluoride, chloride, carbonate, phosphate and sulfate melts, with implications to the origin of natrocarbonatite. Geochim Cosmochim Acta 79:20–40. https://doi.org/10.1016/j.gca.2011.11.035
Wang Q, Deng J, Liu X et al (2010) Discovery of the REE minerals and its geological significance in the Quyang bauxite deposit, West Guangxi, China. J Asian Earth Sci 39:701–712. https://doi.org/10.1016/j.jseaes.2010.05.005
William-Jones AE, Migdisov AA, Samson IM (2012) Hydrothermal mobilisation of the Rare Earth Elements–a Tale of "Ceria" and "Yttria". Elements 8:355–360
Xu C, Kynickỳ J, Smith MP et al (2017) Origin of heavy rare earth mineralization in South China. Nat Commun 8:14598
Yang X-M, Yang X-Y, Zheng Y-F, Le Bas MJ (2003) A rare earth element-rich carbonatite dyke at Bayan Obo, Inner Mongolia, North China. Mineral Petrol 78:93–110
Zaitsev AN, Terry Williams C, Jeffries TE et al (2014) Rare earth elements in phoscorites and carbonatites of the Devonian Kola Alkaline Province, Russia: Examples from Kovdor, Khibina, Vuoriyarvi and Turiy Mys complexes. Ore Geol Rev 61:204–225. https://doi.org/10.1016/j.oregeorev.2014.02.002

Electronic Supplementary Material

Detailed geological background

1. Amis complex, Namibia

Briefly, the Amis complex and the larger Brandberg complex onto which it is juxtaposed are of the same age (132.5 to 130.5 My) and are hosted in metasediments of the Damara orogen (~ 550 My; Miller 1983) and volcanic rocks from the Paraná-Etendeka igneous province. Three granite and 4 pegmatite-aplite samples were used for this study, their localization is provided on Fig 1.

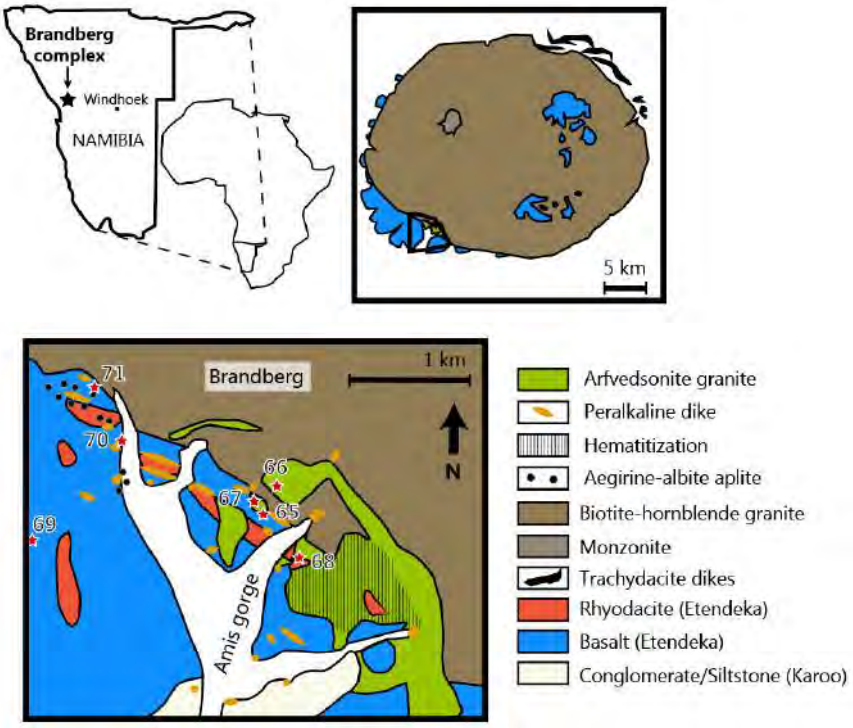

Figure 1 Localization and geological map of the Amis and Brandberg complexes, modified after Schmitt et al. (2002). Stars provide the location of samples analyzed in this study

The Amis complex is made up of about 3 km² of peralkaline rocks, with a main part consisting of arfvedsonite granite, plus pegmatite-aplite occurrences and dykes that have very similar composition to the main granite (Fig 1). The complex is interpreted to originate from a basaltic melt which experienced fractionation and assimilation of crustal material in a rifting context (Schmitt et al. 2000). The Amis complex is highly enriched in REE, other HFSE and volatiles (H_2O, F). Pegmatites and aplites in the north-western part of the Amis complex are particularly enriched in REE mineralizations and uranium. Schmitt et al. (2002) infer that hydrothermal fluids had a very limited impact on

the rocks of Amis complex. They affirm that minerals are all mainly magmatic, with the exception of replacement of arfvedsonite by quartz-hematite overgrowths. Based on the study of melt inclusions, they propose that the main part of REE and other HFSE enrichment is magmatic. In contrast, Diehl (1990) proposed that the influence of hydrothermal fluids was much higher, and inferred the replacement of arfvedsonite by aegirine.

2. Evisa complex, Corsica

The Evisa complex (290 My; Cocherie et al. 2005) is a NE-SW oriented alkaline granitic batholith located above a deep fracture in the northwestern part of Corsica (Quin 1969). It was emplaced among metaluminous granitoids after the Hercynian collision in an extensional post-orogenic or rifting context (Rossi et al. 2010). We collected 7 granite and 5 pegmatite samples from the central part of the complex, their localization is provided on Fig 2.

The complex mainly comprises hypersolvus (perthitic feldspar) and subsolvus (albitic and alkali feldspar) peralkaline granites (Bonin 1990) rich in REE-bearing minerals such as monazite-(Ce), apatite, and allanite-(Ce). Bonin et al. (1978) estimated that the hypersolvus granite was emplaced at about 0.5 kbar and between 900 and 700 °C, which led to formation of chilled margins at the contact with the host rocks. This granite probably experienced two hydrothermal events: a minor, early episode at the end of crystallization, and a more important one, characterized by F-rich fluids, around 200 My (Poitrasson et al. 1998; Bonin et al. 2008). The subsolvus granite is intrusive into the perthitic unit. The subsolvus granite only experienced the second hydrothermal event, which triggered the replacement of the primary zirconosilicate elpidite by a secondary assemblage (Bonin 1990). In addition to these two granite varieties, the Evisa complex contains lindinosite (a peralkaline granite with about 60 % riebeckite amphibole, Le Maitre et al. (2005)) nodules, fayalite-bearing pegmatites, and granitic pegmatites (Bonin 1980). Finally, late dykes of different natures intersect the entire complex. They include basic (dolerites) and acidic (microgranites, rhyodacites, rhyolites) dyke varieties, plus quartz veins (Vellutini et al. 1996; Rossi et al. 2010).

Two hypotheses have been proposed for the source of these granites and are still debated: an under-saturated metasomatized mantle source, or a residual crustal source from which a granitic magma and most of the water had already been removed (Vellutini et al. 1996).

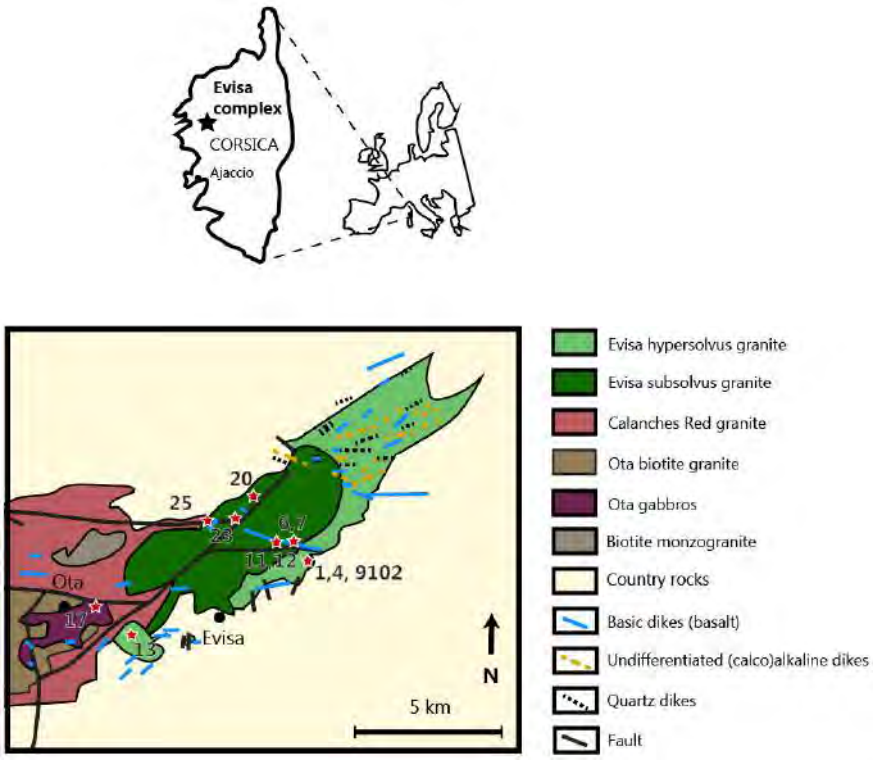

Figure 2 Localization and geological map of the Evisa complex and surrounding granites, modified after Rossi et al. (2010) and Vellutini et al. (1996). Stars provide the location of samples analyzed in this study

3. Khan Bogd complex, Mongolia

The Khan Bogd complex is among the largest alkaline granite plutons in the world, with a surface of 1500 km². It has been investigated for mining purposes and estimates indicate grades between 0.3 and 4.5 % REE, the highest grade being located at the top of the granites plutons (estimation of the tonnage is not available, Kovalenko and Yarmolyuk 1995). To our knowledge, only two publications exist in the western literature on this complex (Kovalenko et al. 2006; Kynicky et al. 2011) and the short description that follows is based on these. It is located in the southern Gobi Desert, at the transition between island-arc calc-alkaline differentiated volcanics (329±5 My) and rift-related bimodal basalt–comendite–alkali granite association (318-290 My), and is dated at approximately 290 Ma (Kovalenko et al. 2006). The pluton consists of two ring bodies: a western peralkaline arfvedsonite-bearing granite, in which many aegirine granitic pegmatites are noticeable and parallel to the external contacts, and an eastern aegirine granite. We collected 3 granite and 7 pegmatite samples, mostly on the sides of the western ring of the complex; their localization is provided on Fig 3.

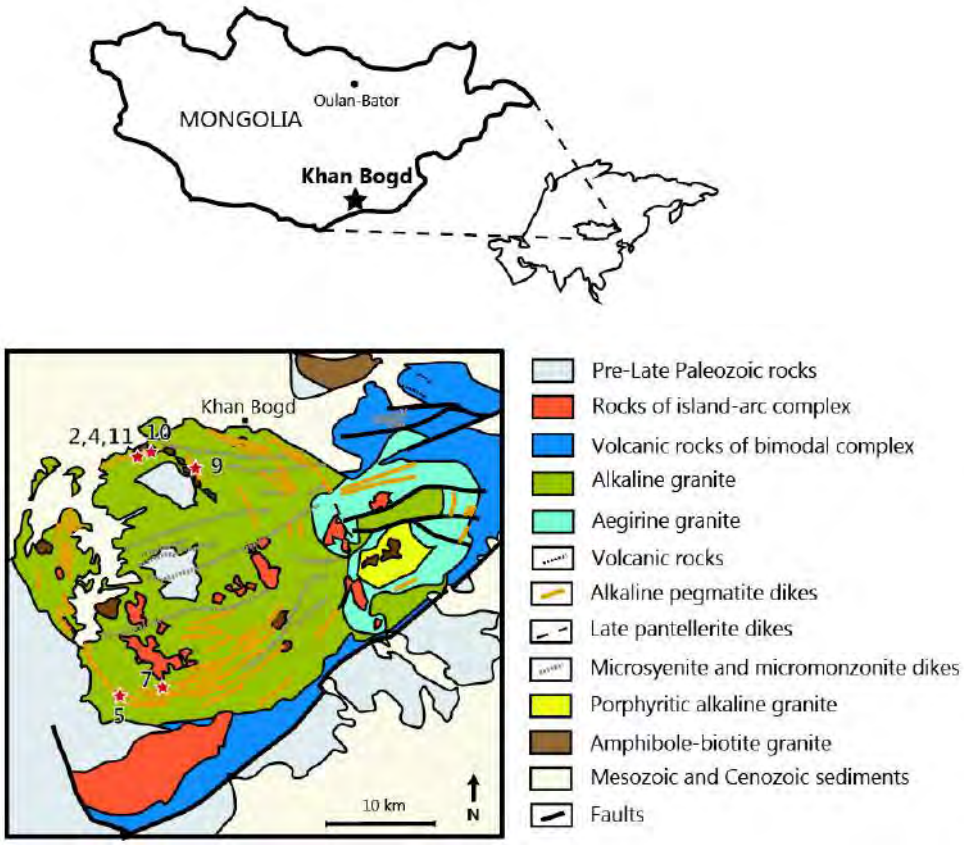

Figure 3 Localization and geological map of the Khan Bogd complex, modified after Kovalenko et al. (2006). Stars provide the location of samples analyzed in this study

The origin of this pluton is linked to a mantle plume and the active continental margin of the South Mongolian Hercynides, but the exact process is still under discussion. A first hypothesis proposes that oceanic islands blocked the subduction and broke the slab, allowing the mantle plume to cross it, forming a structure similar to an asthenospheric window that would have been the source of the rift-related magmatism and the Khan Bogd pluton. A second hypothesis suggests that the mantle plume heated the slab and thereby lowered its sinking angle. This provoked partial melting of the sinking oceanic lithosphere and of the mantle wedge. Either way, geochemical studies indicate that this triggered extensive crustal melting, generating the alkali granitic magma (Kovalenko et al. 2006). The latter authors suggest that to form such a large volume of alkali granite, the volume of parental basaltic magma must have been almost similar to one of medium-sized trap provinces. The eastern aegirine granite is interpreted to have emplaced later, along with pegmatites (Kovalenko et al. 2006; Kynicky et al. 2011). Finally, Kynicky et al. (2011) propose the release of a silica-saturated orthomagmatic fluid that, similarly to Evisa, triggered the replacement of primary elpidite either by a secondary Ca-rich elpidite, or by an assemblage of armstrongite, gittinsite and zircon.

4. Manongarivo and Ambohimirahavavy complexes, Madagascar

Ambohimirahavavy and Manongarivo are the biggest complexes of the Ampasindava province in northwestern Madagascar, yet are not well documented. They were emplaced at 24 Ma into marine-shelf carbonates and marine-fluvial siliciclastic sediments of the Isalo Group (Thomas et al. 2009; Cucciniello et al. 2016). Both complexes are made of two ring-shaped intrusions side by side, composed of nepheline syenite, alkali feldspar syenite, biotite granite, peralkaline pegmatites, and various volcanic rocks. We collected 3 granite and 4 pegmatite samples from the southern part of the Ambohimirahavavy complex. Due to poor outcropping conditions and low occurrence of pegmatites, we could only obtain 3 pegmatite samples from Manongarivo. The samples from Ambohimirahavavy were selected according to previous studies from Estrade et al. (2014a, b); their localization is provided on Fig 4.

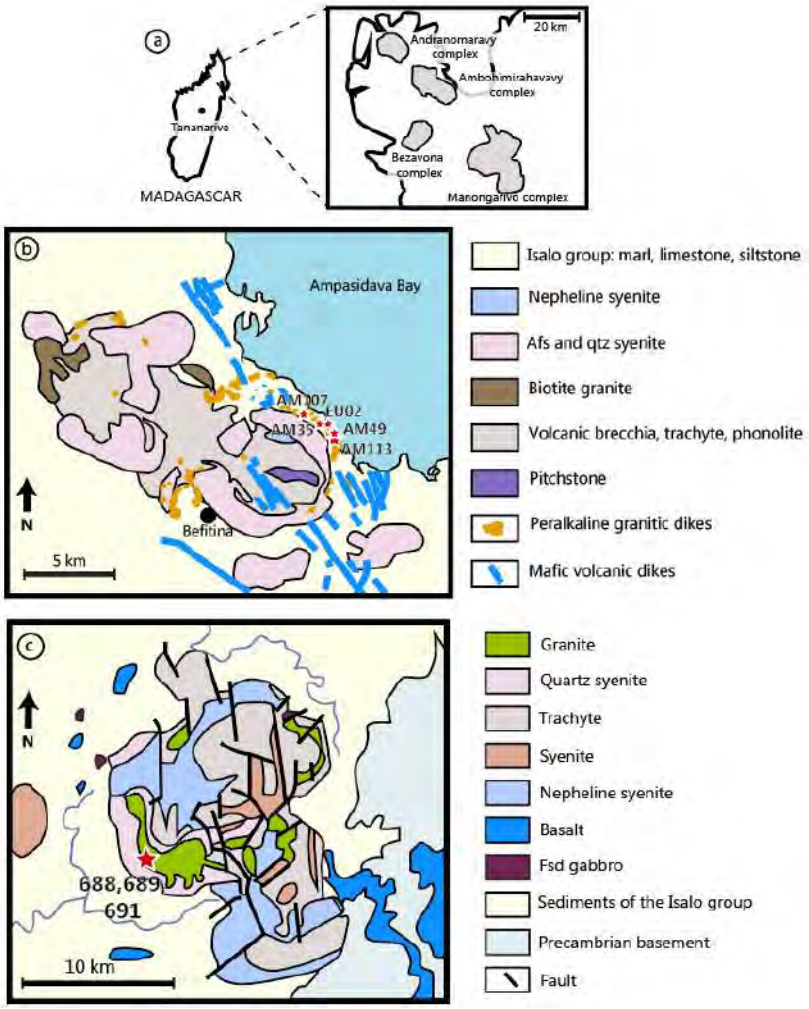

Figure 4 Localization **a** and geological map of the Ambohimirahavavy **b** and Manongarivo **c** complexes, modified after Donnot (1963) and Estrade et al. (2015). Stars provide the location of samples analyzed in this study

Two hypotheses have been proposed to explain the emplacement mode of these complexes. They are believed to have formed in connection with old and deep lithospheric fractures (Nougier et al. 1986) that were found parallel to the Sandrakota shear zone, a major tectonic zone active during the East African Orogeny around 540 Ma (Thomas et al. 2009; Estrade et al. 2014a). The parental melt of the whole complex was probably generated by low degrees of melting (2-10 %) of an incompatible element-enriched metasomatized mantle source with residual minerals enriched in volatiles such as amphibole and phlogopite. Fractional crystallization produced the silica-undersaturated rocks, whereas silica-oversaturated rocks could have originated from the same melt, with crustal contamination. The fractionation of plagioclase and alkali feldspar from an alkaline parental magma formed the most evolved peralkaline rocks of the complexes. An orthomagmatic fluid affected the complexes in the very last stages of magmatic evolution, when low-temperature pegmatites crystallized (Estrade 2014; Cucciniello et al. 2016). The primary zirconosilicates are eudialyte group minerals (EGM) at Ambohimirahavavy, and unknown at Manongarivo. They are replaced by an assemblage of secondary HFSE-bearing minerals, forming pseudomorphs (Lacroix 1923; Estrade et al. 2018). Due to the recent discovery of rare metals in economic concentrations in ion-adsorption clays, the province drew the attention of a mining exploration company (Estrade et al. 2014b). REE and other HFSE are the most enriched in granites and pegmatites, and at their contact with the surrounding limestones (Estrade et al. 2015).

5. Strange Lake complex, Canada

The Strange Lake complex is a well-known resource of critical metals in northeastern Canada, on the border between Quebec and Labrador. Reserves are estimated at 278 Mt grading 0.93% REE_2O_3 of which 39% are HREE, and 214 Mt at 0.85 % REE_2O_3 in total (Gowans et al. 2017). The complex also contains significant amounts of ZrO_2, Nb_2O_5, and BeO. The complex was emplaced 1240 My ago in gneisses and quartz monzonite (Miller 1996) and is considered to represent an extension of the Gardar rift in Greenland (Pillet et al. 1989; Boily and Williams-Jones 1994; Siegel et al. 2017a). It forms a circular body of about 36 km² which contains highly-differentiated peralkaline granitic plutons, partially surrounded by an outwardly-dipping fracture associated with fluorite and hematite breccia. Two zones of pegmatites have been reported: the Main zone in the center of the complex, and the B zone on the northwestern edge. We collected 3 granite and 4 pegmatite samples from the Strange Lake complex. All pegmatite samples come from the Main Zone and their localization is provided on Fig 5. Samples were selected according to previous studies from Salvi and Williams-Jones (1990; 2006; 1995).

The core of the pluton consists of the oldest intrusive part, a hypersolvus granite, while a largely metasomatized transsolvus granite (perthite plus two distinct feldspars) surrounds it, forming the majority of the complex. The latter unit was formerly considered as subsolvus, because perthite only occurs in minor amounts, which was only recently recognized and in which pegmatites concentrate (Gysi et al. 2016; Siegel et al. 2017b). These magmatic events correlate with a progressive enrichment in REE and HFSE mineralizations, from HFSE-poor hypersolvus granite to HFSE-rich transsolvus granite and pegmatites (Miller 1996). Most of the REE are concentrated in the pegmatites.

Two extensive hydrothermal events affected the complex. These have been documented by alteration phases, fluid inclusions in quartz, and O-isotopic values. The first event is attributed to circulation of a near-neutral, hot (≥ 350 °C) orthomagmatic brine consisting of Na-enriched aqueous and carbonic phases (Salvi and Williams-Jones 2006; Vasyukova et al. 2016), and affected the whole complex. The second hydrothermal event consists of a cooler (100 - 200 °C), acidic fluid that circulated mostly in the transsolvus granite and pegmatites. This stage is interpreted to have resulted from mixing of a fluid equilibrated with the paragneiss surrounding the complex and a fluid originating from the granites. It is responsible for the replacement of primary elpidite into a secondary assemblage (Salvi and Williams-Jones 1990), the concentration of REE and other HFSE in pegmatites (Boily and Williams-Jones 1994; Salvi and William-Jones 1997), and the formation of the fluorite breccia (Gysi and Williams-Jones 2013; Gysi et al. 2016).

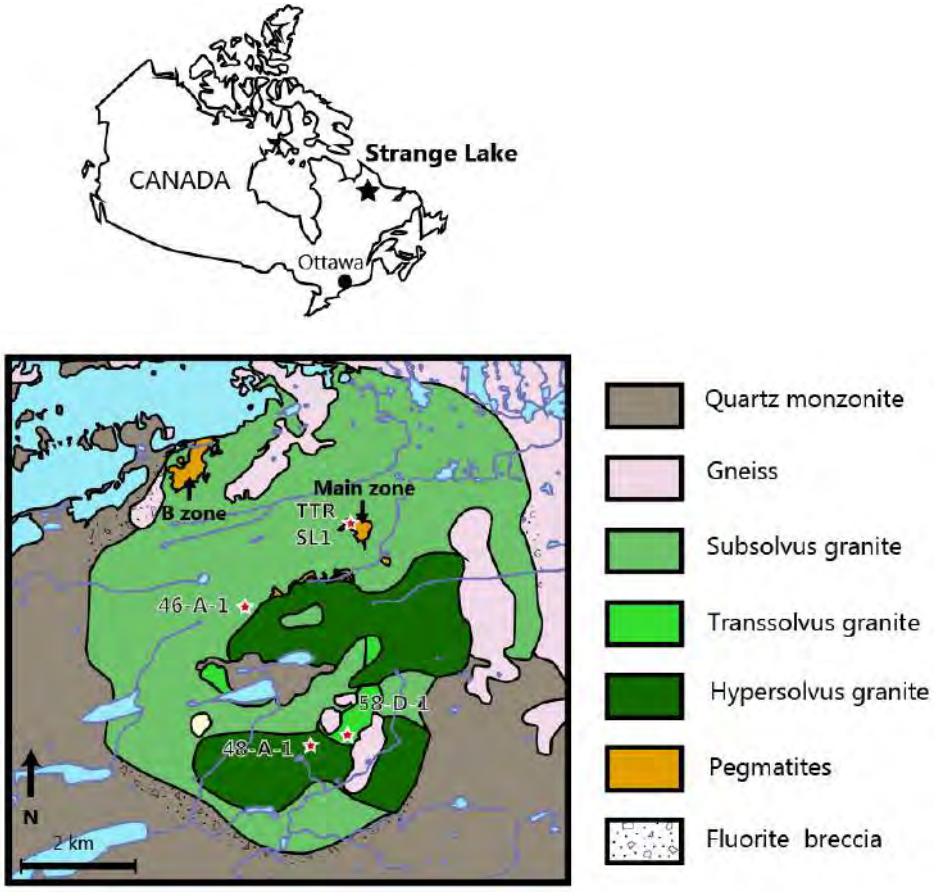

Figure 5 Localization and geological map of the Strange Lake complex, modified after Vasyukova et al., 2015. Stars provide the location of samples analyzed in this study

References

Boily M, Williams-Jones AE (1994) The role of magmatic and hydrothermal processes in the chemical evolution of the Strange Lake plutonic complex, Quebec-Labrador. Contrib Mineral Petrol 118:33–47

Bonin B (1990) Les granites des complexes annulaires, BRGM. Office des publications universitaires

Bonin B (1980) Les complexes acides alcalins anorogéniques continentaux: l'exemple de la Corse. PhD Thesis

Bonin B, Grelou-Orsini C, Vialette Y (1978) Age, origin and evolution of the anorogenic complex of Evisa (Corsica): A K-Li-Rb-Sr study. Contrib Mineral Petrol 65:425–432

Bonin B, Platevoet B, Poitrasson F, Renna MR (2008) Eurogranites-IGCP510 2008 Joint Field-meeting—Alkaline The Permian–Triassic A-type Volcanic–Plutonic Igneous Suite of Corsica. In: 33th International Geological Congress in Oslo, Norway Convention Centre, Lillestrom, Norway

Cocherie A, Rossi P, Fanning CM, Guerrot C (2005) Comparative use of TIMS and SHRIMP for U–Pb zircon dating of A-type granites and mafic tholeiitic layered complexes and dykes from the Corsican Batholith (France). Lithos 82:185–219

Cucciniello C, Tucker RD, Jourdan F, et al (2016) The age and petrogenesis of alkaline magmatism in the Ampasindava Peninsula and Nosy Be archipelago, northern Madagascar | SpringerLink. Mineral Petrol 110:309–331. https://doi.org/10.1007/s00710-015-0387-1

Diehl M (1990) Geology, mineralogy, geochemistry and hydrothermal alteration of the Brandberg alkaline complex, Namibia. Geological Survey of Namibia

Donnot M (1963) Côte Nord-Ouest du complexe intrusif alcalin; Ampasindava-Manongarivo

Estrade G (2014) Le complexe cénozoïque alcalin d'Ambohimirahavavy à Madagascar : origine, évolution et minéralisations en métaux rares. Toulouse 3

Estrade G, Béziat D, Salvi S, et al (2014a) Unusual evolution of silica-under-and-oversaturated alkaline rocks in the Cenozoic Ambohimirahavavy Complex (Madagascar): Mineralogical and geochemical evidence. Lithos 206:361–383

Estrade G, Salvi S, Béziat D, et al (2014b) REE and HFSE mineralization in peralkaline granites of the Ambohimirahavavy alkaline complex, Ampasindava peninsula, Madagascar. J Afr Earth Sci 94:141–155

Estrade G, Salvi S, Béziat D (2018) Crystallization and destabilization of eudialyte-group minerals in peralkaline granite and pegmatite: a case study from the Ambohimirahavavy complex, Madagascar. Mineral Mag 82:375–399. https://doi.org/10.1180/minmag.2017.081.053

Estrade G, Salvi S, Béziat D, Williams-Jones AE (2015) The origin of skarn-hosted rare-metal mineralization in the Ambohimirahavavy alkaline complex, Madagascar. Econ Geol 110:1485–1513

Gowans RM, Lewis WJ, Zalnieriunas RV (2017) Quest Rare Minerals Ltd.: Strange Lake Resource Estimation

Gysi AP, Williams-Jones AE (2013) Hydrothermal mobilization of pegmatite-hosted REE and Zr at Strange Lake, Canada: A reaction path model. Geochim Cosmochim Acta 122:324–352

Gysi AP, Williams-Jones AE, Collins P (2016) Lithogeochemical vectors for hydrothermal processes in the Strange Lake peralkaline granitic REE-Zr-Nb deposit. Econ Geol 111:1241–1276

Kovalenko VI, Yarmoluyk VV, Sal'nikova EB, et al (2006) Geology, geochronology, and geodynamics of the Khan Bogd alkali granite pluton in southern Mongolia. Geotectonics 40:450–466

Kovalenko VI, Yarmolyuk VV (1995) Endogenous rare metal ore formations and rare metal metallogeny of Mongolia. Econ Geol 90:520–529

Kynicky J, Chakhmouradian AR, Xu C, et al (2011) Distribution and evolution of zirconium mineralization in peralkaline granites and associated pegmatites of the Khan Bogd complex, southern Mongolia. Can Mineral 49:947–965

Lacroix A (1923) Minéralogie de Madagascar. A. Challamel, éditeur, Librairie maritime et coloniale

Le Maitre RW, Streckeisen A, Zanettin B, et al (2005) Igneous rocks: a classification and glossary of terms: recommendations of the International Union of Geological Sciences Subcommission on the Systematics of Igneous Rocks. Cambridge University Press

Miller RM (1983) The Pan-African Damara Orogen of South West Africa/Namibia. Evol Damara Orogen South West Afr

Miller RR (1996) Structural and textural evolution of the Strange Lake peralkaline rare-element (NYF) granitic pegmatite, Quebec-Labrador. Can Mineral 34:349–371

Nougier J, Cantagrel JM, Karche JP (1986) The Comores archipelago in the western Indian Ocean: volcanology, geochronology and geodynamic setting. J Afr Earth Sci 1983 5:135–145. https://doi.org/10.1016/0899-5362(86)90003-5

Pillet D, Bonhomme MG, Duthou JL, Chenevoy M (1989) Chronologie Rb/Sr et K/Ar du granite peralcalin du lac Brisson, Labrador central, Nouveau-Québec. Can J Earth Sci 26:328–332

Poitrasson F, Paquette J-L, Montel J-M, et al (1998) Importance of late-magmatic and hydrothermal fluids on the Sm–Nd isotope mineral systematics of hypersolvus granites. Chem Geol 146:187–203

Quin J-P (1969) Les granites alcalins et hyper-alcalins de Nord-Ouest de la Corse. Thèse de doctorat, Université d'Aix-Marseille. Faculté des sciences

Rossi P, Marre J, Cocherie A, Caballero Y (2010) Notice explicative de la feuille Vico-Cargèse à 1/50 000

Salvi S, William-Jones A (1995) Zirconosilicate phase relations in the Strange Lake (Lac Brisson) pluton, Quebec-Labrador, Canada : American Mineralogist. Am Mineral 80:1031–1040. https://doi.org/10.2138/am-1995-9-1019

Salvi S, William-Jones A (1997) Fischer-Tropsch synthesis of hydrocarbons during sub-solidus alteration of the Strange Lake peralkaline granite, Quebec/Labrador, Canada. Geochem Cosmochim Acta 61:83–99. https://doi.org/10.1016/S0016-7037(96)00313-4

Salvi S, Williams-Jones AE (1990) The role of hydrothermal processes in the granite-hosted Zr, Y, REE deposit at Strange Lake, Quebec/Labrador: evidence from fluid inclusions. Geochim Cosmochim Acta 54:2403–2418
Salvi S, Williams-Jones AE (2006) Alteration, HFSE mineralisation and hydrocarbon formation in peralkaline igneous systems: Insights from the Strange Lake Pluton, Canada. Lithos 91:19–34
Schmitt AK, Emmermann R, Trumbull RB, et al (2000) Petrogenesis and 40Ar/39Ar geochronology of the Brandberg Complex, Namibia: evidence for a major mantle contribution in metaluminous and peralkaline granites. J Petrol 41:1207–1239
Schmitt AK, Trumbull RB, Dulski P, Emmermann R (2002) Zr-Nb-REE mineralization in peralkaline granites from the Amis Complex, Brandberg (Namibia): evidence for magmatic pre-enrichment from melt inclusions. Econ Geol 97:399–413
Siegel K, Williams-Jones AE, Stevenson R (2017a) A Nd-and O-isotope study of the REE-rich peralkaline Strange Lake granite: implications for Mesoproterozoic A-type magmatism in the Core Zone (NE-Canada). Contrib Mineral Petrol 172:54
Siegel K, Williams-Jones AE, van Hinsberg VJ (2017b) The amphiboles of the REE-rich A-type peralkaline Strange Lake pluton–fingerprints of magma evolution. Lithos 288:156–174
Thomas RJ, De Waele B, Schofield DI, et al (2009) Geological evolution of the Neoproterozoic Bemarivo Belt, northern Madagascar. Precambrian Res 172:279–300. https://doi.org/10.1016/j.precamres.2009.04.008
Vasyukova OV, Williams-Jones AE, Blamey NJF (2016) Fluid evolution in the Strange Lake granitic pluton, Canada: Implications for HFSE mobilisation. Chem Geol 444:83–100
Vellutini P, Rossi P, Michon G, Hervé J (1996) Notice explicative de la feuille Galeria-Osani à 1/50 000

OR2 Table showing standard and detection limits used for EPMA analyses

Element	Standard	Detection limit pyroxene (ppm)	Detection limit amphiboles (ppm)
Al	Corindon	309	451
Ca	Wollastonite	538	788
Cl	Tugtupite	n.a.	288
F	Topaze	n.a.	5185
Fe	Hematite	848	1228
K	Sanidine	474	741
Mg	Periclase	319	471
Mn	Pyrophanite	618	1096
Na	Albite	685	999
Si	Wollastonite	392	550
Ti	Pyrophanite	267	1060

OR3 Table showing detection limits used for LA-ICP-MS analyses

Element	Detection limit pyroxene (ppm)	Detection limit amphiboles (ppm)
Li	14	5
Be	1	3
Sc	1	1
Zn	1	2
Ga	0.3	0.5
Rb	0.5	1
Sr	12	20
Y	0.2	0.2
Zr	3	3
Nb	0.1	0.1
Sn	1	1
Ba	1	1
La	0.1	0.2
Ce	0.1	0.2
Pr	0.1	0.1
Nd	0.3	0.5
Sm	0.3	0.4
Eu	0.1	0.2
Gd	1	1
Tb	0.1	0.1
Dy	0.2	0.2
Ho	0.04	0.1
Er	0.1	0.2
Tm	0.04	0.1
Yb	0.2	0.3
Lu	0.1	0.1
Hf	0.3	0.3
Ta	0.1	0.1
Pb	0.1	0.1
Th	0.02	0.02
U	0.01	0.01

OR 6 Microprobe maps on a type I aegirine crystal at Amis. 3 zones are distinguished: A, the core rich in Ca, Zr, Sn, Hf and poor in Na, Fe; C, sector zoning rich in Ti, Ca; and D, sector zoning rich in Fe. The thick line represents limits of the map

Alkali pyroxenes and amphiboles: a window on Rare Earth Elements and other High Field Strength Elements behavior through the magmatic-hydrothermal transition of peralkaline granitic systems

Contributions to Mineralogy and Petrology

Cyrielle Bernard, Guillaume Estrade, Stefano Salvi, Didier Béziat , Martin Smith
Corresponding author: Guillaume Estrade, GET, CNRS, UPS, Université de Toulouse III, Toulouse, France
guillaume.estrade@get.omp.eu

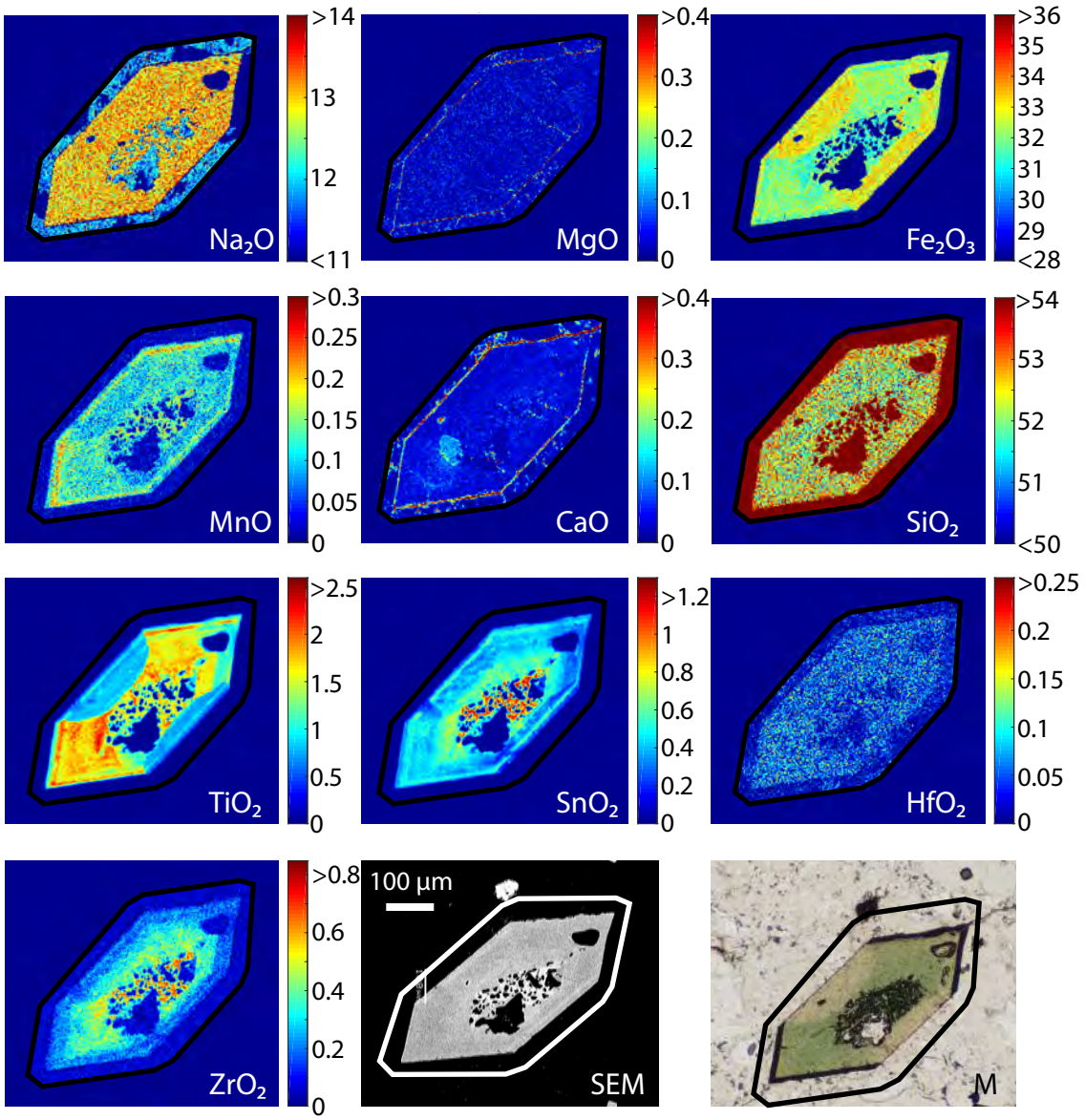

OR 7 Microprobe maps on a type I aegirine crystal at Evisa. 3 zones are distinguished: A, the core rich in Ca, Zr, Sn, Hf and poor in Na, Fe; C, sector zoning rich in Ti, Ca; and D, sector zoning rich in Fe. The thick line represents limits of the map

Alkali pyroxenes and amphiboles: a window on Rare Earth Elements and other High Field Strength Elements behavior through the magmatic-hydrothermal transition of peralkaline granitic systems

Contributions to Mineralogy and Petrology

Cyrielle Bernard, Guillaume Estrade, Stefano Salvi, Didier Béziat , Martin Smith
Corresponding author: Guillaume Estrade, GET, CNRS, UPS, Université de Toulouse III, Toulouse, France
guillaume.estrade@get.omp.eu

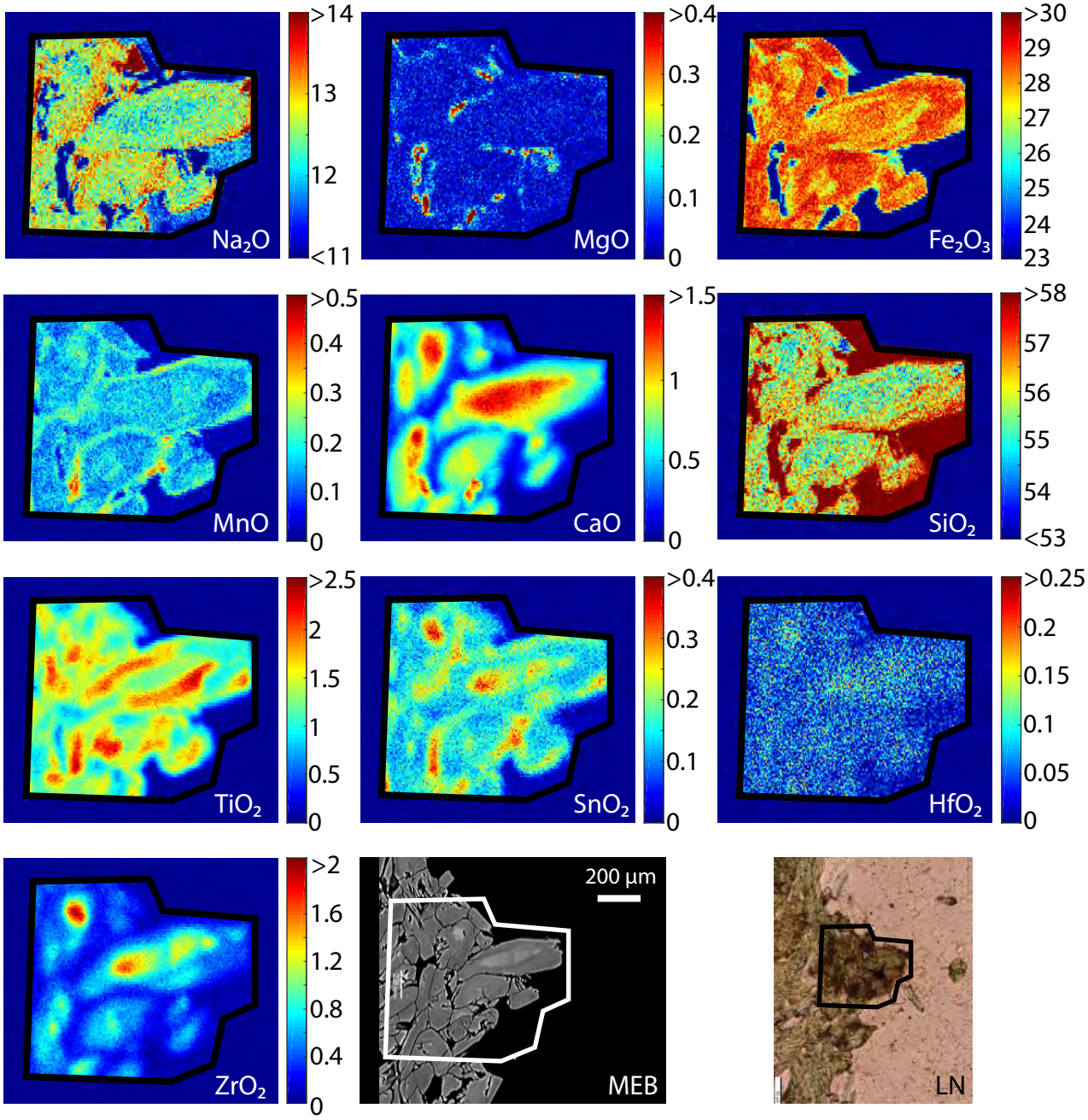

OR 8 Microprobe maps on a type I aegirine crystal at Khan Bogd. 4 zones are distinguished: A, the core rich in Ca, Zr, Sn, Hf and poor in Na, Fe; B; C, sector zoning rich in Ti, Ca; and D, sector zoning rich in Fe

Alkali pyroxenes and amphiboles: a window on Rare Earth Elements and other High Field Strength Elements behavior through the magmatic-hydrothermal transition of peralkaline granitic systems

Contributions to Mineralogy and Petrology

Cyrielle Bernard, Guillaume Estrade, Stefano Salvi, Didier Béziat , Martin Smith
Corresponding author: Guillaume Estrade, GET, CNRS, UPS, Université de Toulouse III, Toulouse, France
guillaume.estrade@get.omp.eu

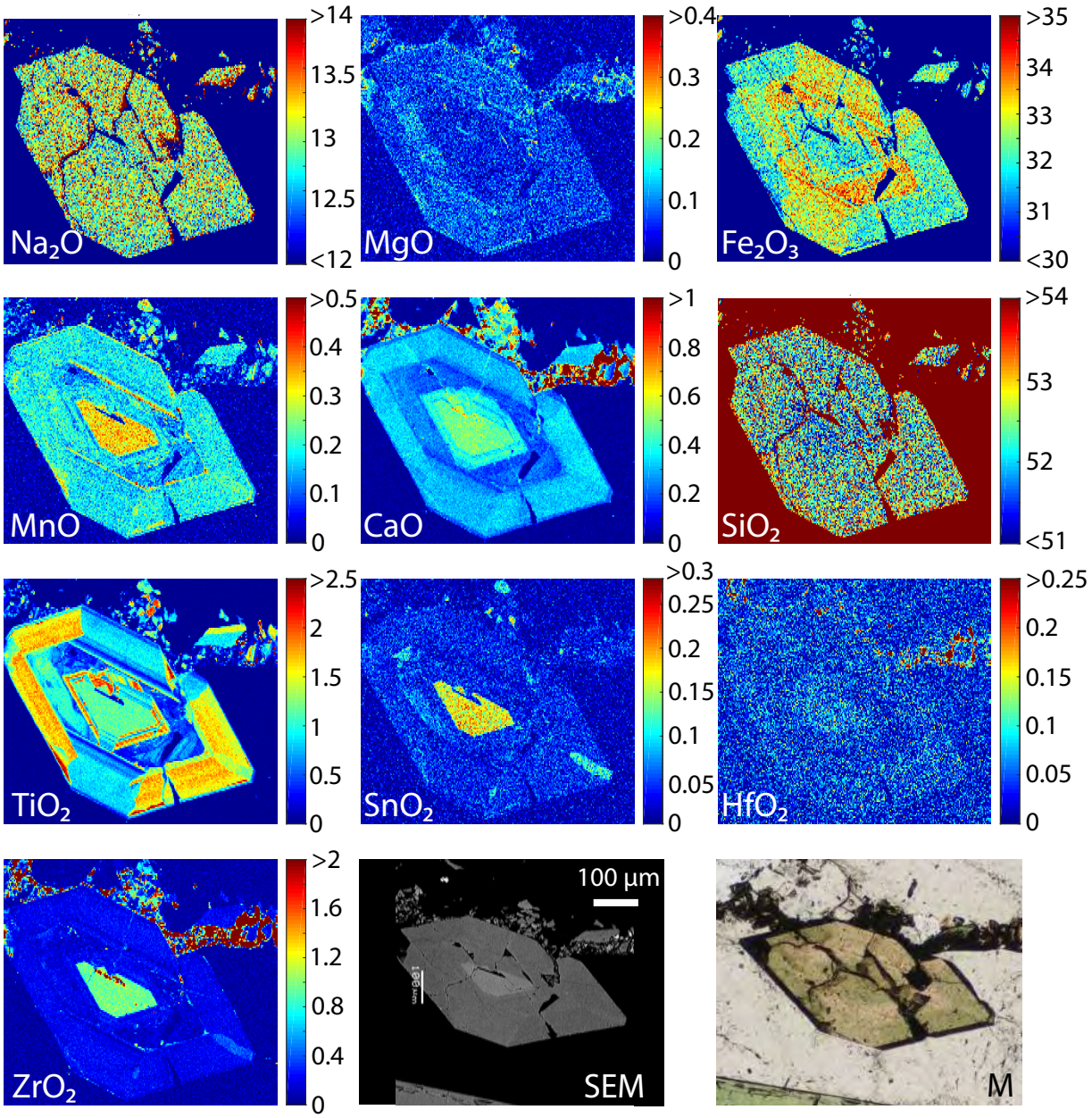

OR 9 Microprobe maps on a type I aegirine crystal at Manongarivo. 3 zones are distinguished: A, the core rich in Ca, Zr, Sn, Hf and poor in Na, Fe; C, sector zoning rich in Ti, Ca; and D, sector zoning rich in Fe

Alkali pyroxenes and amphiboles: a window on Rare Earth Elements and other High Field Strength Elements behavior through the magmatic-hydrothermal transition of peralkaline granitic systems

Contributions to Mineralogy and Petrology

Cyrielle Bernard, Guillaume Estrade, Stefano Salvi, Didier Béziat , Martin Smith
Corresponding author: Guillaume Estrade, GET, CNRS, UPS, Université de Toulouse III, Toulouse, France
guillaume.estrade@get.omp.eu

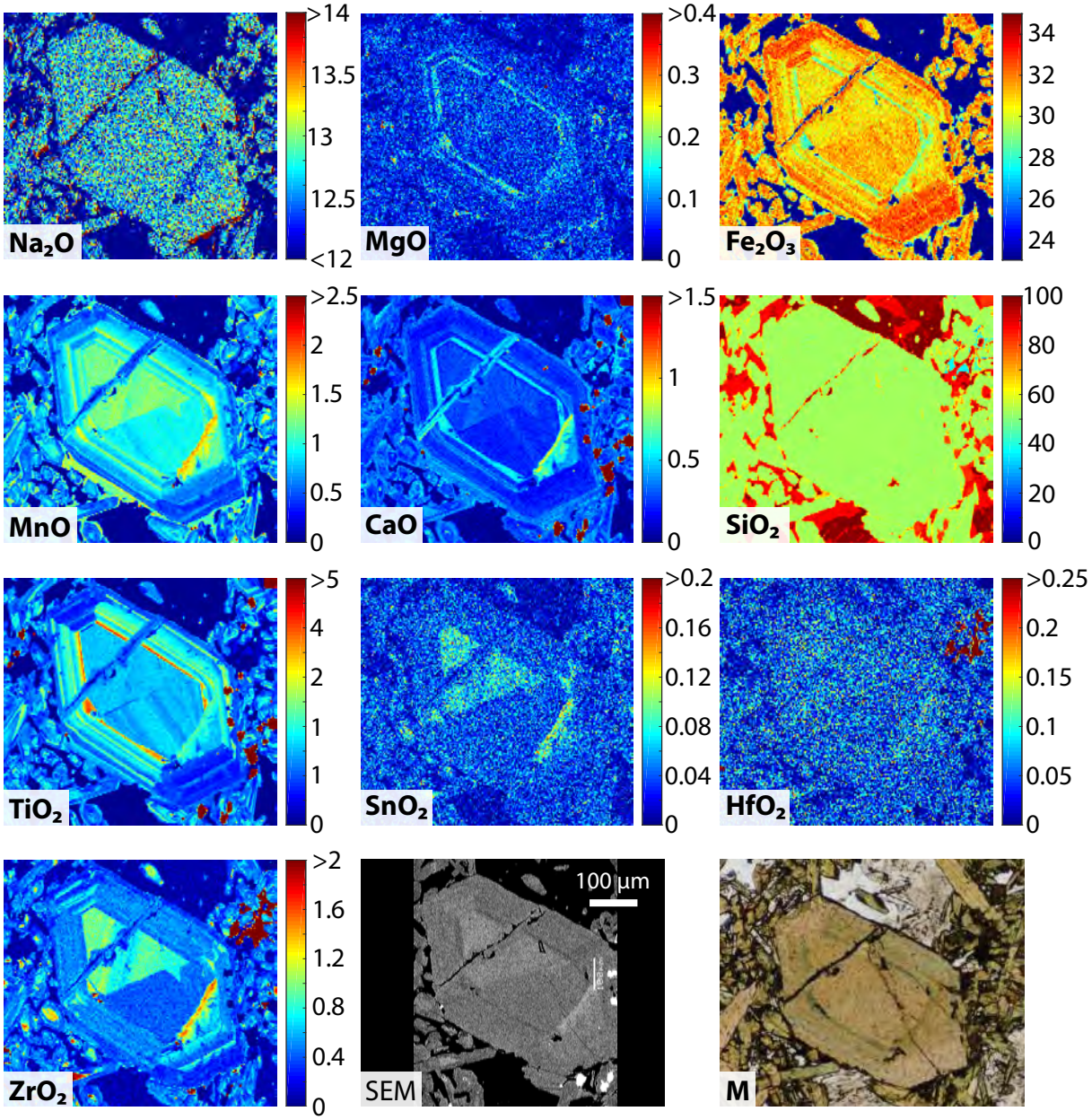

OR 10 Microprobe maps on a type II aegirine crystal at Strange Lake. No core-to-rim zoning is observed, but an oscillatory zoning occurs for most elements

Alkali pyroxenes and amphiboles: a window on Rare Earth Elements and other High Field Strength Elements behavior through the magmatic-hydrothermal transition of peralkaline granitic systems

Contributions to Mineralogy and Petrology

Cyrielle Bernard, Guillaume Estrade, Stefano Salvi, Didier Béziat , Martin Smith
Corresponding author: Guillaume Estrade, GET, CNRS, UPS, Université de Toulouse III, Toulouse, France
guillaume.estrade@get.omp.eu

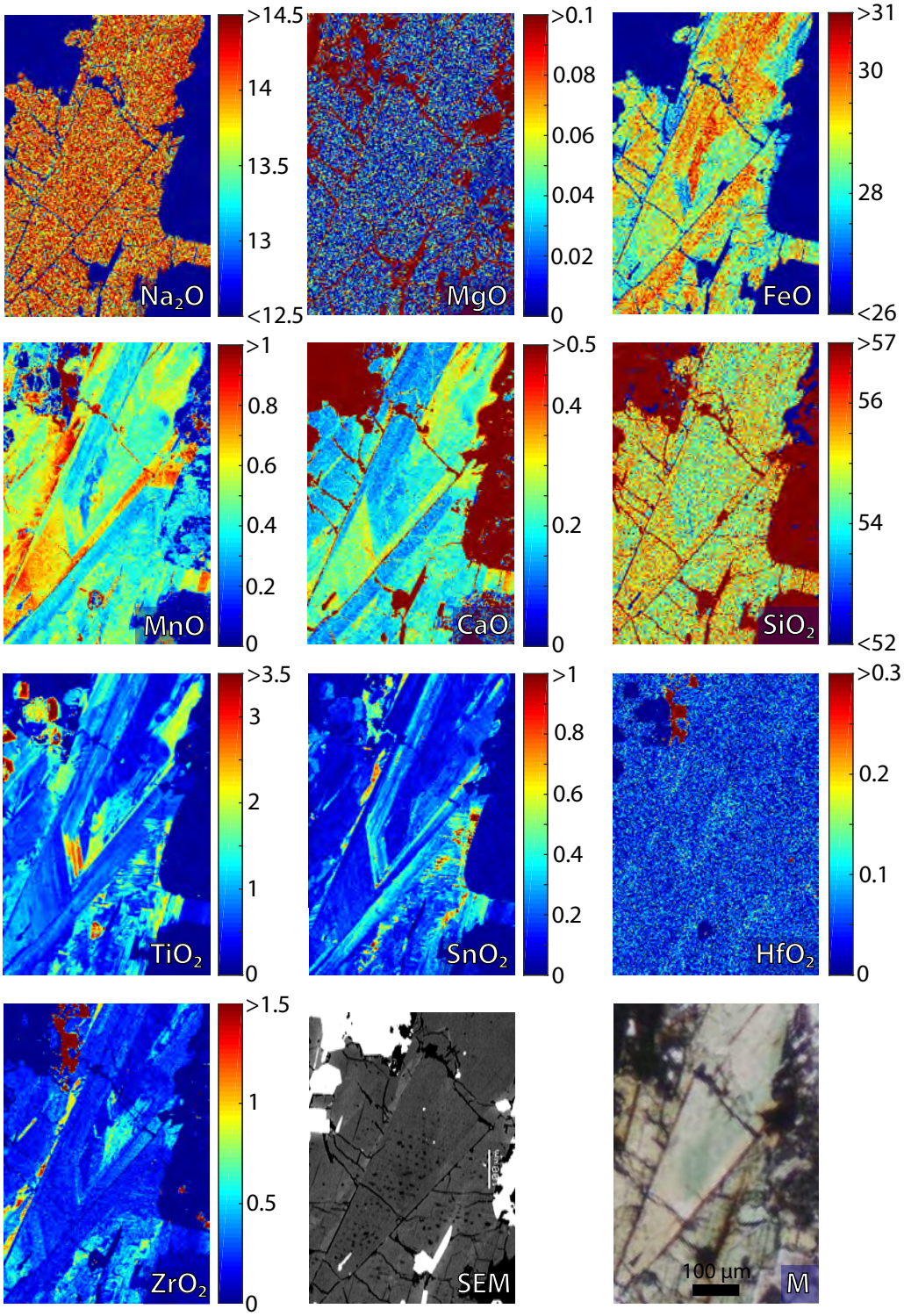

4.2 Oxygen isotopes as tracers for amphiboles and pyroxene origin

In order to further investigate the magmatic origin of amphibole and the magmatic and hydrothermal origin of pyroxene, oxygen stable isotope analyses were performed on these minerals. Oxygen 16 and 18 were chosen as oxygen occurs in both amphibole and pyroxene, unlike H or C. Since hydrothermal processes are known to produce O isotope fractionation, this study was performed with the hope to observe a difference in the $\delta^{18}O$ systematics, from magmatic amphibole and pyroxene to pyroxene of hydrothermal origin (cf section 4.1).

4.2.1 Presentation of O stable isotopes and their applications

Isotopes of one element are atoms with the same number of protons that only differ in their number of neutrons. They can be either stable or radiogenic. In order to be stable, atoms must have an approximately equal number of protons and neutrons (symmetry rule), and atoms with even atomic numbers are more abundant than those with odd numbers (Oddo-Harkins rule, which also applies to the REE).

The variation in abundance of radiogenic isotopes is linked to their radioactive decay. In contrast, the variation of stable isotopes is linked to fractionation related to physical and chemical differences between the isotopes. Fractionation processes mainly result from isotope exchange reactions and kinetic processes. Isotope exchange is a special case of general chemical equilibrium where there is no net reaction, but in which the isotope distribution changes between different chemical substances, between different phases, or between individual molecules. Kinetic fractionation results from different rates of chemical reactions or physical processes between the isotopes. Other factors such as magnetic effect, diffusion, pressure, temperature, crystal structure or sorption can also lead to a difference in isotopes relative abundances (see Hoefs, 2009 for further details).

Although about 300 stable isotopes are known, only a few of them are routinely used, such as hydrogen, carbon and nitrogen. This work focuses exclusively on oxygen. Oxygen has three stable isotopes with the following natural abundances: ^{16}O = 99.757 %; ^{17}O = 0.038 %; ^{18}O = 0.205 % (Rosman and Taylor, 1998). Isotopic

composition is expressed as the ratio R, which is the isotopic abundance of the heavier isotope divided by that of the lighter isotope (Faure and Mensing, 2005). In the case of oxygen, because of the greater mass difference and abundance, the ratio $^{18}O/^{16}O$ is usually measured. Isotopic composition is commonly expressed in delta (δ) value:

$$\delta_x = (\frac{R_x}{R_{std}} - 1) \times 10^3 \tag{4.1}$$

where R is the isotopic ratio; x is the sample; std is the standard, classically SMOW (Standard Mean Ocean Water) for oxygen in silicates analysis; and δ_x is the difference between these R values, expressed in per mil (Hoefs, 2009).

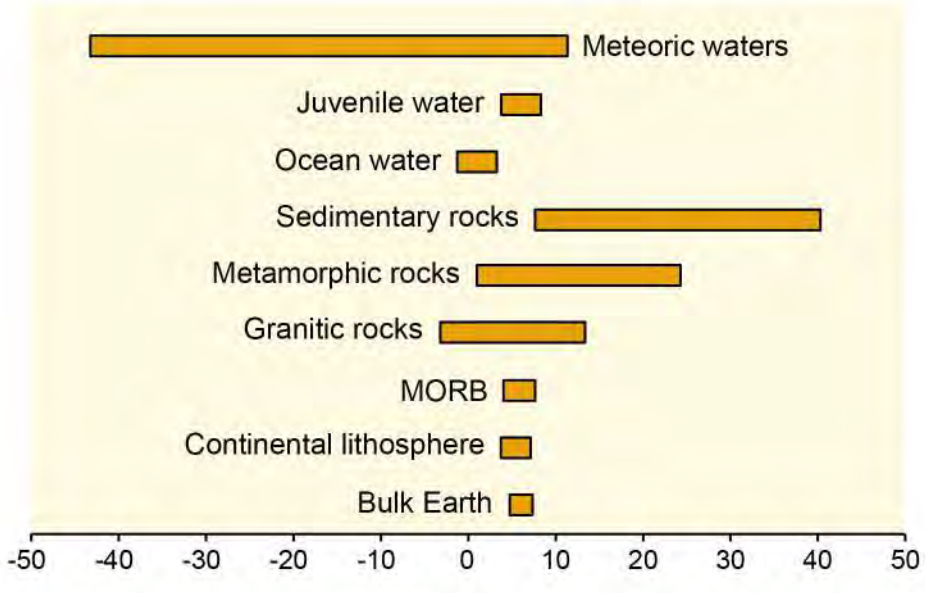

Figure 4.1 $\delta^{18}O$ values of important geological reservoirs, data from Eiler et al., 2000; Hoefs, 2009; Kyser et al., 1981; Mattey et al., 1994; Ohmoto, 1986

Isotopic composition depends, on the first order, on the nature of the rock analyzed (sediment, metamorphic rock, etc; Fig 4.1). On the second order, it depends on processes experienced by the rock. In a purely magmatic rock, the isotopic composition is determined by the nature of the magmatic source, the temperature of magma generation and crystallization, the mineralogical composition of the rock, and the evolutionary history of the magma such as crustal assimilation, magma mixing, etc. Isotopic composition of magmatic rocks is also impacted by hydrothermal circulations (Hoefs, 2009). Based on $^{18}O/^{16}O$ ratios, Taylor (1977, 1978) proposed a division of granitic rocks into three groups: (1) normal ^{18}O-granitic rocks ($\delta^{18}O$ between 7 and 10 ‰); (2) high

^{18}O granitic rocks (δ^{18}O >10 ‰) to be related with a high δ^{18}O in the original magma, a high-temperature exchange between the pluton and adjacent high δ^{18}O country rocks, or with a secondary event such as weathering or low-temperature hydrothermal alteration; (3) low ^{18}O granitic rocks (δ^{18}O < 6 ‰) formed by melting or assimilation of hydrothermally altered roof rocks.

Another significant cause for O isotopes fractionation is hydrothermal alteration. Because of this, O isotopes are widely used in ore deposits studies. Indeed, they can provide information on the circulating fluids characteristics such as their origin, temperatures of mineralization, and physico-chemical conditions of mineral deposition. The main fluid sources identified are ocean water, meteoric waters, and juvenile water (degassed from the mantle; Fig 4.1). Other types of ore fluids, including magmatic waters, are considered recycled from one or more of these three sources and are characterized by their δ^{18}O in association with their δD (Fig 4.2). As such, δ^{18}O analysis commonly provide precious information as to the development of late magmatic fluids and processes occurring during late- to post-magmatic evolution. At this end, some studies based on δ^{18}O and δD in alkaline complexes have been performed (e.g. Ilímaussaq, Marks et al., 2004; Strange Lake, Boily and Williams-Jones, 1994; Siegel et al., 2017; Ambohimirahavavy, Marquis, 2019).

In some cases, it is possible to determine the δ^{18}O of the fluid, either by direct measurement of fluid inclusions contained within hydrothermal minerals, or by analysis of hydroxyl-bearing minerals and calculation of the isotopic composition of fluids from known temperature-dependent mineral-water fractionations, assuming that minerals were precipitated from solutions under conditions of isotope equilibrium (Hoefs, 2009).

4.2.2 Application of O isotopes to alkaline amphibole and pyroxene

In order to validate the magmatic origin of amphibole and the magmatic and hydrothermal origin of pyroxene, O stable isotopes analysis were performed on these minerals. Considering our previous conclusion (Section 4.1) according to which amphiboles and pyroxene from all six complexes grew under the same conditions, only minerals from Ambohimirahavavy were analyzed with this method. The selected samples are AM49, a pegmatite with zoned aegirine and no amphibole, and AM107, a granite with unzoned aegirine and amphibole

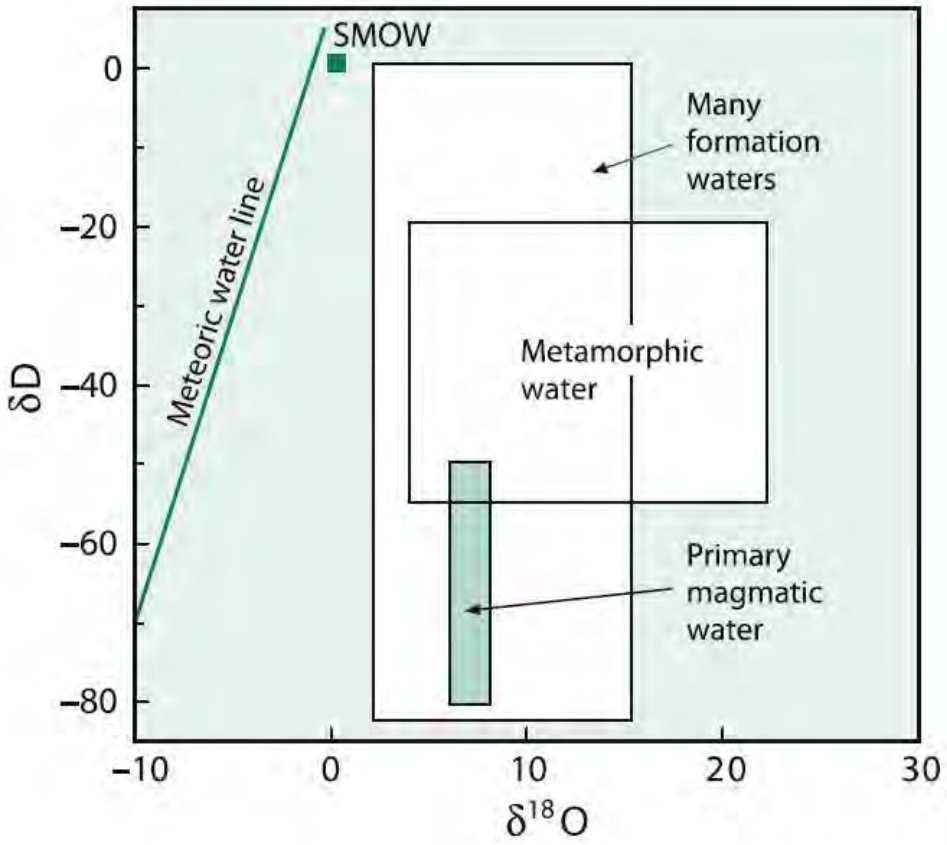

Figure 4.2 Plot of δ^{18}O versus δD of waters of different origins, from Hoefs, 2009

(Tab 4.1). In addition, previous analyses from Strange Lake, taken from Boily and Williams-Jones (1994), and from Ambohimirahavavy, taken from Marquis (2019) were also taken into account. were also taken into account.

Whole-rock samples selected for this study were crushed before being sifted. Magnetite was then removed from the fraction of size 200-125 μm for the granite and 400-200 μmm for the pegmatite with a magnet. The remaining fractions were then introduced in a Frantz magnetic separator with 0.22 Å and an inclination of 20 mm, in order to collect only the slightly magnetic minerals, which include alkali amphibole and pyroxene. The last part of the separation was done by hand, under a binocular microscope, where selection was done based on the color of the crystals (green for aegirine and black for amphibole), which was later verified with the SEM. Approximately 8 mg of each mineral were handpicked. The analyses were performed by Chris Harris at the Stable Isotope Lab of the University of Cape Town (UCT), South Africa, using a fluorination line. He reacted approximately 2 mg of material with BrF_5 using the laser as the source of heat. δ^{18}O values were determined on O_2 gas absorbed onto a molecular sieve in sample bottles. The

standard used was the aegirine sample STFL1B from the Straumsvola complex, Antarctica, described in the paper by Harris et al. (2018). The precision is better than 0.1 ‰. The limitation with this method is that only whole crystals can be analyzed. Hence, the different zones of aegirine cannot be checked separately, but it seems reasonable to expect that the resulting average value of the zoned pegmatitic aegirine would be different from the unzoned granitic one.

Table 4.1 $\delta^{18}O$ values of aegirine and amphibole from Ambohimirahavavy and Strange Lake, acquired on whole crystals. Data are from this study as well as from Boily and Williams-Jones (1994) and Marquis (2019)

Complex		Ambohimirahavavy								Strange Lake		
Rock nature		Pegmatite (AM49)			Granite (AM107)		Pegmatitic afs syenite	Nepheline syenite		Unaltered granites	Altered subsolvus granite	Altered subsolvus granite
Source		This study					Marquis (2019)			Boily & Williams-Jones (1994)		
Mineral		Zoned aegirine			Unzoned aegirine		Unzoned amphibole	Amphibole	Amphibole	Aegirine	Arfvedsonite	Arfvedsonite	Arfvedsonite + aegirine
		Whole	Core	Rim									
Number of analyses		1	16	16	1	18	2	4	2	6	3	3	2
Mean $\delta^{18}O$ (‰)	Whole crystal	6.65 ± 0.1			6.41 ± 0.1		6.52 ± 0.1	5.1 ± 0.3	5.1 ± 0.3	4.8 ± 0.3	5.0 ± 0.1	12.1 ± 0.1	5.7 ± 0.1
	In situ		6.5 ± 0.2	6.5 ± 0.2		7.2 ± 0.2							

From data of this study, it is obvious that there is no real difference between amphibole and aegirine of pegmatite and granite from Ambohimirahavavy, which are all close to $\delta^{18}O$ values of 6.5 ‰. These values are similar to those of amphibole in unaltered granites and of amphibole altered to aegirine in the altered subsolvus granite from Strange Lake ($\delta^{18}O$ values of 5-5.7 ‰). However, $\delta^{18}O$ values of amphibole that are not altered to aegirine are much higher (12.1 ‰ on average). According to Boily and Williams-Jones (1994), this high value is consistent with the circulation of low-temperature (< 200 °C) hydrothermal fluids. It could also simply be the initial value of the melt. Hence, the comparison tends to rule out the circulation of a similar fluid at Ambohimirahavavy. The similarity of $\delta^{18}O$ values between the three crystal types in granite and pegmatite from Ambohimirahavavy prevents any interpretation as to the magmatic or orthomagmatic hydrothermal origin of aegirine. Indeed, as shown in Fig 4.1 and 4.2, the $\delta^{18}O$ values of granitic rocks and magmatic water overlap, hence it is that possible aegirine crystals rims grew from an orthomagmatic fluid, leaving no imprint on their $\delta^{18}O$ value. However, it is also possible that hydrothermal rims of zoned aegirine are too small to impact significantly the $\delta^{18}O$ value. Hence, in situ analyses should be required to rule this possibility out. Data on amphibole and aegirine in nepheline and alkali feldspars syenite (Marquis, 2019) provide lower $\delta^{18}O$ values, close to 5.0. The difference with $\delta^{18}O$ values in pegmatite and granite may be due to crystal fractionation, lower in syenites.

4.2.3 In situ isotopic measurements

A further step is to determine the $\delta^{18}O$ value of specific parts of a crystal, by performing in-situ spot analyses. This should allow to better understand the zonations of aegirine and check whether these analyses provide different values depending on the zone analyzed. To do so, aegirine crystals of samples AM49 and AM107 as well as the aegirine standard that were used for the laser fluorination technique were mounted on aluminum support and polished. They were then sent to Etienne Deloule, in collaboration with Gaston Giuliani and Nordine Bouden, at the Centre de Recherches Pétrographiques et Géochimiques of the University of Nancy, France. They used an IMS 1270 ionic microprobe to perform in situ analyses on the aegirine crystals. The results are provided in Tab 4.1. Unfortunately, similarly to the bulk data, there appears to be no difference in the $\delta^{18}O$ value in core and rims of zoned aegirine. The values found are about 6.5 ‰, which is the same that what was found for amphibole and unzoned aegirine. Considering all the evidences provided in previous sections, according to which amphibole and aegirine core are of magmatic origin whereas aegirine rims formed under hydrothermal conditions, it is likely that aegirine rims grew from an orthomagmatic fluid, which, as shown by Fig 4.2, would lead to no differences in $\delta^{18}O$. The difference between whole crystal and in situ values in granite may be due to analytical processes (Deegan et al., 2016) or to a low purity of aegirine, which would affect only whole crystals analyses.

4.3 Zircon as an indicator of REE enrichment

Zircon is a common mineral in the rocks studied from all complexes, especially in pegmatites. Similarly to amphiboles and aegirine, although this mineral is typical of igneous rocks, it can also grow at the hydrothermal stage. The formula of pure zircon is $ZrSiO_4$, but many elements can enter its structure. The most common elements found in zircon are the REE, and Hf ("Zircon", 2020), because they have an atomic radius close to that of Zr^{4+}. Among the REE, HREE have an even more similar atomic radius than LREE, hence zircon commonly fractionates the REE and is enriched in HREE, presenting REE spectra with steep slopes (Gysi et al., 2016; Hoskin, 2005). As described in Chapter 3, zircon (characteristic of miaskitic rocks) and complex zirconosilicates (characteristic of agpaitic rocks) do not precipitate at

the same time. Hence, in the rocks studied, zircon cannot be early magmatic. In this section, zircon from the six studied complexes are described petrographically and chemically in order to understand the origin of their variety of textures and composition and link them to their REE content. Measurements were performed according to the methods described in Chapter 3.

4.3.1 Petrography of zircon

Based on petrographic observations such as shape, zonation, inclusions, mineral association and presence or not in a pseudomorph, zircons from all six complexes can be classified in three main categories. The first category (type-SG, single grain) is made of euhedral zircon occurring as single grains in equilibrium with quartz and feldspars. The second category (type-P, in pseudomorphs) regroups zircon in pseudomorphs that is systematically associated with quartz and occasionally with elpidite, fluorite, amphibole, or REE-bearing minerals. The third category (type-I, interstitial) is rarer and regroups interstitial anhedral zircon, growing between quartz and feldspars grain boundaries. Table 4.2 synthetizes the characteristics of the zircons present in each complex, in pegmatites and granites.

Table 4.2 A summary of petrographic characteristics of zircon from all six studied complexes

Rock type		Pegmatite					Granite	
Zircon type		Type-I	Type-P			Type-SG	Type-P	Type-SG
Amis	Size	20 - 150 µm	~300 µm			200-700 µm	20-100 µm	100-250 µm
	Shape	Anhedral	Subeuhedral			Euhedral	(Sub)euhedral	Euhedral
	Abundance in the rock	Average	Rare			Abundant	Abundant	Rare
	Zonation	Oscillatory	Weak, core to rim			Core to rim	Weak	No
	Porosity/inclusions	No	No			Yes	No	Yes
	Alteration	No	Low			Rims dissolution	No	Rims dissolution
	CL color	Blue	Yellow, purple			Yellow, purple	Yellow, purple	Yellow, purple
	Mineral association	qtz, afs	qtz			qtz, afs	qtz, bt, Fe-ox	qtz, afs
	Figure	4.3 c	4.3a			4.3b	4.3d	4.3e
Evisa	Size		30-100 µm			100-250 µm	30-100 µm	100-500 µm
	Shape		Subeuhedral			Euhedral	Euhedral with some	Subeuhedral
	Abundance in the rock		Abundant			Average	Abundant	Rare
	Zonation		Weak oscillatory			Oscillatory	Yes	Core to rim
	Porosity/inclusions		No			In the core	In the core	No
	Alteration		Occasional in the core			Along rims	Rims and core	Core and rims
	CL color		Purple			Purple	Yellow, purple	Pink
	Mineral association		qtz			qtz	qtz ± flr	qtz, afs
	Figure		4.4a			4.4b	4.4c, d	4.4e
Khan Bogd	Size		100-200 µm	50-600 µm	10-100 µm			
	Shape		Subeuhedral	Euhedral	Euhedral, botryoidal or dendritic			
	Abundance in the rock		Low	Abundant	Abundant			
	Zonation		Weak, core to rim	Oscillatory in rims	Core to rim			
	Porosity/inclusions		No	No	In the core			
	Alteration		Fractures	Low	Low			
	CL color		Purple, red	Purple	Purple			
	Mineral association		amp	qtz	qtz, elp			
	Figure		4.5a	4.5b	4.5c			
Ambo	Size		50-500 µm	50-500 µm	50-500 µm			150-400 µm
	Shape		Euhedral	Dendritic	Botryoidal			Subeuhedral
	Abundance in the rock		Abundant	Low	Low			Abundant
	Zonation		Oscillatory	No	Core to rim			Oscillatory and sector zoning
	Porosity/inclusions		No	In the core	No			In the core
	Alteration		Low	Low	No			Along rims, fractures
	CL color		Yellow	Yellow, purple				Yellow, purple
	Mineral association		qtz, REE-bearing minerals	qtz, euhedral zrn	qtz, cal, Al-phyllosilicates, euhedral zrn			qtz, REE-bearing minerals
	Figure		4.6a	4.6b	4.6c			4.6d
M	Size		20-200 µm	10-200 µm				
	Shape		Botryoidal	Euhedral				
	Abundance in the rock		Average	Abundant				
	Zonation		Oscillatory	Sector zoning				
	Porosity/inclusions		In the core	No				
	Alteration		Occasional in the core	Low				
	CL color		Yellow	Pink, yellow-green				
	Mineral association		qtz, REE-bearing minerals	qtz				
	Figure		4.7b, c	4.7a				
Strange Lake	Size	~10 µm	20-100 µm	20-100 µm			20-150 µm	20-100 µm
	Shape	Anhedral	Euhedral	Euhedral			Botryoidal	Euhedral
	Abundance in the rock	Low	Low	Low			Low	Low
	Zonation	No	Oscillatory	n.a.			n.a.	n.a.
	Porosity/inclusions	No	No	No			No	No
	Alteration	No	In the core	Locally along rims			Low	Locally along rims
	CL color							
	Mineral association	flr	qtz, flr, hem	qtz, elp, hem, K-phyllosilicate			flr, qtz	qtz, elp, hem, K-phyllosilicate
	Figure	4.8b		4.8c			4.8c	

At Amis, all three categories of zircon are observed in pegmatites, but no type-I zircon was found in the arfvedsonite granite. In pegmatites, type-P zircon is euhedral and associated with quartz (Fig 4.3a). It is also commonly zoned from core to rim, and the zonation is especially visible with CL, from yellow to purple. Although the interpretation of CL colors in zircon is still a matter of debate (Nasdala et al., 2003), one of the most common explanations is the presence of impurities such as the REE, and the organization of the crystallographic cell. The yellow color could be linked to the presence of Yb^{3+}, but Kempe et al. (2000) indicate that this color cannot be seen in zircon unless the crystal has already underwent structural damages of radioactive origin. The purple color is interpreted to come from Tm^{3+} or Gd^{3+} (Blanc et al., 2000; Nasdala et al., 2003). However, in zircon of this study, all three REE are present, hence the reason why one REE is dominant over the others to give CL color remains unknown. In granite, type-P zircon is associated with biotite, quartz and Fe-oxides but has petrographic properties similar to those in pegmatites (Fig 4.3d). It is similar to cluster zircon described by Estrade (2014) at Ambohimirahavavy. Type-SG single zircon grains in pegmatite are especially large compared to other zircons (200-700 μm), contain feldspar inclusions, and are euhedral, zoned, and altered (Fig 4.3b). They also appear yellow and purple in CL, with a layer of deep purple at its rims. They are abundant close to aegirine clusters. Type-SG zircon in granite is also similar to those in pegmatites, although generally smaller. It is porous and can contain inclusions rich in Th or REE (100-250 μm; Fig 4.3e). Type-I zircon occurs in zones of pegmatite where there are no aegirine clusters. It occurs between feldspars, amphibole and quartz crystals and are zoned (Fig 4.3c). They appear blue in CL, which is commonly attributed to the presence of Dy^{3+} (Blanc et al., 2000; Nasdala et al., 2003).

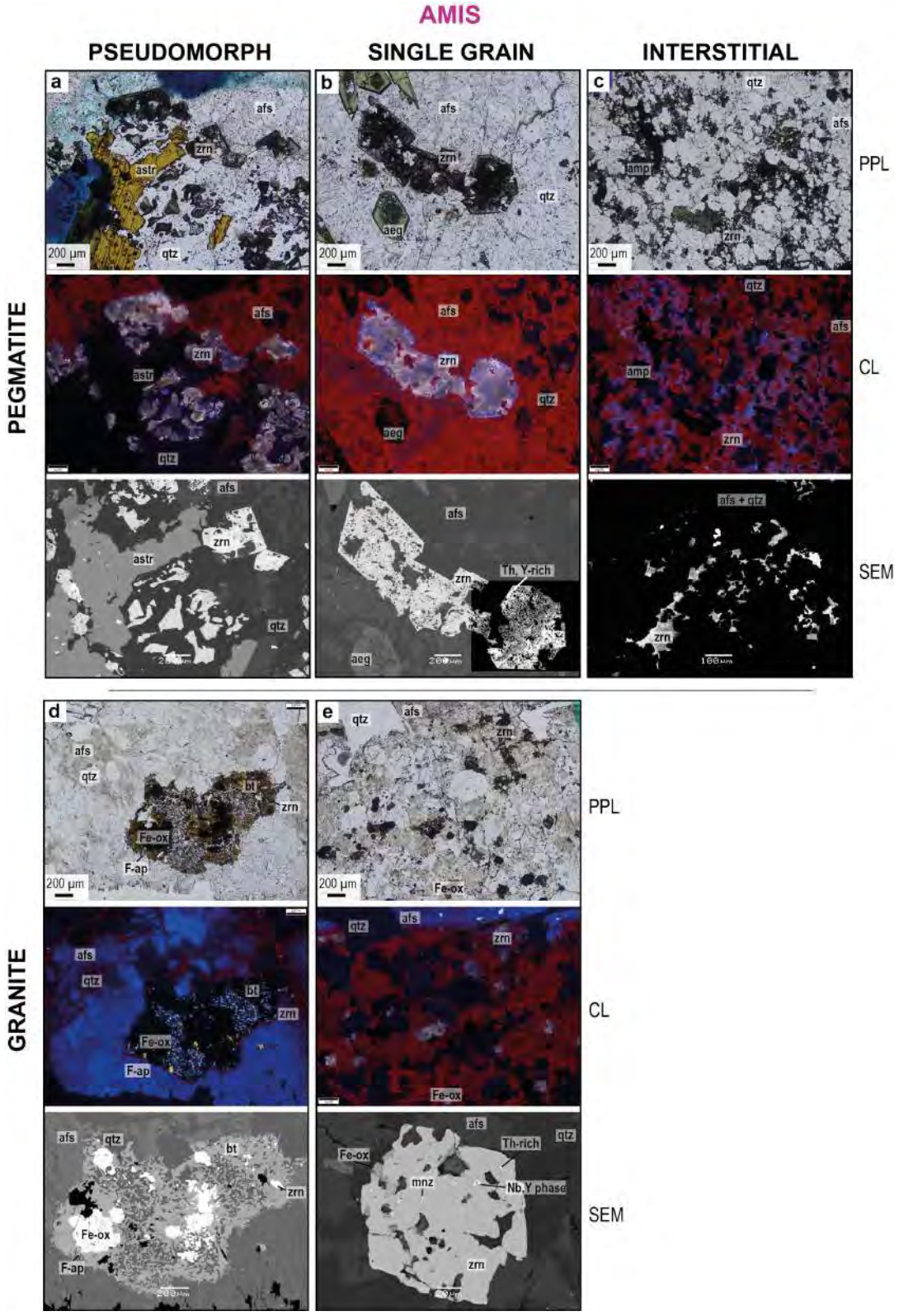

Figure 4.3 Photomicrographs of representative zircons from Amis in pegmatites and granite. Most CL images were acquired by Adrien Prault. (a) Type-P euhedral zircon in pseudomorphs with quartz, sample SOS071; (b) Type-SG euhedral single grain, sample SOS071; (c) Type-I anhedral interstitial zircon, sample SOS071; (d) Type-P euhedral zircon in a pseudomorph with quartz, biotite and Fe-oxides, sample SOS066; (e) Type-SG euhedral single grain, sample SOS066. Abbreviation: afs: alkali feldspar; zrn: zircon; qtz: quartz; astr: astrophyllite; aeg: aegirine; amp: amphibole; bt: biotite; Fe-ox: Fe-oxides; F-ap: fluoro-apatite; mnz: monazite-(Ce)

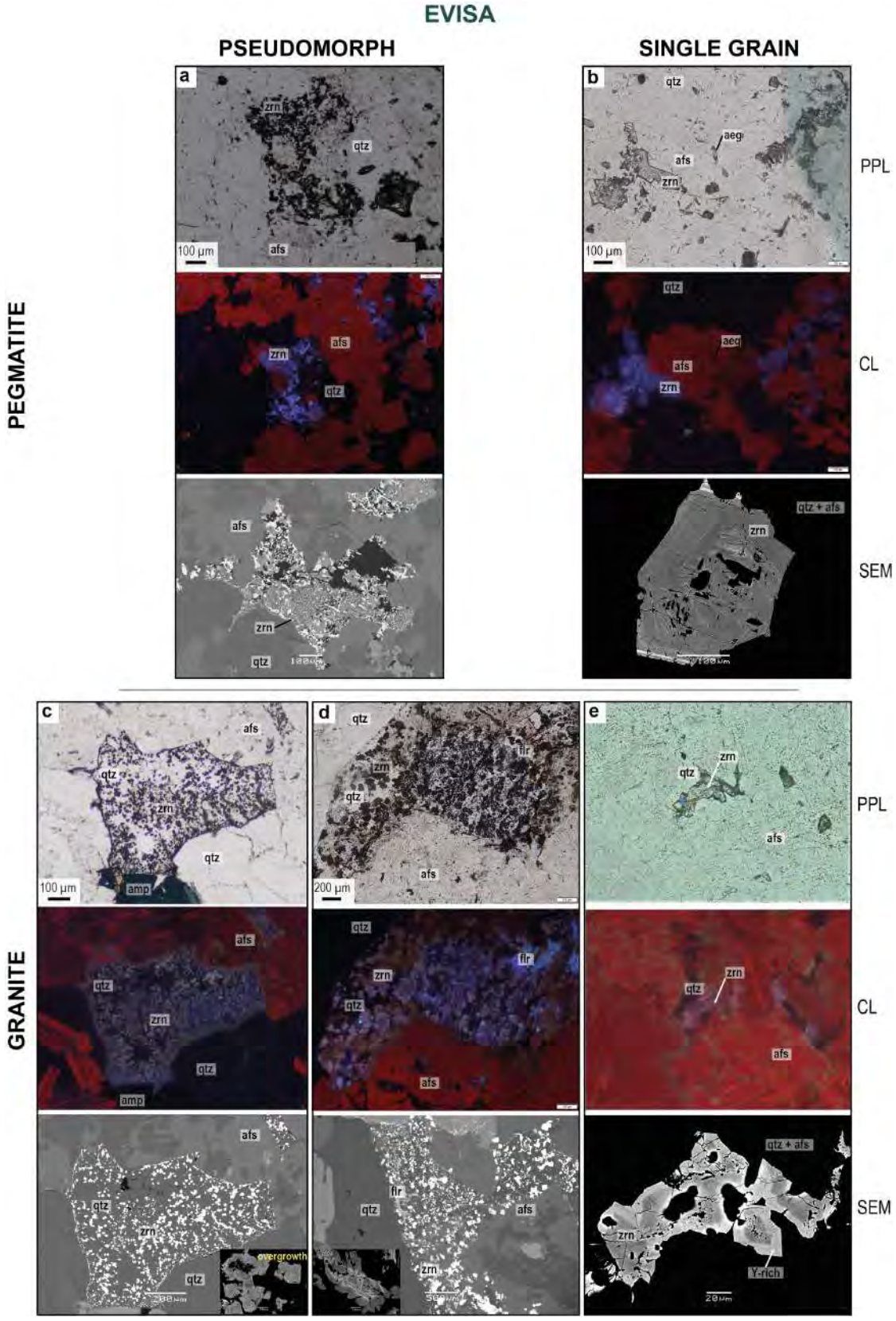

Figure 4.4 Photomicrographs of representative zircons from Evisa in pegmatites and granites. (a) Type-P euhedral zircon in a pseudomorph with quartz and REE-bearing minerals, sample EV1817A; (b) Type-SG euhedral single grain, sample EV1817A; (c) Type-P euhedral zircon in a pseudomorph with occasional overgrowths and associated with quartz, sample EV1820; (d) Type-P euhedral zircon in a pseudomorph with quartz and fluorite, sample EV1823B; (e) Type-SG euhedral single grain, sample EV1823B. Abbreviation: afs: alkali feldspar; zrn: zircon; qtz: quartz;aeg: aegirine; flr: fluorite

At Evisa, type-I zircon was not found. In pegmatites, type-P zircon is similar to type-P zircon from Amis, with the exception that it is associated with REE-bearing minerals and appear exclusively purple (Tm^{3+} or Gd^{3+}) in CL (Fig 4.4a). In granites, two subtypes of zircon in pseudomorphs were found. The first subtype is present in pseudomorphs with quartz only; it is euhedral, zoned, and is yellow (Yb^{3+}) to purple in CL (Fig 4.4c). It locally shows overgrowths made of small dendritic zircon crystals growing perpendicularly to the surface of the first generation of zircon. The second zircon subtype in pseudomorphs occurs associated with quartz and fluorite. Compared to the other pseudomorph zircon subtype, it is weakly zoned, and only shows purple CL (Fig 4.4d). Zircon type-SG in pegmatite is euhedral and presents an important oscillatory zonation. It can contain quartz and feldspar inclusions in its core (Fig 4.4b). In granite, type-SG zircon is euhedral but presents partly dissolved rims and core. It is zoned from core to rim and appears pink in CL, which may indicate the presence of Sm^{3+} (Nasdala et al., 2003; Fig 4.4e).

In samples from Khan Bogd, zircon is abundant only in pseudomorphs formed in pegmatites. However, type-P zircon can be further divided into three subtypes. (1) The first consists of zircon associated with amphibole. It is subhedral, present a weak core to rim zonation, and is highly fractured. It is only rarely found in the rocks. It is purple to red in CL, which indicates the potential presence of Tm^{3+}, Gd^{3+}, Sm^{3+} and Nd^{3+} (Blanc et al., 2000; Nasdala et al., 2003; Fig 4.5a). (2) The second subtype of pseudomorph zircon is similar to that of Amis and Evisa, i.e., euhedral, oscillatory zoned, purple in CL and associated with quartz (Fig 4.5b). (3) The third and last subtype is made of zircon partially replacing elpidite. It can be euhedral, botryoidal or dendritic, and occurs at the center of elpidite crystals, associated with quartz. It can be porous in its core and is mostly purple in CL (Yb^{3+}, Nasdala et al., 2003; Fig 4.5c). All three subtypes can be found in the same pegmatite. Kynicky et al. (2011) report the occurrence of type-SG zircon, but in granite only. It can be zoned from core to rim.

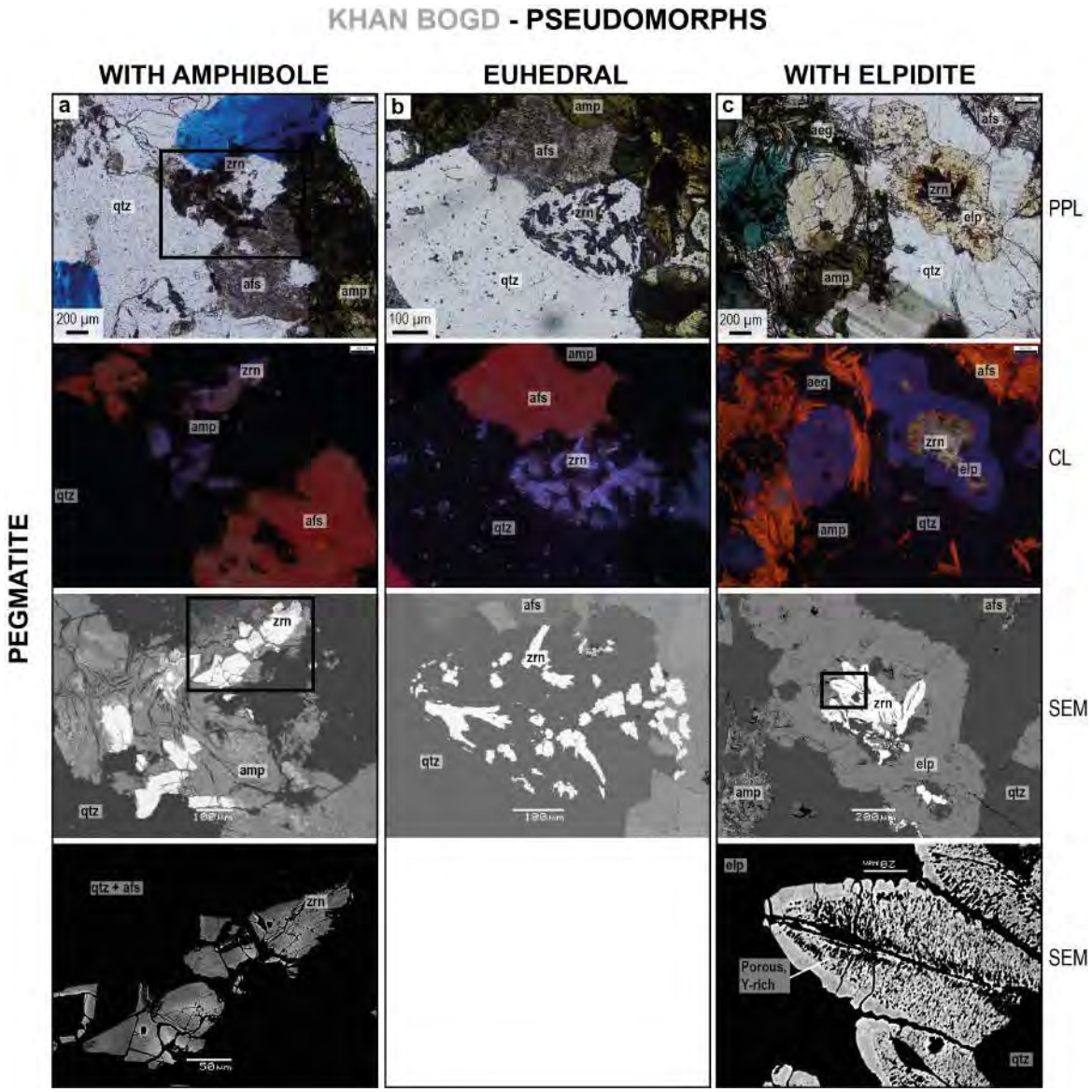

Figure 4.5 Photomicrographs of representative type-P zircons from Khan Bogd in pegmatites. Black squares indicate the position of the photograph underneath. Most CL images were acquired by Adrien Prault. (a) Euhedral zircon in a pseudomorph with amphibole, sample KB04A; (b) Euhedral zircon in a pseudomorph with quartz, sample KB04B; (c) Dendritic porous zircon in a partial pseudomorph after elpidite, sample KB04A. Abbreviation: afs: alkali feldspar; zrn: zircon; qtz: quartz; aeg: aegirine; amp: amphibole; elp: elpidite

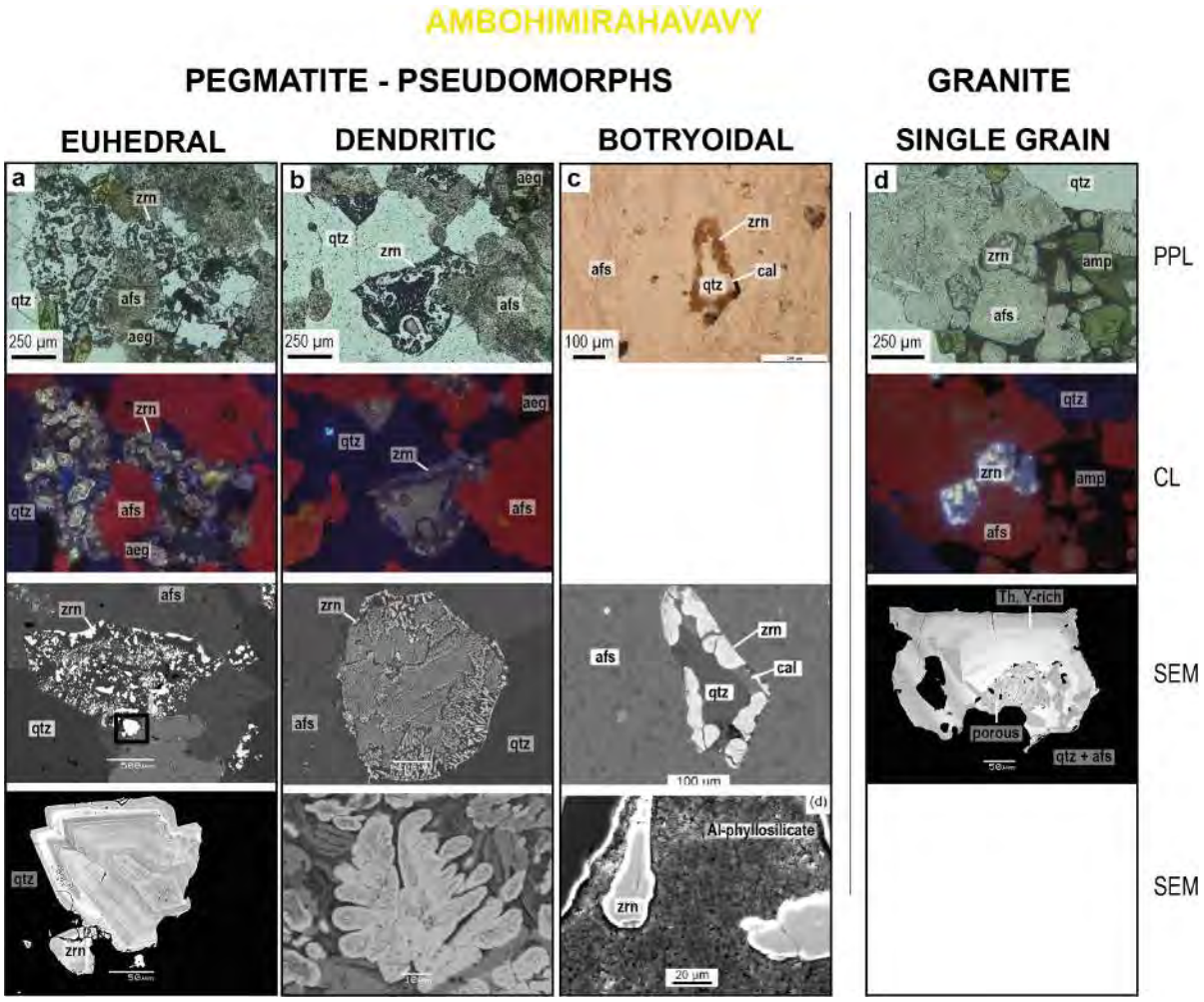

Figure 4.6 Photomicrographs of representative zircons from Ambohimirahavavy in pegmatites and granites. The black square indicates the position of the photograph underneath; if not present, the photomicrograph underneath was taken at a different location. SEM images were acquired by Guillaume Estrade. (a) Type-P euhedral zircon in a pseudomorph with quartz, samples AM113A1 (PPL, CL) and AM35 (SEM); (b) Type-P dendritic zircon in a pseudomorph with quartz and euhedral zircon, samples AMJ05 (PPl, CL) and AMJ12 (SEM); (c) Type-P botryoidal zircon associated with quartz and calcite or with Al-phyllosilicate, sample AMJ12; (d) Type-SG euhedral single grain of zircon, sample AM107. Abbreviation: afs: alkali feldspar; zrn: zircon; qtz: quartz; aeg: aegirine; amp: amphibole; cal: calcite

At Ambohimirahavavy, type-P zircon was only found in pegmatites and type-SG zircon was found only in granites. Three subtypes of type-P zircon are observed. (1) The first one is made of euhedral crystals associated with quartz or REE-bearing minerals. They show oscillatory zoning, visible in CL and SEM. They appear mostly yellow in CL, which is the sign for radioactive damages and Yb^{3+} presence (Fig 4.6a). (2) The second subtype of zircon in pseudomorphs is made of dendritic

zircon. It is commonly associated with quartz, but can also be found in the same pseudomorph than euhedral zircon. No zonation is visible, but it is porous and appears yellow and purple in CL (Tm^{3+} and/or Gd^{3+}; Fig 4.6b). (3) The third subtype of zircon in pseudomorphs is much rarer than the other two. It was described by Estrade (2014) as botryoidal crystals crystallizing along the rims of pseudomorphs made of quartz, calcite, euhedral zircon and/or Al-phyllosilicates. Since I could not find it in the samples from this study, no CL information is provided (Fig 4.6c). In granites, type-SG zircon occurs as single euhedral crystals altered and porous in their core. They are oscillatory and sector-zoned. They appear yellow and purple in CL (Fig 4.6d). In addition, Estrade (2014) described another category of zircon, that occurs only in pegmatites as single grains or in clusters. It is subeuhedral to anhedral, oscillatory and sector-zoned, and not porous.

At Manongarivo, only pegmatite samples are available for this study. Two subtypes of type-P zircon were observed. (1) The first one is made of euhedral crystals associated with quartz and strongly sector-zoned. They appear pink and yellow-greenish in CL. This yellow-green color could be due to Er^{3+}, and the pink color is likely linked to Sm^{3+} (Nasdala et al., 2003; Fig 4.7a). They are similar to cluster zircon described by Estrade (2014). (2) The second one is made of botryoidal zircon associated with quartz and/or REE-bearing minerals. It is core to rim zoned (Fig 4.7b), and can present quartz and feldspar crystals in its core. It appears mostly yellow in CL (Fig 4.7c).

At Strange Lake, zircon is globally scarcer and smaller than zircons from other complexes. Indeed, Strange Lake rocks are agpaitic at magmatic (elpidite) and early hydrothermal (armstrongite, gittinsite) stages, hence zircon grew only as an alteration mineral. No significant amounts of zircon were found in samples from this study, hence the following description is based on observations made by Gysi and Williams-Jones (2013), Gysi et al. (2016) and Salvi and Williams-Jones (1995). At Strange Lake, zircon was found occurring as type-P and type-I. Type-P zircon can be divided in three subtypes. (1) The first one regroups euhedral zircon with oscillatory zoning associated with quartz, fluorite and hematite. Unfortunately, no image of this subtype of zircon was found in the previously mentioned papers. (2) The second subtype is made of botryoidal zircon associated with fluorite and quartz (Fig 4.8a). (3) The third subtype is made of euhedral zircon locally altered and associated with elpidite, hematite and K-phyllosilicate (Fig 4.8c). Type-I zircon was found mostly at grain boundaries of fluorite (Fig 4.8b).

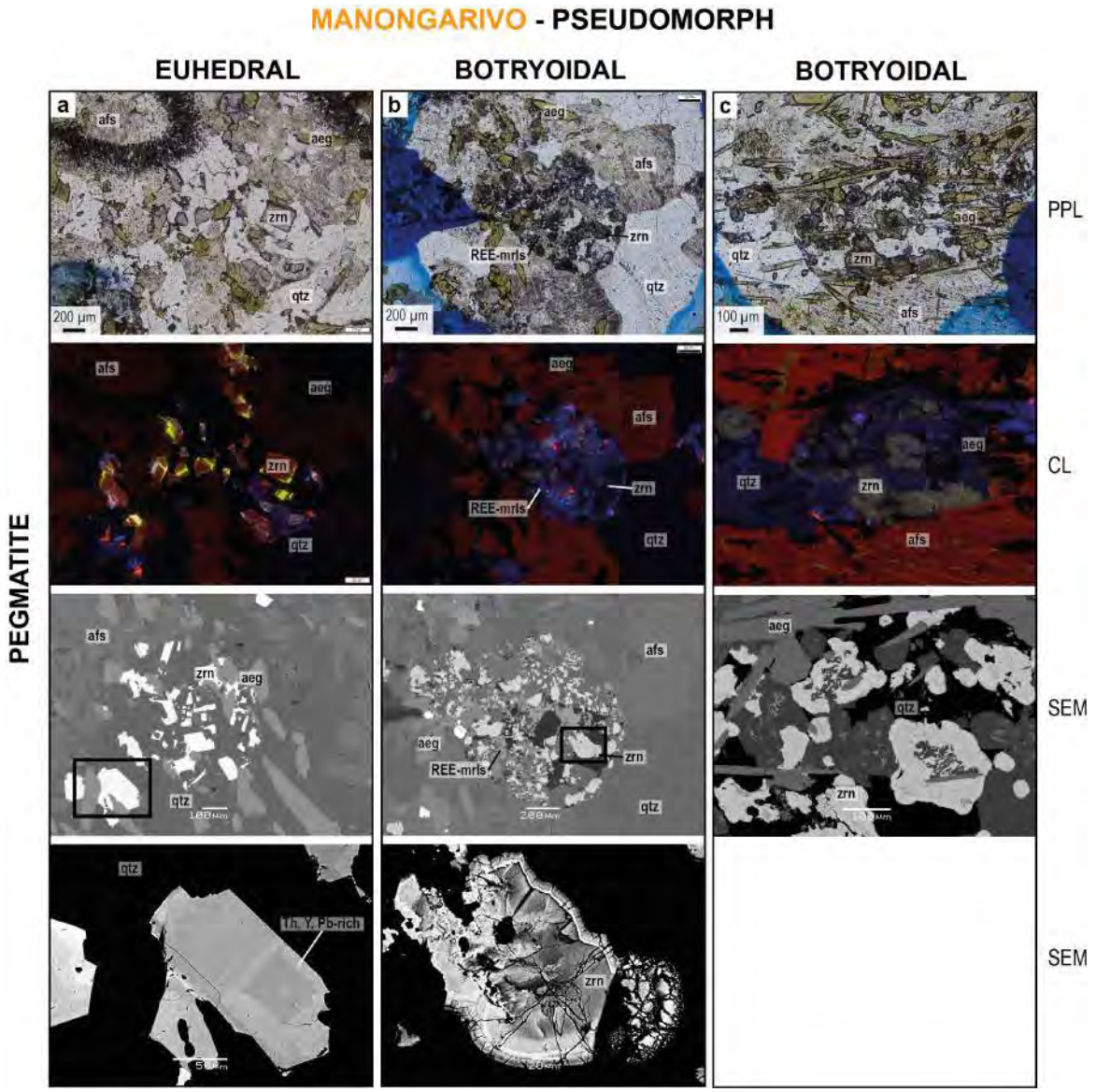

Figure 4.7 Photomicrographs of representative zircons from Manongarivo in pegmatites. Black squares indicate the position of the photograph underneath. Most CL images were acquired by Adrien Prault. (a) Type-P euhedral, sector-zoned zircon in a pseudomorph with quartz, sample 689; (b) Type-P botryoidal, core to rim zoned zircon in a pseudomorph with quartz and REE-bearing minerals, sample 688; (c) Type-P botryoidal zircon associated with quartz, sample 688. Abbreviation: afs: alkali feldspar; zrn: zircon; qtz: quartz; aeg: aegirine

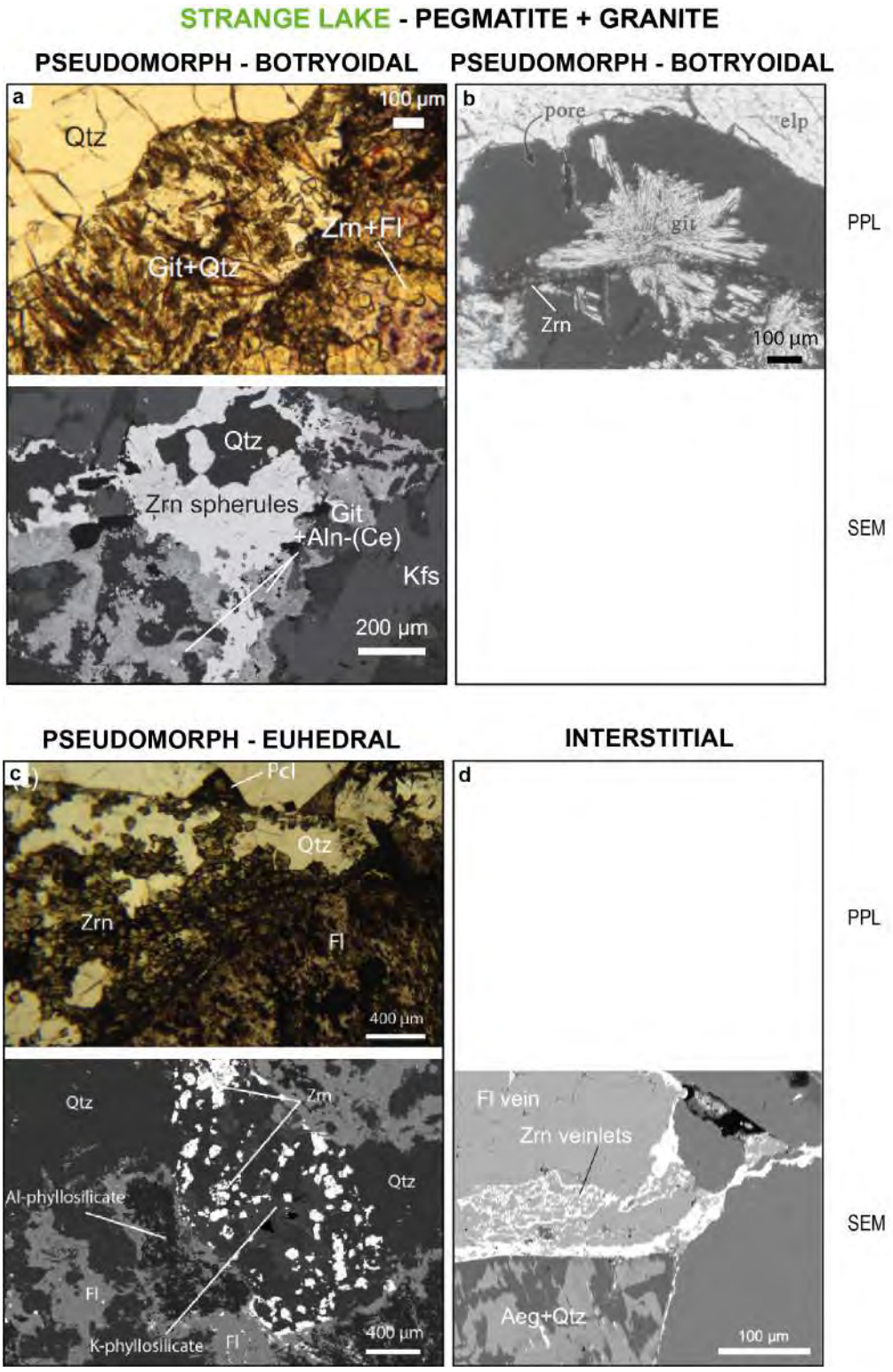

Figure 4.8 Photomicrographs of representative zircons from Strange Lake in pegmatites, (a), (c), (d) from Gysi et al. (2013, 2016) and (b) from Salvi and Williams-Jones (1995). (a) Type-P botryoidal zircon in a pseudomorph with quartz and fluorite; (b) Stringlet of zircon spherules with gittinsite growing on top (c) Type-P euhedral zircon associated with quartz and K-phyllosilicate; (d) Type-I interstitial zircon. Abbreviation: Zrn: zircon; Qtz: quartz; Fl: fluorite; Git: gittinsite; Aln-(Ce): allanite-(Ce); Aeg: aegirine; Pcl: pyrochlore ; elp: elpidite

4.3.2 Major and trace elements in zircon

Zircons of the different petrographic categories are also distinguished by their trace elements chemistry (Tab 4.3). REE content being the core of this study, it will be discussed apart in the next section.

4.3.2.1 Compositional variations within single zircon crystals

In all complexes, most zircon crystals have heterogeneous compositions, independently of their category or the rock they grew in. They can be sector-zoned, present core to rim or oscillatory zoning, or be altered. The zonation is more or less visible under SEM depending on the difference of concentration between trace elements whose concentration varies. In zircon of all complexes, the elements responsible for the zonation visible with the SEM are Y and, for most of them, Th. The concentration of Y and Th varies in a similar manner; both are more abundant in light zones of SEM images (Fig 4.3b,c, 4.4b,e, 4.6a,d, 4.7a,b). Considering that the zonation pattern involving Y and Th is common to all complexes and to most zircon crystals, it is likely that the incorporation of these elements is a property of zircon itself and does not depend on its origin (e.g. Soman et al., 2010). In addition, some other elements can locally vary depending on the complex and the zircon type. The most obvious observed zonations are found at Evisa, Ambohimirahavavy, and Manongarivo. In type-P zircon of pegmatites from Evisa, the concentration of Hf, Pb and U is positively correlated with that of Y and Th. At Ambohimirahavavy, Ce is responsible for the oscillatory zoning of type-P euhedral zircon; and at Manongarivo, Pb is also positively correlated with Th and Y.

4.3.2.2 Comparison of zircon compositions in a same complex

Petrographic categories of zircon are also visible in their composition. However, although the difference between categories is visible inside one complex, no composition pattern is found common between all complexes, with the exception of the REE which will be discussed in the next section.

In pegmatites from Amis, type-I interstitial zircon contains less ZrO_2 (58.8 %) and P (680 ppm), and more ThO_2 (1.36 %), HfO_2 (2.27 %), Rb (186 ppm), and Ba (124 ppm) than other zircons. Light type-SG zircon is rich in P (3938 ppm), Y (12043 ppm) and ThO_2 (1.52 %) whereas dark type-SG is richer in HfO_2 (1.6 %), PbO (0.06 %), Al_2O_3 (0.09 %), K_2O (0.02 %), MnO (0.04 %), FeO (0.07 %), Na_2O (0.09 %),

Table 4.3 Mean major and trace compositions of zircon of all six studied complexes and of different petrographic compositions. Data of SG zircon at Khan Bogd is from Kynicky et al. (2011), and data at Strange Lake is from Gysi et al. (2016). Abbreviations: I: interstitial; P: pseudomorph; SG: single grain; amp: amphibole; edl: euhedral; elp: elpidite; den: dendritic; bot: botryoidals

Complex	Amis						Evisa					Khan Bogd						Ambohimirahavavy				Manongarivo		Strange Lake				
Rock	Pegmatite				Granite		Pegmatite		Granite			Pegmatite					Granite	Pegmatite		Granite		Pegmatite		Pegmatite			Granite	
Zircon type	Type-I	Type-P	Type-SG		Type-P	Type-SG	Type-P	Type-SG	Type-P	Type-SG		Type-P					Type-SG	Type-P		Type-SG		Type-P		Type-I	Type-P		Type-P	
Subtype			Light	Dark		Dark		Dark		Light	Dark	P-amp	P-edl 04A	P-edl 04B	P-elp			P-edl	P-den	Light	Dark	P-edl	P-bot		P-edl	P-elp	P-bot	P-elp
Wt. %																												
Analyses no	**6**	**11**	**5**	**4**	**6**	**22**	**14**	**13**	**11**	**3**	**2**	**4**	**8**	**20**	**26**	**7**		**165**	**16**	**43**	**15**	**14**	**51**	**5**	**19**	**16**	**24**	**27**
SiO_2	30.6	30.4	29.6	31.7	32.0	31.7	31.4	31.4	31.2	31.6	31.4	31.4	32.1	31.8	31.7	31.4		32.1	32.3	31.5	32.3	31.9	31.4	32.9	31.1	30.1	31.8	30.3
ZrO_2	58.8	60.7	58.8	63.4	65.6	65.1	60.3	61.6	62.4	58.2	58.8	61.4	65.0	61.4	63.6	63.8		62.9	61.1	61.5	65.4	65.7	61.3	59.7	57.5	55.0	55.0	58.3
TiO_2	0.05	0.06	0.02	0.06	0.03	0.04	0.03	0.05	0.12	0.44	0.41	0.14	0.23	0.11	0.20	0.15		n.a.	n.a.	n.a.	n.a.	0.04	0.23	0.16	0.14	0.08	0.13	0.07
CaO	0.02	0.02	0.01	0.15	0.06	b.d.l.	0.02	0.02	0.08	0.25	0.12	0.19	0.10	0.22	0.13	1.71		0.13	0.32	0.02	0.02	0.01	0.46	0.10	0.05	0.10	0.84	1.09
Na_2O	0.03	0.01	b.d.l.	0.09	b.d.l.	0.01	0.03	0.03	0.13	0.19	0.40	0.01	0.07	0.07	0.11	b.d.l.		n.a.	n.a.	n.a.	n.a.	0.00	0.08	0.32	0.37	0.32	0.11	0.23
FeO	0.14	0.20	0.03	0.07	0.53	0.08	0.04	0.03	0.27	0.65	0.38	0.20	0.29	0.18	0.33	0.37		0.25	0.99	0.03	0.19	0.21	0.27	0.51	0.48	0.54	0.67	0.59
MnO	0.02	0.02	0.02	0.04	0.02	0.01	0.01	0.02	0.08	0.08	0.13	0.19	0.12	0.18	0.05	0.11		n.a.	n.a.	n.a.	n.a.	0.02	0.26	0.51	0.16	0.09	0.07	0.23
MgO	b.d.l.	b.d.l.	b.d.l.	0.01	0.02	0.01	b.d.l.	0.01	0.01	0.01	b.d.l.	0.02	0.01	0.01	0.01	n.a.		n.a.	n.a.	n.a.	n.a.	0.01	0.01	n.a.	n.a.	n.a.	n.a.	n.a.
K_2O	0.02	0.04	b.d.l.	0.02	0.02	0.01	0.01	0.01	0.03	0.04	0.01	0.01	0.01	0.02	0.02	b.d.l.		n.a.	n.a.	n.a.	n.a.	b.d.l.	0.02	n.a.	n.a.	n.a.	n.a.	n.a.
Al_2O_3	b.d.l.	0.05	b.d.l.	0.09	0.02	0.04	b.d.l.	b.d.l.	0.18	0.44	0.30	0.003	0.06	0.06	0.12	n.a.		0.06	0.24	b.d.l.	0.01	0.09	0.65	0.60	0.56	0.26	0.62	0.08
UO_2	b.d.l.	b.d.l.	0.03	0.05	0.07	0.07	0.17	0.15	0.09	0.14	0.17	0.10	b.d.l.	0.07	0.04	n.a.		0.26	0.19	0.64	0.34	b.d.l.	b.d.l.	n.a.	n.a.	n.a.	n.a.	n.a.
ThO_2	1.36	0.94	1.52	0.26	0.03	0.07	0.06	0.16	0.07	0.02	b.d.l.	0.10	0.07	0.05	0.04	n.a.		0.12	0.10	1.40	0.17	0.26	0.09	n.a.	n.a.	n.a.	n.a.	n.a.
PbO	b.d.l.	0.06	0.01	0.06	0.07	0.05	0.06	0.06	0.09	0.24	0.27	0.12	0.14	0.09	0.07	n.a.		0.05	0.02	0.02	0.02	0.09	0.06	n.a.	n.a.	n.a.	n.a.	n.a.
HfO_2	2.27	1.24	1.00	1.60	1.32	1.75	1.06	1.01	1.29	1.08	1.25	1.12	1.29	1.12	1.27	1.04		1.15	1.22	0.86	0.92	1.18	1.01	1.58	1.47	1.33	1.50	1.40
SnO_2	0.01	0.03	0.01	0.01	b.d.l.	0.01	0.05	0.04	0.21	0.79	0.78	0.01	0.01	0.02	0.01	n.a.		n.a.	n.a.	n.a.	n.a.	0.01	0.02	n.a.	n.a.	n.a.	n.a.	n.a.
ZnO	0.01	0.01	b.d.l.	b.d.l.	0.03	0.01	b.d.l.	b.d.l.	0.05	0.04	0.07	0.02	0.06	0.03	0.03	n.a.		n.a.	n.a.	n.a.	n.a.	0.05	0.07	n.a.	n.a.	n.a.	n.a.	n.a.
ppm																												
Analyses no	**3**	**5**	**3**	**2**	**6**	**22**	**3**	**4**	**20**	**3**	**2**	**4**	**6**	**7**	**4**	**7**		**11**	**13**	**4**	**15**	**14**	**4**	**5**	**19**	**16**	**24**	**27**
Li	50	17	37	15	n.a.	n.a.	b.d.l.	b.d.l.	b.d.l.	n.a.	n.a.	b.d.l.	b.d.l.	b.d.l.	b.d.l.	n.a.		b.d.l.	41	b.d.l.	n.a.	b.d.l.	b.d.l.	n.a.	n.a.	n.a.	n.a.	n.a.
P	680	3029	3938	1720	n.a.	n.a.	b.d.l.	b.d.l.	b.d.l.	n.a.	n.a.	151	b.d.l.	232	108	n.a.		b.d.l.	32	105	n.a.	b.d.l.	b.d.l.	n.a.	n.a.	n.a.	n.a.	n.a.
Sc	643	732	715	635	n.a.	n.a.	827	748	810	n.a.	n.a.	775	1061	800	1112	n.a.		650	871	880	n.a.	892	975	n.a.	n.a.	n.a.	n.a.	n.a.
Rb	186	8	21	36	n.a.	n.a.	5	7	16	n.a.	n.a.	7	1	4	4	n.a.		12	7	1	n.a.	23	4	n.a.	n.a.	n.a.	n.a.	n.a.
Sr	136	132	173	99	n.a.	n.a.	b.d.l.	b.d.l.	b.d.l.	n.a.	n.a.	248	61	213	306	n.a.		75	19	b.d.l.	n.a.	b.d.l.	b.d.l.	n.a.	n.a.	n.a.	n.a.	n.a.
Y	10189	10093	12043	5452	1788	2299	8160	13295	8643	11400	7500	12815	1850	15037	1911	7245		605	591	5667	2700	563	347	7555	20600	32287	26034	15583
Nb	266	155	156	97	n.a.	n.a.	298	230	590	n.a.	n.a.	1329	125	132	290	n.a.		1540	1130	247	n.a.	2255	788	769	3058	1905	2405	1608
Ta	18	8	7	8	n.a.	n.a.	164	103	165	n.a.	n.a.	298	53	31	54	n.a.		586	439	36	n.a.	174	177	n.a.	n.a.	n.a.	n.a.	n.a.
Cs	5	b.d.l.	1	2	n.a.	n.a.	11	b.d.l.	2	n.a.	n.a.	16	1	2	3	n.a.		b.d.l.	b.d.l.	b.d.l.	n.a.	4	1	n.a.	n.a.	n.a.	n.a.	n.a.
Ba	124	3	12	15	n.a.	n.a.	233	24	430	n.a.	n.a.	92	182	68	838	n.a.		68	44	4	n.a.	132	27	n.a.	n.a.	n.a.	n.a.	n.a.
La	145	1	14	50	n.a.	n.a.	10	15	218	n.a.	n.a.	297	10	42	52	117		310	396	4	n.a.	b.d.l.	1	b.d.l.	597	b.d.l.	1348	b.d.l.
Ce	1248	48	199	244	34	222	15	120	911	3800	4400	1524	34	280	423	419		365	674	1027	200	742	604	512	2605	790	6149	726
Pr	47	b.d.l.	6	22	n.a.	n.a.	2	3	153	n.a.	n.a.	220	4	28	43	59		28	62	26	n.a.	3	4	b.d.l.	705	b.d.l.	820	b.d.l.
Nd	202	4	32	91	n.a.	n.a.	7	14	873	n.a.	n.a.	1326	25	145	259	289		56	193	314	n.a.	57	65	b.d.l.	3814	1093	3257	386
Sm	98	19	39	48	n.a.	n.a.	8	22	330	n.a.	n.a.	632	24	160	117	105		11	33	276	n.a.	118	135	b.d.l.	1510	626	725	302
Eu	4	2	2	2	n.a.	n.a.	b.d.l.	2	19	n.a.	n.a.	36	1	17	6	7		1	4	12	n.a.	8	9	b.d.l.	b.d.l.	b.d.l.	b.d.l.	b.d.l.
Σ LREE	*1745*	*74*	*292*	*457*			*41*	*176*	*2504*			*4035*	*98*	*672*	*899*	*996*		*770*	*1362*	*1659*		*928*	*818*	*512*	*9230*	*2508*	*12298*	*1414*
Gd	292	145	210	121	n.a.	n.a.	75	129	372	n.a.	n.a.	892	75	509	215	176		25	39	617	n.a.	552	655	1214	1712	4205	2584	737
Tb	132	100	139	58	n.a.	n.a.	45	98	84	n.a.	n.a.	211	22	179	41	36		8	8	135	n.a.	12	4	n.a.	n.a.	n.a.	n.a.	n.a.
Dy	1882	1843	2449	973	n.a.	n.a.	695	1674	787	n.a.	n.a.	1670	208	1778	300	387		73	71	997	n.a.	81	39	1132	1677	6206	2648	2352
Ho	666	827	1028	436	n.a.	n.a.	302	777	224	n.a.	n.a.	402	61	489	72	132		21	19	223	n.a.	18	12	n.a.	n.a.	n.a.	n.a.	n.a.
Er	2935	4987	5881	2669	n.a.	n.a.	1547	3599	1008	n.a.	n.a.	1500	247	1911	226	566		82	71	670	n.a.	60	48	1313	1466	5709	1855	2450
Tm	570	1329	1497	714	n.a.	n.a.	304	632	171	n.a.	n.a.	293	50	362	33	153		15	13	97	n.a.	11	10	n.a.	n.a.	n.a.	n.a.	n.a.
Yb	4490	12363	13231	6724	n.a.	n.a.	2500	4311	973	n.a.	n.a.	2721	463	2914	234	1934		121	104	653	n.a.	94	82	3073	3819	13324	983	4610
Lu	568	1707	1796	948	n.a.	n.a.	403	592	99	n.a.	n.a.	435	63	443	29	312		17	15	82	n.a.	13	13	527	725	1890	b.d.l.	615
Σ HREE+Y	*21723*	*33393*	*38274*	*18095*			*13955*	*24979*	*11989*			*20939*	*3039*	*23622*	*3061*	*10940*		*967*	*931*	*9141*		*1404*	*1210*	*14814*	*29999*	*63620*	*34104*	*26346*
Σ REE + Y	*23468*	*33467*	*38566*	*18552*			*13996*	*25155*	*14493*			*24973*	*3136*	*24294*	*3960*	*11936*		*1737*	*2294*	*10800*		*2332*	*2028*	*15327*	*39229*	*66129*	*46402*	*27760*
Total wt %	95.92	97.53	95.41	99.73	100.04	99.19	94.84	97.15	97.89	95.73	95.68	97.84	99.98	97.94	98.42	99.74		97.48	96.89	97.18	99.66	100.11	96.32	97.99	95.99	94.59	95.61	95.17

CaO (0.15 %), TiO_2 (0.06 %), ZrO_2 (63.4 %) and SiO_2 (31.7 %; Tab 4.3). Generally, zircon in pegmatites from Amis contain more ThO_2, Y and Ce and less SiO_2 and ZrO_2 than in granites (Fig 4.9).

At Evisa, type-P zircon in pegmatites and granites has high Ba contents (respectively 233 and 479 ppm), while type-SG zircon has high Y contents (respectively 13295 and 17324 ppm). In addition, light type-SG zircon in granite contains more CaO (0.25 %), FeO (0.65 %), K_2O (0.04 %), Al_2O_3 (0.44 %), and Y (11400 ppm) than dark type-SG zircon, which contains more Na_2O (0.4 %), MnO (0.13 %) and HfO_2 (1.25 %; Tab 4.3). Zircon in pegmatites contain more Cs and less TiO_2, FeO, Al_2O_3, SnO_2, Rb, Nb, Ba and Y than in granites (Fig 4.10). Zircon in granite is especially rich in Na_2O (0.13-0.28 %).

At Khan Bogd, only type-P zircon is present in pegmatites. Zircon associated with amphibole have lower Na_2O and Al_2O_3, and higher Nb (1329 ppm), Ta (298 ppm) and Cs (16 ppm) content than other zircons in this complex. Type-P euhedral zircon from sample KB04A, and type-P zircon with elpidite have similar CaO and Y contents (respectively about 0.1 % and 1900 ppm), which are lower than in other type-P zircon of Khan Bogd (respectively 0.2 % and 13000 ppm). In addition, euhedral zircon from sample KB04A also has a low Sr content (61 ppm), and zircon associated with elpidite has less MnO (0.05 %) and more Ba (838 ppm) than other type-P zircons from the same complex (Tab 4.3). Zircon in granite seems to contain much more CaO than zircon in pegmatites (Fig 4.11).

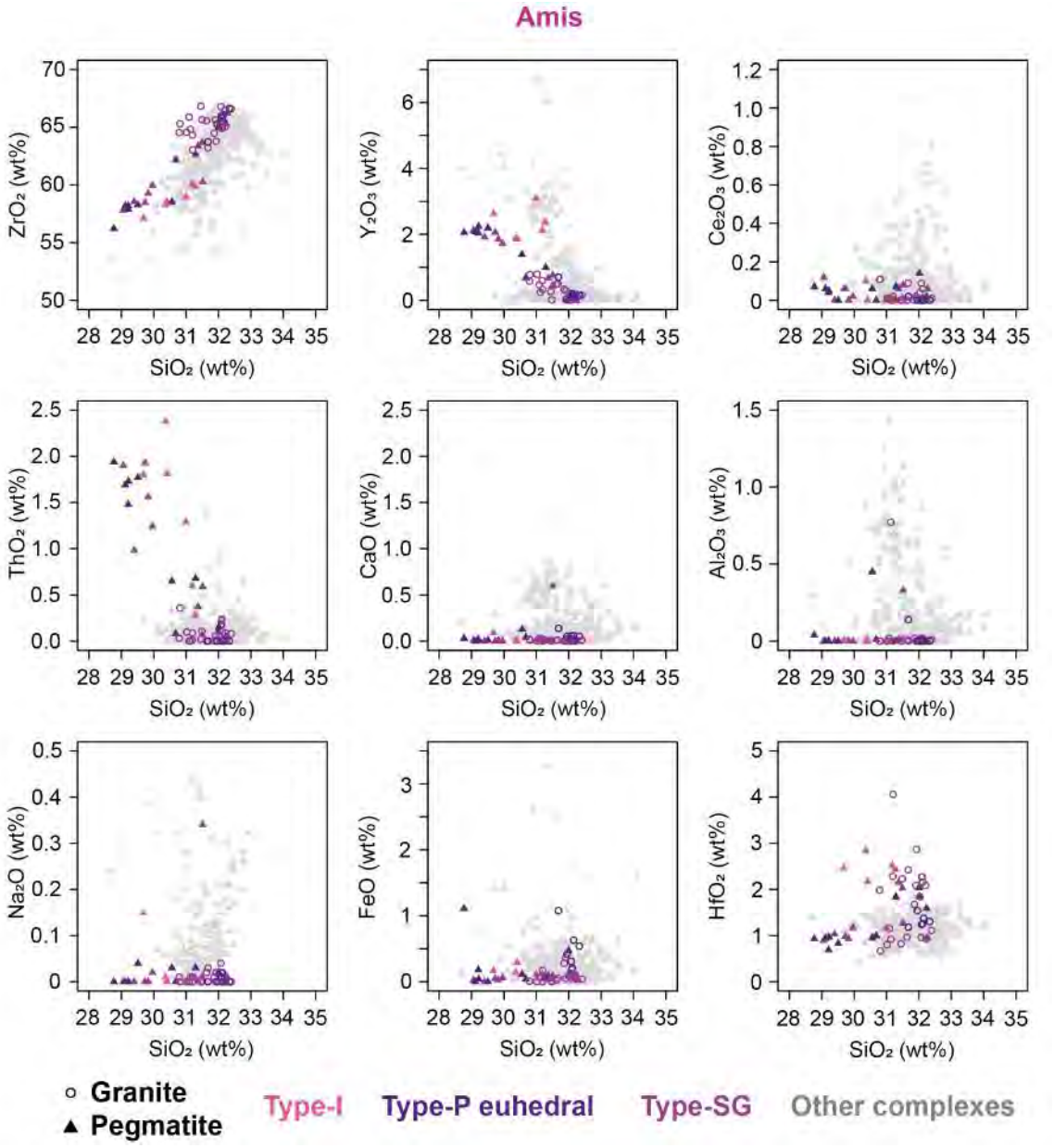

Figure 4.9 Binary diagrams highlighting the main major and trace composition of zircons from different rocks and types as a function of SiO_2 at Amis

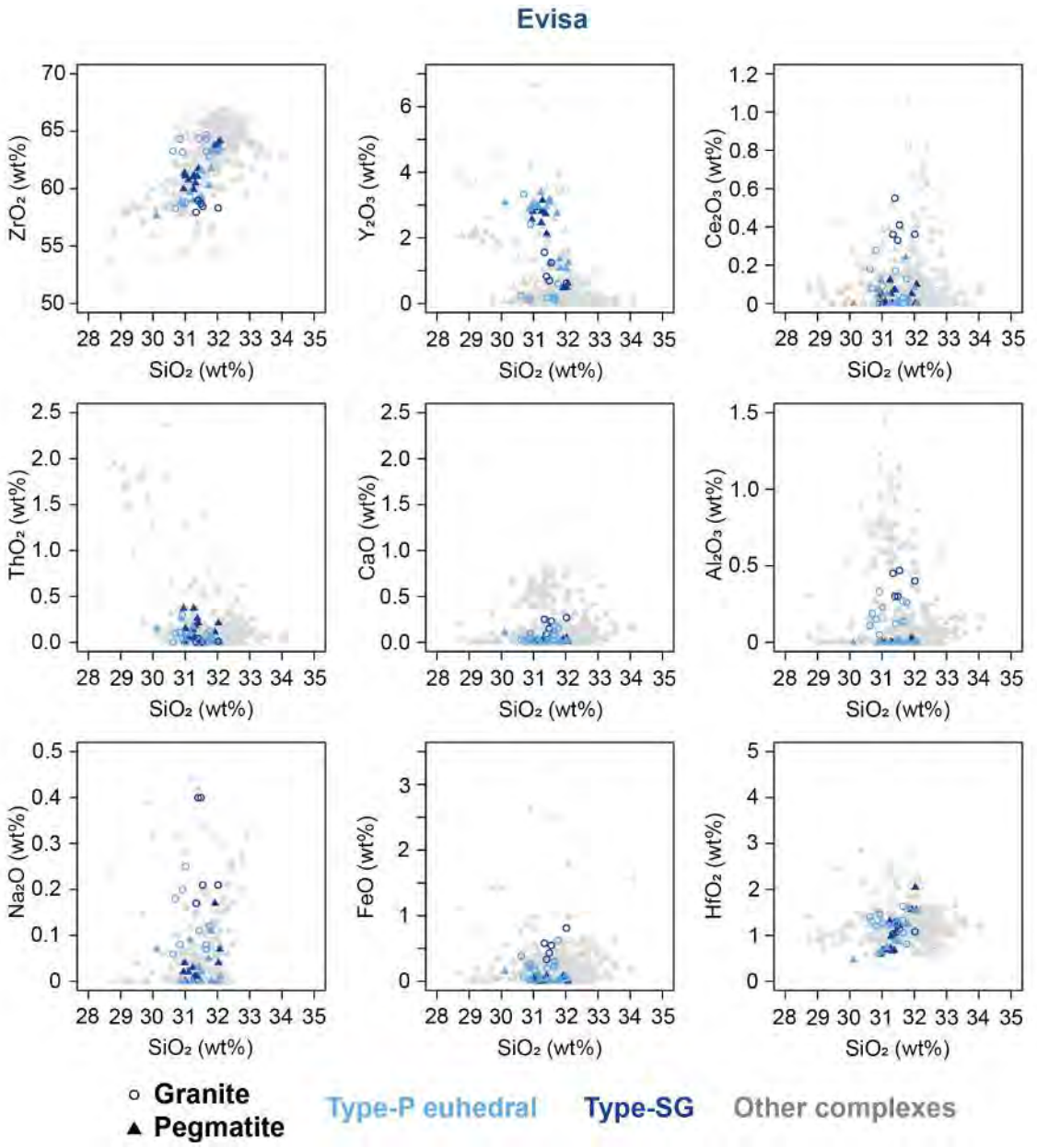

Figure 4.10 Binary diagrams highlighting the main major and trace composition of zircons from different rocks and types as a function of SiO_2 at Evisa

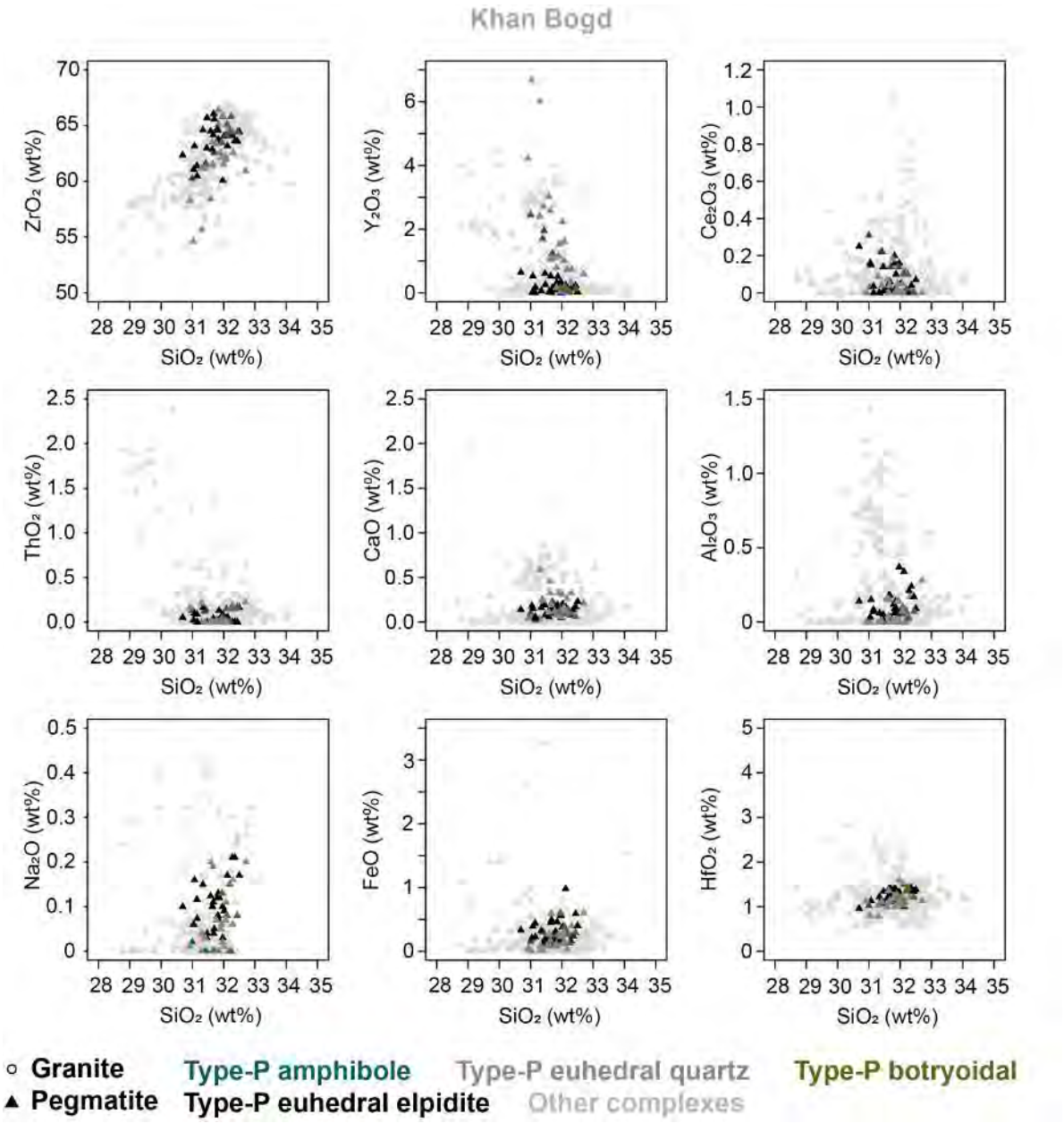

Figure 4.11 Binary diagrams highlighting the main major and trace composition of zircons from different rocks and types as a function of SiO_2 at Khan Bogd

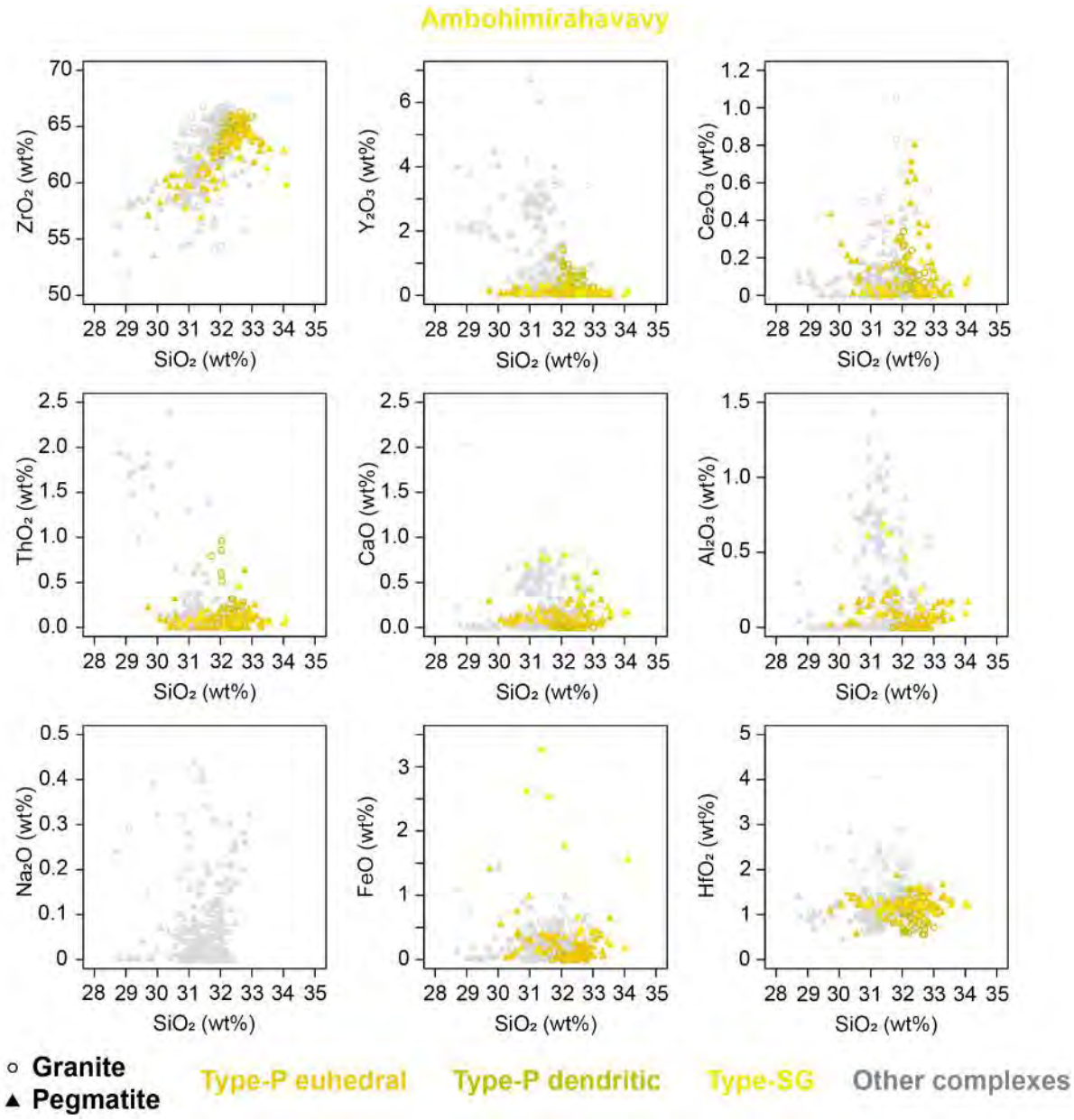

Figure 4.12 Binary diagrams highlighting the main major and trace composition of zircons from different rocks and types as a function of SiO_2 at Ambohimirahavavy

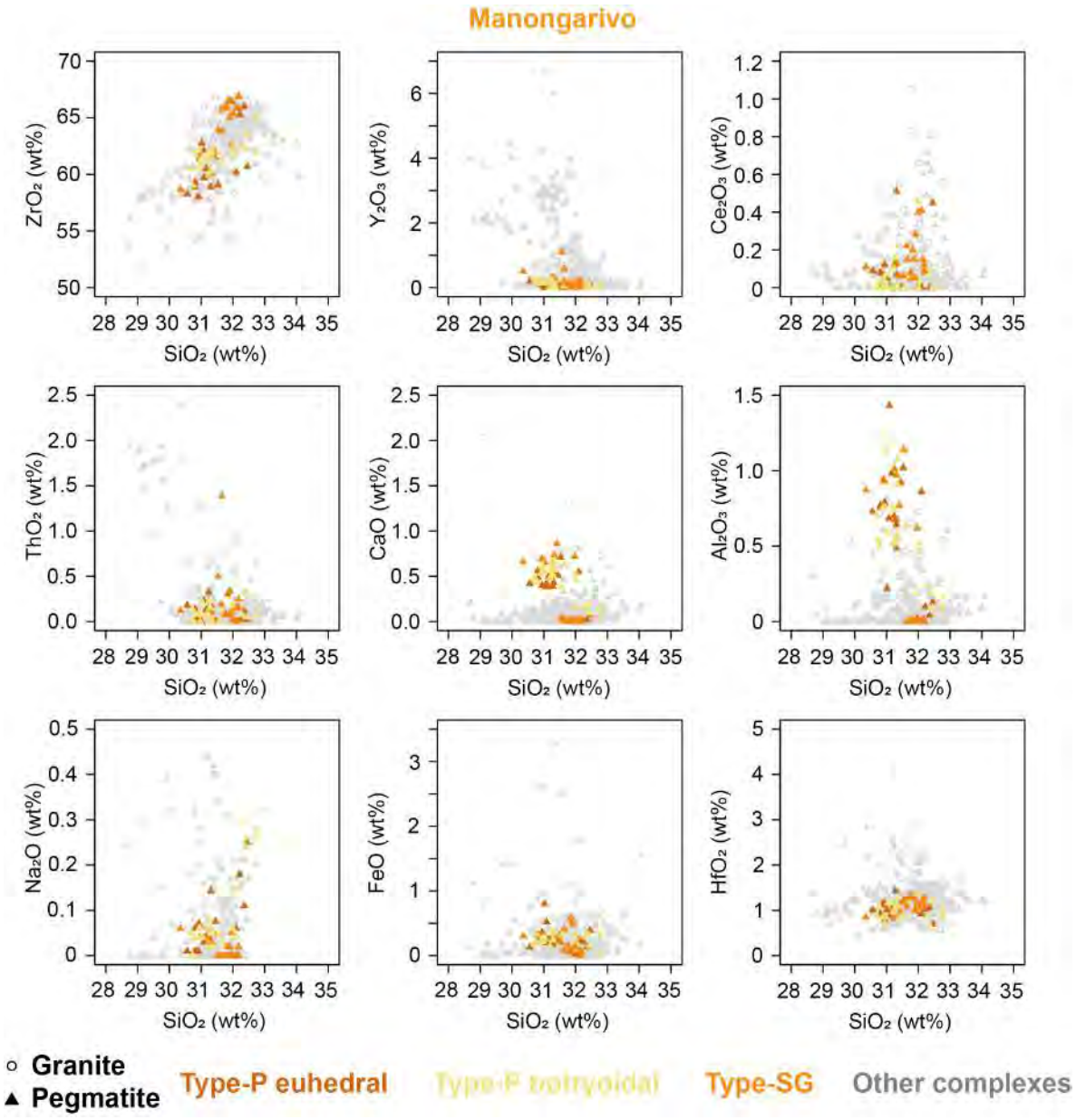

Figure 4.13 Binary diagrams highlighting the main major and trace composition of zircons from different rocks and types as a function of SiO_2 at Manongarivo

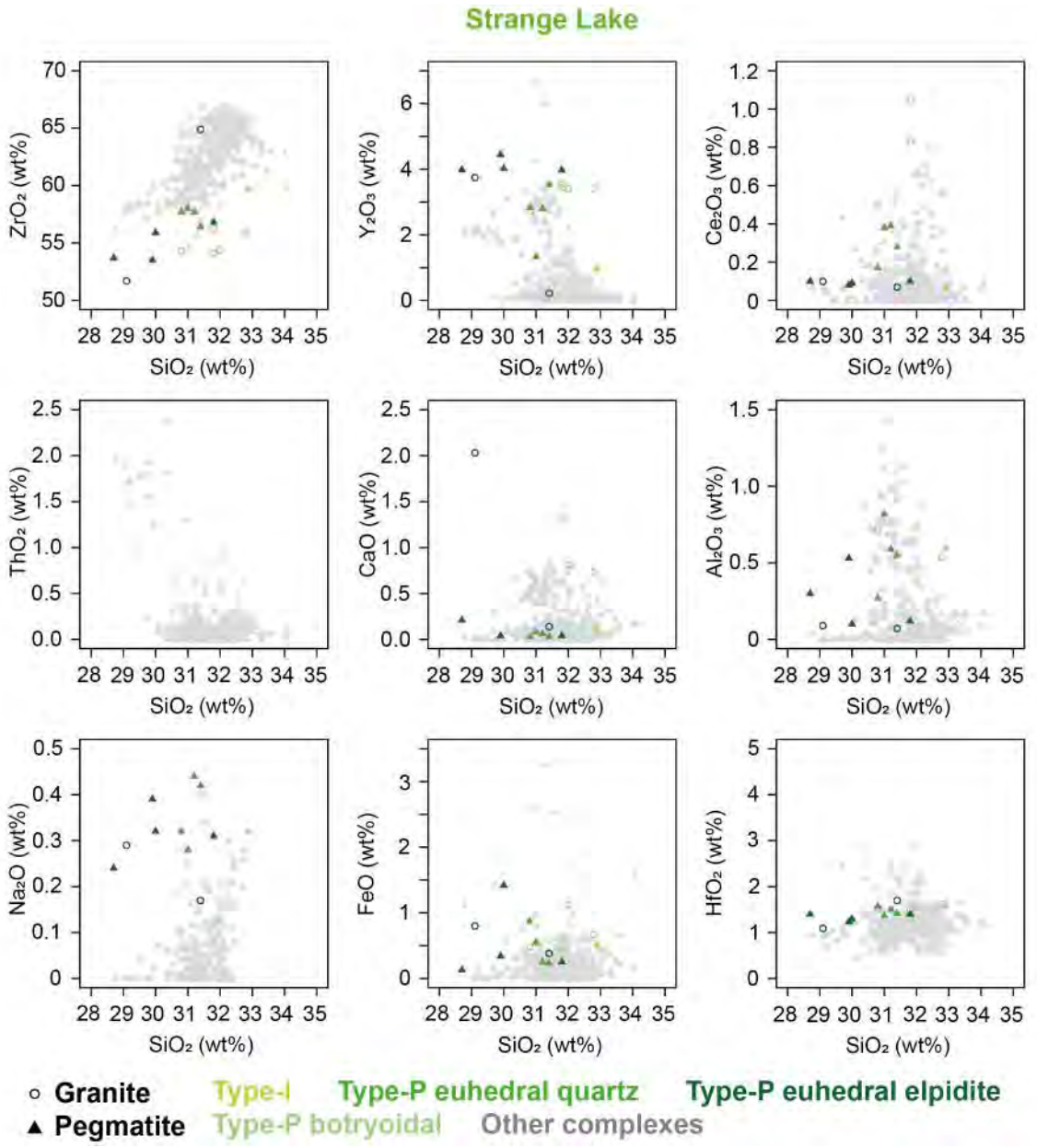

Figure 4.14 Binary diagrams highlighting the main major and trace composition of zircons from different rocks and types as a function of SiO_2 at Strange Lake

In pegmatites from Ambohimirahavavy, botryoidal zircon was not measured. The comparison between type-P euhedral and dendritic zircon shows that dendritic zircon contain more CaO and Al_2O_3 than euhedral one (respectively 0.32 and 0.24 vs 0.13 and 0.06 %; Tab 4.3). Light type-SG zircon in granites are richer in UO_2 (0.64 %) and ThO_2 (1.4 %) and poorer in ZrO_2 (61.5 %) and FeO (0.03 %) than dark type-SG. In addition, zircon in pegmatites contain more FeO, CaO, Al_2O_3, Li, Rb, Sr, Nb, Ta, Ba, and less ZrO_2, Y and ThO_2 than in granites (Fig 4.12).

At Manongarivo, botryoidal type-P zircon contains more TiO_2 (0.23 %), CaO (0.46 %), MnO (0.26 %) and Al_2O_3 (0.65 %) than euhedral type-P zircon. It also contains less ZrO_2 (61.3 %), ThO_2 (0.09 %), Rb (4 ppm), Nb (788 ppm), and Ba (27 ppm; Fig 4.13). No comparison is possible between zircons in pegmatites and granites (Tab 4.3).

At Strange Lake, type-I interstitial zircon is poorer in Y (7555 ppm) and Nb (769 ppm) than other zircons in pegmatites. Type-II euhedral zircon and type-P zircon associated with elpidite have common chemistries in pegmatite. In granite, zircon associated with elpidite is richer in MnO (0.23 %) and poorer in Al_2O_3 (0.08 %), Y (15583 ppm) and Nb (1608 ppm) than type-P botryoidal zircon (Tab 4.3). Globally, zircon in granites is richer in CaO than in pegmatites (respectively 1.0 vs 0.1 %; Fig 4.14).

4.3.2.3 Comparison between complexes

Zircon from the different localities also present global chemistry differences. Zircon from Amis contains more P and Th and less Si, Ca, and Al than in the other complexes. At Evisa, zircon is globally poorer in Ca and richer in Y than the others. Zircon from Khan Bogd shows a wide range for Y concentrations. Zircon from the Malagasy complexes, on the other hand, is quite poor in Y. In addition, zircon from Manongarivo is globally rich in Ca and Al compared to other complexes. At Strange Lake, zircon is poorer in Zr and richer in Hf. Granitic zircon from Strange Lake also shows a high concentration in Ca, up to 2.03 % CaO.

4.3.3 REE in zircon

As mentioned above, zircon has the ability to incorporate significant amounts of REE in its crystallographic structure. In this study, some complexes have zircon with steep slopes towards HREE only (e.g. Amis), some have mostly flat spiderdiagrams (e.g. Strange Lake), and some have both (e.g. Evisa; Fig 4.15). The next paragraphs are dedicated to describe zircon REE compositions of each complex in details, with the exception of inner zonations, which were not investigated.

At Amis, the classic HREE enrichment of zircon is observed in all three zircon types (Fig 4.15). Data are only available for pegmatites, in which the steeper spider diagrams slopes are observed for type-P zircon. Indeed, zircon in pseudomorphs after an unknown primary complex zirconosilicate is poorer in LREE (74 ppm) and

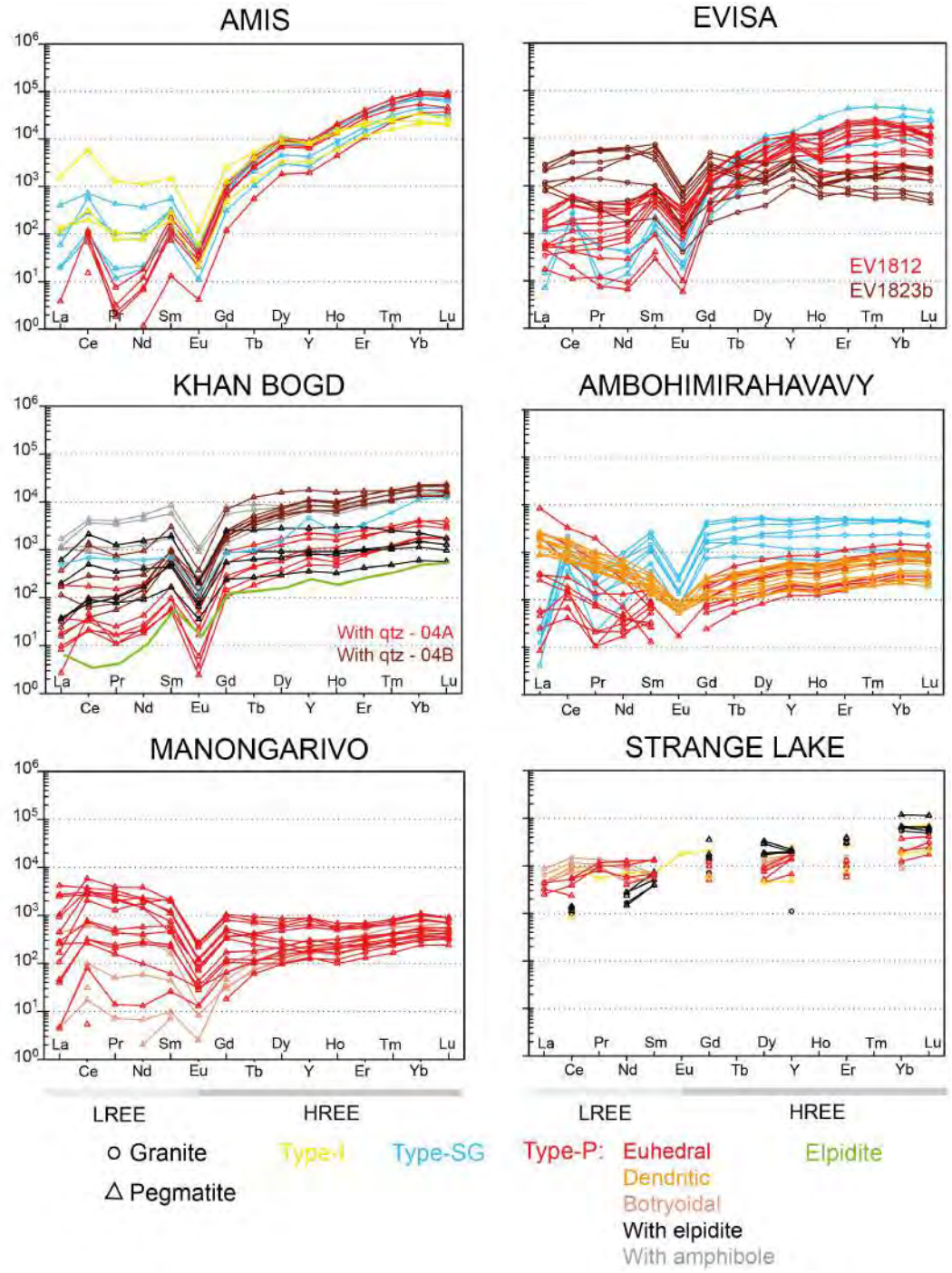

Figure 4.15 Spider diagrams for zircon of the three types in the six studied complexes. Elpidite spectrum is shown at Khan Bogd for comparison. Data at Strange Lake are from Gysi et al. (2016)

richer in HREE (33393 ppm) than other zircons from the Amis complex. Type-I zircon has higher LREE (1745 ppm) and lower HREE amounts (21723 ppm) than the others, and type-SG zircon has intermediate values (358 ppm LREE, 30201 ppm

HREE) Light zones in type-SG zircon are poorer in LREE and richer in HREE than dark zones (Tab 4.3). The maximum concentration range between the three types is about 3 orders of magnitude for LREE, whereas it is less than 1 for HREE. In addition, most zircons from Amis have more or less pronounced Ce positive and Eu negative anomalies (Fig 4.15). These anomalies were also found in amphiboles and aegirine from the same complex (Section 4.1).

At Evisa, type-SG and type-P zircon of pegmatites also show steep, HREE-rich spiderdiagrams. Type-SG zircon in pegmatites contains more LREE (176 ppm) and HREE (24979 ppm) than type-P (41 ppm LREE, 13955 ppm HREE). Light zones in type-SG zircon are poorer in Ce and richer in Y than dark zones (Tab 4.3). Type-P zircon from two subsolvus granites was analyzed. Zircon from sample EV1812 is associated with quartz only, whereas zircon from sample EV1823B is associated with quartz and fluorite. Interestingly, type-P zircon associated with quartz only has a pattern shape similar to that of pegmatites, with an enrichment in HREE (457 ppm LREE, 19097 ppm HREE), whereas type-P zircon from sample EV1823B has a much flatter spider diagram (4553 ppm LREE, 5627 ppm HREE). Europium anomaly is present in all zircons, and Ce anomaly is mostly seen in type-SG zircon. In addition, a positive anomaly in Y is visible in zircons from granites. Zircon in pegmatites is richer in HREE than in granites (Fig 4.15).

At Khan Bogd, type-P zircon is divided in 4 subtypes depending on the minerals it is associated with: with amphibole, with elpidite and quartz in sample KB04A, with quartz-only in sample KB04A, and with quartz-only in sample KB04B. Samples KB04A and B are parts of the same pegmatite, but were collected in different layers. In sample KB04A, not all elpidite was pseudomorphed, whereas in KB04B, all elpidite has been replaced. Type-P zircon associated with amphibole has a flat spider diagram with high concentrations in LREE (4035 ppm) and HREE (8159 ppm). Spider diagrams of zircon associated with elpidite have a similar flat shape but with lower REE contents (899 ppm LREE, 3067 ppm HREE). Spider diagrams of zircon associated with quartz-only have slightly steeper slopes with intermediate REE concentrations. However, zircon associated with quartz-only have lower REE contents in sample KB04A (98 ppm LREE, 3039 ppm HREE), i.e. where some elpidite remains, than in sample KB04B (672 ppm LREE, 23622 ppm HREE), where all elpidite was replaced. It is interesting to note that elpidite of sample KB04A has a spider diagram shape similar to that of zircon associated with quartz-only in the same sample, with lower REE concentrations (29 ppm LREE,

255 ppm HREE on average). REE concentrations in type-SG zircon from the granite reported by Kynicky et al. (2011) are intermediate between those in pegmatites (996 ppm LREE, 10940 ppm HREE; Tab 4.3), and the shape of the spider diagram is similar to that of elpidite-associated type-P. A negative Eu-anomaly is present in all zircons. A positive Ce anomaly is showed by all type-P zircons but the ones associated with amphibole, and a Y positive anomaly is also present in type-SG zircon (Fig 4.15).

At Ambohimirahavavy, type-SG zircon has relatively low LREE (1214 ppm) and high HREE contents (7236 ppm). Type-P zircon has flatter spectra. Euhedral type-P zircon has LREE contents that highly vary (48 to 4527 ppm) and low HREE contents (967 ppm). Dendritic type-P zircon has a very uncommon spectrum V-shape, with an enrichment in LREE (1362 ppm) with respect to HREE (931 ppm; Tab 4.3). Europium negative anomaly is present in all zircons, and type-SG and some type-P euhedral zircons also present a positive Ce anomaly (Fig 4.15).

At Manongarivo, euhedral type-P zircon has the same pattern than at Ambohimirahavavy: a large range of LREE concentrations (3 to 6317 ppm) and a HREE content of 927 ppm on average. Botryoidal type-P zircon has much lower REE contents than euhedral one (227 ppm LREE, 566 ppm HREE; Tab 4.3; Fig 4.15).

At Strange Lake, REE concentrations are very similar between all zircon types, no matter their granitic or pegmatitic host (Fig 4.15). However, type-I zircon in pegmatites has lower REE concentrations (512 ppm LREE, 14814 ppm HREE). Unlike zircon from Khan Bogd, pegmatitic type-P zircon associated with elpidite contain less LREE and more HREE than that associated with quartz, fluorite and/or hematite (respectively 2508 vs 9230 ppm LREE and 63620 vs 29999 ppm HREE). This flatter spider diagram of zircon associated with fluorite was however also observed at Evisa. In granites, botryoidal zircon has higher REE contents than that associated with elpidite (12298 vs 1414 ppm LREE, 34104 vs 26346 ppm HREE; Tab 4.3).

In summary, comparing the REE contents of zircon from the different complexes, it is obvious that type-SG and type-I zircon strongly fractionate the REE by incorporating preferentially HREE. Type-P zircon, except at Amis, has flatter REE spectra. Malagasy zircon has very similar spider diagrams, with a low HREE content leading in some cases to a V-shape spectrum. Zircon from Strange Lake is especially rich in REE, and zircon from Amis has high HREE contents (Fig 4.15).

4.3.4 Discussion on the origin of zircon types highlighting REE enrichment and fractionation processes

Three main types of zircon have been identified in the six complexes of this study. Type-SG (single grain) systematically occurs as euhedral, isolated crystals associated with alkali feldspar and quartz, and is richer in HREE than LREE. Type-P (in pseudomorphs) grew after a primary zirconosilicate, either elpidite of EGM. It can occur as euhedral, dendritic or botryoidal crystals. It is globally richer in Fe, Nb, Ta and Ba than other types and has overall flatter REE spider diagrams than type-SG. It is divided in subtypes according to its shape and minerals it is associated with. Type-I (interstitial) occurs as interstitial anhedral grains filling the space between feldspars and quartz. It is poorer in Zr and richer in trace elements than the other types, and was found only at Amis and Evisa.

4.3.4.1 Type-SG zircon

In all complexes, type-SG zircon occurs systematically as euhedral, isolated crystals associated with magmatic alkali feldspar and quartz. These two primary minerals have also been observed to form inclusions in the core of these zircons at Amis and Evisa, suggesting coeval growth. These petrographic observations point to a magmatic origin for type-SG zircon. The composition of zircon can also be indicative of its origin. Hoskin (2005) and Yang et al. (2014) mentioned that magmatic zircon is systematically oscillatory zoned. However, type-SG zircon in this study is not systematically and not exclusively oscillatory zoned. In addition, other studies (e.g. Estrade, 2014; Gysi et al., 2016; Kynicky et al., 2011) mention magmatic zircon in alkaline rocks with no oscillatory zonation. Hence, this parameter is not necessarily diagnostic of the origin of a zircon crystal, at least in alkaline rocks. Type-SG zircon is globally richer in Zr, Th and P than other types analyzed in this study. Incorporation of trace elements in zircon depends mostly on their valence and atomic size (Finch and Hanchar, 2003). Based on these observations, Estrade (2014) proposed the following coupled substitution:

$$^{A}REE +^{A} Th +^{A} U +^{T} P \leftrightarrow^{T} Si +^{A} Zr +^{A} Hf \tag{4.2}$$

with T and A the two crystallographic sites of zircon. This equation explains the presence of Th and P in higher quantities in type-SG zircon. In this case, substituting

elements are incorporated inside the two crystallographic sites of zircon.

The shape of REE spiderdiagrams is also often used as a tracer for zircon origin (e.g. Gysi et al., 2016; Hoskin, 2005; Pettke et al., 2005). Indeed, as mention in the previous section, zircon incorporates preferentially HREE over LREE. Hence, a purely magmatic zircon generally has a steep REE-spectrum slope with a high enrichment in HREE. This steep slope was observed for all type-SG zircons in this study (Fig 4.15). One more indication of the magmatic origin of a zircon is the positive Ce and negative Eu anomalies. These anomalies are commonly explained by a valence different from the usual 3+. Indeed, because of similar valences, Ce^{4+} substitutes more easily than other REE for Zr^{4+} in zircon. Ce^{4+} being mostly present in oxidized magma, the positive Ce anomaly in zircon is commonly attributed to a magmatic environment. However, Hoskin (2005) also observed small Ce anomalies in hydrothermal zircon. On the other hand, since Eu^{2+} does not easily enter zircon structure, a negative Eu anomaly in zircon is an indication of a reduced magmatic environment (Trail et al., 2012). However, in this study, a positive Ce anomaly is indeed observed in all type-SG zircon, as well as in some zircons of the other types, but a negative Eu anomaly is also present in all zircons, from all types and all complexes. It is therefore necessary that at least one of these anomalies is caused by another process. It is known that at magmatic stage, high concentrations of Eu are incorporated in plagioclase, and this Eu-anomaly is also visible in whole-rock contents (Fig 2.14). Hence, the negative Eu anomaly in zircon results from early fractionation of plagioclase. At Khan Bogd, an additional positive Y anomaly is visible in type-SG zircon. In addition, this anomaly was also observed for some amphibole and aegirine crystals (see section 4.1). To my knowledge, it is the first time that such an anomaly is reported in zircon. Yttrium being commonly associated with HREE, this anomaly could be the sign for a high REE fractionation. The presence of this anomaly in several minerals indicates this is a property of the magma itself.

Type-SG zircon is also commonly porous in its core (e.g. Fig 4.7e), which is poorer in trace elements and contains mineral inclusions such as thorite, monazite-(Ce) or Nb-Y phase (e.g. Fig 4.3e). Indeed, at Amis the core is richer in Al, K, Mn, Fe, Na, Ca, Ti, Hf and Pb; at Evisa the core is reported to be less radiogenic (Poitrasson et al., 1998) and contains more Na, Mn and Hf; at Khan Bogd it is poorer in Y, Ca (Kynicky et al., 2011); and at Ambohimirahavavy, the core is poorer in Th, Y (Estrade, 2014), U and richer in Fe than the rims. These peculiar observations

can be explained by a process of dissolution-reprecipitation under hydrothermal conditions. Indeed, the solubility of zircon in hydrothermal fluids is proportional to its concentration in trace elements such as Y, Th and U as they weaken the crystallographic structure (Geisler et al., 2007). Zircon dissolution hence frees significant amounts of these elements. While zircon reprecipitates without these trace elements, they concentrate and reprecipitate as small inclusions. Since the molar volume of trace element-rich zircon is higher than trace-free zircon, porosity is created during dissolution-reprecipitation processes and elements such as Ca, Al or Fe can be incorporated (Geisler et al., 2007; Soman et al., 2010). The preferential core alteration is explained by the fact that trace elements content decreases as magmatic zircon crystallizes and competes with other minerals accepting these elements (Pettke et al., 2005); magmatic zircon rims are then poorer in trace elements and less subject to hydrothermal dissolution-reprecipitation.Hence, type-SG zircon grew at the magmatic stage, and its core was then hydrothermally altered, leaving the rims as magmatic relicts.

Type-SG zircon also presents composition differences between the six complexes, which can be related to two parameters. The first one is the initial composition of the parental melt, which depends on the nature of its source as well as on the rate of partial melting. The second one is the competition of zircon with other minerals. Indeed, if another mineral with a high affinity for a given element is growing at the same time or before type-SG zircon, this element will not be incorporated in zircon. On the other hand, if an element compatible with zircon is not requisitioned by another mineral, its concentration in type-SG zircon will be higher.

4.3.4.2 Type-P zircon

Type-P zircon is found in pseudomorphs, which suggests it is of hydrothermal origin. It replaces elpidite, EGM, and, at Amis, an unknown zirconosilicate. Its petrographic characteristics are highly variable from one complex to the other, but also inside a same complex. Euhedral shapes are the most common in this category. Dendritic zircon is found at Ambohimirahavavy and as overgrowths at Evisa. This geometry is due to the same fractal phenomenon that forms snowflakes or lightning, called diffusion-limited aggregation (Chopard et al., 1991). In this process, the concentration of atoms is low, hence the growth is limited only by diffusion in the environment. However, in order to explain the different sizes and orientations of zircon dendrites in pseudomorphs, Badin (1996) showed that the

growth must have occurred in an aqueous and siliceous environment. The dendritic shape allows the maximization of the surface area at the crystal-environment interface, hence crystallization kinetic and temperature also play a role in the crystallization of this habit (French, 2010). The fact that dendritic zircon occurs as overgrowths on euhedral zircon at Evisa (Fig 4.4c) and can be in the core of pseudomorphs with euhedral zircon at Ambohimirahavavy (Fig 4.6b) suggests that dendritic zircon postdates euhedral zircon. At Ambohimirahavavy, Estrade (2014) described botryoidal zircon as overgrowths on euhedral zircon. This suggests they also postdate this kind of zircon. The differences in composition between euhedral, dendritic and botryoidal zircon described for each complex hence likely reflects specific evolution of hydrothermal fluids reflected by their composition.

Independently of their habitus, type-P zircon contains more Fe, Nb, Ta and Ba than any other zircon type. Unlike type-SG zircon, these elements are not incorporated in crystallographic sites A or T, but in interstitial sites (Finch and Hanchar, 2003), which causes bigger lattice size of hydrothermal zircon compared with magmatic one (Zeng et al., 2017).

Except at Amis, type-P zircon has flatter REE spiderdiagrams than type-SG one, and is relatively enriched in LREE. This feature is unusual and probably directly related to hydrothermal fluid composition (Gysi et al., 2016). The absence of such flat shape at Amis can be explained by the fact that at hydrothermal conditions, zircon undergoes retrograde solubility, meaning its solubility in an aqueous environment increases while temperature decreases (Gysi et al., 2016). Since LREE are more soluble than HREE at high temperatures (up to 300 °C) and that the opposite is true at low temperatures (Migdisov et al., 2009), hydrothermal zircon that grew at high temperatures incorporates important amounts of HREE. Hence, in this case, hydrothermal zircon can have REE patterns similar to those of magmatic zircon. This also indicates that type-P zircon from Amis likely grew at high temperatures.

At Khan Bogd, 4 subtypes of type-P zircon were found. Zircon associated with amphibole is the richest in REE. Considering that amphiboles contain significant quantities of REE, it is likely that high concentration in zircon is a direct legacy. Zircon associated with elpidite have flat spider diagrams with lower REE contents. As previously mentioned, zircon associated with quartz only have steeper spider diagrams. However, in the sample KB04A where elpidite remains, this zircon contains less REE, and Ca than in the sample KB04B where elpidite was totally

pseudomorphed. This indicates that the Ca and REE content of zircon is directly linked to that of elpidite, at the sample scale. In addition, this process is only local as it does not impact the whole pegmatite. At Ambohimirahavavy, Estrade (2014) also noticed that type-P botryoidal zircon has a REE spectrum similar to that of EGM and suggested this could be the result of the primary, replaced mineral legacy. At Strange Lake however, zircon associated with elpidite does not contain less HREE, indicating a different mechanism, probably in relation with the extremely high REE concentrations, must occur in this complex.

At Evisa, two different trends are visible in REE spectra of type-P zircon. Zircon from sample EV1812, in pseudomorphs with quartz, is much richer in HREE than LREE. On the other hand, zircon from sample EV1823B, in pseudomorphs with quartz and fluorite, have flatter REE spectra. Gysi and Williams-Jones (2016) showed than in addition to a low temperature, high amounts of fluorine also enhance zircon dissolution. This is because Zr hydroxyfluoride complexes are likely to form if enough F is available. The presence of fluorite in pseudomorphs shows that a significant amount of F was available in the environment, limiting zircon crystallization until most F was taken up by fluorite precipitation. In addition, fluorite in granitic rocks can incorporate REE (mostly LREE; Schwinn and Markl, 2005), resulting in less REE available for zircon. Hence, type-P zircon in sample EV1823B likely crystallized later, and hence at a lower temperature, than zircon in sample EV1812. Light REE being more compatible at low temperatures, they entered zircon structure more easily, while most HREE were already incorporated in other minerals such as britholite-(Y), yttrialite-(Y), aeschynite-(Y) or xenotime-(Y). The presence of F in hydrothermal fluids was also reported at Khan Bogd and Strange Lake, probably contributing to the flat shape of type-P zircon spectra by consuming REE in fluorite.

Hence, the composition of type-P zircon is directly influenced by the primary mineral it replaces as it can incorporate the same trace elements and presents a similar spider diagram shape. Its trace elements content also depends on the composition of the hydrothermal fluid it grew from, as ligands in this fluid can enhance or decrease the solubility of trace elements such as the REE.

4.3.4.3 Type-I zircon

Type-I zircon was only found at Amis and Strange Lake in this study. It occurs as interstitial between quartz, feldspars and amphiboles, indicating that they grew after them. They are richer in Mn, Al, Rb, Ba, Th, and Hf and poorer in Zr than other zircon types. The presence of significant amounts of Mn and Al, incorporated in interstitial sites, as well as the flatter spiderdiagram at Amis indicate they are also hydrothermal. They probably grew with the last hydrothermal flows at the late-hydrothermal stage.

4.3.5 What zircon tells us about REE behavior at the magmatic-hydrothermal transition

From magmatic (type-SG) to hydrothermal in pseudomorphs (type-P) zircon, the HREE concentration decreases and the LREE concentration increases in all complexes. Late-hydrothermal interstitial zircon (type-I) at Amis presents even higher LREE and lower HREE concentrations, and type-I zircon from Strange Lake also incorporated less HREE.

The composition of type-SG zircon depends on magmatic processes and on competition with other minerals. Combining the study of these minerals with that of trace elements in type-SG zircon can give information on the behavior of REE at the magmatic stage. The composition of type-P zircon is mostly inherited from the composition of the primary replaced mineral; hence it is not a good indicator of the composition of hydrothermal fluids. However, the shape of the REE spider diagram of type-P zircon indicates the presence, or absence, of ligands such as F in the hydrothermal fluid. The REE composition of type-I zircon seems to be related only to the composition of the late-hydrothermal stage. At Amis, its higher LREE and lower HREE concentration than in type-SG is therefore likely a good indicator that from the magmatic to the late-hydrothermal stage, there is a gain of LREE and a loss of HREE in the environment from which zircon precipitated. However, as type-I zircon was only seen at Amis and Strange Lake, and because this trend is only visible at Amis, it is likely a local information that cannot be applied to all complexes.

4.4 Estimation of the contribution of hydrothermal fluids to the REE budget of alkaline complexes

4.4.1 Mass-balance calculation on pseudomorphs

In complexes where the primary zirconosilicate could be identified and its REE content analyzed, it is possible to perform a calculation to roughly estimate whether the REE were mobilized and to what extent. In this calculation, the amount of LREE, HREE and Y in a primary zirconosilicate is compared with the amount of these elements in the minerals forming the pseudomorphs replacing it. The proportion of the various minerals in pseudomorphs is estimated visually from PPL and SEM images. This work could only be performed at Khan Bogd and Strange Lake, because the REE content of the primary zirconosilicate is unknown in the other complexes. In addition, since pseudomorphs after EGM present a much more diverse mineralogy than those after elpidite, not all of them could be analyzed for traces and therefore the calculation for the Ambohimirahavavy complex cannot be accurate.

The results are presented in Table 4.4. At Khan Bogd, primary elpidite is replaced by an assemblage of zircon plus quartz. Zircon is the only phase containing REE, hence it is the only one taken into account. The results show that there are much more REE, and especially HREE and Y, in pseudomorphs than in magmatic elpidite. This implies that there is a large input of REE by hydrothermal fluids. At Strange Lake, primary elpidite is replaced by gittinsite, quartz, hematite and occasional fluorite and zircon. Gittinsite being the major carrier of REE, it is the only one taken into account. Since REE values measured in this work differ significantly from those found by Gysi et al. (2016), mass-balance calculation was performed with the two dataset. Anyway, calculation with both datasets show that there are much more REE, and especially LREE, in pseudomorphs than in magmatic elpidite. In addition, Salvi and Williams-Jones (1996) performed mass-balance calculation at Strange Lake by comparing fresh and altered subsolvus granite. They found that the high-temperature fluid did not mobilize the REE, but that the Ca-F-rich, low-temperature fluid significantly enriched the rock in HREE. Once again, it implies that hydrothermal fluids contributed a lot to the final REE budget of the

rock. However, the enrichment is calculated as a percentage relatively to the initial REE content of the zirconosilicate. Hence, as elpidite from Strange Lake is already rich in HREE, the relative enrichment by fluids is artificially lower than for LREE. These calculations therefore show that hydrothermal fluids highly contribute to the REE budget of the pseudomorph, but do not indicate the extent to which fluids contributed to fractionating lights from heavy REE.

Table 4.4 Mass-balance calculations between REE in magmatic primary zirconosilicate and REE in minerals in pseudomorphs after this zirconosilicate. The bold numbers represent the percentage of REE brought by hydrothermal fluids; a negative number means there is more REE in the magmatic zirconosilicate than in the hydrothermal pseudomorph

Complex	Khan Bogd			Strange Lake					
Mineral location	Primary zirconosilicate	Pseudomorph	% enrichment from primary mineral to pseudomorph	Primary zirconosilicate	Pseudomorph			% enrichment from primary mineral to pseudomorph	
Mineral	Elpidite	Zircon		Elpidite	Gittinsite	Gittinsite	Zircon		
Source of analyses	*This work*	*This work*		*Vasyukova et al. 2016*	*Gysi et al. 2016*	*This work*	*Gysi et al. 2016*	*Gysi et al. 2016*	*This work*
% in the pseudom	100	40		100	60	60	2		
LREE	18.5	671.9		3.9	2366	22220	512		
HREE	56.9	8601.6		1492.7	2033	6053	14814		
Y	14.0	15037.3		292	1600	24409	7555		
For 100%									
LREE	18.5	268.8	**1353**	3.9	1419.6	13332.0	10.2	**36563**	**342009**
HREE	56.9	3440.6	**5947**	1492.7	1219.8	3631.8	296.3	**2**	**163**
Y	14.0	6014.9	**42864**	292.0	960.0	14645.4	151.1	**281**	**4967**

4.4.2 Estimation of the proportion of REE in hydrothermal minerals

4.4.2.1 Methodology

The detailed study of REE-bearing minerals in Chapters 3 and 4 allows to estimate the fraction of REE hydrothermally concentrated in the six complexes by mass-balance calculation. To do so, the main steps are to identify the magmatic, REE-bearing minerals, estimate the REE amount they carry, and compare it with the total REE concentration in the rock. The remaining REE are assumed to be present in hydrothermal minerals. This procedure is applied for Ce and Yb in order to represent light- and heavy-REE, respectively, and determine if any fractionation occurs. The procedure is inspired by the one described in Schmitt et al. (2002). The detailed process, applied to one granite and one pegmatite of each complex, is as follows:

1. Whole-rock analysis of Nb, ZrO_2, FeO, REE
2. Estimation of the percentage of pyroxene in the sample. Since it is the only green mineral in thin sections, it is possible to estimate its proportion in the sample with accuracy with the help of an image analysis program created for this purpose
3. Attribution of the matching REE amount according to previous analyses in pyroxene
4. Estimation of the percentage of amphibole in the sample by attributing all FeO to amphibole
5. Attribution of the matching REE and Nb amounts according to previous analyses in amphibole
6. Estimation of the percentage of PGM in the sample by assigning all remaining Nb not incorporated in amphibole
7. Attribution of the matching REE amount according to previous analyses in PGM
8. Estimation of the percentage of zircon in the sample by assigning the ZrO_2 of whole-rock analyses
9. Attribution of the matching REE amount according to previous analyses in zircon
10. Comparison of the sum of the REE in these four minerals with the total REE in the rock. The remaining REE is estimated to be concentrated in hydrothermal minerals

The image analysis program to estimate the proportion of pyroxene in the sample was created with the help of Yves Auda at the GET laboratory. The principle is to determine the percentage of pixels of pyroxene, i.e. of green pixels, in a scan of a thin section. The first step is to determine the pixel colors that we want to count by highlighting them in polygons using the software QGIS. Then, using the software GRASS and the computer program written by Yves Auda, a histogram thresholding is performed. The whole program as well as guidelines on how to use it are given in Appendix C.

4.4.2.2 Results and discussion

4.4.2.2.1 Magmatic vs hydrothermal REE budget

Mass-balance calculation was performed on one pegmatite and one granite of each complex, where possible. The results show that in all complexes, the majority of the REE (80 % on average) is contained in hydrothermal minerals (Fig 4.16). This is in accordance with the results of Schmitt et al. (2002) who found that more than 70 % of the REE are in hydrothermal phases at Amis. In most rocks, there is a fractionation between light- and heavy-REE, the proportion of hydrothermal HREE being higher than that of LREE. The complexes of Khan Bogd and Strange Lake are different from the other complexes, as in pegmatites almost all Y is located in hydrothermal minerals and in the pegmatite from Khan Bogd and the granite from Strange Lake no REE fractionation is observed. In the granites from Evisa and Khan Bogd, the proportion of hydrothermal LREE is higher.

In the granite from Evisa, the proportion of hydrothermal Y is very low (2 %), and most of it is incorporated in magmatic zircon. In addition, the calculations showed that even though they can incorporate significant concentrations of REE compared to other minerals, the contribution of amphibole and pyroxene to the REE budget of the rock is very low.

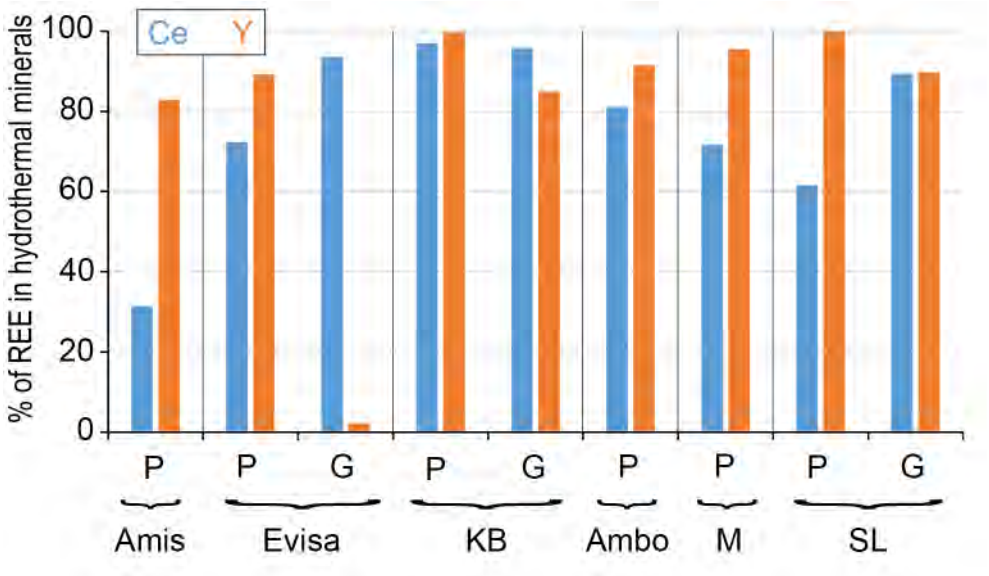

Figure 4.16 Histogram showing an estimation of the percentage of Ce and Y in hydrothermal minerals for the six studied complexes, in pegmatites and granites. Abbreviations: P: pegmatite; G: granite; KB: Khan Bogd; Ambo: Ambohimirahavavy; M: Manongarivo; SL: Strange Lake

4.4.2.2.2 Discussion on the method

Although the method used in this study tries to account for most of the magmatic REE-bearing minerals, some approximations had to be made. Considering pyroxene as a magmatic mineral is not entirely valid, as Section 4.1 provides evidences that pyroxene rims are hydrothermal. In view of this element, the hydrothermal contribution may be slightly underestimated, but since pyroxene does not have a high impact on the global REE budget of the rock, this effect is probably negligible. Likewise, all zircons are not magmatic. In rocks where only type-P or type-I zircon was found, its contribution to the REE budget is entirely counted as hydrothermal, and in rocks where only type-SG was found, it is regarded as only magmatic. In rocks where hydrothermal and magmatic zircon was found, it was all accounted for magmatic contribution, hence once again the hydrothermal contribution is underestimated. This could explain the very low amount of hydrothermal Y in the granite from Evisa. In addition, I only selected samples where either zircon or zirconosilicates are present, to make sure that most ZrO_2 is mostly contained in one of these phases.

Some minerals were also not taken into account. Amphibole is not the only mineral with FeO: astrophyllite and hematite also contain Fe. However, the combination of low concentration of these two minerals and the low impact of amphibole on the REE budget of the rock reveals that this does not change much the results of the calculation. Monazite-(Ce), chevkinite-(Ce), and allanite-(Ce,Nd) are rare magmatic minerals that were also not taken into account. Indeed, they are present in negligible quantities, hence their impact on the global REE budget is very limited. For example, Schmitt and associates propose to attribute all P_2O_5 to magmatic monazite-(Ce); however, not all monazite-(Ce) is magmatic, and P_2O_5 in whole-rock analyses is below the detection limit.

Considering these approximations, the precise results of this calculation must be taken cautiously. However, the percentages of REE in hydrothermal minerals found are so high that there is no doubt as to the significant contribution of fluids to the global REE budget.

Chapter 5

Fluid inclusion study

This Chapter is a draft for a second paper, hence some notions previously mentioned are explained again in the *Introduction* section.

5.1 Introduction

Rare Earth Elements (REE) are among the most critical raw materials today (European Commission, 2018). Their supply is restricted and mostly controlled by China and to a lesser extent, Australia, whereas the demand is growing. They are used in many modern technologies linked to the transition to renewable energy infrastructure (Goodenough et al., 2018; Lucas et al., 2014). REE deposits can be primary (igneous, carbonatites and alkaline systems) or secondary (placers and ion-adsorption) (Chakhmouradian and Wall, 2012) and economic concentrations of heavy REE (HREE, Gd to Lu) are rather rare compared to those of light REE (LREE, La to Eu). Today, ion-adsorption deposits provide most of the global REE (and mostly HREE) production (U.S. Geological Survey, 2019). However, many exploration targets worldwide are carbonatites and alkaline igneous rocks (Bloodworth, 2010). Most alkaline igneous rocks are silica-undersaturated, with the silica-saturated variety (i.e., granitic) being quite rare (e.g. Foland et al., 1993; Kramm and Kogarko, 1994; Larsen and Sørensen, 1987). However, it is the latter that have high Yb/La ratios compared to other varieties. Pegmatites, which form from the last and most evolved part of silica saturated melts, concentrate the highest amounts of REE and other HFSE.

The timing of concentration and fractionation of the REE in alkaline silica-saturated granites and pegmatites is still a matter of debate. Indeed,

although most authors agree on a magmatic pre-enrichment (Marks and Markl, 2017), there is also evidence that hydrothermal processes play a key role in concentrating the REE to ore grades (e.g. Dostal, 2017; Lecumberri-Sanchez et al., 2015; Salvi and Williams-Jones, 1990). However, to date, the importance of hydrothermal processes is still debated, partly because the processes occurring at the magmatic-hydrothermal transition are hard to document and most studies were carried out in the laboratory (e.g. Migdisov et al., 2016). Although punctual studies seem to indicate that the role of hydrothermal fluids in concentrating the REE to ore levels is essential, evidence that would allow to generalize this is lacking.

In the past, several studies of fluid inclusions (FI) have provided crucial information as to temperature, pressure, estimates of concentration and possible ligands of the REE in hydrothermal fluids. Only a restricted number of studies have directly measured REE in FI. Most of them used the crush-leached method in which a small crystal is crushed and the fluid released is analyzed by ICP-MS (Banks et al., 1994; Bühn and Rankin, 1999; Bühn et al., 2002; Ghazi et al., 1993; Norman et al., 1989; Vasyukova and Williams-Jones, 2018). This method has the advantages of being able to measure anionic species (e.g. F-, Cl-) and to detect trace elements more easily than the analysis of single inclusions. Analyses of REE in single inclusions are even rarer in the literature although this method allows precise analyses even in quartz containing inclusions of other minerals and several FI populations. Audétat et al. (2008) measured Ce concentrations of up to 300 ppm in a single FI, with an uncertainty of 20 %. In addition, so far most of these studies focused on silica-undersaturated alkaline rocks (e.g. Graser et al., 2008; Potter, 2000), with the notable exception of Strange Lake (Salvi and Williams-Jones, 1990; Vasyukova and Williams-Jones, 2016). The goal of this study is to compare six alkaline, silica-saturated, REE-rich complexes from different parts of the world, to explore the role of hydrothermal fluids in concentrating and fractionating the REE, and to understand which characteristics (temperature, salinity, composition) are necessary to enrich alkaline complexes in REE to ore grades. Apart from Strange Lake, FI in the five other complexes, namely Ambohimirahavavy and Manongarivo in Madagascar, Amis in Namibia, Evisa in Corsica, and Khan Bogd in Mongolia, have never been studied.

5.2 Geological context

The six alkaline igneous complexes on which this work focuses are: Ambohimirahavavy (Estrade et al., 2014a) and Manongarivo (Donnot, 1963; Rakotovao et al., 2009) in Madagascar, Amis in Namibia (Schmitt et al., 2002), Evisa in Corsica (Bonin et al., 1978), Khan Bogd in Mongolia (Kovalenko et al., 2006), and Strange Lake in Canada (Salvi and Williams-Jones, 1990). These complexes were chosen because all present evidence of hydrothermal circulation, among which the presence of pseudomorphs and primary fluid inclusions, and contain high amounts of REE (from 800 ppm in a granite from Khan Bogd to 12 % in a pegmatite from Strange Lake, personal unpublished data). All complexes contain peralkaline rocks, i.e. their ratio of $(Na_2O+K_2O)/Al_2O_3$ is >1. Some of them have been the subject of in-depth studies, such as the Strange Lake complex which was first studied in the late 1980's (e.g. Miller, 1986; Salvi and Williams-Jones, 1990) and still is today (Vasyukova and Williams-Jones, 2020); others are poorly known, as is the case for the Manongarivo complex, for which the only available information are two documents in French (Donnot, 1963; Rakotovao, 2009).

Although they were emplaced in different geodynamic complexes and at different periods, it appears that the melt source was a metasomatized upper mantle for all six complexes. Crustal contamination and feldspars fractionation, if occurring, are two processes that can enrich alkaline granites in REE. However, the rate of partial melting at the origin of these complexes is still debated, which is an essential parameter given that a lower rate implies a greater accumulation of incompatible elements, REE included, in the newly generated melt. Although their role is debated, all complexes underwent at least one alteration episode from an orthomagmatic fluid, and some of them an additional late hydrothermal event (identified at Amis, Evisa, and Strange Lake).

The composition of the fluids that circulated was measured in fluid inclusions at Ambohimirahavavy and Strange Lake, and inferred from the study of secondary mineral assemblages for the other complexes. The resulting conclusions are similar for all the complexes, although they do not always have the same timing. For example, F- is described in all complexes, but in the orthomagmatic fluid at Khan Bogd and Madagascar, and in the post-magmatic fluid at Amis, Evisa

and Strange Lake. The presence of significant amounts of Na^{+} and Fe^{3+} in an orthomagmatic fluid is reported for Evisa, the two Malagasy complexes and Strange Lake, and Ca^{2+} was identified at Khan Bogd, Madagascar and Strange Lake. Locally, CO_2 and/or CH_4 were reported at Khan Bogd and Strange Lake, and CO_3^{2-} at Amis. The resulting conclusions are similar for all the complexes: independently of its orthomagmatic or late origin, a F-, Ca-rich fluid is systematically observed and inferred to have mobilized and fractionated the REE. The importance of this process compared to magmatic ones in concentrating and fractionating the REE is still a matter of debate. Comparing six complexes that were emplaced in different geodynamic settings and witnessed different fluid conditions (composition, temperature) is a strategy to highlight common features in order to better constrain and generalize the timing of REE and other HFSE enrichment in alkaline complexes. More detailed information about the geological context of each complex is provided in Bernard et al. (2020).

5.3 Sample selection and method

5.3.1 Sample selection

Between 3 and 15 samples of the 6 complexes were studied in order to select the 2 more representative samples each for the FI study. One granite and one pegmatite were chosen to represent each complex, except at Manongarivo where only two pegmatites were available (and no granite) due to bad outcropping conditions in the field. We ensured that the selected samples were representative in terms of mineralogy and rock chemistry, based on petrographic observations and SEM and EPMA analyses as well as on previously published FI descriptions (Salvi and Williams-Jones, 1990; Vasyukova and Williams-Jones, 2016; Vasyukova and Williams-Jones, 2018 at Strange Lake, Estrade et al., 2015 at Ambohimirahavavy, and Schmitt et al., 2002 at Amis). We also made sure, where possible, that selected samples contained numerous FI that are not obviously secondary and large enough to be studied. A summary of the observations on selected samples is provided in Tab 5.1. Considering the extensive fluid inclusion data already existing for Strange Lake (references above), we chose not to study FI in this complex and to rely on those data.

Table 5.1 Samples selected for the FI study and their main characteristics

Complex	Amis		Evisa	Khan Bogd		Ambohimirahavavy		Manongarivo		Strange Lake		
Sample	SOS069	SOS071	EV1823b	EV1825A	KB07A	KB04B	AM107	AM35	688	689	Salvi and Williams-Jones (1990), Vasyukova et al. (2016)	
Sample description	Arfvedsonite granite	Pegmatite with aegirine in clusters	Subsolvus granite with a pseudomorph	Pegmatite with pseudomorphs	Granite with pseudomorphs	Pegmatite with pseudomorphs	Granite	Pegmatite with pseudomorphs	Pegmatite	Pegmatite	Hypersolvus granite	Subsolvus granite	Pegmatite
FIA	LV1, LV2, LV-V, LVS1, LVS2, LVS2-LV	LV1, LV2, LV-V, LVS1, LVS2, LVS2-LV	LV1, LV2, LVS, V, LV1-LVS	LV1, LV2, V	LV2-V2, LV2, L, V1, LV1-V1, LV1-L1	LV2-V2, LV2, L, V1, LV1-V1, LV1-L1, LVS, LVS-LV2	LV1, LV2, LVS, V1, LVS-LV1, V2	LV1, LV2, LVS, V1, LVS-LV1, LVSx, LV1-V1, LVS-V1	LV1, LV2, LVS, V, LV1-V, LV1-LVS, LVSx	LV1, LV2, LVS, V, LV1-V, LV1-LVS, LVSx	LV1-V1	LV3-LVS3	LV1-LVS1, LV1-V1, LV2-V2-LVS2, LV2, LV3-LVS3
FI average size	5 µm	5-15 µm	< 5 µm	< 5 µm	< 5 µm	< 5 µm	10 µm	10-15 µm	10 µm	5-10 µm	5-30 µm	5-10 µm	5-40 µm
FI shape	Rounded, irregular or negative crystal shape	Rounded or irregular	Rounded, irregular or negative crystal shape	Rounded or irregular	Negative quartz crystal shape, irregular or rounded	Negative quartz crystal shape, irregular or rounded	Rounded, irregular or cubic	Rounded or irregular	Rounded or irregular	Rounded or irregular	Irregular, rounded or negative crystal shape	Irregular, rounded or negative crystal shape	Irregular, rounded or negative crystal shape
FI location (general tendency)	Center of quartz crystals	Center of quartz crystals; associated with MI; close to aegirine clusters	Rims of quartz crystals; pseudomorph	Rims of quartz crystals	Sealed fractures; rims of quartz crystals	Sealed fractures; rims of quartz crystals	Rims of quartz crystals	Rims of quartz crystals	Not in quartz core	Not in quartz core	Quartz crystals	Pseudomorphs; sealed fractures	Quartz crystals; pseudomorphs; sealed fractures
Solid search with SEM	Yes	No	Yes	No	Yes	Yes	No	No	No	No	Yes (previous work)	Yes (previous work)	Yes (previous work)

5.3.2 Methods

Detailed petrographic studies were carried out to identify fluid inclusion assemblages (FIA). Primary and secondary fluid inclusions were first identified in 30 μm thick polished thin sections of all rock types from the six complexes using the criteria of Roedder (1984). Doubly polished slices of 100 μm thickness were made out of the selected samples. Microthermometric measurements were performed at the University of Toulouse using a Linkam THMGS 600 heating–freezing stage mounted on a BX-51 Olympus microscope. The stage was calibrated against synthetic pure H_2O inclusions (0.0 and +374.1 °C) supplied by SynFlinc and with natural pure CO_2 inclusions (–56.6 °C) from Camperio (Ticino, Switzerland). Measurements below 0 °C are accurate to ±0.1 °C, whereas at the highest temperature measured (∼400 °C), they are accurate to ±1 °C. Cryogenic experiments were carried out before heating to reduce the risk of decrepitating the inclusions. Salinity (expressed as wt% equivalent NaCl) were calculated using the HokieFlincs-H_2O-NaCl spreadsheet of Steele-MacInnis et al. (2012).

In order to identify the nature of the major components of the fluid, evaporate mounds were analyzed following Kontak (2004). After thorough cleaning, double-polished quartz chips were heated rapidly until the fluid inclusions decrepitated, generally at temperatures in excess of 400 °C but < 550 °C. Salt mounds that precipitated on the surface were examined using optical microscopy and analyzed at the University of Toulouse 3 using a JEOL JSM 6360LV scanning electron microscope (SEM) equipped with a silicon drift detector analysis system and interpreted with the Esprit software at the GET laboratory, using an accelerating voltage of 20 kV, and a detection time of 30 s.

In rocks where quartz grain size was coarse enough to do so, we also analyzed solids in opened fluid inclusions in quartz following a method similar to that described by Kelly and Burgio (1983). We broke small blocks (1-2 cm in size) that were plunged into liquid nitrogen in order to freeze the inclusions and keep solids from popping out. Once frozen, we broke the blocks to expose fresh surface and placed them horizontally on a SEM sample holder. The SEM and analytical conditions were the same as those used to study evaporate mounds.

Entrapment temperature of FI was determined using the programs BULK and ISOC provided in Bakker (2003). Calculations were made for FI with the lowest and the highest T_h for each composition and each complex, provided that these

temperatures were significative regarding the data distribution. The software BULK is based on the empirical thermodynamic model of Naden (1996) for the system NaCl-$CaCl_2$ and Hall et al. (1988) for the system NaCl-KCl. It calculates the proportion of each phase of the inclusion and its bulk density at 20 °C based on the state equation of Krumgalz, (1996) for the system NaCl-$CaCl_2$, Oakes et al. (1990) for the system NaCl-KCl, and Bodnar (1993) for the system NaCl. The information obtained with BULK is then entered in the program ISOC to calculate corresponding isochores based on the equations from Zhang and Frantz (1987). Entrapment pressure was estimated from data in the literature as well as from petrographic evidences such as the presence of volcanic rocks. Since for most cases no hydrates were spotted, the proportion of salts in the inclusion was mostly estimated from eutectic temperatures, using Shepherd et al. (1985).

5.4 Petrography of selected samples

5.4.1 General mineralogical description

Pegmatites in all complexes are heterogeneous in texture, i.e. they show mineralogical layering visible from the scale of the outcrop to that of a thin section, whereas granites are generally homogeneous. In pegmatites, the layers have grain sizes ranging from a few μm to about 40 cm and locally more. Therefore, to obtain meaningful data, samples for this study were selected from zones of relatively fine grain size (less than a few cm).

All pegmatites and granites are dominated by quartz, alkali feldspar (perthites, albite, orthoclase, and/or microcline) that are commonly strongly albitized, plus Na-amphiboles and, mostly in pegmatites, Na-pyroxene (aegirine). Common accessory minerals in both rock types include zircon, pyrochlore group minerals (PGM) and Fe- and Ti-oxides. Other minerals present mostly in pegmatites include Ca and Na zirconosilicates, fluorite, astrophyllite and REE-bearing minerals (typically bastnäsite-(Ce), monazite-(Ce), xenotime-(Y), chevkinite-(Ce), allanite-(Ce), aeschynite-(Y), fergusonite-(Y), britholite-(Y), synchysite-(Ce)). Ti-bearing minerals such as chevkinite-(Ce) and astrophyllite show signs of alteration such as dissolved edges.

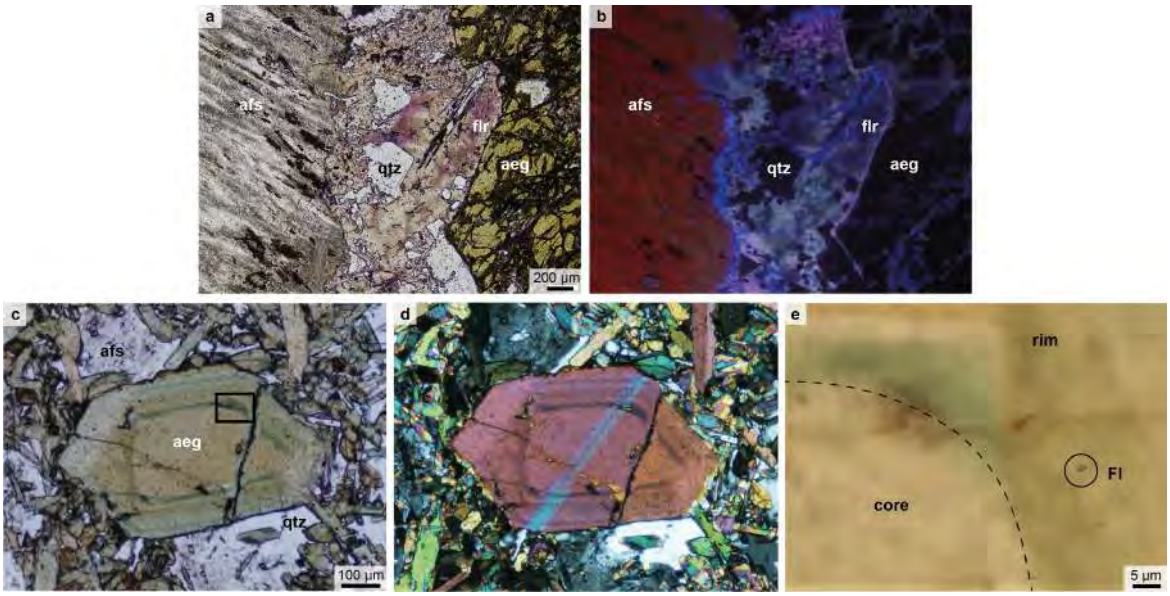

Figure 5.1 Examples of zonations and fluid inclusions in fluorite and aegirine. (a) Optical view of fluorite at Strange Lake, sample SL1-20; (b) Same view of zoned fluorite with cathodoluminescence; (c) Optical view of zoned aegirine at Manongarivo, sample 688; (d) Same view of aegirine with analyzed light; (e) An example of small fluid inclusion in the rim of aegirine from Manongarivo. Abbreviations: afs: alkali feldspar; qtz: quartz; flr: fluorite; aeg: aegirine; FI: fluid inclusion

Ca and Na zirconosilicates are mostly EGM at Ambohimirahavavy (Estrade et al., 2018; Lacroix, 1923), and elpidite at Evisa, Khan Bogd and Strange Lake (Bonin and Platevoet, 1988; Grigor'eva et al., 2011; Salvi and Williams-Jones, 1990). These zirconosilicates were partially to totally hydrothermally replaced by secondary mineral assemblages, which commonly formed pseudomorphs (Estrade et al., 2014b; Gysi et al., 2016; Poitrasson et al., 1998). The mineralogy of the pseudomorphs varies in the different complexes and consists either of different Zr- and/or REE-bearing minerals, or exclusively zircon plus quartz. Both types are found in all complexes, except in Amis where our samples only contain the zircon-quartz pseudomorphs. Elpidite can also be extensively replaced by other zirconosilicates, namely armstrongite and gittinsite (e.g. Salvi and Williams-Jones, 1995), whereas EGM is only partially replaced by these phases. At Khan Bogd, the elpidite is altered from its core, and replaced by zircon and armstrongite.

Fluid inclusions were found in quartz and, less commonly, in fluorite and aegirine. All three minerals are zoned in all complexes (Fig 5.1, 5.3, 5.4). Fluid inclusions in fluorite and aegirine are sparse and generally small (< 5 μm), thereby this study is based only on fluid inclusions found in quartz. Aegirine zonation

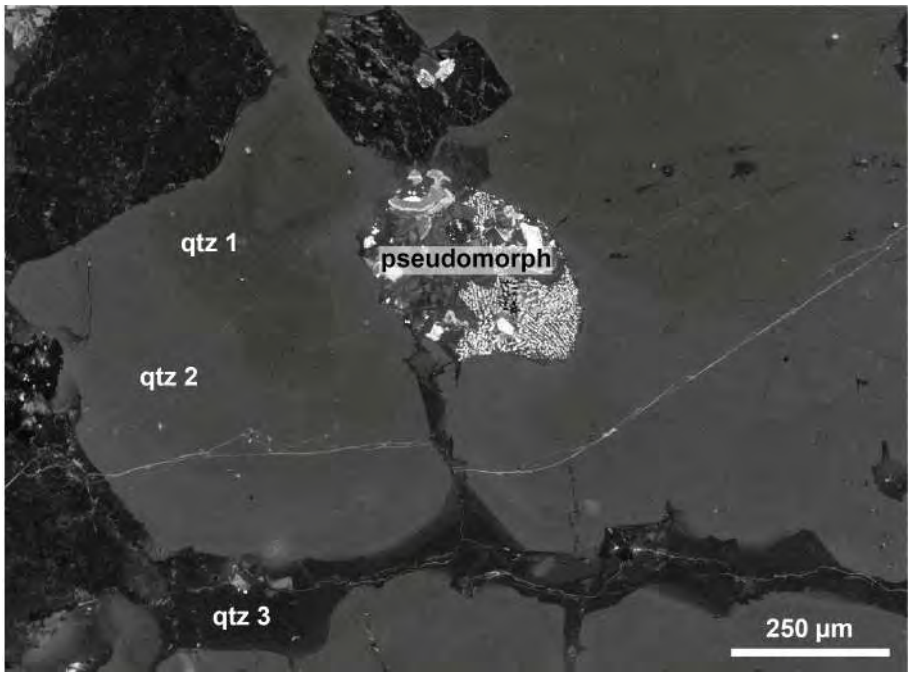

Figure 5.2 Quartz overgrowths SEM-CL

was interpreted by Bernard et al. (2020) as magmatic in origin for their core, with hydrothermal rims that grew in competition with pseudomorphs. Fluid inclusions in aegirine were only found in rims of aegirine crystals (Fig 5.1e). Optical microscopy does not show any zonation in quartz; however, optical CL reveals a generation overgrowing a primary core, a texture commonly observed in granites from all complexes (Fig 5.3), whereas in pegmatites it was only observed at Amis, Evisa and Madagascar (Fig 5.4). In granites, the core appears navy blue while the rims are dark blue, except at Ambohimirahavavy where the opposite occurs. The difference in color is due to different activator elements. In quartz, the nature of activator elements is still debated, but studies point to a high amount of Ti (Rusk et al., 2006), or a high ratio Ti/Fe (Marshall and Mariano, 1988) being responsible for the observed blue color. Quartz rims are thin compared to cores at Amis and Khan Bogd, whilst cores are less developed in the other granites. In addition, quartz core at Ambohimirahavavy is rich in inclusions of alkali feldspar, aegirine and Na-amphibole. At Strange Lake, alkali feldspar inclusions are located close to the core-rim transition, inside the rim. Granites from Ambohimirahavavy and Strange Lake also have quartz cores clearly delimited, in contrast with the other granites where the core-rim limit is blurry. All of these elements indicate that the core grew in two major phases that match the magmatic and hydrothermal zones

previously determined in aegirine. In pegmatites, the same overgrowth is observed only at Amis, Evisa and Madagascar (Fig 5.4). The core at Ambohimirahavavy is also the only one to be darker than the rims. At Khan Bogd and Strange Lake, the quartz close to sealed fractures appears lighter, suggesting a second generation of quartz sealed the first quartz crystals. Given that alkaline pegmatites crystallization processes are complex, it is not surprising to note that quartz zonation/overgrowth relationships are more complex as well. In addition, SEM-CL was performed on a pegmatite sample from Ambohimirahavavy (Fig 5.2). On this image, three generations of quartz are visible, and the third one connects quartz rims to a pseudomorph. This is a clear proof that this generation grew in competition with pseudomorphs and is hydrothermal.

5.4.2 Petrography of fluid inclusions types and assemblages

5.4.2.1 The Amis complex, Namibia

Granites and pegmatites at Amis contain many FI in quartz, with sizes ranging from 5 to 15 μm on average. They commonly occur in a rounded or irregular shape, and occasionally with a negative quartz crystal shape, especially in the arfvedsonite granite. Schmitt et al. (2002) mentioned that FI at Amis are only secondary, but this statement was not supported by any observations. Their disposition outside of fractures and, mostly in pegmatite, their association with melt inclusions (MI), would rather suggest a primary origin for these FI. Melt inclusions are easy to spot as they are filled with many crystals and do not contain any fluid phase, neither liquid nor vapor. Melt inclusions and associated FI are often located in the core of quartz crystals (Fig 5.5a,c). In pegmatite, FI are more abundant close to aegirine clusters.

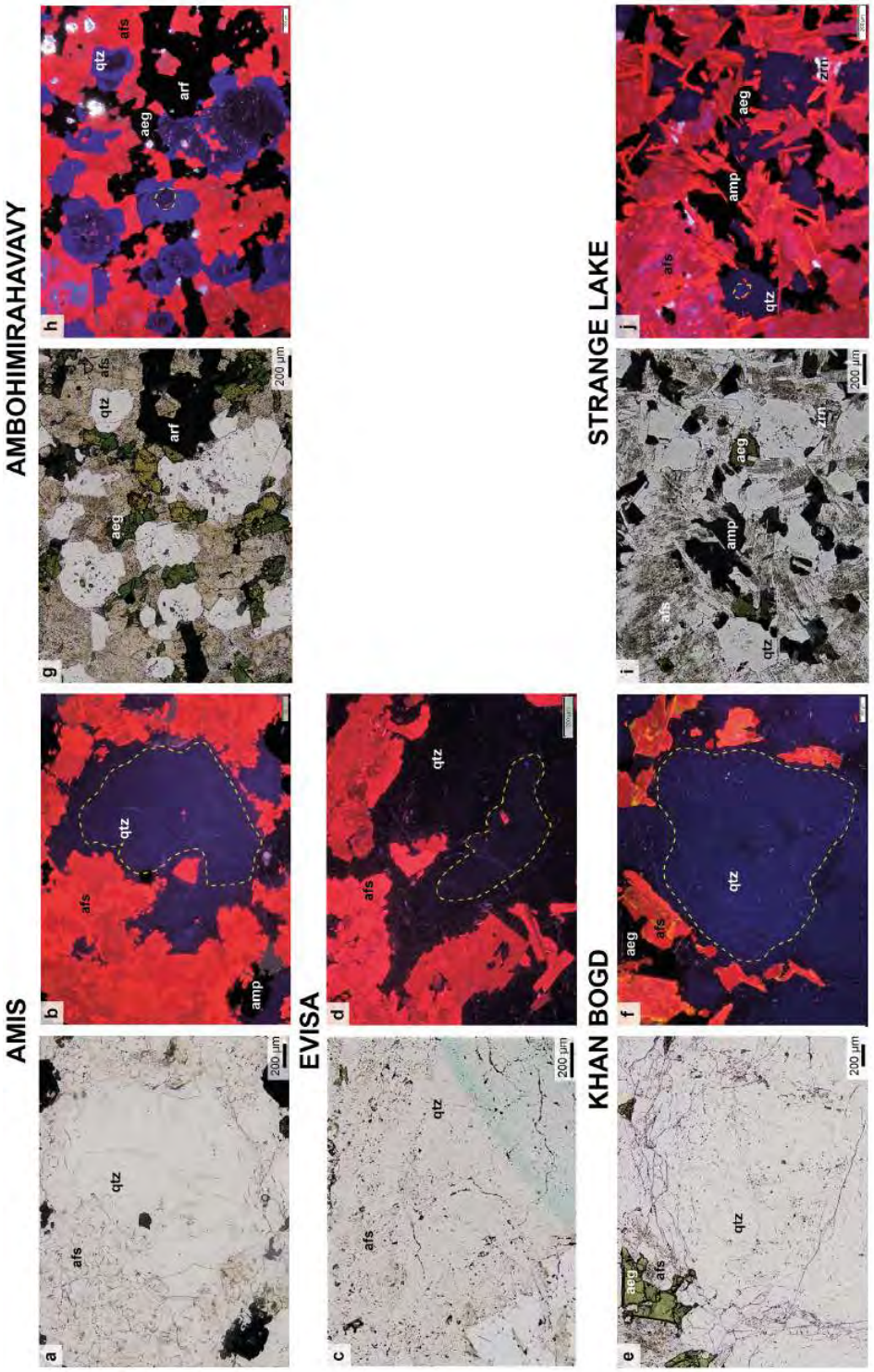

Figure 5.3 Quartz overgrowths in granitic samples. (a), (c), (e), (g), and (i) are transmitted-light views, (b), (d), (f), (h), and (j) are optical-cathodoluminescence images. (a), (b) Amis, sample SOS069; (c), (d) Evisa, sample EV1823B; (e), (f) Khan Bogd, sample KB07A; (g); (h) Ambohimirahavavy, sample AM107; (i), (j) Strange Lake, sample 58-D-1. Abbreviations: qtz: quartz; arf: arfvedsonite; aeg: aegirine; afs: alkali feldspar; amp: amphibole; zrn: zircon

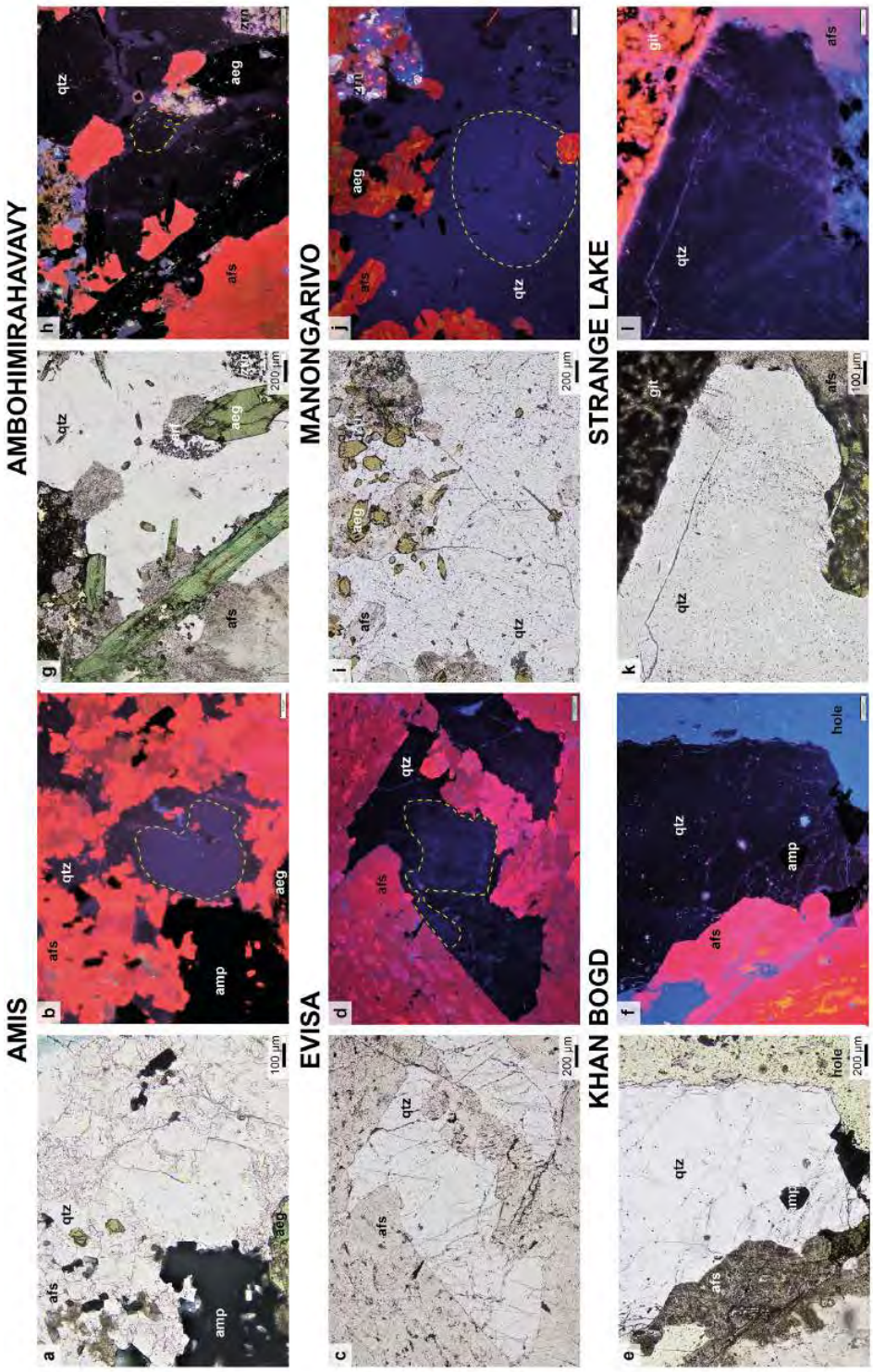

Figure 5.4 Quartz overgrowths and zonations in pegmatitic samples. (a), (c), (e), (g), (i), and (k) are transmitted-light views, (b), (d), (f), (h), (j), and (l) are optical-cathodoluminescence images. (a), (b) Amis, sample SOS071; (c), (d) Evisa, sample EV1825A; (e), (f) Khan Bogd, sample KB04B; (g); (h) Ambohimirahavavy, sample AM35; (i), (j) Manongarivo, sample 688; (k), (l) Strange Lake, sample SL1-20. Abbreviations: qtz: quartz; amp: amphibole; aeg: aegirine; afs: alkali feldspar; zrn: zircon; git: gittinsite

Based on the phases present at room temperature, their location in the samples and their associations, 7 types of FIA were identified. Here as in the following sections, FIA they are labeled by order of abundance, hence an assemblage labeled 1 does not mean it is primary; similarly, an assemblage labeled 2 does not mean it is secondary. The first FIA, the most abundant both in granite and pegmatite, consists of liquid-vapor inclusions (LV) distributed in the whole quartz crystals, often in association with MI (Fig 5.5a). The L/V ratio is constant, around 80/20. In addition, these inclusions occasionally contain one to three unidentified euhedral black opaque crystals (Fig 5.5b). The occurrence of these crystals in only a few FI indicates they are probably accidentally trapped crystals. Liquid only (Fig 5.5c) FI also occur in both the granite and the pegmatite, but they nucleate a vapor bubble after cooling without any volume change. Since microthermometry measurements ruled out the possibility of liquid CH_4, this vapor bubble nucleation is interpreted as a sign for metastability (Roedder, 1971). These FI will therefore be considered as LV in the following sections. The second assemblage regroups liquid-vapor and vapor-rich inclusions systematically found together (LV-V1; Fig 5.5d). The third assemblage is made of liquid-vapor-solid (LVSx1) inclusions with a number x of solids, and is commonly found in close association with MI in pegmatite and granite. Unlike type-1 LV inclusions, these inclusions can be intermediate between fluid and melt, as some of them contain a lot of solids, but also a vapor bubble (Fig 5.5e). Considering the fact that the vapor bubble can be homogenized, we will consider these as FI. However, as the solid content is different from one inclusion to another, this is likely heterogeneous trapping. This type of inclusion was also described by Thomas et al. (2006b) as pegmatite-forming melts having H_2O concentrations >40 wt%.

The fourth assemblage occurs in pegmatite and is made of liquid-vapor-solid (LVS2) inclusions, where the solid is a cube of salt (Fig 5.5f). These inclusions can be found in association with LV FI, forming the fifth assemblage type (LVS2-LV). The sixth assemblage type is found abundant in granite, and is rich in aqueous vapor (V1, Fig 5.5g). Finally, the seventh assemblage is found in sealed fractures cutting across grain boundaries, which indicates they are secondary in origin (Roedder, 1984). As LV, they are commonly found in both rock types, and they are made of vapor-rich inclusions (V2; Fig 5.5h). Assemblages are commonly made of 2-10 FI, except for V2 in fractures which can regroup dozens of FI.

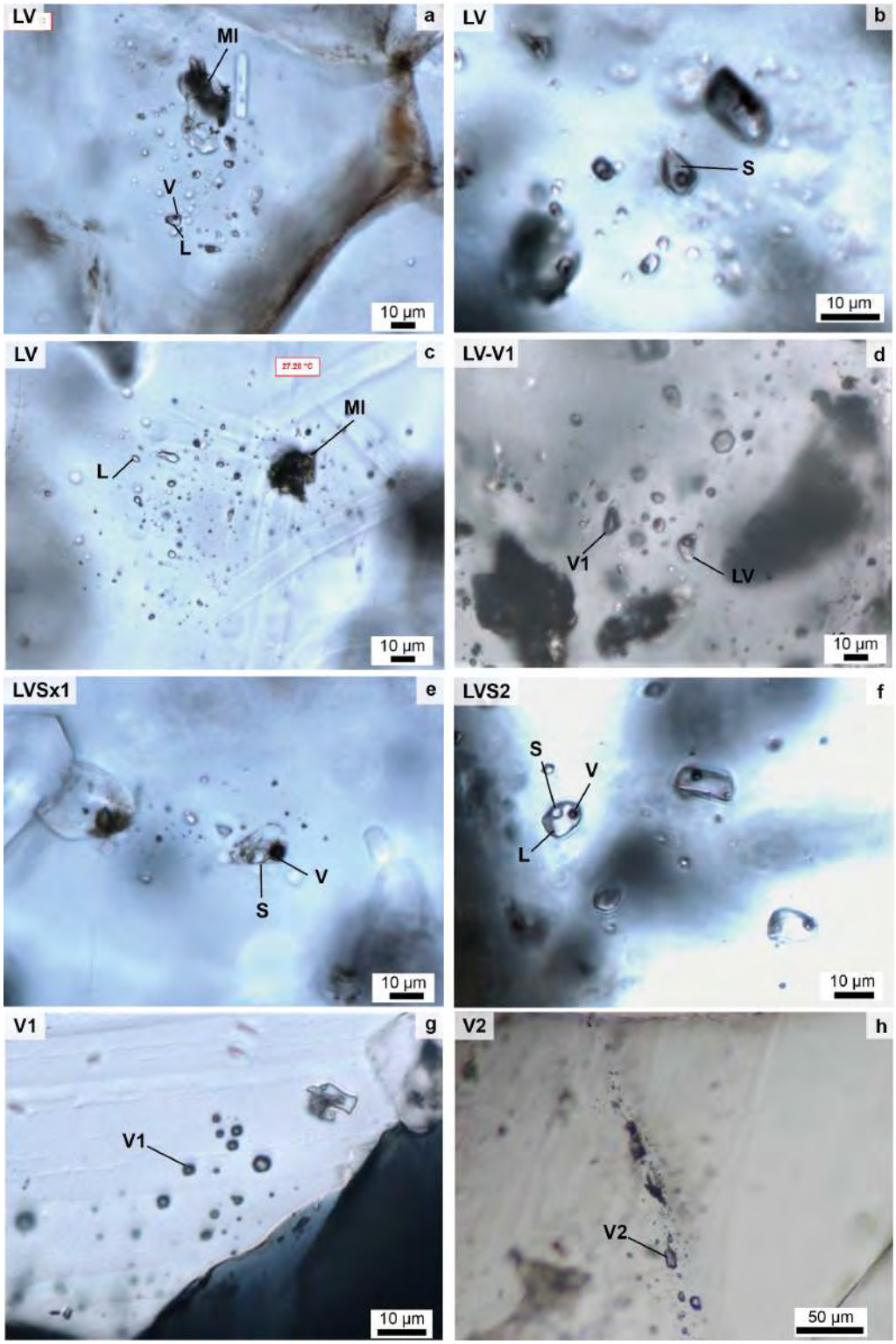

Figure 5.5 Photographs of representative fluid inclusions (FI) in quartz from Amis, Namibia. (a) LV FI associated with a melt inclusion (MI), sample SOS071; (b) LV FI with a black solid, sample SOS071; (c) LV FI under their metastable liquid only conformation, sample SOS069; (d) LV-V1 assemblage, sample SOS071; (e) LVSx1, an inclusion with a majority of solids but also a vapor bubble: it is intermediate between MI and FI, sample SOS071; (f) LVS2, with a cube of salt, sample SOS071; (g) V1 FI close to an arfvedsonite, sample SOS069; (h) V2 secondary FI in a sealed fracture, sample SOS069

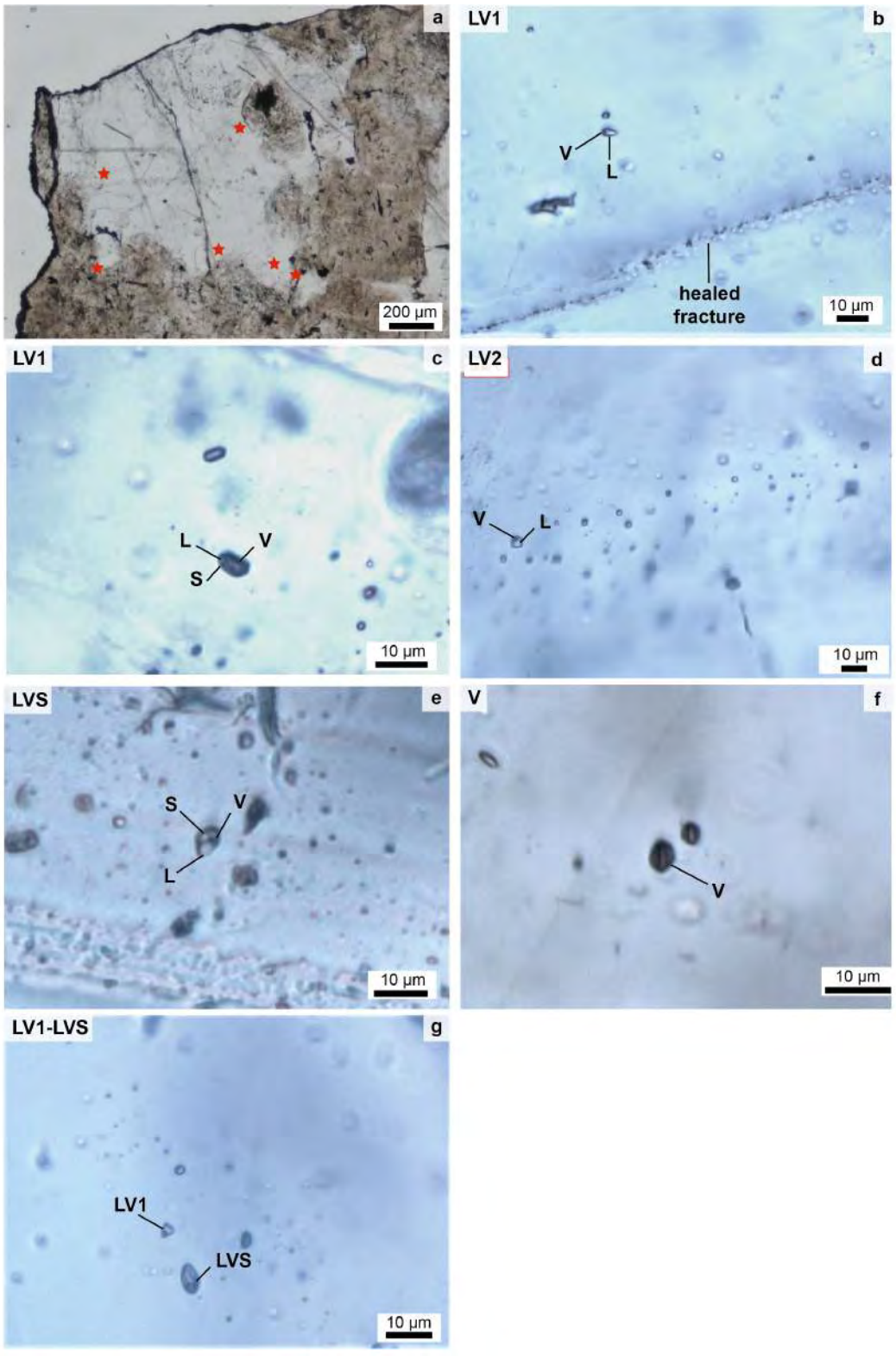

Figure 5.6 Photographs of representative fluid inclusions (FI) in quartz from Evisa, Corsica. (a) View of an entire quartz grain, red stars provide the location of some primary inclusions analyzed in this study, sample EV1823B; (b) LV1 FI, sample EV1825A; (c) LV1 FI with a black solid, sample EV1823B; (d) LV2 FI aligned along a sealed fracture, sample EV1823B; (e) LVS FI, sample EV1823B; (f) Vapor-rich FI, sample EV1825A; (g) LV1-LVS FIA, sample EV1823B

5.4.2.2 The Evisa complex, Corsica

Quartz crystals in granite and pegmatite from Evisa are rich in FI. Their size is small compared to the other complexes (< 5 μm) and they are mostly distributed on the edges of quartz crystals (Fig 5.6a). They commonly occur in a rounded or irregular shape, but they can also present a negative quartz crystal shape in granite. To my knowledge, no description of FI exist for this complex.

This description as well as the followings are based on the same criteria as for Amis. At Evisa, 5 types of FI assemblages were identified. By decreasing order of abundance, they are (1) LV1, regrouping liquid-vapor and metastable liquid FI with an occasional trapped opaque, euhedral black crystal if the FI is in granite (Fig 5.6b,c). The ratio L/V is 80/20; (2) LV2 in sealed fractures cutting several grains, secondary in origin whose L/V ratio varies between 70/30 and 80/20 (Fig 5.6d); (3) LVS with the solid being a cube of salt and present only in granite (Fig 5.6e); (4) vapor-rich aqueous (V; Fig 5.6f); (5) LV1-LVS, only in granite (Fig 5.6g). Assemblage (5) is much less abundant in the studied rocks. The number of FI in the assemblages is similar to that of Amis. In the pseudomorph of the granite, FI are usually bigger than outside of it, and more LVS assemblages are found. The presence of FI in the pseudomorph is an evidence of their primary origin.

5.4.2.3 The Khan Bogd complex, Mongolia

At Khan Bogd, the study of FI is very difficult as the vast majority of FI is located in fractures, and other FI are rare and often too small to be measured (< 5 μm). These FI are located at the rims of quartz crystals (Fig 5.7a), similarly to Evisa, and commonly present a negative crystal shape. They can also in a rounded or irregular shape. To this day, no data was published on the FI at Khan Bogd.

Eight types of FIA are distinguished at Khan Bogd. By decreasing order of abundance, these are: (1) LV2-V2, which commonly contain 70 % LV FI, and 30 % aqueous vapor-dominated FI, together in sealed fractures and hence secondary (Fig 5.7b); (2) LV2, made of secondary FI with an occasional trapped black euhedral opaque crystal (Fig 5.7c) grouped with metastable L, in sealed fractures cutting several crystals and with L/V ratios ranging from 60/40 to 80/20; (3) liquid (L), with a size ranging from 1 to 10 μm (Fig 5.7d); (4) V1, which is aqueous vapor-rich and can be associated with MI (Fig 5.7e); (5) LV1-V1, LV1 FI having a L/V ratio close to 80/20 (Fig 5.7f); (6) LV1-L (Fig 5.7g); (7) LVS, the solid being a cube of salt. This

FIA is found mostly in pegmatites in the rims of quartz (Fig 5.7h); (8) LVS-LV2, also found mostly in pegmatites, in sealed fractures restricted to within a single quartz crystal and hence pseudosecondary (Fig 5.7i). Assemblage types 7 and 8, in sealed fractures, are by far the most widespread at Khan Bogd. Assemblages contain 1-5 FI on average, and dozens if they are in sealed fractures.

5.4.2.4 The Ambohimirahavavy complex, Madagascar

At Ambohimirahavavy, FI are abundant, and relatively large (10-15 μm on average) compared to those in the other complexes. Similarly to Evisa and Khan Bogd, FI are concentrated in sealed fractures and on the edges of quartz crystals (Fig 5.8a). Some FI were also found in pseudomorphs of pegmatite. They occur in a rounded or irregular shape, with the exception of one population in granite (further details below). At Ambohimirahavavy, FI were studied locally in a skarn by Estrade et al. (2015) and will provide an interesting comparison, but no data is available for granite and pegmatite.

In granite and pegmatite of this complex, 9 types of FIA are distinguished petrographically. In an order of decreasing abundance, they are: (1) LV1, with an occasional trapped opaque, euhedral black crystal and a L/V ratio of 70/30 (Fig 5.8b,c); (2) LV2, secondary FI in sealed fractures crossing grains boundaries with a L/V ratio between 60/40 and 80/20 (Fig 5.8d); (3) LVS, the solid being a cube of salt (most likely halite); in some cases, these FI have a square shape in granite (Fig 5.8e); (4) V1, aqueous vapor-rich (Fig 5.8f); (5) LVS-LV1 associated together (Fig 5.8g); (6) LVSx, present only in pegmatite, with FI containing liquid, vapor, and with x representing a number of translucent solids between 2 and 5 on average (Fig 5.8h); (7) LV1-V1, only in pegmatite (Fig 5.8i); (8) LVS-V1, only in pegmatite (Fig 5.8j); (9) V2, made of pure CO_2 based on microthermometry measurements, rarely occurring and present only in granite.

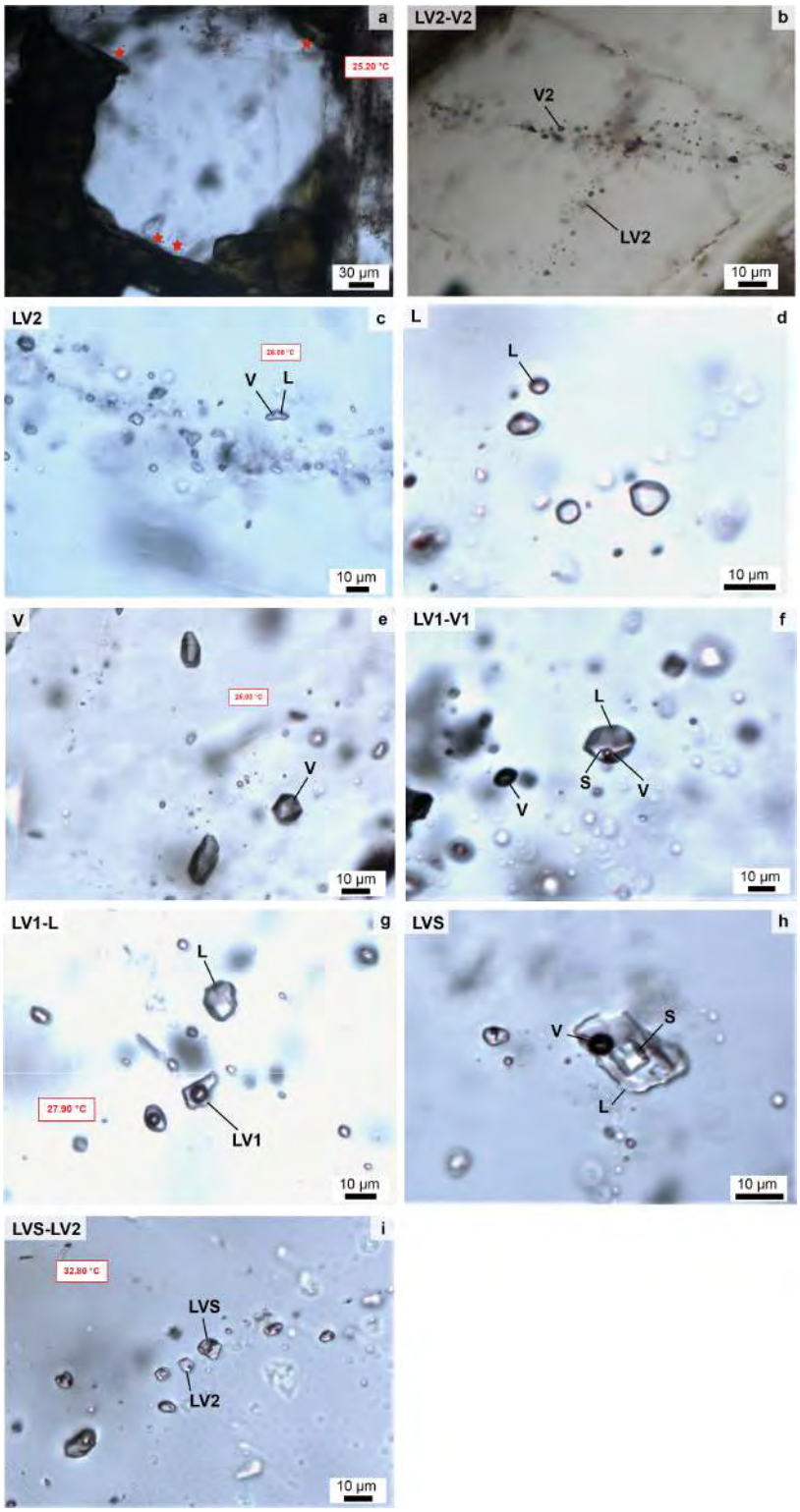

Figure 5.7 Photographs of representative fluid inclusions (FI) in quartz from Khan Bogd, Mongolia. (a) A quartz crystal with analyzed primary FI shown by red stars on its rims, sample KB07A; (b) LV2-V2 FIA in a sealed fracture, sample KB07A; (c) LV2 FIA, sample KB07A; (d) Liquid FI, sample KB04B; (e) Vapor FI with a thick meniscus, sample KB04B; (f) LV1-V1 FIA, with a black crystal in LV1, sample KB07A; (g) LV1-L FIA, sample KB04B; (h) LVS FIA, sample KB04B; (i) An assemblage of pseudosecondary LVS with LV2, sample KB04B

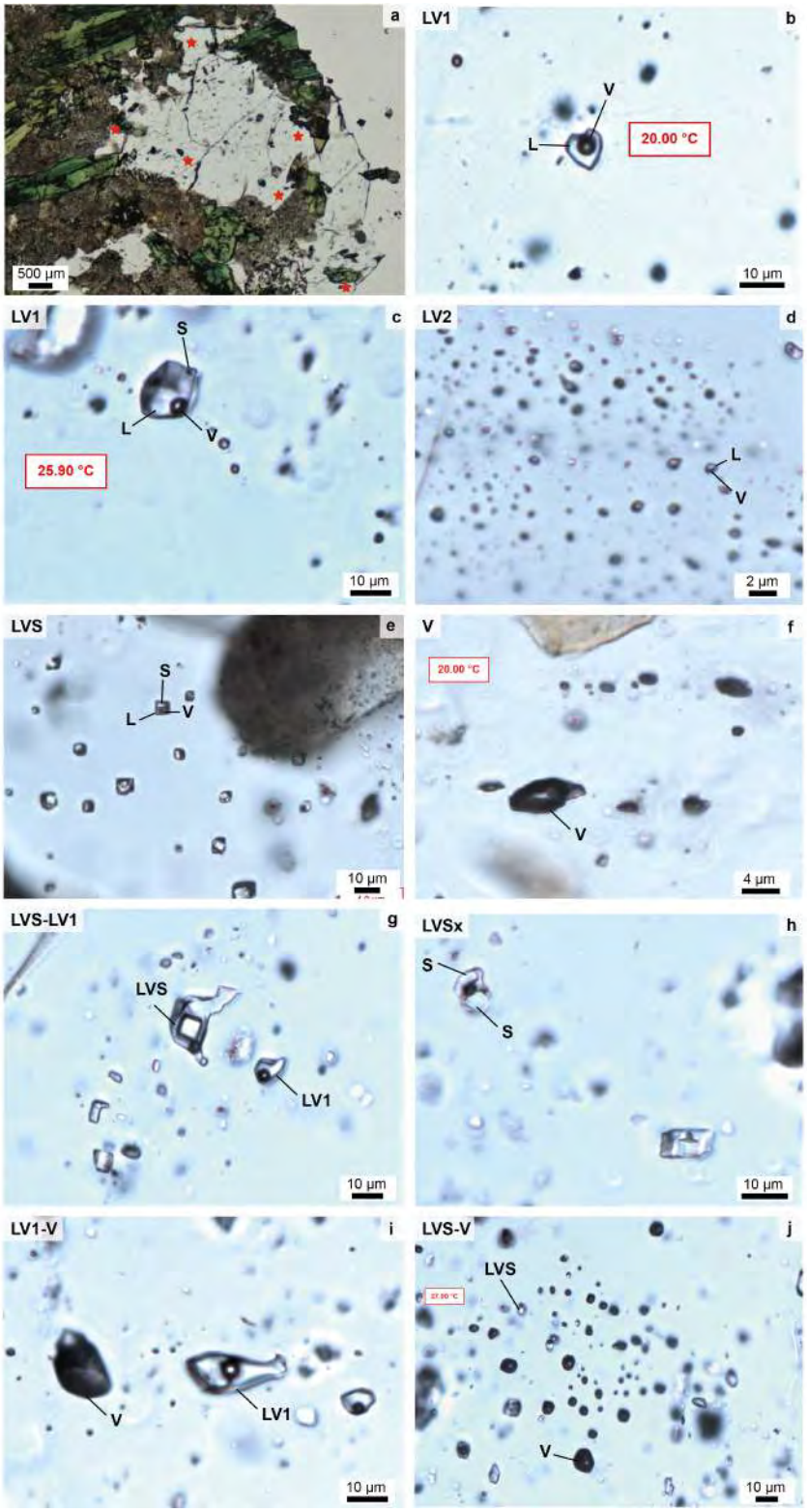

Figure 5.8 Photographs of representative fluid inclusions (FI) in quartz from Ambohimirahavy, Madagascar. (a) A quartz crystal with analyzed primary FI shown by red stars on its rims, sample AM35; (b) LV1 in the shape of a heart, because geology is lovable, sample AM35; (c) LV1 with a black trapped crystal, sample AM35; (d) LV2 FIA in a sealed fracture, sample AM35; (e) LVS FIA, sample AM107; (f) Vapor-rich FI, sample AM35; (g) LVS-LV1 FIA, sample AM35; (h) LVSx assemblage, with two solids, sample AM35; (i) LV1-V FIA, sample AM35; (j) LVS-V FIA, sample AM35

5.4.2.5 The Manongarivo complex, Madagascar

Fluid inclusions at Manongarivo are commonly rounded or irregular in shape and have an average size of 5-10 µm. They occur in all parts of quartz crystals but the core (Fig 5.9a). No data about FI is available in the literature, and unfortunately, due to poor sampling conditions, this study is based only on FI in pegmatites.

In pegmatites from Manongarivo, 7 types of FIA are petrographically distinguishable and very similar to those at Ambohimirahavavy: (1) LV1, with an occasional trapped euhedral black opaque crystal and a constant L/V ratio close to 80/20 (Fig 5.9b,c); (2) LV2, secondary in sealed fractures crossing grain boundaries with a L/V ratio between 70/30 and 90/10 (Fig 5.9d); (3) LVS with a cube of salt (Fig 5.9e); (4) V, aqueous vapor-rich (Fig 5.9f); (5) LV1-V (Fig 5.9g); (6) LV1-LVS (Fig 5.9h); (7) LVSx containing 2 to 5 solids similar to those at Ambohimirahavavy (Fig 5.9i). An aegirine crystal was also found trapped in a LV1 FI (Fig 5.9j).

5.4.2.6 The Strange Lake complex, Canada

As mentioned, the Strange Lake complex has been the subject of several studied, hence the following description is based on preexisting data from those works. The first description of FI in this complex was made by Salvi and Williams-Jones (1990, 1992), while the latest, more detailed one is provided by Vasyukova et al. (2016, 2018). Fluid inclusions were studied in pegmatite, hypersolvus granite, and subsolvus granite. They occur in irregular, rounded, or negative crystal shapes with sizes ranging from 5 to 40 μm, though mostly between 5 and 10 μm (Salvi and Williams-Jones, 1990; Vasyukova and Williams-Jones, 2016). In granite, FI were also found in or at the boundaries of pseudomorphs (Salvi and Williams-Jones, 1990).

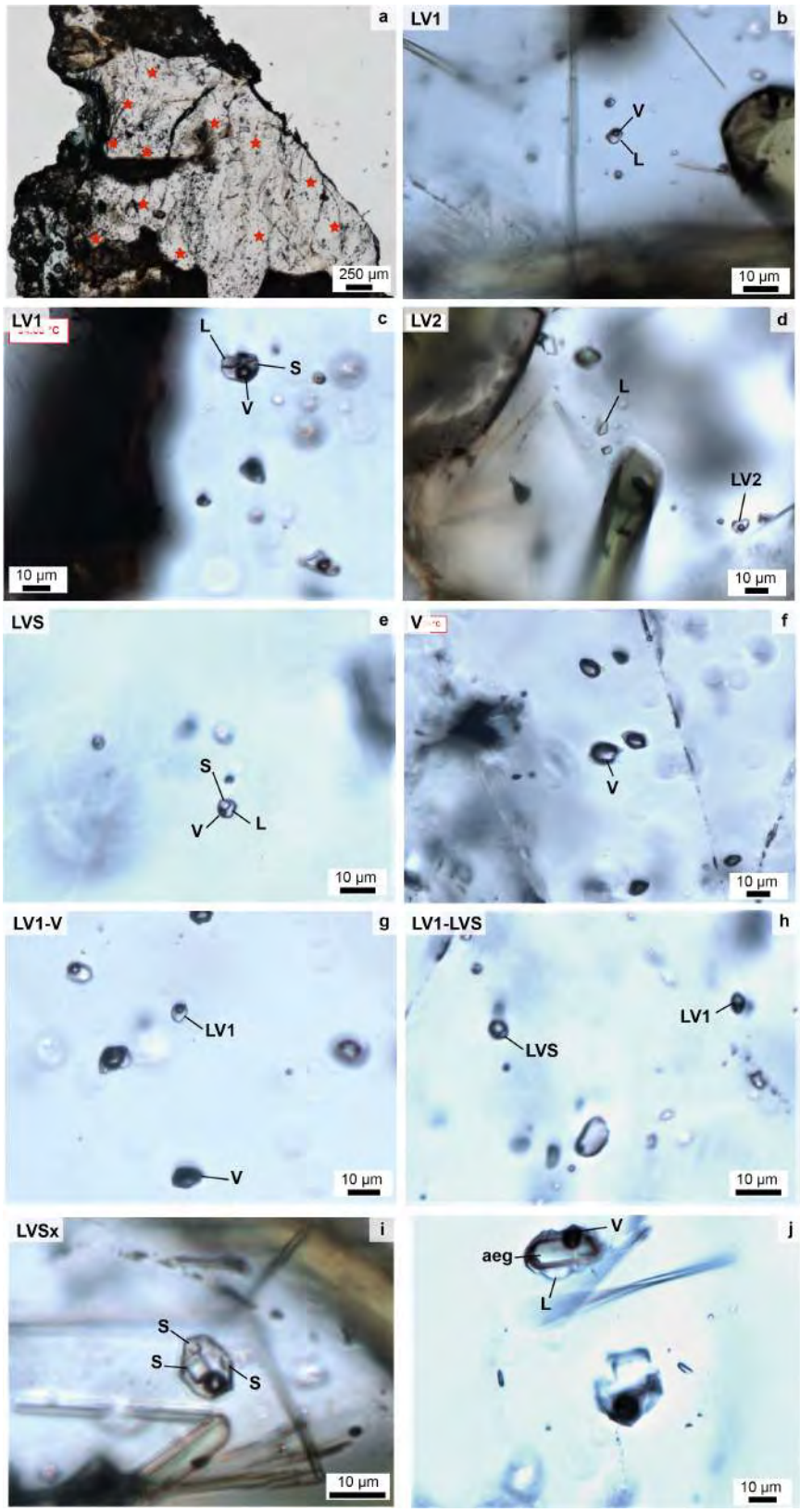

Figure 5.9 Photographs of representative fluid inclusions (FI) in quartz from Manongarivo, Madagascar. (a) A quartz crystal with analyzed primary FI shown by red stars on its rims, sample 688; (b) LV1 FI, sample 688; (c) LV1 FI with a trapped black crystal, sample 688; (d) LV2 FIA in a sealed fracture, sample 688; (e) LVS with a cubic, sample 688; (f) Vapor-rich, sample 688; (g) LV1-V FIA, sample 688; (h) LV1-LVS FIA, sample 688; (i) LVSx FI with 3 translucent solids, sample 689; (j) Aegirine trapped in a liquid-vapor IF, sample 688

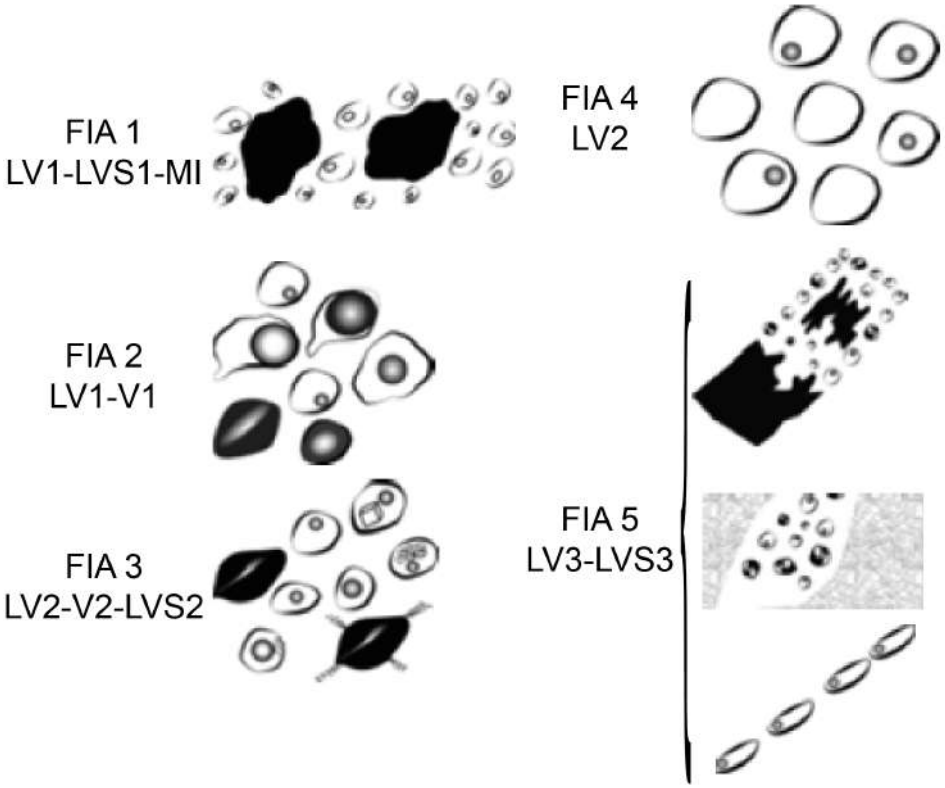

Figure 5.10 Schematic representation of the five FIA types at Strange Lake, modified from Vasyukova et al. (2016)

Five assemblage types are described by Vasyukova et al. (2016) and represented in Fig 5.10: (1) LV1-LVS1, in pegmatites, associated with MI, in which LV1 type occurs as 5-10 μm inclusions with a L/V ratio of 90/10, and the solid in LVS1 is halite; (2) LV1-V1, in pegmatite and hypersolvus granite, and in which LV1 are 5-30 μm in diameter and V1 contain a carbonic phase CH_4-dominated; (3) LV2-V2-LVS2, in pegmatite, in which LV2 have a L/V ratio of 90/10 and a size of 10-20 μm, V2 are CO_2-,CH_4-dominated, and LVS2 are aqueous carbonic with a nahcolite crystal; (4) LV2, in pegmatite; (5) LV3-LVS3, in pegmatites and subsolvus granite, which occur in pseudomorphs and along healed fractures, in which LV3 are 5-10 μm inclusions with a L/V ratio of 95/5 and LVS3 is aqueous and rich in minerals of the pseudomorph they are in (gittinsite-quartz-zircon, titanite-quartz-fluorite) or in albite or microcline.

5.5 Results

5.5.1 Identification of populations and microthermometry data

Microthermometry measurements were challenging in some complexes but also in some FIA, such as vapor-rich ones. Hence, as described in the following paragraphs, only a restricted dataset was acquired for them. For the same reason, although all observed FIA were described in the previous section, not all of them were measured. In addition, only a few secondary FI were measured in this study as they were trapped after the complexes emplacement; some of them were however measured to compare their properties to primary FI.

The following microthermometry measurements focused on 3 specific temperatures. The eutectic temperature (T_e) is the temperature at which the analyzed FI begins to melt; it indicates which are the main salts in the inclusion. The melting temperature (T_m) is the temperature at which the whole inclusion is melted, and it shows the overall salinity of the inclusion. Finally, the homogenization temperature (T_h) is the temperature at which all phases contained in the FI homogenize as only one phase; it indicates the minimum temperature at which the fluid was circulating when it got trapped.

5.5.1.1 The Amis complex, Namibia

In granite as much as in pegmatite from Amis, T_e of LV1 inclusions is between -40 and -55 °C. This indicates that solutes other than NaCl are present (T_e H_2O-NaCl is - 21.2 °C, Linke, 1958). The eutectic temperature of the H_2O-$CaCl_2$ system is at -49.8 °C (Linke, 1958), and T_e until -55 °C indicate there is a mixing with KCl (T_e=-50.5 °C), $MgCl_2$ (T_e=-52.2 °C), or NaCl (T_e=-55 °C). The study of salt mounds with the SEM will help determining which salt is indeed present with NaCl. The eutectic temperature of LVS2, however, is systematically close to -55 °C indicating a probable H_2O-NaCl-$CaCl_2$ composition.

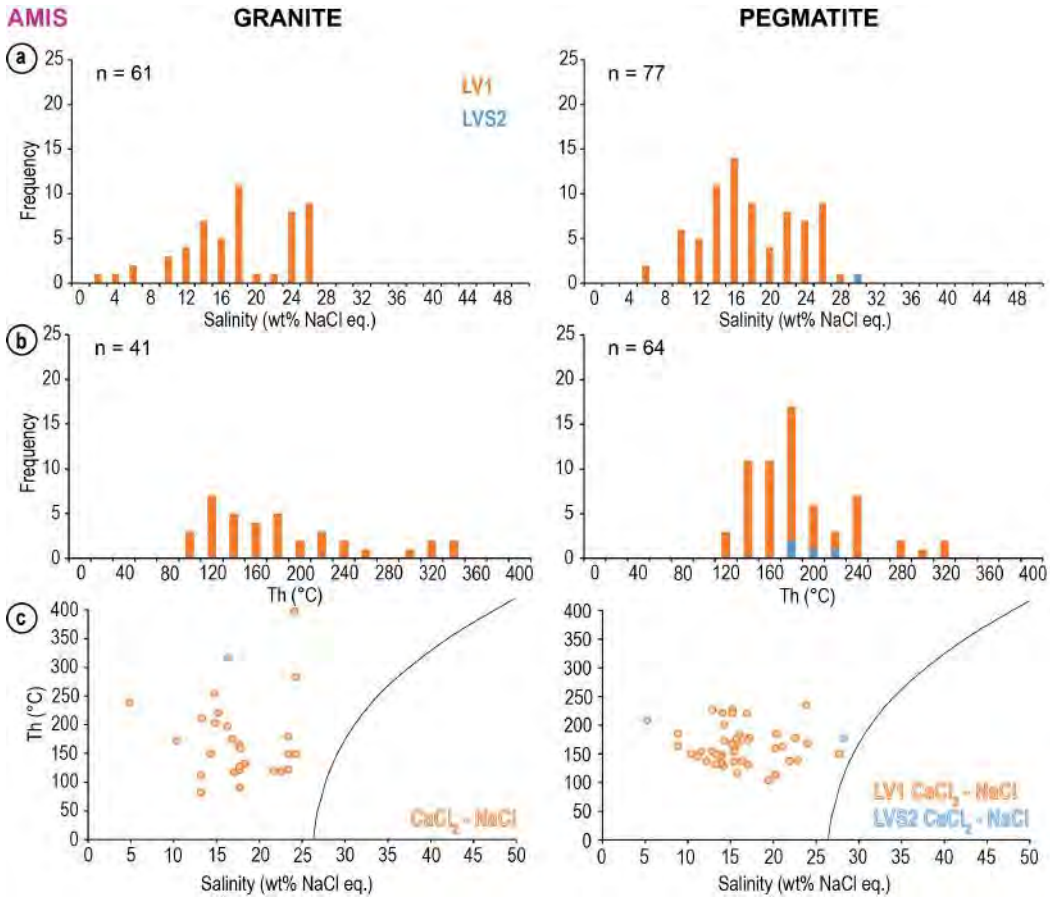

Figure 5.11 Diagrams showing salinities and temperature of FI in pegmatite and granite from Amis, Namibia. (a) Histogram of salinities; (b) Histogram of temperatures; (c) Graphs showing homogenization temperature as a function of salinity; the circled LVS dot shows a maximum temperature (decrepitation); the black curve is the halite liquidus

At Amis, no vapor-dominated FI was measured in the granite, and only a low number of LVS2 in pegmatite were. No hydrates were spotted, hence it is not possible to give the precise proportion between NaCl and $CaCl_2$. Salinities of LV1 in granite range from 2 to 26 wt% NaCl eq., with two peaks at 18 and 24-26 wt% NaCl eq. In comparison, LV1 in pegmatites show a slightly more restricted range of salinity, from 6 to 28 wt% NaCl eq., but with similar peaks at 16 and 26 wt% NaCl eq. In pegmatite, the only LVS2 measured gives a salinity of 30 wt% NaCl eq. (Fig 5.11a). Temperatures of homogenization of LV1 in granite and pegmatite are also similar and bimodal, ranging from 100 to 340 °C with two maximums at 180 and 320-340 °C (Fig 5.11b). However, the data temperatures in granite show a wider spread than in pegmatite, between 100 and 220 °C. LVS2 FI in pegmatite homogenize by halite dissolution from 180 to 220 °C, and a few of them decrepitated at 350 °C after halite dissolution. The few secondary LV2 inclusions measured have moderate

salinities (21 wt% NaCl eq.) and quite low T_h (130-145 °C).

Diagrams of T_h as a function of salinity are provided in Fig 5.11c. Unfortunately, T_h and salinity were not measured in the same LVS2 inclusions in pegmatite, hence only the maximum value (decrepitation) is shown for one inclusion. Inclusions in the granite seem dispersed, while in the pegmatite LV1 inclusions concentrate in a smaller range of temperature, as observed in Fig 5.11b.

5.5.1.2 The Evisa complex, Corsica

Eutectic temperatures data for LV1 inclusions in pegmatite from Evisa form two clusters: one at -23 °C, and one around -48 °C. In granite, only the second cluster was found. In pegmatite, more data needs to be acquired to understand the precise relationship between these two populations. According to Linke (1958), the temperature of -23.5 °C matches a composition of H_2O-NaCl-KCl, and -49.8 °C is the eutectic temperature of a mixture H_2O-$CaCl_2$.

At Evisa, similarly to Amis, most of the FI measured were LV1 type. In granite, some inclusions were measured in pseudomorphs, and they show the same range of temperature and salinity data than FI outside pseudomorphs (Fig 5.12). In granite, LV1 salinities range from 0 to 26 wt% NaCl eq., with two maximums at 2-10 and 16-18 wt% NaCl eq. In pegmatites the range of salinities is similar, with maximums at 2-6, 14, and 18-22 wt% NaCl eq. In addition, one vapor FI was measured in the granite, and its salinity is of 18 wt% NaCl eq., which matches one of the maximums of LV1 inclusions (Fig 5.12a). Homogenization temperature tendencies are reversed compared to Amis, i.e. the range is much higher in pegmatite than in granite. In granite, they range from 120 to 260 °C, with a maximum at 160-180 °C; in pegmatite, they range from 80 to 360 °C with maximums at 100 and 180 °C (Fig 5.12b).

Diagrams T_h-salinity (Fig 5.12c) for granite show FI with a restricted Th range, whereas for pegmatite, two groups are distinguishable: one with salinity <6 wt% NaCl eq. and temperature ranging from 150 to 300 °C, and the other with salinity above 10 wt% NaCl eq. and temperatures between 100 and 200 °C.

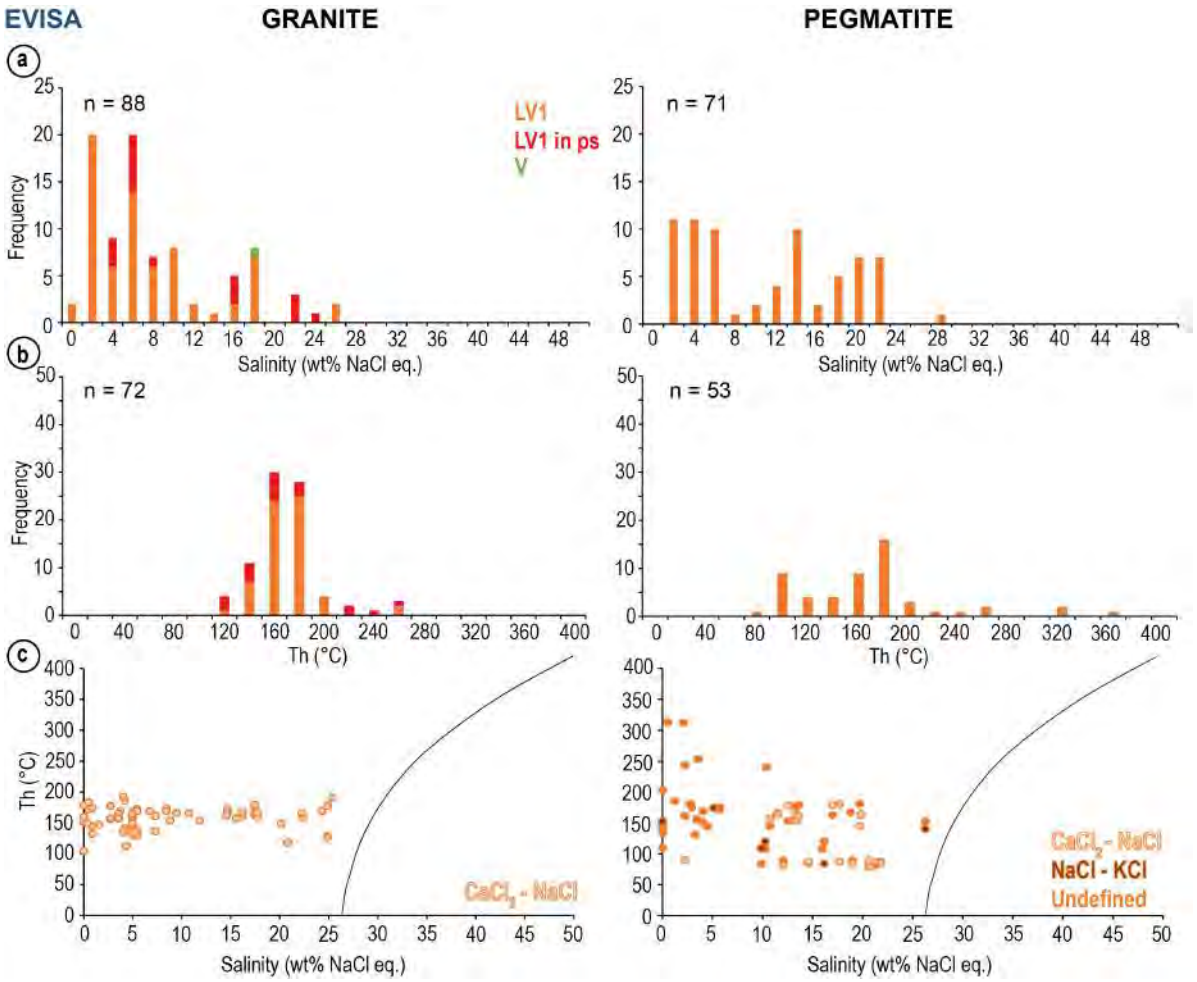

Figure 5.12 Diagrams showing salinities and temperature of FI in pegmatite and granite from Evisa, Corsica. (a) Histogram of salinities; (b) Histogram of temperatures, note that the frequency is more important for the granite; (c) Graphs showing homogenization temperature as a function of salinity; the black curve is the halite liquidus. Abbreviation: ps: pseudomorph

5.5.1.3 The Khan Bogd complex, Mongolia

At Khan Bogd, eutectic temperatures of L inclusions in granite are close to -23 °C, suggesting the system H_2O-NaCl-KCl. In the pegmatite, some L have the same T_e, but others have Te around -48 °C, close to T_e of the system H_2O-$CaCl_2$. Inclusions made of LV and LVS in granite and pegmatite are similar, with T_e ranging from -23 to -32 °C. These temperatures indicate that NaCl is not the only salt, and KCl, $CaCl_2$ and/or $MgCl_2$ are probably also present. The study of salt mounds will help with the determination of the salts actually present.

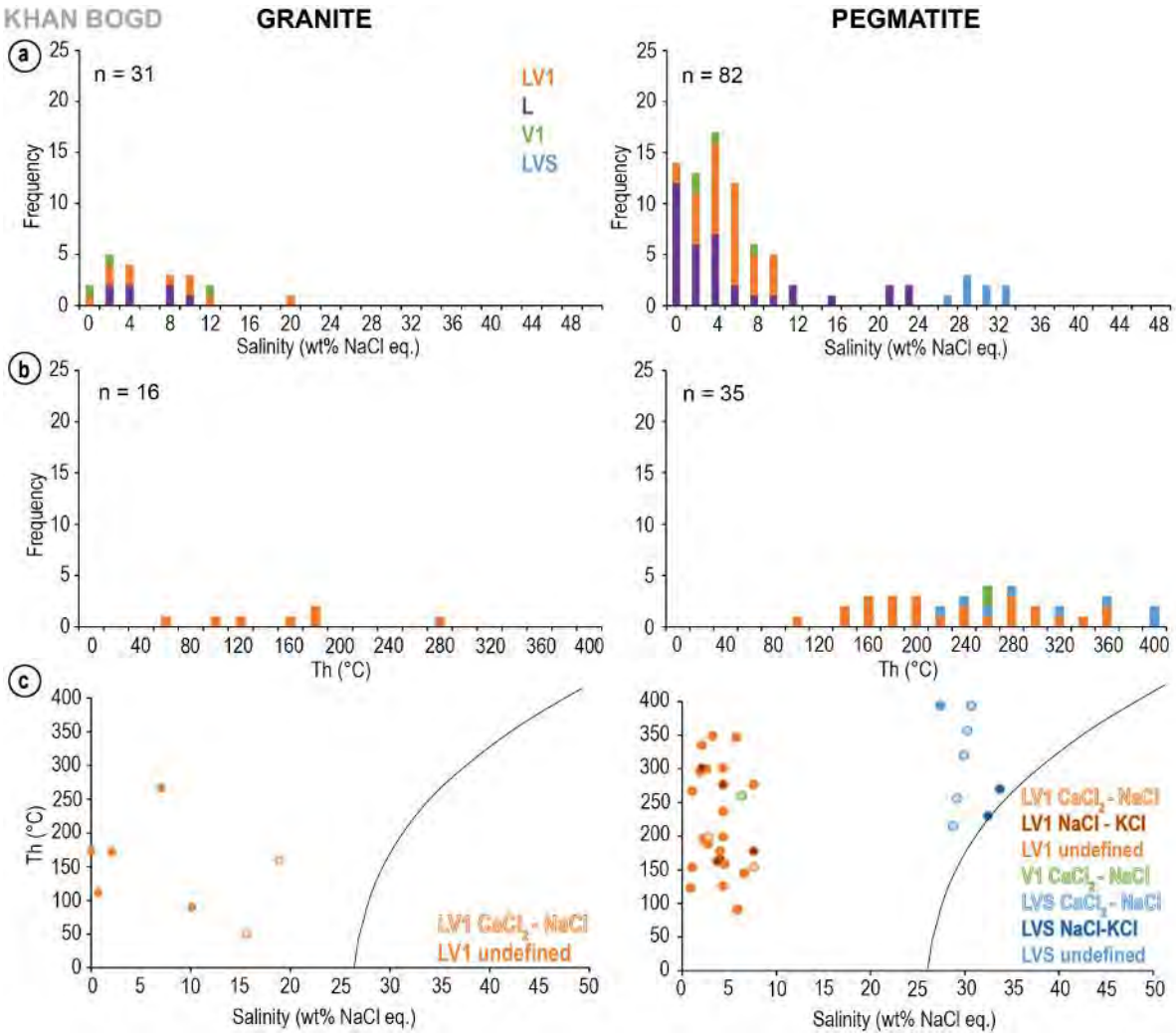

Figure 5.13 Diagrams showing salinities and temperature of FI in pegmatite and granite from Khan Bogd, Mongolia. (a) Histogram of salinities; (b) Histogram of temperatures; (c) Graphs showing homogenization temperature as a function of salinity; the black curve is the halite liquidus

The low number of primary FI as well as their small size led to only a restricted number of microthermometric measurements. In addition, the majority of primary FI is liquid only and a vapor bubble did not appear even upon repeated cooling runs, hence it was impossible to acquire temperature data. LV1 inclusions have mostly low to moderate salinities in granite and pegmatite, from 0 to 12 wt% NaCl eq., with a majority under 6 wt% NaCl eq. Two inclusions, rich in $CaCl_2$, have salinities > 15 wt% NaCl eq. in the granite. Salinities for V1 and L inclusions are similar, and some L FI in the pegmatite have salinities of 22-24 wt% NaCl eq (Fig 5.13a). In the pegmatite, LVS inclusions commonly nucleate hydrohalite around -24 °C at the expense of the salt cube, which is hence halite (Fig 5.14).

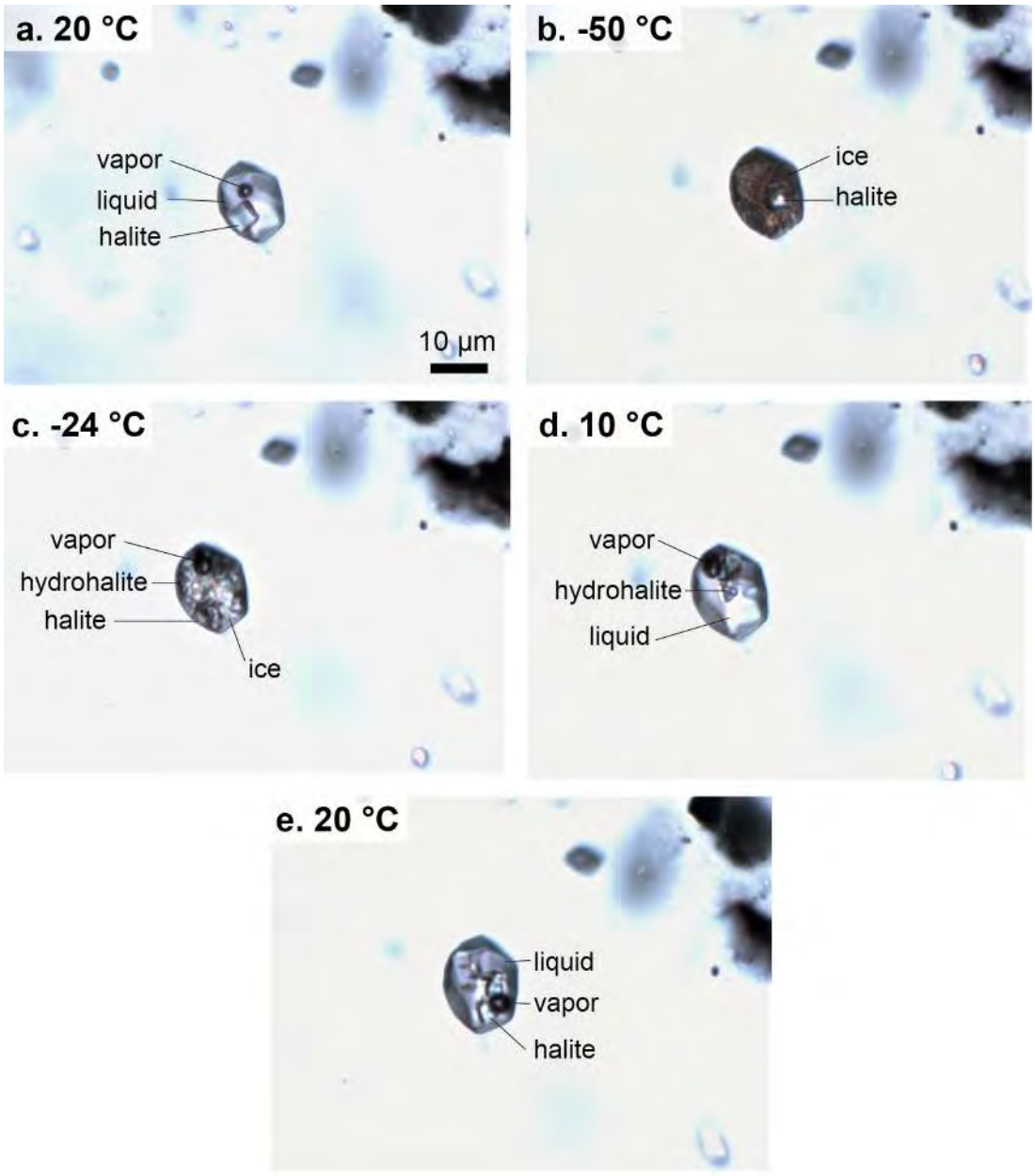

Figure 5.14 Evolution of an LVS FI evolution under cooling at Khan Bogd, sample KB04B. (a) Initial state at 20 °C with a vapor bubble and a cube of halite; (b) Totally frozen inclusion, the vapor bubble disappeared; (c) Ice begins to cool, the vapor bubble reappeared, and hydrohalite begins to replace the cube of halite; (d) Metastable hydrohalite remains above 0 °C; (e) Final state back to 20 °C, hydrohalite disappeared and several halite cube reformed

This replacement allows a precise determination of the salinity of these inclusions, which is 28-34 wt% NaCl eq. Homogenization temperatures of LV1 inclusions may not be very representative, because of the paucity of data, and because the few measurements are highly scattered, from 50 to 280 °C in granite and 100 to 360 °C in pegmatite, with no defined peak (Fig 5.13b). A number of LV FI in granite

decrepitated around 325 °C. Vapor inclusions measured in the pegmatite gave a temperature of 260 °C. In pegmatite, LVS inclusions have higher T_h than LV, but still with a high spreading, from 220 to 400 °C.

The low amount of data does not permit to draw any conclusion from the T_h-salinity diagram in the granite (Fig 5.13c). However, in pegmatite, the difference between LV1 and LVS inclusions is obvious, with a salinity gap of 15 wt% and a higher T_h for LVS inclusions.

5.5.1.4 The Ambohimirahavavy complex, Madagascar

At Ambohimirahavavy, most inclusions, either LV1 or LVS, have T_e at -23 $\pm$ 0.5 °C, indicating they can be modeled in the H_2O-NaCl-KCl system. Salinity data are compact compared to the other studied complexes. LV1 inclusions in granite have salinities between 2 and 6 wt% NaCl eq., with a maximum at 2 wt%. This tendency also occurs for the pegmatite, although some LV1 inclusions have higher salinities, from 16 to 20 wt% NaCl eq. In the pegmatite, V1 inclusions have salinities of 2-4 wt% NaCl, whereas LVS show salinities of 32-48 wt% NaCl eq., with a maximum at 46 wt% (Fig 5.14a). Homogenization temperatures in LV1 in both granite and pegmatite range from 180 to 400 °C, with a peak at 300-340 °C. In pegmatite V1 inclusions have T_h between 300 and 340 °C. LVS inclusions in pegmatite also present high temperatures, 300-400 °C with a maximum at 380 °C (Fig 5.14b). Some LV1 inclusions in the pegmatite decrepitated at 360 °C, and LVS in the granite decrepitated at 400-470 °C.

A plot of T_h as a function of salinity for FI data in the granite shows only one population of LV1 inclusions. For the pegmatite, it is obvious that LV1 and V1 inclusions have the same characteristics. LVS inclusions in pegmatite have much higher salinities and align perfectly along halite liquidus (Fig 5.14c).

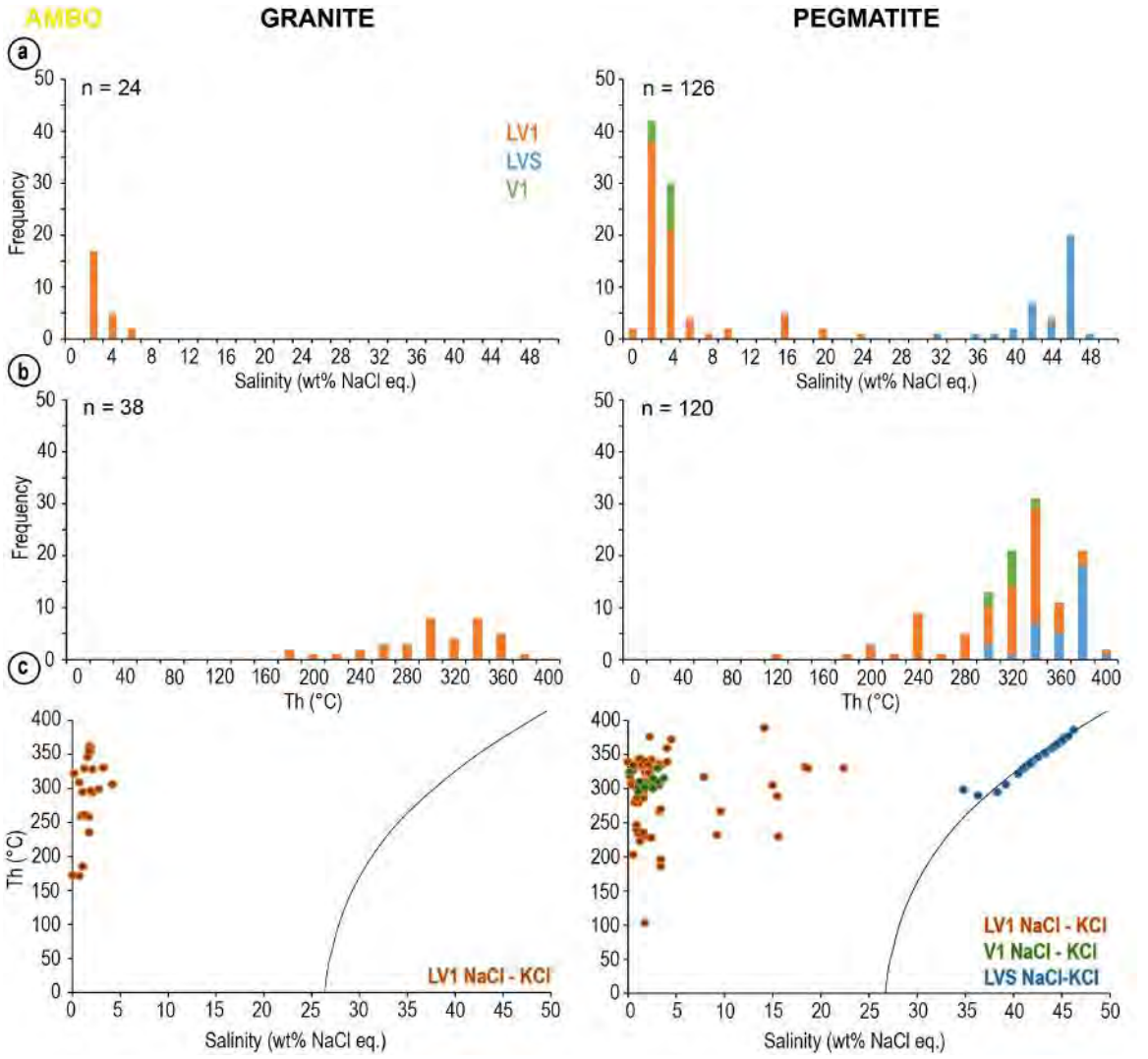

Figure 5.15 Diagrams showing salinities and temperature of FI in pegmatite and granite from Ambohimirahavavy, Madagascar. (a) Histogram of salinities; (b) Histogram of temperatures; (c) Graphs showing homogenization temperature as a function of salinity; the black curve is the halite liquidus

5.5.1.5 The Manongarivo complex, Madagascar

At Manongarivo, two tendencies are observed regarding eutectic temperatures. LV1 inclusions can have T_e close to -23 °C or to -35 °C. Eutectic temperatures of LVS inclusions are mostly close to -35 °C. The value of -23 °C indicates the presence of the system H_2O-NaCl-KCl. The value of -35 °C matches the system H_2O-NaCl-$MgCl_2$, but it is possible that this value is underestimated, hence the presence of KCl and $CaCl_2$ is not excluded and will be determined with the SEM on salt mounds. More data needs to be acquired to understand the precise relationship

between the two populations.

Salinities of LV1 inclusions are spread from 0 to 26 wt% NaCl eq., with maximums at 2 and 16 wt%. Vapor-dominated inclusions have similar salinities of 4-20 wt% NaCl eq. LVS inclusions have much higher salinities, from 36 to 50 wt% NaCl eq., with a maximum at 44-46 wt% (Fig 5.16a). Homogenization temperatures of LV1 inclusions range from 120 to 380 °C, with a net maximum around 300 °C. Vapor inclusions have slightly higher T_h, from 320 to 380 °C. LVS inclusions have even higher T_h, from 360 to 400 °C, with a maximum at 360-380 °C (Fig 5.16b). Many LV1 inclusions decrepitated at 330 °C, and many LVS at 420 °C.

Similarly to Ambohimirahavavy, the diagram T_h-salinity shows that LV1 and V inclusions have similar properties, whereas LVS inclusions have higher T_h and salinities. They also align along halite liquidus (Fig 5.16c).

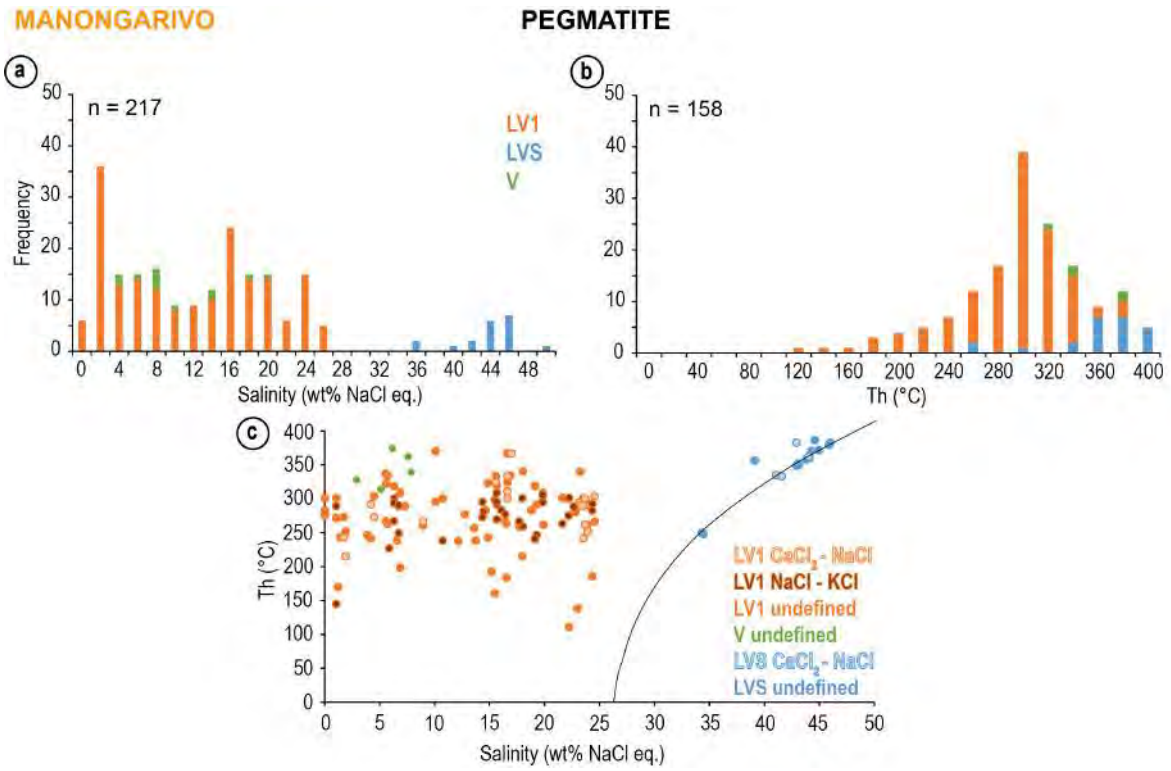

Figure 5.16 Diagrams showing salinities and temperature of FI in pegmatite from Manongarivo, Madagascar. (a) Histogram of salinities; (b) Histogram of temperatures; (c) Graphs showing homogenization temperature as a function of salinity; the black curve is the halite liquidus

5.5.1.6 The Strange Lake complex, Canada

At Strange Lake (Fig 5.17), Vasyukova et al. (2016) found that LV1 inclusions have salinities of 10-34 wt% NaCl eq., with maximums at 25, 23, 16 and 13 wt%. LV2 provide a range of 0.8-21 wt% NaCl eq. with maximum at 10 wt% NaCl eq.

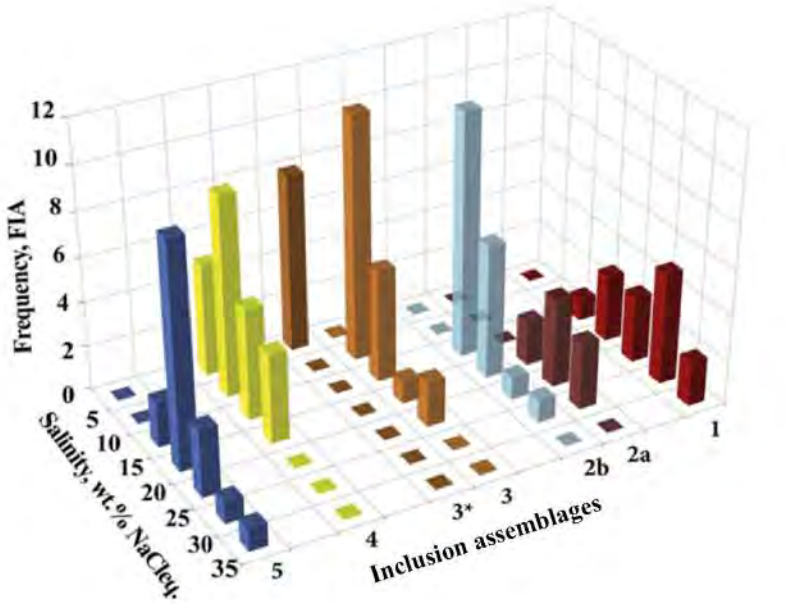

FI type	Salinity (wt% NaCl eq.) Range /Maximums	Th (°C) Range /Maximums	Decre-pitation T (°C)	Te (°C)	Representative petrographic sketch
LV1	10-34 / 25, 23, 16, 16	85-221 / 110, 114, 147, 221	180	-22 to -11	
LV2	0.8-21 / 10	80-180 / 80, 146	150-200		
LV3	17-27 / 18	71-125		-50	
V1 (CH4)		n.d. / -80			
V2 (CO2-CH4)	n.d. / 4	-5.8 to 31 / -5.8, 24-28			
LVS1 (halite)	15-34	n.d. / 185			
LVS2 (nahcolite)	4.2-13.6	70-95			
LVS3 (silicates)	17-27	71-125		-50	

Figure 5.17 Recapitulative of microthermometry data acquired at Strange Lake by Vasykova et al. (2016). Histograms show salinities of the 5 FIA found in this complex. Only aqueous FI are represented. Assemblage 2a has LV1 with higher salinities than 2b, and assemblage 3* represent V2 FI for which salinity was determined from the temperature of clathrate melting. The table summarizes the information about the different FI types, as no histogram for T_h is provided in the paper

LV3 range between 17 and 27 wt% NaCl eq. with a maximum at 18 wt%. V2 inclusions, CH_4 and CO_2-bearing, have a salinity around 4 wt% NaCl eq. Finally, no salinity data is provided for LVS1 (halite) inclusions; LVS2 (nahcolite) have salinities of 4-14 wt% NaCl eq., and LVS3 (various silicates) of 17-27 wt% NaCl eq. Homogenization temperature of LV1 range from 85 to 221 °C, with maximums at 110, 114, 147 and 221 °C; many inclusions decrepitated around 180 °C. LV2 T_h range from 80 to 180 °C, with maximums at 80 and 146 °C; many decrepitated at 150-200 °C. LV3 T_h are low and range from 71 to 125 °C. V1 inclusions (CH_4) have T_h around -80 °C, and V2 with a lot of CO_2 have T_h of -5.8 to 31 °C with maximums at -5.8 and 24-28 °C. Homogenization temperatures of LVS are close to 185 °C on average for type 1, 70-95 °C for type 2, and 71-125 °C for type 3.

Not much information is provided on eutectic temperatures. LV1 inclusions have Te ranging from -22 to -11 °C, most of them being close to -22 °C. This indicates they are probably made of a mix of H_2O-NaCl-KCl. Some LV3 and LVS3 inclusions have T_e close to -50 °C, indicating the presence of $CaCl_2$ (Fig 5.17).

5.5.2 SEM study of solids in fluid inclusions

In rocks where the grain size was big enough to allow it, opened inclusions were analyzed with the SEM to try to identify the solids in LVS FI. Unfortunately, most opened inclusions were empty, and only one solid was found in the granite sample from Khan Bogd (Fig 5.18). This is probably related to the low number of solids observed in FI, enhanced by the opened inclusions technique which mostly relies on luck to find them. In addition, the observed solid is made of round aggregates, hence is different from the opaque black solid described in the previous petrography section. The EDS spectrum of this solid shows it is made of Ca, Ce and C at least (Fig 5.18g). The presence of F is unlikely but not excluded as its main ray, Kα, is close to the Mα ray of Ce. Hence, this mineral could be parisite-(Ce) or synchisite-(Ce) if F were indeed present, which would make sense as these minerals are present elsewhere in the rock. In the more likely absence of F, the identification of this phase is trickier: it could be calcioancylite-(Ce) or galgenbergite-(Ce), two hydrated carbonates of REE.

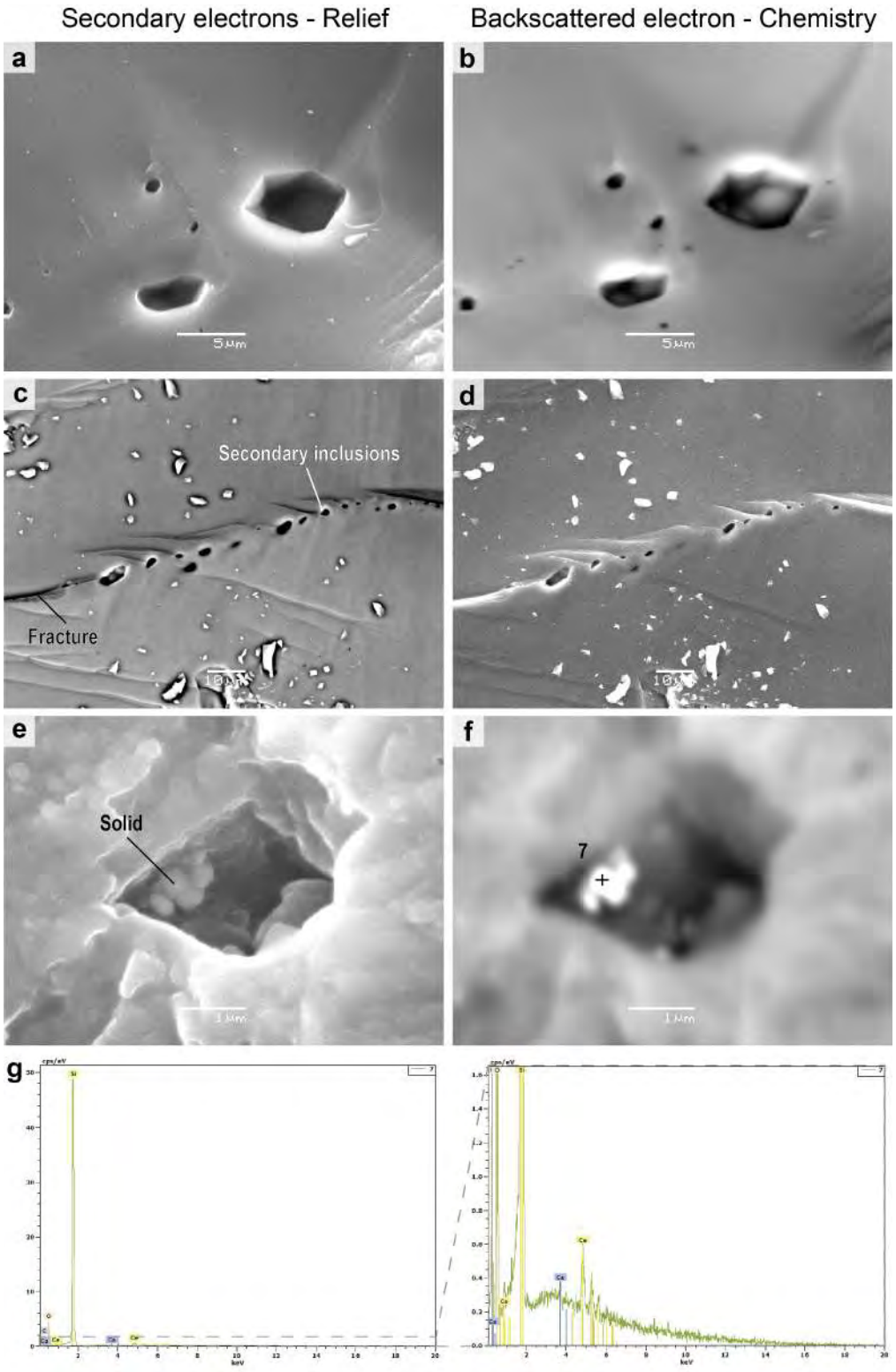

Figure 5.18 SEM photographs and EDS spectra showing opened fluid inclusions at Khan Bogd. (a), (b) Empty primary FI of different sizes and shapes at Khan Bogd (KB04B); (c), (d) Empty secondary FI aligned in a sealed fracture at Khan Bogd (KB04B); (e),(f) Primary FI with a solid inside from Khan Bogd (KB07A); (g) BSE-EDS spectrum of point 7 shown in (f) with a zoom on Ce peaks

5.5.3 Evaporate salt mounds

Although eutectic temperatures provide clues as to the salt composition of FI, these measures can be unprecise and are very difficult to obtain. Hence, a study of decrepitated inclusions and associated salt mounds was performed, using the SEM. With this technique, only atoms are seen, and the way they bond together is an interpretation. The presence of Cl with Na, K or Ca is interpreted as the presence of salt molecules.

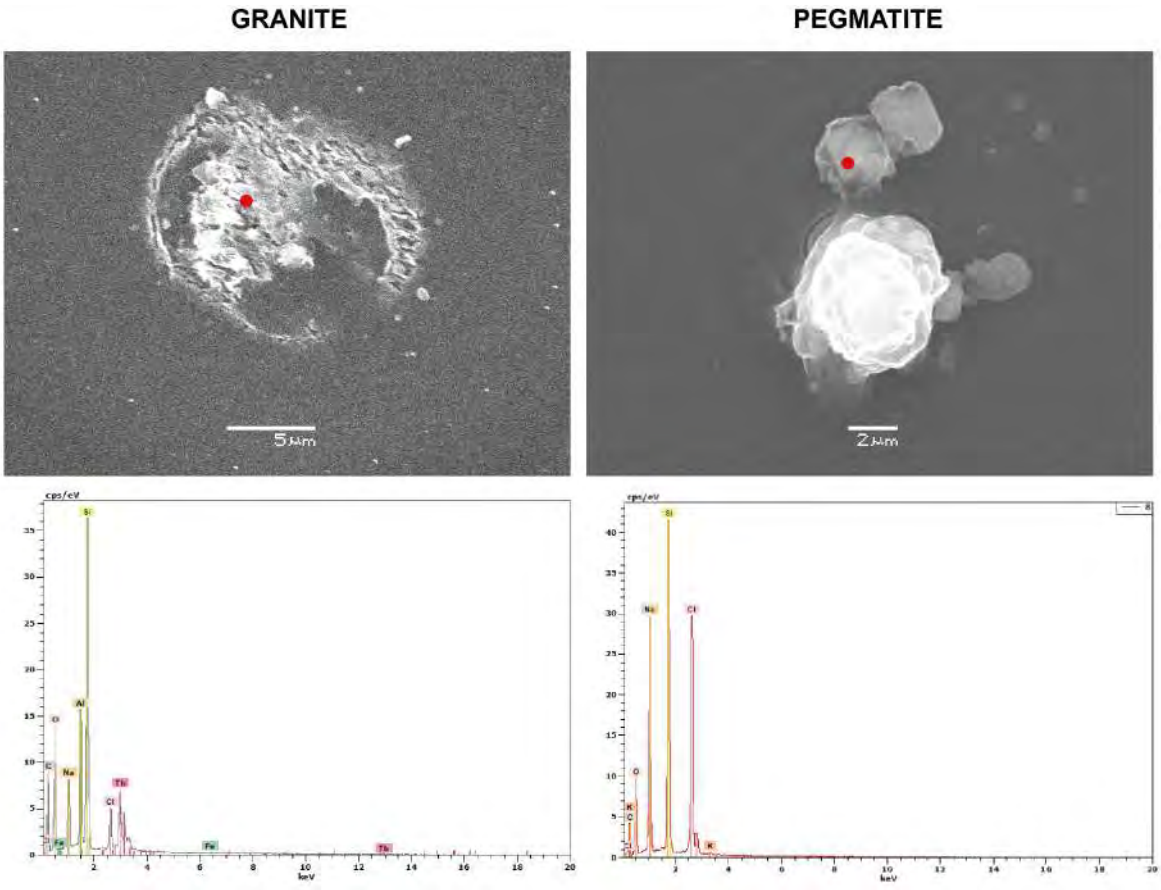

Figure 5.19 Secondary electrons-SEM photographs of decrepited FI forming salt mounds in granite and pegmatite at Amis, Namibia and their matching EDS spectra. The red dot on SEM images match the location of the associated spectrum below

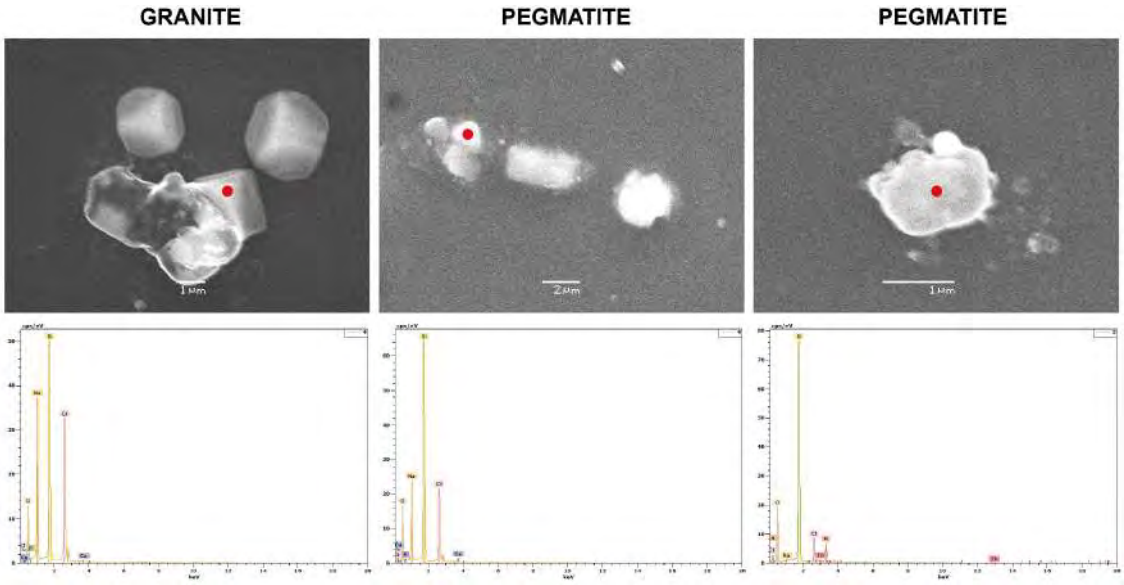

Figure 5.20 Secondary electrons-SEM photographs of decrepited FI forming salt mounds in granite and pegmatite at Evisa, Corsica and their matching EDS spectra. The red dot on SEM images match the location of the associated spectrum below

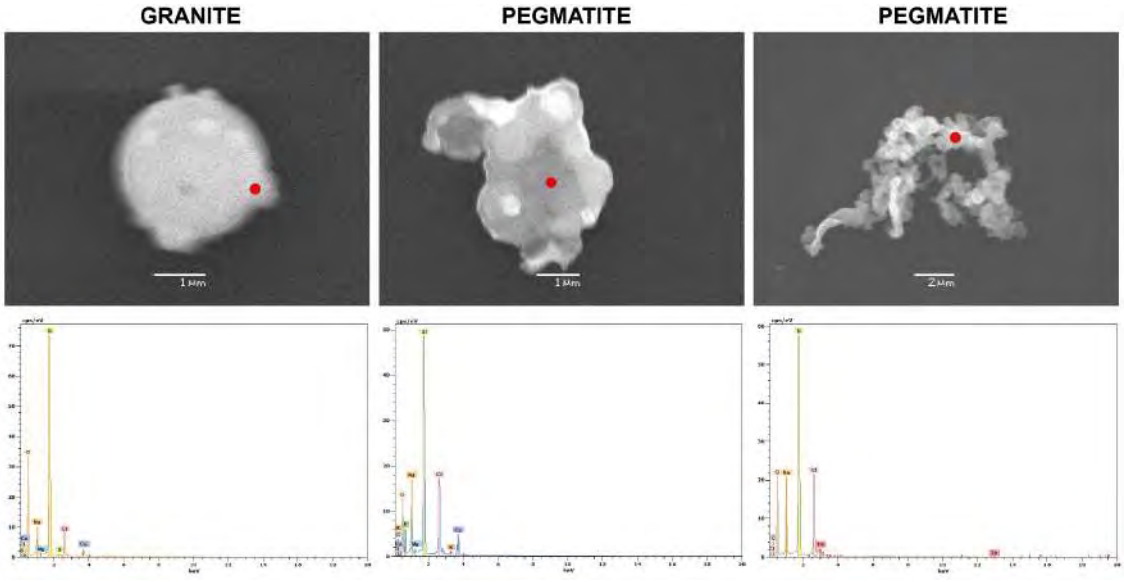

Figure 5.21 Secondary electrons-SEM photographs of decrepited FI forming salt mounds in granite and pegmatite at Khan Bogd, Mongolia and their matching EDS spectra. The red dot on SEM images match the location of the associated spectrum below

At Amis, only a few salt mounds could be observed, in both granite and pegmatite. Most of them contain a majority of NaCl with a bit of KCl; some FI in the granite also contain Al and Th (Fig 5.19). However, T_e (ranging between -40 and -55 °C) indicates the presence of $CaCl_2$, which was not found in these

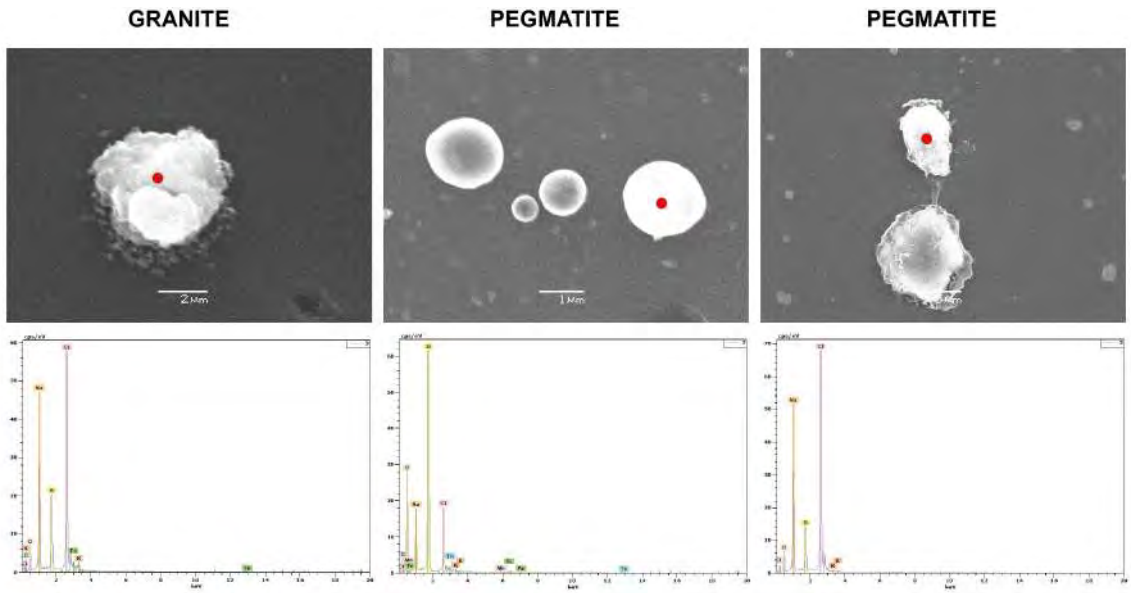

Figure 5.22 Secondary electrons-SEM photographs of decrepited FI forming salt mounds in granite and pegmatite at Ambohimirahavavy, Madagascar and their matching EDS spectra. The red dot on SEM images match the location of the associated spectrum below

salt mounds. At Evisa, two chemistries of FI were found in salt mounds. The first one is common to granite and pegmatite, and consists of NaCl plus $CaCl_2$ in a smaller proportion. F^- was also detected (Fig 5.20). The second chemistry was found only in the pegmatite and consits of a mix of NaCl and KCl, plus Th, occasionally (Fig 5.20). These observations are consistent with the bimodal T_e (respectively -23 and -48 °C) measured by microthermometry. At Khan Bogd, similarly to Evisa, two compositions were found, the first one being common to granite and pegmatite, and the second observed only in the pegmatite. The common chemistry is made of NaCl and $CaCl_2$ mostly, with traces of KCl, $MgCl_2$, F^-, and S^{2-} (Fig 5.21), whereas the chemistry found only in pegmatite is made of NaCl alone, with Th in a few cases (Fig 5.21). These observations mostly match those made with T_e, except for the temperature of -23 °C which suggests the presence of NaCl plus KCl in the inclusions, yet K was not detected in the salt mounds. At Ambohimirahavavy, inclusions with NaCl, KCl and occasional Th were found in granite and pegmatite. In addition, salt mounds where Th was detected can also contain Mn and Fe (Fig 5.22). This matches exactly the conclusions previously drawn from T_e of -23 $\pm$ 0.5 °C. In pegmatites from Manongarivo, the majority of evaporate salt mounds indicate the presence of NaCl, KCl and S^{2-} in FI. However, some mounds consisted of a mix of NaCl, KCl, $CaCl_2$, Al and S^{2-} (Fig 5.23). The

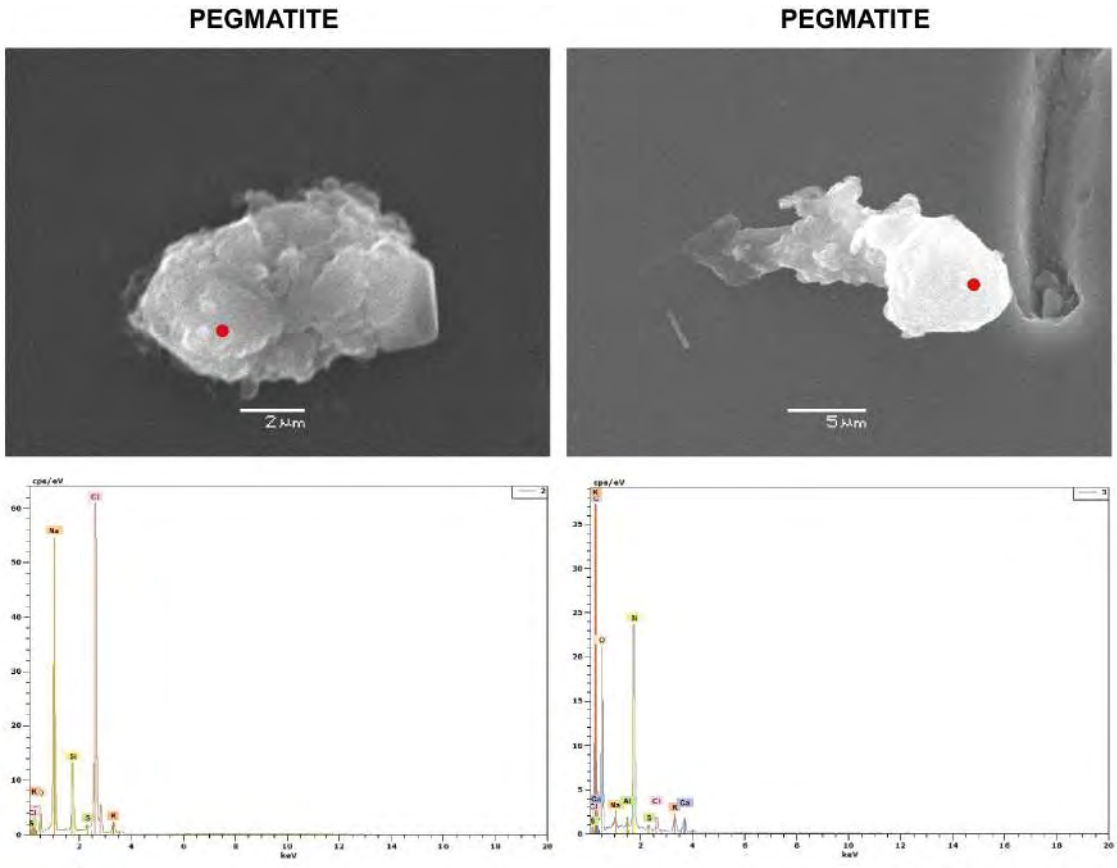

Figure 5.23 Secondary electrons-SEM photographs of decrepited FI forming salt mounds in pegmatite at Manongarivo, Madagascar and their matching EDS spectra. The red dot on SEM images match the location of the associated spectrum below

main composition of these inclusions matches the T_e measurements of -23 and -35 °C. At Strange Lake, Salvi and Williams-Jones (1990, 1992) measured FI with leachate analyses and found that the chemistry of FI is dominated by NaCl, with lower but appreciable amounts of $CaCl_2$ and KCl in some inclusions. In addition, most inclusions also contain small concentrations of Mg and Li, and some of them also contain Fe. A pegmatite (TTR20) and a subsolvus granite (46-I-2) samples may also contain F^- and HCO_3^-. The presence of NaCl only and NaCl with $CaCl_2$ is in accordance with the T_e measured by Vasyukova et al. (2016).

5.6 Discussion

5.6.1 Fluid features common to all complexes from this study

Comparing microthermometric data from the six complexes highlights the fact that not all complexes have similar T_h nor salinity. Of all granites, FI from Amis and Strange Lake have the highest salinities (most inclusions between 12 and 28 wt% NaCl eq.), those from Khan Bogd and Ambohimirahavavy have the lowest (0-12 wt% NaCl eq.), and FI from Evisa has salinity values between them (2-10 and 16-18 wt% NaCl eq.). Pegmatites from Ambohimirahavavy have FI with either very low or very high salinity values. FI in pegmatites from Khan Bogd have low salinity values, from Amis and Evisa medium values, and for Manongarivo and Strange Lake salinity values are scattered across a wide range (Fig 5.24a). Hence, Ambohimirahavavy is the only complex to show a significant difference in salinity between granite and pegmatite.

Homogenization temperatures of FI in granites from Ambohimirahavavy are higher (300-340 °C) than those from Amis, Evisa, Khan Bogd and Strange Lake, which have similar T_h (scattered mostly between 80 and 200 °C). The same trend is observed in pegmatites: T_h from Ambohimirahavavy and Manongarivo are high (260-400 °C) while in the other complexes they are lower (80-260 °C). In granites and pegmatites, T_h from Strange Lake are at the lower end of the trend (Fig 5.24b).

Combining salinity and homogenization temperature data (Fig 5.24c), Amis and Evisa complexes appear similar, as well as Ambohimirahavavy and Manongarivo. However, although it was expected that this second pair would provide similar results considering their common geography and emplacement context, the pair Amis-Evisa is more surprising. Khan Bogd complex is more similar to Amis and Evisa for granites, and to Malagasy complexes for pegmatites.

The main salts present in the six complexes are $CaCl_2$ with NaCl, and NaCl with KCl. The Malagasy complexes contain less Ca and have higher T_h than the other complexes. In addition, at Ambohimirahavavy and Strange Lake, carbon was found in the form of CH_4 and/or CO_2. In addition to the main salts, Al, Th, F, S, Mg and Fe were found in FI of the different complexes. Magnesium and Fe, respectively present at Khan Bogd and Ambohimirahavavy, are quite common in FI as they can

be present as salts $MgCl_2$ and $FeCl_2$ (e.g. Bakker, 2003). Aluminum was found at Amis and Manongarivo, and, although it is considered an immobile element in most environment, it can be soluble in aqueous solutions. In non-complexing, alkaline solutions, it occurs as $Al(OH)_4^-$ (Castet et al., 1993); in high-temperature, high-salinity alkaline aqueous fluids, it occurs as $(Na,K)Al(OH)_4$ (e.g. Anderson et al., 1987; Pascal and Anderson, 1989); and it reaches its higher solubility in the presence of F, as $NaAl(OH)_3F$ or $NaAl(OH)_2F_2$ (Tagirov et al., 2002). Since no F was measured in the FI where it is present, it is likely that in fluids of this study Al occurs as $NaAl(OH)_4$. The presence of F in $CaCl_2$-rich FI from Evisa, Khan Bogd and Strange Lake is important to notice, as F is known to be a transporting ligand for many elements, including the REE. At 25 °C, it forms $REEF^{2+}$ and $REEF_2^+$ complexes, which are stronger with HREE than LREE; at higher temperatures, above 100 °C, it forms mostly $REEF^{2+}$ complexes which are stronger with LREE than HREE (Migdisov et al., 2016). Sulphur was found in FI from Khan Bogd and Manongarivo. Sulphur is known to be a transportation ligand for the REE at 25 °C (Schijf and Byrne, 2004; Wood, 1990), and the few available experimental data at higher temperatures show that it also forms stable complexes with the REE, as $REE(SO_4)_2^-$ at 150-250 °C and $REESO_4^+$ at 25-150 °C (Migdisov and Williams-Jones, 2008). In addition, no S-bearing mineral was found at Khan Bogd, and only pyrite was found at Manongarivo, which rises the question of where S was mobilized from and where it got deposited. Thorium is reported in FI from all complexes but Manongarivo and Strange Lake. Its presence is surprising as it is deemed immobile in hydrothermal fluids (Bailey and Ragnarsdottir, 1994; Pelt et al., 2008). In addition, it is commonly found in association with U, which was not found in FI where it is present, even at Amis despite the global enrichment in U of this complex. A recent study showed that Th can become soluble at temperatures of 175-250 °C in sulfate-bearing aqueous fluids (Nisbet et al., 2019), but sulfate is not systematically found in FI with Th in this study. A recapitulative of FI measurements of the six complexes is provided in Tab 5.2.

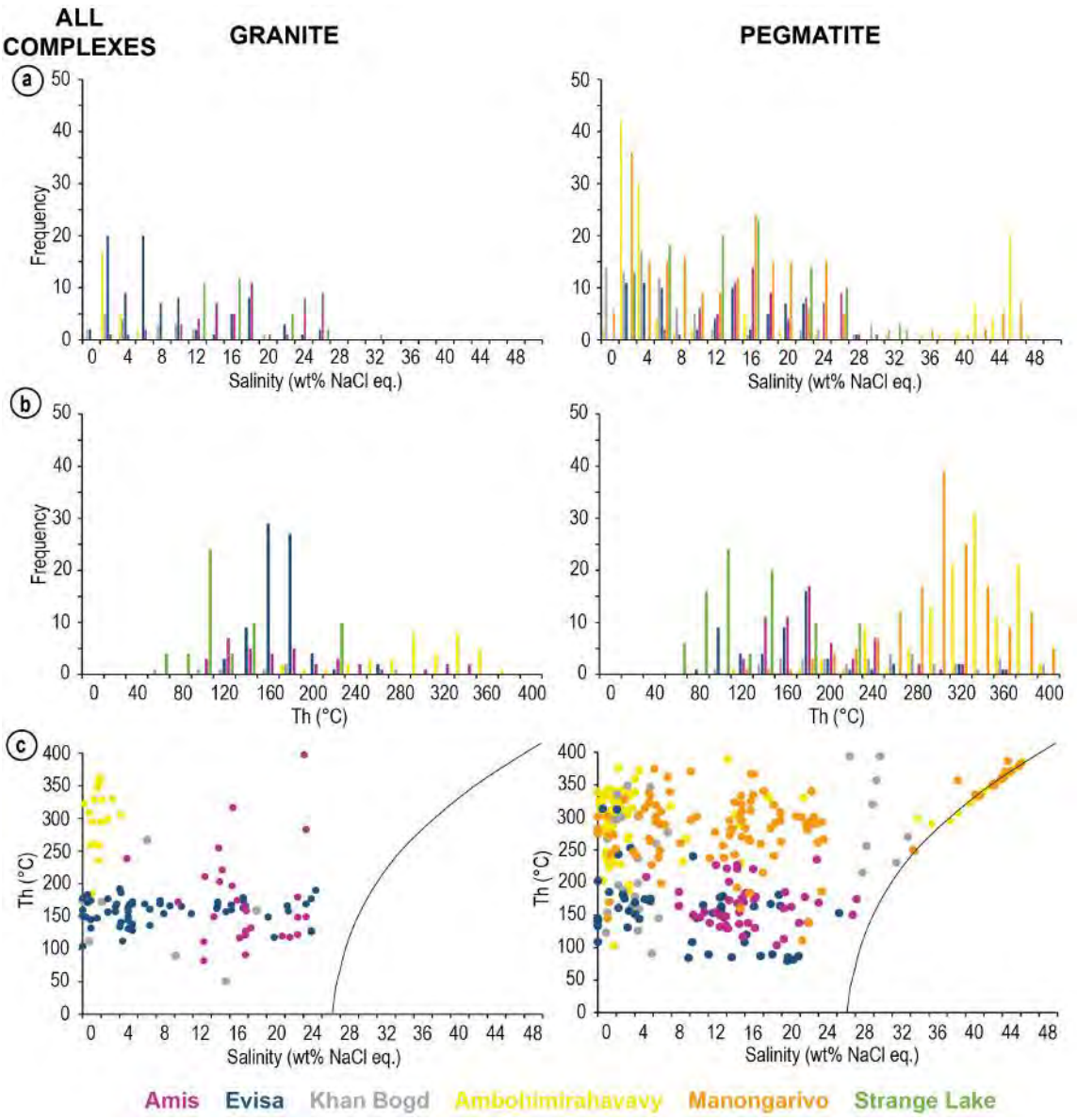

Figure 5.24 Histograms comparing salinities and temperature of FI in pegmatite and granite of the six studied complexes. The black curve is the halite liquidus. Data for Strange Lake were interpreted from Vasyukova et al. (2016) since only ranges and maximums are provided: if the maximum is provided, it is represented by a peak of 10 in frequency; if only the range is given, it is represented by peaks of 2 in frequency along the whole range

Table 5.2 Summary of the main properties of FI measured in this study and their interpretation for the six studied alkaline complexes

Complex	Amis		Evisa		Khan Bogd		Ambohimirahavavy		Manongarivo		Strange Lake	
Sample	SOS069	SOS071	EV1823b	EV1825A	KB07A	KB04B	AM107	AM35	688	689	Salvi and Williams-Jones (1990), Vasyukova et al. (2016)	
Rock type	Granite	Pegmatite	Subsolvus granite	Pegmatite	Granite	Pegmatite	Granite	Pegmatite	Pegmatite	Pegmatite	Hypersolvus granite	Subsolvus granite	Pegmatite
FI chemistry	$CaCl_2$ + NaCl ± Al, Th; NaCl		$CaCl_2$ + NaCl ± F	$CaCl_2$ + NaCl ± F; NaCl + KCl ± Th	$CaCl_2$ + NaCl ± KCl, $MgCl_2$, F, S; NaCl + KCl ± Th		NaCl + KCl ± Th, $FeCl_2$, $MnCl_2$; CO_2	NaCl + KCl ± Th, $FeCl_2$, $MnCl_2$	$CaCl_2$ + NaCl ± KCl, Al, S; NaCl + KCl ± S	NaCl + KCl ± S	KCl ± NaCl; CH_4; NaCl; CO_2; $CaCl_2$ + F + NaCl; CO_2;	
FI salinity (wt% NaCl eq.)	16-26		0-26	10-22; 0-26	15-25; n.d.	0-30; 0-35	2-6		0-46; 0-46	0-46	23; 4; n.d.	
T_h (°C)	100-340		160-180	80-180; 80-180	50-200; n.d.	150-400; 150-360	180-340		120-380; 120-380	120-380		
T entrapment (°C)	120-250 or 210-580	120-250 or 240-560	160-180	80-180; 80-180	260	260; ~260	300-340		320-380; 320-380	320-380	310-425; 290-310; 230-290	
Boiling	Likely		No	No	Yes	Yes	Yes		Yes	Yes	n.d.	
Fluid interpretation	Undetermined				Possible NaCl-KCl orthomagmatic got enriched in Ca		H_2O-CO_2-NaCl-KCl orthomagmatic		NaCl-KCl orthomagmatic got enriched in Ca		KCl -CH_4 orthomagmatic got enriched in Na, Ca, F and oxidized to CO_2	

5.6.2 Fluid circulations in the six complexes

5.6.2.1 The Amis complex, Namibia

At Amis, measured LV1 FI in pegmatite and granite have similar compositions ($CaCl_2$, NaCl, ± Al, Th), salinities (16-26 wt% NaCl eq.), and Th (bimodal between 100 and 340 °C). In both rocks they are commonly associated with MI. The overall common chemistry and salinity in both rocks, as well as the close association of FI with MI, tend to indicate the circulation of a single, orthomagmatic fluid. The origin of the salts would then be the melt itself. However, the rather low T_h could indicate a later origin for the $CaCl_2$-rich fluid. Hence, the origin of this fluid remains undetermined.

In order to determine the entrapment temperature of the measured FI, and hence the circulation temperature of the orthomagmatic fluid, it is important to understand the entrapment conditions of these FI. The wide and continuous salinity range in LV1 FI of pegmatite, its relatively restricted T_h range (Fig 5.11c), and the presence of vapor inclusions associated with LV1 evokes the possibility of boiling during fluid entrapment (Audétat, 2019; Bodnar et al., 1985; Roedder and Bodnar, 1980). However, the lower T_h does not especially match the higher salinities; in order to confirm the occurrence of boiling, it is therefore necessary to verify that T_h of V-rich inclusions are similar to that of LV1, and this data for V-rich inclusions could not be obtained.

In addition, T_h range in granite is wider (Fig 5.11c), with no apparent petrographic explanation for this high difference. This wide range of temperature could be the sign for a long lasting hydrothermal flow during cooling of the rocks, or post-trapping modifications of the FI. Hence, boiling is likely but there is no absolute proof for it. If boiling indeed occurred, then it did at the same temperature range than the Th range in pegmatite (approximately 120-250 °C; Fig 5.11c; Bodnar et al., 1985). In the case boiling did not occur, isochores for minimum and maximum T_h were calculated using the programs BULK and ISOC (Bakker, 2003). They are found similar in the pegmatite and the granite, but emplacement pressure of the Amis complex needs to be estimated in order to find the entrapment temperature in this case. Schmitt et al. (2000) estimated that the Brandberg complex, which is adjacent to the Amis complex (Fig 2.1), emplaced at a pressure of 300 MPa, i.e. approximatively 10 km depth, which is quite deep compared with other alkaline complexes (e.g. 300-600 m at Ambohimirahavavy, Estrade et al., 2015, 3.6 km at

Strange Lake, Vasyukova and Williams-Jones, 2016). This pressure intercepts the previously calculated isochores at 210 and 580 °C in granite and 240 and 560 °C in pegmatite. The lowest values of these temperatures are in accordance with those determined in the case of boiling, but the highest values point to a very hot fluid.

Based on eutectic temperatures, the fluid measured by microthermometry was dominated by $CaCl_2$ with some NaCl. Salt mounds only revealed the presence of NaCl with some KCl, indicating another fluid with a different chemistry circulated. These interpretations are in contradiction with the findings of Schmitt et al. (2002), who based their study on the richness of MI in H_2O, Cl and F and on the behavior of Y in fluids. They do propose two fluids flow at Amis, but with different compositions than what is found in this work. Indeed, they propose a first orthomagmatic, CO_2-rich fluid and a second post-magmatic, F-rich fluid. However, our microthermometric study did not reveal the presence of CO_2, and no F was found in solids nor salt mounds. Secondary carbonate minerals found in this complex could precipitate from a fluid that interacted with host rocks. Fluorite was found as a secondary mineral at Amis, hence it is likely that F is indeed present in fluids.

5.6.2.2 The Evisa complex, Corsica

At Evisa, measured LV1 FI can be split in three groups: (1) in the granite, with a composition dominated by $CaCl_2$, NaCl and F, a salinity of 0-26 wt% NaCl eq., and a T_h of 160-180 °C; (2) in the pegmatite, mostly composed of $CaCl_2$, NaCl and F, a salinity of most inclusions of 10-22 wt% NaCl eq., and a T_h range of 80-180 °C; (3) in the pegmatite, with a composition of NaCl, KCl and Th, a salinity of most inclusions of 0-26 wt% NaCl eq., and a T_h of 80-180 °C (Fig 5.12c). In the pegmatite, group (2) FI generally occurs more commonly in quartz rims than group (3).

At Evisa, no assemblage regrouping LV and V FI was observed, hence boiling is unlikely. In this case, isochores for minimum and maximum T_h were calculated for the pegmatite and granite, but no estimation of the emplacement pressure is given in the literature. However, pegmatites are known to be more abundant at the top of the pluton, and since volcanic rocks have all been eroded and in comparison with other alkaline plutons, it is possible to infer an emplacement depth range for this pegmatite and the granite located at the same pressure. Hence, it is likely that rocks from Evisa emplaced between 1 and 3 km. These estimated depths combined with calculated isochores give an emplacement temperature range of 120 – 320 °C for the

$CaCl_2$-bearing fluid in the granite, 90 – 230 °C for the $CaCl_2$-bearing fluid in the pegmatite, and 95 – 320 °C for the KCl-bearing one in the pegmatite. These ranges are very wide and do not provide reliable information as to the relative circulation timing of the two fluids.

According to Poitrasson et al. (1998) and Bonin et al. (2008), the Evisa complex experienced two major hydrothermal events. The first one was the circulation of a Na-, Fe-rich orthomagmatic fluid that affected only the hypersolvus granite, the second one was a post-magmatic F- and Na-rich fluid. These authors do not mention any fluid enriched in Ca, despite the presence of fluorite-bearing hydraulic breccia, documented by Bonin (1988). In this study, although the presence of two FI compositions points to the circulation of two distinct fluids, Fe was not found in FI. However, it is not excluded that the small black crystals occasionally spotted in FI are hematite.

5.6.2.3 The Khan Bogd complex, Mongolia

At Khan Bogd, based on their chemistry, two groups of FI are distinguished and these are present in the granite as well as in the pegmatite. The first group is made of $CaCl_2$- and NaCl-bearing FI with traces of KCl, $MgCl_2$, F, and S; it includes V1 FI; in the granite it has salinities of 15-25 wt% NaCl eq. and T_h of 50-200 °C; in the pegmatite, it has a wider salinity range of 0-30 wt% NaCl eq. and a T_h range of 150-400 °C. The second group is made of NaCl- and KCl-bearing FI with traces of Th; in the granite its characteristics have not been determined; in the pegmatite it has salinities of 0-35 wt% NaCl eq. and T_h of 150-360 °C. It is difficult to distinguish a clear petrographic location for these two groups in quartz.

The presence of vapor-rich inclusions associated with LV1 FI with similar T_h is a clear indicator of boiling during fluid entrapment. In this case, the real entrapment temperature of $CaCl_2$-, NaCl-bearing fluid is given by the inclusions of this group (vapor-rich and LV1) that homogenized at the lowest temperature. However, because it is difficult to observe the precise T_h in vapor-rich inclusions, the best T_h estimate are obtained from the LV1 group (Diamond, 2001). Hence, the real entrapment temperature is of approximately 150-200 °C in the pegmatite and the granite (Fig 5.13b). For the NaCl-KCl fluid, the entrapment temperature can go up to 300 °C in the pegmatite, and is undetermined in the granite.

Kynicky et al. (2011), based on the presence of Ca in hydrothermally altered elpidite and of hydrothermal calcite, fluorcarbonates and fluorite, proposed that the

Khan Bogd complex experienced the circulation of a Ca-CO_2-F-rich fluid. This fluid separated from the melt at the final stages of its evolution, with a possible crustal input indicated by the Ca enrichment. Based on microthermometric measurements no CO_2 was found in FI of this study, but in view of the low amount of vapor-rich inclusions measured, its presence as a vapor phase cannot be ruled out. It is possible that the fluid described by Kynicky et al. (2011) matches the $CaCl_2$- and NaCl-bearing inclusions measured in this study. In addition, traces of KCl, $MgCl_2$, F and S were found in these inclusions, and elpidite is hydrothermally altered to its Ca-rich zirconosilicate equivalent, armstrongite. Similarly to Evisa, there is no indication as to the relative timing of circulation of the two fluids. However, in comparison with the Malagasy and Strange Lake complexes as well as with the interpretation of Kynicky, it is possible to infer that the Ca-rich fluid is not orthomagmatic and occurred after the NaCl-, KCl-rich fluid. Since the Ca-rich fluid does not have a significantly lower salinity than the NaCl-, KCl-rich one, it is unlikely that it is only a meteoric fluid. Instead, this fluid could be the result of the interaction of the NaCl-, KCl-rich fluid with country rocks.

5.6.2.4 The Ambohimirahavavy complex, Madagascar

At Ambohimirahavavy, all aqueous FI measured are made of NaCl and KCl, with traces of Th, $MnCl_2$, and $FeCl_2$. Salinities and T_h are similar in granite and pegmatite, with respectively 2-6 wt% NaCl eq. and 180-340 °C. Only LVS FI have higher salinities, of 32-48 wt% NaCl eq. In addition, some CO_2 vapor inclusions were found in the granite. they were identified with their T_m of 56 ± 1 °C.

Similarly to Khan Bogd, the presence of vapor-rich inclusions associated with LV1 FI with comparable T_h is good evidence for boiling of the fluid during trapping. Hence, trapping conditions are given by T_h of LV1 inclusions (Roedder, 1984), i.e. 300-340 °C in the pegmatite and the granite (Fig 5.15b).

According to the study of FI in skarn by Estrade (2014), the Ambohimirahavavy complex experienced the circulation of an orthomagmatic, NaCl, $FeCl_2$, $CaCl_2$, F-rich fluid. The presence of $CaCl_2$ and F was not detected in FI from this study, but Ca could come from carbonate-rich horizons in the host rocks and be only local. Hence, I interpret this H_2O-CO_2-NaCl-KCl-bearing fluid as orthomagmatic. The similarity of entrapment temperatures between the granite and the pegmatite is another argument in favor of an orthomagmatic origin.

5.6.2.5 The Manongarivo complex, Madagascar

In pegmatites from Manongarivo, two chemistries were found in FI: $CaCl_2$-, NaCl-rich with traces of KCl, Al, and S; and NaCl-, KCl-rich with traces of S. They show a similar salinity range of 0-26 wt% NaCl eq. for LV1 and V FI, and 44-46 wt% NaCl eq. for LVS FI. Homogenization temperatures are also similar between the two chemistries and all FI types, from 120 to 380°C with a maximum at 300 °C. It is difficult to distinguish a clear petrographic location for the two chemistries in quartz, but it seems that NaCl-, KCl-rich FI are located closer to the core of the quartz crystal than $CaCl_2$-, NaCl-rich FI. In addition, $CaCl_2$-, NaCl-rich FI are mostly found in one pegmatite sample.

Similarly to Khan Bogd and Ambohimirahavavy, the presence of vapor-rich inclusions associated with LV1 FI with similar T_h is a clear indicator of boiling. Hence, the entrapment temperature is that of LV1 inclusions (Roedder, 1984), and is around 300 °C (Fig 5.16b).

No study of circulating fluids is available for the Manongarivo complex, but it appears similar to the Ambohimirahavavy complex in terms of geological context and nature and Th of FI. Following this similarity as well as the fact that $CaCl_2$-, NaCl-rich FI petrographically seem to have been trapped later, I propose that a NaCl-, KCl-rich fluid exsolved at the magmatic stage and got enriched in Ca later, probably while interacting with host rocks.

5.6.2.6 The Strange Lake complex, Canada

At Strange Lake, Vasyukova and Williams-Jones (2019) proposed a very detailed model for fluids circulation, presented in Section 2.5.3. To summarize, they propose the exsolution of a salt-rich (23 wt% NaCl eq.), hot (425-360 °C) fluid from the melt. This fluid was made of H_2O, CH_4 and rich in KCl, until it cooled down to 310 °C. On further cooling, CH_4 got oxidized to CO_2, and the fluid got less saline (4 wt% NaCl eq.) and richer in NaCl compared with other salts due to nahcolite dissolution. Still cooling down, the fluid got richer in $CaCl_2$ and F, until 230 °C. At this point, CO_2 escaped from the fluid, and at 180 °C, this oxidizing fluid caused hematization of granites and pegmatites.

5.6.3 Comparison of the characteristics of complexes of this study with the literature

5.6.3.1 Summary of fluid properties in silica-saturated alkaline complexes

From the study of the six complexes presented in this work, it appears that alkaline complexes experienced the circulation of mostly aqueous fluids with highly variable salinities, with FI from 0 up to 48 wt% NaCl eq. This is in agreement with the study of Konnerup-Madsen and Rose-Hansen (1984) who found aqueous fluids with salinities varying from 2 to 64 wt% in an alkaline granite from Ilímaussaq. Homogenization temperatures range from 80 to 400 °C, and all complexes experienced the circulation of at least two fluids, one NaCl- and KCl-dominated and the other $CaCl_2$- and NaCl-dominated. At Ambohimirahavavy, Manongarivo and Strange Lake, the NaCl-KCl fluid is orthomagmatic, and the $CaCl_2$-NaCl one is late magmatic and interacted with host rocks. At Amis, Evisa and Khan Bogd, the timing of the two fluids remains undetermined, although comparison with the other complexes of this study as well as with the literature make it likely that the NaCl-KCl fluid is orthomagmatic and the $CaCl_2$-NaCl one circulated later. The relatively low T_h is consistent with the alkaline environment, and especially in pegmatites, in which many fluxing elements are present and can cause a liquidus undercooling. The determination of the characteristics of these fluids is an important result, as no other study has been made on FI from multiple silica-saturated alkaline complexes.

5.6.3.2 Comparison with the literature: fluids in silica-undersaturated alkaline complexes and peraluminous pegmatites

Marks and Markl (2017) propose a review of fluid inclusions properties in miaskitic and agpaitic rocks, based on silica-undersaturated alkaline rocks and on Strange Lake. They show that orthomagmatic fluids forming agpaitic minerals are commonly rich in CH_4, while fluids forming miaskitic minerals are made of H_2O or H_2O-CO_2. Late-magmatic to secondary fluids seem to get richer in H_2O than in carbon species than orthomagmatic ones. However, no generalization can be made on the property of the fluids; salinity seems to be determined by the pressure at which the fluid circulates, temperature depends on the orthomagmatic or secondary origin of the fluid, and salts composition depends on the composition

of the magmatic source, magmatic processes and host rocks. The major difference with silica-saturated rocks from this study is that CH_4 was not found (except at Strange Lake), despite the circulation of a fluid forming agpaitic minerals at Khan Bogd (replacement of elpidite by armstrongite).

Fluid inclusions in peraluminous pegmatites also consist mostly of H_2O and CO_2 (e.g. Thomas et al., 2006b), but generally they have a more varied cation contents compared to alkaline pegmatites. They can contain NaCl, KCl and $CaCl_2$, similarly to rocks in this study, but can also be rich in $MgCl_2$ and $FeCl_2$. They also commonly contain solids rich in B and Sn (e.g. Omsuckchan, Russia, Kamenetsky et al., 2004; Tanco, Canada, London, 1986; Ehrenfriedersdorf, Germany, Thomas et al., 2003; Thomas et al., 2006a), which were not found in FI of alkaline pegmatites. Peraluminous pegmatites FI have broad P-T ranges, depending once again on local emplacement conditions. However, many FI studies report entrapment temperatures between 300 and 500 °C, hence comparable to those in Malagasy complexes or higher. Similarly to alkaline pegmatites, boiling seems to be a common process (Thomas et al., 2006b).

5.6.4 Other mineralized systems with interaction of a granitic melt with hydrothermal fluids: epithermal and porphyry deposits

Porphyry deposits, similarly to alkaline complexes, have a dual magmatic and hydrothermal origin and concentrate many metals including Au, Cu, Mo, Sn, and W. They can commonly be associated with epithermal deposits, which emplace near the surface at relatively low temperatures and concentrate mostly Au and Ag. Bodnar et al. (2014) compiled thousands of FI analyses performed in epithermal and porphyry deposits.

It appears that FI in porphyries, similarly to alkaline complexes, present a large range of salinities, from 0 to 60 wt% NaCl eq. Homogenization temperatures are between 100 and 900 °C, with a majority of FI homogenizing between 200 and 450 °C, which is comparable with T_h in Malagasy complexes or higher. Mineralizing fluids in porphyries are considered to be a mix between an orthomagmatic and a meteoric fluid. The main salts they contain are NaCl, KCl and $FeCl_2$, and in some cases they contain significant concentrations of F, S and/or B. Boiling is common in porphyry deposits, resulting in the entrapment of LV, V-rich, and LV-halite FI. Hence, physical properties of fluids circulating in porphyries are similar to those in

alkaline granites (salinity, T_h). The main difference is the composition of fluids. In porphyries, S is very common in fluids, whereas it is much rarer in fluids associated with alkaline granites. Calcium and carbonate ions are common in alkaline granites, which is not the case in porphyries. These composition differences highlight the importance of the nature of ligands to fractionate and enrich REE in alkaline granites more than in porphyries.

Epithermal deposits form at lower temperatures, mostly between 120 and 310 °C, which is comparable to the complexes of Amis, Evisa, Khan Bogd and Strange Lake. Metal deposition phase is estimated to take place around 240-250 °C. Epithermal deposits also display a wide range of salinities, between 0 and 40 wt% NaCl eq., but the vast majority of the occurrences provide salinities between 0 and 17 wt% NaCl eq. Similarly to porphyries, mineralizing fluids are orthomagmatic and meteoric. The main difference with porphyries and alkaline complexes of this study, in addition with the composition of the fluids, is the large amount of various gases. The dominant gas is CO_2, but significant amounts of H_2S, CH_4, N_2 and SO_2 can also be found in FI. The mineralization is commonly transported by S and NH_3. Hence, the presence of vapor phases as well as the different compositions are the main differences with alkaline granites, and lead to the formation of different mineralizations.

5.7 Conclusion

As a conclusion, the six studied alkaline complexes in this study are mostly made of the same type of FI (LV, LVS, V), but their size, number and the relative importance of secondary FI makes them more or less difficult to measure. Fluid inclusions at the Malagasy complexes are easier to measure, probably because of their young age (25 Ma) which does not allow much tectonics or fluids modification to overprint primary FI. Signs of ebullition in most complexes evokes the formation of porphyry and epithermal deposits, in which vapor is a key factor in ore concentration. However, T_h and/or main salts are different from these deposit types. Salinities vary a lot inside one complex in connection with ebullition, but T_h are similar at Evisa and Khan Bogd on one hand, and in the Malagasy complexes on the other hand. The latter show higher T_h, which match common T_h of peraluminous pegmatites. Either way, T_h is never higher than 400 °C, which

remains quite low compared with other mineralized deposits such as porphyries. No significant difference was found in order to explain the HREE enrichment higher in silica-saturated than silica-undersaturated alkaline rocks, but this work is only preliminary and needs further investigation. The composition of aqueous FI is similar in most complexes, the main salts being either $CaCl_2$ and NaCl, or NaCl and KCl. The latter fluid is orthomagmatic at Ambohimirahavavy, Manongarivo and Strange Lake, and its origin remains undetermined at Amis, Evisa and Khan Bogd. The presence of other elements is interesting, such as S and F which have the ability to mobilize the REE, and Th and Al which are not commonly found in fluids.

Chapter 6

Thesis synthesis: contribution of magmatic and hydrothermal stages on REE behavior in alkaline granitic complexes

This work focused on six silica-saturated alkaline complexes worldwide. Granites and pegmatites in these complexes are comparable in mineralogy, textures, mineral composition, and REE enrichment and fractionation ways. The similarities of these complexes allow to draw general conclusions about alkaline granitic complexes.

6.1 Magmatic vs hydrothermal mineral paragenesis

The six silica-saturated alkaline complexes in this study all have the same main mineralogy. It consists of quartz, alkaline feldspars, and alkaline amphiboles and/or aegirine. Based on textures, relations with other minerals, composition, zonations, and the presence or absence of FI, a paragenesis has been established. In all complexes, alkaline feldspars, quartz core, alkaline amphiboles, aegirine core, some PGM, and the zirconosilicates elpidite and EGM (depending on the complex) are early magmatic. At the late-magmatic stage, it is likely that most of these minerals kept growing, with the exception of amphiboles, elpidite and EGM. At this stage, zircon began to crystallize (except at Strange Lake), along with allanite-(Ce,Nd), astrophyllite, chevkinite-(Ce), stilpnomelane, and/or monazite-(Ce) depending on the complex.

Moving on to hydrothermal stage, quartz and aegirine rims grew, along with zircon and a wide diversity of minerals forming pseudomorphs after the primary zirconosilicates elpidite and EGM. These minerals present a wide chemical variety, with silicates (e.g. gittinsite, låvenite), carbonates (e.g. bastnäsite-(Ce)), halides (e.g. fluorite), oxides (e.g. hematite, ilmenite), phosphates (e.g. monazite-(Ce), apatite). In addition, some magmatic minerals were altered at the hydrothermal stage and their texture and composition changed. This is the case for alkaline feldspars that were albitized, magmatic PGM that gained Pb and Y, and elpidite that, where not replaced, became enriched in Ca. Although alkaline melts are highly differentiated and hence globally poor in Ca, many secondary minerals are rich in Ca (e.g. bastnäsite-(Ce), gittinsite, armstrongite, apatite, fluorite). This is probably due to the interaction of hydrothermal fluids with surrounding rocks that are rich in Ca, such as gabbros and basalts at Amis, Khan Bogd and Evisa, limestones at Madagascar, and monzonite at Strange Lake.

6.2 REE concentration at magmatic and hydrothermal stages

It is accepted in the literature that purely magmatic processes play an important role in concentrating the REE in silica-saturated alkaline complexes. Those include a low rate of partial melting of the source, fractional crystallization, and melt-melt or melt-fluid immiscibility. The source of alkaline complexes also plays a role in the high REE concentration in these complexes, as it is a metasomatically REE-enriched mantle or a mantle plume (e.g. Chakhmouradian and Zaitsev, 2012; Vasyukova and Williams-Jones, 2020). The relative importance of fluids in concentrating and fractionating the REE is still debated, and the comparison of magmatic and hydrothermal minerals in this work allows an estimation of the relative importance of the contribution of the two stages in the REE-enrichment of granitic alkaline complexes.

The study of minerals that grew during both the magmatic and hydrothermal stages provides an insight on the relative contributions of the two stages. Aegirine is such a mineral, for which the magmatic core is systematically richer in REE than hydrothermal rims, of 20 to 80 % depending on the complex and the REE.

In addition, no link was found between FI properties (temperature, salinity, composition) and whole-rock REE content variations between the different rocks and the different complexes. The influence of the geodynamic context of the different complexes (they were emplaced in a rifting, subduction and hot-spot, or post-collision context) appears to be minimal, as there are many similarities between the six alkaline complexes in this study. However, and though restricted, local parameters such as the melt source and host rocks still play a role in the final composition of the complex, as it is observed with the Malagasy complexes that are geographically close and emplaced in the same conditions. In addition, as orthomagmatic fluids exsolve from the melt, their concentration in REE also depends on the concentration of these elements in the melt. These data seem to indicate that the high absolute quantity of REE in alkaline complexes is mostly linked to magmatic processes and melt source.

Nevertheless, there are numerous evidences that hydrothermal fluids can mobilize and concentrate the REE. Minerals that grew during magmatic and hydrothermal stages provide some evidences. In aegirine, although the rims are poorer in REE than the core, concentrations in the rims are of dozens of ppm, which remains not negligible. In addition, aegirine rims grew in competition with REE-bearing minerals in pseudomorphs, which have much higher affinities for the REE. This could be another explanation as to the depletion in REE of aegirine rims, which does not imply that hydrothermal fluids mobilize only restricted amounts of REE. Hydrothermal zircon also contains tens to hundreds of REE. The alteration of magmatic minerals, either total or partial, also indicates a mobilization and concentration of REE by hydrothermal fluids. The most eloquent example are the pseudomorphs after primary zirconosilicates, in which REE concentrate in higher quantities than in the original zirconosilicate. This process is also observable in hydrothermally altered magmatic PGM that get richer in Y. At Khan Bogd, obvious proofs of the mobilization of REE by a hydrothermal fluid are a REE-, Zr-phase found in fractures crossing several minerals, and a carbonate of Ce that was found in a FI. Estimation of the fraction of REE in hydrothermal minerals provide quantitative evidences of the mobilization of the REE by fluids, with 30 to almost 100 % of Ce and Y present in hydrothermal minerals. Hence, although the absolute amounts of REE in alkaline complexes depends on the magmatic source and processes, there is an extensive input, remobilization and concentration by hydrothermal fluids.

The scale over which the REE are mobilized by fluids is still an open question, as shown by the occurrence of evidences for both local and global influence found in the complexes. Local evidence, at the sample scale, is provided by the pseudomorphs. Indeed, pseudomorphs after EGM, which can contain up to 10 % REE, consist of a large variety of minerals, most of them being REE-rich; conversely, pseudomorphs after elpidite, which contains only traces of REE, are mostly made only of gittinsite and quartz plus or minus zircon. The hypothesis of a local remobilization is also supported by the shape of the REE spectrum of hydrothermal zircon. The REE spectrum of zircon in pseudomorphs varies from one layer to another in a same pegmatite at Khan Bogd, and from one granite sample to another at Evisa. This indicates that REE were not homogenized at the scale of the complex. These features even provide a base to identify the primary zirconosilicate in a complex, even where it has been totally replaced. For example, at Amis, the occurrence of pseudomorphs only with zircon and quartz as well as the shape of the spider diagram of this zircon make it likely that elpidite used to occur in the complex. However, evidences of global, complex-scale hydrothermal mobilization of the REE are also visible. The occurrence of a REE-, Zr-phase in fractures crossing several minerals, and of the carbonate of Ce in a FI in quartz, indicate that the REE can be mobilized on a bigger scale than pseudomorphs. The occurrence of altered PGM enriched in Y also shows that Y was transported from elsewhere and precipitated in these minerals. In addition, mass-balance calculation on pseudomorphs shows that REE were broadly brought by the circulating fluids. Hence, it seems that hydrothermal fluids contain significant concentrations of REE and can mobilize and concentrate them in minerals, both locally, in pseudomorphs, and globally, in fractures and minerals of different geographic areas.

The scale over which the REE are mobilized also depends on the quantity of fluid flows. As shown by the restricted alteration halo around pegmatites, less fluid circulated in alkaline complexes than in porphyries or carbonatites. However, even inside a same complex, there can be a significant variation of fluid flows. This is shown at Malagasy and Khan Bogd complexes, in which the primary zirconosilicate remains in some pegmatites, and has been totally replaced in others. Hence, in accordance with the findings of Migdisov et al. (2016), the more fluid flows, the more the REE are remobilized.

6.3 REE fractionation by hydrothermal fluids

Silica-saturated alkaline complexes are notably enriched in HREE compared with silica-undersaturated alkaline complexes. Although magmatic processes do lead to a REE fractionation as HREE are more compatible than LREE, this work provides evidences that hydrothermal fluids enhance this fractionation. As previously mentioned, altered PGM is enriched in Y, which is commonly associated with HREE, but not in LREE compared with fresh PGM. Similarly, the calculated percentage REE loss from magmatic core to hydrothermal rims of aegirine shows that, except at Ambohimirahavavy, this loss is more important for LREE than for HREE. This shows that the amounts of LREE and HREE transported by hydrothermal fluids are different. In this case, HREE seem to be transported in relatively higher quantities than LREE. This trend is also shown by estimation of the proportion of REE in hydrothermal minerals in which, except in the granites of Evisa and Khan Bogd, a higher percentage of HREE than LREE is concentrated in hydrothermal minerals. The study of zircon shows a reverse trend: from magmatic to hydrothermal zircon in pseudomorphs, the HREE concentration decreases and the LREE concentration increases. However, it has been demonstrated that the REE signature of zircon in pseudomorphs depends mainly on that of the primary mineral it replaces, i.e. it does not represent the hydrothermal fluid composition. At Amis, late-hydrothermal zircon contains more LREE and less HREE than other zircon grains in this complex. Amis is also the complex in which REE fractionation between aegirine core and rims is the most visible (40 % of difference). Hence, it is likely that competition between aegirine and zircon plays a role in controlling the REE composition of these minerals.

6.4 Properties of fluids in alkaline systems

In order to determine a common pattern of hydrothermal REE concentration and fractionation in silica-saturated alkaline complexes, it is important to understand the properties of the fluids circulating in each complex. Fluid inclusions in the different complexes can provide such evidence. FI data from the 6 complexes indicate various

entrapment temperatures and pressures, as well as different salinities for each locality. Hence, it can be concluded that these parameters do not have a specific impact on the transportation of REE in hydrothermal fluids.

Nevertheless, the composition of fluid inclusions from the six complexes do have similitudes. They show that two fluids circulated in all complexes: one NaCl-KCl-rich, and one $CaCl_2$-NaCl-rich. At Ambohimirahavavy, $CaCl_2$ was only found in skarn associated with the complex (Estrade et al., 2015). At Ambohimirahavavy, Manongarivo and Strange Lake, the NaCl-KCl-rich fluid is determined to be orthomagmatic, and the $CaCl_2$-NaCl-rich fluid is low-temperature secondary. In the other complexes, the relative timing is unclear. However, the comparison with other complexes as well as the poverty of the melt in Ca suggest a similar timing in all complexes, with the NaCl-KCl fluid being orthomagmatic, i.e., early, and the $CaCl_2$-NaCl fluid being secondary.

Vasyukova and Williams-Jones (2020) propose that a high concentration of Ca in the melt is partly responsible for the formation of two immiscible melts, a silicate one that would concentrate HREE, and one rich in fluoride that would concentrate LREE and Y instead. In this study, F was only found in the $CaCl_2$-NaCl-rich fluid at Evisa, Khan Bogd and Strange Lake. Fluorite is however found in all complexes but Khan Bogd. This is an important finding and indicates that the role of a fluoride melt must be nuanced. The other difference with the model proposed by Vasyukova and Williams-Jones (2020), is that, with microthermometric analyzes, carbonic phases are not common and were only found at Ambohimirahavavy (CO_2) and Strange Lake (CH_4 and CO_2).

Known ligands of REE in fluids are also present in the complexes The major ones are F at Evisa, Khan Bogd and Strange Lake, S at Khan Bogd and Manongarivo, and CO_3^{2-}, Cl and OH in the six complexes. Fluorine is known to be a strong REE ligand, and it has higher affinity with LREE at temperatures above 100 ∘C and with HREE under 100 ∘C. Calcium likely plays an indirect role as it permits the sequestration of F in fluorite, depleting the fluid in F and thereby allowing massive deposition of the REE. Sulfur is also a strong ligand but does not fractionate the REE. Carbonate ions are strong ligands, especially at low temperatures, and likewise do not seem to fractionate the REE. Chlorine does not have a strong affinity for the REE, but because it is very abundant anion, it is an important ligand; it forms more stable complexes with the light than the heavy REE (Migdisov et al., 2016). The behavior of OH as a ligand is not precisely determined, but it is very abundant and the few

studies indicate that it forms more stable complexes with Y at high pressures (up to 4.5 GPa; Stefanski, 2020). Granites from complexes where F was found match the samples in which the proportion of hydrothermal Ce are equal or higher than hydrothermal Y. This is in accordance with microthermometric data that point to a fluid circulating at a temperature above 100 °C, and shows the importance of F in the formation of mineralization. The general observation that HREE are more mobilized than LREE in fluids of the six complexes of this study is however not explained by present-day knowledge of REE ligands.

6.5 The mobility of other HFSE in fluids of alkaline systems

This study also provides evidences as to the mobility of HFSE (namely U, Zr, Hf, Nb, Ta, Sn, Th, Ti) and Al in hydrothermal fluids. In this study, Zr and Hf are present in aegirine rims and secondary zirconosilicates such as gittinsite or zircon; Nb and Ta were found among others in fractures in aegirine; Sn was also found in aegirine rims; Th is present in many FI; hydrothermal pyrochlore and aegirine are highly enriched in Ti; and Al was found in hydrothermal zircon and in FI. Among HFSE, only U was not found in hydrothermal minerals, but absence of evidence is not evidence of absence. Until recently, several of these elements were deemed immobile in fluids, and the complexes they form in aqueous fluids are still debated. For example, Ayers et al. (2012) determined that Zr mostly forms complexes with OH, while Tarnopolskaia and Bychkov (2019) estimated that it forms complexes with F. Another example is provided by Nisbet et al. (2019) who showed that Th is soluble in fluids rich in SO_4^{2-}. However, sulfate was not systematically found in FI with Th in this study, hence the behavior of Th in fluids still needs further studies. Hence, although the modalities are not fully understood, this work shows that along with the REE, hydrothermal fluids also have the ability to transport significant amounts of HFSE and Al.

6.6 A recipe for REE enrichment and fractionation in alkaline granites and associated pegmatites

From the study of six alkaline complexes worldwide enriched in HREE, it appears that they experienced common events that can be generalized to propose a global recipe for REE enrichment and fractionation in alkaline granites and associated pegmatites. Similarly to this work, Vasyukova and Williams-Jones (2020) provide a recipe for REE-enrichment of alkaline complexes, but their conclusions rely mostly on the Strange Lake complex, hence a more diverse dataset is required and provided by this work. The steps witnessed by the different common minerals of the complexes of this work are summarized in Fig 6.1.

1. Enrich your melt in REE, through a source rich in REE, a low rate of partial melting, and/or fractionate crystallization.
2. Exsolve a NaCl-KCl-rich orthomagmatic fluid with a significant REE, and mostly HREE, content. Add salt to taste.
3. Enrich the fluid in Ca and REE-ligands such as S, CO_3^{2-} by country rocks contamination during cooling. Choose preferentially HREE-ligands.
4. Mix this Ca-rich fluid with magmatic minerals, alter them, and enrich secondary minerals in REE, and mostly HREE. Form as many pseudomorphs as you see fit.
5. Let it rest until cooled.
6. Enjoy!

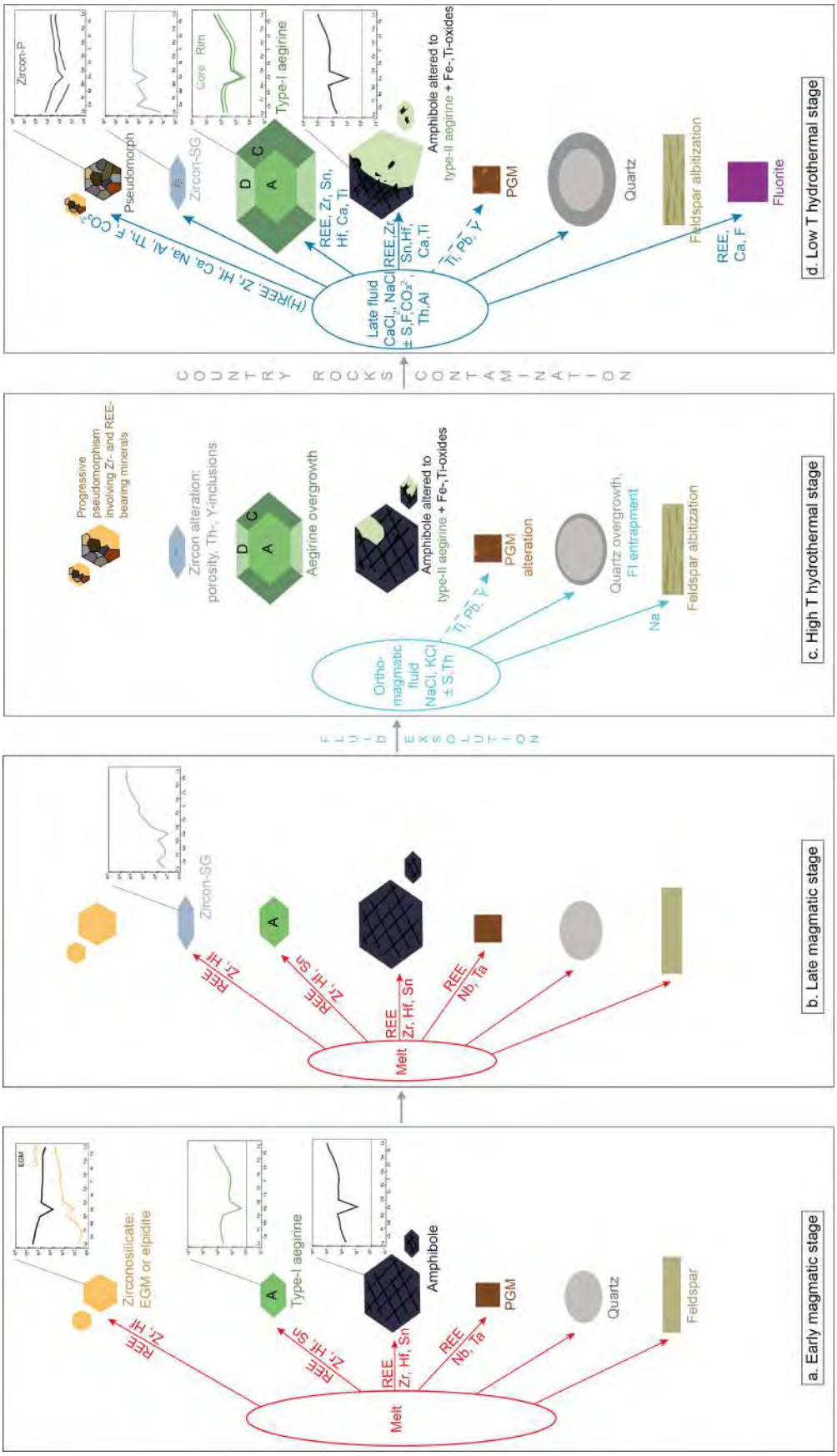

Figure 6.1 Synthesis of the steps for REE enrichment and fractionation of alkaline granitic complexes from magmatic to late-hydrothermal stage, witnessed by common minerals. The dashed blue arrows indicate the timing is undefined between the two hydrothermal stages

Conclusions and perspectives

Because of their evolved nature, alkaline complexes are known to host important primary concentrations of rare earth elements (REE). Thus, alkaline rocks represent potentially viable alternatives to ion-adsorption deposits, which currently account for most of the REE production. Most studies on alkaline rocks focus on silica-undersaturated rocks, hence silica-saturated alkaline complexes remain mostly undocumented. Yet, silica-saturated rocks are particularly enriched in heavy REE (HREE), which are rarer and have more industrial applications than light REE (LREE). Pegmatites concentrate these elements even more, as they form from most evolved parts of a melt. In the scientific community, debates are still ongoing as to the origin of REE enrichment and their fractionation. Although magmatic processes such as partial fusion and fractional crystallization are known to play a role, more and more studies point out the importance of hydrothermal processes.

This thesis uses 6 world-class alkaline complexes as field laboratory to investigate the role of fluids in concentrating and fractionating the REE. A first major result was provided by the study of minerals commonly found in these rocks, i.e. amphiboles, aegirine and zircon. It could be establish that hydrothermal fluids, either orthomagmatic or post-magmatic, have the ability to mobilize and concentrate significant amounts of REE. These REE are mostly concentrated in secondary minerals such as bastnäsite-(Ce), armstrongite or fluornatropyrochlore. Hydrothermal fluids also fractionate the REE by remobilizing the HREE more than the LREE, as shown by the composition of hydrothermal aegirine and by quantitative estimation of the proportion of REE-bearing hydrothermal minerals. This work also shows that the REE composition of secondary minerals, commonly forming pseudomorphs in these rocks, depends on the composition of the replaced primary mineral. However, the remobilization of REE by hydrothermal fluids is also effective at a larger scale as REE-bearing phases were found in fractures cross-cutting several minerals and the amount of REE in pseudomorphs is higher than in the primary zirconosilicate.

Another major aspect of this thesis is the study of fluid inclusions in all complexes, in order to document the properties of the fluids that remobilized and fractionated the REE. It appears that fluids circulate at relatively low temperatures, under 400 °C, with salinities varying widely from one complex to another as well as within a single complex. Despite these variations, two fluid compositions were systematically found in the complexes: a NaCl-KCl-rich fluid and a $CaCl_2$-NaCl-rich one. At Ambohimirahavavy, Manongarivo and Strange Lake, it has been established that the NaCl-, KCl-rich fluid is orthomagmatic; at Amis, Evisa and Khan Bogd, its origin remains undetermined. In addition, evaporate salt mounds analyses showed the common presence of anions such as F^-, SO_4^{2-}, CO_3^{2-} in fluid inclusions, in addition to OH^- and Cl^- that are classically present in hydrothermal fluids. All these anions have the potential to form stable REE complexes. Although REE fractionation by the fluid is not explained by our current knowledge of these ligands, their presence in most alkaline complexes of this study indicates that they play a key-role at least in mobilizing and concentrating the REE.

In light of the data provided by this work, it appears that more data on each fluid in the complexes need to be acquired in order to better constrain their timing of circulation. In addition, LA-ICPMS measurements on single fluid inclusions would precisely document the amounts and the ligands of each REE transported by the fluids. As such, they would help to better constrain the observed light-heavy REE fractionation that is indeed operated by hydrothermal fluids in alkaline granitic complexes. The study of pyrochlore group minerals (PGM) and feldspars, two magmatic minerals hydrothermally altered, would supplement this work. These minerals are likely to provide valuable information on the mobility of REE and other HFSE (e.g. Ti in PGM) in hydrothermal fluids.

Conclusions et perspectives

Étant issus de magmas très différenciés, les complexes alcalins sont enrichis en terres rares (TR). De ce fait, ils représentent une alternative viable aux argiles ioniques, dont sont actuellement extraites la majorité des TR. La majorité des études sur les roches alcalines ont été menées sur des roches sous-saturées en silice, et de nombreuses zones d'ombre subsistent pour les roches sur-saturées. Pourtant, les roches alcalines sur-saturées sont enrichies en TR lourdes, qui sont plus rares mais qui permettent plus d'applications industrielles que les TR légères. Les pegmatites, se formant à partir des magmas les plus évolués, sont encore plus concentrées en ces éléments. L'origine de l'enrichissement et du fractionnement des TR dans ces roches continue de faire débat de nos jours. En effet, bien que les processus magmatiques tels que le taux de fusion partielle et la cristallisation fractionnée jouent un rôle, un nombre croissant d'études montrent le rôle majeur joué par les fluides hydrothermaux.

Dans ce manuscrit, 6 complexes alcalins sont comparés pour comprendre le rôle des fluides hydrothermaux dans la concentration et le fractionnement des TR. Un premier résultat majeur est fourni par l'étude de minéraux communément trouvés dans ces roches, i.e. les amphiboles, les aégyrines et les zircons. Il a été établi que les fluides hydrothermaux, qu'ils soient orthomagmatiques ou post-magmatiques, peuvent mobiliser et concentrer les TR en grande quantité. Les TR sont concentrées principalement dans des minéraux secondaires tels que la bastnaësite-(Ce), l'armstrongite ou le fluornatropyrochlore. L'étude de la composition des aégyrines hydrothermales et le calcul de l'estimation de la proportion de TR présentes dans les minéraux hydrothermaux montre que les fluides fractionnent également les TR en remobilisant plus facilement des lourdes que les légères. L'étude de la composition des minéraux secondaires, communément trouvés dans les pseudomorphoses, a aussi montré que celle-ci dépend de la composition du minéral qu'ils remplacent. Cependant, la présence de phases à TR dans des fractures ainsi que la quantité de TR plus importante dans les pseudomorphoses que dans le zirconosilicate primaire indiquent que la

remobilisation des TR a aussi lieu à grande échelle.

Le deuxième aspect majeur de ce travail est l'étude des inclusions fluides. Elle a été réalisée dans les 6 complexes alcalins afin de documenter les propriétés du/des fluide(s) qui ont remobilisé et fractionné les TR. Les résultats montrent que les fluides circulent à une température relativement basse de 400 °C, et que leur salinité varie grandement, à la fois d'un complexe à l'autre et dans un même complexe. Malgré ces variations, deux compositions ont été systématiquement identifiées dans les 6 complexes : un fluide riche en NaCl et KCl, et un fluide riche en $CaCl_2$ et NaCl. À Ambohimirahavavy, Manongarivo et Strange Lake, le fluide riche en NaCl et KCl est orthomagmatique ; à Amis, Evisa et Khan Bogd, son origine est indéterminée. L'étude des décrépitats a en outre montré la présence d'anions dans des inclusions fluides tels que F^-, SO_4^{2-}, CO_3^{2-}, en plus de OH^- et Cl^- qui sont classiquement présents dans les fluides hydrothermaux. Tous ces anions sont de bons ligands pour les TR. Bien que le fractionnement des TR par le fluide ne soit pas explicable par nos connaissances actuelles de ces ligands, leur présence dans la majorité des complexes alcalins de cette étude indique qu'ils jouent un rôle clé, sinon dans le fractionnement, au moins dans la mobilisation et la concentration des TR.

Il ressort de ce travail que plus de données sur chaque fluide doivent être acquises afin de mieux comprendre leur chronologie relative. Des données LA-ICPMS localisées sur des inclusions seules permettraient de plus de documenter précisément les quantités de TR et les ligands associés dans les deux types de fluides, et par là-même comprendre l'origine du fractionnement TR légères-lourdes observé dans les complexes alcalins granitiques. L'étude des pyrochlores et des feldspaths, deux minéraux magmatiques altérés par des fluides hydrothermaux, permettrait de donner encore plus d'informations sur la mobilité des TR, mais également des HFSE (e.g. Ti dans les pyrochlores) dans les fluides hydrothermaux.

Bibliography

Allanite-(Ce). (2020). Retrieved May 6, 2020, from http://www.webmineral.com/data/Allanite-(Ce).shtml

Ancey, M., Bastenaire, F., and Tixier, R. (1978). Application des méthodes statistiques en microanalyse. *Microanalyse, microscopie électronique à balayage*, *323*(347), 11–16.

Anders, E., and Grevesse, N. (1989). Abundances of the elements: Meteoritic and solar. *Geochimica et Cosmochimica Acta*, *53*(1), 197–214. https://doi.org/10.1016/0016-7037(89)90286-X

Anderson, G. M., Pascal, M. L., and Rao, J. (1987). Aluminum Speciation in Metamorphic Fluids. In H. C. Helgeson (Ed.), *Chemical Transport in Metasomatic Processes* (pp. 297–321). Springer Netherlands. https://doi.org/10.1007/978-94-009-4013-0_12

Annen, C., Blundy, J. D., Leuthold, J., and Sparks, R. S. J. (2015). Construction and evolution of igneous bodies: Towards an integrated perspective of crustal magmatism. *Lithos*, *230*, 206–221.

Armstrongite. (2020). Retrieved May 6, 2020, from http://webmineral.com/data/Armstrongite.shtml

Atencio, D., Andrade, M. B., Christy, A. G., Gieré, R., and Kartashov, P. M. (2010). The pyrochlore supergroup of minerals: Nomenclature. *The Canadian Mineralogist*, *48*(3), 673–698.

Audétat, A. (2019). The Metal Content of Magmatic-Hydrothermal Fluids and Its Relationship to Mineralization Potential. *Economic Geology*, *114*(6), 1033–1056. https://doi.org/10.5382/econgeo.4673

Audétat, A., Pettke, T., Heinrich, C. A., and Bodnar, R. J. (2008). Special Paper: The Composition of Magmatic-Hydrothermal Fluids in Barren and Mineralized Intrusions. *Economic Geology*, *103*(5), 877–908. https://doi.org/10.2113/gsecongeo.103.5.877

Ayers, J. C., Zhang, L., Luo, Y., and Peters, T. J. (2012). Zircon solubility in alkaline aqueous fluids at upper crustal conditions. *Geochimica et Cosmochimica Acta*, *96*, 18–28. https://doi.org/10.1016/j.gca.2012.08.027

Badin, J. (1996). Observation sur la croissance fractale des cristaux de pyridinate de mercure engendrés dans un gel d'Agar. *Bulletin de liaison de la société Française de Minéralogie et de Cristallographie*, *8*, 30–34.

Bailey, E. H., and Ragnarsdottir, V. K. (1994). Uranium and thorium solubilities in subduction zone fluids. *Earth and Planetary Science Letters*, *124*(1), 119–129. https://doi.org/10.1016/0012-821X(94)00071-9

Baker, D. R. (1998). The escape of pegmatite dikes from granitic plutons; constraints from new models of viscosity and dike propagation. *The Canadian Mineralogist*, *36*(2), 255–263.

Bakker, R. J. (2003). Package FLUIDS 1. Computer programs for analysis of fluid inclusion data and for modelling bulk fluid properties. *Chemical Geology*, *194*(1), 3–23. https://doi.org/10.1016/S0009-2541(02)00268-1

Balashov, Y. A., and Glaznev, V. N. (2006). Cycles of alkaline magmatism. *Geochemistry International*, *44*(3), 274–285.

Banks, D. A., Yardley, B. W. D., Campbell, A. R., and Jarvis, K. E. (1994). REE composition of an aqueous magmatic fluid: A fluid inclusion study from the Capitan Pluton, New Mexico, U.S.A. *Chemical Geology*, *113*(3), 259–272. https://doi.org/10.1016/0009-2541(94)90070-1

Bédard, J. H. (2006). Trace element partitioning in plagioclase feldspar. *Geochimica et Cosmochimica Acta*, *70*(14), 3717–3742.

Bernard, C., Estrade, G., Salvi, S., Béziat, D., and Smith, M. (2020). Alkali pyroxenes and amphiboles: A window on rare earth elements and other high field strength elements behavior through the magmatic-hydrothermal transition of peralkaline granitic systems. *Contributions to Mineralogy and Petrology*, *175*(9). https://doi.org/10.1007/s00410-020-01723-y

Binnemans, K., Jones, P. T., Blanpain, B., Van Gerven, T., Yang, Y., Walton, A., and Buchert, M. (2013). Recycling of rare earths: A critical review. *Journal of cleaner production*, *51*, 1–22.

Birkett, T. C., Miller, R. R., Roberts, A. C., and Mariano, A. N. (1992). Zirconium-bearing minerals of the Strange Lake intrusive complex, Quebec-Labrador. *The Canadian Mineralogist*, *30*(1), 191–205.

Blanc, P., Baumer, A., Cesbron, F., Ohnenstetter, D., Panczer, G., and Rémond, G. (2000). Systematic Cathodoluminescence Spectral Analysis of Synthetic Doped Minerals: Anhydrite, Apatite, Calcite, Fluorite, Scheelite and Zircon. In M. Pagel, V. Barbin, P. Blanc, and D. Ohnenstetter (Eds.), *Cathodoluminescence in Geosciences* (pp. 127–160). Springer. https://doi.org/10.1007/978-3-662-04086-7_5

Bloodworth, A. (2010). Rare earth elements: A beginner's guide from the BGS | British Geological Survey (BGS). https://www.bgs.ac.uk/research/highlights/2010/rare_earth_elements.html

Bodnar, R. J. (1993). Revised equation and table for determining the freezing point depression of H2O-NaCl solutions. *Geochimica et Cosmochimica acta*, *57*(3), 683–684.

Bodnar, R. J., Lecumberri-Sanchez, P., Moncada, D., and Steele-MacInnis, M. (2014). Fluid inclusions in hydrothermal ore deposits. *Treatise on Geochemistry, Second Editionth edn. Elsevier, Oxford* (pp. 119–142).

Bodnar, R. J., Reynolds, T. J., and Kuehn, C. (1985). Fluid inclusion systematics in epithermal systems. *Reviews in Economic Geology* (pp. 73–97). Society of Economic Geology.

Boily, M., and Williams-Jones, A. E. (1994). The role of magmatic and hydrothermal processes in the chemical evolution of the Strange Lake plutonic complex, Quebec-Labrador. *Contributions to Mineralogy and Petrology*, *118*(1), 33–47.

Bollaert, Q. (2019, July). *Petrogenesis, Mineralisation and Remobilisation of Rare Metals of the Manongarivo Alkaline Complex, Madagascar* (Master) [Master].

Bonin, B. (1988). Peralkaline granites in Corsica: Some petrological and geochemical constraints. *Rendiconti della Società italiana di Mineralogia e Petrologia*, *43*(2), 281–306.

Bonin, B., Grelou-Orsini, C., and Vialette, Y. (1978). Age, origin and evolution of the anorogenic complex of Evisa (Corsica): A K-Li-Rb-Sr study. *Contributions to Mineralogy and Petrology*, *65*(4), 425–432.

Bonin, B., Platevoet, B., Poitrasson, F., and Renna, M. R. (2008). Eurogranites-IGCP510 2008 Joint Field-meeting-Alkaline The Permian–Triassic A-type Volcanic–Plutonic Igneous Suite of Corsica, Universite de Paris-Sud Paris. *33th International Geological Congress in Oslo, Norway Convention Centre, Lillestrom, Norway*.

Bonin, B. (1980). *Les complexes acides alcalins anorogéniques continentaux: L'exemple de la Corse* (PhD Thesis).

Bonin, B. (1990a). From orogenic to anorogenic settings: Evolution of granitoid suites after a major orogenesis. *Geological Journal*, *25*(3-4), 261–270.

Bonin, B. (1990b). *Les granites des complexes annulaires* (BRGM). Office des publications universitaires.

Bonin, B., and Platevoet, B. (1988). Interactions solide-fluide et phenomenes de fenitisation dans le magmatisme alcalin de Corse; l'exemple de l'association du Vieux Pont d'Ota. *Bulletin de la Société Géologique de France*, *4*(4), 571–578.

Borst, A. M., Friis, H., Andersen, T., Nielsen, T. F., Waight, T. E., and Smit, M. A. (2016). Zirconosilicates in the kakortokites of the Ilímaussaq complex, South Greenland: Implications for fluid evolution and high-field-strength and rare-earth element mineralization in agpaitic systems. *Mineralogical Magazine*, *80*(1), 5–30.

Bowen, N. L. (1945). Phase equilibria bearing on the origin and differentiation of alkaline rocks. *American Journal of Science*, *243*, 75–89.

Brisbin, W. C. (1986). Mechanics of pegmatite intrusion. *American Mineralogist*, *71*(3-4), 644–651.

British Geological Survey. (1998). *World mineral production 1992-1996*.

British Geological Survey. (2003). *World mineral production 1997-2001*.

British Geological Survey. (2008). *World mineral production 2002-2006*.

British Geological Survey. (2013). *World mineral production 2007-2011*.

British Geological Survey. (2018). *World mineral production 2012-2016*.

British Geological Survey. (2019). *World mineral production 2013-2017*.

Broom-Fendley, S., Brady, A. E., Wall, F., Gunn, G., and Dawes, W. (2017). REE minerals at the Songwe Hill carbonatite, Malawi: HREE-Enrichment in late-stage apatite. *Ore Geology Reviews*, *81*, 23–41. https://doi.org/10.1016/j.oregeorev.2016.10.019

Broom-Fendley, S., Styles, M. T., Appleton, J. D., Gunn, G., and Wall, F. (2016). Evidence for dissolution-reprecipitation of apatite and preferential LREE mobility in carbonatite-derived late-stage hydrothermal processes. *American Mineralogist*, *101*(3), 596–611. https://doi.org/10.2138/am-2016-5502CCBY

Bühn, B., and Rankin, A. H. (1999). Composition of natural, volatile-rich Na–Ca–REESr carbonatitic fluids trapped in fluid inclusions. *Geochimica et*

Cosmochimica Acta, *63*(22), 3781–3797. https://doi.org/10.1016/S0016-7037(99)00180-5

Bühn, B., Rankin, A. H., Schneider, J., and Dulski, P. (2002). The nature of orthomagmatic, carbonatitic fluids precipitating REE,Sr-rich fluorite: Fluid-inclusion evidence from the Okorusu fluorite deposit, Namibia. *Chemical Geology*, *186*(1), 75–98. https://doi.org/10.1016/S0009-2541(01)00421-1

Burnham, C. W., and Nekvasil, H. (1986). Equilibrium properties of granite pegmatite magmas. *American Mineralogist*, *71*(3-4), 239–263.

Calciohilairite. (2020). Retrieved May 6, 2020, from http://www.webmineral.com/data/Calciohilairite.shtml

Cameron, E. N. (1949). Internal structure of granitic pegmatites. *Econ. Geol., Monograph*, *2*, 115.

Carignan, J., Hild, P., Mevelle, G., Morel, J., and Yeghicheyan, D. (2001). Routine Analyses of Trace Elements in Geological Samples using Flow Injection and Low Pressure On-Line Liquid Chromatography Coupled to ICP-MS: A Study of Geochemical Reference Materials BR, DR-N, UB-N, AN-G and GH. *Geostandards Newsletter*, *25*(2-3), 187–198. https://doi.org/10.1111/j.1751-908X.2001.tb00595.x

_eprint: https://onlinelibrary.wiley.com/doi/pdf/10.1111/j.1751-908X.2001.tb00595.x

Castet, S., Dandurand, J.-L., Schott, J., and Gout, R. (1993). Boehmite solubility and aqueous aluminum speciation in hydrothermal solutions (90–350°C): Experimental study and modeling. *Geochimica et Cosmochimica Acta*, *57*(20), 4869–4884. https://doi.org/10.1016/0016-7037(93)90126-H

Castor, S. B., and Hedrick, J. B. (2006). Rare earth elements. *Industrial minerals and rocks*, 769–792.

Černy, P. (1991). Rare-element granitic pegmatites. Part I: Anatomy and internal evolution of pegmatitic deposits. *Geoscience Canada*.

Černy, P., and Ercit, T. S. (2005). The classification of granitic pegmatites revisited. *The Canadian Mineralogist*, *43*(6), 2005–2026.

Chakhmouradian, A. R., and Wall, F. (2012). Rare earth elements: Minerals, mines, magnets (and more). *Elements*, *8*(5), 333–340.

Chakhmouradian, A. R., and Zaitsev, A. N. (2012). Rare earth mineralization in igneous rocks: Sources and processes. *Elements*, *8*(5), 347–353. Retrieved

October 9, 2017, from http://elements.geoscienceworld.org/content/8/5/347.abstract

Chengyu, W., Dianhao, H., and Zhongxun, G. (1990). REE geochemistry in the weathered crust of granites, Longnan area, Jiangxi Province. *Acta Geologica Sinica-English Edition*, *3*(2), 193–209.

Chevkinite-(Ce). (2020). Retrieved May 6, 2020, from http://webmineral.com/data/Chevkinite-(Ce).shtml

Chopard, B., Herrmann, H. J., and Vicsek, T. (1991). Structure and growth mechanism of mineral dendrites. *Nature*, *353*(6343), 409–412.

Christophe-Michel-Lévy, M. (1961). Reproduction artificielle de quelques minéraux riches en zirconium (zircon, eudialyte, catapléite, elpidite) ; comparaison avec leurs conditions naturelles de formation. *Bulletin de Minéralogie*, *84*(3), 265–269. https://doi.org/10.3406/bulmi.1961.5487

CNMC. (2020). *IMA Mineral List with Database of Mineral Properties*. Retrieved May 6, 2020, from https://rruff.info/ima/

Cocherie, A., Rossi, P., Fanning, C. M., and Guerrot, C. (2005). Comparative use of TIMS and SHRIMP for U–Pb zircon dating of A-type granites and mafic tholeiitic layered complexes and dykes from the Corsican Batholith (France). *Lithos*, *82*(1-2), 185–219.

Crosby, W. O., and Fuller, M. L. (1897). Origin of pegmatite. *The American Geologist*, *19*(3), 147.

Cucciniello, C., Tucker, R. D., Jourdan, F., Melluso, L., and Morra, V. (2016). The age and petrogenesis of alkaline magmatism in the Ampasindava Peninsula and Nosy Be archipelago, northern Madagascar. *Mineralogy and Petrology*, *110*(2-3), 309–331.

Davris, P., Balomenos, E., Taxiarchou, M., Panias, D., and Paspaliaris, I. (2017a). Current and Alternative Routes in the Production of Rare Earth Elements. *BHM Berg-und Hüttenmännische Monatshefte*, *162*(7), 245–251.

Davris, P., Stopic, S., Balomenos, E., Panias, D., Paspaliaris, I., and Friedrich, B. (2017b). Leaching of rare earth elements from eudialyte concentrate by suppressing silica gel formation. *Minerals Engineering*, *108*, 115–122.

Deegan, F. M., Whitehouse, M. J., Troll, V. R., Budd, D. A., Harris, C., Geiger, H., and H\ aalenius, U. (2016). Pyroxene standards for SIMS oxygen isotope analysis and their application to Merapi volcano, Sunda arc, Indonesia. *Chemical Geology*, *447*, 1–10.

de Saint Blanquat, M., Horsman, E., Habert, G., Morgan, S., Vanderhaeghe, O., Law, R., and Tikoff, B. (2011). Multiscale magmatic cyclicity, duration of pluton construction, and the paradoxical relationship between tectonism and plutonism in continental arcs. *Tectonophysics*, *500*(1-4), 20–33.

de Wit, M. J. (2003). Madagascar: Heads it's a continent, tails it's an island. *Annual Review of Earth and Planetary Sciences*, *31*(1), 213–248.

Diamond, L. W. (2001). Review of the systematics of CO2–H2O fluid inclusions. *Lithos*, *55*(1-4), 69–99.

Diehl, M. (1990). Geology, mineralogy, geochemistry and hydrothermal alteration of the Brandberg alkaline complex, Namibia. *Memoir-Geological survey. South West Africa, Namibia*, (10).

Dill, H. G. (2015). Pegmatites and aplites: Their genetic and applied ore geology. *Ore Geology Reviews*, *69*, 417–561.

Donnot. (1963). *Complexes intrusifs alcalins de la province pétrographique d'Ampasindava (Côte N.O. de Madagascar)* (TAN-63/A.1). Bureau de recherches géologiques et minières.

Dostal, J. (2017). Rare Earth Element Deposits of Alkaline Igneous Rocks. *Resources*, *6*(3), 34. https://doi.org/10.3390/resources6030034

Eiler, J. M., Crawford, A., Elliott, T. I. M., Farley, K. A., Valley, J. W., and Stolper, E. M. (2000). Oxygen isotope geochemistry of oceanic-arc lavas. *Journal of Petrology*, *41*(2), 229–256.

Elliott, H. A. L., Wall, F., Chakhmouradian, A. R., Siegfried, P. R., Dahlgren, S., Weatherley, S., Finch, A. A., Marks, M. A. W., Dowman, E., and Deady, E. (2018). Fenites associated with carbonatite complexes: A review. *Ore Geology Reviews*, *93*, 38–59. https://doi.org/10.1016/j.oregeorev.2017.12.003

Elpidite. (2020). Retrieved May 6, 2020, from http://webmineral.com/data/Elpidite.shtml

Emerick, C. M., and Duncan, R. A. (1982). Age progressive volcanism in the Comores Archipelago, western Indian Ocean and implications for Somali plate tectonics. *Earth and Planetary Science Letters*, *60*(3), 415–428.

Estrade, G. (2014, January). *Le complexe cénozoïque alcalin d'Ambohimirahavavy à Madagascar : Origine, évolution et minéralisations en métaux rares*. Paul Sabatier - Toulouse 3. Toulouse.

Estrade, G., Béziat, D., Salvi, S., Tiepolo, M., Paquette, J.-L., and Rakotovao, S. (2014a). Unusual evolution of silica-under-and-oversaturated alkaline rocks

in the Cenozoic Ambohimirahavavy Complex (Madagascar): Mineralogical and geochemical evidence. *Lithos*, *206*, 361–383.

Estrade, G., Salvi, S., and Béziat, D. (2018). Crystallization and destabilization of eudialyte-group minerals in peralkaline granite and pegmatite: A case study from the Ambohimirahavavy complex, Madagascar. *Mineralogical Magazine*, *82*(2), 375–399.

Estrade, G., Salvi, S., Béziat, D., Rakotovao, S., and Rakotondrazafy, R. (2014b). REE and HFSE mineralization in peralkaline granites of the Ambohimirahavavy alkaline complex, Ampasindava peninsula, Madagascar. *Journal of African Earth Sciences*, *94*, 141–155.

Estrade, G., Salvi, S., Béziat, D., and Williams-Jones, A. E. (2015). The origin of skarn-hosted rare-metal mineralization in the Ambohimirahavavy alkaline complex, Madagascar. *Economic Geology*, *110*(6), 1485–1513.

Eudialyte. (2020). Retrieved May 6, 2020, from http://www.webmineral.com/data/Eudialyte.shtml

European Commission. (2018). Report: Critical raw materials and the circular economy. https://ec.europa.eu/commission/publications/report-critical-raw-materials-and-circular-economy_en

Faure, G., and Mensing, T. M. (Eds.). (2005). *Isotopes : Principles and applications*. Wiley. Retrieved June 2, 2020, from http://www.documentation.ird.fr/hor/fdi:010064579

Accession Number: fdi:010064579

Finch, R. J., and Hanchar, J. M. (2003). Structure and chemistry of zircon and zircon-group minerals. *Reviews in mineralogy and geochemistry*, *53*(1), 1–25.

Fitton, J. G., and Upton, B. G. J. (1987). Alkaline igneous rocks.

Foland, K. A., Landoll, J. D., Henderson, C. M. B., and Chen, J. (1993). Formation of cogenetic quartz and nepheline syenites. *Geochimica et Cosmochimica Acta*, *57*(3), 697–704.

French, J. E. (2010). Dendritic zircon formation by deterministic volume-filling fractal growth: Implications for the mechanisms of branch formation in dendrites. *American Mineralogist*, *95*(5-6), 706–716. https://doi.org/10.2138/am.2010.3320

Garcier, R. J., and Verrax, F. (2017). Critiques mais non recyclées: Expliquer les limites au recyclage des terres rares en Europe. *Flux*, (2), 51–63.

Geisler, T., Schaltegger, U., and Tomaschek, F. (2007). Re-equilibration of Zircon in Aqueous Fluids and Melts. *Elements*, *3*(1), 43–50. https://doi.org/10.2113/gselements.3.1.43

Gerdes, A., Kogarko, L. N., and Vladykin, N. V. (2017). New data on the age and nature of the Khan–Bogd alkaline granites, Mongolia. *Doklady Earth Sciences*, *477*, 1320–1324.

Ghazi, A. M., Vanko, D. A., Roedder, E., and Seeley, R. C. (1993). Determination of rare earth elements in fluid inclusions by inductively coupled plasma-mass spectrometry (ICP-MS). *Geochimica et Cosmochimica Acta*, *57*(18), 4513–4516. https://doi.org/10.1016/0016-7037(93)90500-V

Gittinsite. (2020). Retrieved May 6, 2020, from http://www.webmineral.com/data/Gittinsite.shtml

Goldschmidt, V. M. (1925). Geochemische Verteilungsgesetze der Elemente, Part V. Isomorphie und Polymorphie der Sesquioxyde. *Die Lanthaniden-Kontraktion und ihre Konsequenzen, Oslo*.

Goodenough, K. M., Schilling, J., Jonsson, E., Kalvig, P., Charles, N., Tuduri, J., Deady, E. A., Sadeghi, M., Schiellerup, H., and Müller, A. (2016). Europe's rare earth element resource potential: An overview of REE metallogenetic provinces and their geodynamic setting. *Ore Geology Reviews*, *72*, 838–856.

Goodenough, K. M., Shaw, R. A., Smith, M., Estrade, G., Marqu, E., Bernard, C., and Nex, P. (2019). Economic mineralization in pegmatites: Comparing and contrasting NYF and LCT examples. *The Canadian Mineralogist*, *57*(5), 753–755.

Goodenough, K. M., Wall, F., and Merriman, D. (2018). The rare earth elements: Demand, global resources, and challenges for resourcing future generations. *Natural Resources Research*, *27*(2), 201–216.

Gowans, R. M., Lewis, W. J., and Zalnieriunas, R. V. (2017). *Technical report for the updated mineral resource estimate for the Strange Lake property, Québec, Canada* (NI 43-101). Micon International Ltd. for Quest Rare Minerals Ltd. www.sedar.com

Graser, G., Potter, J., Köhler, J., and Markl, G. (2008). Isotope, major, minor and trace element geochemistry of late-magmatic fluids in the peralkaline Ilímaussaq intrusion, South Greenland. *Lithos*, *106*(3), 207–221. https://doi.org/10.1016/j.lithos.2008.07.007

Green, T. H., and Ringwood, A. E. (1968). Genesis of the calc-alkaline igneous rock suite. *Contributions to Mineralogy and Petrology*, *18*(2), 105–162.

Grigor'eva, A. A., Zubkova, N. V., Pekov, I. V., Kolitsch, U., Pushcharovsky, D. Y., Vigasina, M. F., Giester, G., Dordević, T., Tillmanns, E., and Chukanov, N. V. (2011). Crystal chemistry of elpidite from Khan Bogdo (Mongolia) and its K-and Rb-exchanged forms. *Crystallography Reports*, *56*(5), 832.

Grosse, F. (2010). Is recycling "part of the solution"? The role of recycling in an expanding society and a world of finite resources. *SAPI EN. S. Surveys and Perspectives Integrating Environment and Society*, (3.1).

Gysi, A. P., and Williams-Jones, A. E. (2013). Hydrothermal mobilization of pegmatite-hosted REE and Zr at Strange Lake, Canada: A reaction path model. *Geochimica et Cosmochimica Acta*, *122*, 324–352.

Gysi, A. P., Williams-Jones, A. E., and Collins, P. (2016). Lithogeochemical vectors for hydrothermal processes in the Strange Lake peralkaline granitic REE-Zr-Nb deposit. *Economic Geology*, *111*(5), 1241–1276.

Hall, D. L., Sterner, S. M., and Bodnar, R. J. (1988). Freezing point depression of NaCl-KCl-H 2 O solutions. *Economic Geology*, *83*(1), 197–202.

Harkins, W. D. (1917). The evolution of the elements and the stability of complex atoms. I. A new periodic system which shows a relation between the abundance of elements and the structure of the nuclei of atoms. *Journal of the American Chemical Society*, *39*(5), 856–879.

Harris, C., Dreyer, T., and le Roux, P. (2018). Petrogenesis of peralkaline granite dykes of the Straumsvola complex, western Dronning Maud Land, Antarctica. *Contributions to Mineralogy and Petrology*, *173*(1), 8.

Hatch, G. (2015). *TMR advanced rare-earth projects index: Technology Metals Research Web page*. Retrieved May 6, 2020, from https://www.techmetalsresearch.com/guide/what-are-rare-earth-metals/

Hoefs, J. (2009). *Stable isotope geochemistry* (8th ed.). Springer. https://doi.org/10.1007/978-3-319-78527-1

Hoskin, P. W. O. (2005). Trace-element composition of hydrothermal zircon and the alteration of Hadean zircon from the Jack Hills, Australia. *Geochimica et Cosmochimica Acta*, *69*(3), 637–648. https://doi.org/10.1016/j.gca.2004.07.006

Humphries, M. (2013). Rare Earth Elements: The Global Supply Chain. *Congresional Research Service. Disponível em:< https://fas. org/sgp/crs/natsec*, *41347*.

Ichihara, M., and Harding, A. (1995). Human Rights, the Environment and Radioactive Waste: A Study of the Asian Rare Earth Case in Malaysia. *Review of European Community and International Environmental Law*, *4*(1), 1–14. https://doi.org/10.1111/j.1467-9388.1995.tb00190.x _eprint: https://onlinelibrary.wiley.com/doi/pdf/10.1111/j.1467-9388.1995.tb00190.x

Ishihara, S., Hua, R., Hoshino, M., and Murakami, H. (2008). REE abundance and REE minerals in granitic rocks in the Nanling range, Jiangxi Province, southern China, and generation of the REE-rich weathered crust deposits. *Resource Geology*, *58*(4), 355–372.

Jahn, B.-m., Wu, F., Capdevila, R., Martineau, F., Zhao, Z., and Wang, Y. (2001). Highly evolved juvenile granites with tetrad REE patterns: The Woduhe and Baerzhe granites from the Great Xing'an Mountains in NE China. *Lithos*, *59*(4), 171–198. https://doi.org/10.1016/S0024-4937(01)00066-4

Jahns, R. H. (1953). The genesis of pegmatites II. Quantitative analysis of lithium-bearing pegmatite, Mora County, New Mexico. *American Mineralogist: Journal of Earth and Planetary Materials*, *38*(11-12), 1078–1112.

Jahns, R. H., and Burnham, C. W. (1969). Experimental studies of pegmatite genesis; l, A model for the derivation and crystallization of granitic pegmatites. *Economic Geology*, *64*(8), 843–864.

Jain, S. C., and Hughes, A. E. (1978). Ostwald ripening and its application to precipitates and colloids in ionic crystals and glasses. *Journal of Materials Science*, *13*(8), 1611–1631.

Jébrak, M., Marcoux, É., des ressources naturelles et de la faune, Q. (M., and Québec, G. (2008). *Géologie des ressources minérales*. Ministère des ressources naturelles et de la faune.

Kamenetsky, V. S., Naumov, V. B., Davidson, P., van Achterbergh, E., and Ryan, C. G. (2004). Immiscibility between silicate magmas and aqueous fluids: A melt inclusion pursuit into the magmatic-hydrothermal transition in the Omsukchan Granite (NE Russia). *Chemical Geology*, *210*(1), 73–90. https://doi.org/10.1016/j.chemgeo.2004.06.016

Kanazawa, Y., and Kamitani, M. (2006). Rare earth minerals and resources in the world. *Journal of alloys and compounds*, *408*, 1339–1343.

Keith-Roach, M., Grundfelt, B., Kousa, A., Pohjolainen, E., Magistrati, P., Aggelatou, V., Olivieri, N., and Ferrari, A. (2015). Past experience of environmental, health and safety issues in REE mining and processing industries and an

evaluation of related EU and international standards and regulations. *Final Report of the EuRare Project; Kemakta Konsult AB: Stockholm, Sweden; Geological Survey of Finland: Espoo, Finland*.

Kelly, W. C., and Burgio, P. A. (1983). Cryogenic scanning electron microscopy of fluid inclusions in ore and gangue minerals. *Economic Geology*, *78*(6), 1262–1267.

Kempe, U., Gruner, T., Nasdala, L., and Wolf, D. (2000). Relevance of cathodoluminescence for the interpretation of U-Pb zircon ages, with an example of an application to a study of zircons from the Saxonian Granulite Complex, Germany. *Cathodoluminescence in geosciences* (pp. 415–455). Springer.

Kogarko, L. N. (1990). Ore-forming potential of alkaline magmas. *Lithos*, *26*(1-2), 167–175.

Kogarko, L. N., Williams, C. T., and Woolley, A. R. (2002). Chemical evolution and petrogenetic implications of loparite in the layered, agpaitic Lovozero complex, Kola Peninsula, Russia. *Mineralogy and Petrology*, *74*(1), 1–24.

Konnerup-Madsen, J., and Rose-Hansen, J. (1984). Composition and significance of fluid inclusions in the Ilímaussaq peralkaline granite, South Greenland. *Bulletin de Minéralogie*, *107*(2), 317–326.

Kontak, D. J. (2004). Analysis of evaporate mounds as a complement to fluid-inclusion thermometric data: Case studies from granitic environments in Nova Scotia and Peru. *The Canadian Mineralogist*, *42*(5), 1315–1329.

Kovalenko, V. I., Yarmoluyk, V. V., Sal'nikova, E. B., Kozlovsky, A. M., Kotov, A. B., Kovach, V. P., Savatenkov, V. M., Vladykin, N. V., and Ponomarchuk, V. A. (2006). Geology, geochronology, and geodynamics of the Khan Bogd alkali granite pluton in southern Mongolia. *Geotectonics*, *40*(6), 450–466.

Kovalenko, V. I., and Yarmolyuk, V. V. (1995). Endogenous rare metal ore formations and rare metal metallogeny of Mongolia. *Economic Geology*, *90*(3), 520–529.

Kramm, U., and Kogarko, L. N. (1994). Nd and Sr isotope signatures of the Khibina and Lovozero agpaitic centres, Kola Alkaline Province, Russia. *Lithos*, *32*(3-4), 225–242.

Krumgalz, B. S., Pogorelsky, R., and Pitzer, K. S. (1996). Volumetric Properties of Single Aqueous Electrolytes from Zero to Saturation Concentration at 298.15 K Represented by Pitzer's Ion-Interaction Equations. *Journal of Physical and Chemical Reference Data*, *25*(2), 663–689.

Kynicky, J., Chakhmouradian, A. R., Xu, C., Krmicek, L., and Galiova, M. (2011). Distribution and evolution of zirconium mineralization in peralkaline granites and associated pegmatites of the Khan Bogd complex, southern Mongolia. *The Canadian Mineralogist*, *49*(4), 947–965.

Kyser, T. K., O'Neil, J. R., and Carmichael, I. S. (1981). Oxygen isotope thermometry of basic lavas and mantle nodules. *Contributions to Mineralogy and Petrology*, *77*(1), 11–23.

Lacroix, A. (1923). *Minéralogie de Madagascar*. A. Challamel, éditeur, Librairie maritime et coloniale.

Landes, K. K. (1933). Origin and classification of pegmatites. *American Mineralogist: Journal of Earth and Planetary Materials*, *18*(2), 33–56.

Larsen, L. M., and Sørensen, H. (1987). The Ilímaussaq intrusion—progressive crystallization and formation of layering in an agpaitic magma. *Geological Society, London, Special Publications*, *30*(1), 473–488.

Le Maitre, R. W. (2002). *A classification of igneous rocks and glossary of terms* (Vol. 193). Blackwell Scientific Publications.

Le Maitre, R. W., Streckeisen, A., and Zanettin, B. (2004). *Igneous rocks: IUGS classification and glossary: Recommendations of the International Union of Geological Sciences, Subcommission on the Systematics of Igneous Rock*. University of Cambridge.

Lecumberri-Sanchez, P., Steele-MacInnis, M., Weis, P., Driesner, T., and Bodnar, R. J. (2015). Salt precipitation in magmatic-hydrothermal systems associated with upper crustal plutons. *Geology*, *43*(12), 1063–1066. https://doi.org/10.1130/G37163.1

Li, X.-H., Li, W.-X., Li, Q.-L., Wang, X.-C., Liu, Y., and Yang, Y.-H. (2010). Petrogenesis and tectonic significance of the 850 Ma Gangbian alkaline complex in South China: Evidence from in situ zircon U–Pb dating, Hf–O isotopes and whole-rock geochemistry. *Lithos*, *114*(1-2), 1–15.

Linke, W. F. (1958). *Solubilities, inorganic and metal organic compounds: A compilation of solubility data from the periodical literature* (Vol. 1). Van Nostrand.

Linnen, R. L., Samson, I. M., Williams-Jones, A. E., and Chakhmouradian, A. R. (2014, January 1). Geochemistry of the Rare-Earth Element, Nb, Ta, Hf, and Zr Deposits. In H. D. Holland and K. K. Turekian (Eds.), *Treatise on Geochemistry (Second Edition)* (pp. 543–568). Elsevier. https://doi.org/10.1016/B978-0-08-095975-7.01124-4

Liu, Y., Zhu, Z., Chen, C., Zhang, S., Sun, X., Yang, Z., and Liang, W. (2015). Geochemical and mineralogical characteristics of weathered ore in the Dalucao REE deposit, Mianning–Dechang REE Belt, western Sichuan Province, southwestern China. *Ore Geology Reviews*, *71*, 437–456.

London, D. (1986). Magmatic-hydrothermal transition in the Tanco rare-element pegmatite: Evidence from fluid inclusions and phase-equilibrium experiments. *American Mineralogist*, *71*(3-4), 376–395.

London, D. (2008). Pegmatites. *The Canadian Mineralogist*, *10*.

London, D. (2014). A petrologic assessment of internal zonation in granitic pegmatites. *Lithos*, *184*, 74–104.

London, D. (2015). Reply to Thomas and Davidson on "A petrologic assessment of internal zonation in granitic pegmatites"(London, 2014a). *Lithos*, (212-215), 469–484.

London, D. (2018). Ore-forming processes within granitic pegmatites. *Ore Geology Reviews*, *101*, 349–383.

London, D., and Morgan, G. B. (2017). Experimental crystallization of the Macusani obsidian, with applications to lithium-rich granitic pegmatites. *Journal of Petrology*, *58*(5), 1005–1030.

Lottermoser, B. G. (1992). Rare earth elements and hydrothermal ore formation processes. *Ore Geology Reviews*, *7*(1), 25–41. https://doi.org/10.1016/0169-1368(92)90017-F

Lucas, J., Lucas, P., Le Mercier, T., Rollat, A., and Davenport, W. G. (2014). *Rare earths: Science, technology, production and use*. Elsevier.

Markl, G., Marks, M. A. W., and Frost, B. R. (2010). On the Controls of Oxygen Fugacity in the Generation and Crystallization of Peralkaline Melts. *Journal of Petrology*, *51*(9), 1831–1847. https://doi.org/10.1093/petrology/egq040

Marks, M., Vennemann, T., Siebel, W., and Markl, G. (2004). Nd-, O-, and H-isotopic evidence for complex, closed-system fluid evolution of the peralkaline Ilımaussaq intrusion, South Greenland. *Geochimica et Cosmochimica Acta*, *68*(16), 3379–3395.

Marks, M. A., Hettmann, K., Schilling, J., Frost, B. R., and Markl, G. (2011). The mineralogical diversity of alkaline igneous rocks: Critical factors for the transition from miaskitic to agpaitic phase assemblages. *Journal of Petrology*, *52*(3), 439–455.

Marks, M. A., and Markl, G. (2015). The ilímaussaq alkaline complex, South Greenland. *Layered Intrusions* (pp. 649–691). Springer.

Marks, M. A., and Markl, G. (2017). A global review on agpaitic rocks. *Earth-Science Reviews*, *173*, 229–258.

Marquis, E. (2019). *Rare Earth Element (REE) mobility in alkaline igneous rocks and the potential impact on the formation of ion adsorption type ree ores of the Ambohimirahavavy Alkaline Complex*. University of Brighton.

Marshall, D. J., and Mariano, A. N. (1988). *Cathodoluminescence of geological materials*. Taylor and Francis.

Mattey, D., Lowry, D., and Macpherson, C. (1994). Oxygen isotope composition of mantle peridotite. *Earth and Planetary Science Letters*, *128*(3-4), 231–241.

McDonough, W. F., and Sun, S.-S. (1995). The composition of the Earth. *Chemical geology*, *120*(3-4), 223–253.

Menand, T., Annen, C., and de Saint Blanquat, M. (2015). Rates of magma transfer in the crust: Insights into magma reservoir recharge and pluton growth. *Geology*, *43*(3), 199–202.

Mesto, E., Kaneva, E., Schingaro, E., Vladykin, N., Lacalamita, M., and Scordari, F. (2014). Armstrongite from Khan Bogdo (Mongolia): Crystal structure determination and implications for zeolite-like cation exchange properties. *American Mineralogist*, *99*(11-12), 2424–2432.

Migdisov, A. A., and Williams-Jones, A. E. (2008). A spectrophotometric study of Nd(III), Sm(III) and Er(III) complexation in sulfate-bearing solutions at elevated temperatures. *Geochimica et Cosmochimica Acta*, *72*(21), 5291–5303. https://doi.org/10.1016/j.gca.2008.08.002

Migdisov, A. A., and Williams-Jones, A. E. (2014). Hydrothermal transport and deposition of the rare earth elements by fluorine-bearing aqueous liquids. *Mineralium Deposita*, *49*(8), 987–997. https://doi.org/10.1007/s00126-014-0554-z

Migdisov, A. A., Williams-Jones, A. E., van Hinsberg, V., and Salvi, S. (2011). An experimental study of the solubility of baddeleyite (ZrO2) in fluoride-bearing solutions at elevated temperature. *Geochimica et Cosmochimica Acta*, *75*(23), 7426–7434. https://doi.org/10.1016/j.gca.2011.09.043

Migdisov, A. A., Williams-Jones, A. E., and Wagner, T. (2009). An experimental study of the solubility and speciation of the Rare Earth Elements (III) in

fluoride-and chloride-bearing aqueous solutions at temperatures up to 300 C. *Geochimica et Cosmochimica Acta*, *73*(23), 7087–7109.

Migdisov, A., Williams-Jones, A. E., Brugger, J., and Caporuscio, F. A. (2016). Hydrothermal transport, deposition, and fractionation of the REE: Experimental data and thermodynamic calculations. *Chemical Geology*, *439*, 13–42.

Mikhailova, J. A., Pakhomovsky, Y. A., Ivanyuk, G. Y., Bazai, A. V., Yakovenchuk, V. N., Elizarova, I. R., and Kalashnikov, A. O. (2017). REE mineralogy and geochemistry of the Western Keivy peralkaline granite massif, Kola Peninsula, Russia. *Ore Geology Reviews*, *82*, 181–197.

Miller, R. M. (1983). The Pan-African Damara Orogen of South West Africa/Namibia. *Evolution of the Damara Orogen of South West Africa/Namibia*. Geological Survey.

Miller, R. R. (1986). Geology of the Strange Lake alkalic complex and the associated Zr-Y-Nb-Be-REE mineralization. *Newfoundland Department of Mines and Energy, Mineral Development Division, Report*, *86*(1), 11–19.

Miller, R. R. (1996). Structural and textural evolution of the Strange Lake peralkaline rare-element (NYF) granitic pegmatite, Quebec-Labrador. *The Canadian Mineralogist*, *34*(2), 349–371.

Monazite-(Ce). (2020). Retrieved May 6, 2020, from http://www.webmineral.com/data/Monazite-(Ce).shtml

Moore, M., Chakhmouradian, A. R., Mariano, A. N., and Sidhu, R. (2015). Evolution of rare-earth mineralization in the Bear Lodge carbonatite, Wyoming: Mineralogical and isotopic evidence. *Ore Geology Reviews*, *64*, 499–521.

Mueller, S. R., Wäger, P. A., Widmer, R., and Williams, I. D. (2015). A geological reconnaissance of electrical and electronic waste as a source for rare earth metals. *Waste Management*, *45*, 226–234.

Naden, J. (1996). CalcicBrine; a Microsoft Excel 5.0 add-in for calculating salinities from microthermometric data in the system NaCl-CaCl2-H2O. *PACROFI VI, Madison, WI*.

Nasdala, L., Zhang, M., Kempe, U., Panczer, G., Gaft, M., Andrut, M., and Plötze, M. (2003). Spectroscopic methods applied to zircon. *Reviews in Mineralogy and Geochemistry*, *53*(1), 427–467.

Nicholls, J., and Carmichael, J. S. E. (1969). Peralkaline acid liquids: A petrological study. *Contributions to mineralogy and petrology*, *20*(3), 268–294.

Nisbet, H., Williams-Jones, A. E., Xu, H., Van Hinsberg, V., and Roback, R. (2019). The Behavior of Th in REE-Bearing Hydrothermal Fluids, 2448. Retrieved August 5, 2020, from https://goldschmidt.info/2019/abstracts/abstractView?id=2019001263

Norman, D. I., Kyle, P. R., and Baron, C. (1989). Analysis of trace elements including rare earth elements in fluid inclusion liquids. *Economic Geology*, *84*(1), 162–166. https://doi.org/10.2113/gsecongeo.84.1.162

Nougier, J., Cantagrel, J. M., and Karche, J. P. (1986). The Comores archipelago in the western Indian Ocean: Volcanology, geochronology and geodynamic setting. *Journal of African Earth Sciences (1983)*, *5*(2), 135–145.

Oakes, C. S., Bodnar, R. J., and Simonson, J. M. (1990). The system NaCl CaCl2 H2O: I. The ice liquidus at 1 atm total pressure. *Geochimica et Cosmochimica Acta*, *54*(3), 603–610.

Oddo, G. (1914). Die molekularstruktur der Radioaktiven atome. *Zeitschrift für anorganische Chemie*, *87*(1), 253–268.

Ohmoto, H. (1986). Stable isotope geochemistry of ore deposit. in Stable Isotopes in High Temperature Geological Processes. *Review in Mineralogy*, *16*, 491–559.

Pascal, M. L., and Anderson, G. M. (1989). Speciation of Al, Si, and K in supercritical solutions: Experimental study and interpretation. *Geochimica et Cosmochimica Acta*, *53*(8), 1843–1855. https://doi.org/10.1016/0016-7037(89)90305-0

Pelt, E., Chabaux, F., Innocent, C., Navarre-Sitchler, A. K., Sak, P. B., and Brantley, S. L. (2008). Uranium–thorium chronometry of weathering rinds: Rock alteration rate and paleo-isotopic record of weathering fluids. *Earth and Planetary Science Letters*, *276*(1), 98–105. https://doi.org/10.1016/j.epsl.2008.09.010

Pettke, T., Audétat, A., Schaltegger, U., and Heinrich, C. A. (2005). Magmatic-to-hydrothermal crystallization in the W–Sn mineralized Mole Granite (NSW, Australia): Part II: Evolving zircon and thorite trace element chemistry. *Chemical Geology*, *220*(3), 191–213. https://doi.org/10.1016/j.chemgeo.2005.02.017

Pillet, D., Bonhomme, M. G., Duthou, J. L., and Chenevoy, M. (1989). Chronologie Rb/Sr et K/Ar du granite peralcalin du lac Brisson, Labrador central, Nouveau-Québec. *Canadian Journal of Earth Sciences*, *26*(2), 328–332.

Pirajno, F. (2015). Intracontinental anorogenic alkaline magmatism and carbonatites, associated mineral systems and the mantle plume connection. *Gondwana Research*, *27*(3), 1181–1216.

Poitrasson, F. (2002). In situ investigations of allanite hydrothermal alteration: Examples from calc-alkaline and anorogenic granites of Corsica (southeast France). *Contributions to Mineralogy and Petrology*, *142*(4), 485–500.

Poitrasson, F., Duthou, J.-L., and Pin, C. (1995). The relationship between petrology and Nd isotopes as evidence for contrasting anorogenic granite genesis: Example of the Corsican Province (SE France). *Journal of Petrology*, *36*(5), 1251–1274.

Poitrasson, F., Paquette, J.-L., Montel, J.-M., Pin, C., and Duthou, J.-L. (1998). Importance of late-magmatic and hydrothermal fluids on the Sm–Nd isotope mineral systematics of hypersolvus granites. *Chemical Geology*, *146*(3), 187–203.

Ponthus, L. (2018). *Origine, évolution et mise en place d'un pluton récent en contexte intraplaque océanique. Exemple du complexe sud de Rallier du Baty, Kerguelen (TAAF)* (PhD Thesis).

Potter, J. (2000). *The characterisation and origin of hydrocarbons in alkaline rocks of the Kola alkaline province* (Doctoral dissertation). Kingston University. Retrieved July 14, 2020, from http://ethos.bl.uk/OrderDetails.do?uin=uk.bl.ethos.323560

Quin, J.-P. (1969). *Les granites alcalins et hyper-alcalins de Nord-Ouest de la Corse* (PhD Thesis). Univ. d'Aix-Marseille.

Rakotovao, A. P. (2009). *Contexte géologique et métallogénique des minéralisations en émeraude du gisement de Ianapera, bloc du Vohibory, Sud-Ouest de Madagascar* (PhD Thesis). Université de Toulouse, Université Toulouse III-Paul Sabatier.

Rakotovao, S., Rakotondrazafy, R., Beziat, D., Salvi, S., and Rasolomanana, E. (2009). Pétrologie du complexe alcalin cénozoïque d'Ambohimirahavavy, presqu'île d'Ampasindava, nord-ouest de Madagascar. *Mada-Géo*, *13*, 2–19.

Ridolfi, F., Renzulli, A., Santi, P., and Upton, B. G. J. (2003). Evolutionary stages of crystallization of weakly peralkaline syenites: Evidence from ejecta in the plinian deposits of Agua de Pau volcano (São Miguel, Azores Islands). *Mineralogical Magazine*, *67*(4), 749–767.

Roedder, E. (1971). Metastability in fluid inclusions. *Soc. Mining Geol. Japan, Spec. Issue*, *3*, 327–34.

Roedder, E. (1984). Fluid inclusions. *Mineralogical Society of America*, *12*, 644.

Roedder, E., and Bodnar, R. J. (1980). Geologic pressure determinations from fluid inclusion studies. *Annual review of earth and planetary sciences*, *8*(1), 263–301.

Roelofsen, J. N., and Veblen, D. R. (1999). Relationships among zirconosilicates: Examination by cathodoluminescence and transmission electron microscopy. *Mineralogy and Petrology*, *67*(1-2), 71–84.

Rosman, K. J. R., and Taylor, P. D. P. (1998). Isotopic compositions of the elements 1997 (Technical Report). *Pure and Applied Chemistry*, *70*(1), 217–235. https://doi.org/10.1351/pac199870010217

Rossi, P., Marre, J., Cocherie, A., and Caballero, Y. (2010). Notice explicative de la feuille Vico-Cargèse (1113).

Rudnick, R. L., and Gao, S. (2003). Composition of the continental crust. *The crust*, *3*, 1–64.

Rusk, B., Reed, M. H., Dilles, J. H., and Kent, A. J. R. (2006). Intensity of quartz cathodoluminescence and trace-element content in quartz from the porphyry copper deposit at Butte, Montana. *American Mineralogist*, *91*(8-9), 1300–1312. Retrieved May 20, 2020, from https://www.semanticscholar.org/paper/Intensity-of-quartz-cathodoluminescence-and-content-Rusk-Reed/96ada00a7db0c946667f4dd5090b2485e210a7b8#paper-header

Salvi, S., and Williams-Jones, A. E. (1990). The role of hydrothermal processes in the granite-hosted Zr, Y, REE deposit at Strange Lake, Quebec/Labrador: Evidence from fluid inclusions. *Geochimica et Cosmochimica Acta*, *54*(9), 2403–2418.

Salvi, S., and Williams-Jones, A. E. (1992). Reduced orthomagmatic C-O-H-N-NaCl fluids in the Strange Lake rare-metal granitic complex, Quebec/Labrador, Canada. *European Journal of Mineralogy*, 1155–1174. https://doi.org/10.1127/ejm/4/5/1155

Salvi, S., and Williams-Jones, A. E. (1995). Zirconosilicate phase relations in the Strange Lake (Lac Brisson) Pluton, Quebec-Labrador, Canada. *American Mineralogist*, *80*(9-10), 1031–1040. https://doi.org/10.2138/am-1995-9-1019

Salvi, S., and Williams-Jones, A. E. (1996). The role of hydrothermal processes in concentrating high-field strength elements in the Strange Lake peralkaline complex, northeastern Canada. *Geochimica et Cosmochimica Acta*, *60*(11), 1917–1932.

Salvi, S., and Williams-Jones, A. E. (1997). Fischer-Tropsch synthesis of hydrocarbons during sub-solidus alteration of the Strange Lake peralkaline granite, Quebec/Labrador, Canada. *Geochimica et Cosmochimica Acta*, *61*(1), 83–99.

Salvi, S., and Williams-Jones, A. E. (2006). Alteration, HFSE mineralisation and hydrocarbon formation in peralkaline igneous systems: Insights from the Strange Lake Pluton, Canada. *Lithos*, *91*(1), 19–34.

Salvi, S., Williams-Jones, A. E., Linnen, R. L., and Samson, I. M. (2005). Alkaline granite-syenite deposits. *Geological Association of Canada Short Course Notes*, *17*, 315–341.

Sanematsu, K., Kon, Y., Imai, A., Watanabe, K., and Watanabe, Y. (2013). Geochemical and mineralogical characteristics of ion-adsorption type REE mineralization in Phuket, Thailand. *Mineralium Deposita*, *48*(4), 437–451.

Schijf, J., and Byrne, R. H. (2004). Determination of SO41 for yttrium and the rare earth elements at I = 0.66 m and t = 25°C—implications for YREE solution speciation in sulfate-rich waters1 1Associate editor: D. J. Wesolowski. *Geochimica et Cosmochimica Acta*, *68*(13), 2825–2837. https://doi.org/10.1016/j.gca.2003.12.003

Schmitt, A. K., Emmermann, R., Trumbull, R. B., Bühn, B., and Henjes-Kunst, F. (2000). Petrogenesis and 40Ar/39Ar geochronology of the Brandberg Complex, Namibia: Evidence for a major mantle contribution in metaluminous and peralkaline granites. *Journal of Petrology*, *41*(8), 1207–1239.

Schmitt, A. K., Trumbull, R. B., Dulski, P., and Emmermann, R. (2002). Zr-Nb-REE mineralization in peralkaline granites from the Amis Complex, Brandberg (Namibia): Evidence for magmatic pre-enrichment from melt inclusions. *Economic Geology*, *97*(2), 399–413.

Schwinn, G., and Markl, G. (2005). REE systematics in hydrothermal fluorite. *Chemical Geology*, *216*(3), 225–248. https://doi.org/10.1016/j.chemgeo.2004.11.012

Shannon, R. D. (1976). Revised effective ionic radii and systematic studies of interatomic distances in halides and chalcogenides. *Acta crystallographica section A: crystal physics, diffraction, theoretical and general crystallography*, *32*(5), 751–767.

Sheoran, V., Sheoran, A. S., and Poonia, P. (2009). Phytomining: A review. *Minerals Engineering*, *22*(12), 1007–1019.

Shepherd, T. J., Rankin, A. H., and Alderton, D. H. (1985). *A practical guide to fluid inclusion studies*. Blackie.

Siegel, K., Williams-Jones, A. E., and van Hinsberg, V. J. (2017). The amphiboles of the REE-Rich A-Type peralkaline Strange Lake pluton–fingerprints of magma evolution. *Lithos*, *288*, 156–174.

Sirbescu, M.-L. C., Schmidt, C., Veksler, I. V., Whittington, A. G., and Wilke, M. (2017). Experimental crystallization of undercooled felsic liquids: Generation of pegmatitic texture. *Journal of Petrology*, *58*(3), 539–568.

Smith, M. P., Moore, K., Kavecsánszki, D., Finch, A. A., Kynicky, J., and Wall, F. (2016). From mantle to critical zone: A review of large and giant sized deposits of the rare earth elements. *Geoscience Frontiers*, *7*(3), 315–334. https://doi.org/10.1016/j.gsf.2015.12.006

Soman, A., Geisler, T., Tomaschek, F., Grange, M., and Berndt, J. (2010). Alteration of crystalline zircon solid solutions: A case study on zircon from an alkaline pegmatite from Zomba–Malosa, Malawi. *Contributions to Mineralogy and Petrology*, *160*(6), 909–930.

Sørensen, H. (1974). Alkaline rocks. Retrieved May 6, 2020, from https://agris.fao.org/agris-search/search.do?recordID=US201300505898

Sørensen, H. (1997). The agpaitic rocks-an overview. *Mineralogical Magazine*, *61*(407), 485–498.

Sørensen, H., and Larsen, L. M. (1987). Layering in the Ilímaussaq alkaline intrusion, South Greenland. *Origins of igneous layering* (pp. 1–28). Springer.

Steele-MacInnis, M., Lecumberri-Sanchez, P., and Bodnar, R. J. (2012). HokieFlincs_H2O-NaCl: A Microsoft Excel spreadsheet for interpreting microthermometric data from fluid inclusions based on the PVTX properties of H2O-NaCl. *Computers and Geosciences*, *49*, 334–337.

Stefanski, J. (2020). *Thermodynamic Properties and Structure of Aqueous Fluids in Geological Processes*. Universität zu Köln.

Sun, S.-S., and McDonough, W. F. (1989). Chemical and isotopic systematics of oceanic basalts: Implications for mantle composition and processes. *Geological Society, London, Special Publications*, *42*(1), 313–345.

Tagirov, B., Schott, J., Harrichourry, J.-C., and Salvi, S. (2002). Experimental study of aluminum speciation in fluoride-rich supercritical fluids. *Geochimica et Cosmochimica Acta*, *66*(11), 2013–2024.

Tarnopolskaia, M. E., and Bychkov, A. Y. (2019). Experimental study of fluoride complexes of zirconium and hafnium in hydrothermal solutions, 1.

Taylor, H. P. (1977). Water/rock interactions and the origin of H2O in granitic batholiths: Thirtieth William Smith lecture. *Journal of the Geological Society*, *133*(6), 509–558. https://doi.org/10.1144/gsjgs.133.6.0509

Taylor, H. P. (1978). Oxygen and hydrogen isotope studies of plutonic granitic rocks. *Earth and Planetary Science Letters*, *38*(1), 177–210. https://doi.org/10.1016/0012-821X(78)90131-0

Thomas, R., and Davidson, P. (2016). Revisiting complete miscibility between silicate melts and hydrous fluids, and the extreme enrichment of some elements in the supercritical state—consequences for the formation of pegmatites and ore deposits. *Ore Geology Reviews*, *72*, 1088–1101.

Thomas, R., and Davidson, P. (2015). Comment on" A Petrologic Assessment of Internal Zonation in Granitic Pegmatites" by David London (2014). *Lithos*, *212*, 462–468.

Thomas, R., Davidson, P., and Beurlen, H. (2012). The competing models for the origin and internal evolution of granitic pegmatites in the light of melt and fluid inclusion research. *Mineralogy and Petrology*, *106*(1-2), 55–73.

Thomas, R., Förster, H.-J., and Heinrich, W. (2003). The behaviour of boron in a peraluminous granite-pegmatite system and associated hydrothermal solutions: A melt and fluid-inclusion study. *Contributions to Mineralogy and Petrology*, *144*(4), 457–472.

Thomas, R., Webster, J. D., and Heinrich, W. (2000). Melt inclusions in pegmatite quartz: Complete miscibility between silicate melts and hydrous fluids at low pressure. *Contributions to Mineralogy and Petrology*, *139*(4), 394–401.

Thomas, R., Webster, J. D., Rhede, D., Seifert, W., Rickers, K., Förster, H. .-J., Heinrich, W., and Davidson, P. (2006a). The transition from peraluminous to peralkaline granitic melts: Evidence from melt inclusions and accessory minerals. *Lithos*, *91*(1), 137–149. https://doi.org/10.1016/j.lithos.2006.03.013

Thomas, R., Webster, J. D., and Davidson, P. (2006b). Understanding pegmatite formation: The melt and fluid inclusion approach. *Melt inclusions in plutonic rocks*, *36*, 189–210.

Thomas, R. J., De Waele, B., Schofield, D. I., Goodenough, K. M., Horstwood, M., Tucker, R., Bauer, W., Annells, R., Howard, K., and Walsh, G.

(2009). Geological evolution of the Neoproterozoic Bemarivo Belt, northern Madagascar. *Precambrian Research*, *172*(3-4), 279–300.

Timofeev, A., and Williams-Jones, A. E. (2015). The origin of niobium and tantalum mineralization in the Nechalacho REE Deposit, NWT, Canada. *Economic Geology*, *110*(7), 1719–1735.

Titanite. (2020). Retrieved May 15, 2020, from http://webmineral.com/data/Titanite.shtml

Trail, D., Bruce Watson, E., and Tailby, N. D. (2012). Ce and Eu anomalies in zircon as proxies for the oxidation state of magmas. *Geochimica et Cosmochimica Acta*, *97*, 70–87. https://doi.org/10.1016/j.gca.2012.08.032

Trumbull, R. B., Harris, C., Frindt, S., and Wigand, M. (2004). Oxygen and neodymium isotope evidence for source diversity in Cretaceous anorogenic granites from Namibia and implications for A-Type granite genesis. *Lithos*, *73*(1-2), 21–40.

U.S. Geological Survey. (2019). *Mineral Commodity Summaries 2019* (USGS Unnumbered Series).

U.S. Geological Survey. (2020). *Mineral Commodity Summaries 2020* (USGS Unnumbered Series).

Ussing, N. V. (1912). *Geology of the country around Julianehaab, Greenland* (Vol. 38). Bianco Luno.

Vaglio, D., Chiaradia, M., and Garamjav, D. (2007). *Mineralogy, geochemistry and geochronology of pegmatites and associated alkaline granite rocks of the Khan Bogd complex: South Mongolia*. Section des Sciences de la terre [de] l'Université.

Vasyukova, O., and Williams-Jones, A. E. (2016). The evolution of immiscible silicate and fluoride melts: Implications for REE ore-genesis. *Geochimica et Cosmochimica Acta*, *172*, 205–224.

Vasyukova, O. V., and Williams-Jones, A. E. (2018). Direct measurement of metal concentrations in fluid inclusions, a tale of hydrothermal alteration and REE ore formation from Strange Lake, Canada. *Chemical Geology*, *483*, 385–396.

Vasyukova, O. V., and Williams-Jones, A. E. (2019). Closed system fluid-mineral-mediated trace element behaviour in peralkaline rare metal pegmatites: Evidence from Strange Lake. *Chemical Geology*, *505*, 86–99.

Vasyukova, O., and Williams-Jones, A. (2020). Partial melting, fractional crystallisation, liquid immiscibility and hydrothermal mobilisation–A

'Recipe'for the formation of economic A-Type granite-hosted HFSE deposits. *Lithos*, *356*, 105300.

Vasyukova, O., and Williams-Jones, A. E. (2014). Fluoride–silicate melt immiscibility and its role in REE ore formation: Evidence from the Strange Lake rare metal deposit, Québec-Labrador, Canada. *Geochimica et Cosmochimica Acta*, *139*, 110–130.

Veksler, I. V., Dorfman, A. M., Dulski, P., Kamenetsky, V. S., Danyushevsky, L. V., Jeffries, T., and Dingwell, D. B. (2012). Partitioning of elements between silicate melt and immiscible fluoride, chloride, carbonate, phosphate and sulfate melts, with implications to the origin of natrocarbonatite. *Geochimica et Cosmochimica Acta*, *79*, 20–40.

Vellutini, P., Rossi, P., Michon, G., and Hervé, J. (1996). Notice explicative de la feuille Galeria-Osani (1109).

Verplanck, P. L., and Van Gosen, B. S. (2011). *Carbonatite and Alkaline Intrusion-Related Rare Earth Element Deposits: A Deposit Model*. US Department of the Interior, US Geological Survey.

Vlasov, K. A. (1961). Principles of classifying granite pegmatites and their textural–paragenetic types. *Transactions of the Academy of Sciences, USSR, Geologic Series*, *1*, 5–20.

Vlasovite. (2020). Retrieved May 6, 2020, from http://www.webmineral.com/data/Vlasovite.shtml

Wall, F., and Zaitsev, A. N. (2004). Rare earth minerals in Kola carbonatites. *Phoscorites and carbonatites from mantle to mine: the key example of the Kola Alkaline Province*, 43–72.

Wall, F. (2014). Rare earth elements. *Critical metals handbook*, 312–339.

Wang, Q., Deng, J., Liu, X., Zhang, Q., Sun, S., Jiang, C., and Zhou, F. (2010). Discovery of the REE minerals and its geological significance in the Quyang bauxite deposit, West Guangxi, China. *Journal of Asian Earth Sciences*, *39*(6), 701–712.

Weber, R. J., and Reisman, D. J. (2012). Rare earth elements: A review of production, processing, recycling, and associated environmental issues. *US EPA Region*.

Wilkinson, J. J., Nolan, J., and Rankin, A. H. (1996). Silicothermal fluid: A novel medium for mass transport in the lithosphere. *Geology*, *24*(12), 1059–1062.

Wood, S. A. (1990). The aqueous geochemistry of the rare-earth elements and yttrium: 1. Review of available low-temperature data for inorganic

complexes and the inorganic REE speciation of natural waters. *Chemical Geology*, *82*, 159–186.

Woolley, A. R. (2001). Alkaline rocks and carbonatites of the world: Part 3. *Africa: London, Geological Society of London*.

Workman, R. K., and Hart, S. R. (2005). Major and trace element composition of the depleted MORB mantle (DMM). *Earth and Planetary Science Letters*, *231*(1-2), 53–72.

Xu, C., Kynick, J., Smith, M. P., Kopriva, A., Brtnick, M., Urubek, T., Yang, Y., Zhao, Z., He, C., and Song, W. (2017). Origin of heavy rare earth mineralization in South China. *Nature communications*, *8*(1), 1–7.

Yang, W.-B., Niu, H.-C., Shan, Q., Sun, W.-D., Zhang, H., Li, N.-B., Jiang, Y.-H., and Yu, X.-Y. (2014). Geochemistry of magmatic and hydrothermal zircon from the highly evolved Baerzhe alkaline granite: Implications for Zr–REE–Nb mineralization. *Mineralium Deposita*, *49*(4), 451–470.

Yang, X.-M., Yang, X.-Y., Zheng, Y.-F., and Le Bas, M. J. (2003). A rare earth element-rich carbonatite dyke at Bayan Obo, Inner Mongolia, North China. *Mineralogy and Petrology*, *78*(1-2), 93–110.

Zaitsev, A. N., Williams, C. T., Jeffries, T. E., Strekopytov, S., Moutte, J., Ivashchenkova, O. V., Spratt, J., Petrov, S. V., Wall, F., and Seltmann, R. (2015). Rare earth elements in phoscorites and carbonatites of the Devonian Kola Alkaline Province, Russia: Examples from Kovdor, Khibina, Vuoriyarvi and Turiy Mys complexes. *Ore Geology Reviews*, *64*, 477–498.

Zeng, L.-J., Niu, H.-C., Bao, Z.-W., and Yang, W.-B. (2017). Chemical lattice expansion of natural zircon during the magmatic-hydrothermal evolution of A-type granite. *American Mineralogist*, *102*(3), 655–665.

Zhang, Y.-G., and Frantz, J. D. (1987). Determination of the homogenization temperatures and densities of supercritical fluids in the system NaClKClCaCl2H2O using synthetic fluid inclusions. *Chemical Geology*, *64*(3-4), 335–350.

Zircon. (2020). Retrieved July 8, 2020, from http://www.webmineral.com/data/Zircon.shtml

Appendix A

List of minerals mentioned in the manuscript

Name	Formula	Abbreviation
Aegirine	$NaFe^{3+}Si_2O_6$	aeg
Aenigmatite	$Na_4Fe^{2+}{}_{10}Ti_2O_4Si_{12}O_{36}$	
Aeschynite-(Y)	$(Y,Ln,Ca,Th)(Ti,Nb)_2(O,OH)_6$	aes
Alamosite	$PbSiO_3$	
Albite	$NaAlSi_3O_8$	ab
Allanite-(Ce)	$CaCeAl_2Fe^{2+}Si_3O_{12}(OH)$	aln
Apatite	$Ca_5(PO_4)_3(OH,F,Cl)$	ap
Arfvedsonite	$Na_3Fe^{2+}{}_4Fe^{3+}Si_8O_{22}(OH)_2$	arf
Armstrongite	$CaZrSi_6O_{15}\cdot 2H_2O$	arm
Astrophyllite	$K_2NaFe^{2+}{}_7Ti_2Si_8O_{26}(OH)_4F$	astr
Baddeleyite	ZrO_2	
Barite	$BaSO_4$	
Bastnäsite-(Ce)	$CeCO_3F$	bsn
Biotite	$K(Mg,Fe^{2+})_3AlSi_3O_{10}(OH,F)_2$	
Britholite-(Ce)	$(Ce,Ca)_5(SiO_4)_3(OH)$	brh
Britholite-(Y)	$(Y,Ca)_5(SiO_4)_3(OH)$	brh
Calcioancylite-(Ce)	$(Ce,Ca,Sr)(CO_3)(OH,H_2O)$	
Calciocatapleiite	$CaZrSi_3O_9\cdot 2H_2O$	
Calciohilairite	$CaZrSi_3O_9\cdot 3H_2O$	Ca-hlr
Calcite	$CaCO_3$	
Cassiterite	SnO_2	
Catapleiite	$Na_2ZrSi_3O_9\cdot 2H_2O$	
Cerite-(Ce)	$(Ce,La,Ca)_9(Mg,Fe^{3+})(SiO_4)_3(SiO_3OH)_4(OH)_3$	
Chalcopyrite	$CuFeS_2$	
Chevkinite-(Ce)	$Ce_4(Ti,Fe^{2+},Fe^{3+})_5O_8Si_4O_{14}$	chk
Chloritoid	$Fe^{2+}Al_2OSiO_4(OH)_2$	
Cryolite	Na_3AlF_6	
Dalyite	$K_2ZrSi_6O_{15}$	
Elpidite	$Na_2ZrSi_6O_{15}\cdot 3H_2O$	elp
Epidote	$Ca_2Al_2Fe^{3+}Si_3O_{12}(OH)$	
Eudialyte	$Na_{15}(Ca,REE)_6(Fe,Mn)_3Zr_3Si_{26}O_{73}(O,OH,H_2O)_3(Cl,OH)_2$	EGM
Fayalite	$Fe^{2+}{}_2SiO_4$	fay
Fergusonite-(Ce)	$CeNbO_4\cdot 0.3H_2O$	
Ferriallanite-(Ce)	$CaCeFe^{3+}AlFe^{2+}Si_3O_{12}(OH)$	
Ferroceladonite	$KFe_2Si_4O_{10}(OH)_2$	Fe-Cel
Ferro-ferri leakite	$Na_3Fe^{2+}{}_2Fe^{3+}{}_2LiSi_8O_{22}F_2$	
Ferro-ferri-katophorite	$Na_2CaFe^{2+}{}_4Fe^{3+}Si_7AlO_{22}(OH)_2$	
Fluocerite-(Ce)	CeF_3	flc
Fluorbritholite-(Ce)	$(Ce,Ca)_5(SiO_4)_3F$	
Fluorite	CaF_2	flr
Fluornatropyrochlore	$(Na,Pb,Ca,REE,U)_2Nb_2O_6F$	
Gadolinite-(Ce)	$Ce_2Fe^{2+}Be_2O_2(SiO_4)_2$	
Gagarinite-(Ce)	$NaCaCeF_6$	
Gagarinite-(Y)	$NaCaYF_6$	

Galena	PbS	
Galgenbergite-(Ce)	$CaCe_2(CO_3)_4 \cdot H_2O$	
Gerenite-(Y)	$(Ca,Na)_2(Y, REE)_3Si_6O_{18} \cdot 2H_2O$	
Gittinsite	$CaZrSi_2O_7$	git
Hastingsite	$NaCa_2Fe^{2+}{}_4Fe^{3+}Si_6Al_2O_{22}(OH)_2$	
Hematite	Fe_2O_3	hem
Hilairite	$Na_2ZrSi_3O_9 \cdot 3H_2O$	hlr
Ilmenite	$Fe^{2+}Ti^{4+}O_3$	ilm
Kaersutite	$NaCa_2(Mg_3Fe^{3+}Ti)(Si_6Al_2)O_{22}O_2$	krs
Kainosite-(Y)	$Ca_2Y_2(SiO_3)_4CO_3 \cdot H_2O$	
Laptevite-(Ce)	$NaFe^{2+}REE_7Ca_5Y_3(SiO_4)_4Si_3B_2PO_{18}(BO_3)F_{11}$	lpt
Låvenite	$(Na,Ca)_4(Mn^{2+},Fe^{2+})_2(Zr,Ti,Nb)_2(Si_2O_7)_2(O,F)_4$	lvn
Leakeite	$Na_3(Mg_2Fe^{3+}{}_2Li)Si_8O_{22}(OH)_2$	lkt
Leifite	$Na_7Be_2Si_{15}Al_3O_{39}(F,OH)_2$	
Magnetite	$Fe^{2+}Fe^{3+}{}_2O_4$	
Maoniupingite-(Ce)	$(Ce,Ca)_4(Fe^{3+},Ti,Fe^{2+},\square)(Ti,Fe^{3+},Fe^{2+},Nb)_4Si_4O_{22}$	mnp
Microcline	$KAlSi_3O_8$	
Monazite-(Ce)	$CePO_4$	mnz
Nacareniobsite-(Ce)	$Ca_3REENa_3Nb(Si_2O_7)_2(OF)F_2$	ncr
Nahcolite	$NaH(CO_3)$	nah
Narsarsukite	$Na_2(Ti,Fe^{3+})Si_4(O,F)_{11}$	nrs
Okanoganite-(Y)	$(Y,REE,Ca,Na,Th)_{16}(Fe^{3+},Ti)(Si,B,P)_{10}(O,OH)_{38}F_{10}$	
Orthoclase	$KAlSi_3O_8$	
Parisite-(Ce)	$CaCe_2(CO_3)_3F_2$	
Pyrite	FeS_2	
Pyrochlore group minerals	$A_{2-m}Nb_2O_{6-w}F_{1-n}$ with A = Ca or Na	PGM
Pyrophanite	$Mn^{2+}TiO_3$	
Pyrrhotite	Fe_7S_8	
Quartz	SiO_2	qtz
Rutile	TiO_2	
Sphalerite	ZnS	
Stilpnomelane	$(K,Ca,Na)(Fe,Mg,Al)_8(Si,Al)_{12}(O,OH)_{36} \cdot nH_2O$	
Synchysite-(Y)	$CaY(CO_3)_2F$	
Thorite	$ThSiO_4$	thr
Titanite	$CaTiSiO_5$	ttn
Turkestanite	$(K,\square)(Ca,Na)_2ThSi_8O_{20} \cdot nH_2O$	
Uranosilite	$(UO_2)Si_7O_{15}$	
Vlasovite	$Na_2ZrSi_4O_{11}$	
Wollastonite	$CaSiO_3$	
Wulfenite	$PbMoO_4$	
Xenotime-(Y)	YPO_4	xnt
Yttriaite-(Y)	Y_2O_3	
Yttrialite-(Y)	$Y_2Si_2O_7$	ytl
Zajacite-(Ce)	$NaREE_{0.75}Ca_{1.25}F_6$	
Zircon	$ZrSiO_4$	zrn

Appendix B

Glossary of unusual terms used in the manuscript

A-type granite A stands for anorogenic, it is then a granite occuring in rift zones and intraplate that is usually alkaline (Le Maitre et al., 2004).
Agpaite an igneous alkaline rock in which REE occur in complex Zr-Ti-silicate minerals (e.g. EGM) (Marks and Markl, 2017).
Fenite a metasomatic rock, normally associated with carbonatites and occasionally with nepheline syenites and peralkaline granites. It is composed of alkali feldspar, sodic pyroxene, and/or alkali amphibole (Le Maitre et al., 2004).
Lindinosite peralkaline granite containing nearly 60 % riebeckite (Le Maitre et al., 2004).
Miaskite an igneous alkaline rock in which REE occur in simple silicates like zircon and titanite (Marks and Markl, 2017).
Porphyry any igneous rock that contains phenocrysts in a finer-grained groundmass. Often for rocks that contain two generations of the same mineral (Le Maitre et al., 2004).

Appendix C

Program used to determine the proportion of pyroxene in a thin section

Délimitation des zones de pyroxène sur des lames minces

9 juillet 2019
Par Yves Auda

1. Contexte

La délimitation des zones de pyroxène sur des lames minces est réalisée avec la seule connaissance de la délimitation de quelques zones de pyroxène par des polygones. Une seule classe étant définie, une analyse fondée sur le seuillage d'histogramme s'applique.

2. Matériel

Les lames minces sont photographiées et enregistrées au format jpg ou tif. Les polygone entourant des zones de pyroxène sont digitalisée sous QGIS. Ce logiciel n'est pas le mieux adapté car les SIG demandent que les données soient localisées à la surface terrestre dans un système de coordonnées géographiques ou cartographiques. La superposition des polygones et de l'image pose donc des difficultés résolues par un recalage manuel (fonction transform de GRASS).
Une chaîne de traitement interactif est développée sous R du CRAN et GRASS. La chaîne doit être paramétrée pour chaque image selon la procédure suivante :
Sous GRASS
1. créer une location plane/mapset pyroxene
2. copier les fichiers vecteurs (shape) et image dans un dossier appelé dossier maître
3. affecter le nom de ce dossier à la variable dirSrc de PROG/environnement.R
4. copier le fichier parametre.txt dans le dossier maître
5. donner un nom à l'analyse en affectant une valeur à la variable name du fichier parametre.txt. Choisir par exemple le même nom que celui du dossier maître
6. affecter à shape la racine des fichiers shape
7. affecter à image2 le nom de l'image (photographie de la lame mince)
8. exécuter source(« script1.R ») pour importer les données
8a. Si l'image est coupée, modifier la zone de calcul
9. afficher l'image (name.red) et le vecteur (shape)
10. définir une région de calcul englobant l'image (name.red)
11. déterminer le décalage et l'affecter à yshift. Utiliser QGIS pour identifier les zones homologues. Une valeur de 3950 convient pour les deux images testés.
12. décaler le shape en exécutant source(« script2.R »). Un fichier shapeTran
13. préparer les données pour le dessin d'histogramme source(« script3.R »)
14. modifier interactivement les bornes utilisées pour le seuillage d'histogramme en visualisant l'image name.pyr visualisant les pixels identifiés comme pyroxène. Utiliser source(« script4.R »). Ne pas oublier de rafraîchir l'affichage.
15. Le programme permet également un lissage mode majoritaire activé en positionnant la variable filtrage du fichier parametre.txt à yes. Fen est la taille de la fenêtre mobile.

Une fois l'image créée, différentes statistiques proportion des pixels de pyroxène, taille des amas de pyroxène, nombre d'amas… pourront être calculés.

Annexe
installation GRASS
https://grass.osgeo.org/download/software/ms-windows/#stand-alone

Script 1:

```
source("environnement.R")
source("gestPar.R")
initPar()

cmd("g.region res=1")

image2 <- litPar("image2")
name <- litPar("name")
shape <- litPar("shape")
cmd("r.in.gdal --overwrite input=" %+% dirSrc %+% "/" %+% image2 %+% " output=" %+% name)
cmd("r.composite --overwrite red=" %+% name %+% ".red green=" %+% name %+% ".green blue=" %+%
name %+% ".blue output=" %+% name)
cmd("v.in.ogr -o --overwrite input=" %+% dirSrc %+% "/" %+% shape %+% ".shp output=" %+% name)
```

Script 2:

```
source("environnement.R")

name <- litPar("name")
xshift <- litPar("xshift")
yshift <- litPar("yshift")

cmd("v.transform --overwrite input=" %+% name %+% " output=shapeTran xshift=" %+% xshift %+% "
yshift=" %+% yshift)
```

Script 3:

```
source("environnement.R")
source("gestPar.R")

source(dirLib %+% "/cookieCutter.R")

name <- litPar("name")
cmd("v.to.rast --overwrite input=shapeTran output=rastTran use=val")
cmd('r.mapcalc --overwrite expression="rastU = if(isnull(rastTran), 2, 1)"')
cmd("g.copy --overwrite raster=" %+% name %+% ".red,namered")
cmd('r.mapcalc --overwrite expression="rastU2 = if(isnull(namered), null(), rastU)"')

cookieCutter(layerMono="rastU2", varMono="pyroxene", listVar=name %+% ".", dateList="red blue
green",
 fileOut=dirTrav %+% "/result.csv")

print("fin extraction, memoire OK")
d2 <- read.csv(dirTrav %+% "/result.csv")
colnames(d2) <- c("pyroxene","can","pix")
d3 <- subset(d2, pyroxene == 1)
d4 <- subset(d2, pyroxene == 2)
ii <- sample(1:nrow(d4),nrow(d3)*2)
d5 <- d4[ii,]
d2 <- rbind(d3,d5)
write.csv(d2, dirSrc %+% "/resultS.csv", row.names=FALSE)
```

Script 4:

```
source("environnement.R")
source(dirLib %+% "/cookieCutter.R")
source("gestPar.R")
name <- litPar("name")

affich <- function(ci, d2i, d3i, fact) {
m1 <- mean(d2i)
s1 <- sd(d2i)
int1 <- m1 - fact * s1
int2 <- m1 + fact * s1
IMi <- readRAST9(name %+% "." %+%  ci)
dni <- IMi$CELL
dnib <- dni
dnib[!is.na(dnib)] <- 0
dni3 <- dni > int1 & dni < int2
dnib[dni3] <- 1

hist(d3i, main=ci, xlab='', ylab='', col='black')
hist(d2i, main=ci, xlab='', ylab='', col=ci, add=T)
ord1 <- length(d2i)
lines(data.frame(c(int1,int1),c(0,ord1)), col='pink', lwd=2)
lines(data.frame(c(int2,int2),c(0,ord1)), col='pink', lwd=2)

IMi$CELL <- dnib
imageC <- name %+% ".pyr"
writeRAST(IMi, imageC ,overwrite=TRUE)
imageF <- name %+% ".pyrF"


if(litPar("filtrage") == 'yes') {
print("filtrage mC)thode mode majoritaire")
fen <- litPar("fen")
cmd("r.neighbors --overwrite input=" %+% imageC %+% " output=" %+% imageF %+% " method=mode
size=" %+% fen)
}
}
```

```
# Debut programme

d2 <- read.csv(dirSrc %+% "/resultS.csv")
colnames(d2) <- c("pyroxene","can","pix")
canaux <- c("red","green","blue")

nopremfois <- FALSE
for (ci in canaux) {
d2i <- subset(d2, (pyroxene == 1) & (can == ci))[,"pix"]
d3i <- subset(d2, (pyroxene == 2) & (can == ci))[,"pix"]
if (nopremfois) dev.off()
nopremfois <- TRUE

repeat {
nameFact <- paste0("fact",ci)
fact2 <- as.numeric(litPar(nameFact))

affich(ci, d2i, d3i, fact2)

fact <- as.double(readline("facteur multiplicatif canal  (suivant -1) " %+% ci %+% " : " %+% fact2 %+% " ?
"))
if (is.na(fact)) fact <- fact2
if (fact == -1) break

affich(ci, d2i, d3i, fact)
ecritPar(nameFact,fact)
}
}
dev.off()
```

Script 5:

```
source("environnement.R")
source(dirLib %+% "/cookieCutter.R")
source("gestPar.R")
name <- litPar("name")

# Debut programme
imageF <- name %+% ".pyrF"
cmd("g.region zoom=" %+% imageF)
#r.report -i map=EV1807.pyrF units=c

IMi <- readRAST9(imageF)
dni <- IMi$CELL
tab2 <- table(dni)
tab2 <- matrix(tab2,nrow=1)
colnames(tab2) <- c("matrix", "pyroxen")
write.csv(tab2, dirRes %+% "/statitic.csv",row.names=FALSE)
```

Concentration et fractionnement des Terres Rares dans les complexes alcalins : le rôle des fluides

Les terres rares (TR) sont un groupe de métaux utilisés dans de nombreuses nouvelles technologies. Leur production est limitée, il est donc important de trouver de nouvelles sources d'approvisionnement. Les TR sont divisées en TR légères et lourdes, ces-dernières étant plus rares et ayant plus d'applications. Les granites et pegmatites alcalins sont des roches riches en TR lourdes. Une partie de cet enrichissement est d'origine magmatique, mais le rôle des fluides hydrothermaux (i.e. eau, CO_2, méthane surtout) pose question.

Ce manuscrit se concentre sur l'étude de minéraux communs (amphiboles, pyroxène, zircon) et des inclusions fluides de six zones du monde pour comprendre l'impact des fluides hydrothermaux par rapport à celui des processus magmatiques dans les granites et pegmatites alcalins. Les résultats montrent que la concentration et le fractionnement des TR sont liés à la circulation de fluides hydrothermaux riches en Na et K ou Ca et Na à des températures inférieures à 400 °C.

Mots-clés : terres rares, granite peralcalin, minéralisations, hydrothermal, pegmatites, HFSE, inclusions fluides, métallogénie

---

Concentration and fractionation of Rare Earth Elements in alkaline complexes: the role of fluids

The rare earth elements (REE) are a group of metallic elements used in many modern technologies. Their worldwide production is limited, hence it is necessary to find more sources. The REE are divided in light REE and heavy REE, the latter being rarer and with more industrial uses. Alkaline granites and associated pegmatites are rocks rich in heavy REE. Part of this enrichment is known to be magmatic, but the role of hydrothermal fluids (mostly water, CO_2 and/or methane) in concentrating and fractionating these elements remains unclear.

This work focuses on the study of minerals (amphiboles, pyroxene, zircon mostly) and fluid inclusions in six locations. The influence of hydrothermal fluids on REE relatively to magmatic processes is investigated in alkaline granites and associated pegmatites. The results show that REE concentration and fractionation is indeed linked to the circulation of hydrothermal fluids that are Na-K-rich or Ca-Na-rich and circulate at temperatures below 400 °C.

Keywords: rare earth elements, peralkaline granite, mineralizations, hydrothermal, pegmatites, HFSE, fluid inclusions, metallogeny